LEGIBILITY NOTICE

A major purpose of the Technical Information Center is to provide the broadest dissemination possible of information contained in DOE's Research and Development Reports to business, industry, the academic community, and federal, state and local governments.

Although a small portion of this report is not reproducible, it is being made available to expedite the availability of information on the research discussed herein.

ORNL-6233
Distribution Category
UC-34

ORNL--6233

DE86 008944

PHYSICS DIVISION

PROGRESS REPORT

for Period Ending September 30, 1985

J. B. Ball Director

S. Datz	Section Head
E. E. Gross	Section Head
C. M. Jones	Section Head
J. B. McGrory	Section Head
F. Plasil	Act. Sect. Head
R. L. Robinson	Section Head

Edited by: A. B. Livingston

Date Published: April 1986

OAK RIDGE NATIONAL LABORATORY
Oak Ridge, Tennessee 37831
operated by
MARTIN MARIETTA ENERGY SYSTEMS, INC.
for the
U. S. DEPARTMENT OF ENERGY
under Contract No. DE-AC05-84OR21400

Reports previously issued in this series are as follows:

ORNL-2718	Period Ending March 10, 1959
ORNL-2910	Period Ending February 10, 1960
ORNL-3085	Period Ending February 10, 1961
ORNL-3268	Period Ending January 31, 1962
ORNL-3425	Period Ending May 21, 1963
ORNL-3582	Period Ending January 31, 1964
ORNL-3778	Period Ending December 13, 1964
ORNL-3924	Period Ending December 31, 1965
ORNL-4082	Period Ending December 31, 1966
ORNL-4230	Period Ending December 31, 1967
ORNL-4395	Period Ending December 31, 1968
ORNL-4513	Period Ending December 31, 1969
ORNL-4659	Period Ending December 31, 1970
ORNL-4743	Period Ending December 31, 1971
ORNL-4844	Period Ending December 31, 1972
ORNL-4937	Period Ending December 31, 1973
ORNL-5025	Period Ending December 31, 1974
ORNL-5137	Period Ending December 31, 1975
ORNL-5306	Period Ending June 30, 1977
ORNL-5498	Period Ending December 31, 1978
ORNL-5787	Period Ending June 30, 1981
ORNL-6004	Period Ending September 30, 1983
ORNL-6120	Period Ending September 30, 1984

CONTENTS

2. EXPERIMENTAL NUCLEAR PHYSICS

NUCLEAR STRUCTURE STUDIES VIA ELASTIC AND INELASTIC SCATTERING

NUCLEAR STRUCTURE STUDIES VIA CHARGE-EXCHANGE REACTIONS

NUCLEAR STRUCTURE STUDIES VIA TRANSFER AND CAPTURE REACTIONS

NUCLEAR STRUCTURE STUDIES VIA COMPOUND NUCLEUS REACTIONS

QUASI-ELASTIC HEAVY-ION REACTIONS

STRONGLY DAMPED HEAVY-ION REACTIONS, FUSION, FISSION

EMISSION OF LIGHT IONS, NEUTRONS, PIONS, AND PHOTONS IN HEAVY-ION REACTIONS

MISCELLANEOUS TOPICS

INSTRUMENTATION

ACCELERATOR-BASED ATOMIC PHYSICS

LOW-ENERGY HEAVY-ION PHYSICS

NUCLEAR STRUCTURE

THE UNISOR NUCLEAR STRUCTURE THEORY PROGRAM

POSITRON PRODUCTION IN STRONG ELECTROMAGNETIC FIELDS

RELATIVISTIC NUCLEAR MODELS

INTERMEDIATE-ENERGY HEAVY-ION PHYSICS

ULTRA-RELATIVISTIC HEAVY-ION COLLISIONS

ATOMIC PHYSICS

MATHEMATICAL PHYSICS

6. NUCLEAR SCIENCE APPLICATIONS

INTRODUCTION

This report covers the research and development activities of the Physics Division for the 1985 fiscal year, beginning October 1, 1984, and ending September 30, 1985.

The research activities of the Division remain centered on experimental nuclear physics, experimental atomic physics, and theoretical nuclear and atomic physics. The largest of these programs, experimental nuclear physics, is dominated by the heavy ion research program. A major part of this effort is the responsibility for operating the Holifield Heavy Ion Research Facility as a national user facility. The operation of the Facility and the associated internal research programs are described in Chapters 1 — 3 of this report.

The activities of the nuclear research staff, while centered at the Holifield Facility, also involve the utilization of many other research facilities throughout the world. This work is also included in Chapter 2. A major new activity described here is the preparation for participation in an ultrarelativistic heavy ion experiment to be performed at CERN in 1986.

The experimental atomic physics program has two components: the accelerator-based studies of basic collisional phenomena and the studies in support of the controlled fusion program. These efforts are described in Chapter 4. Also associated with the fusion-related studies are a plasma diagnostics program and the operation of an atomic physics data center. The former is described in Chapter 7, and the latter is discussed in Chapter 9, along with our effort in support of the nuclear data compilation effort.

The theoretical physics program, both nuclear and atomic, is covered in Chapter 5. This chapter also includes the theory effort associated with the UNISOR program.

Smaller programs in applications and high-energy physics are summarized in Chapters 6 and 8.

Development work on new booster accelerator concepts to provide a significant increase in ion energy performance for the Holifield Facility has continued actively throughout this period. A preliminary design was prepared for a booster synchrotron, having a bending power of 8 Tm, to be injected by the Holifield tandem accelerator. This study is described in Chapter 10. At the end of this reporting period, a workshop was held to explore research opportunities in "intermediate energy" heavy ion physics. In response to the results of this workshop, the size of the booster will be increased. As this report goes to press, a design and proposal for a 15-Tm synchrotron booster accelerator is being prepared. Included also in Chapter 10 is a description of the efforts presently under way to design a 2-Tm synchrotron booster/cooler ring for the accelerator-based atomic physics program.

Finally, this report concludes with some general information on publications, Division activities, and personnel changes.

1. HOLIFIELD HEAVY ION RESEARCH FACILITY

OVERVIEW

J. A. Martin C. M. Jones
R. L. Robinson

Holifield Facility accelerator operation continued to show significant improvement this year. Operational highlights in this reporting period include provision of 3904 research hours (an increase of 23%), improved tandem accelerator voltage performance, and provision of twenty-eight ion species ranging from ^{1}H to ^{238}U.

Research hours per month since the first beam was available for research from the tandem accelerator are shown in Fig. 1.1. Beginning in January 1984, we have been using a cycle which has three to four months of research followed by about a month for minor accelerator development and programmed maintenance, which is denoted by "PM" in Fig. 1.1. The division of time between research- and machine-related activities appears to be near optimum.

Technical highlights in this period include demonstration of tandem accelerator operation with macropulsed beams, completion of a computer controlled emittance measurement system, installation of new control system computers for both the tandem accelerator and ORIC, development of a new tandem accelerator beam bunch phase-lock system, development of a new and more effective procedure for setting up coupled beams in ORIC, and development of a new aperture geometry for NEC acceleration tubes which provides improved electron and ion suppression. Details of these developments are reported in later sections.

Statistics on research activities are given in Tables 1.1-1.3. The spin spectrometer continues to be the most heavily used experimental device in the facility. Half of the research hours on this device were for studies of high-spin states utilizing up to eleven Ge detectors with up to nine of these being encompassed with Compton suppression annuli.

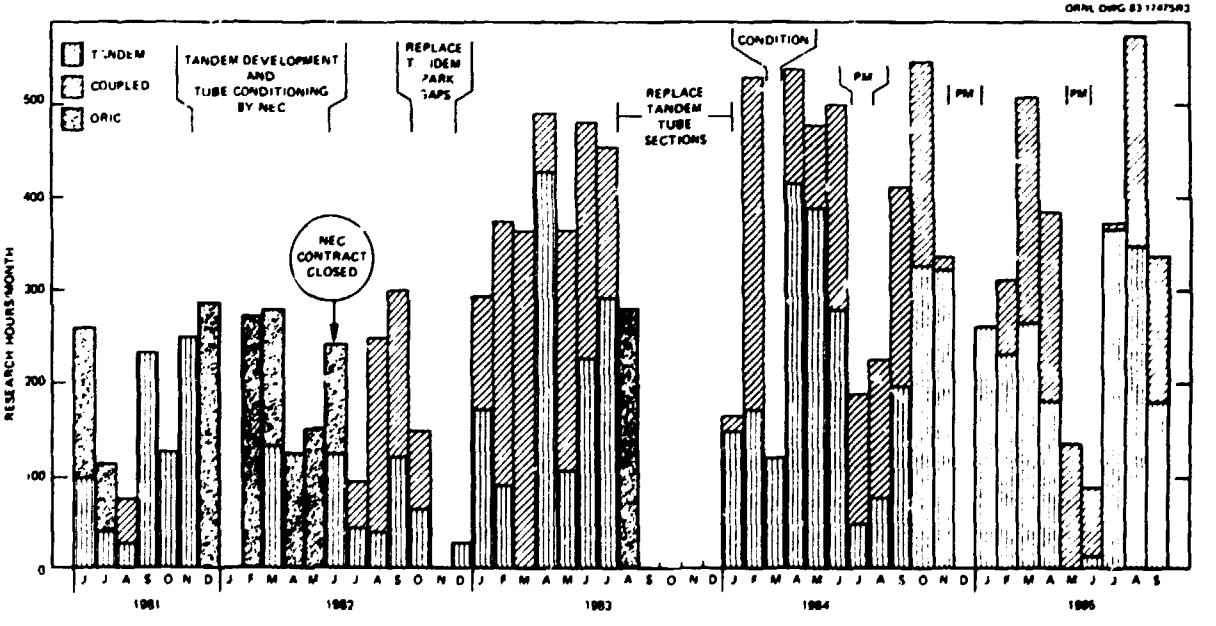

Fig. 1.1 Research hours per month for experiments utilizing the HHIRF accelerators. The intervals denoted as PM are programmed maintenance periods.

Table 1.1. Use of experiment target stations for the period October 1, 1984 through September 30, 1985

Target Station	Research Hours (No. of Runs)		
	Tandem	Coupled	Total
γ-ray spectrometer (tandem)	534(10)	na	534(10)
γ-ray spectrometer (coupled)	na	0	0
Velocity filter	183(4)	na	183(4)
Atomic physics (tandem)	89(2)	na	89(2)
Split-pole magnet	191(7)	na	191(7)
Applications (Beam line 31)	0	na	0
Beam line C-2	na	320(2)	320(2)
0.8-m chamber	na	41(2)	41(2)
Broad-range magnet	123(1)	488(6)	611(7)
Time-of-flight facility	50(3)	0	50(3)
1.6-m scattering chamber	84(3)	125(2)	209(5)
UNISOR	494(24)	0	494(24)
Spin spectrometer	766(11)	395(4)	1,161(15)
Beam line 17	21(1)	na	21(1)
Total	2,535(66)	1,369(16)	3,904(82)

na = not accessible to beam

Table 1.2. Division of research hours by research activities for the period October 1, 1984 through September 30, 1985

Activity	Research Hours		
	Tandem	Coupled	Total
High-spin states	755	135	890
Low-lying level properties	436		436
Giant resonances	18	146	164
Quasi-elastic	268	377	645
Damped reactions	143		143
Fusion	368		368
Fission	81	16	97
Reaction mechanisms	43	223	266
Pion production		320	320
Atomic	110	78	188
Applications	153		153
Tests of apparatus	134		134
Tests of detectors	26	74	100
Total	2,535	1,369	3,904

The broad range magnetic spectrometer with its associated vertical drift detector has proven to be a remarkably high resolution device. When operating in the dispersion matched mode with the ORIC cyclotron, the FWHM of a directly observed 1000-MeV ^{58}Ni beam was 160 keV ($\Delta E/E = 1/6000$). This system was also demonstrated to have mass resolution $\Delta M/M$ of 1:60.

The Joint Institute for Heavy Ion Research in its first year of operation carried out its mission of enhancing the research activities of the Holifield Facility principally by support of visitors - forty-six since July 1984. Another activity was the support of six workshops. The largest of these, which dealt with the topic of intermediate energy heavy ion physics, was held to examine the physics opportunities that might be made available if a large synchrotron booster were put at the Holifield Facility in place of the ORIC cyclotron.

ACCELERATOR OPERATIONS

G. D. Alton
J. A. Biggerstaff
S. L. Birch
M. R. Dinehart
D. T. Dowling
H. D. Hackler
C. L. Haley
D. L. Haynes
D. E. Hoglund[1]
E. D. Hudson
C. A. Irizarry
N. L. Jones
C. M. Jones
R. C. Juras[2]
S. W. Lane
C. T. LeCroy
C. A. Ludemann
C. A. Maples
J. A. Martin
R. L. McPherson
G. D. Mills
S. W. Mosko
S. N. Murray
D. K. Olsen
E. G. Richardson
N. F. Ziegler

In the current reporting period, FY 1985, "typical operation" of the Holifield Facility was provided for the entire year. As shown in Tables 1.4 and 1.5, beam was provided for research during this period for a total of more than 3900 h, an increase of 23% over 1984. Other important achievements during

Table 1.3. Number of researchers from different institutions who participated in experiments at the HHIRF in the twelve-month period between October 1, 1984 and September 30, 1985

Institutions	Number of Researchers
U.S. UNIVERSITIES	
Georgia State Univ.	1
Georgia Inst. of Tech.	8
JIHIF	1
Louisiana State Univ.	1
Massachusetts Inst. of Tech.	3
Michigan State Univ.	7
Mississippi College	1
ORAU	5
State University of New York	5
Tennessee Tech. Univ.	2
Texas A&M Univ.	6
Univ. of Florida	3
Univ. of Kentucky	1
Univ. of Pittsburg	2
Univ. of Rochester	6
Univ. of Tennessee	12
Univ. of Virginia	2
Vanderbilt Univ.	10
Washington Univ.	7
Western Kentucky Univ.	2
Yale Univ.	1
	86
NATIONAL LABORATORIES	
EG&G Idaho	1
NASA	3
Naval Research Center	1
Naval Surface Weapons Lab.	1
Nuclear Research Center	1
ORNL	53
	60
NON-U.S. INSTITUTES	
Hahn-Meitner Institute (Germany)	1
Institut fur Kernphysik (Germany)	1
Liverpool Univ. (England)	1
Manchester Univ. (England)	1
McMaster Univ. (Canada)	1
Neils Bohr Institute (Denmark)	1
Research Inst. of Physics (Sweden)	1
Univ. de Sao Paulo (Brazil)	1
Univ. of Aarhus (Denmark)	1
Univ. of Bielefed (Germany)	1
Univ. of Cologne (Germany)	1
Univ. of Delhi (India)	1
	12

Table 1.4. Tandem accelerator utilization for the period October 1, 1984 through September 30, 1985

	Hours	Percent
Beam available for research (tandem-alone and coupled operation)	3904	45
Beam available during ORIC tuning (coupled operation)	303	3
Accelerator tuning (includes scheduled startup-shutdown)	1167	13
Machine studies (includes conditioning not required for specific experiments)	439	5
Unscheduled maintenance	874	10
Scheduled maintenance	1727	20
Scheduled shutdown	346	4

Table 1.5. Cyclotron utilization for the period October 1, 1984 through September 30, 1985

	Hours	Percent
Beam available for research (coupled operation)	1369	16
Accelerator tuning (includes scheduled startup-shutdown and operation during tandem tuning)	444	5
Machine studies	73	1
Unscheduled maintenance	139	2
Scheduled maintenance	1478	17
Scheduled shutdown	5257	60

this period include reduction of tandem accelerator unscheduled maintenance by almost a factor of two to 874 h, reduction of ORIC unscheduled maintenance by 33% to 139 h, and reduction of ORIC tuning time by 33% to 2i h/run. Coupled operation continues to be limited by budgetary considerations.

A summary of beams provided in FY 1985, including eight new ion species, is presented in Table 1.6. The most notable of these are ^{1}H and ^{7}Li, which are the lightest ion species yet provided; ^{58}Ni, which was provided for three experiments at energies exceeding 1 GeV; and ^{238}U, which is the heaviest ion species yet provided. A significant improvement in operating efficiency during this period resulted from the use of the ORNL axial geometry cesium sputter sources described in the previous Physics Division Progress Report[3] and later in this section.

As part of our continued focus on training, a formal training and certification program for ORIC operators was implemented during FY 1985. In addition, one additional operator was certified for tandem accelerator operation and one additional operator was certified for ORIC operation.

Table 1.6. Beams provided for research for the period October 1, 1984 through September 30, 1985

Ion Species	Maximum Energy (MeV)	Mode	Provided for first time in this period
^{1}H	25	T	x
^{7}Li	80	T	x
^{12}C	300	T,C	
^{13}C	67	T	x
^{16}O	403	T,C	
^{17}O	376	T,C	
^{19}F	170	T	
^{24}Mg	138	T	
^{26}Mg	160	T	
^{28}Si	265	T	
^{32}S	725	T,C	
^{34}S	145	T	
^{35}Cl	240	T	
^{37}Cl	187	T	
^{40}Ca	210	T	x
^{45}Sc	200	T	
^{46}Ti	280	T	
^{48}Ti	220	T	
^{50}Ti	200	T	
^{52}Cr	230	T	x
^{58}Ni	1010	T,C	
^{64}Ni	235	T	
^{63}Cu	126	T	
^{90}Zr	395	T	x
^{93}Nb	276	T	x
^{116}Sn	634	C	
^{197}Au	357	T	
^{238}U	119	T	x

*T = Tandem alone; C = Coupled mode.

1. Co-op student, Virginia Polytechnic Institute and State University, Blacksburg, VA 24061.
2. Instrumentation and Controls Division.
3. G. D. Alton, Physics Division Progress Report for Period Ending September 30, 1984, ORNL-6120 (1985), p. 9.

TANDEM ACCELERATOR

G. D. Alton
J. A. Biggertaff
D. L. Haynes
D. E. Hoglund[1]
C. M. Jones
R. C. Juras[2]
J. E. Mann[3]
R. L. McPherson
G. D. Mills
E. G. Richardson
N. F. Ziegler

Voltage Performance

As shown in Fig. 1.2, voltage performance of the tandem accelerator continued to improve during FY 1985. During this period, the tandem accelerator was operated routinely at 20 MV and was operated for one scheduled experiment at 21.5 MV, a new world's record.

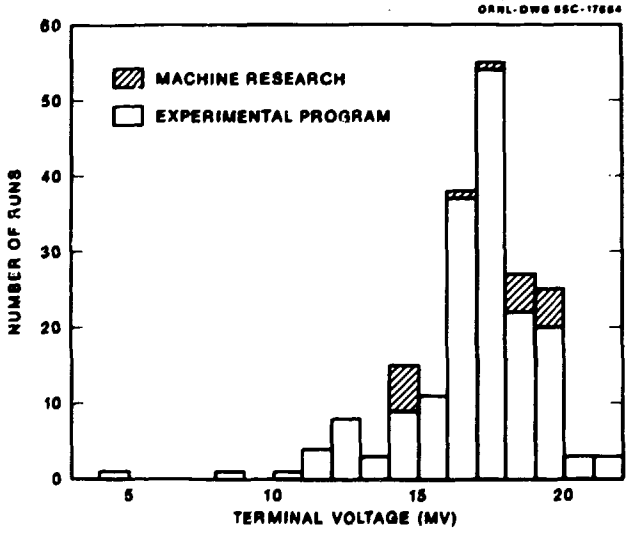

Fig. 1.2. The number of runs in 1-MV-wide intervals is shown as a function of tandem accelerator terminal potential for the period October 1, 1984 through September 30, 1985.

While the frequency of full column sparks increased slightly to an average of eight/month, only 7% of full column sparks resulted in observed deconditioning. As a result of our encouraging experience, the routine voltage limit for the experimental program was raised from 20 to 21 MV at the end of FY 1985.

As part of our effort to improve voltage performance of the accelerator, a test of the hydrogen arc discharge cleaning technique described in the previous Physics Division progress report[4] was performed on the top five units of the accelerator. Unfortunately, this test, which is described in detail later in this section, was inconclusive.

Development work in preparation for the planned FY 1986 Accelerator Improvement and Modification (AIM) project, which will provide for reconfigured acceleration tubes, has continued. As described later in this section, this work has resulted in an improved tube design which will be tested in FY 1986.

Improvements and Modifications

The efficiency and quality of tandem accelerator operation were further improved by the routine use of the axial geometry cesium surface ionization sources described in the previous Physics Division progress report[5] and later in this Section. Also described below are the development and testing of a macropulsed ion source (for synchrotron injection) and development of apparatus for measuring the emittance of negative ion source beams.

The now-obsolete Perkin-Elmer 7/32 computer used for real-time operation of the tandem accelerator control system was replaced with a surplus Perkin-Elmer 8/32D computer obtained from the ORNL Fusion Energy Division. With this change, both computers used in the tandem control system have now been upgraded to Perkin-Elmer type 8/32D. In addition, surplus components obtained from the Fusion Energy Division were used to (1) upgrade the control system shared memory from 32 kB to 128 kB, (2) upgrade the CSC (control and supervisory computer) fast memory from 512 kB to 768 kB, and (3) configure a third off-line 8/32D computer. The result of these changes, which were made with only minimal cost, will be improved reliability, easier maintenance, and increased system speed and capacity. In addition to the hardware changes noted above, work also continued on system software. The most important effort in this area was an extensive revision and improvement of the program which is used for recording accelerator parameters and setup of new beams.

The quality of coupled operation was further improved by development of a new phase-lock circuit. This circuit, which stabilizes the phase of beam bunches injected into the ORIC, utilizes a tuned resonant circuit which is excited by beam pulses passing through a cylindrical capacitive pickup element located in the transfer line between the tandem accelerator and ORIC. A phase error signal, which is generated by comparing the phase in the tuned resonant circuit with the ORIC rf phase, is used to control the pre-accelerator buncher phase so as to reduce time jitter in the injected beam. The effectiveness of this system is shown in Fig. 1.3 where we show the time dispersion of bunched beams with and without the phase-lock circuit. Two of the most important features of this circuit are that it functions with beam currents as low as 10 enA — a factor of five lower than the original phase-lock circuit, and that it operates over a frequency range of 4 to 16 MHz.

Engineering of the new beam buncher-chopper system was completed. Installation has been postponed to coincide with a major maintenance period for the accelerator when the low-energy tube will be at atmospheric pressure. One possibility is the interval during which the compressed geometry tubes will be installed. In the interim, this system will be tested off-line.

ORNL-PHOTO 1672-85

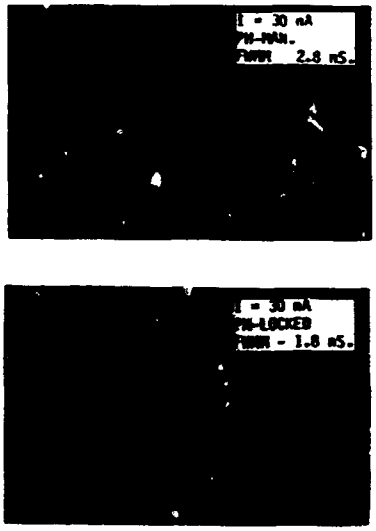

Fig. 1.3. Total time dispersion of bunched beams measured with a time-to-pulse-height converter for which the start signal is provided by gamma rays generated by the beam and the stop signal is provided by the ORIC rf. The upper figure is without phase-lock while the lower figure is with phase-lock. The examples shown were measured for a 30 enA, 125 MeV $^{32}S^{6+}$ beam for a period of four minutes each.

SF_6 System Operation

Operation of the SF_6 storage and recirculation system in FY 1985, including 15 transfers to and from storage, was without incident.

---

1. Co-op student, Virginia Polytechnic Institute and State University, Blacksburg, VA 24061.
2. Instrumentation and Controls Division.
3. Consultant.
4. P. H. Stelson, J. E. Raatz, and R. D. Rathmell, Physics Division Progress Report for Period Ending September 30, 1984, ORNL-6120 (1985), p. 14.
5. G. D. Alton, Ibid, p. 9.

ORIC ACCELERATOR

D. T. Dowling C. A. Ludemann
E. D. Hudson J. A. Martin
S. N. Lane S. W. Mosko
R. S. Lord[1] D. K. Olsen

Operation Highlights

During the period of this report, 21 runs were completed with coupled operation of the cyclotron and tandem accelerator. The stand-alone mode of cyclotron operation, using the cyclotron internal ion source, was not used during the year. The heaviest ion accelerated was $^{116}Sn^{+27}$ (634 MeV). The highest energy beam was 1010 MeV $^{58}Ni^{+24}$, which was used in three experiments. A performance summary for runs of the past year is given in Table 1.7. The accuracy of achieving the desired energy was within ~ 1% RMS. Beam extraction efficiency averaged about 70%. Beam stability was much improved as a result of the addition of a new phase-lock circuit to the tandem beam buncher system. Operational efficiency increased between FY 1984 and FY 1985: Tuning time was reduced from 31 h/run to 21 h/run; unscheduled maintenance time per research hour was reduced from 0.15 h to 0.10 h; the ratio of research time to total scheduled time increased from 62% to 68%. These improvements were realized as a result of better setup of the cyclotron and the continuing program of replacing unreliable and obsolete equipment.

Improved ORIC Setup Calculations

During this reporting period, a clearer understanding of the factors coupling beam extraction and first-harmonic balance of the ORIC magnetic field has been achieved. From this understanding, a consistent methodology for setup calculations has been developed. This work has resulted in more predictable, reproducible, and stable ORIC operation.

The compensated-iron magnetic extraction channel has both inside and outside coil currents which must be set during ORIC setup. These currents determine the channel's field contribution, both internal and external to the channel. The internal field of the channel must be adjusted to give the correct extracted beam path; whereas, the external field of the channel must be adjusted to give the correct first-harmonic field component for enhanced turn separation at extraction. To first order, the internal and external fields from the channel are linearly dependent on the inside and outside coil currents.

Table 1.7. Coupled operation for research for the period October 1, 1984 through September 30, 1985

Date	Ion	Desired Energy (MeV)	Measured Energy (MeV)	Error* (%)	Extraction Efficiency (%)	Injected Ion	Injection Energy (MeV)	Tandem Voltage (MV)
10/6/84	$^{32}S^{+15}$	720	715.1	- 0.7	80	$^{32}S^{+6}$	131.7	18.8
10/11/84	$^{58}Ni^{+23}$	930	910.0	- 2.1	75	$^{58}Ni^{+9}$	167.4	16.7
10/17/84	$^{58}Ni^{+23}$	930	910.0	- 2.1	50	$^{58}Ni^{+9}$	167.4	16.7
11/2/84	$^{58}Ni^{+23}$	930	907.8	- 2.4	90	$^{58}Ni^{+9}$	167.2	16.6
2/21/85	$^{58}Ni^{+23}$	930	933.9	+ 0.4	70	$^{58}Ni^{+9}$	179.8	18.0
2/26/85	$^{17}O^{+8}$	375	376.7	+ 0.4	85	$^{17}O^{+3}$	71.9	17.9
2/28/85	$^{17}O^{+8}$	325	326.0	+ 0.3	70	$^{17}O^{+3}$	71.9	17.9
3/1/85	$^{32}S^{+15}$	700	700.8	+ 0.1	75	$^{32}S^{+6}$	125.3	17.9
3/3/85	$^{116}Sn^{+27}$	630	634.4	+ 0.7	55	$^{116}Sn^{+7}$	138.5	17.3
3/27/85	$^{16}O^{+7}$	215	212.3	- 1.3	85	$^{16}O^{+2}$	53.4	17.8
3/29/85	$^{12}C^{+6}$	300	299.6	- 0.1	75	$^{12}C^{+2}$	53.9	17.8
4/10/85	$^{17}O^{+8}$	375	375.1	+ 0.0	60	$^{17}O^{+3}$	71.9	17.9
4/30/85	$^{32}S^{+15}$	700	703.5	+ 0.5	75	$^{32}S^{+6}$	133.7	17.9
6/25/85	$^{58}Ni^{+24}$	1005	1009.8	+ 0.5	90	$^{58}Ni^{+9}$	177.8	17.7
8/8/85	$^{32}S^{+15}$	700	713.7	+ 2.0	75	$^{32}S^{+6}$	126.2	18.0
8/26/85	$^{16}O^{+8}$	400	403.3	+ 0.8	75	$^{16}O^{+3}$	71.3	17.7
8/30/85	$^{58}Ni^{+23}$	930	917.7	- 1.3	55	$^{58}Ni^{+9}$	179.9	18.0
9/2/85	$^{32}S^{+15}$	720	725.2	+ 0.7	70	$^{32}S^{+6}$	127.0	18.1
9/4/85	$^{58}Ni^{+24}$	1005	1008.5	+ 0.3	75	$^{58}Ni^{+9}$	178.2	17.8
9/9/85	$^{58}Ni^{+24}$	1005	1010.6	+ 0.6	70	$^{58}Ni^{+9}$	178.8	17.9
9/11/85	$^{58}Ni^{+22}$	600	597.6	- 0.4	70	$^{58}Ni^{+9}$	179.9	18.0

*Error (%) = (Measured/desired - 1.00) x 100.

Therefore, there exists a unique pair of channel currents for any desired extraction path and first-harmonic balance.

In actual practice, this simple picture is confused because the channel's contribution to ORIC's first-harmonic balance is strongly dependent on the channel position, which in turn depends on the required extraction path, which in turn depends on the K ($K = ME/q^2$) and q/M of the beam. The balance is also strongly affected, of course, by the harmonic coil settings. In addition, the setup codes cannot correctly predict the inside- and outside-coil currents. In order to reduce this confusion, channel entrance and exit positions were found by calculation which readily allow extraction of all beams with $60 < K < 100$ and $0.25 < q/M < 0.5$. The channel has been fixed at this position for all ORIC runs during this reporting period. Beams have been extracted only through adjustment of the extraction channel coil currents and electrostatic deflector and coaxial magnetic channel strengths and positions.

Fixing the channel position has allowed a systematic study of the coil currents. The straight line in Fig. 1.4 shows the measured first-harmonic balance line; that is, any pair of coil currents on this line give the same first-harmonic component to the ORIC field. Different points along this line give different internal channel field strengths. The data points are the coil currents used for the last 17 ORIC runs. The points clustered around 2400 A of inside current are from K = 100 runs. The setup code for the same channel position tends to give a parallel balance line with ~ 300 A more outside current. In any event, Fig. 1.4 gives the approximate channel currents required for extraction.

All other injection parameters, extraction parameters, and trim-coil and harmonic-coil currents have been calculated following a

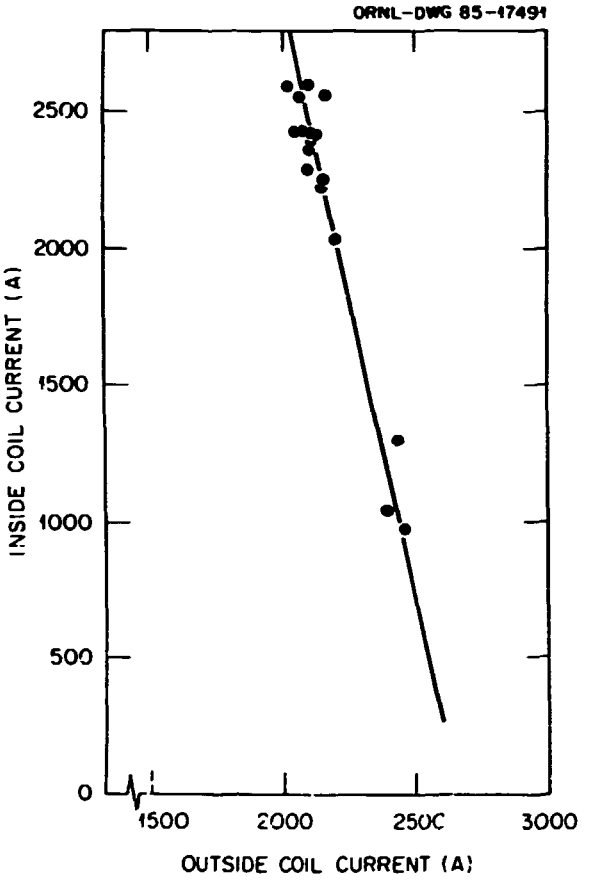

Fig. 1.4. The straight line is from measured pairs of inside- and outside-coil currents which give the required first-harmonic component to the ORIC field to deflect a K = 100, q/M = 0.23 beam at an extraction radius of 29.6 inches. The lower channel entrance and exit positions were set at 33.8 and 36.4 inches. The data points show the coil currents for all ORIC runs since October 1984.

fixed methodology with the goal of reducing the parameter differences from run to run. Following these procedures with strict adherence to calculated settings, a more predictable, reproducible, and stable operation has resulted. The time spent tuning the beam through ORIC in coupled operation has been reduced significantly.

Other operating improvements have included: turning trim coils 1, 2, and 3 off during normal operation, giving a simplified, more efficient cyclotron; including the injection foil energy loss in setup calculations; and measuring and including in the setup calculations possible beam obstructions in the dee structure.

New ORIC Control Computer

The new ORIC control computer, a MODCOMP Classic/55, was brought into operation, on schedule, in June 1985. The new hardware will insure the long-range availability of spare components as well as reliability of the system. Furthermore, the increased size of memory and disk storage will enhance the capability for software development.

Two areas of program development at this time are designed to improve on-line monitoring of operation as well as evaluation of machine performance. A voice-synthesized annunciator will augment CRT readout of errors detected in operating parameters. CRT graphics will aid analysis of beam-energy resolution as well as the internal distribution of ion current in the machine.

Two operator-assistance features that are expected to reduce occasional setup errors are also being developed. Operating parameters will be set directly from values computed from our setup code with minimal manual intervention. Furthermore, the independent controls for the currents in the inside and outside coils of our compensated-iron extraction channel will be replaced by the more appropriate physical parameters "strength" and "balance." This transformation will mathematically constrain the two currents and provide better control of the first-harmonic field component produced by the channel.

Cyclotron Improvements

Power Supplies. A program for upgrading magnet power supplies and replacement of obsolete or unreliable units is continuing. Nevertheless, power supply breakdowns were a major contributor to accelerator outages during the past year. Some of the most troublesome units included the valley harmonic coil power supplies, which have vacuum tube amplifiers, saturable reactor pre-regulators, and germanium-pass transistors. These power supplies will

soon be replaced by a group of newly purchased SCR-regulated units, which are now being installed.

The coaxial beam extraction magnet power supply is another unit receiving considerable attention. The main contactor and several control-circuit components for this 6000-ampere unit were replaced, and a new "dc transformer current sensor" will soon replace a badly deteriorated "freon-cooled shunt." This power supply has many good design features and it would be costly to replace. Consequently, it is hoped that these improvements will extend its useful life for several years.

A group of eight steering-magnet power supplies in the cyclotron control panel are being replaced by a new set of computer-controlled bipolar units and a handy patch panel for simplification of load assignment and connection. The original units were unipolar, vacuum-tube regulated, power supplies which have been in service for over 25 years. Six of the new units are already in use, and the remainder will follow soon.

It was found that one of our older switching-magnet power supplies was having frequent breakdowns due to improper load matching. Other power supplies of this same transistor regulated design series are very reliable. We have now exchanged loads between the troublesome unit and another more flexible power supply. Both units are performing satisfactorily.

RF System. The ORIC rf system has operated quite reliably during the past several years, but tuning range limitations prevented operation at frequencies above 18.0 Hz. We have reduced the dee aperture by 2.5 mm to increase the dee-to-ground clearance and thereby reduce capacitive loading. The net result is a usable tuning range of 6.70 MHz to 20.1 MHz, or a full 3:1 span. The rf system now uses less power at the upper end of the tuning range and stability is substantially improved. A potentially costly plan to modify the resonator for extending the rf-tuning range is no longer necessary. There is no evidence of loss of beam transmission resulting from the reduced dee aperture. The present aperture is 2 cm.

Vacuum System. The cyclotron vacuum system has received several improvements during the past year which are leading to better vacuum and easier maintenance.

Automatic controls and valves were added to the ion source/foil positioner vacuum lock which throttle pump and vent lines so as to avoid damaging stripper foils during foil carrier installation.

The cryopanels have been removed from the main magnet gap to improve gas conduction through the region. The cryopanels were originally intended for central region pumping when internal ion sources are in use. The panels were not effective for ion injection operation and they required excessive maintenance.

The 20-inch cryopump on the rear of the rf resonantor is still unable to perform according to expectation. We have tried throttling the pump with a baffle plate, which permits some operation, however, the pumping head tends to overload after a few days of operation. Most recently, Air Products sent a new cold head which is said to be of an improved design. So far, the new head looks better on cool-down rate, but proof of performance will require several weeks of testing.

Main Magnet Coil Conductor Passivation. The cyclotron's main magnet coils are fabricated from aluminum, which requires periodic passivation treatment to prevent destructive corrosion. This treatment should be done annually but has not been permitted in the last few years because of environmental restrictions on disposal of the passivation solution. The treatment produces a waste product consisting of several thousand gallons of water containing 2.25 kg of dissolved potassium dichromate. The disposal cost for such a quantity of waste material is not acceptable.

Recently, we learned that we could remove potassium dichromate from water in a resin-bed deionizer. A set of deionizer tanks was purchased and one successful passivation

treatment has been completed. The deionizer has sufficient capacity for two additional treatments. Following these treatments, we will have to purchase additional resin and dispose of a small volume of "filled" resin.

Instrumentation and Controls. Several refinements were implemented in the cyclotron's extraction system and injection system controls. Linear potentiometers were added to several positioner devices to improve position readout resolution and accuracy. Position calibrations were verified for the range of positions required by our new setup procedures.

New positioner readouts were provided on the stripping foil viewing mirror. We are now able to set mirror positions appropriate for any foil location without going through the former procedure of substituting an LED for the foil and pre-setting the viewing mirror. This reduces cyclotron setup time by more than one hour.

A new programmable multichannel chart recorder has been added to the main control panel. This recorder is replacing an obsolete unit, but it is adding several new capabilities to the cyclotron control system. The recording channels have programmable alarm levels which are being used to advise operators of undesirable operating conditions such as high water temperatures.

Utilities. Installation of a new compressed air dryer and distribution system was completed. The new dryers are somewhat smaller than the original units, but they are more efficient and have an improved control system. A humidity sensor determines when dryer tower switching is required and extends the operating cycle as appropriate. The original dryer system switched its dryer towers at four-hour intervals, but the new system delays switching for periods of several hours to several days. We have operated through the first summer in several years without a major compressed-air system breakdown. We have also experienced a substantial improvement in the reliability of air-actuated controls components, which formerly sustained frequent damage due to a wet-air supply.

Several changes and modifications in water coolant systems were implemented in the interest of energy conservation. A significant fraction of electrical energy consumption at HHIRF goes into pumping coolant through equipment. Consequently, improvements in the efficiency of the water system make a significant contribution toward reduction of HHIRF operating costs. We are operating the cooling tower with a single 150-hp circulation pump rather than with two pumps, when ORIC is shut down. A low-flow "throttle line" was added to the main deionized-water heat exchanger to permit operation with reduced flow. Also, a set of special operating procedures was developed for reducing coolant flow to inactive areas and for maintaining adequate system pressure in the cooling-tower loop when only one pump is operating. The net result is a reduction of electric power consumption by 2.5 to 3.0 MWh per day during periods when ORIC is shut down.

A cartridge-type deionizer was added to the 300-psi water system for maintaining low conductivity. Formerly, this system could be cleaned only by flushing with deionized water from the 150-psi water system. The 300-psi system serves areas subject to radiation activation and includes cyclotron extraction system components and the cyclotron beam probe. Reduced conductivity improves beam-current monitoring in these components and reduces electrolysis damage in water-cooled electrical leads.

---

1. Consultant.

NEGATIVE ION SOURCE DEVELOPMENT

High-Intensity Pulsed Beam Testing of the 25 MV Tandem Accelerator

G. D. Alton C. M. Jones

Efforts were continued during this reporting period to develop high-intensity,

pulsed-mode negative ion sources and the associated pulsing technology for synchrotron applications. Our interest in development of such capabilities has been stimulated by consideration of an 8-Tesla-meter synchrotron-cooler ring as a possible addition to the Holifield Heavy Ion Research Facility and, more recently, by consideration of a 2-Tesla-meter synchrotron-cooler atomic physics facility for which the HHIRF tandem accelerator would also serve as an injector. Typical pulse widths and repetition rates for synchrotron injection applications are ~ 100 μsec and a few Hz, respectively.

The cylindrical ionizer geometry negative ion source[1] was evaluated for pulsed mode operation and found to produce high-intensity, square waveform, negative ion beams at repetition rates of a few Hz from a variety of elements including Ag^-, Au^-, Cu^-, Ni^-, and O^- with peak intensities ranging from 100 to 350 μA.[2,3] Furthermore, the dc and pulsed beam components were found to be essentially independent of each other, i.e., the dc component could be adjusted without significantly affecting the pulsed beam component. The independence of the dc and pulsed beams is important for tandem accelerator applications in that a small dc beam is required for tandem terminal voltage control and for adjustment of beam line transport components (lenses, steerers, etc.) to assist in transport of the superposed pulsed beam through the accelerator and beam transport system.

After successful demonstration of pulsed negative ion beams with intensities, waveforms, and repetition rates commensurate with synchrotron applications, the question of whether such beams could be injected into the HHIRF tandem accelerator without detrimental effects on the operational stability of the accelerator was addressed. High-intensity, pulsed $^{16}O^-$ beams were injected into the HHIRF tandem accelerator in order to evaluate operation of the accelerator in this mode. Parameters chosen for this evaluation were: pulse length 100 μs, repetition rate 8 Hz, and average pulse amplitude 100 μA. A 6 μg/cm^2 carbon terminal foil stripper and a terminal potential of 14.1 MV were chosen for the evaluation. Examples of the injected $^{16}O^-$ (300 keV) and accelerated $^{16}O^{6+}$ (99 MeV) beams are shown in Fig. 1.5. No evidence of voltage instabilities or terminal voltage droop were detected during these tests.

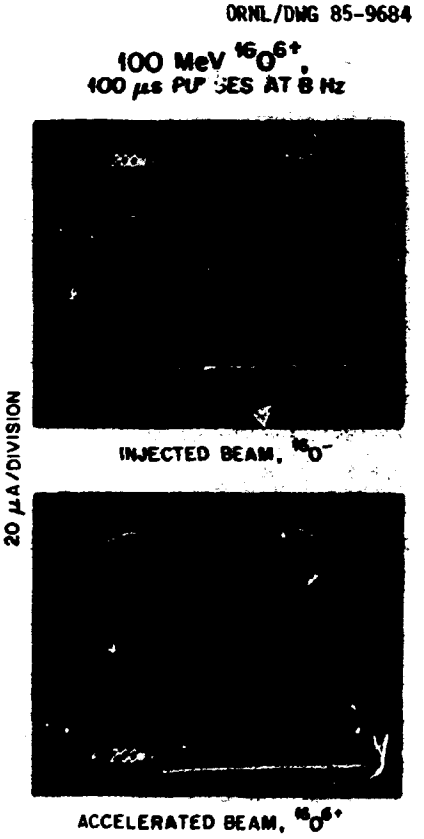

Fig. 1.5. Waveforms of ^{16}O beams injected into and accelerated by the Holifield Heavy Ion Research Facility tandem accelerator.

However, the percentage transmission of the pulsed component of the beam was observed to be slightly lower than that of the dc component, indicating perhaps the presence of space charge effects which are expected during low-velocity transport of such high-density negative ion beams in the injector. We also noted that the transport lenses required slightly increased potentials for the pulsed beam over those required required for transport of the dc beam.

The cylindrical ionizer geometry source has proven to be an excellent choice for pulsed mode operation, producing high intensities of negative ion beams from a spectrum of elements. The absence of any observable deleterious effects during operation of HHIRF tandem accelerator with intense pulsed ^{16}O beams indicates that the tandem accelerator can be used effectively as a synchrotron injector.

The Spherical Ionizer Geometry Negative Ion Source

G. D. Alton

The radial geometry cesium plasma[4] ion source and the cylindrical ionizer geometry[1,5] cesium sputter ion source used for routine tandem accelerator operation share in common the same mechanical features. The sources can be converted one to the other by the interchange of essentially one component. Thus, the basic source design permits easy and inexpensive change of the method and geometry for producing the cesium ion beam used for sputtering the material of interest.

The results of computer simulation studies of positive ion trajectories in the cylindrical ionizer geometry source show the positive ion distribution at impact with the cathode to be composed of two parts: a region concentrated on axis with diameter of 0.75 mm and a low-density uniform region with diameter of 4.5 mm. Sample wear patterns observed in practice are found to agree almost exactly with those predicted.

The presence of a two-component beam prompted computer simulation studies of a spherical ionizer geometry source, which would, in principle, not exhibit the halo beam effect and perhaps have a lower emittance as a consequence. The spherical geometry is readily amenable to simulation by solving Poisson's equation for the electrode configuration. An example of positive ion trajectories through the ionizer/sputter probe region of the source after optimization of the cathode region for negative ion extraction is shown in Fig. 1.6; the computed ion current density resulting from positive ion impact at the sample surface is shown in

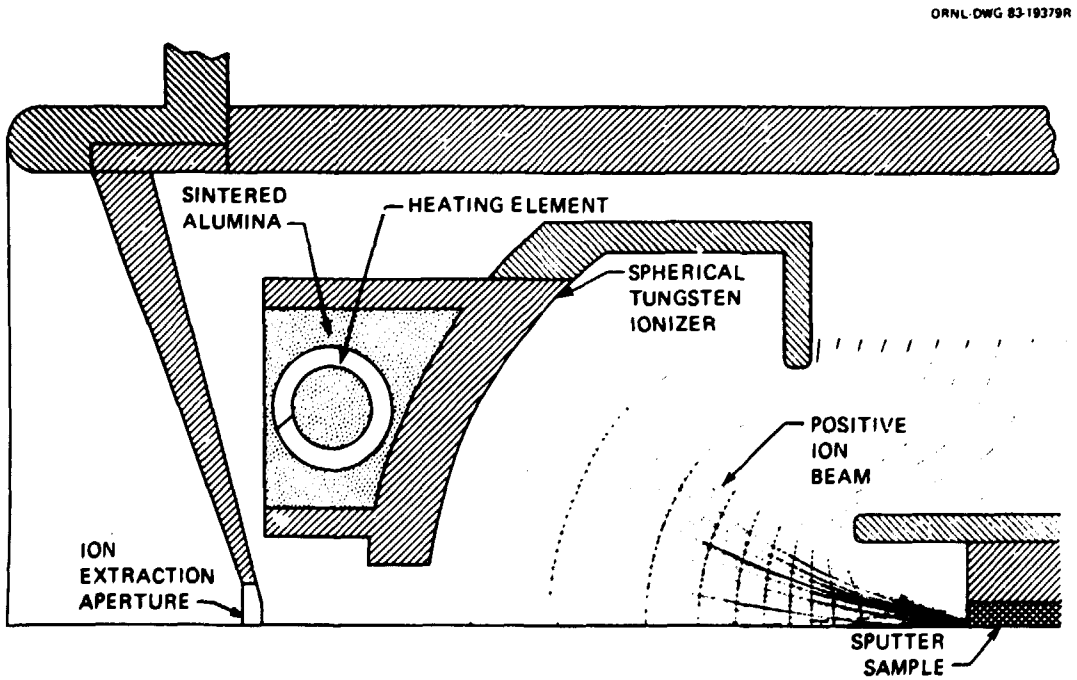

Fig. 1.6. Calculated positive ion trajectories in the ionizer/sputter probe region of the spherical ionizer geometry cesium sputter negative ion source.

Fig. 1.7. As noted, there is no evidence of a halo beam; these simulations predict a wear pattern on axis of ~ 0.75 mm diameter.

The ionizer support housing and cathode shapes and electrode positions were determined iteratively during positive and negative ion beam simulation studies through the chosen electrode configuration. The radius of curvature of the ionizer was arbitrarily chosen to be 25.4 mm.

Based on the results of the computer simulation studies, a spherical geometry ionizer was procured, and an ionizer support housing and a cathode electrode were fabricated. These components were assembled to form the spherical ionizer geometry cesium sputter negative ion source[6] and installed in the common housing for testing and evaluation.

Important operational parameters such as ionizer heater current versus ionizer temperature, negative ion yield versus cesium oven temperature, and negative ion yield versus cathode probe voltage were determined. The source was evaluated extensively during test stand operation and subsequently used as an "on line" source for routine tandem accelerator operation. The cathode wear patterns observed in practice are identical to those predicted by computer simulation studies, again pointing out the value of this technique.

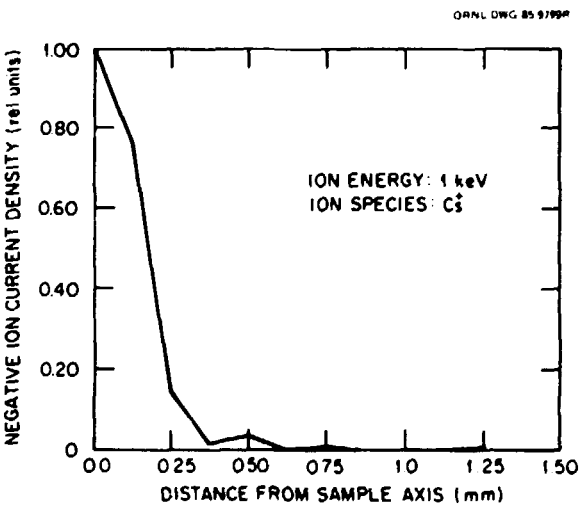

Fig. 1.7. Calculated positive ion current density distribution at the sputter probe region of the spherical geometry ionizer source.

Preliminary results indicate that the emittances of the spherical and annular geometry sources are almost identical. The source has been used to generate negative ion beams of Au^-, C^-, Ni^-, O^- and TiH^- with maximum observed intensities of 41 μA, 6 μA, 93 μA, 6 μA, and 600 nA, respectively. The C^-, O^- and TiH^- ion beams were recorded during "on-line" tandem accelerator operation and do not necessarily reflect optimized values.

Evaluation studies of this source will be continued during the next fiscal year. Presently a multiple sample indexing mechanism is being evaluated for use with both the spherical and cylindrical ionizer geometry sources.

The Emittance Measurement Facility

G. D. Alton J. W. McConnell
S. Tajima[7]

During this reporting period, an IBM personal computer (PC) was interfaced to an emittance measuring device[8] by means of a Transiac 6001 CAMAC crate controller.[9] The interface is effected through a plug-in card designed for use with the IBM PC. The crate controller acts as an external register to hold CAMAC N, F, A commands and to transfer data to and from the CPU of the computer. The driver-call programs, which address the CAMAC modules (input/output register, analog-to-digital converter, stepping motor controller), which, in turn, communicate with the emittance hardware through an external electronics unit, are written in the high-level computer language Basic.

The emittance measurement device consists of a vacuum housing, two identical steering motor driver-detector units for determining the emittances of an ion beam in either the

x or y directions and a control unit for driving the detector hardware. The control unit consists of a CAMAC crate with a crate controller, input/output register, stepping motor controller, and 12 bit analog-to-digital converter (ADC). The CAMAC crate control modules communicate with the emittance measurement hardware via an external electronics unit. The electronics unit consists of a relay unit for x,y direction selection, fast switches for stepping motor brake control, a current-to-voltage converter for processing detector current signals, current range logic circuitry, current integrators and an analog multiplexer.

The ion beam diagnostic unit (Fig. 1.8) consists of an electrically isolated slit aperture, positioned 0.4 m in front of a detector unit which is made up of 32 electrically isolated plates. The current striking each of the detectors is used to determine the differential angular divergence of the ion beamlet which is allowed to pass through the slit aperture at a given x or y position.

An emittance measurement consists of stepping the slit-detector system through the ion beam in a chosen direction while monitoring the total ion current striking the slit unit and the differential ion currents striking each of the 32 detectors during a

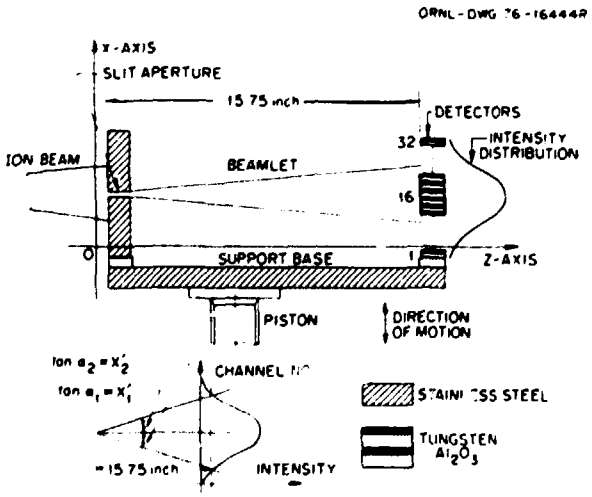

Fig. 1.8. Schematic drawing of the emittance measurement detector unit.

fixed integration time period (~ 5 ms). The position at which data is accumulated is determined by the voltage signal from a precision linear potentiometer. The ion currents from the slit unit and each of the 32 detection plates are converted to voltage signals and, along with the position voltage signals for each of 50 positions, are digitized and stored as a file on hard disk.

The control program is written in an interactive menu-driven format and can be executed by running the program MEASURE·BAS and selecting one of the following menu options: (1) data acquisition (single mode); (2) data acquisition (double mode); (3) store data to file; and (4) end.

A flow diagram for the data acquisition portion of the program is shown in Fig. 1.9. The data set can be called from file for data analysis. A complete set of x or y data, including background data, can be acquired and stored in memory in less than 20 minutes. An additional 20 minutes is required to process the data and extract emittance values. To date, the emittance measuring facility has been used to study emittance versus ion mass and ion beam intensity for the cylindrical and spherical ionizer geometry sources. Future plans include modifications to the electronics and control program and measurement of the emittances from negative ion sources operated in pulsed mode. The procedures and programs used for reducing the data and producing hard copy emittance information are discussed in the following report.

Emittance Data Analysis

G. D. Alton G. J. Nelson[10]

Several programs, interface programs and modifications to existing programs have been written, all in Basic, for processing raw emittance data. The programs, like the hardware control program, are executed on an IBM PC-XT equipped with 10 megabyte hard-disk storage. These programs are either written or exist in interactive menu driven format.

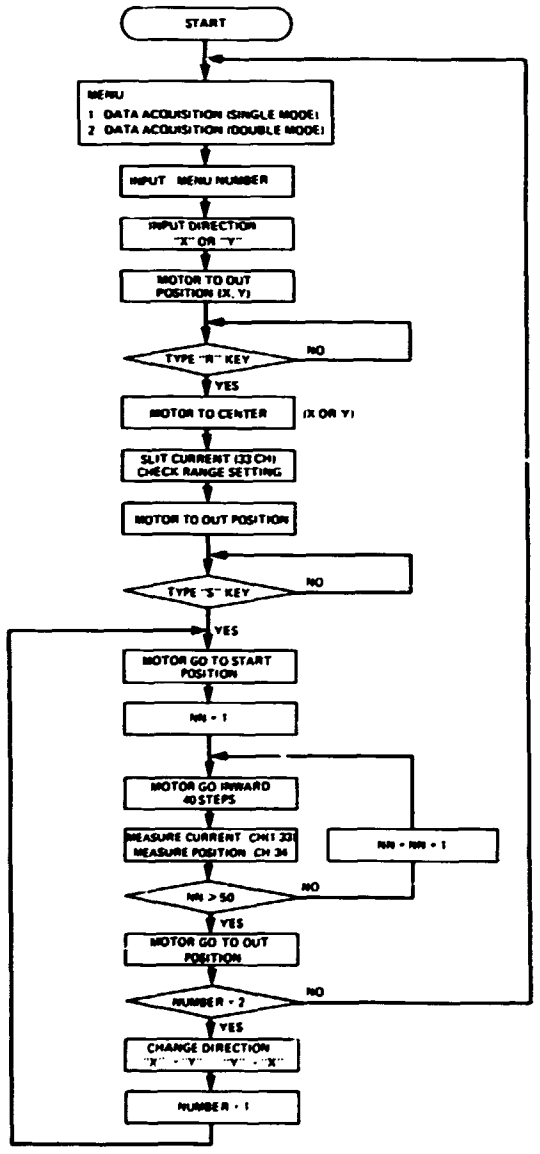

Fig. 1.9. Flow diagram for emittance data acquisition.

Prior to data storage or analysis, a menu selectable option permits a three-dimensional monitor display of the xx' or yy' versus intensity data set. By visually inspecting the raw data, a decision can be made whether to keep or erase the particular data file. If the data set is considered worthy of keeping, it is, first of all, subjected to point-by-point background subtraction by use of a background data file taken immediately after the beam measurement. This procedure is necessary because of the difficulty of electronically reducing the residual background to zero in each of the 32 detector channels.

In order to compensate for variations in beam intensity during a particular measurement, the data set is then normalized by multiplying each of the 32 detector channel readings by the ratio of the maximum slit current reading to the slit current reading at each of 50 positions. The data set is then ready for extraction of emittance information.

By selecting the appropriate option, emittance contours are calculated and automatically plotted. The contour levels are determined by performing a Simpson's rule volume integration over the xx' or yy' versus intensity data set. Contour levels which contain 10% through 80% of the total beam are calculated iteratively in increments of 10% to an accuracy of 0.1%.

The contour level information is then passed to a topographical graphics program[11] which produces contour plots from the data. The area within a particular contour is just the emittance for this particular beam fraction.

Emittance is defined by the relation

$$\varepsilon_x = A_x = \pi xx' \ [\pi \cdot mm \cdot mrad]$$
$$\varepsilon_y = A_y = \pi yy' \ [\pi \cdot mm \cdot mrad]$$

where A_x and A_y are the respective areas in the x or y directions defined by the percentage beam contours. Examples of contour plots along with y direction emittance data for the cylindrical geometry ionizer negative ion source are shown in Fig. 1.10.

Normalized emittances are obtained by multiplying each emittance value by the square root of the particle energy in MeV and may be plotted versus percentage total beam by execution of the plot routine.[11] A comparison of normalized emittance versus percentage total beam current from the cylindrical and spherical ionizer geometry negative ion sources is made in Fig. 1.11.

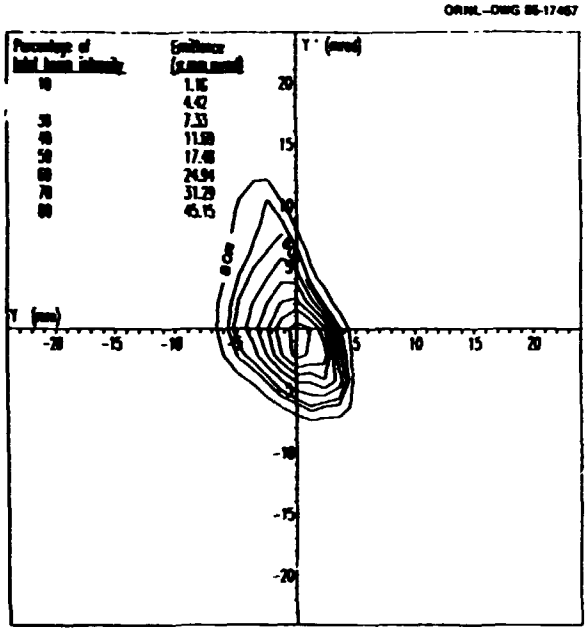

Fig. 1.10. Y-direction emittance contours for the cylindrical geometry ionizer negative ion source. Beam intensity: 6 μA.

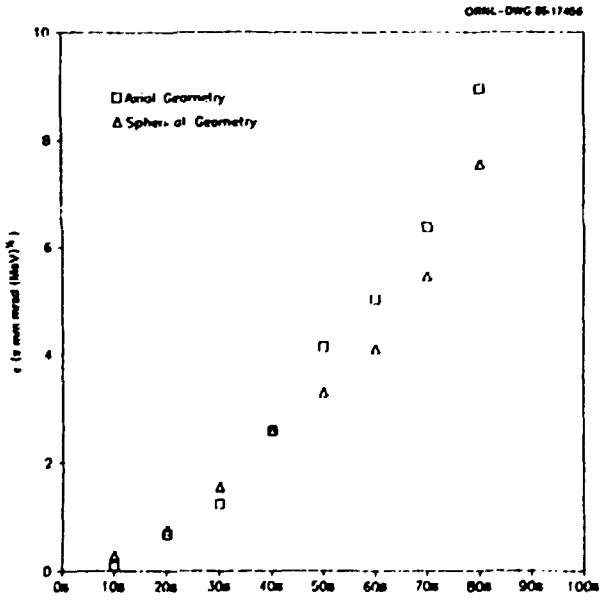

Fig. 1.11. Comparison of the normalized emittances versus percentage beam intensity for the cylindrical and spherical geometry ionizer negative ion sources.

Studies such as these have been made as function of mass and ion beam intensity for each of the two sources. No strong mass or beam intensity effects were observed.

---

1. G. D. Alton, Physics Division Progress Report for Period Ending September 30, 1984, ORNL-6120 (1985), p. 9.
2. G. D. Alton, Ibid., p. 10.
3. G. D. Alton and C. M. Jones, Proceedings of the Fourth International Conference on Electrostatic Accelerator Technology, Buenos Aires, April 1985 (to be published in Nuclear Instruments and Methods in Physical Research).
4. G. D. Alton, R. M. Beckers, and J. W. Johnson, Ibid.
5. G. D. Alton, Ibid.
6. G. D. Alton and G. D. Mills, IEEE Trans. Nucl. Sci., NS-22, No. 5 (1985), 1822.
7. Guest scientist from Japan Atomic Energy Research Institute, Japan.
8. NTG Nuklear Technik, West Germany.
9. Transiac, Inc., Mountain View, CA.
10. ORAU Student Research Participant from Gustavus Adolphus College, St. Peter, MN.
11. Golden Software, Inc., Golden, CO.

TANDEM ACCELERATOR TUBE DEVELOPMENT

Efforts to improve voltage performance of the tandem accelerator tubes continued during this reporting period. In this section, we summarize a hydrogen arc discharge conditioning test on the tandem accelerator and work on optimization of the design of the compressed geometry acceleration tubes which will be installed as part of the planned FY 1986 AIM project.

Arc Discharge Conditioning Test on the Tandem Accelerator

N. F. Ziegler P. H. Stelson
J. E. Raatz[1] C. M. Jones

In December 1984, a test of the hydrogen arc discharge cleaning technique[2,3] was performed on the acceleration tubes of the top five units of the tandem accelerator. This test was motivated by our desire to evaluate this technique as a possible way to improve the performance of our present acceleration tubes and as a method which might be used in

cleaning the compressed geometry tubes[4] which we plan to install in the accelerator as part of the FY 1986 AIM project.

Arc discharge cleaning of acceleration tubes was first attempted by Isoya et al.[5] of Kyushu University, Japan, and has been tested in several other accelerators[6,7,8] with varying degrees of success. Results achieved in small accelerators have been encouraging, but in larger machines, the results have not been as conclusive.

In both the low- and high-energy tubes the arc discharge was operated for a period of six hours with an arc current of about 4 A and a voltage drop of about 60 V per 20 cm tube section. The hydrogen flow was about 10 atmospheric liters per hour and the pressure varied from nominally 200 mT (inlet) to 100 mT (outlet) for the low-energy tube and from 260 mT (inlet) to 150 mT (outlet) for the high-energy tube. Ceramic temperatures were monitored at two typical positions during the discharge and reached values of 170°C and 155°C. Light emitted by the discharge was easily visible through the tube ceramic and appeared to change color during the course of the discharge. In general, the color changed from a pinkish-orange to a purplish-pink. Gap resistance measurements following the arc discharge indicated only minimal, if any, deposition of metal on the ceramic insulators due to sputtering.

The arc discharge test was performed during a scheduled maintenance period for the tandem accelerator. During this period the terminal gas stripper leak valve was repaired. Following the arc discharge, the gas stripper system was tested. The leak valve, which was thought to be closed, flooded the vacuum system with nitrogen to a pressure of about 600 Torr. The rapid gas flow blew titanium dust from the sublimator pump into the foil changer just above the top of the low-energy tube and, very likely, into the tube itself. This possibility initially was viewed with consternation, but it now appears to have had little, if any, effect on accelerator performance. The vacuum accident, however, has cast doubt on the results achieved by the arc discharge.

Following the scheduled maintenance period, the accelerator tank was pressurized in January 1985, and a preliminary check of tube conditioning was made. In February, a more detailed conditioning test was completed. The results of these tests may be summarized as follows. The maximum indicated stable voltage of the top five units of the accelerator after the arc discharge cleaning procedure was 4.45 MV, a value essentially equal to the maximum indicated stable voltage prior to the test. Thus, the arc discharge cleaning procedure resulted in no apparent improvement in voltage performance. In contrast, a striking difference was noted in the pre- and post-discharge conditioning behavior of the acceleration tubes. Prior to the discharge, the tubes exhibited a typical conditioning pattern for the 25URC accelerator. This pattern has two features. The first is a "continuous" X ray, thought to be associated with field emission, which is strongly but smoothly gradient dependent. The second feature is characterized by pulsed X rays and vacuum bursts which have a sharp gradient threshold that increases with time, i.e., which "conditions" upward as the gradient is slowly increased. This feature is thought to be the familiar microdischarge phenomena resulting from positive-negative ion exchange.

After the discharge, the pulsed X-ray conditioning was absent and the continuous, time-independent X ray was markedly reduced. Instead, we observed continuous X-ray production, with corresponding vacuum activity, which responded to gradient increases and then quickly conditioned away at fixed gradient. This behavior persisted until June 1985, when pulsed X-ray conditioning was again observed. At the end of this reporting period, these units exhibited "normal" pulsed X-ray

conditioning, but no continuous X-ray background.

As indicated above, the results of this test are somewhat clouded by the vacuum accident described above. At the present time, we plan to postpone consideration of further arc discharge tests until a determination can be made of the gradient limits imposed by the column structure. Such a determination is planned for May 1986, as part of the AIM-1986 project.

Compressed Geometry Accelerator Tube Design

K. A. Erb J. T. Mitchell[9]
C. M. Jones J. E. Raatz[1]
R. D. Rathmell[1]

The overall effective insulator length of acceleration tubes in the tandem accelerator can be increased by approximately 18%, by eliminating the heatable apertures provided as part of the original design. This modification would not only reduce the voltage gradient for a given total voltage, and thus improve performance, but would also eliminate a large number of potentially troublesome vacuum feedthroughs and mechanical components.

A compressed tube design meeting the above objectives was reported by Assmann et al.[10] and tests of this tube were carried out in a 3 MV accelerator at the National Electrostatics Corporation by HHIRF and NEC personnel.[11,12] While this tube performed satisfactorily, we have subsequently found that the apertures in this configuration can be shaped to achieve improved trapping of electrons and secondary ions. Associated changes in the adjacent insert electrodes are also required to shield the insulators.

Trajectories of secondary ions released from the aperture with various initial conditions were calculated for a design similar to that of Ref. 3. As the results shown in Fig. 1.12A. indicate, a significant number of these rays are accelerated into subsequent tube sections, where their increased energies render them progressively more troublesome.

We have found that this problem can be reduced significantly by introducing vee-shaped apertures, as shown in Fig. 1.12B. It is interesting to note that essentially complete one-tube suppression can be achieved when the apertures are pitched at even greater angles, but at the risk of possibly enhanced ion-exchange microdischarges. The geometry shown represents our best compromise between these two factors, and we intend to test the design under realistic conditions in May 1986, as part of the AIM-1986 project.

---

1. National Electrostatics Corporation, Middleton, WI.
2. P. H. Stelson, J. E. Raatz, and R. D. Rathmell, Physics Division Progress Report for Period Ending September 30, 1984, ORNL-6120 (1985), p. 14.
3. N. F. Ziegler, P. H. Stelson, C. M. Jones, and J. E. Raatz, Proceedings of the Fourth International Conference on Electrostatic Accelerator Technology and Associated Boosters, Buenos Aires, April 1985 (to be published in Nuclear Instruments and Methods in Physical Research).
4. J. E. Raatz, R. D. Rathmell, P. H. Stelson and N. F. Ziegler, Ibid.
5. A. Isoya, Y. Nakajima, T. Nakashima, N. Kato, K. Kobayashi, T. Sugimitsu, K. Kimura, S. Mitarai, T. Maeda and Y. Miyake, Proc., Third Int. Conf. on Electrostatic Accelerator Technology, Oak Ridge, Tennessee (April 13-16, 1981), p. 98.
6. G. Korschinek, J. Held, A. Isoya, W. Assmann, and H. Münzer, Nucl. Instrum. Methods, Phys. Res. A220 (1984) 82.
7. N. F. Ziegler, P. H. Stelson, W. Carli, H. Münzer, and G. Korschinek, Proc., Symposium of Northeastern Accelerator Personnel (SNEAP), Stony Brook, New York, 1984 (to be published).
8. E. Minehara, private communication.
9. Summer research participant, Oak Ridge Associated Universities.
10. W. Assmann, G. Korschinek, H. Münzer, Nucl. Instrum. Methods, Phys. Res. 220 (1984) 86.
11. J. E. Raatz, R. D. Rathmell, P. H. Stelson, and N. F. Ziegler, Physics Division Progress Report for Period Ending September 30, 1984, ORNL-6120 (1985), p. 15.
12. J. E. Raatz, R. D. Rathmell, P. H. Stelson, and N. F. Ziegler, Proceedings of the Fourth International Conference on Electrostatic Accelerator Technology and Associated Boosters, Buenos Aires, April 1985 (to be published in Nuclear Instruments and Methods in Physical Research).

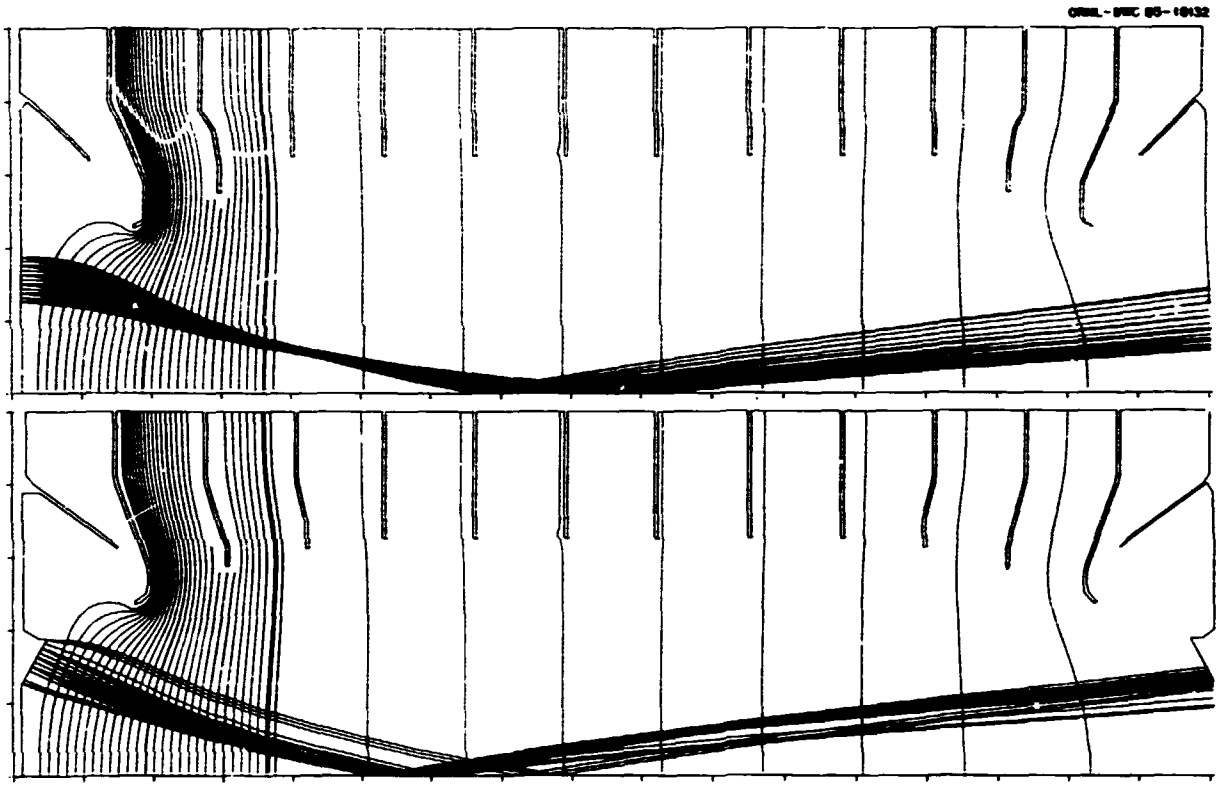

Fig. 1.12. Two possible compressed accelerator tube geometries: (a) top, a design similar to that proposed by Assmann et al.[10]; and (b) bottom, the geometry with vee-shaped apertures developed for the HHIRF tandem accelerator. Trajectories of secondary ions released from the apertures at the left are shown. Better ion-trapping is achieved with the vee-shaped apertures.

CHARGE-STATE DISTRIBUTIONS OF 100, 175, 275, AND 352 MeV GOLD IONS EMERGING FROM THIN CARBON FOILS

J. A. Martin K. A. Erb
R. L. Auble C. M. Jones
D. K. Olsen

These measurements were undertaken as a consequence of our failure early this year to accelerate Au^{+45} ions in the ORIC using an injected beam of 352 MeV $^{197}Au^{+17}$ from the tandem accelerator. Following that unsuccessful test, we made a preliminary measurement of the charge-state distribution of 352 MeV ^{197}Au ions emerging from a carbon foil using the bending magnet that is a part of the cyclotron beam injection system. The measured mean charge was ~ 38.5, about 4.5 charge-states lower than predicted by the Sayer[1] semi-empirical formula.

In these measurements, gold ions at 100, 175, 275 and 352 MeV were obtained from the tandem accelerator and the 90° double-focusing tandem accelerator energy analyzing magnet was used to separate the charge-states following stripping in the post-accelerator foil stripper. Carbon foil thicknesses of 10, 20, 40, and 80 $\mu g/cm^2$ were used depending on the beam energy. At least two different foil thicknesses were used at each energy to insure that equilibrium distributions were measured.

Table 1.8 summarizes the results of 12 measurements. The charge transmission percentage is the ratio of the sum of the currents measured following the analyzing magnet image slit for the several charge-states divided by the current measured in the Faraday cup just downstream from the stripping foil. Ideally, the charge-transmission ratio would be 100% but the measurements show values ranging from 89% to 132%. This may be due to incomplete suppression of electrons from the foil by the suppressor (1000 V) of

Table 1.8. Summary of ^{197}Au Charge-State Distribution Measurements

Meas. No.	Energy (MeV)	Foil Thickness ($\mu g/cm^2$)	Charge Transmission (%)	$\bar{q}$
1	352	40	117.4	38.3
2	352	40	110.2	33.3
3	352	80	105.6	38.2
4	352	20	132.5	37.8
5	275	40	88.9	35.3
6	275	40	109.9	35.3
7	275	20	112.8	35.6
8	175	20	97.1	31.9
9	175	10	97.2	31.4
10	175	20	95.5	31.8
11	100	20	97.7	28.0
12	100	10	117.0	27.6

Table 1.9. Charge-state distributions for ^{197}Au Ions

Ion Charge q	Ion Energy (MeV) 100	175	275	352
	Charge Fractions F_q (%)			
45				0.4
44				1.3
43			0.3	2.7
42			0.5	5.2
41			1.1	8.0
40			2.6	11.8
39			5.1	14.8
38		0.4	9.2	16.2
37		1.1	13.3	15.2
36		2.8	16.3	11.0
35		6.3	17.5	7.5
34	0.4	11.2	14.7	4.2
33	1.2	16.0	10.0	1.8
32	3.0	19.1	5.5	
31	7.0	17.7	2.6	
30	12.0	13.2	1.0	
29	18.0	7.6	0.2	
28	19.1	3.3		
27	16.4	1.2		
26	11.5			
25	6.5			
24	3.1			
23	1.3			
22	0.5			
21				

the cup located just beyond the stripping foil. Charge-distribution curves for a given energy, normalized to 100% transmission, are essentially identical for all of the thicker foils suggesting that the variation in transmission ratio is not significant. Normalized charge-state fractions for measurement No's. 1, 6, 10, and 11 are given in Table 1.9.

The mean charge derived from these measurements is plotted in Fig. 1.13 and compared with the prediction of the Sayer, Nikolaev and Dmitriev,[2] and Shima et al.[3] semi-empirical charge-state prediction formulas. These data agree with the average of the three formulas at 100 MeV but deviate systematically at higher energies. As shown in Fig. 1.13, data measured at Brookhaven National Laboratory[4] at 235 MeV agrees with the trend of the present results.

These measurements for ^{197}Au and the measurements of other groups for several heavy ions have been compared with the charge-state predictions of Sayer, Nikolaev and Dimetriev, and Shima et al. For ^{40}Ar, ^{63}Cu, and ^{84}Kr, the measurements and predictions of mean charge typically agree within 0.5 charge state whereas the measurements and predictions of mean charge for ^{132}Xe, ^{197}Au, ^{208}Pb, and ^{238}U show consistently larger discrepancies at energies greater than ~ 1 MeV/nucleon. These comparisons are reported in detail in the published paper.[5] We have not attempted to develop a new semi-empirical formula to describe the present measurements and those noted above since we believe that additional measurements are probably needed before an adequate semi-empirical formula can be devised. In the meantime, we note that the currently used charge-state prediction formulas should be used with caution for ions with $Z > \sim 36$ and energies above ~ 1 MeV/nucleon.

1. R. O. Sayer, Revue de Physique Appliquée 12 (1977) 1543.
2. V. S. Nikolaev and I. S. Dmitriev, Phys. Lett. 28A (1968) 277.
3. K. Shima, T. Ishihara and T. Mikumo, Nucl. Instrum. Methods 200 (1982) 605.
4. P. Thieberger, private communication.
5. J. A. Martin, R. L. Auble, K. A. Erb, C. M. Jones and D. K. Olsen, Proceedings of the Fourth International Conference on Electrostatic Accelerator Technology and Associated Boosters, Buenos Aires, April 1985 (to be published in Nuclear Instruments and Methods in Physical Research).

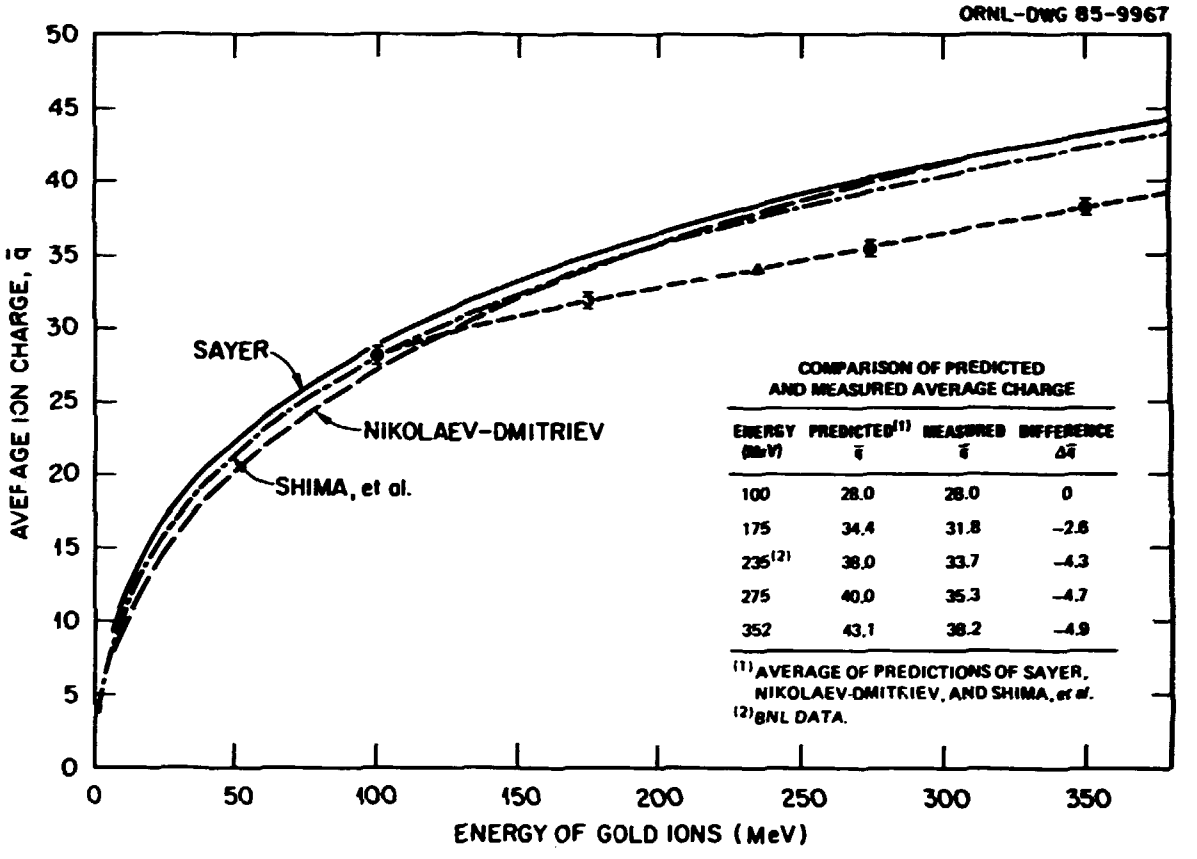

Fig. 1.13. Comparison of mean-charge derived from these measurements with the prediction of Sayer, Nikolaev-Dmitriev, and Shima et al. semi-empirical formulas.

EXPERIMENTAL APPARATUS

R. L. Auble
J. L. Blankenship[1]
H. K. Carter[2]
M. L. Halbert
H. J. Kim
J. W. Johnson
N. R. Johnson
R. L. Robinson

A list of the major experimental devices available to HHIRF users is given in Table 1.10. All of these devices have been in routine operation during the past year and most have required little or no modification. Brief discussion of the exceptions are given here. Additional details on specific projects are given elsewhere in this report.

Spin Spectrometer

Last year we reported that the average resolution of the NaI crystals of the spin spectrometer had slipped from the original value of 8.4% to 9.2%. This degradation has continued with the most recent measurement yielding an average resolution of 10.4%. Orders have been placed for rebuilding or replacing 40 of the 72 units. It is estimated that this will restore the average resolution to 9.0%.

The number of Ge detectors which are available for insertion into the spin spectrometer has been increased to eleven. Nine NaI and one BGO Compton suppression shields are presently available for use with these detectors. Liquid nitrogen fill systems for cooling the Ge-detectors are being improved to overcome problems caused by ice formation.

Velocity Filter

The major improvement to the velocity filter was the installation of newly designed and fabricated high voltage power supplies for the electrostatic deflectors. These have been tested at voltages up to 230 KV.

Table 1.10. Major experimental devices available to HHIRF users

Device	Beam Line	Beams[a]
Spin Spectrometer	C15	T,C
1.6-m Scattering Chamber	C16A	T,C
UNISOR	C16B	T,C
Time-of-Flight Facility	C17	T,C
Broad-Range Magnetic Spectrometer	C18	T,C
0.8-m Scattering Chamber	C20	C
Gamma-Ray Spectrometer	C7	C
80-cm Spherical Chamber	C9[b]	C[b]
Split-Pole Magnetic Spectrometer	33	T
Velocity Filter	21	T
Gamma-Ray Spectrometer	23	T
Atomic Physics Station	35	T

a. Accessible to beams from T = tandem accelerator only; C = ORIC or coupled accelerators only; T,C = both accelerators.

b. Normal location; can be moved to other beam lines if required.

Other improvements were the installation of a 3-jaw "clean-up" slit and a cryopump placed at the entrance of the velocity filter and addition of a microprocessor control system for the power supplies to facilitate setup.

Broad-Range Spectrometer

The excellent performance of the BRS detector system was demonstrated using a well collimated, low intensity, 1-GeV ^{58}Ni beam. The BRS was positioned at 0°, allowing the direct beam to enter the detectors thereby eliminating target-dependent contributions. The vertical drift chamber (VDC) exhibited a position resolution of 0.25 mm (FWHM); this corresponds to an energy resolution of approximately 1:6000. The angular resolution of the VDC was determined to be 0.3° (FWHM), which, due to the angular magnification of the BRS, implies a resolution of 0.08° in the measured scattering angle.

Some specific improvements to the broad range magnetic spectrometer are:

1. A viewer was installed which allows more precise dispersion matching of the BRS and the 153° analyzing magnet.
2. A 4-jaw collimator was added on the beam line to the BRS to limit the angular divergence of the beam and to allow direct viewing of incident beam by the focal plane detectors.
3. The vacuum control/display system was replaced to provide easier and more reliable operation.

---

1. Instrumentation and Controls Division, ORNL.
2. UNISOR, Oak Ridge Associated Universities.

ATOMIC PHYSICS AND APPLICATIONS ANNEX

R. L. Robinson D. L. Haynes

Support has been obtained for the addition of an experimental target room adjoining the tandem tower as shown in Fig. 1.14. Included in this project is a corridor between the new room and the tandem counting room. The target room provides sufficient space for four target stations to meet present and anticipated growing needs of researchers in the area of atomic physics and applications.

The design of this addition is 90% complete. The present schedule calls for start of construction early in 1986 and completion of the building before the end of the year.

COMPUTER SYSTEMS

J. A. Biggerstaff J. B. McGrory
W. H. Atkins[1] W. T. Milner
J. R. Beene R. O. Sayer[1]
J. W. McConnell C. N. Thomas[2]

Data Acquisition/Reduction Computer System

We now have 8 megabytes of memory in each of our three central processors. Half of this

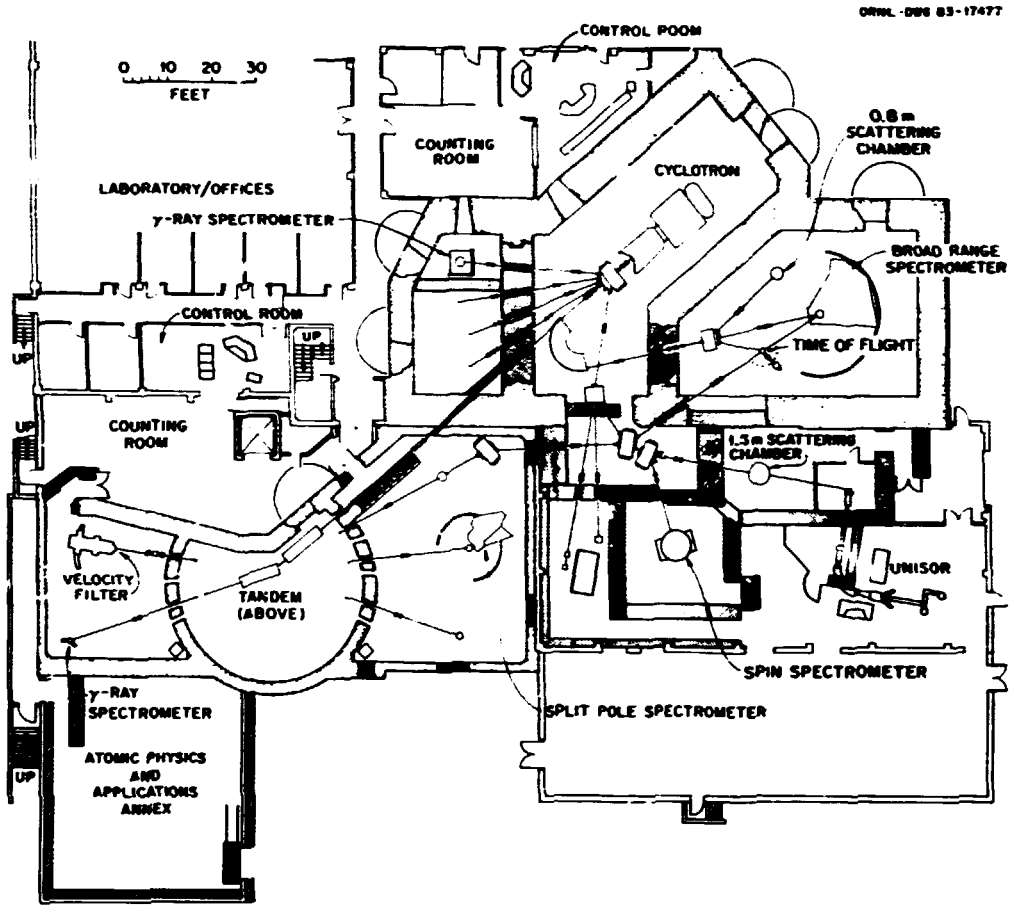

Fig. 1.14. Floor plan of the experimental areas at the HHIRF showing the location of the new atomic physics and applications annex planned for construction in 1986.

memory in each machine cannot be used by our aging CAMAC interfaces and must be given special treatment by the operating system. Two megabytes in each machine are reserved for histogramming use by the on-line acquisition task. The remaining two megabytes are reserved for future use by parallel-data-processing tasks (see below). One processor ("CPU-C") now has two new fixed-media disk drives (each 630 Mbyte) and a 240-Mbyte removable-media drive. CPU-A and CPU-B each have three of the 240-Mbyte disk drives. An additional 6250-bpi tape drive (#8) was installed. A Tektronix 4695 color copier was installed with a CAMAC interface accessible from any CPU. We no longer support color hard-copy on our three original Trilog printer/plotters, each of which is still accessible for monochrome plots from at least two CPU's. A memory module in our 3-way shared CAMAC crate now provides convenient and reliable means of transferring files between systems.

The most spectacular hardware accomplishment was the expansion of CPU-C to a two-processor system. Perkin-Elmer has offered the 3200 MPS multiple processor system for some time. This system, based on the (then) top-of-the-line 3250 CPU and using auxiliary processors (APU's) essentially identical to our 3230 processors, was beyond our means and would not have permitted us to use our Writeable Control Store (WCS) data processing microcode on the main CPU. We developed instead a significantly less expensive system using our existing 3230 as the main CPU configured with standard Perkin-Elmer components. The components required for adding a single APU were procured and installed in less

than one week. No significant problems were encountered; a functionally equivalent system is now offered by Perkin-Elmer as a standard product. The system fully meets our expectations -- two concurrent "tape-scan" tasks run in essentially the same time as one such task on a uniprocessor system. We have demonstrated that we still have reserve I/O capacity to serve additional APU's. Ultimately we will want to develop software to provide parallel processing within a single task but our present load is such that, with the assistance of the system load-levelling executive, we make effective use of the additional capacity by simultaneous execution of different tasks. The improved interactive response time during periods of heavy load has been especially gratifying.

Software developments include addition of procedures, for control of experimental apparatus, to acquisition packages and the generation of a new, single-user, acquisition and display package for testing and medium-scale off-line experiments (off-line means "not using the accelerators"). We have ported our data processing procedures and many of our utility programs to the VAX computer. Part of the reason for this work was to generate FORTRAN-language equivalents of our lower-level (assembly language and microcode) procedures to aid users who wish to study our techniques for data processing; the primary motive was to generate programs for export to users' home facilities. The graphics software package used on our VAX computer has been converted for use on the Perkin-Elmer computers.

The VAX 11/780, FPS-164 Array Processor Computer System

The scientific computing needs of the Physics Division have been met, in large part, by the VAX/AP system which is operated by the Physics Division. The computer system was heavily utilized (> 60% of total available CPU time on the VAX and the AP). The VAX is known for its reliability. The FPS-164 had significant reliability problems early in the fiscal year, but the substitution of a hard disc for a floppy disc for error logging apparently fixed the problem, and the AP has since been highly reliable.

One major modification of the system this year was the upgrade of the VAX 11/780 to a VAX 11/785. This yields a 50-70% enhancement in execution time for a given operation. The other major modification was to add one matrix accelerator board to the array processor. This gives a large enhancement for a small number of operations which involve a product of a matrix times a vector. As an example, with the accelerator board and the use of a new read-only table memory, the multiplication of a 120 x 120 matrix times a 120-dimensional vector was achieved at a rate of 22 million floating point operations per second (megaflops) as compared to 2.2 megaflops achieved without the new equipment. The 22-megaflop rate is very close to the rate for the original CRAY. Since much of the computing on the AP involves such operations, it is hoped that the throughput of the VAX/AP will increase significantly for some of the "stock" calculations. The accelerator board capability was added to the VAX/AP system by the Engineering Physics Division, which will now have access to the array processor from their newly acquired VAX 11/785. The hardware configuration of the system is shown here.

VAX

- 11/785 processor
- 12 megabytes fast memory
- ~ 1.5 gigabytes disc storage
- 1 800/1600 b.p.i., 125 i.p.s. tape drive
- 1 800/1600/6250 b.p.i., 125 i.p.s. tape drive
- 1 900 l.p.m. printer
- 1 TRILOG printer-plotter

FPS-164 Attached Processor

- 1 megaword of 64-bit fast memory
- 1 matrix accelerator board
- 270 megawords local disc storage

---

1. Computing and Telecommunciations Division.
2. Oak Ridge Associated Universities.

USERS SUPPORT

R. L. Auble
R. P. Cumby
R. W. Miles
C. A. Reed[1]
C. N. Thomas[1]
M. E. Whitley

The Users Support Group consists of several technicians who assist HHIRF users with the setup of experimental apparatus. Because of the demand for beam time and the consequently tight operating schedule for the HHIRF accelerators, it is extremely important that each experiment be ready to start at the designated time. This goal has been met through the combined efforts of the experimentalists and the users support group.

Assistance with vacuum systems and mechnical design is provided by Bob Miles and Charles Reed. Maintenance of the HHIRF electronics pool and testing of detectors is covered by Richard Cumby and Mark Whitley. Interfacing of the experimental apparatus with the HHIRF data acquisition computers is handled by Charles Thomas.

In addition, the Support Group provides the in-house staff with technical assistance in the modification of existing, and the design of new, experimental apparatus.

---

1. Oak Ridge Associated Universities.

JOINT INSTITUTE FOR HEAVY ION RESEARCH

R. L. Robinson
J. H. Hamilton[1]
L. L. Riedinger[2]

In July 1985 the Joint Institute for Heavy Ion Research (JIHIR) completed its first year of operation as a funded organization. Because the Institute is a new concept for the managing institutes (ORNL, University of Tennessee, and Vanderbilt University), this has been a year in which the JIHIR Policy Council has been developing guidelines for best utilizing the resources of the JIHIR in fulfilling its mission of enhancing the research programs of the Holifield Heavy Ion Research Facility. The major use of the funds has been for support of guests. Between July 1984 and September 1985, there have been 46 guests with an average length of stay of 2½ months. The Policy Council has attempted to choose persons, both experimentalists and theorists, with a wide range of professional experience (from renowned scientists to promising post-docs) and with strengths in different subdisciplines (nuclear structure, reaction mechanisms, atomic physics, etc.). Table 1.11 lists the guests who began their JIHIR appointment during the July 1984–September 1985 period.

A second way in which the JIHIR is contributing to the HHIRF program is through its sponsorship and organization of meetings. Some specifics on the meetings are given in Table 1.12. These were held in the conference room of the JIHIR.

The JIHIR continues to provide dormitory accommodations for HHIRF users. At the beginning of FY 1985 the number of available beds was increased from 8 to 10. The number of overnight guests was 218 during FY 1985 and the average length of stay was 6 days.

During most of the year, the only regular employee of the JIHIR was a half-time secretary. This was clearly inadequate secretarial support and the position has recently been increased to full time.

---

1. Vanderbilt University, Nashville, Tennessee.
2. University of Tennessee, Knoxville, Tennessee.

USERS GROUP ACTIVITIES

R. L. Auble

During 1985, members of the HHIRF Users Group were requested to renew their membership, in keeping with the Users Group Charter. A total of 385 users renewed their memberships and the total membership presently stands at 407.

Since October 1, 1984, the Executive Committee has held five meetings to provide input to the HHIRF operations staff and management and to keep abreast of developments on the HHIRF accelerators and experimental apparatus.

Table 1.11. Visiting scientists at the Joint Institute for Heavy Ion Research during the period of July 1984 - September 1985

Name	Institute
A. Arima	Univ. Tokyo (Japan)
S. Ayik	Western Kentucky Univ.
M. A. Beckerman	Joint Institute for Heavy Ion Research
R. Bengtsson	Lund Univ. (Sweden)
D. R. Bes	Univ. Argentina (Argentina)
A. Bracco	Univ. Milano (Italy)
R. A. Braga	Georgia Inst. of Tech.
D. Brink	Oxford Univ. (England)
R. Broglia	Niels Bohr Institute (Denmark)
P. A. Butler	Univ. of Liverpool (England)
F. Canto	Lawrence Berkeley Laboratory
Y. S. Chen	Inst. of Atomic Energy (Beijing, China)
N. Cindro	Ruder Boskovic Inst. (Yugoslavia)
J. D. Cole	INEL
J. Eberth	Univ. Cologne (West Germany)
A. Faessler	Univ. Tubingen (West Germany)
J. D. Garrett	Niels Bohr Institute (Denmark)
W. Greiner	Univ. Frankfort (West Germany)
I. Hamamoto	Lund Univ. (Sweden)
P. G. Hansen	Aarhus Univ. (Denmark)
F. Iachello	Yale Univ.
M. Irvine	Manchester Univ. (England)
C. M. Ko	Texas A&M Univ.
S. Koonin	Cal. Inst. of Tech.
R. Liotta	Res. Inst. of Physics (Sweden)
D. J. Love	Univ. Liverpool (England)
C. Mahaux	Univ. Liege (Belgium)
J. A. Maruhn	Univ. Frankfort (West Germany)
E. Migneco	Univ. Catania (Italy)
H. P. Morsch	Inst. fur Kernphysik (West Germany)
U. Mosel	Univ. Giessen (West Germany)
W. Nazarewicz	Lund Univ. (Sweden)
P. Nolan	Univ. of Liverpool (England)
S. Pancholi	Univ. Delhi (India)
F. Paulano	Niels Bohr Institute (Denmark)
L. Peker	Brookhaven National Laboratory
P. Quentin	Univ. Bordeaux (France)
J. O. Rasmussen	Lawrence Berkeley Laboratory
P. G. Reinhard	Univ. Erlangen (West Germany)
P. Semmes	Georgia Inst. Tech.
K. Schmid	Univ. Tubingen (West Germany)
K. Taulbjerg	Aarhus Univ. (Denmark)
K. Teh	Vanderbilt Univ.
C. L. Wu	Jilin Univ. (Jilin, China)
Y. Yamazaki	Tokyo Inst. of Tech. (Japan)
J. Y. Zhang	Inst. of Modern Phys. (Lanzhou, China)

The dates and locations of the meetings were:

October 19, 1984 at Nashville, Tennessee;
February 15, 1985 by telephone conference;
April 26, 1985 at Crystal City, Virginia;
June 24, 1985 at HHIRF;
September 25, 1985 at JIHIR.

Members of the Executive Committee are listed in Table 1.13. They are elected by the Users Group, with two new members being elected each year for a three-year term. The slate of candidates is selected by a Nominating Committee whose members for 1985 were Doug Cline (Chairman), Joe Natowitz, Demetrios Sarantites, Glenn Young, and Ed Zganjar.

The annual meeting of the Users Group was held in Nashville, Tennessee on October 19, 1984, with approximately 50 persons in attendance. In addition to serving as a convenient mechanism for keeping users informed of happenings at HHIRF, this meeting provided a forum for users to express their questions and concerns regarding the operation of the HHIRF.

PROGRAM ADVISORY COMMITTEE

R. L. Robinson

An indicator of the normality of facility operation has been the regularity of the meeting times for the Program Advisory Committee. As shown by the statistics given in Table 1.14, the time interval between the last four PAC meetings was approximately six months. Statistics in this table also suggest that the number of requested hours has equilibrated at about 3000. If the Holifield Facility can achieve near 4000 hours of research per year, as is the current projection, about 60% of these requested hours can be approved. This allows for 10-15% of the research hours being reserved for discretionary time.

Table 1.12. Meetings sponsored by JIHIR during FY 1985

Meeting	Date	Approximate Attendance	Organizer
Holifield Theory Users Group Meeting	Oct. 12-13, 1984	40	J. McGrory G. Leander M. Strayer
Symposium on Directions in Nuclear Structure Research	Oct. 15-16, 1984	120	JIHIR
Holifield Theory Users Group Meeting	May 10-11, 1985	40	J. McGrory G. Leander M. Strayer
Workshop on Future Directions for UNISOR	June 26-27, 1985	40	K. Carter
High Spin Workshop	July 11-16, 1985	40	N. Johnson L. Riedinger
Workshop on Intermediate Energy Heavy Ion Physics	Sept. 23-25, 1985	140	ORNL Physics Division and JIHIR

Table 1.13. Users Group Executive Committee Members for 1984-86

1984*

C. K. Gelbke, Michigan State University
D. C. Hensley, Oak Ridge National Laboratory
J. B. Natowitz, Texas A&M University
D. G. Sarantites,† Washington University
E. H. Spejewski, Oak Ridge Associated Universities
S. G. Steadman, Massachusetts Institute of Technology
J. L. Wood, Georgia Institute of Technology

1985

M. W. Guidry, University of Tennessee
D. C. Hensley, Oak Ridge National Laboratory
A. C. Mignerey, University of Maryland
D. G. Sarantites, Washington University
S. G. Steadman,† Massachusetts Institute of Technology
J. L. Wood, Georgia Institute of Technology

1986

J. R. Beene, Oak Ridge National Laboratory
M. W. Guidry, University of Tennessee
I. Y. Lee, Oak Ridge National Laboratory
A. C. Mignerey, University of Maryland
S. G. Steadman, Massachusetts Institute of Technology
J. L. Wood,† Georgia Institute of Technology

* Seven members due to change from 2-year to 3-year tenure.

† Chairperson.

The last column of Table 1.14 gives the hours of the recommended experiments which remain, as of September 30, 1985, to be scheduled. The intention is to complete the majority of experiments within a year after approval.

Table 1.15 lists the participants on the PAC's which met during FY 1985. Harvey Gould (Lawrence Berkeley Laboratory) is a new member of the committee. George Bertsch (Michigan State University) and Joe McGrory (Oak Ridge National Laboratory) were substituting for regular members who were unable to attend.

Table 1.14. Statistics on PAC's as of September 30, 1985

	Meeting Time	Requested	Recommended	Rec/Req.	Yet to be Run (hrs)
PAC-1	Nov. 80	4840	2120	44%	0
PAC-1A	Jun. 81	2164	1032	47%	0
PAC-2	Feb. 83	5120	1656	32%	0
PAC-3	Apr. 84	5288	2232	42%	32
PAC-4	Sept. 84	3272	2048	63%	334
PAC-5	Apr. 85	3368	2056	61%	1301
PAC-6	Sept. 85	2976	1776	60%	1776

Table 1.15. Participants on PAC meetings held in FY 1985

PAC-5
(April 15-16, 1985)

G. F. Bertsch, Michigan State University
C. K. Gelbke, Michigan State University
H. A. Gould, Lawrence Berkeley Laboratory
E. E. Gross, Oak Ridge National Laboratory
R. Nix, Los Alamos National Laboratory
P. H. Stelson, Oak Ridge National Laboratory
D. Ward, Chalk River Nuclear Laboratory

PAC-6
(Sept. 26-27, 1985)

C. K. Gelbke, Michigan State University
H. A. Gould, Lawrence Berkeley Laboratory
O. Hansen, Brookhaven National Laboratory
J. B. McGrory, Oak Ridge National Laboratory
R. Nix, Los Alamos National Laboratory
P. H. Stelson, Oak Ridge National Laboratory
D. Ward, Chalk River National Laboratory

2. EXPERIMENTAL NUCLEAR PHYSICS

NUCLEAR STRUCTURE STUDIES VIA ELASTIC AND INELASTIC SCATTERING

MEASUREMENT OF THE SPIN-ROTATION PARAMETER FOR p + ^{208}Pb ELASTIC SCATTERING AT 300 MeV

C. W. Glover, C. A. Miller[1], D. J. Horen, R. Sawafta[1], O. Hausser[1], C. Gunther[2], K. Hicks[1], J. Lisantti[3], K. P. Jackson[1], D. K. McDaniels[3], A. Cellar[1], L. W. Swenson[4], R. Henderson[1], W. P. Aflord[5], R. Abegg[1], R. Helmer[5], C. Broude[6]

Over the past few years there has been a growing concern among some physicists that the Schrodinger equation of motion is not valid and that the Dirac equation of motion may be needed in solving the nuclear many-body problem.[7] The most striking evidence in favor of the Dirac equation of motion has been in the study of proton elastic scattering spin observables.[8] By measuring the cross section, analyzing power, and the spin-rotation function Q, one can completely specify the proton-nucleus elastic scattering S-matrix. Thus, it is important that the measurement of these observables be made in order to constrain any model of elastic scattering. The calculations suggest that the spin-rotation data will display the most sensitivity to the differences between the relativistic (RIA) and the non-relativistic (NRIA) models. To date, only a few measurements have been performed in order to determine all the elastic scattering observables. Of those measurements which have been made, the RIA provides a better description of all the data above 500 MeV. There are several measurements from IUCF at 200 MeV of the spin-rotation function. Neither the RIA nor the NRIA are in satisfactory agreement with all the data from the IUCF work.

In order to span the energy gap in the data between 200 and 500 MeV, we[9] have designed and built a focal plane polarimeter (FFP) for the medium resolution spectrometer (MRS) at TRIUMF. Using this facility, we have measured the spin-rotation function for ^{208}Pb($\vec{p}$,$\vec{p}$) at 300 MeV.

The principle of measuring Q is shown schematically in Fig. 2.1. In elastic scattering no spin transfer is possible to a spin-zero nucleus. Thus the polarization vector for the scattered proton is of equal length, but can be rotated by an angle β in the scattering plane with respect to the incoming proton's in-plane components of the polarization vector (see Fig. 2.1a). The Q-function is related to β via the expression $Q = \sqrt{1 - P^2}\sin\beta$. Therefore, to determine Q, we must measure the change of the in-plane components of the polarization vector.

In this experiment a beam of polarized protons with the polarization vector normal (N) to the reaction plane and perpendicular to beam's momentum ($\hat{k}$) emerges from the cyclotron and is injected into a superconducting solenoid. The superconducting solenoid rotates the polarization vector into the sideways (S) direction (i.e., where the polarization vector is in the scattering plane and perpendicular to the beam's momentum vector $\hat{k}$). An in-beam polarimeter between the solenoid and the Pb target provides a constant measure of the beam's transverse polarization. The interaction of the proton beam with the nuclear field of the target causes a rotation of the initial polarization vector. The scattered protons emerging from the target with momentum $\hat{k}'$ have polarization components in the longitudinal (L'), normal (N'), and sideways (S') direction. The MRS focuses the scattered beam into the FFP. However, the magnetic field of the MRS dipole magnet precesses the scattered proton's spin vector about the S'-axis by an angle ξ, thus, bringing it into the (S'', N'', L'') coordinate system. These coordinate systems are related by

$$S'' = S'$$
$$N'' = L'\sin\xi + N'\cos\xi$$
$$L'' = L'\cos\xi - N'\sin\xi$$

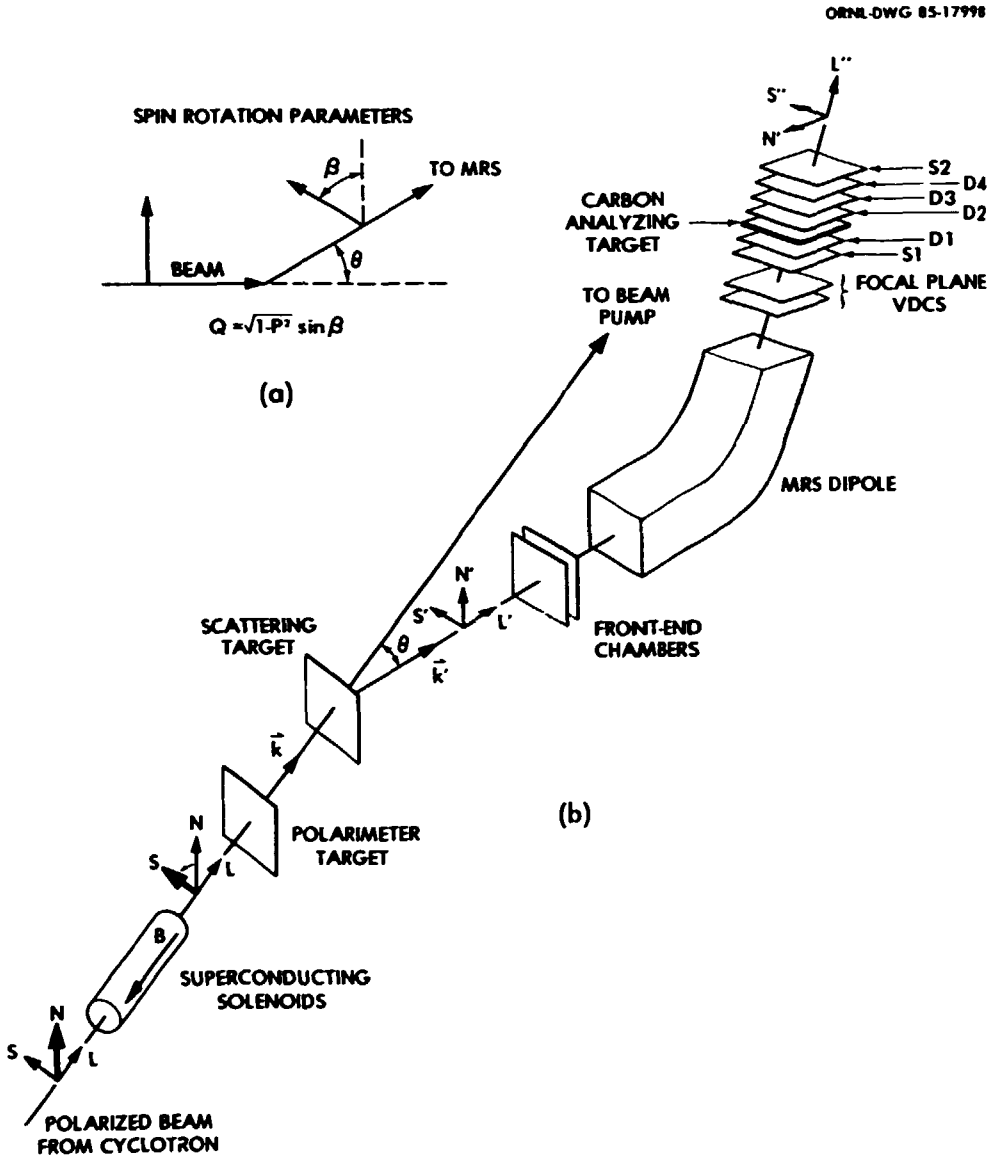

Fig. 2.1. (a) Shows that spin rotation function Q is a measure of the rotation of the in-plane components of the proton's spin vector. (b) Displays schematically the TRIUMF MRS-FFP facility used in the measurement for the spin rotation function Q.

where the precession angle ξ is 130° at this energy and converts about 76% of the longitudinal component (L') into the normal (N'') direction. After the precessed scattered beam emerges from the MRS dipole it enters the focal plane VDCs which are used to ray-trace its trajectory into the FFP. The particles are then scattered in the FFP a second time by a 7 cm (thick) x 1 m x 1 m secondary carbon target with a known analyzing power. The trajectory of the secondary scattered particles are determined by ray-tracing, using a stack of delay-line detectors. These measurements determine the transverse polarization components (S' and N'') of the particles emerging from the MRS dipole. Separation of the L' and N' components is achieved by reversing the solenoid's current to flip the spin of the incident beam (S → -S; this causes L' component to change sign and leaves N' component unaffected).

This method is clearly vulnerable if an unknown longitudinal component exists in the incident beam. For this reason, different combinations of spin directions of the incoming

beam (up/down or ±N) and solenoid currents (positive/negative) must be used in order to prepare a beam with the same sideways polarization, but having longitudinal polarizations with opposite signs. A fifth independent measurement per scattering angle will be obtained by using an unpolarized beam. From a total of 10 measurements of N'' and S' combined with results for S and N from the in-beam polarimeter, we derive four independent quantities: the polarization P, the spin transfer coefficients $D_{SS'}$ and $D_{SL'}$, and the longitudinal component for the incident beam P_L. The spin rotation parameter is calculated using the expression

$$Q = D_{SS'} \sin\theta - D_{SL'} \cos\theta.$$

In Fig. 2.2, we compare the data against the NRIA and RIA models of elastic scattering. The cross section and analyzing power data displayed in this figure is from Hutcheon et al.[10] The RIA calculation displayed in the figure is from Ray et al.[11] The NRIA calculations were performed using a folding optical model where the same ground state density used by Ray et al. was averaged over the target's volume with one of two different nucleon-nucleon (NN) interactions. The folding model calculation employing the density-dependent (DD) NN-interaction of von Geramb[12] is shown by a dashed curve in the figures. The folding model calculation using the free effective NN-interaction of Franey and Love[13] is shown by the dotted curve. From the Fig. 2.2, one can see that the NRIA calculations provide a better description of tne cross section and analyzing power data than the RIA calculations. In the calculations for the spin rotation parameter, the forward angle ($\theta < 15°$) data agrees better with the RIA model whereas the NRIA-DD calculations are far superior to all the other calculations for angles > 15°. From these calculations the NRIA-DD folding model provides the best description of the data.

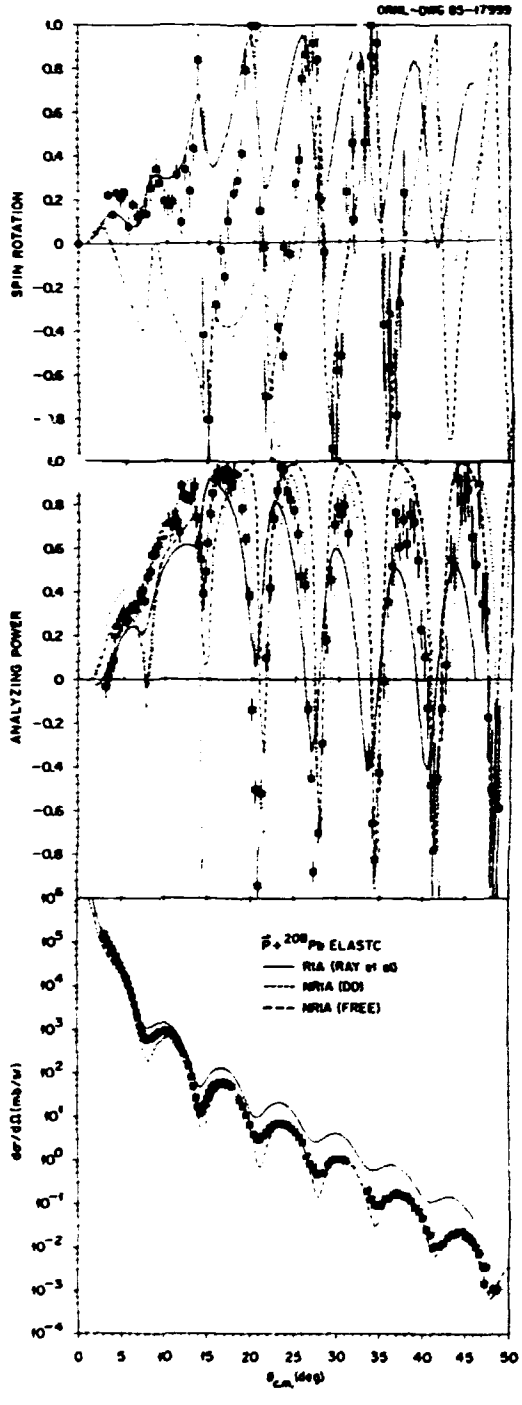

Fig. 2.2. The new Q data at 290 MeV from this experiment is displayed along with the 300 MeV cross section and analyzing power data from Hutcheon et al. The solid curve represents the RIA prediction from Ray et al. The short dashed curve represents a NRIA folding model prediction using the same ground state density for ^{208}Pb as Ray et al. and the 200 MeV density-dependent NN-interaction from von Geramb. The long dashed curve is a NRIA folding model calculation using same ground state density as the other calculation and the free NN-interaction from Franey and Love.

---

1. TRIUMF, Vancouver, B.C. V6T 2A3, Canada.
2. University of Bonn, Bonn, West Germany.
3. University of Oregon, Eugene, OR 97403.
4. Oregon State University, Corvallis, OR 97331.

5. University of Western Ontario, London N6A 3K7, Ontario, Canada.
6. Weizmann Institute, Rehovot, Israel.
7. J. R. Shepard, C. Y. Cheung, and R. L. Boudrie, eds., Proceedings of the LAMPF Workshop on Dirac Approaches to Nuclear Physics, Los Alamos National Laboratory, Los Alamos, NM, May 19[illegible]5.
8. G. W. Hoffmann, in Ref. 7.
9. Otto Hausser et al., to be published.
10. D. Hutcheon et al., private communication (TRIUMF).
11. L. Ray and G. W. Hoffmann, Phys. Rev. C 31, 538 (1985).
12. H. V. von Geramb, Table of Effective Density and Energy Dependent Interactions for Nucleons, Part A: Central Potential, Universitat Hamburg report, 1980; W. Bauhoff and H. V. von Geramb, Table of Effective Density and Energy Dependent Interactions for Nucleons, Part B: Spin-Orbit Potential, Universitat Hamburg report, 1980.
13. M. A. Franey and W. G. Love, Phys. Rev. C 31, 488 (1985).

ELASTIC AND INELASTIC POLARIZED PROTON SCATTERING FROM ^{6,7}Li at 200 MeV

C. W. Glover
J. Rapaport[1]
T. N. Taddeucci[1]
D. Wong[1]
C. C. Foster[2]
P. Schwandt[2]
G. J. Wagner[3]
J. Seubert[4]
J. R. Comfort[5]
J. A. Carr[6]
A. Carpenter[6]
F. Petrovich[6]

In an effort to test our understanding of the evolution of the proton-nucleus reaction mechanism from low to intermediate proton bombarding energies, we have measured elastic and inelastic cross section and analyzing power angular distributions for 200-MeV polarized protons scattered from ^{6,7}Li. Data were obtained for the inelastic transitions leading to the 3^+, T = 0 state at 2.184-MeV and the 0^+, T = 1 spin-flip state at 3.56 MeV in ^{6}Li and the $1/2^-$, T = 1/2 state at 0.478 MeV in ^{7}Li. The measurements were made at IUCF using the QDDM spectrometer and the associated focal plane detector system.[7] The analysis of these data are compared with the analysis by Petrovich et al.[8] of the same transitions for proton energies of 24-50 MeV.

The distorted-wave approximation (DWA) is used both by us and by Petrovich et al.[8] In order to facilitate a comparison with the lower-energy data, the same spectroscopic amplitudes used in Ref. 8 are used here. Transition densities generated from these spectroscopic amplitudes reproduce electromagnetic static moments, transition probabilities, electron scattering form factors. The proton form factors are constructed by folding these transition densities with an effective nucleon-nucleon (NN) interaction. Two different effective NN-interactions are considered here. They are the parameterizations of the NN-interaction in free space (labeled IA) by Franey and Love[9] and the density-dependent (DD) interaction of von Geramb.[10] The DD interaction is a free effective interaction modified to account for the effects of Pauli blocking in the nuclear medium.

Three sets of distorted waves were used in the DWA calculations which were generated from three different optical potentials. One optical potential was found phenomenologically by adjusting the geometries of Woods-Saxon (WS) potential wells. The other two optical potentials were obtained by averaging the IA or DD NN-interactions over the ground state density distribution. From Fig. 2.3, one can see that the WS optical potential provides the best reproduction of the elastic data and that the DD folding model optical potential gives a better description of the data than the IA potential, this is particularly evident in the analyzing power data.

In Fig. 2.4 shows the contributions due to higher-order multipoles for elastic scattering from ^{7}Li. It can be seen that the forward angle cross section is due to scattering from a spherical potential, while the data beyond 30° is due to the J = 2 quadrupole moment term. This suggests that a coupled channels analysis must be performed in order to describe the ^{7}Li elastic data. Thus, one should be aware that any phenomenological spherical optical potential will lead to unusual well geometries in order to account for the deformation.

Two different form factors for each transition and three sets of distorted waves will be considered in the analysis of the inelastic data. The two form factors were obtained by folding the IA or DD NN-interactions with each of the transition densities. The effects due to distortions were investigated by combining in a self-consistent manner the distorted-waves

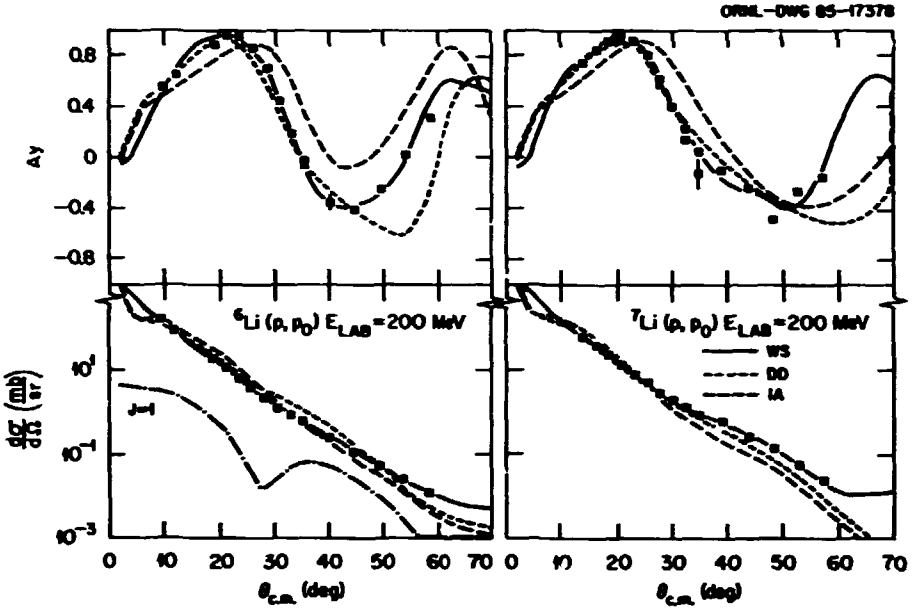

Fig. 2.3. The results from the standard WS phenomenological (solid curve) and folding optical model analyses are compared with the ^{6,7}Li elastic scattering data. The long- and short-dashed curves represent folding model predictions from averaging the DD- and free NN-interaction, respectively, over the same ground state densities.

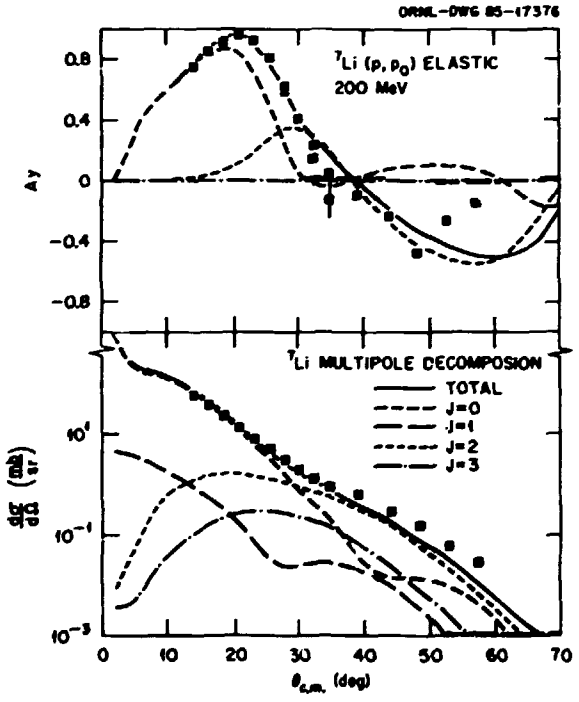

Fig. 2.4. The multipole contributions to ^{7}Li elastic scattering are displayed. The curves are labeled by their multipolarity. The dominate J = 0 and J = 2 are the contributions from the spherical and quadrupole terms and the J = 1 and J = 3 arise from "spin-flip" transitions.

obtained from the IA folding model optical potential. The calculations used factors calculated using the same IA NN-interaction (labeled IA in the figures). This same type of microscopic parameter-free self-consistent calculation was performed using the DD interaction (labeled DD). Also, calculations are presented where each of the different form factors are used in conjunction with the distorted waves generated from the phenomenological optical potential (labeled WS). The results of these calculations are compared to the data in Figs. 2.5 and 2.6.

Displayed in Fig. 2.5 are the data and calculations for the $(1^+;0) \rightarrow (3^+;0)$ transition in ^{6}Li and the $(3/2^-;1/2) \rightarrow (1/2^-;1/2)$ transition in ^{7}Li. These transitions proceed primarily by transferring two units of angular momentum ($L = 2\hbar$) to the target. From Fig. 2.6, one can see that all calculations overpredict the magnitude of the peak in the cross section and underpredict the magnitude of the data at the larger angles. The underprediction of the data at the larger angles is likely due to inadequacies in the transition densities because

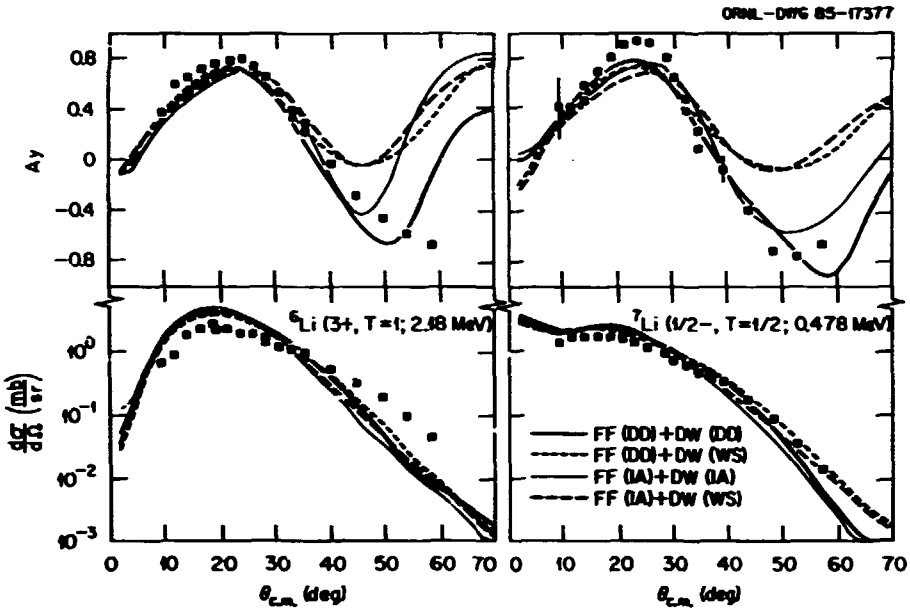

Fig. 2.5. The DWA calculations for the predominately L = 2 transitions are compared with the data. The label FF(DD) + DW(DD) corresponds to a calculation in which the form factor was calculated by folding the inelastic transition density from Ref. 5 with the DD-effective NN-interaction and the distorted-waves were calculated microscopically by folding the ground state density with the same DD effective NN-interaction. Consequently, the FF(DD) + DW(WS) means that this same form factor was used in conjunction with distorted waves generated from the phenomenological WS optical model parameters. The IA label means that these same types of calculations were performed using the free NN-effective interaction rather than the DD interaction.

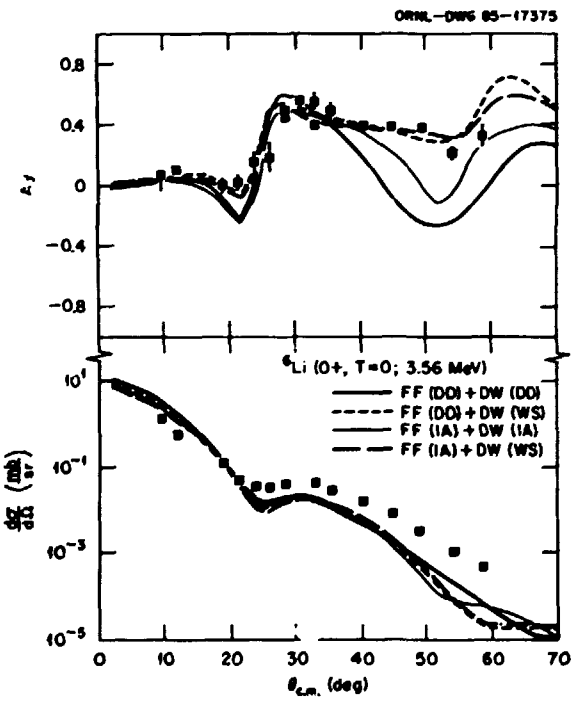

Fig. 2.6. The same labeling scheme used in Fig. 2.5 is used here for the 0^+, T = 0 transition in ^{6}Li.

these transition densities also underpredict the magnitude of the electron scattering form factors data at large values of momentum transfer (q). The calculations overpredict, by a factor of 2 and 1.45, the peak of the 3^+ and $1/2^-$ cross sections, respectively. The overprediction of the data is hard to understand because these transition densities describe the low-q electron scattering data quite well. This leaves as suspect our description of the reaction mechanism and/or the effective NN-interaction. It is thought that the effective NN-interactions used here are accurate at the 30-40% level and are probably not responsible for the total discrepancy between the data and calculations. For the $1/2^-$ transition in ^{7}Li we know that we have not taken into proper account the distortions via a coupled channels description. But this is not the case for ^{6}Li. Thus, it is suggested that the discrepancy may be explained by one or more of the following effects: (1) The first term in the Born series may not be sufficiently

accurate, where rescattering effects with the dense ^{4}He core may need to be considered. (2) Coupling through the break-up channel may not be negligible. With respect to the first point, Comparat et al.[11] have shown that higher-order terms in the multiple scattering expansion are needed in the IA description of p + ^{4}He elastic scattering data at 156 MeV.

Finally, from Figs. 2.5 and 2.6, the effects due to distortions can clearly be seen in the analyzing power calculations. The analyzing power data are best described by calculations using the DD NN-interaction for both the folded optical potential and the form factor. This can be understood by considering the overlap between the form factor and the distorting potential in the calculation of the scattering amplitude. The form factors tend to be localized in a particular region in R-space. As a consequence of this radial localization, the form factor places more weight on the shape and magnitude of the distorting potential in the region of R-space, where the overlap is the greatest, whereas, elastic scattering is averaged over the entire nuclear volume. Thus, the distortions experienced by a proton for this transition is in closer agreement with that predicted by the density-dependent optical potential and is not very well approximated by the phenomenological WS optical potential which gives the best reproduction of the elastic scattering data. This form of radial localization has been noticed for other nuclear systems[12-16] and has been discussed extensively by Kelly.[16]

The data and calculations for the cross section and analyzing power angular distributions for the 0^+; T = 1 spin-flip state at 3.56 MeV in ^{6}Li are displayed in Fig. 2.6. This figure is organized the same way as Fig. 2.5 for the L = 2ħ transitions.

The transition density extracted by Petrovich et al.[8] for the 0^+, T = 1 state only reproduces the magnitude and shape of the B(M1,q) distribution for momentum transfers q < 1 fm^{-1}. Beyond this, the model predicts a diffractive minimum at a smaller momentum transfer than the data indicates and, for the most part, underestimates the strength in the second diffractive lobe in the B(M1;q) distribution. A discussion of this deficiency has been given by Bergstrom[17-20] and others,[21-24] where it was shown that the M1 form factor can be described by modifying the p-shell radial wave function. The resulting transition densities suggest that the valence nucleons in the T = 1 state are pushed further out and have a longer tail than that given by the 1p harmonic oscillator description used here.

From Fig. 2.6, one can see that the IA and DD cross section and analyzing power calculations are approximately the same at low-q and overpredict the cross section data by 1.4 for the most forward data point. All calculations underestimate the cross section data beyond q ~ 1.2 fm^{-1}, probably due to defects in the description of the transition density at these momentum transfers. The analyzing power angular distributions are well described when phenomenological distorted waves are used, as compared with those obtained from the microscopic folded optical potential. This can be understood by noting that the 0^+, T = 1 state is simply a spin-isospin flip state of the ground state. Therefore, the transition density should have a similar shape to that of the ground state. Thus, from our previous arguments about the radial localization of inelastic transitions, one can see that the distortions experienced by a proton should be approximated by elastic scattering and that the phenomenological optical potential gives the best reproduction of the elastic data.

The results from the present experiments demonstrate that the discrepancy in magnitude between the DWIA calculations and the measurements of the the inelastic proton cross sections for ^{6,7}Li cannot be explained by employing a density-dependent effective NN-interaction in the lowest order DWA calculations. However, it was shown that for the elastic and the L = 2 transitions the DWA calculations using the density-dependent NN-interaction were in better agreement with all the observables measured than the IA calculations. This was especially evident in the analyzing power angular distributions. And, as expected, the IA and the density-dependent DWA calculations give similar

results for 0^+, T = 1 spin-flip state. These results suggest that the consequences of Pauli blocking must be taken into account even for a nucleus as diffuse as ^{6}Li. Also, these results indicate that the lowest order DWA is not adequate enough to describe the data, and the effects from higher-order processes need to be investigated.

---

1. Ohio University, Athens, OH 45701.
2. Indiana University Cyclotron Facility, Bloomington, IN 47405.
3. Physikalisches Institut der Universitat Tubingen, 7400 Tubingen, West Germany.
4. Indiana University-Purdue University at Indianapolis, Indianapolis, IN 46223.
5. Arizona State University, Tempe, AZ 85287.
6. Florida State University, Tallahassee, FL 32306.
7. C. W. Glover et al., submitted to Physical Review C.
8. F. Petrovich et al., Nucl. Phys. A383, 355 (1982).
9. M. A. Franey and W. G. Love, Phys. Rev. C 31, 488 (1985).
10. H. V. von Geramb, Table of Effective Density and Energy Dependent Interactions for Nucleons, Part A: Central Potential, Universitat Hamburg report, 1980; W. Bauhoff and H. V. von Geramb, Table of Effective Density and Energy Dependent Interactions for Nucleons, Part B: Spin-Orbit Potential, Universitat Hamburg report, 1980.
11. V. Comparat et al., Phys. Rev. C 12, 251 (1975).
12. C. W. Glover, submitted to Physical Review C.
13. C. Olmer et al., Phys. Rev. C 29, 361 (1984).
14. J. Kelly et al., Phys Rev. Lett. 45, 2012 (1980).
15. M. Hugi. W. Bauhoff, and H. O. Meyer, Phys. Rev. C 28, 1 (1983).
16. J. Kelly, Ph.D. thesis, Massachusetts Institute of Technology (1981).
17. J. C. Bergstrom and E. I. Tomusiak, Nucl. Phys. A262, 196 (1976).
18. J. C. Bergstrom, I. P. Auer, and R. S. Hicks, Nucl. Phys. A251, 401 (1975).
19. J. C. Bergstrom, Nucl. Phys. A327, 458 (1979).
20. R. Neuhausen and R. M. Hutcheon, Nucl. Phys. A164, 497 (1971).
21. R. M. Hutcheon, O. Sundberg, and G. Tibell, Nucl. Phys. A154, 261 (1970).
22. D. F. Jackson and J. Mahalanabis, Nucl. Phys. 64, 97 (1965).
23. D. F. Jackson, Nucl. Phys. 35, 194 (1962).
24. R. S. Henderson et al., Nucl. Phys. A372, 117 (1981).

ELASTIC AND INELASTIC SCATTERING OF 500 MeV PROTONS FROM ^{40}Ca AND EXCITATION OF GIANT MULTIPOLE RESONANCES

B. L. Burks, F. E. Bertrand, R. L. Auble, E. E. Gross, D. J. Horen, R. O. Sayer[1], L. W. Swenson[2], D. K. McDaniels[3], J. Lisantti[3], K. W. Jones[4], J. B. McClelland[4], S. Seestrom-Morris[5]

Investigations of the 12- to 30-MeV excitation energy region in sd-shell nuclei using 60-MeV protons[6] and 120-MeV alphas[7] have found a complicated fine structure of giant resonance strength, in contrast to the broad (2-6 MeV FWHM) peaks formed by isoscalar giant resonances in heavier nuclei. Although previous studies have been made, a comparison of results from several different reactions is needed to unfold the complicated observed resonance structures in the sd-shell nuclei.

We have measured cross sections and analyzing powers for elastic and inelastic scattering of 500-MeV protons from ^{40}Ca at the HRS facility at LAMPF. The elastic scattering data were obtained in ±0.5° bins for 1° steps between 3.5° and 22° laboratory angle. The inelastic scattering data were obtained in ±0.5° bins for 14 angles between 3.5° and 20.5°. Two settings of the magnetic field were required to obtain composite inelastic scattering spectra for excitation energies up to about 40 MeV (see Fig. 2.7). Elastic scattering data were measured in shorter runs at separate magnetic field settings. The typical energy resolution for all spectra was 80 keV FWHM.

Although the giant resonance region in ^{40}Ca has been studied with a variety of probes, intermediate energy proton scattering has the advantage of providing good discrimination between excitations of different multipolarities, since significant differences exist between the shapes of cross section angular distributions for neighboring L-transfer values. An example is given in Figure 2.8 where cross section data are plotted for several low-lying excited states and compared to DWBA calculations for L transfers between L = 1 and L = 5. With the range of

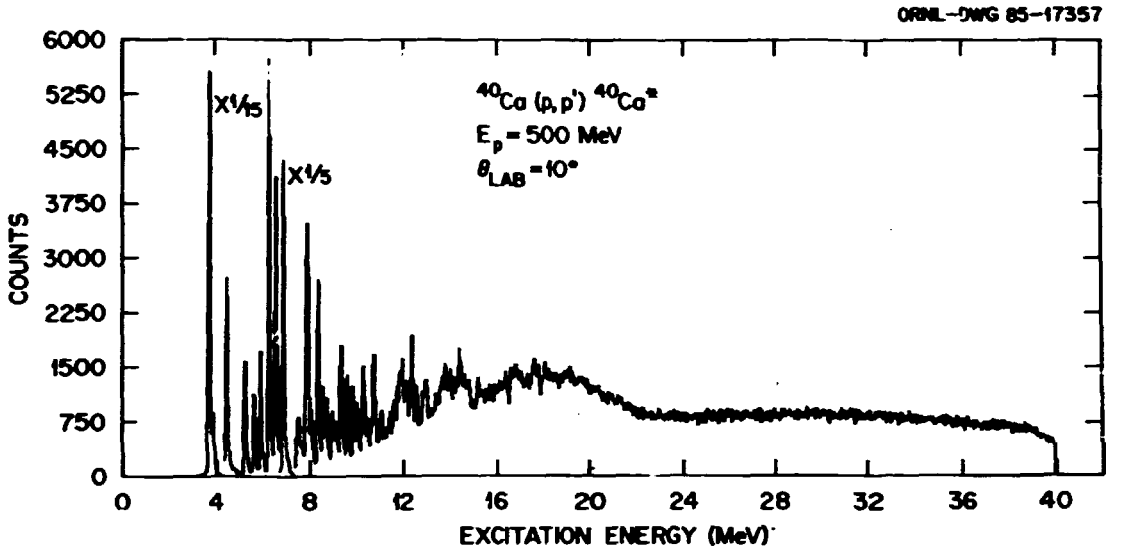

Fig. 2.7. An excitation energy spectrum for $^{40}Ca(p,p')^{40}Ca^*$ at E_p = 500 MeV and θ_{lab} = 10°.

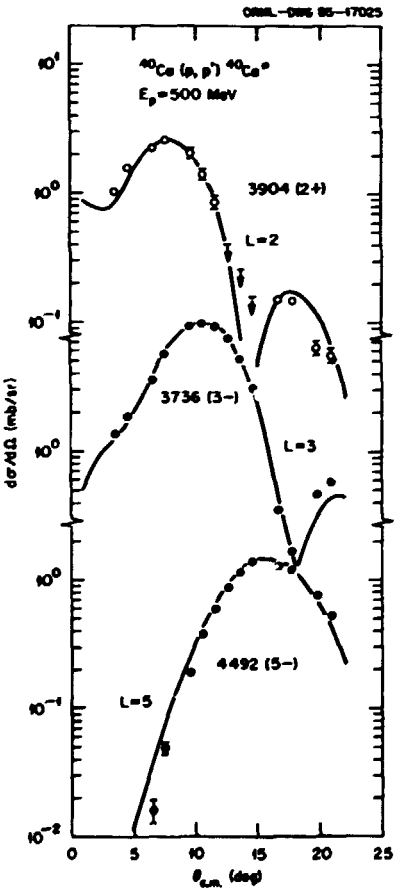

Fig. 2.8. Cross section angular distributions for several low-lying states in ^{40}Ca from the $^{40}Ca(p,p')^{40}Ca^*$ reaction at E_p = 500 MeV. The solid curves are DWBA predictions for the indicated L-transfer values.

angles covered in this measurement, our analysis should unfold the contributions to the fine structure in the giant resonance region of ^{40}Ca from excitations with multipolarities up to L = 5.

---

1. Computing and Telecommunications Division, ORNL.
2. Oregon State University, Corvallis, OR 97331.
3. University of Oregon, Eugene, OR 97403.
4. Los Alamos National Laboratory, Los Alamos, NM 87545.
5. University of Minnesota, Minneapolis, MN 55455.
6. F. E. Bertrand et al., "Inelastic Proton Excitation of Giant Resonances in sd-Shell Nuclei," Phys. Div. Ann. Prog. Rept., Dec. 31, 1975, ORNL-5137, p. 63.
7. F. E. Bertrand et al., Phys. Rev. Lett. 40, 635 (1978). K. Van der Borg et al., Phys. Lett. 67B, 105 (1977). K. Van der Borg et al., Nucl. Phys. A365, 243 (1981).

ELASTIC AND INELASTIC SCATTERING OF 250- AND 500-MeV PROTONS FROM ^{28}Si AND EXCITATION OF GIANT MULTIPOLE RESONANCES

B. L. Burks[1]
F. E. Bertrand[1]
R. L. Auble[1]
E. E. Gross[1]
C. W. Glover[1]
D. J. Horen[1]
R. O. Sayer[1]
L. W. Swenson[2]
X. Y. Ciao[2]
D. K. McDaniels[3]
J. Lisantti[3]
O. Hauser[4]
K. Hicks[4]
G. A. Miller[4]
K. W. Jones[5]
J. B. McClelland[5]
S. Seestrom-Morris[6]

In addition to the $^{40}Ca(p,p')$ measurements reported in the previous article we have also

studied giant resonance structures in the sd-shell nucleus ^{28}Si. These elastic and inelastic scattering data were measured with 500-MeV polarized protons at LAMPF and with 250-MeV unpolarized protons at TRIUMF. As shown in Fig. 2.9, the excitation energy region from about 12 to 30 MeV in ^{28}Si is populated by many narrow structures rather than the broad isoscalar giant resonance peaks observed for inelastic proton scattering from heavier targets. Data from several reactions must be compared in order to understand the complicated fine structure in the giant resonance region of these nuclei.

A limited set of data was obtained at the HRS facility at LAMPF, including elastic scattering cross sections and analyzing powers in ±0.5° bins for 1° steps from 3.5° to 22.5° laboratory angles. Inelastic scattering cross sections and analyzing powers were obtained at 4 angles between 3.5° and 12.5° for an excitation energy range up to about 22 MeV. For 4 additional angles between 6.5° and 10.5°, the data extend up to an excitation energy of about 40 MeV. A more complete set of cross section data was obtained at TRIUMF for elastic and inelastic scattering of 250-MeV protons. These data span an angular range from about 4° to 40° for the elastic scattering and have ample statistics in the inelastic scattering data for an angular range of about 4° to 27°, including excitations up to about 50 MeV. Although the data obtained at LAMPF are incomplete and suffer in some instances from poor statistics, they have been useful to compare to the TRIUMF data since the energy resolution for the HRS data is typically 80 keV FWHM compared to 150 keV FWHM for the TRIUMF data.

The advantage of intermediate-energy proton scattering over lower-energy proton and alpha scattering measurements is that the cross section angular distributions differ markedly for neighboring L-transfers. Therefore, the multipolarities of giant resonance excitations may be determined by comparison of differential cross sections to DWBA calculations. The range of angles at which we have cross section data includes the first maximum in yield for L-transfers up to L = 5. When the analysis of these data is complete we should be able to unfold the contributions to the fine structure in the giant resonance region of ^{28}Si from excitations with multipolarities up to L = 5.

---

1. Computing and Telecommunications Division, ORNL.

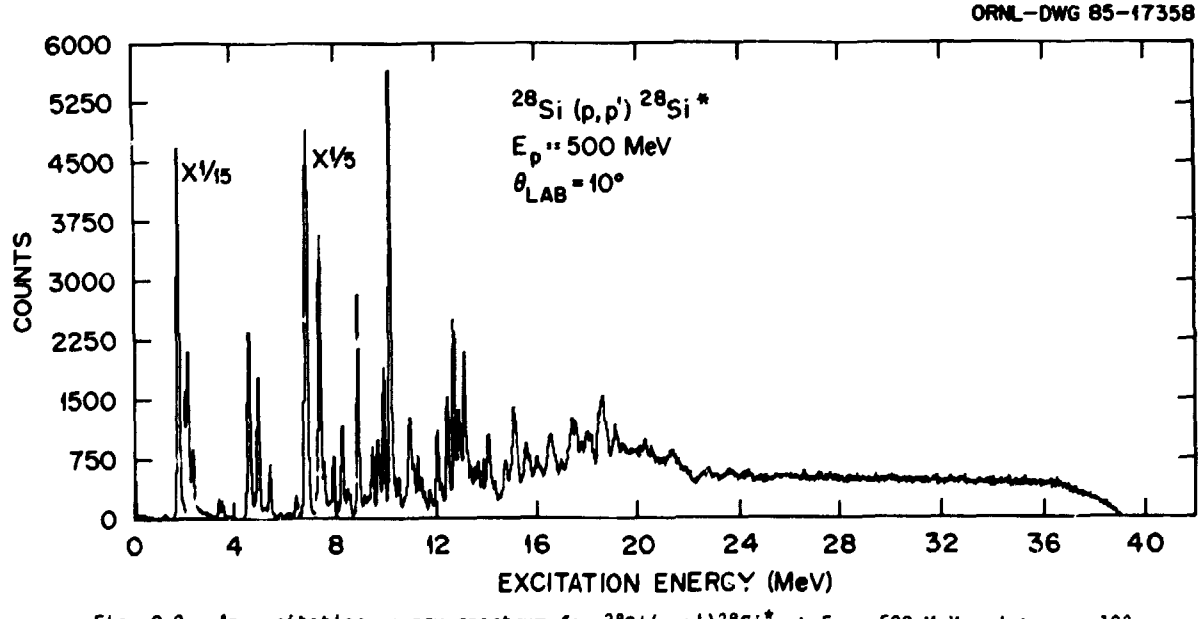

Fig. 2.9. An excitation energy spectrum for $^{28}Si(p,p')^{28}Si^*$ at E_p = 500 MeV and θ_{lab} = 10°.

2. Oregon State University, Corvallis, OR 97331.
3. University of Oregon, Eugene, OR 97403.
4. TRIUMF, Vancouver, B.C. V6T 2A3 Canada.
5. Los Alamos National Laboratory, Los Alamos, NM 87545.
6. University of Minnesota, Minneapolis, MN 55455.

ANALYZING POWER FOR THE INELASTIC CONTINUUM WITH 200-MeV PROTONS[1]

J. Lisantti[2] D. K. McDaniels[2]
J. R. Tinsley[2] F. E. Bertrand
D. M. Drake[3] E. E. Gross
I. Bergqvist[4] D. J. Horen
L. W. Swenson[5] T. P. Sjoreen[6]

Inelastic proton scattering from targets of ^{60}Ni, ^{90}Zr, and ^{208}Pb has been studied using 200-MeV polarized and unpolarized protons. The behavior with angle of a narrow region at the peak of the continuum underneath the giant resonance spectra follows that expected for free nucleon-nucleon scattering, modified by an energy shift dependent on target mass. Analyzing power results support the hypothesis that single-step quasifree scattering represents a significant fraction of the overall inelastic scattering for the excitation region near the proposed quasifree peak, but indicate that other processes start to dominate above this excitation region.

---

1. Abstract of published paper: Phys. Lett. 147B, 23 (1984).
2. University of Oregon, Eugene, OR 97403.
3. Los Alamos National Laboratory, Los Alamos, NM 87545.
4. University of Lund, Lund, S-223 62, Sweden.
5. Oregon State University, Corvallis, OR 97330.
6. Solid State Division, ORNL.

CROSS SECTIONS AND ANALYZING POWERS FOR QUENCHED SPIN EXCITATIONS IN ^{40,48}Ca AT E_p = 334 MeV[1]

D. J. Horen J. Lisantti[3]
F. E. Bertrand L. W. Swenson[4]
E. E. Gross J. B. McClelland[5]
T. P. Sjoreen[2] T. A. Carey[5]
D. K. McDaniels[3] S. J. Seestrom-Morris[5]
J. R. Tinsley[3] K. Jones[5]

The inelastic cross sections and analyzing powers for spin excitations in ^{40,48}Ca have been measured at E_p = 334 MeV. The data for excited states in ^{40}Ca at 8.424 MeV (2^-) and 10.31 MeV (1^+) and the 10.22-MeV (1^+) state in ^{48}Ca are fairly well described by microscopic distorted-wave impulse approximation calculations. Normalizations of the calculated cross sections to the experimental data show that these spin excitations are quenched. We deduce $B(M2)\uparrow = 281\ \mu_N^2 fm^2$ for the 8.42-MeV 2^- state in ^{40}Ca.

---

1. Abstract of published paper: Phys. Rev. C 31, 2049 (1985).
2. Solid State Division, ORNL.
3. University of Oregon, Eugene, OR 97403.
4. Oregon State University, Corvallis, OR 97330.
5. Los Alamos National Laboratory, Los Alamos, NM 87545.

CROSS SECTION AND ANALYZING POWER MEASUREMENTS FOR THE GIANT RESONANCE REGION IN ^{208}Pb WITH 200-MeV PROTONS[1]

D. K. McDaniels[2] F. E. Bertrand
J. R. Tinsley[2] E. E. Gross
J. Lisantti[2] D. J. Horen
D. M. Drake[3] T. Sjoreen[6]
I. Bergqvist[4] R. Liljestrand[7]
L. W. Swenson[5] H. Wilson[7]

The giant resonance region in ^{208}Pb has been studied using inelastic scattering of 200-MeV polarized and unpolarized protons. Both differential cross section $\sigma(\theta)$ and analyzing power $Ay(\theta)$ measurements were made. The isoscalar quadrupole resonance at 10.6 ± 0.5 MeV, the isovector dipole resonance at 13.6 ± 0.5 MeV, and the isoscalar monopole resonance at 14.1 ± 0.5 MeV are clearly observed. Data for a peak at 20.9 ± 1.0 MeV are found to be consistent with an isoscalar giant octupole resonance. This conclusion is based on a comparison of the $\sigma(\theta)$ and $Ay(\theta)$ data with distorted wave born approximation (DWBA) predictions. Evidence is found for an L = 4, $2\hbar\omega$ peak with an excitation energy of about 12.0 MeV, just above the strong giant quadrupole peak. The continuum spectra and $\sigma(\theta)$ data for scattering angles less than 20° are consistent with dominance of single-scattering processes for that portion of the spectrum below about 25 MeV of excitation. The $Ay(\theta)$ data give further support for this hypothesis and indicate

that multiple-scattering processes dominate at higher excitation energies.

---

1. Abstract of paper submitted to Physical Review C.
2. University of Oregon, Eugene, OR 97403.
3. Los Alamos National Laboratory, Los Alamos, NM 87545.
4. University of Lund, Lund, S-223 62, Sweden.
5. Oregon State University, Corvallis, OR 97330.
6. Solid State Division, ORNL.
7. University of Alberta, TRIUMF, Vancouver, British Columbia V6T 2A3, Canada.

ON THE VALIDITY OF MICROSCOPIC CALCULATIONS FOR INELASTIC PROTON SCATTERING[1]

D. K. McDaniels[2] L. W. Swenson[4]
J. Lisantti[2] F. E. Bertrand
J. Tinsley[2] E. E. Gross
I. Bergqvist[3] D. J. Horen

Recent measurements of transition rates for low-lying collective states and giant resonances in ^{208}Pb using inelastic scattering of 200- and 300-MeV protons are in accord with accepted values. This is in sharp disagreement with earlier medium-energy proton inelastic scattering studies in which the validity of the collective model formalism was questioned. Combining these results with measurements at other energies, we conclude that the extraction of deformation lengths with the collective distorted wave Born approximation formalism is satisfactory to at least 800 MeV. The present results bring into question the microscopic calculations of inelastic scattering using RPA wave functions.

---

1. Abstract of paper accepted for publication in Physics Letters.
2. University of Oregon, Eugene, OR 97403.
3. Lund Institute of Technology, Lund, S-223 62, Sweden.
4. Oregon State University, Corvallis, OR 97330.

COMPUTER CODES FOR INTERMEDIATE ENERGY PROTON REACTIONS

C. W. Glover

The following is a list and a brief description of computer codes available on the MHIRF VAX 11/785 for calculating proton reactions at intermediate energies. The user guides and sample input files are available upon request from C. W. Glover (615-574-4729).

ALLWRLD

(Authors: J. A. Carr, J. Kelly, and F. Petrovich; modified by C.W. Glover)

This is a general purpose code that calculates transition densities in a harmonic oscillator basis from shell model spectroscopic amplitudes (the transition densities may also be read in point-wise from another file). From the transition densities the code calculates electromagnetic static moments, transition probabilities, and electron scattering form factors. For charge exchange reactions, the Fermi or GT matrix elements are calculated. For proton reactions, the code folds the transition density with a nucleon-nucleon (NN) interaction and returns a PWIA angular distribution and form factor for use in the distorted-wave code TAMVAX. The ALLWRLD code can use two different NN-interactions. One is the free-space effective interaction of Love and Franey[1] or the density-dependent interaction of von Geramb.[2] If the proton reaction is elastic scattering, the code will calculate a folding model optical potential from the ground state density using either one of the two NN-interactions. This optical potential can be used by TAMVAX for distorted waves. This allows one to perform a completely consistent, microscopic, parameter-free calculation for proton reactions. This same sort of analysis can be done for pion reactions, except that the πN-interaction is used and the form factors and optical potential are used in the code MSUDWPI.

TAMVAX

(Authors: J. A. Carr, J. Kelly, and F. Petrovich; modified by C. W. Glover)

This is a distorted-wave code which calculates proton scattering observables. The code is designed to accept microscopic form factors and microscopic folded optical potentials from ALLWRLD. Although, it will accept standard Woods-Saxon optical model parameters, the code

can also calculate proton scattering observables for the standard collective model by deforming the WS optical potential.

NOTE: This code employs the zero-range single-nucleon knockout exchange approximation.

MSUDWPI

(Authors: J. A. Carr and F. Petrovich)
This code performs the type of calculations for pions as TAMVAX does for protons.

SNOOPY

(Author: P. Schwandt)
This is an optical model code for spin 0, 1/2, and 1 projectiles. It calculates all elastic scattering observables. A complete description of the code is found in IUCF Report No. 81-3 by P. Schwandt. The elastic scattering data may be analyzed terms of a local, spin-dependent optical potential with relativistic kinematics. The code allows for automatic searches on potential parameters which give the best fit to the elastic scattering observables, with up to eight parameters varied simultaneously to minimize the chi-square. Grid calculations and automatic searches may be combined. Other options available include: input or generation of "external" (e.g., non-Woods-Saxon) potentials form factors, notch perturbations of potentials, and the generation of excitation of functions using energy-dependent potential parameters.

DWBA80

(Original Authors: J. Raynal; Modified by G. W. Love)

This code calculates proton scattering observables in the distorted-wave impulse approximation using a finite range single-nucleon knockout exchange mechanism. The code will accept transition densities or form factors along with folded optical potentials from ALLWRLD or it will build its own form factors by folding the Love-Franey free NN-interaction with shell model spectroscopic amplitudes. Also, standard Woods-Saxon optical potentials may be used.

NOTE: The main difference between this code and TAMVAX is in the exchange. This code calculates the six dimensional exchange integral in a multipole expansion.

DWBA81

(Original Authors: J. Raynal; Modified by J. R. Comfort)

This code is a DWUCKized version of DWBA80, except it will not accept transition densities or form factors and folded optical potentials from ALLWRLD. The code utilizes a DWUCK-like input and some subroutines from DWUCK. This code restricts the user to using transition densities generated from a harmonic oscillator basis, standard Woods-Saxon optical potentials, and free NN-interactions, only.

EFIT

(Author: A. Carpenter)
This is a search code. It takes shell model spectroscopic amplitudes in a harmonic oscillator basis and calculates electromagnetic transition densities. It uses these transition densities to calculate electromagnetic static moments, transition probabilities, and electron scattering form factors and compares these observables to the known data. Then it adjusts the transition densities until the best chi-square is reached between all the data and the model. The results of the "best fit" densities can be used as input to ALLWRLD.

RIA

(Authors: J. Shepard and E. Rost)
This code is based on the formalism developed by Shepard, Rost, and others for the relativistic impulse approximation (RIA); see for example: Phys. Rev. C 30, 1604 (1984), Phys. Rev. C 29, 209 (1984), Phys. Rev. C 27, 2123 (1983). This code calculates a completely covariant NN-interaction in a Breit frame from phase-shift data and folds this with a four-component spinor in the target space for the relativistic form factor. This form factor is then averaged with the projectile's distorted wavefunctions to produce the transition amplitude. The distorted wavefunction is obtained from a Dirac eikonal approximation using effective central and spin-orbit distortions which, in turn, are derived from the covariant NN-interaction. This code allows input of nonrelativistic spectroscopic amplitudes and then assumes that the lower components have the same radial shape as the upper

components. The code outputs proton inelastic scattering observables.

NOTE: There is no allowance made for an exchange term in the theory.

DROP

(Authors: J. Shepard and E. Rost)

This code is the same as RIA, except it is an earlier version used to calculate elastic scattering only.

RUNT

(Author: E.D. Cooper)

This code calculates a relativistic optical potential for proton scattering by adjusting Woods-Saxon shaped scalar vector potentials until a fit to the experimental data is found. The formulism can be found in the article by B. C. Clark, in Interactions Between Medium Energy Nucleons and Nuclei-1983, edited by H. O. Meyer, AIP Conf. Proc. No. 97 (American Institute of Physics, New York, New York) and references contained within.

PHASESHIFT

(Author: C. W. Glover)

This code calculates all nucleon-nucleon elastic scattering observables as a function lab or C.M. angle at a given lab energy using Ardt's October 1977 phaseshifts.

PLOTIT

(Author: C. W. Glover)

This is a user friendly color graphics code. It will plot up to 10 sets of data and 10 sets of curves per graph. The graph may include: a title, axes labels, a legend, and additional labels placed anywhere on the graph with the cursor. The code can create an output file which stores all plotting parameters. The code prompts the user for all input.

---

1. M. A. Franey and W. G. Love, Phys. Rev. C 31, 488 (1985).
2. H. V. von Geramb, Table of Effective Density and Energy Dependent Interactions for Nucleons, Part A: Central Potential, Universitat Hamburg report, 1980; W. Bauhoff and H. V. von Geramb, Table of Effective Density and Energy Dependent Interactions for Nucleons, Part B: Spin-Orbit Potential, Universitat Hamburg report, 1980.

ℓJ-DEPENDENCE OF THE EFFECTIVE REAL OPTICAL POTENTIAL NEAR NEUTRON THRESHOLD[1]

D. J. Horen A. D. MacKellar[2]
C. H. Johnson

Considerable effort has been expended in attempts to use microscopic principles to calculate an optical model potential which will describe the scattering of a single nucleon in finite nuclei.[3] In recent years a number of works have concentrated in an energy region close to the Fermi surface. A common procedure is to attempt to calculate corrections to the Hartree-Fock (HF) potential for each ℓJ, and then deduce an average potential (i.e., independent of ℓJ). Within ~20 MeV of the Fermi energy, it has been suggested that these corrections can be represented by a local surface imaginary potential from which one can deduce the corrections to V_{HF} by means of dispersion relations.[4] Hence, in this energy domain it might be expected that the real part of the optical potential could be expressed as

$$V(r,E) = V_{HF}(r,E) + V_S(r,E),$$

where $V_{HF}(r,E)$ is taken as a W-S volume potential and $V_S(r,E)$ is a surface potential. Mahaux and Ngo suggested that $V_S(r,E)$ can be obtained from the imaginary part of the empirical local optical potential using a dispersion relationship.[4] Furthermore, if $W_S(r,E)$ had a derivative W-S form, they showed that $V(r,E)$ would have a W-S form similar to $V_{HF}(r,E)$ but with a different radius. That is to say, $V(r,E)$ would have an energy dependent radius. This would then lead to a deviation of the volume integral of $V(r,E)$ from that of $V_{HF}(r,E)$ in the region of the Fermi surface (i.e., the so-called "Fermi surface anomaly").

We have used the unique features of low-energy neutron scattering to investigate the behavior of the "effective" real optical potential near the neutron threshold for the system $^{208}Pb + n$.

From high resolution measurements of total and differential elastic scattering cross sections for E = 0.050-1.005 MeV, we have determined sets of R-matrix parameters which describe

the data for the partial waves $s_{1/2}$, $p_{1/2}$, $p_{3/2}$, and $d_{5/2}$. From these, for a given radius we are able to deduce "effective" real potentials for these partial waves at the same energy. A discussion of how we deduce OMP from the experimentally determined partial wave scattering functions has been given elsewhere.[5] (Technically, our one datum relating to the real potential is incapable of distinguishing between r_v and $V_{\ell J}$. In fact, we find the data can be reasonably described by a function Vr_v^n with $n \approx 1.5$.) In Fig. 2.10 we plot the depths of the "effective" real optical potential for $^{208}Pb + n$ versus energy. In this figure, we include points which correspond to potentials required to reproduce binding energies for bound states and differential neutron scattering data[6] at higher energies using the same geometry. We observe that at $E \approx 0.5$ MeV, the "effective" real potential for s- and d-waves appears deeper than that for p-waves.

The surface part of $V(r,E)$ at these energies is believed to arise mainly from particle-vibration excitations which are localized near the nuclear surface. It is possible to simulate part of $V_s(r,E)$ by the utilization of the coupled-channel formalism. We have performed coupled-channel calculations using the code[7] ECIS for the s-, p-, and d- partial waves in order to obtain a physical insight as to the behavior of the "effective" $V_{\ell J}$. We find that the coupled-channel calculations can reproduce fairly well the neutron strengths and $R^{ext}_{\ell J}$ deduced from the data. We observed that the neutron widths calculated with ECIS were sensitive to the depth of the scattering potential employed, especially for the p-wave channels. In fact, it was found that for resonances associated with the $3d_{3}^{-}$ particle vibration, the neutron width went through a null as a function of the scattering potential.

To better understand this, we have examined the individual functions which enter into the coupled-channel equations. In addition to the vibrational deformation parameter, the strength of the effective coupling potential is related to an overlap integral of the amplitude of the scattered wave, a bound-state wave function and the derivative of the optical potential (which is localized near the nuclear surface). In particular, for lead we find that the amplitude of the scattered p-wave neutron in a real potential with $V_{\ell J} \approx 40$ MeV has a node near the nuclear surface. Some of the bound-state wave functions (e.g., $3d_{5/2}$) also have nodes in the surface region. As a result, the overlap integrals (or strengths of the particle-vibration couplings) can vary markedly for the different scattering channels, and change with neutron energy.

An important result of the coupled-channel calculations is that the strength of the particle-vibration couplings at a given energy strongly depends upon the amplitude of the scattered wave in the vicinity of the nuclear surface. The presence of a node near the surface has the effect of decoupling the motion of the scattered particle from the surface vibrations. We believe that this phenomenon might explain the variations with energy of the "effective" volume potentials in the region near the neutron threshold, and be the basis for the behavior of our deduced $V_{\ell J}$.

---

1. Based upon a paper to be published in Physics Letters B.
2. University of Kentucky, Lexington, KY 40506.
3. See, e.g., C. Mahaux et al., Phys. Repts. 120, 1 (1985).
4. C. Mahaux and H. Ngo, Nucl. Phys. A378, 205 (1982).
5. Phys. Div. Prog. Rept. for Period Ending Sept. 30, 1984, ORNL-6120, p. 54.
6. J. R. M. Annand, R. W. Finlay, and F. S. Dietrich, Nuclear Physics, to be published.
7. J. Raynal, ECIS 79 (private communication); the present version was modified by R. L. Hershberger.

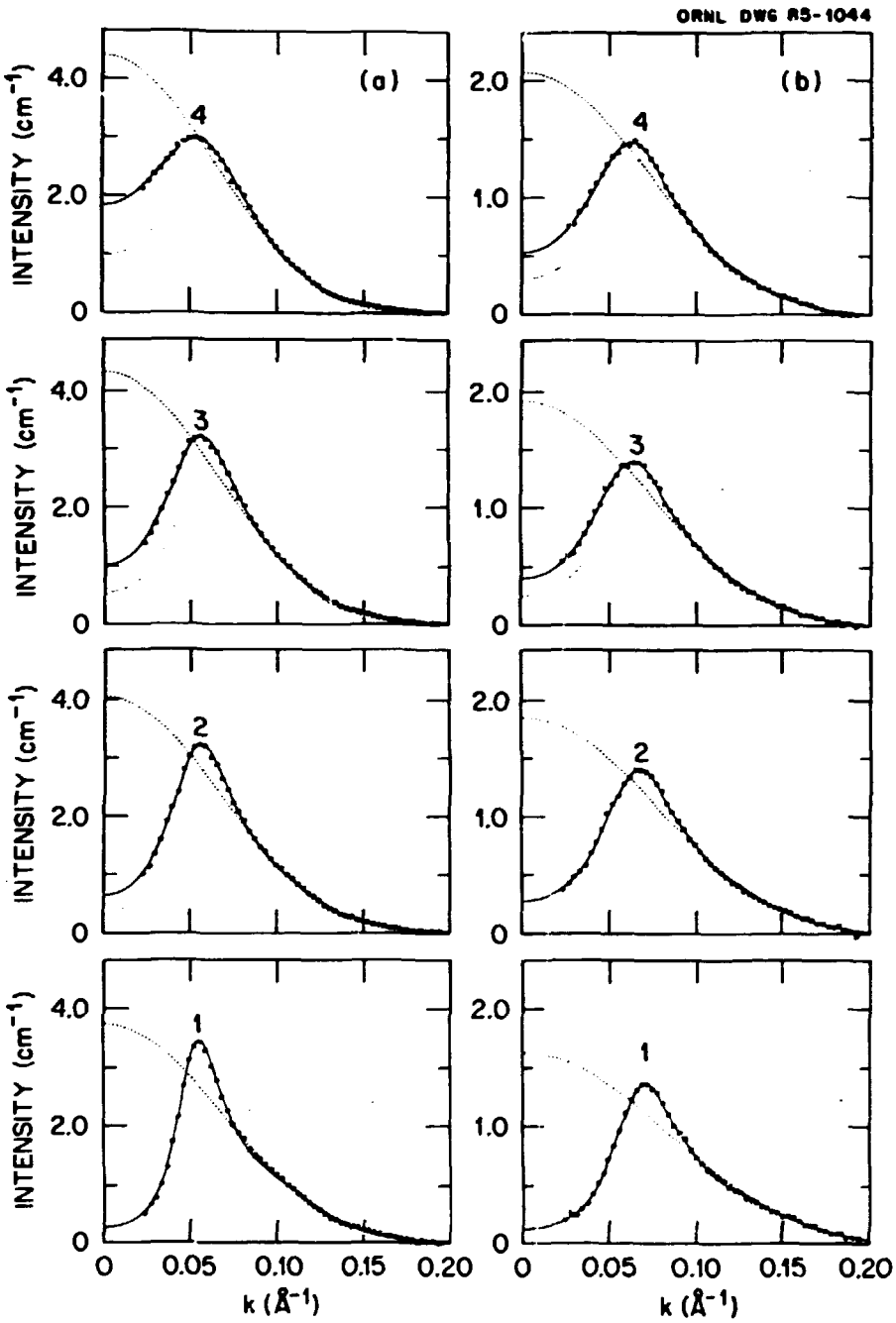

Fig. 2.10. Effective real potential for motion of a single neutron in ^{208}Pb + n system versus energy. The energy of the Fermi surface is taken as ε_F = -6.0 MeV. The potentials for E<0 were deduced from bound state orbitals. A constant real radius parameter r_R = 1.17 fm was used in determining the real well depths at all energies. The potentials shown at 4 and 7 MeV were deduced by "fitting" differential scattering cross sections calculated using OMP from Ref. 6 with a parity dependent potential. The data above 10 MeV are from Ref. 6.

HIGH RESOLUTION NEUTRON CROSS SECTION FOR ^{48}Ca

C. H. Johnson J. A. Harvey[2]
R. F. Carlton[1] R. L. Macklin[2]

Earlier measurements[3] at ORELA of the neutron total cross section of ^{48}Ca revealed an unusually simple structure which indicated ^{48}Ca is essentially a doubly-closed-shell nucleus. The main features observed for neutron energies up to 2 MeV are three broad $d_{5/2}$ states; these consume about 50% of the $2d_{5/2}$ strength and are described by shell-model-in-the-continuum calculations.[4]

Unfortunately, the large statistical uncertainties of those data prevented detailed analyses, except for the broad $d_{5/2}$ resonances. We have repeated the measurements with improved techniques. As previously, we used the 200-m flight path and a burst width of about 7 nsec. But this time we made the beam incident on the edge rather than the face of the scattering sample in order to increase the sample thickness by about a factor of 7 (from 126 b/a to 17.3 b/a). Also, we used compensators to cancel (nearly) the effects of C and O in the $CaCO_3$ sample. The compensators were BeO and C for the "out-beam" and Be for the "in-beam". The effect of these compensators was such that the measured transmissions are for a sample of 89.1% ^{48}Ca, 3.7% ^{40}Ca, and 7.2% ^{16}O. The corrections for the small amounts of ^{40}Ca and ^{16}O were then calculated accurately from known cross sections. That is in contrast to the earlier data analysis which involved subtraction of all of the CO_3 cross section.

These new data allow a more accurate R-Matrix analysis to be made for energies from 0.1 MeV to above 2 MeV. In Fig. 2.11 the points show the cross sections observed below 500 keV and the curve is an R-Matrix fit. Four well-resolved resonances are seen at 302, 401, 415, and 451 keV. From the peak heights we can immediately assign J = 1/2, 3/2, 5/2, and 1/2, respectively. The widths and shapes of the 401- and 415-keV resonances require the respective assignments, $p_{3/2}$ and $d_{5/2}$. The two J = 1/2 resonances cannot both have the same ℓ-value because their

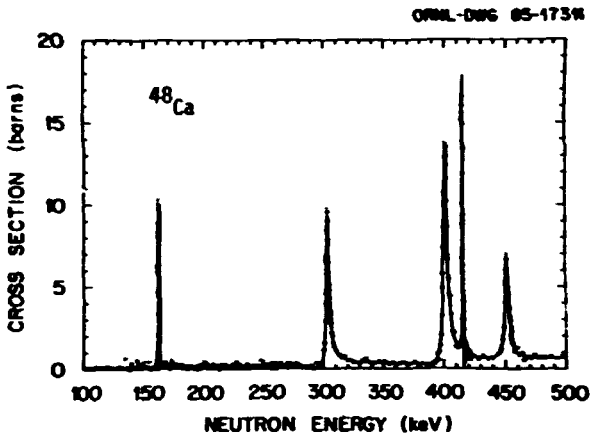

Fig. 2.11 Neutron total cross section for ^{48}Ca below 500 keV. The curve is an R-matrix fit with the indicated resonance J^{π} assignments and appropriate nonresonance phase shifts.

interference patterns are quite different. By appropriate choice of the nonresonance phase shifts one could fit the data with either of the alternate assignments, i.e., either $p_{1/2}$ and $s_{1/2}$, as shown in Fig. 2.11, or the alternate $s_{1/2}$ and $p_{1/2}$. Our assignments in Fig. 2.11 are based on the following arguments.

One reason for assigning $p_{1/2}$ to the resonance at 302 keV rather than to the one at 451 keV is based on comparisons of the interference patterns to that of the $p_{3/2}$ resonance. Spin-orbit effects, which are evidenced by the observed splitting of the bound 2p states, are expected to give a more negative phase shift for $p_{1/2}$ than for $p_{3/2}$. From the observed asymmetries of the two J = 1/2 resonances we see that our assignments are consistent with this expectation whereas the alternate assignment is not.

A second reason comes from the observed[5] delayed neutron spectrum from the β-decay of $^{49}K(I = 3/2^+)$. The β-decay has a strong branch with log ft = 5.0 to the level corresponding to the 451-keV resonance. Therefore, the transition has a high probability of being allowed and the state has even parity, i.e., $1/2^+$.

The scattering functions obtained by averaging[6] for each partial wave can be compared to those for an optical model potential. Since the s-and p-wave strength functions are very small

for this nucleus the averaging can be omitted and the off-resonance phase shifts can be fit, using a real potential. Using a Woods-Saxon well with r_0 = 1.21 fm and a = 0.66 fm and a 7-MeV spin-orbit surface potential with the same r_0 and a, we find the observed shifts are fit with central depths of $V_{1/2^+}$ = 50 MeV, $V_{3/2^-}$ = 50 MeV and $V_{1/2^-}$ = 46.5 MeV. The value for $V_{1/2^+}$ is about 3.5 MeV less than for ^{40}Ca and this is expected because of the isospin term of about 25(N-Z)/A. However, the fact that the p-wave potentials tend to be shallower than for s-waves is in contrast to ^{40}Ca, where they were deeper. A further analysis to higher energies is in progress and should reduce the uncertainties in the optical model parameters.

---

1. Middle Tennessee State University, Murfreesboro, TN.
2. Engineering Physics and Mathematics Division.
3. J. A. Harvey, C. H. Johnson, R. F. Carlton, and B. Castel, Physics Division Progress Report for period ending September 30, 1984, ORNL-6120, p. 50.
4. J. A. Harvey, C. H. Johnson, R. F. Carlton, and B. Castel, Phys. Rev. C 32, 1114 (1985).
5. L. C. Carraz, et al., Phys. Lett. 109B, 419 (1982).
6. C. H. Johnson, C. Mahaux, and R. R. Winters, Phys. Rev. C 32, 359 (1985).

ENERGY AVERAGE OF THE SCATTERING MATRIX IN PICKET FENCE MODELS

C. H. Johnson C. Mahaux[1]
R. R. Winters[2]

From high resolution neutron cross section measurements at facilities such as ORELA one can obtain scattering functions for individual partial waves for energies up to about 2 MeV. By subsequent averaging, one finds scattering functions which are to be described by an optical model potential (OMP) for each partial wave. This ability to study the OMP partial waves at a single energy is a unique feature of high resolution work.

To illustrate the averaging process we consider s-wave neutrons on a spin-zero target. The scattering function in the R-matrix formalism reads

$$S(E) = e^{-2ika}\,\frac{1 + ika\,R(E)}{1 - ika\,R(E)} \qquad (1)$$

where a is the boundary radius and where the R-function includes terms of the form $\gamma_\lambda^2/(E_\lambda - E)$ summed over all levels both internal and external to the experimental region E_ℓ to E_u,

$$R(E) = R^{int}(E) + R^{ext}(E). \qquad (2)$$

The scattering function is unitary. Averaging produces a non-unitary <S> with a complex R-function

$$\mathcal{R}(E) = \bar{R}(E) + i\pi s(E) \qquad (3)$$

Following Lane and Thomas,[3] we find[4] that the quantities in Eq. (3) are given to a good approximation by simple prescriptions. The strength function s(E) is approximately the average reduced width per energy interval near E,

$$s(E) = \frac{\langle\gamma^2\rangle}{D}\Big|_E, \qquad (4)$$

and $\bar{R}$ is found approximately from R^{ext},

$$\bar{R}(E) = R^{ext}(E) + P\int_{E_\ell}^{E_u} \frac{\tilde{s}(E')dE'}{E' - E}. \qquad (5)$$

Here P denotes the principle value of the integral and $\tilde{s}(E)$ is the experimental strength function from the right-hand side of Eq. (4). The experimental quantity on the right-hand side of Eq. (5) is denoted $\tilde{R}(E)$.

The derivation of Eqs. (4) and (5) is not trivial; it involves analytical extensions to complex energies. In fact, recent papers[5-8] show disagreement on the subject. We have checked the approximation by performing straightforward numerical averages with simple picket fence models. For example, Fig. 2.12 shows "data" for a rising picket fence of reduced widths and an R^{ext}. We average the scattering function of Eq (1) numerically,

$$\bar{S}(\bar{E}) = \int_{E_\ell}^{E_u} W_I(E,E')S(E')dE' \qquad (6)$$

where W_I is a normalized weighting function of width I and $\bar{E}$ is the corresponding averaged energy. In so doing we introduce the variable E' only in the R-function part of S(E). If the above prescriptions are correct, we expect the resulting average quantities, $\bar{R}$ and s, to agree

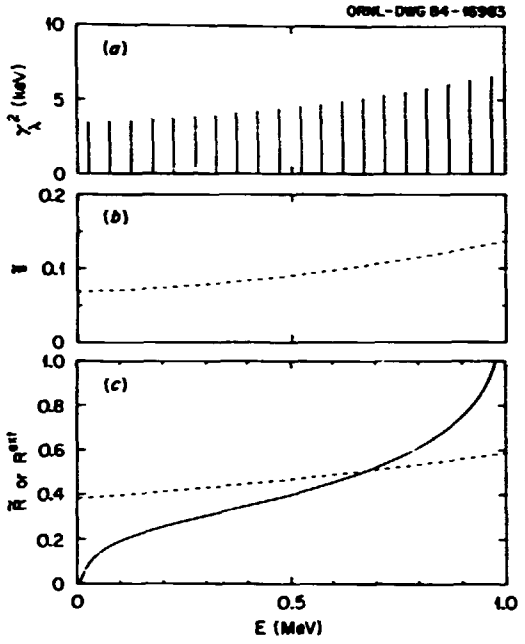

Fig. 2.12 Rising picket fence model: (a) reduced widths, (b) the strength function, (c) the external R function (solid) and $\tilde{R}$ (dashed).

well with the "data", $\tilde{s}$ and $\tilde{R}$. In Fig. 2.12 the dashed curves show $\tilde{s}$ and $\tilde{R}$. Indeed, numerical averages show excellent agreement with these dashed curves. Further details and examples are given in Ref. 4.

1. Consultant from Université de Liège, 4000 Liège, Belgium.
2. Denison University, Granville, Ohio.
3. A. M. Lane and R. G. Thomas, Rev. Mod. Phys. 30, 257 (1958).
4. C. H. Johnson, C. Mahaux, and R. R. Winters, Phys. Rev. C 32, 359 (1985).
5. C. H. Johnson, N. M. Larson, C. Mahaux, and R. R. Winters, Phys. Rev. C 27, 1913 (1983).
6. W. M. MacDonald and M. C. Birse, Nucl. Phys. A403, 99 (1983).
7. W. M. MacDonald and M. C. Birse, Phys. Rev. C 29, 1560 (1984).
8. C. H. Johnson, N. M. Larson, C. Mahaux, and R. R. Winters, Phys. Rev. C 29, 1563 (1984).

ISOSPIN EFFECT IN $\pi^{\pm}$ ^{14}C ELASTIC SCATTERING AT 50 MeV[1]

C. S. Mishra[2], M. V. Hynes[4], B. M. Preedom[2], E. Piasetzky[4], B. G. Ritchie[2], N. S. Chant[5], R. S. Moore[2], P. G. Roos[5], M. Blecher[3], F. E. Bertrand, K. Gotow[3], T. Sjoreen[6], R. L. Burman[4], F. E. Obenshain, E. E. Gross

Angular distributions have been measured for $\pi^{\pm}$ elastic scattering at 50 MeV from ^{14}C. Comparison with previously measured distributions for ^{12}C shows a significant isotopic difference for π^- scattering. The data were analyzed using the second order MSU optical potential proposed for low energy pion nucleus elastic scattering. Agreement with the data was obtained using the same density distributions for the protons and neutrons.

1. Abstract of a paper submitted to Physical Review C.
2. University of South Carolina, Columbia, SC 29208.
3. Virginia Polytechnic Institute and State University, Blacksburg, VA 24061.
4. Los Alamos National Laboratory, Los Alamos, NM 87545.
5. University of Maryland, College Park, MD 20742.
6. Solid State Division, ORNL.

ELASTIC AND INELASTIC SCATTERING OF 158 MeV ^{9}Be IONS[1]

C. B. Fulmer[2], R. L. Auble, G. R. Satchler, J. B. Ball, K. A. Erb, F. E. Bertrand, D. C. Hensley, E. E. Gross

The elastic scattering of 158 MeV ^{9}Be ions was measured for seven targets ranging in mass from 12 to 197. Inelastic data for exciting the lowest 2^+ states of ^{12}C, ^{26}Mg, and ^{60}Ni were also obtained. The elastic data for ^{12}C and ^{16}O show pronounced structures at the most forward

angles which are rapidly damped as the scattering angle increases. The distributions for ^{26}Mg and ^{27}Al show marked structure with significant odd-even differences that can be ascribed to quadrupole scattering from the ^{27}Al ground state. The elastic data were analyzed using the optical model with both Woods-Saxon and folding-model potentials. The folded potentials are too strong and require renormalization; they do not give good fits to the data for the lighter targets. The inelastic data were compared to distorted-wave calculations.

---

1. Abstract of published paper: Nucl. Phys. A427, 545 (1984).
2. Deceased.

ELASTIC AND INELASTIC SCATTERING OF ^{16}O FROM ^{182,184,186}W

R. L. Auble
C. E. Bemis, Jr.
F. E. Bertrand
J. L. Blankenship[1]
E. E. Gross
H. J. Kim
F. K. McGowan
R. O. Sayer[2]

Multidimensional barrier penetration calculations in the quantum mechanical coupled-channels formalism offer the promise of a more complete understanding of the "enhanced" subbarrier fusion cross sections observed experimentally for many heavy-ion reaction systems. One such system of interest is for ^{16}O + ^{184}W, where "particular enhancements" to the subbarrier fusion cross sections have been suggested and are associated with large negative static hexadecapole deformations.[3] A rigorous coupled-channels calculation would include couplings to all inelastic and transfer reaction channels and would use a realistic ion-ion potential derived from experimental elastic and inelastic scattering data.

Comparative fusion cross sections for the ^{16}O + ^{182,184,186}W systems are under experimental investigation in efforts to understand the predicted relationship between "enhanced" subbarrier fusion cross sections and static negative hexadecapole deformations.[4] To complement these studies, we have performed precision elastic and inelastic scattering measurements for these same systems in the angular range 38°-74° for 100-MeV ^{16}O ions. This energy is in the nuclear-Coulomb interference region, and detailed knowledge of the ion-ion potential and matrix elements between states may be derived from the inelastic and elastic angular distribution data.

The elastic and inelastic scattering experiments were completed at HHIRF using the broad-range spectrometer (BRS) equipped with the vertical drift chamber (VDC) in the focal plane. The principles and operating characteristics of this detector have been reported[5,6] previously. The analyses of data from these experiments are far from complete, and careful optimization of the parameters of the VDC is required in order to extract the elastic and inelastic differential cross sections. Initial scans of the data have indicated that the energy resolution is adequate to permit separation of the elastic and 2^+ inelastic groups (~100 keV) and that statistics are adequate to allow binning of the differential cross section data into 0.25°-angle bins. However, an additional short calibration experiment is required to provide an internal normalization of the data, due to the lack of sufficient angular overlap in the BRS settings used in our experiments. Extraction of the ion-ion potentials and coupling matrix elements will be performed after the data analyses are completed.

---

1. Instrumentation and Controls Division, ORNL.
2. Computing and Telecommunications Division, ORNL.
3. M. J. Rhoades-Brown and V. E. Oberacker, Phys. Rev. Lett. 50, 1435 (1983).
4. H. J. Kim et al., Phys. Div. Prog. Rep., Sept. 30, 1983, ORNL-6004, p. 136.
5. M. V. Hynes et al, Nucl. Instrum. Methods Phys. Res., Sect. A, 224, 89 (1984).
6. T. P. Sjoreen et al., Nucl. Instrum. Methods Phys. Res., Sect. A, 224, 421 (1984).

OPTICAL MODEL AND COUPLED CHANNEL ANALYSES OF ELASTIC AND INELASTIC SCATTERING OF ^{18}O FROM ^{28}Si AT 352 MeV

B. L. Burks
M. A. G. Fernandes[1]
D. J. Horen
R. L. Auble
F. E. Bertrand
J. L. Blankenship[2]
J. L. C. Ford, Jr.[3]
E. E. Gross
D. C. Hensley
R. O. Sayer[4]
D. Shapira
T. P. Sjoreen[5]
G. R. Satchler

In a previous report,[6] the experimental procedures for a measurement of elastic and inelastic scattering of ^{18}O from ^{28}Si at 352 MeV were presented. In this section we discuss the analysis of the elastic and inelastic scattering data; the reaction data analysis is presented in the following sections of this report.

An optical model analysis of the elastic scattering data was performed using the code PTOLEMY.[7] Three sets of optical model parameters, each obtained by fitting cross section data, were used as starting points for the parameter search. These three sets of optical model parameters are designated in the literature as: A-type,[8] E-18,[9] and S-7.[10] The well-known first and second potentials have been used to describe ^{16}O + ^{28}Si elastic scattering over a large incident energy range; the S-7 set was obtained from the fit of ^{18}O + ^{28}Si elastic and transfer data at E_{inc} = 56 MeV. The optical parameters derived from each initial potential set, in a search allowing r_V, r_W, a_V, and a_W to vary while keeping V and W fixed, are listed in Table 2.1. Figure 2.13 shows the good agreement between the optical model predictions and data. The fits with S-7F and A-F potentials differ little over the entire angular range. Comparable descriptions of the data were obtained with other parameter sets derived from the same three initial optical model potentials.

The inelastic ^{28}Si(1.78 MeV, 2^+) data were analyzed using the coupled channel code ECIS,[11] assuming the axially symmetric rotational model. The Coulomb deformation parameter was derived from the B(E2↑) value with $R_C = r_{CO} \cdot A_T^{1/3}$ fm, corresponding to the experimental intrinsic quadrupole moment.[12] The nuclear deformation parameters of the real and imaginary parts of the optical potential, β_{2V}^N and β_{2W}^N, were derived by equating nuclear and charge deformation

Table 2.1. Optical model parameters extracted from ^{18}O + ^{28}Si elastic scattering. These parameters were used in DWBA calculations described in the following two reports.

Set	V (MeV)	r_V (fm)	a_V (fm)	W (MeV)	r_W (fm)	a_W (fm)	χ^2 (per point)[a]
E-18F[b]	10.0	1.291	0.725	23.40	1.191	0.599	3.1
E-18F CC	10.0	1.29	0.689	23.69	1.191	0.561	4.3
A-F[c]	100.0	0.971	0.652	44.1	1.043	1.051	4.8
A-F CC	100.0	0.97	0.674	43.51	1.043	1.961	6.0
S-7F[d]	50.0	1.077	0.641	43.0	1.041	1.004	5.0

CC identifies potentials derived by coupled-channel calculations.

[a]The values shown were obtained assuming a 10% overall uncertainty in the experimental elastic cross sections.

[b]r_{OC} = 1.0 fm

[c]r_{CO} = 1.30 fm

[d]r_{CO} = r_V

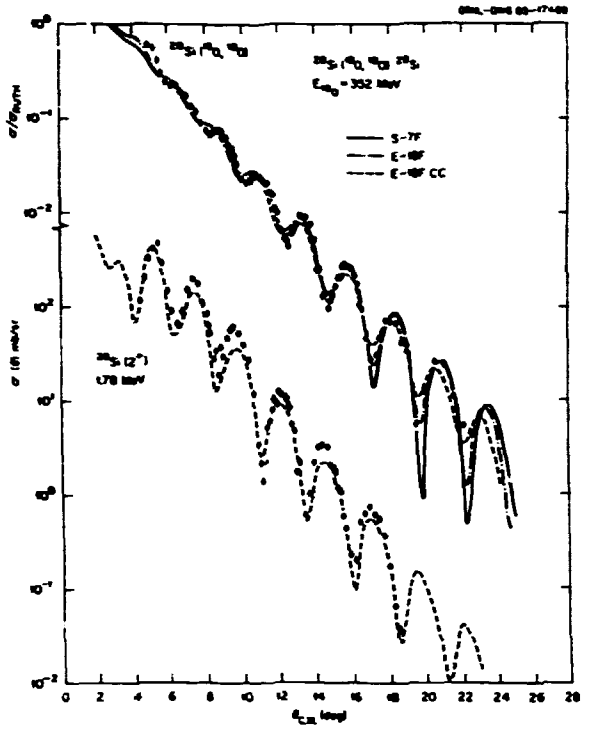

Fig. 2.13. Elastic and inelastic angular distributions. The solid (dot-dashed) curves are optical model predictions with S-7F(E-18F) potentials given in Table 2.1. The dashed curves are coupled channel predictions with E-18F CC given in Table 2.1.

lengths. Only quadrupole deformation was assumed for the optical potentials.

Potentials A-F CC and E-18F CC (Table 2.1) were obtained by fitting the elastic and 2^+ inelastic cross sections. The starting optical potential sets were A-F and E-18, respectively, and in the search only the parameters a_V, W, and a_W were allowed to vary in a 0^+-2^+ coupling calculation. The coupled-channel calculations are seen to fit the elastic and inelastic cross section data very well over the angular range measured (see dashed lines in Fig. 2.13). The deformation parameters used in the calculations with both potentials are presented in Table 2.2.

---

1. Universidade de Sao Paulo, Sao Paulo, Brazil.
2. Instrumentation and Controls Division, ORNL.
3. Deceased.
4. Computing and Telecommunications Division, ORNL.
5. Solid State Division, ORNL.
6. B. L. Burks et al., Phys. Div. Prog. Rept. for Period Ending Sept. 30, 1984, ORNL-6120, p. 47 (1985).
7. D. H. Gloeckner, M. H. Macfarlane, and S. C. Pieper, Argonne National Laboratory Report No. ANL-76-11, 1976 (unoublished).

Table 2.2. Spectroscopic values used in the coupled channels calculations.

Nucleus	E_x (MeV)	J^π	$B(E2)\uparrow$ e^2b^2 [a]	β_2^C [b]	β_{2V}^N	β_{2W}^N
^{28}Si	1.780	2^+	0.0370	-0.369[c]	-0.265[c]	-0.247[c]
				-0.624[d]	-0.259[d]	-0.281[d]

[a] Ref. 12.

[b] Deduced using $\beta_L^C = \frac{4\pi}{3Z_T R_C^L} [B(EL;\uparrow)]^{1/2}$.

[c] A-F CC.

[d] E-18 CC.

8. G. R. Satchler, Nucl. Phys. A279, 493 (1977).
9. J. G. Cramer et al., Phys. Rev. C 14, 2158 (1976).
10. B. T. Kim et al., Phys. Rev. C 20, 1396 (1979).
11. J. Raynal, private communication.
12. W. J. Thompson and J. S. Eck, Phys. Lett. 67B, 151 (1977).

TWO-OCTUPOLE PHONON STATES IN ^{208}Pb

J. R. Beene M. L. Halbert
F. E. Bertrand I. Y. Lee
R. O. Sayer[1]

The study of low lying surface vibrational states in nuclei has played an important role in the development of our understanding of elementary modes of nuclear excitation. The study of the interaction between simple excitation modes continues to be an active field of investigation. One aspect of this field is the study of multi-phonon vibrational states. A reasonable body of data has been assembled for two-quadrupole-phonon states but data on two-octupole-phonon states is almost nonexistent.

^{208}Pb, whose first excited state is a strongly collective (~39 s.p.u.) 3^- state, would appear to be a good place to look for two-octupole (n = 2) phonon states, and considerable effort has been expended in searching for candidates, but no convincing data exists.

In the course of studies of the gamma decays of unbound states[2] in ^{208}Pb, we have acquired data which suggest the existence of states near 5.2 MeV (i.e., twice the energy of the 2.6 MeV 3^- state) which have many properties expected of the n = 2 octupole states. The experiment was not optimized for the study of this problem and therefore our data are inadequate in many respects. In early 1986 we will perform a straightforward extension of our previous experiment to follow up on these results.

States of ^{208}Pb were excited by inelastic scattering of 380-MeV ^{17}O. The inelastically scattered ^{17}O ions were detected in six Si surface barrier telescopes at θ_{Lab} = 13°. Associated gamma radiation was detected in 70 elements of the ORNL Spin Spectrometer. Data on the relative gamma decay strengths to various low lying states as a function of ^{208}Pb excitation energy is reproduced in Fig. 2.14. The excitation energy plotted was obtained from the summed gamma-ray energy in the Spin Spectrometer, but was required to agree, within experimental resolution, with the excitation energy obtained from energy of scattered ^{17}O ion.[2]

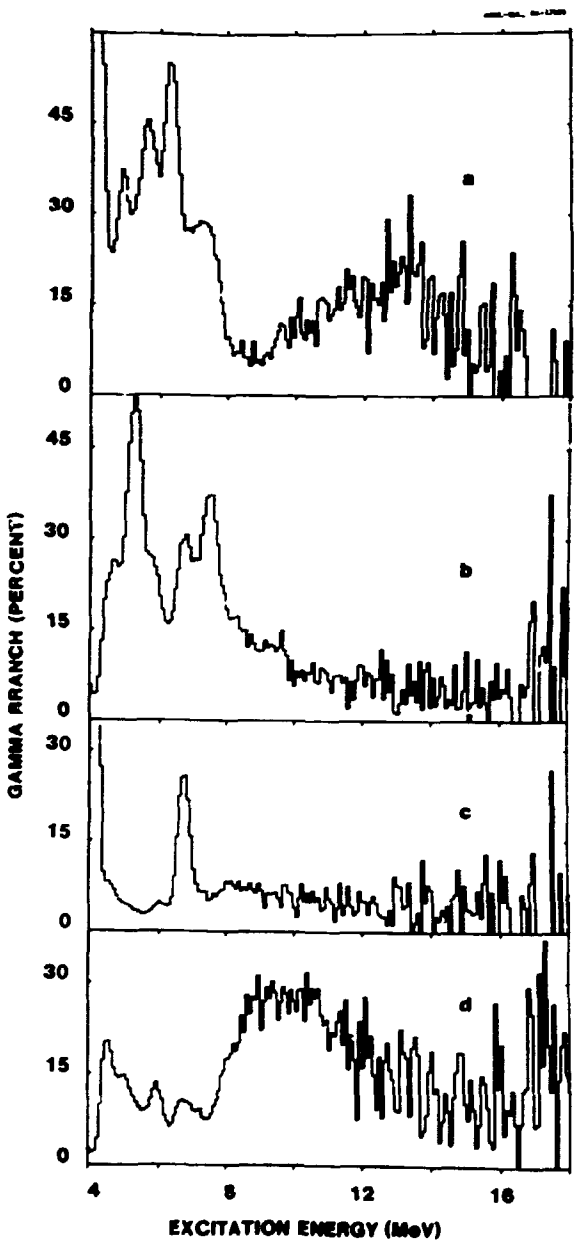

Fig. 2.14. Relative gamma-decay strengths for transitions to a number of low-lying levels in ^{207}Pb: (a) for ground-state decays; (b) for transitions to the 2.61-MeV, 3^- state; (c) the 4.08-MeV, 2^+ state; (d) the 4.97-MeV, 3^- state.

A strong peak centered near 5.3 MeV excitation is the dominant feature of Fig. 2.14b (decays to the 2.6-MeV 3^- state) and noticeably absent in the other plots. These data reveal a structure near 5.2 MeV which has a strong branch to the 2.6-MeV state and no significant branch to the ground state or 4.08-MeV 2^+ state. The plots in Fig. 2.14 show gamma branching (gamma yield to specified final states divided by total gamma yield). In Fig. 2.15 the total yield of gamma decays directly populating the 2.6-MeV 3^- state is plotted, demonstrating that the structure of interest is reasonably strongly excited ($d\sigma/d\Omega$ > 1 mb/sr).

The n = 2 octupole manifold should consist of states with $J^\pi = 0^+ - 6^+$. According to the simplest models the $\Delta n = 2$ decays of these states to the ground state should be forbidden. The state should have strongly enhanced E3 transitions to the 3^- 2.6-MeV state,[3] but it seems likely that E1 decays of the 2^+ and 4^+ members to the 3^- state will probably be their dominant decay modes. The 6^+ member will also have allowed E1 transitions to the 5^- states below 5.2 MeV.

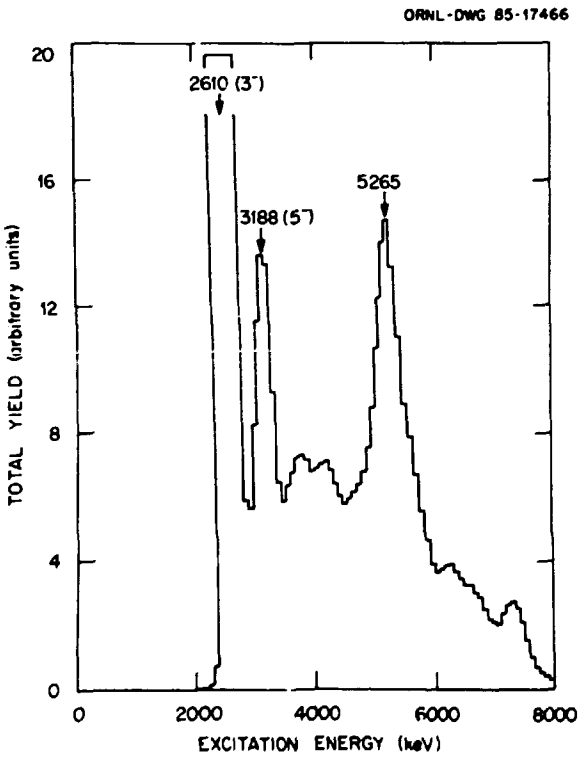

Fig. 2.15. Distribution of strength directly populating the 2.6-MeV 3^- state in ^{208}Pb as a function of ^{208}Pb excitation energy.

We will investigate the gamma decays of the region around 5.2 MeV in detail by repeating our previous experiments with the addition of 8 to 11 Compton suppressed Ge gamma detectors replacing elements of Spin Spectrometer. From the high resolution Ge data we will obtain precise values for the excitation energy of states of the potential n = 2 manifold and also determine the spins of the candidates from $\gamma\gamma$ (Ge-NaI) angular correlations.

---

1. Computing and Telecommunications Division, ORNL.
2. J. R. Beene et al., p. 503 in Nuclear Structure 1985 (Proceedings of the Niels Bohr Centennial Conference, Copenhagen, May 20-24, 1985), edited by R. Broglia, G. Hagemann, and B. Herskind (North-Holland, 1985).
3. A. Bohr and B. Mottelson, Nuclear Structure, Vol. II (W. A. Benjamin, Reading, Mass., 1975).

INELASTIC SCATTERING OF ^{28}Si AND ^{32}S ON ^{208}Pb STUDIED IN THE SPIN SPECTROMETER

D. C. Hensley, J. R. Beene, F. E. Bertrand, M. L. Halbert, D. Humphrey[1], G. Vourvopoulos[1]

Heavy ion inelastic scattering has been shown to be useful in studying collective nuclear structure properties.[2,3] The analysis of such experiments with the coupled-channel rotational model formalism can provide information on deformation parameters β_2 and β_4, static quadrupole moments of 2^+ states, triaxial shape parameters, and the relative phases of matrix elements.

Although collective nuclear structure properties can be studied via other methods such as (e,e'), (p,p'), or (α,α'), there are certain advantages to the use of heavy ions. For example, values for B(E2↑), Q_{4O}, and Q_2 may be derived simultaneously, and heavy ion inelastic scatter provides information on the $2^+ \rightarrow 4^+$ matrix element – the light ion reactions study only the matrix elements $0^+ \rightarrow 2^+$ and $0^+ \rightarrow 4^+$. And it is possible that fitting the differential cross sections helps establish the magnitude of the spin-orbit part of the heavy ion potential.

Previous heavy ion studies based their results on the analysis of elastic scattering data and data for the excitation of the first 2^+ collective state. It has been shown in the scattering of ^{20}Ne[2] and ^{28}Si[4,5] on ^{208}Pb, however, that the 2^+ angular distribution in the region of the grazing angle is very sensitive to the addition of β_4 deformation. Furthermore, for the case of ^{28}Si, it was found that a range of values for the hexadecapole deformation parameter β_4 gave excellent fits to both the elastic and the 2^+ inelastic angular distributions. It is apparently necessary to have information on higher collective states in order to determine deformation parameters uniquely.

Due to the existence of overlapping charged-particle peaks in the vicinity of the peak for the 4^+ state, it has not been possible to extract reliable experimental values for the 4^+ cross section for the cases studied. Although magnetic spectrographs provide intrinsic resolution sufficiently good to separate the states of interest in most cases, the fact that the detected particle is excited and emits γ rays in flight causes the observed groups to be Doppler broadened so as to obscure the states of interest. We have chosen, consequently, to perform the experiments in the Spin Spectrometer using position-sensitive charged-particle detectors in coincidence with the NaI detectors of the spectrometer. The good γ-ray efficiency and resolution of the Spin Spectrometer enable us to identify the states of interest via their γ decay while the charged-particle detectors provide the data for the needed inelastic-scattering angular distributions.

We have now studied the $^{208}Pb(^{28}Si,^{28}Si^*)$ and $^{208}Pb(^{32}S,^{32}S^*)$ reactions at 8.5 MeV/nucleon. The initial results for the ^{28}Si experiment will be described; the ^{32}S results are very similar. A beam of 2 pna on a 440 $\mu g/cm^2$ ^{208}Pb target was sufficient to provide adequate counting rates in the charged-particle detectors which spanned the angular region from 22° to 65° (the grazing angle was near 42°). The counting rates in the NaI detectors were typically about 20 kHz.

A great asset of the Spin Spectrometer for reactions producing few γ rays is its ability to "count" the γ rays. This is done by finding and summing the pulse heights from isolated clusters of detectors. (A cluster involves about 1.5 detectors, on the average.) As long as the number of γ rays is small, the probability that two clusters interfere is correspondingly small. Thus one can separate the various parts of the reaction into components with no γ ray (chiefly the ground state), one γ ray (chiefly the ^{28}Si 2^+ state and the ^{208}Pb 3^- state), two γ rays, etc. In addition, since the direction and velocity of both the projectile and the recoil are known as is the angle at which each γ ray was detected, it is possible to correct the γ-ray spectrum for the effect of any Doppler shift. The γ-ray spectra shown in Fig. 2.16

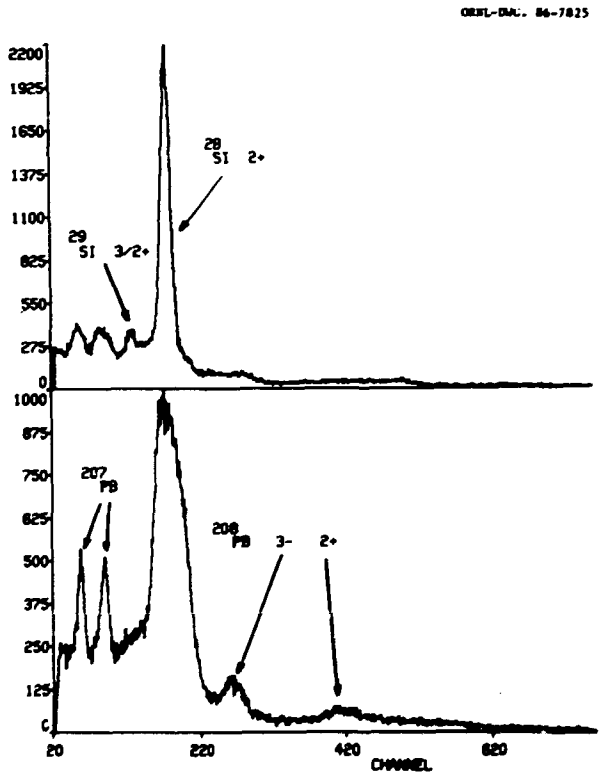

Fig. 2.16. One cluster γ-ray spectra measured in the Spin Spectrometer for the $^{208}Pb(^{28}Si,^{28}Si^*)$ reaction. The upper spectrum has been corrected for Doppler shifts assuming the γ ray came from the detected Si nucleus. For the lower spectrum it was assumed that the γ ray came from the recoil Pb nucleus. Peaks arising from the $^{208}Pb(^{28}Si,^{29}Si)^{207}Pb$ reaction have been indicated also.

are single cluster spectra from the Spin Spectrometer for the ^{28}Si reaction. The upper spectrum was obtained by assuming that the γ ray was emitted by the scattered ^{28}Si, while the lower spectrum was obtained by assuming that the γ ray was emitted by the recoil ^{208}Pb nucleus. The effect of this "Doppler focusing" is quite dramatic, especially for the higher energy γ rays. As was expected, the 2^+ state of ^{28}Si accounts for much of the one-cluster spectrum.

In Fig. 2.17 a two-cluster plot is shown where the axes of the histogram reflect the energies of the two clusters. The histogram has been made symmetric by histogramming the two clusters first as #1 vs #2 and then as #2 vs #1. It was assumed for this figure that both γ rays were emitted by ^{28}Si. Figure 2.18 shows the same data where it was assumed that one γ ray was emitted by ^{28}Si and the other by ^{208}Pb. The region of interest for the 4^+ state of ^{28}Si is indicated in Fig. 2.17. The corresponding

ORNL-DWG. 86-7826

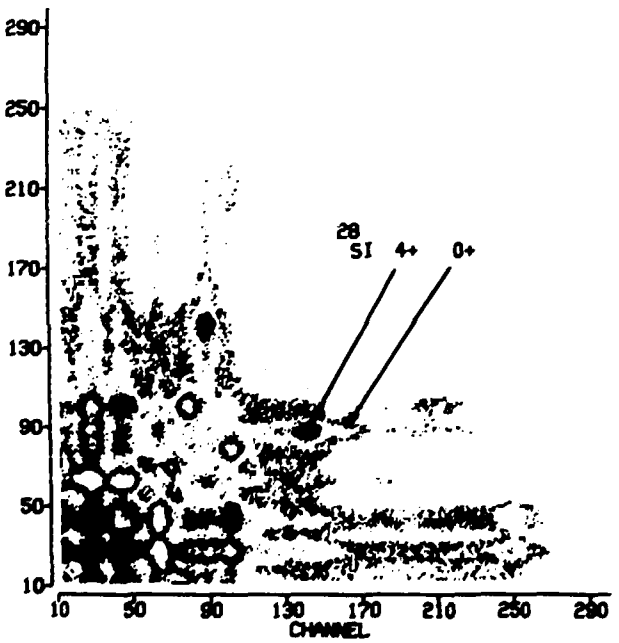

Fig. 2.17. A two cluster γ-ray histogram measured in the Spin Spectrometer for the $^{208}Pb + ^{28}Si$ reaction. The two clusters have been plotted as (1,2) and (2,1) so as to make the display symmetric. Both clusters were corrected for a Si Doppler shift. ^{28}Si groups are indicated. Most of the peaks near the axes came from the $^{208}Pb(^{28}Si,^{29}Si)$ reaction.

ORNL-DWG. 86-7827

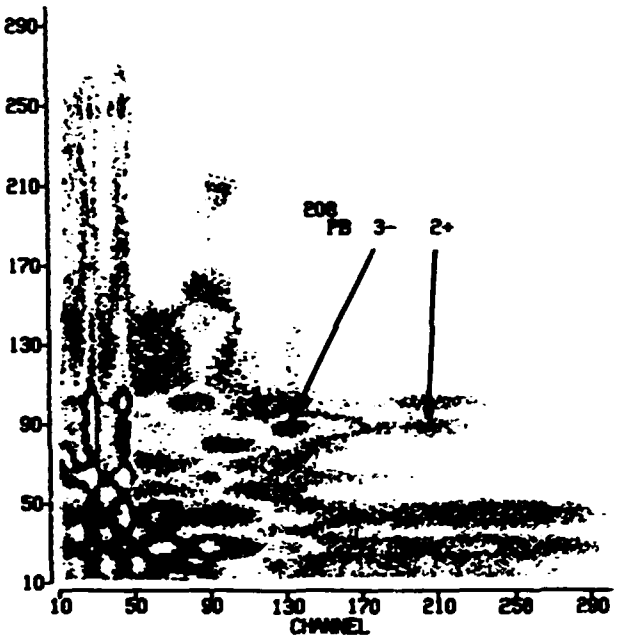

Fig. 2.18. This histogram differs from that of Fig. 2.17 in that the larger cluster (#1) was Pb Doppler corrected, the smaller cluster (#2) Si Doppler corrected, and plotted as (1,2). Then the larger was Si Doppler corrected, the smaller Pb Doppler corrected, and plotted as (2,1). The histogram is now no longer symmetric about the 45° axis. Note that the ^{28}Si 4^+ group indicated in Fig. 2.17 has washed out and the ^{208}Pb 3^- group has come into focus.

region in Fig. 2.18 is seen to be shifted slightly to lower energy, indicating the presence of the γ ray from the 3^- state of ^{208}Pb mutually excited along with the 2^+ state of ^{28}Si. (The energy of the ^{28}Si 4^+ γ ray is 2.84 Mev, and the energy for the ^{208}Pb 3^- γ ray is 2.62 Mev.) The Spin Spectrometer cleanly resolves the two contributions, allowing the angular distribution for the ^{28}Si 4^+ state to be obtained along with that for the mutual excitation of ^{208}Pb 3^- and ^{28}Si 2^+. Most of the counts in Figs. 2.17 and 2.18 arise from the $^{208}Pb(^{28}Si,^{29}Si)$ neutron pick-up reaction in which a γ ray from ^{29}Si is in coincidence with γ rays from the lowest excited states of ^{207}Pb.

A close examination of the γ-ray spectrum in coincidence with the ^{28}Si 2^+ γ ray shows clearly that we can measure the angular distribution for the ^{28}Si 4^+ state, for the 0^+ state just above it, and for the mutual excitation of the ^{28}Si 2^+

state with both the 3^- (2.61 Mev) and 2^+ (4.09 MeV) states of ^{208}Pb. Even though these states have peak differential cross sections of less than a few mb/sr, we are able to obtain detailed information over the whole angle range largely because of the very high efficiency of the Spin Spectrometer.

On the other hand, the scattering chamber in the Spin Spectrometer is relatively small, and a precise determination of the charged-particle scattering angle from this experiment is impossible to obtain. Consequently, a short run in a larger scattering chamber has been planned during which we will measure the elastic angular distribution and the 2^+ angular distribution for both the ^{28}Si and ^{32}S beams. From these data it will be possible to normalize the data taken in the Spin Spectrometer, so that angular distributions for all of the more weakly excited states can be obtained.

As a final note, we are able to obtain γ-ray angular correlation information for many of the states, from which we will be able to deduce m-substate populations for the reaction. This will provide one more piece of information to help the coupled-channel code make a unique determination of the nuclear structure properties of the nuclei being studied.

---

1. Western Kentucky University, Bowling Green, KY 42101.
2. E. E. Gross et al., Phys. Rev. C 17, 1665 (1978).
3. E. E. Gross et al., Nucl. Phys. A401, 362 (1983).
4. J. J. Kolata et al., Phys. Rev. C 30, 125 (1984).
5. P. R. Christensen et al., Phys. Rev. C 29, 455 (1984).

EXCITATION OF THE HIGH ENERGY NUCLEAR CONTINUUM IN ^{208}Pb BY 22 MeV/NUCLEON ^{17}O AND ^{32}S[1]

F. E. Bertrand
R. O. Sayer[2]
R. L. Auble
M. Beckerman[3]
J. L. Blankenship[4]
B. L. Burks
M. A. G. Fernandes[5]
C. W. Glover
E. E. Gross
D. J. Horen
D. Shapira
H. P. Morsch[6]

The ^{208}Pb high excitation continuum has been studied using inelastic scattering of 22 MeV/nucleon ^{17}O and ^{32}S. The spectra, taken with a magnetic spectrograph, show no evidence for peaks in the 30-100 MeV region of excitation. This is in contradiction to recently published results. The ^{17}O spectra are found to be remarkably similar to those from medium energy proton scattering, thus showing the "cleanliness" of ^{17}O as a probe for heavy-ion excitation of giant resonances.

---

1. Abstract of paper submitted to Physical Review C.
2. Computing and Telecommunications Division, ORNL.
3. Joint Institute for Heavy Ion Research, Oak Ridge, TN 37831.
4. Instrumentation and Controls Division, ORNL.
5. Universidade de Sao Paulo, Sao Paulo, Brazil.
6. Institut fur Kernphysik, Julich, West Germany and Joint Institute for Heavy Ion Research, Oak Ridge, TN 37831.

ELECTROMAGNETIC DECAY OF GIANT RESONANCES

J. R. Beene
F. E. Bertrand
B. L. Burks
M. L. Halbert
D. C. Hensley
R. L. Auble
D. J. Horen
R. L. Robinson
T. P. Sjoreen[1]
R. O. Sayer[2]
R. L. Varner

During the last two years, we have carried out a series of experiments designed to investigate the electromagnetic decays of giant resonances (GR), primarily in ^{208}Pb and ^{90}Zr.[3,4] An extensive report on the current status of these experiments, including a discussion of the procedures we have developed for data analysis, can be found in Ref. 3.

In these experiments we attempt to obtain as complete a set of data as possible on the decay of the region of excitation energy dominated by the T = 0, E2 and E0 resonances and the T = 1, E1 resonance (~9-15 MeV in ^{208}Pb, 12-21 MeV in ^{90}Zr). Utilizing the ORNL Spin Spectrometer, we have been able to isolate and quantitatively study decay branches to the ground state and low-lying excited states. These data stimulated a number of calculations of the giant resonance decay properties.[5,6] One interesting aspect of these calculations, which is borne out by the data, is the extreme suppression of the E1

gamma-decay branch from the T = 0, E2 resonance (GQR) in ^{208}Pb to the 3$^-$, 2.61-MeV state. These same calculations, on the other hand, predict a strong enhancement of the E1 decay from the T = 1 GQR (E_x = 22 MeV) to the 3$^-$, 2.61-MeV state. Later in this report there is a brief discussion of plans for an experiment stimulated by this prediction.

A major development during the last year has been an improved understanding of the ground-state decays from the T = 0 GQR.[3,7] The experiments give ground-state decay probabilities for the GQR of

$$\frac{\Gamma_{\gamma 0}}{\Gamma\Gamma} = (3.27 \pm 0.45) \times 10^{-4} \qquad (^{208}\text{Pb,GQR}) \ ;$$

$$\frac{\Gamma_{\gamma 0}}{\Gamma\Gamma} = (6 \pm 3) \times 10^{-5} \qquad (^{90}\text{Zr,GQR}) \ .$$

The Zr result suffers from very poor statistics. This will be much improved when the analysis of a new experiment on Zr is completed. We estimate that we have increased the amount of data available by a factor of 20-50.

The results for $\Gamma_{\gamma 0}$ can be compared to expectation based on the energy-weighted sum rule (EWSR). If we consider the ground-state gamma decay to occur directly from the GR doorway state, then it should be considered as occurring in competition with the damping process, characterized by $\Gamma^\downarrow$. (See Ref. 3 for a more detailed discussion.) We identify $\Gamma^\downarrow$ with the experimentally observed resonance widths Γ_{exp} (2.0 MeV in ^{208}Pb and 3.4 MeV in ^{90}Zr). The ground-state gamma width for a state exhausting 100% of the isoscalar L = 2 EWSR[8] is

$$\Gamma_{\gamma 0}(\text{EWSR}) = 8.07 \times 10^{-7} \, E_{\gamma 0}^5 \, B(E2\downarrow)_{\text{EWSR}} \ \text{W} \ ;$$

$$B(E2\downarrow)_{\text{EWSR}} = 5B(E2\downarrow)_{\text{EWSR}} = \frac{49.88 \, Z^2R^2}{A \, E_{GQR}} \, e^2fm^4 \ .$$

Using these expressions we find for the direct ground-state branch

$$\left.\frac{\Gamma_{\gamma 0}(D)}{\Gamma^\downarrow}\right]_{100\% \text{ EWSR}} = 8.62 \times 10^{-5} \qquad (^{208}\text{Pb}) \ ;$$

$$\left.\frac{\Gamma_{\gamma 0}(D)}{\Gamma^\downarrow}\right]_{100\% \text{ EWSR}} = 4.6 \times 10^{-5} \qquad (^{90}\text{Zr}) \ .$$

Taken at face value, this implies that the $\Gamma_{\gamma 0}$ strength in ^{208}Pb corresponds to 379% of the EWSR and that in ^{90}Zr to ~130%! Apparently, we should look either for some process associated with the reaction mechanism which might enhance the ground-state decay or for some process other than the direct process which might contribute to it. The simplest explanation falls in the latter category and involves the decay of the compound states into which the GQR is damped. We can estimate this effect:

$$\frac{\Gamma_{\gamma 0}}{\Gamma}(\text{CN}) = \left.\frac{\langle\Gamma_{\gamma 0}\rangle_{2^+}}{\langle\Gamma_n\rangle_{2^+}}\right|_{E_{GQR}} \ ,$$

where $\langle\Gamma_{\gamma 0}\rangle$ is the average ground-state branch of the individual compound states and $\langle\Gamma_n\rangle$ is the corresponding average neutron width.[9]

$$\langle\Gamma_{\gamma 0}(E_\gamma)\rangle = \frac{E_{\gamma 0}^5 \, f_{E2}(E_{\gamma 0})}{\rho(J = 2, \, E_{GQR})} \ ,$$

where $f_{E2}(E_\gamma)$ is the E2 gamma strength function and ρ is the density of states.

Similar expressions can be given for the average neutron width,[10]

$$\langle\Gamma_n\rangle = \frac{\sum_f \left(\frac{(2\ell + 1)}{g} \, S_\ell v_\ell \sqrt{E_n \times 10^3 \text{ MeV}}\right)}{\rho(J = 2, \, E_{GQR})} \ ,$$

where the sum is over final states (spin I) in the A - 1 nucleus, v_ℓ is the penetrability factor,[10,11] E_n is the neutron kinetic energy (MeV), and S_ℓ is the neutron strength function[10-12] for orbital angular momentum ℓ.

Since both the CN and direct contributions depend on the EWSR strength, our data can be compared with the sum of the two to give

^{208}Pb E2 γ0 strength ~ (107 ± 13)% EWSR,

and

^{90}Zr E2 γ0 strength ~ (113 ± 60)% EWSR.

The quoted uncertainties do not include the uncertainty in the calculated relative neutron widths.

Note that in earlier reports,[4] due to an error in our expression for the direct $\Gamma_{\gamma 0}$ sum rule of a factor of $(A/Z)^2$, we quoted values of ~85% of the EWSR for the EWSR for the direct component alone in ^{208}Pb.

The strength of the ground-state E2 gamma branch from the GQR of both ^{208}Pb and ^{90}Zr is accounted for reasonably well if effects of compound decay are included. Quantitative conclusions are hampered by the limitations of our estimate of the compound-state $\langle\Gamma_n\rangle$, but this estimate offers a straightforward explanation of the much greater importance of compound decays in ^{208}Pb than in ^{90}Zr. The total gamma-decay strength, given by the EWSR, controls both the direct and compound gamma widths. The direct gamma yield is thus completely determined by the EWSR and the spreading width, both of which vary slowly and systematically with nuclear species. The CN gamma yield, however, depends, in addition, on the average neutron width at the GQR, which can vary enormously from nucleus to nucleus. Calculations can guide us to systems for which, like ^{90}Zr, the direct branch dominates. Bismuth-209 is an example in the Pb region.[7]

Some interesting inconsistencies still remain when these ideas are applied to some other GQR gamma-decay branches. The absence of a direct E1 branch from the GQR to the 2.61-MeV, 3^- state in ^{208}Pb is well accounted for by calculations;[5,6] however, we must also consider the compound contribution to this decay, and in a purely statistical decay, this branch should be about 30% as large as the E2 ground-state branch. The compound decay to this state is apparently also suppressed.

Calculations[5,6] stimulated by this work have shown that the T = 1 GQR in ^{208}Pb (E_x = 22 MeV) should have an extremely large decay branch to the 3^-, 2.61-MeV state. We have determined that this isovector resonance can be strongly excited (mostly by Coulomb excitation) with 100-MeV/nucleon ^{17}O ions. We have proposed an experiment, to be carried out at the GANIL facility in France, to use the strong excitation and distinctive gamma-decay mode to isolate the T = 1 GQR, a state for which almost no reliable experimental data exist.

---

1. Solid State Division, ORNL.
2. Computing and Telecommunications Division, ORNL.

3. J. R. Beene, in Proceedings of the Niels Bohr Centennial Conference on Nuclear Structure, Copenhagen, Denmark, May 1985, to be published.
4. J. R. Beene, Phys. Div. Prog. Rep., Sept. 30, 1984, ORNL-6120, p. 32.
5. P. F. Bortignon, R. A. Broglia, and G. F. Bertsch, Phys. Lett. 148B, 20 (1984).
6. J. Speth et al., Phys. Rev. C 31, 2310 (1985).
7. J. R. Beene et al., Physics Letters B, in press.
8. A. Bohr and B. R. Mottelson, Nuclear Structure, Vol. I, Benjamin, Reading, Mass., 1969; A. Bohr and B. R. Mottelson, Nuclear Structure, Vol. II, Benjamin, Reading, Mass., 1975.
9. G. A. Bartholomew et al., in Advances in Nuclear Physics, Vol. 7, ed. E. Vogt and M. Baranger, Plenum Press, New York, 1973.
10. S. G. Mughabghab, M. Divadeenam, and N. E. Holden, Neutron Cross Sections, Academic Press, New York, 1981.
11. D. J. Horen, J. A. Harvey, and N. W. Hill, Phys. Rev. C 18, 722 (1978).
12. J. E. Lynn, Theory of Neutron Resonance Cross Reactions, Oxford University Press, Oxford, 1968.

NEUTRON DECAY OF GIANT RESONANCES

J. R. Beene — R. L. Auble
A. Bracco[1] — D. J. Horen
F. E. Bertrand — R. L. Robinson
M. L. Halbert — T. P. Sjoreen[2]
D. C. Hensley — R. O. Sayer[3]

The giant electric multipole resonances in heavy nuclei are simple nuclear states embedded in a dense spectrum of more complex states, with which they mix. The consequent damping of the giant resonances (GR) offers an excellent test of our understanding of many-body physics in atomic nuclei. The questions now being asked[4,5] concerning the microscopic structure and the damping of these resonances require more detailed experiments than those which have served to build up the systematic catalog of gross properties of the resonances over the last decades.[6-8] The data required are coincidence data on the particle and gamma decay of the resonances, which can probe aspects of the resonance structure not addressed by the existing systematics.[6-8]

We have carried out a series of experiments which provide important data on the neutron decay of giant resonances (primarily the T=0 E2 and E0 resonances) in ^{90}Zr and ^{208}Pb.[9,10] In these systems neutron decay accounts for the bulk of all decays (>99.9%) in the excitation

energy region of interest. Experimental techniques and data analysis procedures are discussed at some length in Ref. 9.

The analysis of experimental data on the distribution of neutron-decay strength among various low lying states of the A-1 system is now complete for both ^{208}Pb and ^{90}Zr. We also have extracted neutron angular distributions for strong transitions in the Pb system. The interpretation of these data is not straightforward. Our goal is to identify and study any "nonstatistical" neutron emission. In order to do this we require extremely careful statistical model calculations, including thorough exploration of the reasonable parameter space of the model, if conclusions are to have any real significance. Cursory calculations employed to extract small nonstatistical effects — or even worse — simple subtraction of assumed Maxwell Boltzmann statistical neutron spect have been, unfortunately, all too common a characteristic of previous work in this field.

Our goal over the next several months is to carry out statistical calculations of sufficient quality and detail that we can identify genuinely nonstatistical characteristics in the data, and be able to address questions of significance and uniqueness of our analysis in a quantitative way.

---

1. Universita Degli Studi di Milano, 20133 Milano, Italy.
2. Solid State Division, ORNL.
3. Computing and Telecommunications Division, ORNL.

4. G. F. Bertsch, P. F. Bortignon, and R. A. Broglia, Rev. Mod. Phys. 55, 287 (1983).
5. P. F. Bortignon and R. A. Broglia, Nucl. Phys. A371, 405 (1981).
6. F. E. Bertrand, Annu. Rev. Nucl. Sci. 26, 457 (1976).
7. Giant Multipole Resonances, ed. F. F. Bertrand (Harwood Academic, New York, 1980).
8. F. E. Bertrand, Nucl. Phys. A354, 129c (1981).
9. J. R. Beene et al., p. 503 in Nuclear Structure 1985 (Proceedings of the Niels Bohr Centennial Conference, Copenhagen, May 20-24, 1985), edited by R. Broglia, G. Hagemann, and B. Herskind (North-Holland, 1985).
10. J. R. Beene et al., p. 34 in Phys. Div. Prog. Rept. for Period Ending Sept. 30, 1984, ORNL-6120 (1985).

TEST OF THE TRIAXIAL ROTOR MODEL AND THE IBFA MODEL DESCRIPTION OF COLLECTIVE STATES IN ^{193}Ir

F. K. McGowan, C. Roulet[1], N. R. Johnson, Y. A. Ellis-Akovali, I. Y. Lee, R. M. Diamond[2], W. T. Milner, F. S. Stephens[2], M. W. Guidry[3]

Coulomb excitation of states in ^{193}Ir up to J = 21/2 have been observed with 160-MeV ^{40}Ar and 617-MeV ^{136}Xe ions. Most of these states are grouped into three rotational-like bands based on the $3/2^+$ ground state, the $1/2^+$ first excited state, and the $7/2^+$ γ-vibrational-like state at 621 keV. The average deviation between experimental and theoretical energies for 17 states is 54 keV for the particle-asymmetric-rigid-rotor model and 66 keV for the IBFA model (limited to broken Spin(6) symmetry and only the $d_{3/2}$ orbital is considered). The overall agreement of both model predictions with experimental γ-ray yields for transitions within the $3/2^+$ band is quite good. For interband transitions originating in the $K = 1/2^+$ and $7/2^+$ bands, the IBFA model tends to underestimate the γ-ray yields by one to two orders of magnitude. There are five moderately collective transitions corresponding to $\Delta\tau_1 = 2$ transitions in the U(6/4) and U(6/20) supersymmetry schemes[4,5] and are strictly forbidden in these schemes. The U(6/4) supersymmetry scheme assumes that the proton moves only in the single-j orbital $d_{3/2}$. the multi-j U(6/20) supersymmetry scheme includes all four positive parity single-particle orbitals, viz., $g_{7/2}$, $d_{5/2}$, $d_{3/2}$, and $s_{1/2}$. The predictions of excitation energies are virtually identical in U(6/4) and U(6/20).

There is one transition $3/2 \rightarrow 3/2$ of 180 keV in ^{193}Ir with a $B(E2, 3/2 \rightarrow 3/2) = 14\ B(E2)_{sp}$ which is a strictly forbidden $\Delta\tau_1 = 2$ transition in both supersymmetry schemes. This collective E2 transition is not a special situation in ^{193}Ir but a general feature in ^{191}Ir and ^{197}Au.[6] Table 2.3 presents a comparison of the experimental and model-predicted B(E2) values for ^{193}Ir. The B(E2) values predicted by U(6/20) and U(6/4) supersymmetry schemes differ by only about 25%. For both supersymmetry schemes there is a lack of detailed agreements with the B(E2) values for the $\Delta\tau_1 = 1$ transitions from the

Table 2.3 Comparison between experimental and model-predicted B(E2) values for ^{193}Ir.

The B(E2) values are given in units of $B(E2)_{sp} = .00662e^2b^2$ for A = 193. The adjustable constant in the E2 operator deduced from $B(E2)_{exp}$ for ^{192}Os is $\chi^2 = 3.32\ B(E2)_{sp}$. In U(6/20) $\sigma_1 = 17/2$ and in U(6/4) $\sigma_1 = 15/2$.

Nucleus	τ_{1i}	J_i	τ_{1f}	J_f	E_γ (keV)	$B(E2)^a_{exp}$	B(E2) Calculated U(6/20)	U(6/4)	Broken Spin(6)	Triaxial Rotor
^{193}Ir	3/2	1/2	1/2	3/2	73.0	41.4 ± 4.8	69.	56.	32.8	14.4
	3/2	5/2	1/2	3/2	138.9	77.0 ± 1.5	69.	56.	63.0	74.1
	3/2	7/2	1/2	3/2	357.7	38.5 ± 0.8	69.	56.	45.2	38.1
	5/2	3/2	1/2	3/2	180.0	13.9 ± 1.1	0.0	0.0	0.27	16.5
	5/2	5/2	1/2	3/2	361.8	1.40 ± 0.60	0.0	0.0	0.5	5.7
	5/2	7/2	1/2	3/2	621.	8.7 ± 0.3	0.0	0.0	0.08	3.6
	3/2	7/2	3/2	5/2	218.8	22.7 ± 5.4	15.4	12.6	23.9	18.0
	5/2	3/2	3/2	1/2	107.0	$40.8^{+16.6}_{-13.6}$	32.5	25.9	27.3	41.3
	5/2	5/2	3/2	1/2	289.	71.0 ± 12.1	55.8	44.4	39.0	34.5
	5/2	7/2	3/2	5/2	482.	20.4 ± 3.0	47.4	37.7	28.5	14.1
	5/2	9/2	3/2	5/2	382.9	74.9 ± 2.7	73.0	58.1	53.6	68.3
	5/2	11/2	3/2	7/2	499.	50.3 ± 3.5	93.0	74.0	78.7	68.0
σ_{1i}=13/2	1/2	3/2	1/2	3/2	460.	3.5 ± 0.3	0.0	0.0	0.02	6.3
σ_{1i}=13/2	1/2	3/2	3/2	1/2	387.	0.62 ± 0.41	0.0	0.0	0.54	5.6
σ_{1i}=13/2	1/2	3/2	3/2	5/2	321.	0.74 ± 0.26	0.0	0.0	0.09	4.7
σ_{1i}=13/2	1/2	3/2	5/2	3/2	280.	$0.21^{+0.29}_{-0.17}$	0.0	0.0	11.1	0.27
	5/2	5/2	5/2	3/2	182.	28.7 ± 6.0	1.8	1.4	0.02	3.2
	1/2	3/2	1/2	3/2	0.0	(42.4 ± 1.1)[b]	73.	60.	53.6	31.7
^{192}Os	1	2	0	0	205.8	(63.8 ± 0.6)[c]				

[a]Ref. 7 and 8
[b]Ref. 9
[c]Ref. 10

decay of the $\tau_1 = 3/2$ states to the 3/2 ground state. These features are, however, reproduced to a much better degree by the broken spin(6) calculations. Besides the five moderately collective transitions with $\Delta\tau_1 = 2$, there are four transitions in Table 2.3 with $\Delta\sigma_1 = 1$ which are strictly forbidden in the U(6/20) and U(6/4) supersymmetry schemes. By far the most successful interpretation of the B(E2) values in ^{193}Ir is the particle-asymmetric rigid rotor model.

---

1. Present address: Etudes et Productions, Schlumberger, Clamar, France.

2. Lawrence Berkeley Laboratory, Berkeley, CA.
3. Adjunct staff member from University of Tennessee, Knoxville, TN.
4. A. B. Balantekin et al., Nucl. Phys. A370, 284 (1981).
5. Yin-Sheng Ying et al., Phys. Lett. 148B, 13 (1984).
6. F. K. McGowan et al., Ann. Phys. (N.Y.) 63, 549 (1971).
7. V. S. Shirley, Nucl. Data Sheets 32, 593 (1981).
8. J. X. Saladin et al., Bull. Am. Phys. Soc. 27, 705 (1982).
9. Y. Tunaka et al., Phys. Rev. Lett. 51, 1633 (1983).
10. M. V. Hoehn et al., Phys. Rev. C 24, 1667 (1981).

TEST OF THE TRIAXIAL ROTOR MODEL AND THE IBFA MODEL DESCRIPTION OF COLLECTIVE STATES IN ^{191}Ir[1]

F. K. McGowan, N. R. Johnson, I. Y. Lee, W. T. Milner, C. Roulet[2], J. Hattula[3], M. P. Fewell[4], Y. A. Ellis-Akovali, R. M. Diamond[5], F. S. Stephens[5], M. W. Guidry[6]

Coulomb excitation of states in ^{191}Ir up to J = 21/2 have been observed with 160-MeV ^{40}Ar and 617-MeV ^{136}Xe ions. Most of these states are grouped into three rotational-like bands based on the $3/2^+$ ground state, the $1/2^+$ first excited state, and the $7/2^+$ γ-vibrational-like state at 686 keV. The average deviation between experimental and theoretical energies for 20 states is 45 keV for the particle-asymmetric-rigid-rotor model and 125 keV for the IBFA model (limited to broken Spin(6) symmetry and only the $d_{3/2}$ orbital is considered). The overall agreement of both model predictions with experimental γ-ray yields for transitions within the $3/2^+$ band is quite good. For interband transitions originating in the $K = 1/2^+$ and $7/2^+$ bands, the IBFA model tends to underestimate the γ-ray yields by one to two orders of magnitude. These six moderately collective transitions correspond to $\Delta\tau_1=2$ transitions in the U(6/4) and U(6/20) supersymmetry schemes and are strictly forbidden in these schemes. For both supersymmetric schemes[7,8] there is a lack of detailed agreement with the very collective E2 transitions which have $\Delta\tau_1=0,\pm1$ in Table 2.4. The triaxial rotor model description of the experimental energies and the collective E2 transitions is the most successful approach.

---

1. Summary of a paper to be published in Phys. Rev. C.
2. Present address: Etudes et Productions, Schlumberger, Clamar, France.

Table 2.4 Comparison between experimental and model-predicted B(E2) values for ^{191}Ir.

The B(E2) values are given in units of $B(E2)_{sp}$ and $B(E2)_{sp} = .00652\ e^2b^2$ for A = 191. The adjustable parameter in Eq. (2) deduced from $B(E2)_{exp}$ for ^{190}Os is $\gamma^2 = 3.25B(E2)_{sp}$. In U(6/20) $\sigma_1 = 19/2$ and in U(6/4) $\sigma_1 = 17/2$.

Nucleus	τ_{1i}	J_i	τ_{1f}	J_f	E_γ (keV)	$B(E2)_{exp}$	B(E2) Calculated U(6/20)	U(6/4)	Broken Spin(6)	Triaxial Rotor
^{191}Ir	3/2	1/2	1/2	3/2	82.5	20.9 ± 2.4	82	68	28.5	17.9
	3/2	5/2	1/2	3/2	129.4	91.7 ± 2.6	82	68	95.6	88.2
	3/2	7/2	1/2	3/2	343.2	42.6 ± 0.9	92	68	55.2	46.3
	5/2	3/2	1/2	3/2	179.0	16.6 ± 1.4	0.0	0.0	2.0	34.4
	5/2	5/2	1/2	3/2	351.1	3.1 ± 0.8	0.0	0.0	0.5	4.4
	5/2	7/2	1/2	3/2	686.3	9.7 ± 0.3	0.0	0.0	1.2	3.5
	3/2	5/2	3/2	1/2	46.9	6.6 ± 3.4	12.3	10.3	3.1	12.0
	3/2	7/2	3/2	5/2	213.8	44.5 ± 6.1	18.0	15.1	41.1	26.5
	5/2	3/2	3/2	1/2	96.5	54 ± 11	39	32	38.2	32.7
	5/2	5/2	3/2	1/2	268.6	>89	67	55	48.0	48.5
	5/2	7/2	3/2	5/2	556.8	19.5 ± 3.4	57	46	34.2	14.0
	5/2	9/2	3/2	5/2	373.1	102 ± 3	88	72	74.4	78.7
	5/2	11/2	3/2	7/2	489.0	72 ± 4	111	91	80.8	80.4
$\sigma_{1i}=15/2$	1/2	3/2	1/2	3/2	539.	(1.5 ± 0.7)[c]	0.0	0.0	0.02	5.6
$\sigma_{1i}=15/2$	1/2	3/2	3/2	1/2	457.	0.6 ± 0.6	0.0	0.0	0.55	5.0
$\sigma_{1i}=15/2$	1/2	3/2	3/2	5/2	409.	0.6 ± 0.3	0.0	0.0	0.09	3.8
$\sigma_{1i}=15/2$	1/2	3/2	5/2	3/2	360.	0.5 ± 0.3	0.0	0.0	11.3	0.21
$\sigma_{1i}=15/2$	1/2	3/2	5/2	5/2	188.	$2.4^{+13.}_{-1.8}$	0.0	0.0	4.0	2.4
	1/2	3/2	1/2	3/2	0.0	(50.8 ± 1.1)[a]	85	71	69	21.0
^{190}Os	1	2	0	0	186.7	(76.0 ± 0.6)[b]				

[a] Ref. 9
[b] Ref. 10
[c] Refs. 11 and 12

3. On leave from University of Jyväskyla, Jyväskyla, Finland.
4. Present address: Australian National University, Canberra, Australia.
5. Lawrence Berkeley Laboratory, Berkeley, CA.
6. Adjunct staff member from University of Tennessee, Knoxville, TN.
7. A. B. Balantekin et al., Nucl. Phys. A370, 284 (1981).
8. Yin-Sheng Ling et al., Phys. Lett. 148B, 13 (1984).
9. Y. Tunaka et al., Phys. Rev. Lett. 51, 1633 (1983).
10. M. V. Hoehn et al., Phys. Rev. C 24, 1667 (1981).
11. E. Browne, Nucl. Data Sheets 30, 653 (1980).
12. K. S. Krane, At. Data Nucl. Data Tables 18, 137 (1976).

NUCLEAR STRUCTURE STUDIES VIA CHARGE-EXCHANGE REACTIONS

GAMOW-TELLER STRENGTH FUNCTION IN ^{71}Ge VIA THE (p,n) REACTION AT MEDIUM ENERGIES[1]

D. Krofcheck[2] C. C. Foster[5]
E. Sugarbaker[2] C. D. Goodman[5]
J. Rapaport[3] I. J. Van Heerden[5]
D. Wang[3] C. Gaarde[6]
J. N. Bahcall[4] J. S. Larsen[6]
R. C. Byrd[5] D. J. Horen
T. N. Taddeucci[3,5]

The GT strength function in ^{71}Ge has been measured using the ^{71}Ga(p,n) reaction at E_p = 120 and 200 MeV. While a significant fraction of the total strength is associated with excited states located below particle emission threshold, the first excited state exhibits little GT strength. Excited state contributions to the total solar neutrino capture rate for a ^{71}Ga detector are about 14 SNU for the neutrino spectrum of the standard solar model and about 3-4 SNU for representative nonstandard solar models.

---

1. Abstract of published paper: Phys. Rev. Lett. 55, 1051 (1985).

2. Ohio State University, Columbus, OH 43210.
3. Ohio University, Athens, OH 45701.
4. Institute for Advanced Study, Princeton, NJ 08540.
5. Indiana University, Bloomington, IN 47405.
6. Niels Bohr Institute, Copenhagen, Denmark.

SPIN-FLIP DECOMPOSITION OF THE SPECTRUM FOR ^{90}Zr(p,n) AT E_p = 160 MeV[1]

T. N. Taddeucci[2,3] D. J. Horen
C. D. Goodman[3] J. S. Larsen[5]
R. C. Byrd[3] C. Gaarde[5]
I. J. Van Heerden[3] J. Rapaport[2]
T. A. Carey[4] T. P. Welch[2]
E. Sugarbaker[6]

The transverse polarization transfer for the ^{90}Zr(p,n) reaction has been measured for E_p = 160 MeV and $\theta = 0°$. A sequence of alternating unnatural parity and natural parity excitations is clearly revealed. Some of the observed features are consistent with the known or predicted excitation energies of 0^+, 0^-, 1^+, and 1^- resonances.

---

1. Abstract of paper submitted to Physical Review C.

2. Ohio University, Athens, OH 45701.
3. Indiana University Cyclotron Facility, Bloomington, IN 47405.
4. Los Alamos National Laboratory, Los Alamos, NM 87545.
5. Niels Bohr Institute, Copenhagen, Denmark.
6. Ohio State University, Columbus, OH 43214.

THE ^{19}F(p,n)^{19}Ne AND ^{39}K(p,n)^{39}Ca REACTIONS AT INTERMEDIATE ENERGIES AND QUENCHING OF THE GAMOW-TELLER STRENGTH[1]

J. Rapaport[2] C. Foster[5]
C. Gaarde[3] D. J. Horen
J. Larsen[3] T. Masterson[6]
C. Goulding[4] E. Sugarbaker[7]
C. D. Goodman[5] T. N. Taddeucci[2,5]

The (p,n) reactions on ^{19}F and ^{39}K targets were studied at 120 MeV and 160 MeV using the Indiana University Cyclotron time-of-flight facility. States up to 12-MeV excitation energy were observed and angular distributions for these neutron groups are presented. The ground-state mirror transitions have accurately measured ft values. This information is used to normalize the zero-degree energy spectra to a scale of Gamow-Teller (GT) transition probability to obtain GT strengths to excited states. The experimental sum GT strengths are smaller than the sum-rule-limit values, showing strong evidence for GT quenching.

1. Abstract of published paper: Nucl. Phys. A431, 301 (1984).
2. Ohio University, Athens, OH 45701.
3. Niels Bohr Institute, Copenhagen, Denmark.
4. Los Alamos National Laboratory, Los Alamos, NM 87545.
5. Indiana University Cyclotron Facility, Bloomington, IN 47401.
6. Colorado University, Boulder, CO 80309.
7. Ohio State University, Columbus, OH 43201.

THE $^{51}V(p,n)^{51}Cr$ REACTION AT E_p = 160 MeV[1]

J. Rapaport[2] C. D. Goodman[5]
R. Alarcon[2] C. C. Foster[5]
B. A. Brown[3] D. Horen
C. Gaarde[4] T. Masterson[6]
J. Larsen[4] E. Sugarbaker[7]
T. N. Taddeucci[2,5]

The $^{51}V(p,n)^{51}Cr$ reaction was studied at E_p = 160 MeV using the Indiana University beam-swinger facility. Data were obtained at several angles up to θ_L = 20°. The 0° spectrum was used to obtain a ΔL = 0 response function from which Gamow-Teller strength was derived. A shell-model calculation of the GT strength distribution was presented and compared with the experimental results. The M1 strength was also calculated and compared with available results from (e,e') and (p,p') experiments. A comparison was made with other N = 28 nuclei. Effects of a truncated shell-model space are presented.

1. Abstract of published paper: Nucl. Phys. A427, 332 (1984).
2. Ohio University, Athens, OH 45701.
3. Michigan State University, East Lansing, MI 48824.
4. Niels Bohr Institute, Copenhagen, Denmark.
5. Indiana University, Bloomington, IN 47405.
6. University of Colorado, Boulder, CO 80309.
7. Ohio State University, Columbus, OH 43214.

SOLAR-NEUTRINO DETECTION: EXPERIMENTAL DETERMINATION OF GAMOW-TELLER STRENGTHS VIA THE ^{98}Mo AND $^{115}In(p,n)$ REACTIONS[1]

J. Rapaport[2] C. D. Goodman[5]
P. Welch[2] C. F. Foster[5]
J. Bahcall[3] D. Horen
E. Sugarbaker[4] C. Gaarde[6]
T. N. Taddeucci[2,5] J. Larsen[6]
T. Masterson[7]

The empirical distribution of Gamow-Teller strengths in ^{98}Tc and ^{115}Sn have been obtained via the (p,n) reaction at E_p = 120 Mev and E_p = 200 MeV on ^{98}Mo and ^{115}In targets. This information is used to calculate the cross sections for absorption of solar neutrinos in ^{98}Mo and ^{115}In, nuclides which are being considered as neutrino detectors to accomplish solar-neutrino spectroscopy.

1. Abstract of published paper: Phys. Rev. Lett. 54, 2325 (1985).
2. Ohio University, Athens, OH 45701.
3. Institute for Advanced Study, Princeton, NJ 08540.
4. Ohio State University, Columbus, OH 43201.
5. Indiana University, Bloomington, IN 47401.
6. Niels Bohr Institute, Copenhagen, Denmark.
7. University of Colorado, Boulder, CO 80309.

MEASUREMENTS OF GAMOW-TELLER STRENGTH DISTRIBUTIONS IN MASSES 13 AND 15

C. D. Goodman[2] J. S. Larsen[4]
R. C. Byrd[2] C. Gaarde[4]
I. J. Van Heerden[2] J. Rapaport[5]
T. A. Carey[3] T. P. Welch[5]
D. J. Horen E. Sugarbaker[6]
T. N. Taddeucci[2,5]

The differential cross section and the transverse spin-flip probability have been measured for the dominant transitions in $^{13}C(p,n)^{13}N$ and $^{15}N(p,n)^{15}O$ at E_p = 160 MeV. The Gamow-Teller transition strengths deduced from the data show

that the major $\frac{1^-}{2} \rightarrow \frac{3^-}{2}$ transitions are strongly quenches relative to the $\frac{1^-}{2} \rightarrow \frac{1^-}{2}$ mirror transitions, in strong disagreement with simple shell-model expectations.

---

1. Abstract of published paper: Phys. Rev. Lett. 54, 877 (1985).
2. Indiana University Cyclotron Facility, Bloomington, IN 47401.
3. Los Alamos National Laboratory, Los Alamos, NM 87545.
4. Niels Bohr Institute, Copenhagen, Denmark.
5. Ohio University, Athens, OH 45701.
6. Ohio State University, Columbus, OH 43201.

AN INVESTIGATION OF THE $^{28}Si(^{18}O,^{18}F)^{28}Al$ SINGLE CHARGE EXCHANGE REACTION AT 19.5 MeV/NUCLEON

D. J. Horen
B. L. Burks
M. A. G. Fernandes[1]
R. L. Auble
F. E. Bertrand
J. L. Blankenship[2]
J. L. C. Ford, Jr.[3]
E. E. Gross
D. C. Hensley
F. Petrovich[4]
R. O. Sayer[5]
G. R. Satchler
D. Shapira
T. P. Sjoreen[6]

Measurements on the $^{28}Si(^{18}O,^{18}F)^{28}Al$ charge-exchange reaction at E_{lab} = 352 MeV have been completed[7] for θ_{CM} ≈4°-12°, and the data have been analyzed. The target used was a self-supported foil of 117 μg/cm² of natural silicon. An experimental energy resolution of ~265 keV was attained. A spectrum obtained by setting mass and charge gates to identify ^{18}F ions detected with the broad-range spectrograph focal plane detector system is shown in Fig. 2.19. The peaks centered near channels 1190 and 1145 correspond to excitations in ^{28}Al where the ^{18}F ejectile was left in its ground state. The peak at channel 1190 arises from transitions to the ground (3⁺) and first excited (2⁺) states in ^{28}Al. The peak at channel 1145 could be associated with excitation of states in ^{28}Al at 2.139 (2⁺), 2.202 (1⁺), and 2.27 (4⁺) MeV.

In Fig. 2.20 are plotted the charge-exchange differential cross sections for excitation of these two multiplets. We have performed single-step DWBA calculations using microscopic form factors and optical model parameters deduced from fits to elastic scattering data (described

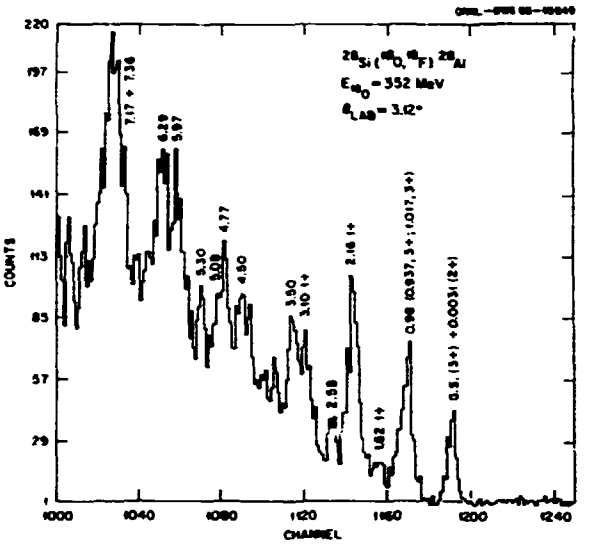

Fig 2.19. $^{28}Si(^{18}O,^{18}F)^{28}Al$ spectrum at θ_{lab} = 3.12°.

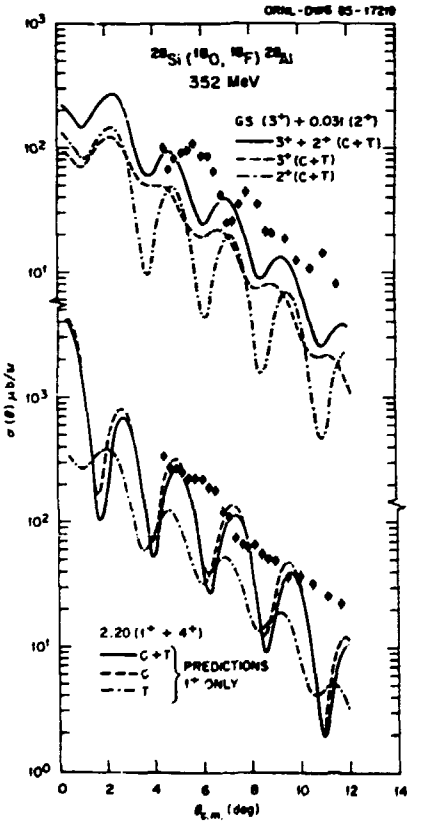

Fig. 2.20. Comparison of $^{28}(^{18}O,^{18}F)^{28}Al$ data with the microscopic DWBA predictions for the (g.s. + 0.031 MeV) and 2.20 MeV doublet transitions. The S-7F optical model potential derived from fitting the ^{18}O + ^{28}Si elastic data and used in the one-nucleon transfers (contributions in the present report) was used in the entrance and exit channels.

by Burks et al., "Optical Model and Coupled Channels Analyses of Elastic and Inelastic Scattering of ^{18}O from ^{28}Si at 352 MeV," earlier in this section). The form factors were calculated using a double folding model with harmonic oscillator wave functions and transition amplitudes provided by Wildenthal,[8] and the M3Y effective nucleon-nucleon interaction. The calculated cross sections are also shown in Fig. 2.20. For the ground and first excited state doublet, the calculated cross sections for each state are plotted separately. The reason that the cross section for the 3^+ state is less diffractive than that for the 2^+ state can be traced to the fact that the amplitudes of the central plus exchange (+E) and tensor (T) components are nearly equal for the 3^+ state, whereas the 2^+ state is mainly excited via the C+E force. The calculated cross sections leading to excitation of the 2^+ and 4^+ states near 2.2 MeV were negligible relative to that for the 1^+ state. In the lower portion of Fig. 2.20 we show the calculated cross section for the 1^+ state as well as the separate C+E and T components of the interaction.

At the present time, we do not believe that the relatively good agreement in magnitude between the experimental and calculated cross sections can be taken as an indication that the reaction takes place entirely by a one step process. First, we know from intermediate energy (p,n) measurements that the spin-isospin GT transitions are quenched. It is generally believed that a major part of this quenching arises from configuration mixing which is not taken into account in our calculation. Furthermore, it has been suggested[9] that the strength of the central part of the M3Y interaction might be too large by about a factor of two. Hence, we suspect that at least half of the experimental cross section to the 2.2-MeV peak arises from other than a one step process.

The same microscopic form factors for excitation of the ground-state doublet were also utilized with the S-7 OMP of Ref. 10 to calculate the charge-exchange cross section at 3.1 MeV/nucleon. The calculated cross section was found to be two orders of magnitude smaller than that experimentally observed.[10]

In summary, we interpret these results as indicating that in the $^{28}Si(^{18}O,^{18}F)^{28}Al$ charge-exchange reaction the one-step contribution is insignificant at 3.1 MeV/nucleon but is becoming comparable to other reaction paths at 19.5 MeV/nucleon. Further experimentation is required to determine whether this reaction at ~20 MeV/nucleon will prove useful in deducing GT matrix elements.

---

1. Universidade de Sao Paulo, Departamento de Fisica Nuclear, Sao Paulo, Brazil.
2. Instrumentation and Controls Division, ORNL.
3. Deceased.
4. Florida State University, Tallahassee, FL 32306.
5. Computing and Telecommunications Division, ORNL.
6. Solid State Division, ORNL.
7. Phys. Div. Prog. Rept. for Period Ending Sept. 30, 1983, ORNL 6004, p. 73.
8. B. H. Wildenthal, private communication.
9. F. Petrovich, in the (p,n) Reaction and the Nucleon-Nucleon Force, edited by C. D. Goodman et al. (Plenum, New York, 1980), p. 115.
10. B. T. Kim et al., Phys. Rev. C 20, 1396 (1979).

NUCLEAR STRUCTURE STUDIES VIA TRANSFER AND CAPTURE REACTIONS

SPINS AND PARITIES OF LOW-LYING STATES IN ^{81}Kr FROM THE $^{80}Kr(\vec{d},p)^{81}Kr$ REACTION AND IMPLICATIONS FOR A ^{81}BR SOLAR NEUTRINO DETECTOR[1]

B. L. Burks T. B. Clegg[3]
R. E. Anderson[2] E. J. Ludwig[3]
R. L. Varner

The structure of ^{81}Kr has been investigated via the $^{80}Kr(\vec{d},p)^{81}Kr$ reaction using an 11.0-MeV vector-polarized deuteron beam. Differential cross sections, σ, and vector analyzing powers, A_y, have been measured from 20° to 90° for 17 excited states below 3.0-MeV excitation energy. Comparisons of these distributions to DWBA calculations and empirical shapes were made to extract spectroscopic factors and values of spin and parity for these states. The significance of these measurements to the design of a bromine solar neutrino detector is discussed.

1. Abstract of published paper: Nucl. Phys. A442, 300 (1985).
2. Rockwell International Corp., Golden, CO 80401.
3. University of North Carolina, Chapel Hill, NC 27514 and Triangle Universities Nuclear Laboratory, Durham, NC 27706.

ALPHA-PARTICLE D-STATE AND CONFIGURATION-MIXING EFFECTS IN THE $^{89}Y(d,\alpha)^{87}Sr$ REACTION[1]

B. C. Karp[2] B. L. Burks
E. J. Ludwig[3] T. B. Clegg[3]
J. E. Bowsher[3] F. D. Santos[4]
A. M. Eiro[4]

Angular distributions and cross sections of vector and tensor analyzing powers have been measured for low-lying levels populated by the $^{89}Y(d,\alpha)^{87}Sr$ reaction at 9.0, 12.0, and 16.0 MeV. Full finite-range DWBA calculations that include the effects of an alpha-particle D-state component and (L,J)-mixing have been performed. The ground-state transition indicates that the D-state parameter $D_2 = -0.35 \pm 0.1$ fm^2. The angular distributions of the tensor analyzing powers are very sensitive to the magnitude and sign of the mixing amplitudes and can be used to determine the neutron-proton configurations transferred. The mixing amplitudes for the 0.388-MeV and 0.873-MeV states in ^{87}Sr are established from the analysis.

1. Abstract of paper submitted to Nuclear Physics A.
2. AT&T Bell Laboratories, Holmdel, NJ 07723.
3. University of North Carolina, Chapel Hill, NC 27514 and Triangle Universities Nuclear Laboratory, Durham, NC 27706.
4. Centro de Fisica Nuclear da Universidade de Lisboa, Av. Gama Pinto, 2, 1699 Lisbon Codex, Portugal.

A DWBA ANALYSIS OF THE $^{86}Sr(\vec{d},p)^{87}Sr$ REACTION[1]

B. L. Burks E. J. Ludwig[3]
R. E. Anderson[2] B. C. Karp[4]
T. B. Clegg[3] Y. Aoki[5]

The structure of ^{87}Sr has been investigated via the $^{86}Sr(\vec{d},p)^{87}Sr$ reaction using an 11.0-MeV vector-polarized deuteron beam. Differential cross sections, σ, and vector analyzing powers, A_y, have been measured from 20° to 105° for 18 excited states below 4.0 MeV excitation energy. Comparisons of these distributions to DWBA calculations and empirical shapes were made to extract neutron spectroscopic factors and values of spin and parity for these states. Angular distributions of σ and A_y were also measured from 25° to 165° for $^{86}Sr(\vec{d},d)^{86}Sr$ elastic scattering. An optical-model analysis of these data provided deuteron potential parameters for the DWBA calculations. The significance of these measurements to the design of a rubidium solar neutrino detector is discussed.

1. Abstract of paper submitted to Nuclear Physics A.
2. Rockwell International Corp., Golden, CO 80401.
3. University of North Carolina, Chapel Hill, NC 27514 and Triangle Universities Nuclear Laboratory, Durham, NC 27706.
4. AT&T Bell Laboratories, Holmdel, NJ 07723.
5. University of Tsukuba, Ibaraki, Japan.

STATES OF ^{38}S FROM THE $^{36}S(t,p)^{38}S$ REACTION[1]

N. J. Davis[2] M. C. Vetterli[2]
J. A. Kuehner[2] C. Bamber[2]
A. A. Pilt[2] E. K. Warburton[3]
A. J. Trudel[2] J. W. Olness[3]
S. Raman

The $^{36}S(t,p)^{38}S$ reaction was studied at 18-MeV bombarding energy with an overall energy resolution of 55 keV. Excited states of ^{38}S were identified at energies (uncertainties in parentheses) of 1295(10), 2835(14), 3375(17), 3690(17), 4336(20), 4478(22), 4955(25), 5064(27), 5278(28), 6000(30), and 6605(60) keV. Angular distributions were measured for protons leading to the ground state and ten lowest excited states. The data are compared with distorted-wave Born approximation calculations in which a microscopic two-nucleon form factor was employed. On this basis spin assignments have been made for several states. A comparison is made between levels observed in ^{38}S and those predicted by the weak coupling and shell models.

1. Abstract of published paper: Phys. Rev. C 32, 713 (1985).
2. McMaster University, Hamilton, Ontario, Canada L8S 4K1.
3. Brookhaven National Laboratory, Upton, NY 11973.

ONE-NUCLEON-TRANSFER REACTIONS INDUCED BY 352-MeV ^{18}O ON ^{28}Si

M. A. G. Fernandes[1]
B. L. Burks
D. J. Horen
R. L. Auble
F. E. Bertrand
J. L. Blankenship[2]
J. L. C. Ford, Jr.[3]
E. E. Gross
D. C. Hensley
R. O. Sayer[4]
G. R. Satchler
D. Shapira
T. P. Sjoreen[5]

Previous one-nucleon transfer studies induced by heavy ions have shown that DWBA calculations reproduce reasonably well the magnitude and shape of angular distributions for transitions to states with strong single-particle or single-hole components.

In the present $^{28}Si(^{18}O,^{17}O)$ and $^{28}Si(^{18}O,^{19}F)$ transfer studies, finite-range DWBA calculations were performed with the code PTOLEMY. Data taken previously[6] for these same reactions at $E_{^{18}O}$ = 56 MeV were reanalyzed with PTOLEMY, in order to compare the incident energy dependence of the experimental cross sections with that predicted by the DWBA. Therefore, the same bound-state parameters were used at 56 MeV and 352 MeV for all transitions: $r = r_{so}$ = 1.20, $a_o = a_{so}$ = 0.65 fm and $V_{s.o.}$ = 7 MeV.

In the case of the 56-MeV data analysis, only the S-7 parameter set obtained in Ref. 6, was tried in the present calculations. For the $(^{18}O,^{17}O)$ and $(^{18}O,^{19}F)$ transfers at 352 MeV, the three optical potentials (S-7F, A-F, and E-18F) deduced from the elastic data analysis[7] were investigated. The same optical potential was used in the entrance and exit channels in each case.

DWBA predictions and measured $(^{18}O,^{17}O)$ angular distributions for well known predominantly single-particle states in ^{29}Si are compared in Fig. 2.21. Potentials S-7F and A-F reproduce the magnitude and shape of the data reasonably well. On the contrary, DWBA predictions with the E-18F potential overestimate the magnitude of the measured cross sections by a factor of two at 352 MeV. The spectroscopic factors of ^{29}Si states obtained using the various optical parameters sets, and assuming $S_1(^{18}O\text{-}^{17}O)$ = 1.53 (Ref. 8) are given in Table 2.5. The values listed are normalized to $S_{g.s}(d,p)$ = 0.53 (Ref. 9), and agree with the (d,p) (Ref. 9), $(^{18}O,^{17}O)$ at 56 MeV (Ref. 6), and $(^{15}N,^{14}N)$ (Ref. 10) studies.

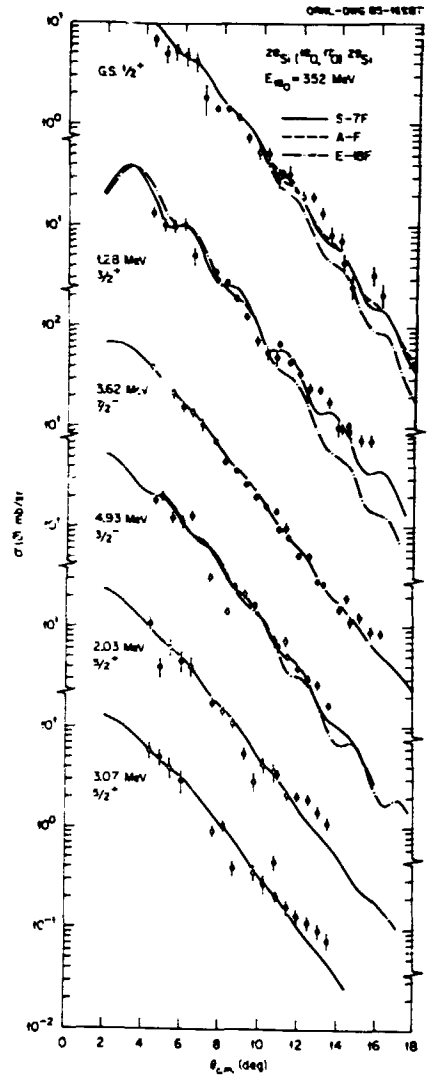

Fig. 2.21. $^{28}Si(^{18}O,^{17}O)^{29}Si$ angular distributions. The solid curves are DWBA predictions using S-7F optical potential. The dot-dashed curve was obtained with the E-18F optical potential.

In the case of the $(^{18}O,^{19}F)$ reaction, the ^{19}F(0.199 MeV, 5/2+) state is strongly excited in comparison with the ^{19}F ground state. Such behavior is in agreement with $^{18}O(^{3}He,d)^{19}F$ results (Ref. 11). The several measured and calculated angular distributions displayed in Fig. 2.22, represent mutual excitations of the ^{19}F state at 0.199 MeV and the various predominantly single-hole states in ^{27}Al listed in the figure. As was the case for the $(^{18}O,^{17}O)$

Table 2.5. Comparison of the spectroscopic factors S_2 for ^{29}Si states extracted in the present $(^{18}O,^{17}O)$ DWBA calculations with results from other work.

Ex (MeV)	J^π	$(^{18}O,^{17}O)$ Present Work[a] A-F	E-18F	S-7F	56 MeV[b] S-7	S(d,p)[c]	$S_2(^{15}N,^{14}N)$[d]
0.0	$1/2^+$	0.53(0.81)	0.53(0.28)	0.53(0.66)	0.53(0.66)	0.53	0.525
1.28	$3/2^+$	0.73(1.11)	0.63(0.33)	0.72(0.91)	1.24(1.56)	0.74	1.154
2.03	$5/2^+$	0.13(0.19)		0.13(0.17)	Not resolved	0.12	0.155
3.07	$5/2^+$	0.08(0.12)		0.08(0.10)	Not resolved	0.06	0.060
3.62	$7/2^-$	0.30(0.45)		0.32(0.40)	0.46(0.57)	0.40	0.546
4.93	$3/2^-$	0.50(0.77)		0.53(0.67)	0.41(0.51)	0.55	

[a]Assuming $S_1(^{18}O,^{17}O)$ spectroscopic factors $S_1(d_{5/2}) = 1.59$ (Ref. 8). On each column the first values were obtained by normalizing to the the $S_{g.s.}(d,p) = 0.53$ (Ref. 9), resulting in N = 1.26 (S-7f), N = 1.52 (A-F), and N = 0.53 (E-18F) for the different potentials. In parentheses are listed the values obtained for N = 1.

[b]Data from Ref. 6 and reanalyzed in the present work using the procedure in a.

[c]Ref. 9.

[d]Ref. 10.

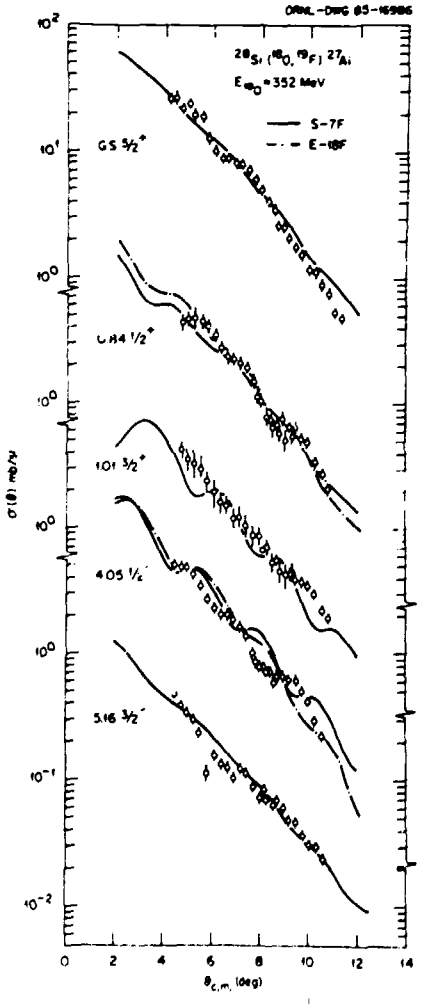

Fig. 2.22. $^{28}Si(^{18}O,^{19}F)^{27}Al$ angular distributions. See legend of Fig. 2.21.

transfer, DWBA predictions with S-7F and A-F potentials describe in magnitude and shape the $(^{18}O,^{19}F)$ data but the shallow E-18F potential again overestimates the measured cross sections by a factor of about two. Table 2.6 shows the good agreement between the ^{27}Al spectroscopic factors extracted in the present work and those from $(d,^3He)$ (Ref. 12) and $(^{15}N,^{16}O)$ (Ref. 10).

Previous studies of the incident energy dependence of transfer cross sections were performed with closed-shell systems: $^{16}O + ^{208}Pb$ (Refs. 13, 14) and $^{16}O + ^{48}Ca$ (Ref. 15). In the case of $^{16}O + ^{208}Pb$ for incident energies spanning the $E/E_B \sim 1$-4 region in relation to the Coulomb barrier, the DWBA predictions at the higher energies overestimate the data by factors 2-3, whereas no such discrepancy between experimental and calculated cross sections was observed for the $^{16}O + ^{48}Ca$ systems at $E/E_B \approx 4$. The present DWBA calculations using the E-18F potential show similar behavior as in the case of $^{16}O + ^{208}Pb$.

---

1. Universidade de Sao Paulo, Sao Paulo, Brazil.
2. Instrumentation and Controls Division, ORNL.
3. Deceased.
4. Computing and Telecommunications Division, ORNL.
5. Solid State Division, ORNL.

Table 2.6. Comparison of the spectroscopic factors S_2 for ^{27}Al states extracted from the present (^{18}O,^{19}F) UMBA analysis with results from other work.

Ex (MeV)	J^π	Present Work[a] A-F	Present Work[a] E-18F	Present Work[a] S-7F	56 MeV[b] S-7	$S(d,^3He)$[c]	$S_2(^{15}N,^{16}O)$[d]
0.0	$5/2^+$				4.02	3.76	3.80
0.84	$1/2^+$	0.49(0.61)	0.49(0.20)	0.49(0.51)		0.49	1.02
1.01	$3/2^+$	0.89(1.12)		1.00(1.04)		0.56	1.03
2.21	$7/2^+$					(<0.4)	0.71
2.73	$5/2^+$	0.70(0.87)		0.65(0.68)		0.61	
4.05	$1/2^-$	2.06(2.57)		1.93(2.00)		1.80	
4.41	$5/2^+$			0.38(0.39)		0.35	
5.16	$3/2^-$	1.16(1.45)		1.08(1.12)		1.0	

[a]The first values on each column were obtained by normalizing to the $S_{0.84}(d,^3He = 0.49$ (Ref. 11), and assuming for the (^{18}O,^{19}F) system $S_{0.199}(^3He,d) = 0.408$ (Ref. 6).

[b]Data from Ref. 6, where only the $^{27}Al_{g.s}$ transition was studied. In the present reanalysis of these data, we assumed $S_{g.s}(^{18}O,^{19}F) = 0.21$ (Ref. 11).

[c]Ref. 12.

[d]Ref. 5.

6. B. T. Kim et al., Phys. Rev. C 20, 1396 (1979).
7. B. L. Burks et al., "Optical Model and Coupled Channels Analyses of Elastic and Inelastic Scattering of ^{18}O from ^{28}Si at 352 MeV," this section.
8. R. D. Lawson, Theory of the Nuclear Shell Model (Oxford University, London, 1980).
9. M. C. Mermaz et al., Phys. Rev. C 4, 1778 (1971).
10. J. C. Peng et al., Phys. Rev. C 18, 2179 (1978).
11. F. Ajzenberg-Selove, Nucl. A300, 1 (1978).
12. B. H. Wildenthal and E. Newman, Phys. Rev. 167, 1027 (1968).
13. S. C. Pieper et al., Phys. Rev. C 18, 180 (1978).
14. C. Olmer et al., Phys. Rev. C 18, 205 (1978).
15. T. J. Humanic et al., Phys. Rev. C 26, 993 (1982).

TEST OF FERMI GAS MODEL PREDICTIONS OF LEVEL DENSITY IN ^{137}Xe[1]

B. Fogelberg[2] M. Mizumoto[4]
J. A. Harvey[3] S. Raman

We have studied the unbound levels of ^{137}Xe via neutron resonance reactions and β decay of ^{137}I. High-resolution neutron transmission data revealed a total of 35 resonances below a neutron energy of 500 keV. At least 27 of the resonances are p-wave resonances. The near absence of s-wave resonances in this energy region resulted in an extremely low value for the s-wave neutron strength function. The current γ-ray data complement earlier studies of γ rays and delayed neutrons following the β decay of ^{137}I. By combining all data, we have obtained a detailed picture of the level density in ^{137}Xe for a wide range of angular momenta. With the exception of $\frac{1}{2}^+$ and $\frac{1}{2}^-$ levels, the overall agreement is good between the current data and predictions of the Fermi gas model.

---

1. Abstract of published paper: Phys. Rev. C 31, 2041 (1985).

2. The Studsvik Science Research Laboratory, S-611 82 Nykoping, Sweden.
3. Engineering Physics and Mathematics Division, ORNL.
4. Guest scientist from the Japan Atomic Energy Research Institute, Tokai-mura, Naka-gun, Ibraki-ken, Japan under the 1984 JAERI/USDOE Agreement on Cooperation in Research in the area of Nuclear Physics.

THERMAL NEUTRON CAPTURE GAMMA RAYS FROM SULFUR ISOTOPES: EXPERIMENT AND THEORY[1]

S. Raman J. C. Wells[3]
R. F. Carlton[2] E. T. Jurney[4]
J. E. Lynn[5]

We have carried out a systematic investigation of γ rays after thermal neutron capture by all stable sulfur isotopes (^{32}S, ^{33}S, ^{34}S, and ^{36}S). The measurements were made at the internal target facility at the Los Alamos Omega West Reactor. We detected a larger number of γ rays: ~100 in ^{33}S, ~270 in ^{34}S, ~60 in ^{35}S, and ~15 in ^{37}S. Before developing detailed level schemes, we culled and then consolidated the existing information on energies and J^{π} values for levels of these nuclides. Based on the current data, we have constructed detailed decay schemes which imply that there are significant populations of 26 excited states in ^{33}S, 70 states in ^{34}S, 20 states in ^{35}S, and 7 states in ^{37}S. By checking the intensity balance for these levels and by comparing the total intensity of primary transitions with the total intensity of secondary γ rays feeding the ground state, we have demonstrated the relative completeness of these decay schemes. For strongly populated levels, the branching ratios based on the current measurements are generally better than those available from previous measurements. In all four cases, a few primary electric dipole (E1) transitions account for a large fraction of the capture cross section for that particular nuclide. To understand and explain these transitions, we have recapitulated and further developed the theory of potential capture. Toward this end, we reviewed the theory relating off-resonance neutron capture to the optical-model capture. We studied a range of model-dependent effects (nature and magnitude of imaginary potential, surface diffuseness, etc.) on the potential capture cross section, and we have shown how experimental data may be analyzed using the expression for channel capture suitably modified by a factor that takes into account the model-dependent effects. The calculations of cross sections for most of the primary transitions in the sulfur isotopes are in good agreement with the data. Some discrepancies for weaker transitions can be explained by an interfering compound-nucleus contribution to capture. This contribution is of the magnitude expected from statistical surveys of resonance capture data. Estimates of the cross section due to the valence-capture mechanism in s-wave resonances show that this cross section should dominate the more complicated compound-nucleus contributions.

---

1. Abstract of published paper: Phys. Rev. C 32, 18 (1985).
2. Middle Tennessee State University, Murfreesboro, TN 37132.
3. Adjunct staff member from Tennessee Technological University, Cookeville, TN 38501.
4. Los Alamos National Laboratory, Los Alamos, New Mexico 87545.
5. Atomic Energy Research Establishment, Harwell, England OX11 ORA.

NUCLEAR STRUCTURE STUDIES VIA COMPOUND NUCLEUS REACTIONS

SINGLE-PARTICLE STATES IN ^{149}Er AND ^{149}Ho,[1] AND THE EFFECT OF THE Z = 64 CLOSURE

K. S. Toth J. M. Nitschke[3]
Y. A. Ellis-Akovali P. A. Wilmarth[3]
F. T. Avignone, III[2] P. K. Lemmertz[3]
R. S. Moore[2] D. C. Sousa[4]
D. M. Moltz[2] A. L. Goodman[5]

Earlier we presented[6] data on the decay of ^{149}Er produced in bombardments of ^{144}Sm by 135-MeV ^{12}C ions from the Oak Ridge Holifield Heavy Ion Research Facility tandem accelerator. Products recoiling out of the target were thermalized in helium gas and transported to a shielded area for singles and coincidence measurements with γ- and X-ray detectors. To obtain more definitive information, particularly for the ^{149}Er isomeric decay, we produced the isotope in the ^{94}Mo(^{59}Ni, n2p) reaction at the Lawrence Berkeley Laboratory SuperHILAC and mass separated it with the OASIS on-line separator.[7]

Table 2.7 summarizes energies and relative intensities for transitions that were assigned unequivocally to ^{149}Er decay on the basis of measured half-lives, γ-ray coincidence relationships, and energies of coincident K X rays.

Table 2.7 Transition energies and intensities.

Nucleus	E_γ(keV)	Relative Intensities I_γ	Relative Intensities $I_\gamma + I_{ce}$
^{149}Er	111.0 ± 0.1	100[a]	316
^{149}Er	630.5 ± 0.3	248 ± 25	329 ± 33
^{149}Ho	171.2 ± 0.1	100[a]	158[b]
^{149}Ho	343.9 ± 0.2	58 ± 5	63 ± 6[b]
^{149}Ho	436.9 ± 0.2	33 ± 5	35 ± 6[b]

[a]Normalization points for ^{149}Er and ^{149}Ho transitions.
[b]Assumed M1 multipolarity for I_{ce} determination.

A cascade of three γ rays (171.2, 343.9, and 436.9 keV) follows ^{149}Er β decay while two transitions (111.0 and 630.5 keV) in coincidence with one another are ascribed to ^{149}Er isomeric deexcitation. The proposed partial decay scheme for ^{149}Er is shown in Fig. 2.22.

Based on single-proton-level systematics for N = 82 isotones (see Refs. 1 and 6) we found that the ^{149}Ho states fit the overall trends and that the effect of the Z = 64 closure is clearly not as pronounced as had been concluded by Nagai et al.[8] Rather our data support a more modest gap at Z = 64 as also implied by α-decay energy systematics (see e.g. Ref. 9) and α-decay transition rates.[10]

Single particle energies for nuclei in this mass region have been calculated previously (see e.g. Refs. 8, 11, and 12) by using phenomenological interactions with adjustable parameters. We performed spherical Hartree-Fock-Bogoliubov (HFB) calculations with realistic interactions in a core-plus-particle description for N = 82 odd-Z and N = 81 even-Z isotones. Equations are given in Ref. 13, while the model space and core energies are in Ref. 14. The interaction is the Brueckner G matrix derived from the Reid soft-core potential.[15] Pairing gaps and single nucleon energies are calculated with this interaction. Core energies were chosen so that the HFB single-particle energies coincide with the deduced[16] single-particle energies in ^{146}Gd.

The theoretical trends, particularly for the single-proton levels, agreed with experiment. For the neutron states, the calculations reproduce the experimental behavior of the splitting between the $h_{11/2}$ and $d_{3/2}$ neutron orbitals. This splitting increases with increasing Z, reaches a maximum at Z = 56-58, and then begins to decrease as a result of proton pairs filling first the $g_{7/2}$ and then the $d_{5/2}$ orbitals. However, the calculations do not explain why the experimental $h_{11/2}$ levels have a constant excitation energy for Z > 58.

1. Summary of published paper: Phys. Rev. C 32, 342 (1985).
2. University of South Carolina, Columbia, SC.
3. Lawrence Berkeley Laboratory, Berkeley, CA.
4. Eastern Kentucky University, Richmond, KY.
5. Tulane University, New Orleans, LA.
6. K.S. Toth et al., Phys. Div. Prog. Rep., Sept. 1984, ORNL-6120, p. 71.
7. J. M. Nitschke, Nucl. Instrum. Methods 206, 341 (1983).
8. Y. Nagai et al., Phys. Rev. Lett. 47, 1259 (1981).
9. K.S. Toth, R. L. Hahn, M. A. Ijaz, and W.M. Sample, Phys. Rev. C 2, 1480 (1970).
10. W.-D. Schmidt-Ott and K.S. Toth, Phys. Rev. C 13, 2574 (1976).
11. G. Wenes, K. Kayde, M. Waroquier, and P. Van Isacker, Phys. Rev. C 26, 1692 (1982).
12. L. Silverberg, Nucl. Phys. 60, 483 (1964).
13. A.L. Goodman, Nucl. Phys. A287, 1 (1977).

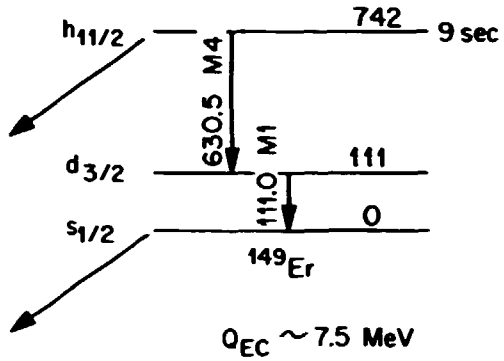

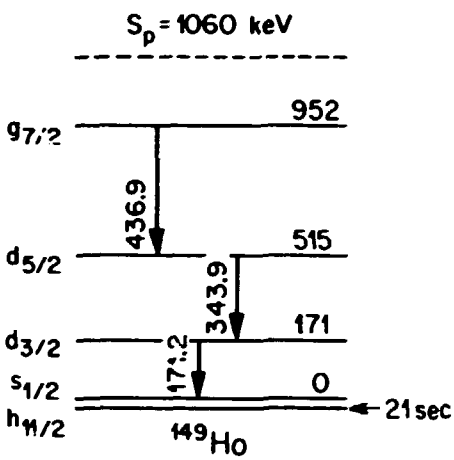

Fig. 2.23 Partial decay scheme for ^{149}Er. The isomeric branch is estimated to be 2.7%.

14. A.L. Goodman, Nucl. Phys. A331, 401 (1979).
15. A.L. Goodman, J.P. Vary, and R.A. Sorenson, Phys. Rev. C 13, 1674 (1976).
16. P. Kleinheinz et al., Z. Phys. A290, 279 (1979).

STRUCTURE IN β-DELAYED PROTON SPECTRA OF N = 81 PRECURSORS

K. S. Toth
Y. A. Ellis-Akovali
F. T. Avignone, III[1]
J. M. Nitschke[2]
P. A. Wilmarth[2]
P. K. Lemmertz[2]
D. M. Moltz[2]

Recently we measured[3] the delayed-proton spectra of ^{147}Dy and of ^{149}Er. The ^{147}Dy spectrum, was found to be dominated by distinct peaks below 4 MeV, while the ^{149}Er spectrum had much less structure in it. The difference between the two spectra was attributed to the difference in level densities in the β-decay daughters: ^{147}Tb has just one proton beyond the (N = 82 + Z = 64) core of ^{146}Gd, while ^{149}Ho has two additional protons. To understand better the nature of this peak structure we extended the investigation to the next N = 81 isotone, i.e., ^{151}Yb.

A target of ^{96}Ru was bombarded by 252-MeV ^{58}Ni ions accelerated in the LBL SuperHILAC. Following mass separation at the OASIS on-line facility, the A = 151 products were assayed with a solid state ΔE-E particle telescope, a plastic scintillator, and γ- and X-ray germanium detectors.

Figure 2.24(a) shows the accumulated delayed-proton spectrum. The half-life of these protons was measured to be 1.6 ± 0.1 s. We conclude that they follow the β decay of the new isotope ^{151}Yb on the basis of a new half-life in the isobaric chain, and coincidences with

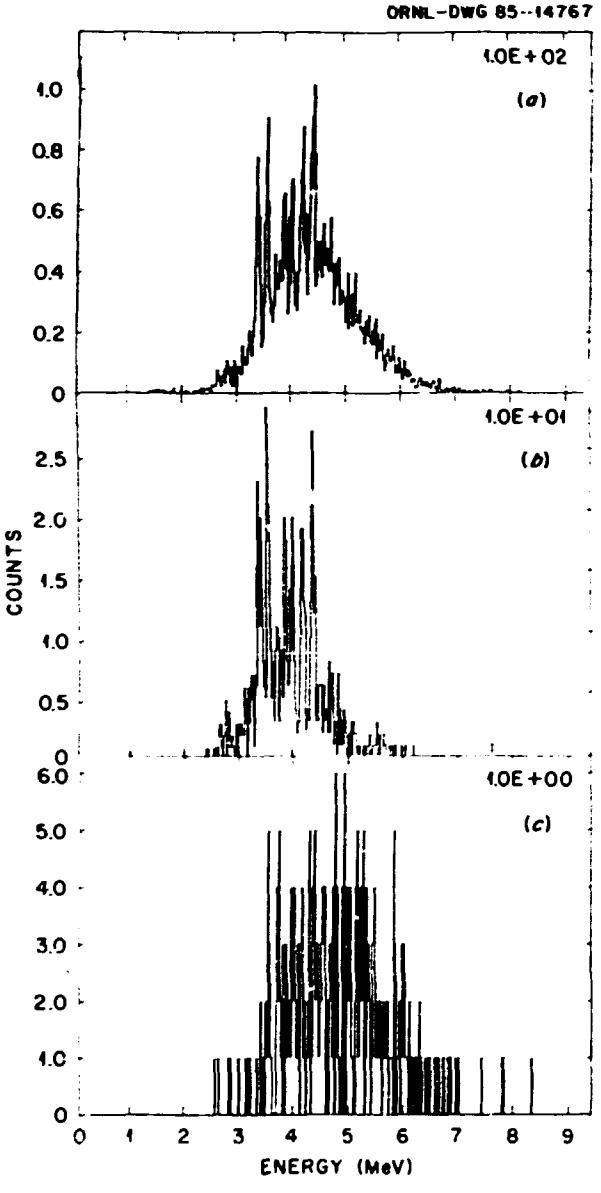

Fig. 2.24 ^{151}Yb β-delayed protons: (a) singles spectrum, (b) spectrum in coincidence with positrons, and, (c) spectrum in coincidence with Tm x rays.

Tm K X rays and with several ^{150}Er γ rays observed in-beam.[4] Note that intense peaks are still present despite the fact that the β-decay daughter, ^{151}Tm, has five protons above the Z = 54 sub-shell. The structure is therefore associated primarily with the N = 82 shell. The apparent suppression[3] of the peaks in going from ^{149}Dy to ^{149}Er was the result of an increase in the Q_{EC} which opened to β-decay feeding a larger number of high-lying states and added to the statistical component in the ^{149}Er spectrum.

In even-Z, N = 81 isotones,[5] there are $h_{11/2}$ isomers located ~ 0.75 MeV above the $s_{1/2}$ ground states. Since high-spin isomers are produced preferentially in heavy-ion reactions one would assume that the delayed protons originate mainly from the $h_{11/2}$ level in ^{151}Yb - and in fact, our proton-γ coincidence data show that protons do indeed populate the first 2^+, 3^-, 5^-, 4^+, and 6^+ states in ^{150}Er.[4] However, these excited-state proton decays account for only 40% of all observed delayed protons; the remainder proceed directly to ground. From consideration of angular momentum hindrances the ground-state protons come mostly from the $s_{1/2}$ state. Statistical model calculations agree: ground-state protons comprise 96% and 6% of protons originating from the $s_{1/2}$ and $h_{11/2}$ ^{151}Yb levels, respectively. The remaining 94% of the $h_{11/2}$ protons are predicted to be distributed amongst the 2^+, 3^-, 5^-, 4^+, and 6^+ levels.

Figures 2.24(b) and 2.24(c) show proton spectra in coincidence with positrons and Tm K X rays, respectively. The peaks in Fig. 2.24(a) are present in Fig. 2.24(b) but not in Fig. 2.24(c). Also, there is a displacement in the average (recoil corrected) proton energies: 4.05 MeV [Fig. 2.24(b)] and 4.86 MeV [Fig. 2.24(c)]. This second energy is close to that measured for protons [see Fig. 2.25 inset (a)] in coincidence with the $3^- \rightarrow 2^+$, 208-keV γ ray, i.e., 4.77 MeV. Additionally, both spectra are structureless, suggesting that the same ^{151}Tm states are involved.

Figure 2.25 shows the ^{151}Yb delayed-proton decay sequence. Protons in coincidence with the 208-keV γ ray determine the average excitation energy of their parent ^{151}Tm states to be 6.95 MeV; at this energy the EC/β+ ratio for ^{151}Yb β decay is 3.3. On the other hand, protons in Fig. 2.24(b) [also shown in Fig. 2.25 inset (b)], being in coincidence with positrons, must be connected to lower-lying ^{151}Tm levels. We suggest that they proceed to the ^{150}Er ground

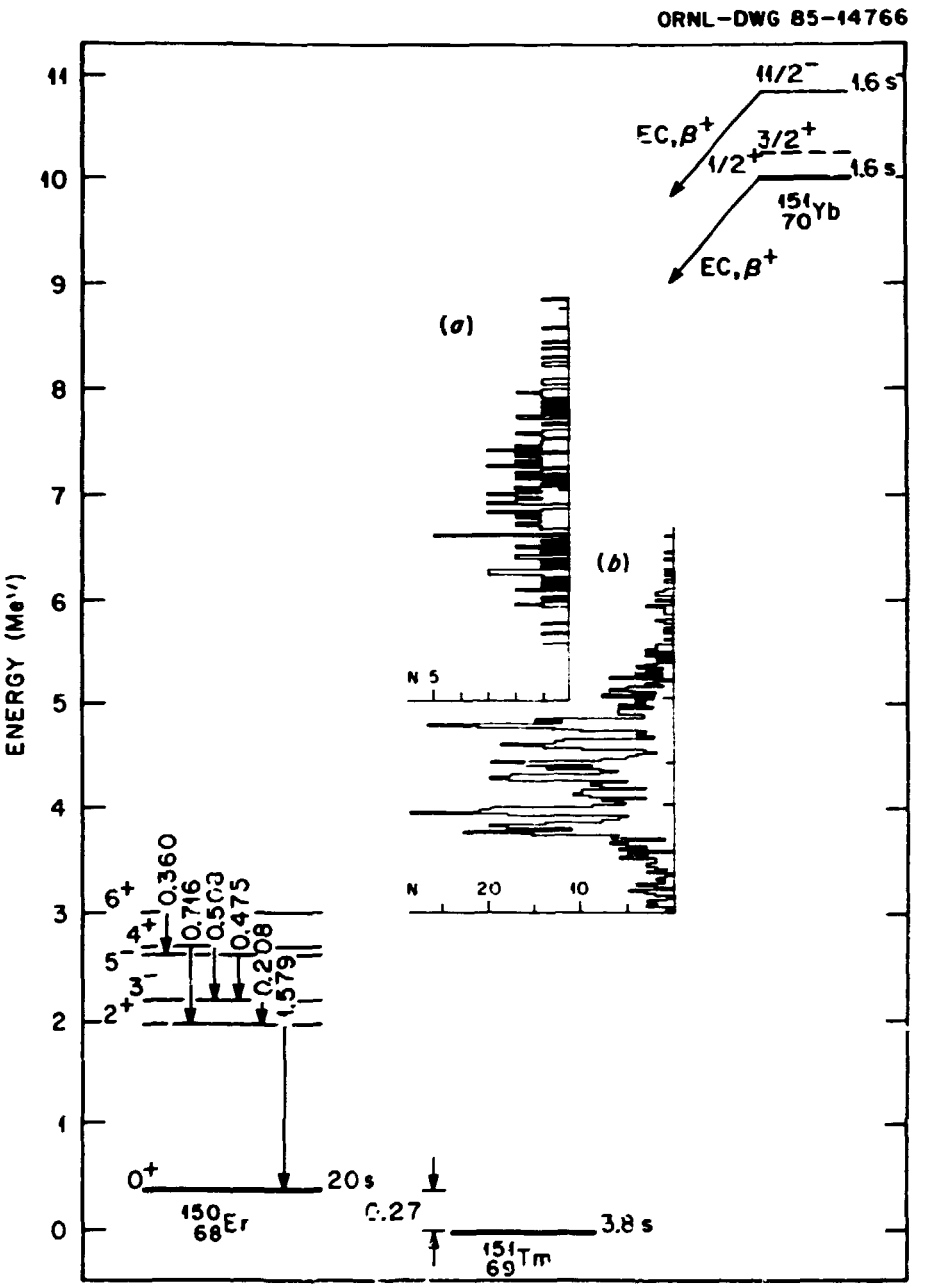

Fig. 2.25 Energy level diagram for ^{151}Yb β-delayed-proton decay. Insets represent protons in coincidence with: (a) the ^{150}Er 208-keV γ ray, and, (b) positrons [see Fig. 2.24(b)]. Within error limits no difference could be measured for the half-lives of the $s_{1/2}$ and $h_{11/2}$ ^{151}Yb levels; the isomeric decay of the $h_{11/2}$ state is estimated to have a branch of ~ 6 x 10^{-4}.

state from ^{151}Tm states at 4.32 MeV (EC/β+ ~ 0.3) and follow the decay of the ^{151}Yb $s_{1/2}$ level. This β decay populates a region in ^{151}Tm where the level density is apparently low, as reflected by the structure in the accompanying proton spectrum.

1. University of South Carolina, Columbia, SC 29208.
2. Lawrence Berkeley Laboratory, Berkeley, CA 94720.
3. K.S. Toth et al., Phys. Rev. C 30, 712 (1984).

4. Y.H. Chung et al., Phys. Rev. C 29, 2153 (1984).
5. K.S. Toth et al., Phys. Rev. C 32, 342 (1985).

SEARCH FOR SUPERDEFORMED SHAPES IN ^{144}Gd[1]

Y. Schutz[2] R. Ribas[4]
C. Baktash J. C. Lisle[5]
I. Y. Lee L. Adler[6]
M. L. Halbert K. Honkanen[6]
D. C. Hensley D. G. Sarantites[6]
N. R. Johnson A. J. Larabee[7]
M. Oshima[3] J. X. Saladin[8]

Evolution of nuclear shapes with angular momentum has become a focus of nuclear structure studies in recent years. Nuclei are expected to become oblate under the stress of the centrifugal force according to the rotating liquid drop model, and change-over to a triaxial shape before fissioning at very high angular momentum. This general behavior, however, will be modified by shell effects. Applying the Strutinsky method to calculate the potential energy surfaces of rapidly rotating nuclei, Neergard and Pashkevich[9] concluded that shell corrections can stabilize superdeformed shapes at high spins in some nuclei. In a more detailed study, Andersson et al.[10] pointed out that these shell corrections are particularly important in the light rare-earth nuclei (Z = 64, N = 82) and may result in a transition from oblate shapes at low spins to superprolate (β = 0.6) shapes at high spins. In the most recent theoretical study of shape evolution in the rare-earth region, Dudek and Nazarewicz[11] have performed cranked shell model calculations with a deformed Woods-Saxon potential. Their calculations suggest that ^{144}Gd is potentially the most favorable case for observing superdeformation.

The γ-γ energy correlation technique is particularly suited for the study of superdeformed shapes. Since, for an ideal rigid rotor, no two γ-ray coincidences have the same energy, in E_{γ_1} vs E_{γ_2} space one observes a valley that runs parallel to the $E_{\gamma_1} = E_{\gamma_2}$ diagonal and separates the two ridges formed by coincidences between neighboring γ rays. The moment of inertia of the rotating body is then related to the width of this valley, W, through $2\mathcal{J}^{(2)}/\hbar^2 = 16/W$. The method can be improved considerably if Compton-suppressed Ge-detectors, which have both good energy resolution and high peak-to-total ratios, are used. Employing multi-element Ge-detection systems, two groups[12,13] have reported observation of correlated γ rays in ^{152}Dy. The deduced moments of inertia are very close to the values predicted for superdeformation.

In the present experiment, the residual ^{144}Gd nucleus was formed in the fusion-evaporation reaction induced by a 145-MeV ^{28}Si beam from the HHIRF tandem accelerator. The target consisted of a 1.5-mg/cm^2-thick isotopically enriched ^{120}Sn target evaporated on a 20-mg/cm^2-thick ^{208}Pb backing. The γ-γ coincidences were recorded with nine Ge detectors each of which replaced a single element of the Spin Spectrometer. Six detectors were inserted in annular truncated conical Compton suppression shields of NaI with pentagonal cross sections. The average of the peak-to-total ratios for the suppressed detectors was approximately 0.4 for 1-MeV γ rays. During data acquisition, the 4n exit channel was selected with nearly 100% efficiency by requiring in the Spin Spectrometer at least three delayed γ rays which tagged the 10^+, $T_{1/2}$ = 131 ns isomer assigned to ^{144}Gd. In this experiment a total of over 30 million pairs of γ rays were recorded with the six suppressed detectors. From a Monte-Carlo simulation (JULIAN-PACE) of the deexcitation of the compound nucleus formed in this reaction, we deduced that the entry state spin distribution for ^{144}Gd spans I-values between 26 and 56, with the mean value at I = 41.

In the off-line analysis all the detector gains were matched and two γ-ray energy correlation matrices (E_{γ_1} vs E_{γ_2}) were constructed for all possible coincidences between any pair of these detectors. One matrix was not Doppler-shift corrected, assuming that all of the γ-ray lifetimes are large compared with the slowing down time of the recoiling nucleus in the lead backing. The second matrix was Doppler-shift corrected to take into account that γ rays cascading along possible superdeformed rotational bands would be emitted before the nucleus

comes to rest in the backing. The matrices were then unfolded to remove the remaining contribution from Compton-scattered events and the resulting data were corrected for the photopeak efficiency of the Ge detectors.

Figure 2.26 shows a number of energy slices projected perpendicularly to the $E_{\gamma_1} = E_{\gamma_2}$ diagonal. They correspond to the average energy intervals of 200 keV between 1.1 MeV and 1.5 MeV. The two projections in Fig. 2.26(a) are taken from the unfolded matrix without Doppler correction. A very weak ridge structure is observed in the lower panel and would correspond, if due to transitions within a rotational band, to a moment of inertia $2\mathcal{I}^{(2)} = 120\hbar^2\ \mathrm{MeV}^{-1}$. The projections in Fig. 2.26(b) are taken from the matrix with the Doppler-shift corrections. The ridge structure is apparently enhanced. It could thus be concluded that the transitions building up this ridge structure are fast compared with the slowing down time of nearly 1 ps of the recoiling nucleus in the lead backing. Nevertheless, a close examination of the γ-γ correlation matrix suggests that the ridge structure is not continuous. Even after applying the method proposed in Ref. 14, which would enhance correlated events over uncorrelated ones, no obvious continuous ridge structure was observed. We therefore suspected that the ridges seen in the projections may be due to

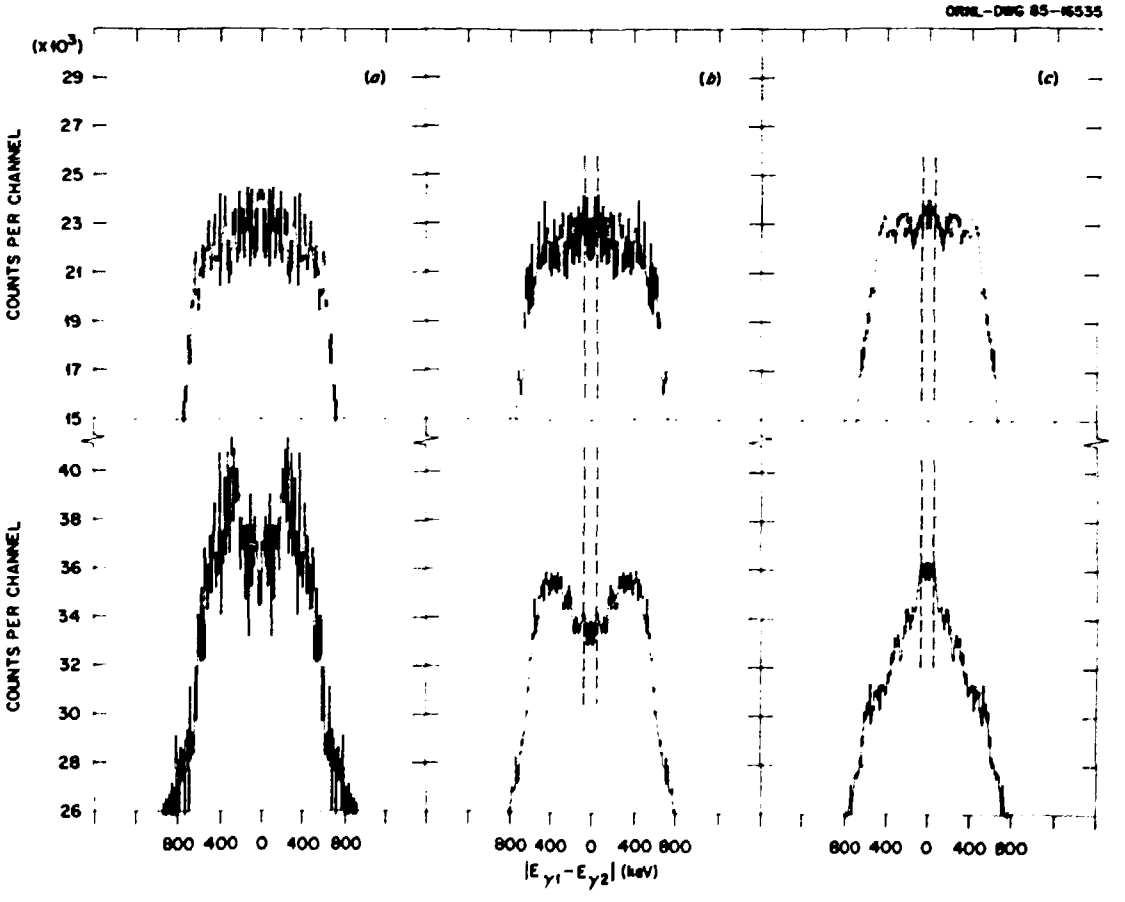

Fig. 2.26 ^{144}Gd: Projections perpendicular to the diagonal valley in the $E_{\gamma_1} - E_{\gamma_2}$ energy correlation map for two average energy intervals $1.1 < (E_{\gamma_1} + E_{\gamma_2})/2 < 1.3$ MeV (lower spectrum in each case) and $1.3 < (E_{\gamma_1} + E_{\gamma_2})/2 < 1.5$ MeV:

(a) from the unfolded and efficiency corrected matrix;
(b) from the Doppler-shift corrected matrix;
(c) from the matrix obtained after discrete lines removal. The dashed vertical lines point to the position of the ridges in panel (b) and correspond to $(2\mathcal{I}^{(2)}/\hbar^2) = 120\ \mathrm{MeV}^{-1}$.

discrete lines. To test this hypothesis, we removed from the matrix the contributions due to the discrete peaks. Figure 2.26(c) shows the projections from the matrix following this subtraction. The ridge structure completely disappears in both energy slices from the γ-γ matrix, thus confirming our hypothesis regarding their origin.

With the present data it would be very hazardous to interpret this negative result as proving the non-existence of superdeformation in ^{144}Gd. The fact that the predicted superdeformation has been observed in ^{152}Dy and that calculations predict ^{144}Gd to be the most favorable case in the rare earth region calls for a critical assessment of the experimental technique which has been used. The main difference between the experiment of Ref. 13 and the present one is the choice of the lead-backed target in the present experiment instead of a self-supporting thin target. If the effective feeding time is comparable to the stopping time in the lead backing, the Doppler shift will wash out the ridge structure so that it cannot be recovered by means of off-line corrections. To arrive at a definitive conclusion regarding the presence of superdeformed structures at high spins in ^{144}Gd, this experiment should be repeated with a thin, unbacked target.

---

1. Summary of a paper to be published.
2. On leave from CRN, Strasbourg, France. Present address: GANIL, Caen, France.
3. On leave from Japan Atomic Energy Research Institute, Tokai, Japan.
4. On leave from Universidade De Sao Paulo, Sao Paulo, Brazil.
5. On leave from Schuster Laboratory, University of Manchester, England.
6. Washington University, St. Louis, MO.
7. University of Tennessee, Knoxville, TN.
8. University of Pittsburgh, Pittsburgh, PA.
9. K. Neergård and V. V. Pashkevich, Phys. Lett. 59B, 218 (1975).
10. C. G. Anderson, et al., Phys. Scripta 24, 266 (1981).
11. J. Dudek and W. Nazarewicz, Phys. Rev. C 31, 298 (1985).
12. Y. Schutz, et al., Phys. Rev. Lett. 48, 1535 (1982).
13. B. M. Nyakó, et al., Phys. Rev. Lett. 52, 507 (1984).
14. O. Andersen et al., Phys. Rev. Lett. 43, 687 (1979).

DISCRETE AND CONTINUUM γ RAY STUDY OF ^{154}ER AT HIGH SPINS[1]

C. Baktash, I. Y. Lee, Y. Schutz[2], N. R. Johnson, M. Oshima[3], C. Y. Chen[4], O. Dietzsch[4], J. X. Saladin[4], E. der Mateosian[5], O. C. Kistner[5], A. W. Sunyar[5], C. J. Lister[5], D. Horn[5], D. G. Sarantites[6], T. Semkow[6], K. Honkanen[6], A. J. Larabee[7]

Study of the interplay between the macroscopic and microscopic effects in nuclei as a function of angular momentum has become the focus of nuclear structure studies in recent years. Theoretically, cranked shell model calculations by several groups predict shape transition patterns in the light rare-earth nuclei which depend sensitively on the neutron number.[9] For example, the Er isotopes with $N < 86$ are predicted to have nearly spherical shapes at low spins and gradually become oblate at higher angular momenta (Fig. 2.27). In contrast, for neutron number $N > 88$, the equilibrium shapes are expected to change from prolate at spins $I < 40$ to triaxial at $I > 50$. Of particular interest is the predicted transition to superprolate ($\beta = 0.6$) shapes for $N = 82$ isotopes at very high spins. Experimental verification of these predictions provides a very stringent test of the validity of these calculations, which have been very successful in describing the nuclear behavior at high angular momenta. To investigate these predicted spin-induced shape changes in ^{154}Er, we used the ^{124}Te (^{34}S, 4n) reaction to populate the high spin states in this nucleus. The ^{34}S beam (170 MeV) was obtained from the double tandem facility at Brookhaven National Laboratory. The experimental setup consisted of six Ge and eleven NaI detectors which served as a multiplicity filter. Four of the Ge detectors were surrounded by annular NaI Compton-suppression shields which gave a suppression factor of better than 2.5 for the ^{60}Co source. By demanding a coincidence of at least two Ge and two NaI detectors, high multiplicity events were emphasized. Nearly 140 million such events were collected on an event-by-event basis.

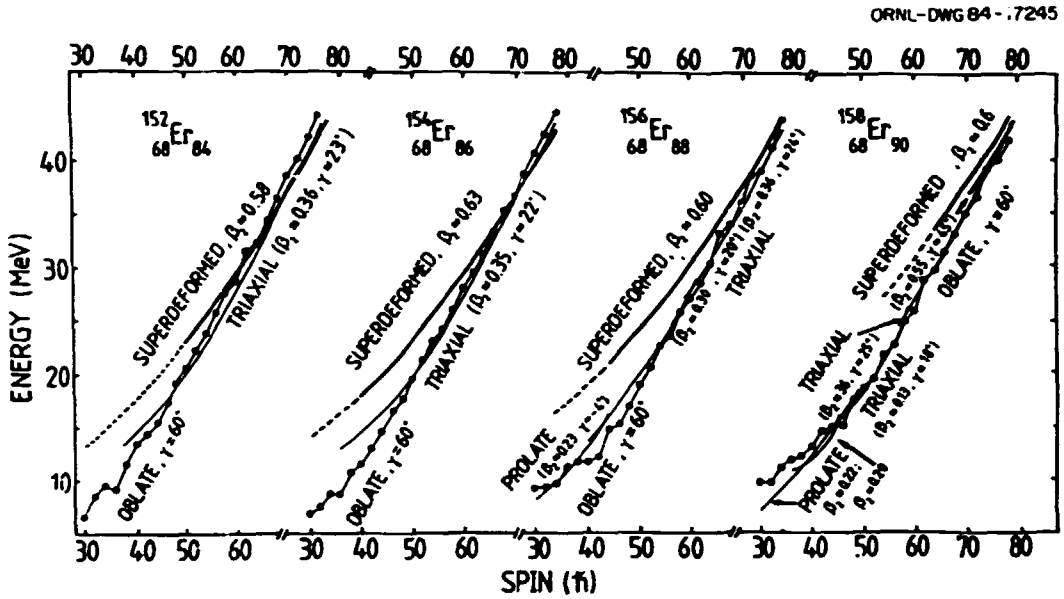

Fig. 2.27 Predicted equilibrium shapes as a function of angular momentum and excitation energy for erbium-isotopes (Ref. 8).

In the off-line analysis, the gains of all Ge detectors were equalized and the Ge-Ge coincidence data were scanned to generate an Eγ-Eγ matrix. This matrix contained nearly 12 million photo peak-photo peak counts before symmetrization, of which approximately 40% belong to ^{154}Er. These data formed the basis for an expended decay scheme of ^{154}Er. Angular correlation information were used to deduce the multipolarity of the newly found transitions. The noteworthy features of the decay scheme include:

(1) The level scheme shows a shell model structure up to the maximum observed spin of 39.

(2) All of the expected optimal states generated by the alignment of the valence nucleons around the oblate symmetry axis are clearly established in the decay scheme.

(3) Existence of high energy γ rays feeding the highest optimal sate, $I^{\pi} = 36^{+}$, reflects the fact that above this state core excitation becomes necessary. Consistent with this picture is fragmentation of the feeding into this state that was experimentally observed.

(4) The level spacings of states with $I^{\pi} = 27^{-}$, 29^{-}, 31^{-}, and 33^{-} closely resemble those of the $I^{\pi} = 10+$, 12+, 14+, and 16+, states in ^{150}Er formed by $(h^{4}_{11/2})$ proton-excitation. Also, the 1467-keV γ ray between $I^{\pi} = 36^{+}$ and 33^{-} optimal states is very similar to the octupole transition that connects the corresponding optimal states in ^{153}Ho. They both arise from $i_{13/2} \rightarrow f_{7/2}$ neutron transition, and reflect the excitation energy of the $i_{13/2}$ neutron orbital.

The above observations are in good agreement with theoretical predictions that noncollective excitations dominate the yrast structure of ^{154}Er below spin 50. To verify the predicted onset of collectivity at higher spins, we have searched for the ridge-valley structure in the unfolded Eγ-Eγ correlation maps. Such a structure has been observed in ^{152}Dy,[9] and interpreted to arise from collective rotation of a superdeformed shape. We have found no evidence for such structures in the Eγ = 1000-1400 keV range, where a strong quadrupole structure has been observed in the energy spectrum. This implies that either the predicted collective bands are not fed even at the highest angular momentum populated in this reaction (60 ħ), or the use of backed target might have washed out the expected weak ridge-valley structure. In the latter case, the combined feeding plus state

lifetimes would have to be comparable to the stopping time of the recoiling nucleus in the lead backing.

---

1. Summary of a paper to be published.
2. On leave from CRN, Strasbourg, France. Present address: GANIL, Caen, France.
3. On leave from Japan Atomic Energy Research Institute, Tokai, Japan.
4. University of Pittsburgh, Pittsburgh, PA.
5. Brookhaven National Laboratory, Upton, NY.
6. Washington University, St. Louis, MO.
7. University of Tennessee, Knoxville, TN.
8. J. Dudek and W. Nazarewicz, Phys. Rev. C 31, 298 (1985).
9. B. M. Nyako et al., Phys. Rev. Lett. 52, 507 (1984).

ON THE PROLATE-OBLATE TRANSITION AND THE PRONOUNCED COLLECTIVITY OF THE SIDE BANDS IN RAPIDLY ROTATING N = 88, 90 NUCLEI

Y. S. Chen[1] L. L. Riedinger[2]

Nuclei with N > 90 behave as prolate rotors while nuclei with 82 < N < 86 at I < 10 ħ behave as oblate rotors. The N = 88, 90 nuclei are transitional nuclei in which there may be prolate-oblate transitions facilitated by a sequence of triaxial shapes. The experimental evidence is (1) the quenching of signature splitting in $h_{11/2}$ proton bands, (2) the reduction of E2 transition probabilites, (3) the loss of the collectivity of the yrast sequence and (4) the pronounced collectivity of the side bands.

All these experiments may be interpreted in terms of multiquasiparticle-induced triaxial shapes. The model used is high-j orbits coupled to a γ-polarizable superfluid core.[3,4] The total Routhian for a given configuration is calculated as:

$$E'_{conf.}(\gamma,\omega) = \frac{1}{2}V_{po}\cos(3\gamma) + E'_{rot}(\gamma,\omega) + \sum_{conf.} e'_{\nu}(\gamma,\omega)$$

where V_{po} is a potential parameter representing the energy difference between the prolate and oblate shapes. The collective rotational energy E'_{rot} may be calculated microscopically.[5]

Letters have been assigned to the various configurations. A, B, C and D are the four lowest quasineutron orbitals of the $i_{13/2}$ shell. E and F are the two lowest quasineutron orbitals of the $h_{9/2}$ shell and a and b are the two lowest quasiproton orbitals of the $h_{11/2}$ shell. The one q. p. Routhians as functions of the γ deformation are calculated at ħω = 0.225 MeV for ^{156}Er and are shown in Fig. 2.28. The total Routhians seen in Fig. 2.29 are built by summing the appropriate one - quasiparticle Routhians. The minimum of the total Routhian gives the equilibrium γ-deformation. An ~ 20° change in γ deformation from the ground configuration [o] to configuration [AB] is due to the drive of orbitals A and B towards positive γ values (see Fig. 2.28). Since both E and F have a very strong γ-driving force towards 60° (oblate), configuration [ABEF] has a triaxial shape with a very small prolate-oblate barrier (P08) and therefore is almost unstable towards oblate shapes. Thus the gentle positive γ-drive of the

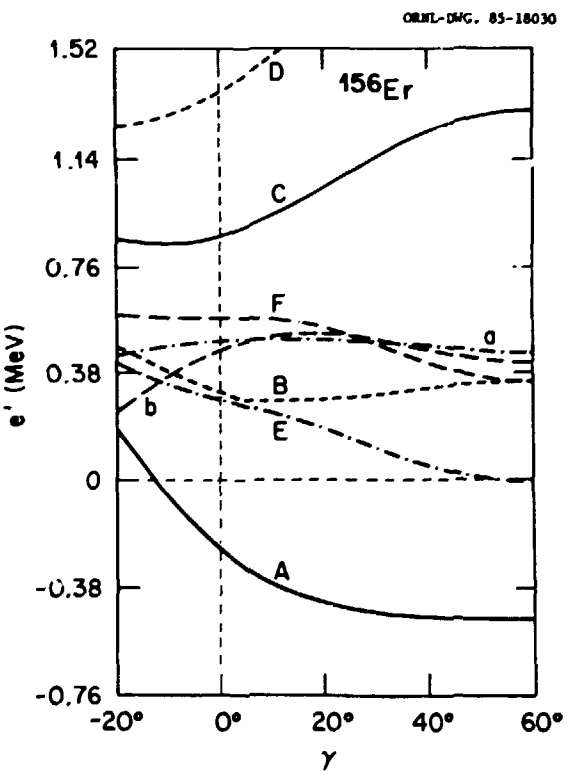

Fig. 2.28 The quasiparticle Routhians calculated as functions of the γ deformation at ħω = 0.225 MeV in ^{156}Er. A, B, C and D are the lowest four $i_{13/2}$ quasineutrons, E and F are the lowest two $h_{9/2}$ quasineutrons and a and b are the lowest two $h_{11/2}$ quasiprotons.

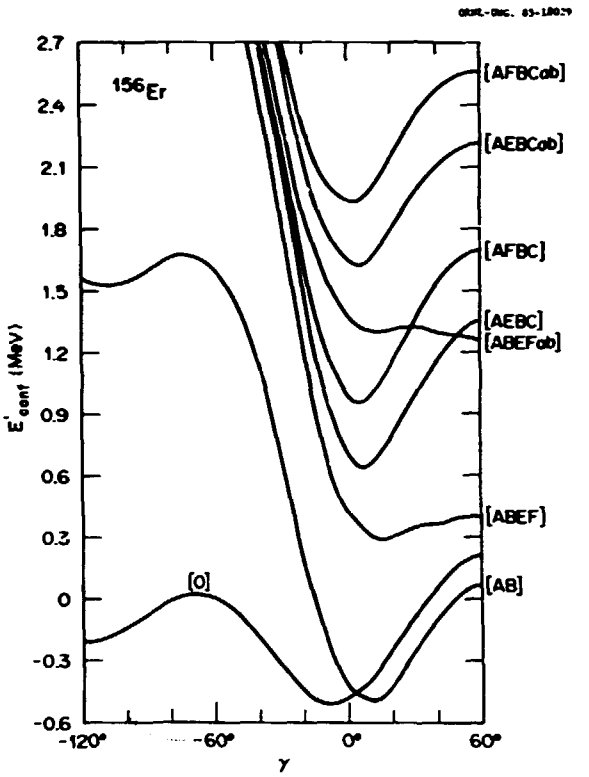

Fig. 2.29 The calculated total Routhians as functions of the γ deformation at $\hbar\omega = 0.225$ MeV in ^{156}Er for given configurations indicated by the letters in parentheses.

a and b orbitals could finally complete the shape transition to the oblate through [ABEFab] which has 30 ħ units of aligned angular momentum. This explains in a natural way the loss of the collective rotational structure of the yrast sequence at spin I = 30 ħ observed in ^{156}Er.[5] The same kind of calculation is carried out for other N = 88 and N = 90 nuclei. It is found that the angular momentum at which oblate shapes are reached is strongly N-dependent, with I = 30 ħ for N = 88 and I = 40 ħ for N = 90 nuclei.[6]

A striking feature in Fig. 2.29 is the fact that the configuration involving the C orbital has essentially a prolate shape and large POB in contrast to the instability of [ABEF] and [ABEFab] towards the oblate shape. This feature is attributed to the very strong negative γ-drive from 60° to 0°, generated by both the C orbital itself and its taking the place of E or F in configurations [ABEF] and [ABEFab], i.e., the replacement of the strong positive γ-drive of E or F by the strong negative γ-drive of C must initiate a doubly strong negative γ-drive. This feature explains the pronounced rotational collectivity of the side bands AE or AF. The triaxiality, together with the extremely shallow minimum of the total Routhian [ABEF], may be responsible for the so-called quasivibrational band observed for the first time in the yrast sequence of ^{158}Yb after the second discontinuity at spin 24 where the extreme form of the vertical rise of the moment of inertia $J^{(1)}$ takes place, exceeding the rigid-rotor value by about 40%.[7] On the other hand, the pronounced collective rotational behavior of the AE band in the same nucleus after its first band crossing (AE → AEBC) at $\hbar\omega \approx 0.36$ MeV [indicated by the almost constant $J^{(1)}$] is well understood by the nearly prolate deep minimum of the total Routhian [AEBC]. The nearly prolate deep minimum of the total Routhians [AFBC] and [AFBCab] explains the fact that the observed AF band in ^{156}Er extends the collective rotational structure up to spin I = 36 ħ, far above the last collective rotational state $I^{\pi} = 30^{+}$ in the yrast sequence.[8]

Further study concludes that the positive γ-driving feature of A and B is due to the triaxiality-induced K-coupling and the negative γ-driving behavior of C is attributed to the γ-dependent j-mixture, which must be considered in solving a deformed Hamiltonian.[8] The features discussed above should be general in the case of any high-j shell.

---

1. Joint Institute for Heavy Ion Research, Oak Ridge National Laboratory, Oak Ridge, TN. Permanent address: Institute of Atomic Energy, Beijing, P. R. C.
2. Adjunct staff member from the Physics Department, University of Tennessee, Knoxville, TN.

3. S. Frauendorf and F. R. May, Phys. Lett. 125B, 245 (1983).
4. Y. S. Chen, Nucl. Phys. A421, 403c (1984).
5. F. S. Stephens et al. Phys. Rev. Letters 54, 2584 (1985).
6. Y. S. Chen, S. Frauendorf and L. L. Riedinger, to be published.
7. C. Baktash et al., Phys. Rev. Lett. 54, 978 (1985).
8. Y. S. Chen and L. L. Riedinger, to be published.

QUASIVIBRATIONAL BANDS AT HIGH SPINS IN ^{158}Yb[1]

C. Baktash — M. P. Fewell[3]
Y. Schutz[2] — L. Courtney[4]
I. Y. Lee — A. J. Larabee[4]
F. K. McGowan — L. L. Riedinger[5]
N. R. Johnson — A. W. Sunyar[6]
M. L. Halbert — E. der Mateosian[6]
D. C. Hensley — O. C. Kistner[6]
D. G. Sarantites[7]

High-spin states in the transitional nucleus ^{158}Yb were populated via several (HI,4n) reactions. Two yrast bands were established up to $I^{\pi} = (40^+)$ and (31^-). In contrast to the negative-parity band up to I = 31 and the positive-parity states up to I = 24, both of which show collective rotational patterns, states with $I^{\pi} = 26^+$-36^+ exhibit a nearly vibrational excitation mode. Such a quasivibrational pattern suggests a gradual transition toward oblate shapes and is the first evidence for a "band termination" in a heavy nucleus.

---

1. Abstract of published paper: Phys. Rev. Lett. 54, 978 (1985).
2. On leave from CRN, Strasbourg, France. Present address: GANIL, Caen, France.
3. Present address: The Australian National University, Canberra, Australia.
4. University of Tennessee, Knoxville, TN.
5. Adjunct staff member from the University of Tennessee.
6. Brookhaven National Laboratory, Upton, NY.
7. Washington University, St. Louis, MO.

THE EVOLUTION OF NUCLEAR SHAPES AT HIGH SPINS AND TEMPERATURES IN ^{158}Yb[1]

Y. Schutz[2] — D. C. Hensley
C. Baktash — L. Courtney[3]
I. Y. Lee — A. J. Larabee[3]
F. K. McGowan — L. L. Riedinger[4]
N. R. Johnson — D. G. Sarantites[5]
M. L. Halbert — Y. S. Chen[6]

Discrete-line spectroscopy in ^{158}Yb (Ref. 7) suggests coexistence of two different band structures at high spins. While the energies of the positive-parity band up to I = 24 and the negative-parity band up to its maximum observed spin of I = 31 show collective rotational patterns, γ rays deexciting states with $I^{\pi} = 24^+$ to 36^+ have nearly equal energies. The latter behavior is interpreted[8] as due to termination of a band wherein the nucleus continuously adjusts its shape parameters while gradually evolving toward an oblate shape. To ascertain which band structure dominates above the yrast line and beyond spin 40, we have examined the continuum γ ray data.

The experimental setup consisted of six Ge detectors placed in the Spin Spectrometer as described in Ref. 7. Use of the Spin Spectrometer allows a detailed characterization of continuum γ-ray spectra by their multiplicity, total energy, and angular-distribution coefficients. Therefore, it is possible to study the evolution of the γ-ray spectra as a function of spin or temperature for constant values of excitation energy or spin, respectively.

The high-spin states in ^{158}Yb were populated via the ^{98}Mo(^{64}Ni,4n) reaction at 285-MeV beam energy. To reduce the severe Doppler broadening, a 1-mg/cm^2-thick target backed with approximately = 15 mg/cm^2 of natural lead was used. All of the energy and timing information of the NaI-and Ge-detectors were recorded event by event on magnetic tapes.

In the off-line analysis of the data, the gains of all NaI detectors were matched, and pulses due to neutrons were removed by their time of flight. The corrected data were then scanned to generate a series of NaI spectra that were simultaneously gated by: (a) discrete γ rays that deexcite states with $I^{\pi} = 2^+$ through 12^+ in ^{158}Yb for channel selection; (b) total pulse height (H) in steps of ΔH = 1.6 MeV; (c) total coincidence fold (K) in steps of ΔK = 1; and (d) azimuthal angle of the NaI detectors (θ = 0°, 24°, 41°, 49°, 64°, 68°, 78°, 88°). The resulting spectra were then corrected for double hits, and unfolded using the measured response functions of the individual NaI elements. The response functions were also used to transform the coincidence fold to multiplicity (M) and total pulse height into excitation energy (E). The values of the excitation energy above the yrast line (E^*) obtained in this manner fall within 20% of the values estimated by fitting an exponentially decaying curve to the high energy tail ($E_\gamma > 3$ MeV) of the γ-ray

spectra. For each distinct set of (E,M) gate-values, the unfolded spectra were sliced into bins of 100 keV and the angular distribution of the intensity in each bin was fitted to the expression

$W(\theta) = A_0 (1 + a_2 P_2 (\cos\theta) + a_4 P_4 (\cos\theta))$.

Using the fitted values of the $a_2(E\gamma)$ coefficients, and assuming that all transitions are of the stretched character, we were able to decompose the energy spectra into two spectra of stretched dipole and stretched quadrupole γ rays. The spin values (I) were estimated from the relative strengths of these two multipolarity spectra and the corresponding multiplicity values. In the following, we shall examine the evolution of these multipolarity spectra as a function of both spin and excitation energy.

The quadrupole γ-ray spectra show two distinct structures. First, there exists a strong and narrow peak around $E\gamma = 750$ keV which is rather stable with increasing I and E^* (See Fig. 2.30). It contains mostly the yrast transitions that deexcite states in the I = 26-36 spin range. The higher edge of this peak falls rapidly and does not move noticeably with increasing M or E^*. Instead, a second and much broader structure gradually develops around 1.15 MeV at high multiplicities and at excitation energies in excess of several MeV above the yrast line. From Fig. 2.30, it is apparent that the intensity of this structure grows with increasing excitation energy and persists up to about $E^* = 10$ MeV. Comparisons of the spectra corresponding to angles of $\theta = +24°$ and

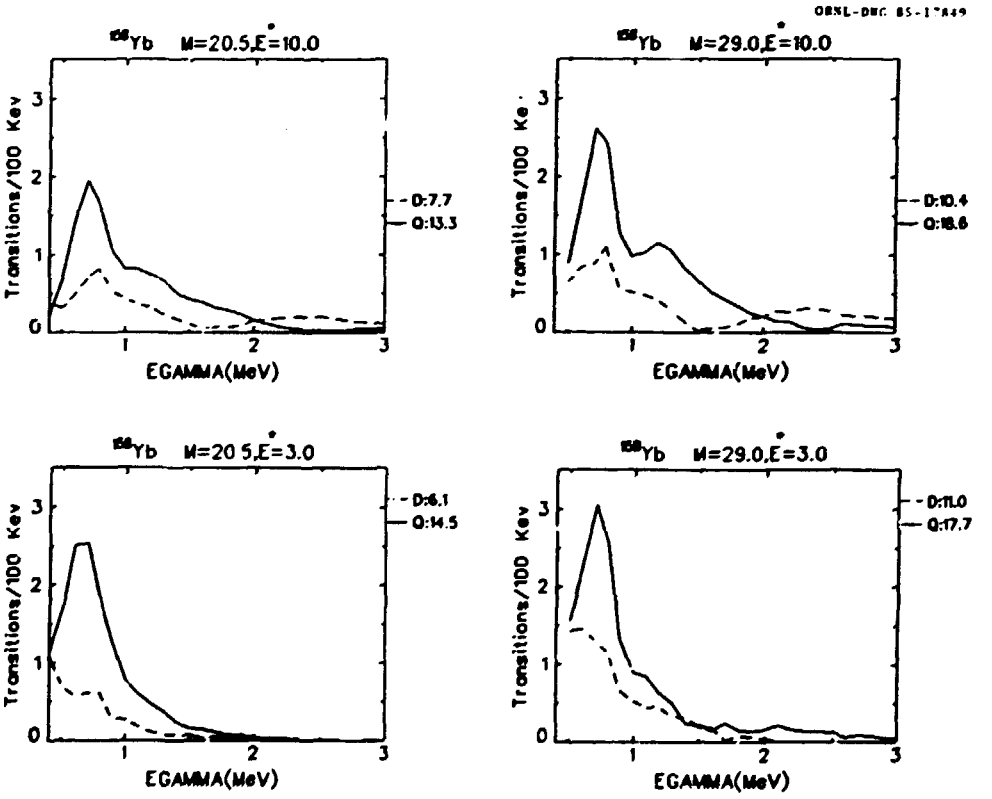

Fig. 2.30 Evolution of the quadrupole (solid lines) and dipole (dashed lines) spectra with excitation energy (E^*) and multiplicity (M). Each panel is labeled with the corresponding values of E^* and M. The strong quadrupole peak at $E\gamma = 750$ keV is mostly due to discrete yrast transitions. Noteworthy structures that become strong at high multiplicities are: A quadrupole bump ($E\gamma = 1.15$ MeV) at high E^*; a broad dipole structure ($E\gamma = 1.5$-3 MeV) at high E^*; and a low energy continuum dipole ($E\gamma < 750$ keV) at low E^*.

$\theta = -24°$ indicate that this structure is fully Doppler shifted. Since the stopping time of the recoiling nuclei in the lead backing of the target is less than 1 ps, this observation implies that these transitions are collective.

The dipole γ-ray spectra also show two distinct features. First, at energies of less than ≈ 750 keV, we observe a continuum of γ rays whose intensity grows with increasing multiplicity, but diminishes with E^*. This clearly identifies the near-yrast high-spin states as their origin. In contrast, a very broad structure, with a centroid at about 2.5 MeV, develops at high spins and high excitation energies as seen in Fig. 2.30. Again, these γ rays are fully Doppler-shifted, indicating that they are most likely Mi in character (B(M1) ≈ 1 W.U.).

Taken together, these observations point to the existence of two very different structures at high spins in ^{158}Yb nucleus: In the vicinity of the yrast line, the presence of low-energy dipole γ rays (most likely M1) rather than strong E2 transitions indicate that these states are only weakly collective. Possible candidate structures are: (1) The continuation of the terminating bands which have been observed at spins I ≈ 40 in the discrete γ ray spectroscopy data (Ref. 7); or (2) weakly collective, triaxial bands. In contrast, at high excitation energies, the presence of collectively enhanced E2 transitions at ≈ 1.15 MeV, and M1 γ rays with Eγ ≈ 2-3 MeV signal the onset of collectivity well above the yrast line. The latter observation clearly indicates that shell effects both survive and dominate the structure of high spin states in ^{158}Yb up to the highest temperatures (≈ 1 MeV) observed in this experiment.

---

1. Summary of a paper to be published.
2. On leave from CRN, Strasbourg, France. Present address: GANIL, Caen, France.
3. University of Tennessee, Knoxville, TN.
4. Adjunct staff member from the University of Tennessee, Knoxville, TN.
5. Washington University, St. Louis, MO.
6. Joint Institute for Heavy-Ion Research, Oak Ridge National Laboratory, Oak Ridge, TN. Permanent address: Institute of Atomic Energy, Beijing, P.R.C.
7. C. Baktash et al., Phys. Rev. Lett. 54, 978 (1985).
8. I. Ragnarsson et al., Phys. Rev. Lett. 54, 982 (1985).

HIGH-SPIN STATES OF ^{159}Yb

L. H. Courtney[1], A. J. Larabee[1], C. Baktash, I. Y. Lee, L. Adler[2], F. K. McGowan, M. P. Carpenter[1], M. Oshima[3], M. L. Halbert, R. Ribas[4], D. C. Hensley, L. L. Riedinger[5], K. Honkanen[2], J. X. Saladin[6], N. R. Johnson, D. G. Sarantites[2], Y. Schutz[7]

A discrete-line spectroscopy experiment has been performed using the Spin Spectrometer. This measurement was performed in order to see if the termination seen in ^{158}Yb (Ref. 8) is present in ^{159}Yb. A 268-MeV ^{64}Ni beam was used to bombard a ^{98}Mo target. Incorporated into the experiment were NaI Compton suppressor shields around six of the nine Ge detectors used to replace NaI counters in the Spin Spectrometer.

In the analysis of the data, two gates were set on (H,K), i.e., the total gamma-ray energy and the total fold, respectively, for each event, to separate the two major reaction products, ^{158}Yb and ^{159}Yb. Ge-Ge coincidence matrices were produced based on these gates. On the basis of these data and data from a previous ^{159,160}Yb Spin Spectrometer experiment, a level scheme has been constructed. Spins for the side bands have been assigned based on data taken in an angular distribution experiment performed at McMaster University with an oxygen-induced reaction.

The assignment of quasiparticles to the observed bands in ^{159}Yb is based on the systematics of the region. The $vi_{13/2}$ orbitals lying lowest relative to the Fermi surface are denoted by A, B, C and D, while the lowest $vh_{9/2}$ orbitals are denoted by E, F, G and H. For protons, the lowest $h_{11/2}$ orbitals, relative to the Fermi surface are called a, b, c and d. The yrast band has a high degree of rotational alignment and is assigned to the $vi_{13/2}$ configuration denoted by A. It is observed up to the $I^\pi = 65/2^+$ level. As shown in Fig. 2.31, this band has an upbend around $\hbar\omega = 0.4$ MeV, with an alignment gain of roughly 8 ħ. As in the isotone ^{157}Er (Ref. 9) this crossing is interpreted as resulting from both the $vi_{13/2}$ alignment, BC, and the $vh_{11/2}$ alignment, ab. Also present are

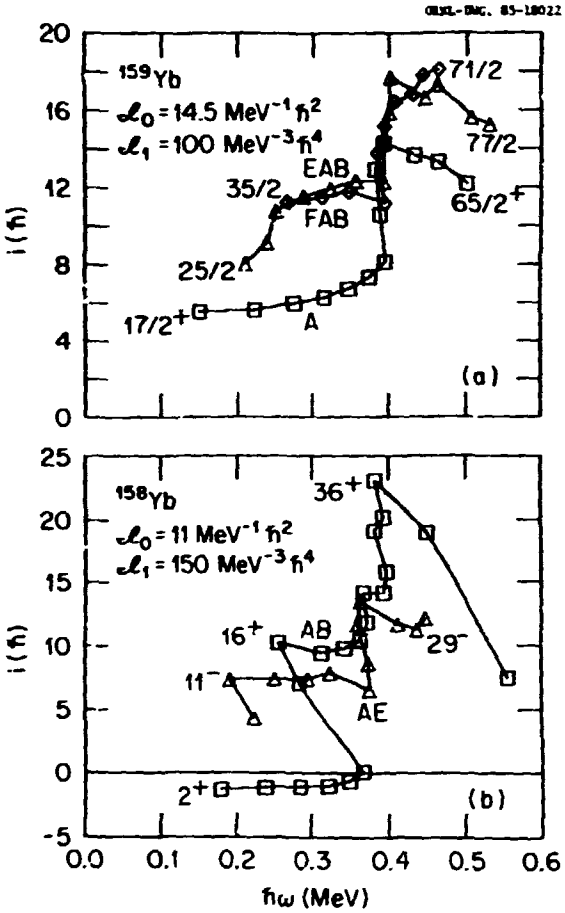

Fig. 2.31. Plot of the particle alignment, i, versus angular frequency, ω, for various bands in (a) ^{159}Yb and (b) ^{158}Yb. The core angular momentum has been extracted using the Harris parameters $\mathcal{J}_0$ and $\mathcal{J}_0$ (Ref. 12). In (a) squares denote the $\nu i_{13/2}$ yrast band with I = even integer + 1/2. The $\nu h_{9/2}$ band is denoted by triangles for I = even integer + 1/2 and diamonds for I = even integer - 1/2. In (b) squares denote the $(\nu i_{13/2})^2$ band with I = even integer and triangles the $\nu i_{13/2}\nu h_{9/2}$ band with I = even integer + 1.

bands built on the $\nu h_{9/2}$ quasiparticles, denoted by E and F, observed mostly after the alignment of the $\nu i_{13/2}$ pair AB (as in ^{157}Er (Ref. 9) and in ^{161}Yb (Ref. 10)). The $\nu h_{11/2}$ alignment at $\hbar\omega \sim 0.4$ MeV, affects both these bands, producing five quasiparticle strucutres EABab and FABab.

The observed structures in ^{159}Yb are therfore understood on the basis of band crossings expected in the N = 89 region. Even after the multiple crossing at $\hbar\omega \sim 0.4$ MeV, the rotational pattern seems to continue up to a frequency of 0.55 MeV, similar to the yrast sequence of ^{160}Yb (Ref. 11). The ^{159}Yb bands show a behavior different from the yrast line of ^{158}Yb, as indicated in Fig. 2.31b. There the yrast line has a major change in structure around $\hbar\omega$ = 0.4 MeV, which is interpreted as the termination of the collective structure.[8] However, the AE side band in ^{158}Yb shows no such tendency, indicating that the band termination is very sensitive to the quasiparticle structure.

---

1. University of Tennessee, Knoxville, TN.
2. Washington University, St. Louis, MO.
3. On leave from Japan Atomic Energy Research Institute, Tokai, Ibaraki 319-11, Japan.
4. Present address: Universidade De Sao Paulo, Sao Paulo, Brazil.
5. Adjunct staff member from University of Tennessee, Knoxville, TN.
6. University of Pittsburgh, Pittsburgh, PA.
7. On leave from CRN, Strasbourg, France. Present address: GANIL, Caen, France.
8. C. Baktash et al., Phys. Rev. Lett. 54 978 (1985).
9. A.A. Riley et al., Phys. Lett. 135B 275 (1984).
10. L.L. Riedinger, Nucl. Phys. A347 141 (1980).
11. L.L. Riedinger et al., Phys. Div. Prog. Rep., Sept. 30, 1983, ORNL-6004, p. 96.
12. S.M. Harris, Phys. Rev. B138 509 (1965).

SPECTROSCOPIC STUDY OF THE HIGH-SPIN STATES IN ^{135}Pr

T. M. Semkow[1] N. R. Johnson
D. G. Sarantites[1] I. Y. Lee
C. Baktash M. Oshima[4]
Y. S. Chen[2] Y. Schutz[5]
K. Honkanen[1] C. Y. Chen[6]
V. Abenante[1] O. Dietzsch[6]
L. A. Adler[1] J. X. Saladin[6]
A. J. Larabee[3] H. C. Griffin[7]
L. L. Riedinger[8]

In-beam spectroscopic investigation of ^{135}Pr was done in order to study the γ-deformation of this nucleus at high spins. The experiment was done at the Brookhaven National Laboratory using the 91-MeV ^{120}Sn(^{19}F,4n) reaction. Coincidence data were recorded between 4 Compton-suppressed Ge detectors at ~ 40° relative to the beam and 2 unsuppressed Ge detectors at ~85°. In addition,

an array of 11 NaI detectors around the target were used as a multiplicity selector.

The ^{135}Pr decay scheme shown in Fig. 2.32 was constructed from the γ-coincidence, intensity, and angular correlation information. A pair of decoupled rotational bands is observed with $(\pi,\alpha) = (+, \pm 1/2)$. Also a strong negative parity band $(-, -1/2)$ is observed. There is some indication for a decoupled $(-, +1/2)$ band (sequence 482, 725, 843, 956, and 1112 keV). A plot of the experimental aligned angular momentum is shown in Fig. 2.33. These features were compared with the cranking shell model calculations. The positive parity bands are based on the $[413\ 5/2]^2 g_{7/2}$ proton configuration. The first backbending at $\hbar\omega_{AB} = 0.32$ MeV is due to the alignment of the $h_{11/2}$ protons and the second backbending at $\hbar\omega_{ab} = 0.49$ MeV is due to the alignment of the $h_{11/2}$ neutrons. In addition, the $(-, -1/2)$ band is based on the $[541\ 3/2]h_{11/2}$ proton configuration. The first backbending at $\hbar\omega_{BC} = 0.46$ MeV is caused by the alignment of $h_{11/2}$ protons. The shifting of the crossing frequency to a relatively large value is due to the blocking of the A proton orbital. The small upbend in the $(-, -1/2)$ band is caused by the alignment of the $h_{11/2}$ neutron orbitals (ab), similar to the second backbending in the positive-parity band.

The alignment of the protons from the beginning of $h_{11/2}$ shell at the first backbending in both parity bands moves γ towards

ORNL-DWG 85-17847

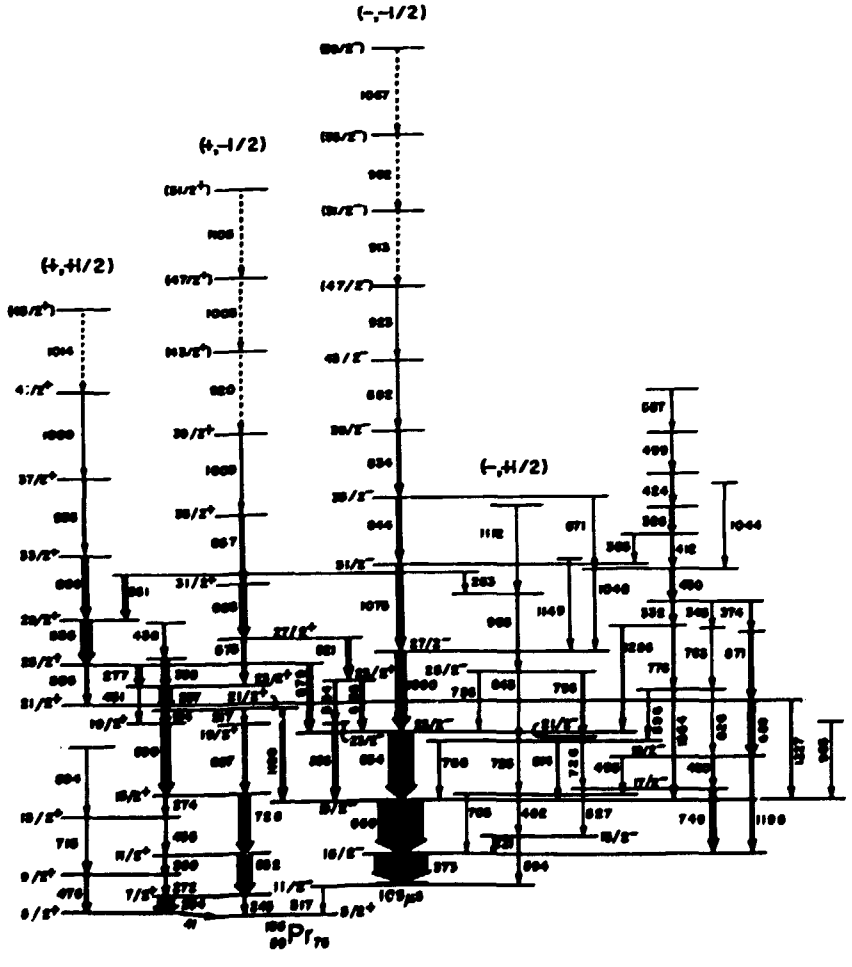

Fig. 2.32 Decay scheme of ^{135}Pr. The rotational bands are identified by the (π,α) numbers.

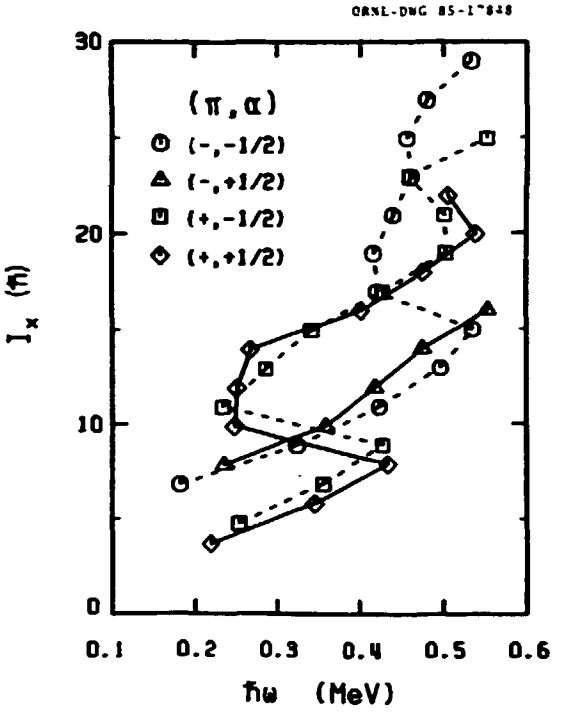

Fig. 2.33 Experimental aligned angular momentum vs the rotational frequency for the positive and negative parity bands in ^{135}Pr.

~ 15°, causing the signature inversion in the positive parity bands. The essentially prolate shapes at high spins in ^{135}Pr are in contrast with the ^{134}Ce core, where the $h_{11/2}$ neutron holes were interpreted to align, causing oblate shapes.[9] ^{133}Pr behaves similarly to ^{135}Pr, except that the crossing frequencies are slightly lower and there is no inversion of signature splitting in positive parity bands.[10]

---

1. Washington University, St. Louis, MO.
2. Joint Institute for Heavy Ion Research, Oak Ridge National Laboratory, Oak Ridge, TN. Permanent address: Institute of Atomic Energy, Beijing, P. R. C.
3. University of Tennessee, Knoxville, TN.
4. On leave from Japan Atomic Energy Research Institute, Tokai, Ibaraki 319-11, Japan.
5. On leave from CRN, Strasbourg, France. Present address: GANIL, Caen, France.
6. University of Pittsburgh, Pittsburgh, PA.
7. University of Michigan, Ann Arbor, MI.
8. Adjunct staff member from the Physics Department, University of Tennessee, Knoxville, TN.
9. M. Müller-Veggian et al., Nucl. Phys. A417, 189 (1984).
10. L. Hildingsson et al., private communication (1985).

HIGH-SPIN STRUCTURE OF ^{163}Lu

K. Honkanen[1] M. L. Halbert
H. C. Griffin[2] D. C. Hensley
D. G. Sarantites[3] N. R. Johnson
V. Abenante[3] A. Larabee[6]
L. A. Adler[3] I. Y. Lee
C. Baktash L. L. Riedinger[7]
Y. S. Chen[4] J. X. Saladin[5]
O. Dietzsch[5] T. M. Semkow[1]
Y. Schutz[8]

The population of rotationally aligning high-j orbitals in nuclei may provide a sensitive probe of the triaxiality parameter γ, and could be used to trace the evolution of γ with angular momentum.[9-11] These observations are based on the fact that a particle (hole) in a high-j orbital polarizes the core toward oblate (prolate) shape; whereas, a quasi-particle in a half-filled high-j orbital shell generates the intermediate situation leading to a triaxial shape. These expectations were confirmed in a cranked shell-model calculation by Leander[11] who concluded that, in a γ-soft nucleus, the presence of a high-j quasi-particle with favored signature will stabilize the shape of the nucleus at a γ value that depends initially on the position of the Fermi level in the shell. For non-γ-soft nuclei that have a potential-energy minimum at some other γ value, the quasi-particle exerts a driving force toward positive γ values when the shell is less than half-full or toward negative γ values when it is more than half-full. In contrast the unfavored signature states are much less sensitive to variations of γ and λ, the position of the Fermi level in the shell. This results in signature splittings that become a sensitive measure of the variation of γ-deformation with spin and λ. Inversion of signature splitting above the backbend in $^{157}_{67}Ho_{90}$ (Ref. 12) and in $^{159}_{69}Tm_{90}$(Ref. 13) in the π7/2-[523] band was explained by the positive driving influence of the two $i_{13/2}$ neutrons above the backbend, resulting in a change from negative to slightly positive γ above the backbend.

To explore the possibility of similar changes in γ as a function of the proton number, we have studied the high spin structure of $^{163}_{71}Lu_{92}$ which has two protons and two neutrons more than ^{159}Tm.

The high spin states in ^{163}Lu were populated via the ^{122}Sn(^{45}Sc,4n) reaction at 192 MeV with the tandem accelerator at the Holifield Heavy Ion Facility. The γ-ray spectroscopic information was obtained using an array of five Ge detectors with pentagonal NaI anti-Compton shields, all located at 63° to the beam, and three additional Ge detectors at 24°. Two-fold or higher coincident events from these detectors were used as event triggers for the NaI detectors of the Spin Spectrometer.

In Fig. 2.34 are shown three band structures believed to be associated with ^{163}Lu. Energy systematics in the heavier odd-A Lu isotopes show that the π9/2⁻[514] band should be the yrast band, although the π1/2⁺[411] decreases rapidly in energy with decreasing A relative to the π7/2⁺[404] state, and in the ^{165}Lu and ^{163}Lu may become the ground state. In ^{165}Lu the π9/2⁻[514] band is yrast[14] and in ^{163}Lu is also the strongest band populated. The decay scheme shown in Fig. 2.34 is preliminary and further analysis is in progress to connect the different structures based on observed coincident γ-rays.

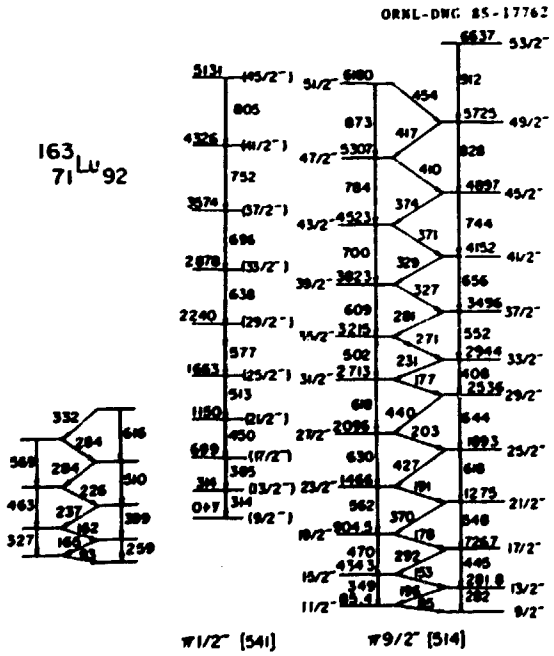

Fig. 2.34 Tentative decay scheme for the three band structures assigned to ^{163}Lu. The spin 9/2⁻ for the lowest observed level in the π9/2⁻[514] band was assumed based on systematics.

The transitions from all these structures have yields associated with (H,k) distributions characteristic of the (^{45}Sc,4n) reaction and, thus, were assigned to ^{163}Lu.

There is a striking similarity between some of the bands in ^{163}Lu and ^{165}Lu. In ^{165}Lu the 9/2⁻[514] band was seen up to I = 43/2⁻ and it has a significant signature splitting.[14] Based on systematics from the odd-A Lu isotopes, we have assigned the yrast band as the π9/2⁻[514]. The backbending in this region is due to breaking and alignment of an $i_{13/2}$ neutron pair, which places the backbending at about 12 units of rotational angular momentum. A second band was assigned as π1/2⁻[541] based on systematics and in analogy with ^{165}Lu. A third band structure shown in Fig. 2.34 is most likely a part of the 7/2⁺[404] band.

The favored and unfavored bands (α = -1/2 and 1/2) gain 7.2 and 8.2 units of angular momentum above the backbend, respectively (Fig. 2.35). This is consistent with the decoupling and alignment of an $i_{13/2}$ neutron pair. The crossing frequencies for the α = -1/2 and α = 1/2 bands are 0.263 and 0.280 MeV, respectively, as is seen from Fig. 2.35b. Below the backbend the π9/2⁻[514] band shows a large negative signature splitting which increases with ω from ~ 55 to 120 keV (Fig. 2.35b), but above the backbend a signature inversion occurs with a splitting of 10 keV which remains constant with increasing ω.

A cranked shell-model calculation for ^{163}Lu gave an ~80-keV negative signature splitting for the quasi-protons for a γ value of -10° at ħω = 0.24 MeV. A signature inversion is predicted for the quasi-proton configuration at γ = 0°. Above the backbend the two $i_{13/2}$ quasi-neutrons are driving toward positive γ values. When the Routhians for these 3-quasiparticles are added and the effect of the core is included, a γ value for this configuration can be obtained. Qualitatively, it appears that a significant shape change from negative to slightly positive γ values is present in this case. Thus, the signature inversion in the π9/2⁻[514] band is quite similar to that observed in ^{155}Ho on ^{159}Tm where the 7/2⁻[523] quasi-proton configuration was pushed toward

ORNL-DWG 85-17763

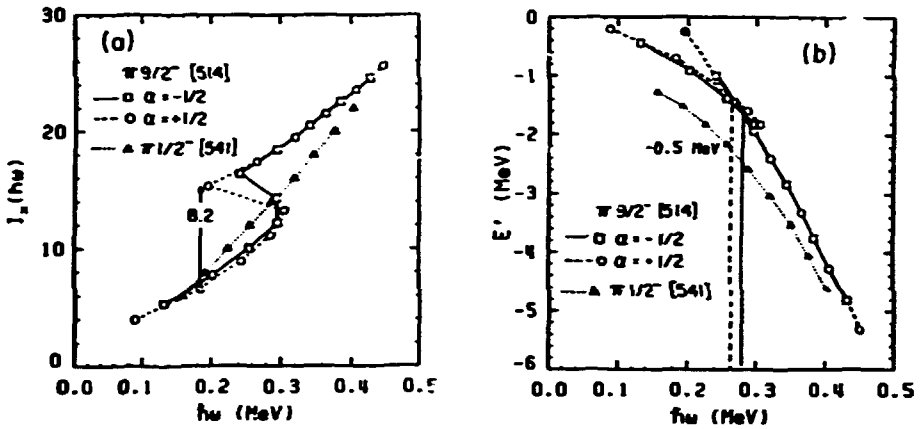

Fig. 2.35 Panels a and b show the aligned angular momentum and the energy in the rotating frame $E' = E_{Level} - \hbar\omega I_x$) for the bands indicated.

slightly positive γ values by the positive driving influence of the two strongly aligning $i_{13/2}$ quasi-neutrons.

The gradual gain in alignment of the π1/2⁻[541] band with increasing ω (Fig. 2.35a) suggests that either the aligning quasiparticles exhibit a strong interaction, or that an ϵ_2 value larger than 0.2 and possibly a different γ value are needed for the π9/2⁻[514] band in order to explain its behavior.

---

1. Washington University, St. Louis, MO 63130. Present address: University of Jyvaskyla, Jyvaskyla, Finland.
2. University of Michigan, Ann Arbor, MI 48109.
3. Washington University, St. Louis, MO 63130.
4. Joint Institute for Heavy Ion Research, Oak Ridge, TN 37831. Permanent address: Institute of Atomic Energy, Beijing, P. R. C.
5. University of Pittsburgh, Pittsburgh, PA 15260.
6. University of Tennessee, Knoxville, TN 37996.
7. Adjunct staff member from the University of Tennessee, Knoxville, TN 37996.
8. On leave from CRN, Strasbourg, France. Present address: GANIL, Caen, France.
9. R. Bengtsson et al., in Proc. Bormio Conf., 1982, p. 144; and p. 161 in High Angular Momentum Properties of Nuclei, ed. N. R. Johnson (Harwood, New York, 1983).
10. S. Frauendorf and F. R. May, Phys. Lett. 125B, 245 (1983).
11. G. A. Leander et al., p. 281 in High Angular Momentum Properties, ed. N. R. Johnson (Harwood, New York, 1983).
12. G. B. Hagemann et al., Phys. Rev. C 25, 3324 (1982).
13. L. L. Riedinger, Physica Scripta T5, 36 (1983).
14. S. Jonsson et al., Nucl. Phys. A422, 397 (1984).

OBSERVATION OF HIGH-SPIN NON-YRAST TWO-QP BANDS γ-γ COINCIDENCE MEASUREMENTS FOLLOWING HEAVY-ION TRANSFER REACTIONS

P. A. Butler[1] S. Juutinen[2]
X. T. Liu[2] S. Sorensen[2]
M. W. Guidry[3] M. P. Carpenter[2]
C. R. Bingham[3] R. W. Kincaid[2]
D. Cline[4] E. Vogt[3]
W. Kernan[4] C. Y. Wu[3]
I. Y. Lee C. Baktash
D. Sarantites[5]

Heavy ion transfer reactions offer the possibility of studying collective bands built upon intrinsic excitations in deformed nuclei. Recently,[6] total γ-ray energy and multiplicity measurements have been made for the system ^{58}Ni + ^{161}Dy, which demonstrates that two regions of multiplicity and energy are populated by 1-neutron pick-up. These results have been explained as a superposition of two populations: the lower multiplicity and sum energy distribution corresponds to direct excitation of the ground-state band, and the higher multiplicity and sum energy distributions corresponds to the transfer to low-lying two-quasi-particle (q.p.) bands in ^{160}Dy.

We have carried out an experiment at the HHIRF in order to obtain further information on the population of non-yrast states in ^{160}Dy via the ^{161}Dy(^{58}Ni, ^{59}Ni)^{160}Dy reaction. The 270-MeV ^{58}Ni beam was supplied by the Holifield Facility tandem accelerator. The measurements were carried out using an array of 10 Ge detectors which are elements within the Spin Spectrometer. Five of the Ge detectors were escape suppressed. Events were collected when a backscattered Ni-like fragment was detected in an array of X and Y position-sensitive, parallel-plate avalanche detector and when any one Ge detector fired.

Figure 2.36a shows the γ-ray spectrum in the Ge detectors when at least two of these were in coincidence. The observed γ-rays come mostly from inelastic scattering and one neutron pick-up; these channels were selected by requiring an energy window in one detector on the strongest ^{161}Dy transitions (Fig. 2.36b) and the strongest ^{160}Dy transitions (Fig. 2.36c). In these spectra, Doppler corrections were made assuming the γ-rays were emitted by the Dy-like fragment. The spectrum of Fig. 2.36c shows that the ground state band in ^{160}Dy is excited strongly up to $J^{\pi} = 10^{+}$, but this drops off rapidly so that the $16^{+} - 14^{+}$ transition is very weak, and that at least three side bands (two negative parity and the γ-band[7]) are weakly populated.

Figure 2.37 shows the spectrum recorded in the NaI detectors, unfolded for energy-dependent response to γ radiation, when in coincidence with the strongest ^{161}Dy and ^{160}Dy transitions which are observed in the Ge detectors. Figure 2.37 reflects the observed strong discrete transitions in the yrast band of ^{161}Dy and the decay of the first excited state of ^{58}Ni. Figure 2.37 is the corresponding spectrum for ^{160}Dy and shows additional features to the observed discrete line intensity. There is a pronounced broad peak at about 1 MeV, the intensity of which is about one-third of the total γ-ray intensity for this reaction. The mean energy of this peak is similar to the observed discrete transitions from the known side bands to the g.s. band in ^{160}Dy.

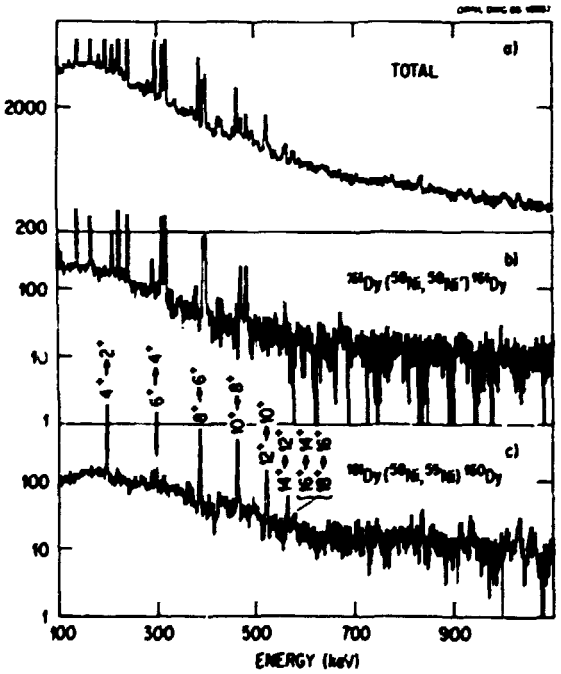

Fig. 2.36 Gamma ray spectrum in the Ge detectors in coincidence with backscattered Ni-like particles. (a) Spectrum corresponding to at least two Ge detectors firing. (b) As (a), spectrum in one Ge detector with energy window on the strongest ^{161}Dy transitions in the other. (c) As (a), spectrum in one Ge detector with energy window on the strongest ^{160}Dy transitions in the other.

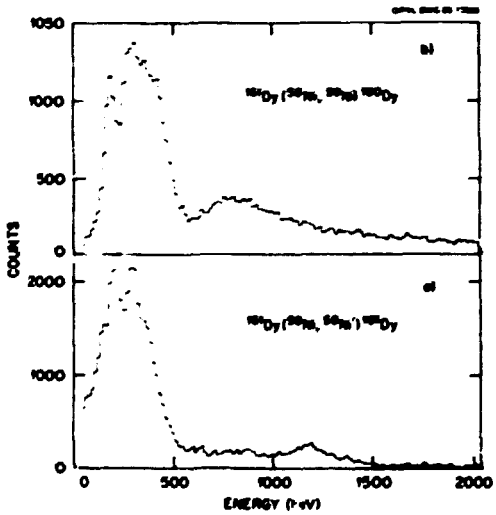

Fig. 2.37 Spectrum recorded in the NaI detectors in coincidence with backscattered Ni-like fragments and energy window in one Ge detector on (a) ^{161}Dy strongest transitions and (b) ^{160}Dy strongest transitions.

These spectra have been interpreted as arising from the decay of many 2 q.p. bands which are populated by the heavy ion transfer reaction. The large distribution of states within these bands will decay to lower lying 2 q.p. or vibrational states (rather than via in-band transitions), which then in turn decay to members of the g.s. band.

---

1. Joint Institute for Heavy Ion Research, Oak Ridge, TN, 37831. Permanent address: Univ. of Liverpool, Liverpool, Great Britain.
2. University of Tennessee, Knoxville, TN.
3. Adjunct staff member from the University of Tennessee, Knoxville, TN.
4. University of Rochester, Rochester, NY.
5. Washington University, St. Louis, MO.
6. M.W. Guidry et al., Phys. Lett., to be published.
7. H.J. Riezebos et al., Groningen annual report.

HIGH-SPIN LEVELS IN DY ISOTOPES MEASURED IN HEAVY-ION INELASTIC SCATTERING EXPERIMENTS

B. Cox[1] S. Juutinen[4]
X. T. Liu[2] M. W. Guidry[4]
I. Y. Lee C. Baktash
D. Cline[3] W. Kernan[3]

The most neutron rich nuclei cannot be studied by means of heavy-ion-induced fusion reactions. In this case Coulomb excitation or inelastic excitation is a possible alternative to study high spin structure.

In work reported elsewhere in this progress report we have recently initiated an extensive series of heavy-ion transfer reaction studies.[5] As a sidelight of those experiments a comprehensive set of heavy-ion inelastic scattering data has been obtained. This inelastic scattering data is of consequence for two reasons. (1) It can be used to determine precise ion-ion potentials in the manner described in Ref. 6. (2) From γ-γ coincidence measurements in the inelastic channels it has been possible to extend the energy level schemes for several deformed nuclei beyond that reported in the literature.

As an illustration of these methods we discuss the extension of the high-spin level schemes of ^{163}Dy and ^{164}Dy. The particle-γ coincidence techniques employed are described in a separate report of this document.[5]

Requiring that no neutrons were detected in the spin spectrometer, that the Q-value is between -30 MeV and + 30 MeV, and that the γ-fold is less than 6, the peak-to-background ratio for inelastic transitions was improved by a factor of 5. This gating method enabled us to construct side bands in ^{163}Dy and ^{164}Dy.

Very little is reported in the literature about the level scheme of ^{163}Dy. The yrast band 5/2 [523] is known to spin 15/2 and side bands even lower. Based on data obtained from the ^{116}Sn + ^{163}Dy experiment, we have been able to extend the favored and unfavored signatures of the 5/2 [523] band to spins $37/2^-$ and $35/2^-$. The 5/2 [642] signatures were observed to spins $29/2^+$ and $27/2^+$, and the 1/2 [521] signatures to spins $23/2^-$ and $21/2^-$. The population of the positive-parity band is mostly feeding from the strongly populated 5/2 [523] band. The level scheme for ^{163}Dy from the present work is shown in Fig. 2.38.

^{164}Dy is much better known than ^{163}Dy. The ground state band is known to spin 14^+ and the γ-band to spin 6^+. In this work we were able to add three more transitions above the 14^+ state and continue the γ-band to the spin 14^+.

The ground-state band and the aligned $i_{13/2}$ band cross at $\hbar\omega$ = 0.3 MeV in these nuclei. Light Dy isotopes show a clear backbending, while ^{160}Dy and ^{162}Dy only upbend due to the large interaction between the ground state band and the s-band. The aligned angular momenta (I_x) in the rotational bands in ^{163}Dy and ^{164}Dy are shown in Fig. 2.39. Both the 5/2 [523] band in ^{163}Dy and the ground state band in ^{164}Dy seem to experience a very gentle upbending at $\hbar\omega \sim$ 0.3 MeV compared with the $i_{13/2}$ band in ^{163}Dy, where band crossing is presumably blocked.

---

1. Bridgewater College, Bridgewater, VA.
2. Adjunct staff member from the University of Tennessee, Knoxville, TN.
3. University of Rochester, Rochester, NY.
4. University of Tennessee, Knoxville, TN.
5. S. Juutinen, et al., separate report in this progress report and to be published.
6. M. W. Guidry, et al., Nucl. Phys. A430, 485 (1984).

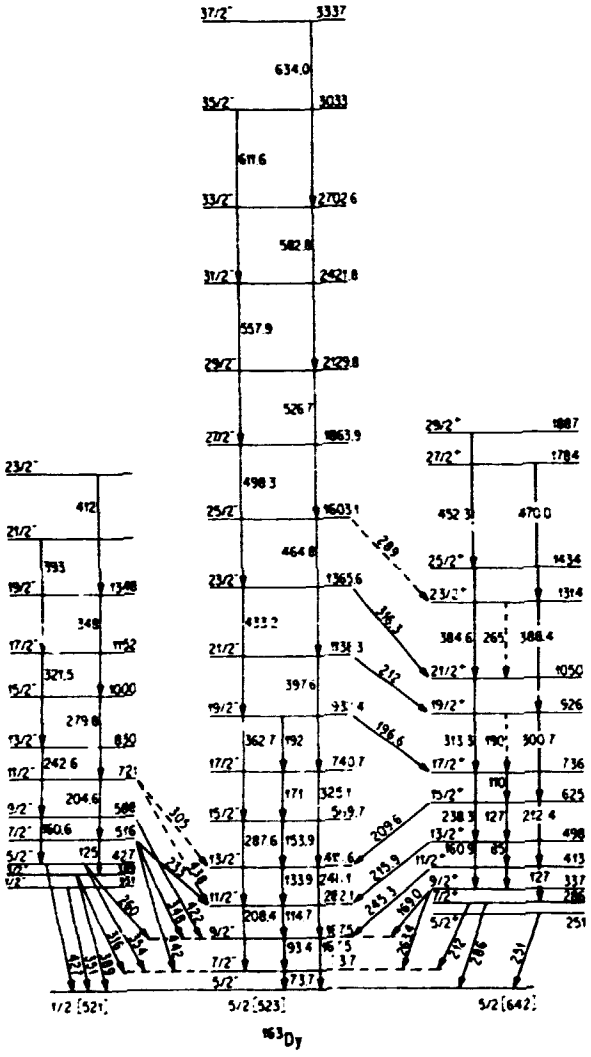

Fig. 2.38 Level scheme for ^{163}Dy deduced from ^{116}Sn + ^{163}Dy inelastic scattering at energies just above the Coulomb barrier.

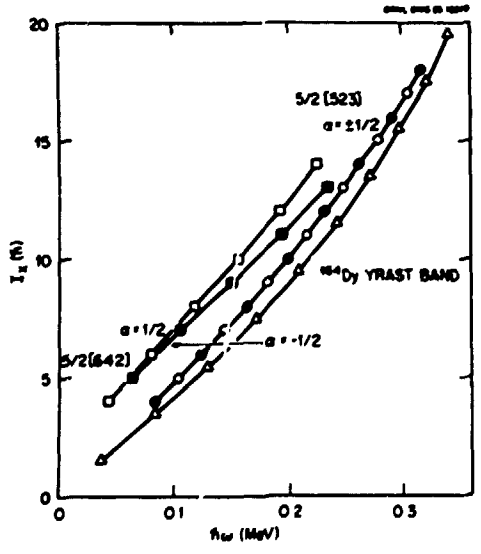

Fig. 2.39 The aligned angular momenta of rotational bands in ^{163}Dy and ^{164}Dy.

FIRST EVIDENCE FOR LOSS OF COLLECTIVITY AT HIGH SPINS IN A STRONGLY DEFORMED NUCLEUS[1]

M. W. Rao[2] M. Oshima[3]
N. R. Johnson J. W. McConnell
F. K. McGowan K. Erb
I. Y. Lee J. C. Wells[4]
C. Baktash A. Larabee[5]
L. L. Riedinger[6]

Recent lifetime measurements[7-9] of N ≈ 90 nuclei have provided transition quadrupole moments (Q_t) which show in the ground band an increase with angular momentum as a result of centrifugal stretching, while in the s-band there is a significant decrease in Q_t. This reduction of Q_t at higher spins has been interpreted with qualitative success on the basis of both cranked Hartree-Fock-Bogoliubov (CHFB)[10-11] and cranked shell-model (CSM)[12,13] calculations. Both approaches depend on the fact that the N ~ 90 nuclei have potential energy surfaces which are very shallow, rendering the nucleus susceptible to the deformation driving influences of the quasiparticles at higher spins. The conclusion for these nuclei near N = 90 is that they are driven to triaxial shapes (+γ in the s-band with a resulting loss of collectivity.

Inherent in the CSM perspective is the fact that as the neutron Fermi surface approaches the middle of the $i_{13/2}$ neutron shell, the driving force towards positive γ values reverses and moves towards the collective sector (-γ). This fact, coupled with the more strongly deformed nature of these nuclei, leads one to assume that these mid-shell nuclei will not demonstrate the dramatic loss of collectivity in the s-band as we have observed for ^{160,161}Yb (Ref. 8) and ^{158}Er (Ref. 9). To test these ideas we have carried out Doppler-shift recoil-distance lifetime measurements on the N = 98 nucleus ^{172}W.

Excited ^{172}W nuclei were produced by the ^{124}Sn(^{52}Cr, 4n) reaction at an incident beam energy of 230 MeV. The recoil velocity of the W nuclei was 0.02*c. Details of the recoil distance device used are discussed in Ref. 14. Data were recorded with a BGO Compton suppressed Ge detector at 0° to the beam direction under the coincidence requirement that at least one of an array of six large volume Ge detectors (positioned at 90° to the beam) be triggered. Coincidence spectra were thus obtained for a total of 18 target-stopper separations ranging

from 16 μm to 7 mm and the data were stored in an event-by-event mode on magnetic tape.

Lifetimes for the yrast sequence of ^{172}W were determined from spectra generated in three ways: (1) by gating on the γ-ray transition above a group of several transitions of interest [gated-above (GA) type data]; (2) from the sum of spectra obtained by gating on individual γ-rays in cascade below the transitions of interest [sum-gated-below (SGB) type data]; and (3) with the entire 90° spectrum below 1.5 MeV as the gate [total-projected (TP) type data]. The data from the GA-type spectra are of relatively poor statistical quality, but they provide decay curves free from contributions of direct side feeding to the levels under study. For the analysis of the spectra of the latter two types, wherein the problems of the unknown side feeding are not eliminated, two-step-cascade side feeding was modeled to each of the levels under study. In all cases, a rotational band was used to model the feeding into the top level of the sequence.

Lifetimes were extracted by using the computer program LIFETIME (Ref. 15) which applies all the usual corrections[16,17] to the data and handles the problem of feeding by direct solution of the Bateman equations. The initial populations and transition rates are adjusted by the program to obtain the best fit to both the shifted and unshifted intensities as a function of target-stopper separation.

Typical fits to the corrected experimental decay curves are shown in Fig. 2.40. The results obtained for the lifetimes are displayed in Table 2.8. The experimental transition quadrupole moments, Q_t, listed in column 4 of Table 2.8, were obtained from the reduced transition probabilities according to the expression

$$B(E2;\ I \rightarrow I\text{-}2) = \frac{5}{16\pi} \langle I\ 2\ 0\ 0 \mid I\text{-}2\ 0\rangle^2\ Q_t^2$$

The uncertainties in the lifetimes and Q_t values quoted in Table 2.8 were determined by the method of the subroutine MINOS described in Ref. 18.

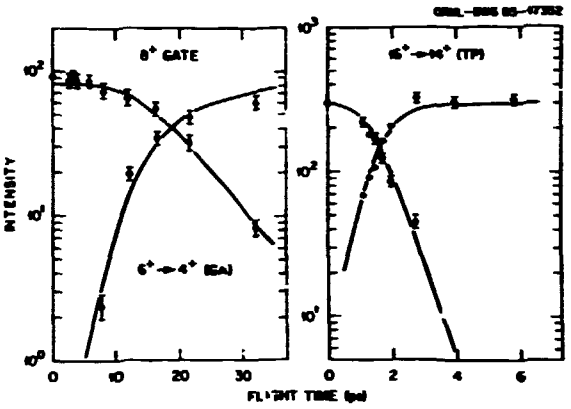

Fig. 2.40 Illustrative decay curves showing unshifted (open circles) and shifted (solid circles) γ-ray intensities as a function of flight time. The solid curves are the fitted time distributions.

Table 2.8. Lifetimes and transition quadrupole moments in ^{172}W

I_i^π	E_γ^a (keV)	τ^b(ps)	Q_t^b(eb)
2^+	123.4	892 ± 56 [c]	7.62 ± 0.24[c]
4^+	254.0	44.5 ± 2.1[c]	7.29 ± 0.18[c]
6^+	350.6	7.18 ± 0.56	8.03 ± 0.31
8^+	419.6	3.40 ± 0.12	7.38 ± 0.15
10^+	470.7	1.92 ± 0.21	7.31 ± 0.46
12^+	513.0	1.57 ± 0.10	6.44 ± 0.28
14^+	549.9	1.10 ± 0.10	6.45 ± 0.29
16^+	576.9	0.82 ± 0.06	6.60 ± 0.28
18^+	598.3	0.72 ± 0.18[d]	6.52 ± 0.81[d]
20^+	644.3	$0.53\ ^{+\ 0.14}_{-\ 0.13}$[e]	$6.21\ ^{+\ 0.90}_{-\ 0.81}$[e]
22^+	711.1	$0.39\ ^{+\ 0.17}_{-\ 0.14}$[e]	$5.65\ ^{+\ 1.56}_{-\ 1.09}$[e]

[a]The uncertainty in transition energies is ± 0.1 keV.

[b]Value represents a weighted average of two numbers; the first, an unweighted arithmetic average of the results of TP and SGB data and the second, an unweighted arithmetic average of GA results.

[c]TP and GA results only.

[d]TP and SGB results only.

[e]TP results only.

It is clear from Fig. 2.41, in which the Q_t values are plotted as a function of the rotational frequency, that there is a reduction of ~ 15% in the Q_t values for spins $I > 12$. From the present data it is not possible to conclude whether this drop occurs suddenly at $I = 12$ or if there is a general downward tendency of the Q_t values throughout the yrast band to spin 22.

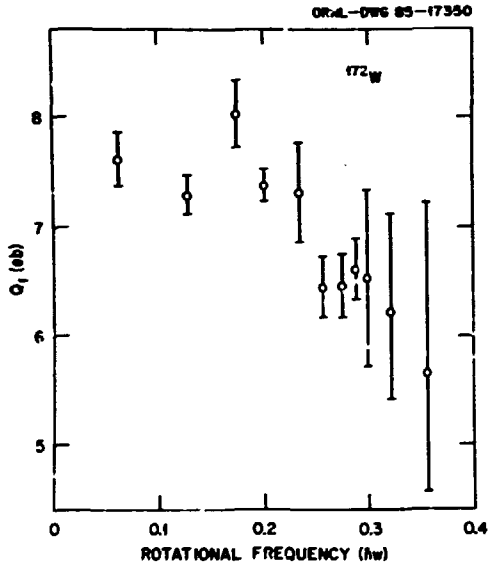

Fig. 2.41 Transition quadrupole moments of the yrast sequence of ^{172}W as a function of rotational frequency.

In either case, this is a surprising and very interesting result, and certainly was not the expected outcome based on previously held ideas about such "strongly" deformed nuclei. At this point we do not have a theoretical explanation for this behavior, but calculations are in progress by several groups.

---

1. Summary of paper to be published; abstract of the work appeared in Bull. Am. Phys. Soc. 30, 1275 (1985).
2. On leave from University of Sao Paulo, Sao Paulo, Brazil.
3. On leave from Japan Atomic Energy Research Institute, Tokai, Ibaraki 319-11, Japan.
4. Adjunct staff member from Tennessee Technological University, Cookeville, TN.
5. University of Tennessee, Knoxville, TN.
6. Adjunct staff member from University of Tennessee, Knoxville, TN.

7. H. Emling et al., Nucl. Phys. A419, 187 (1984).
8. M. P. Fewell et al., Phys. Rev. C 31, 1057 (1985).
9. M. Oshima et al., Bull. Am. Phys. Soc. 29, 1043 (1984); and to be published.
10. R. Bengtsson, in Proceedings of the Conference on High Angular Momentum Properties of Nuclei, Oak Ridge, TN, November 1982, edited by N. R. Johnson, Nuclear Science Research Conference Series, Vol. 4 (Harwood Academic, NY, 1983), p. 161.
11. R. Bengtsson, Y.-S. Chen, J.-Y. Zhang, and S. Aaberg, Nucl. Phys. A405, 221 (1983).
12. G. A. Leander, S. Frauendorf, and F. R. May, in Proceedings of the Conference on High Angular Momentum Properties of Nuclei, Ref. 10, p. 281.
13. S. Frauendorf and F. R. May, Phys. Lett. 125B, 245 (1983).
14. N. R. Johnson et al., Physics Division Progress Report for period ending June 30, 1981, ORNL-5787 (1981), 147.
15. J. C. Wells, M. P. Fewell, and N. R. Johnson, "LIFETIME": A Computer Program for Analyzing Doppler-Shift Recoil-Distance Lifetime Data, ORNL/TM-9105 (1985).
16. N. R. Johnson et al., Phys. Rev. C 12, 1927 (1975).
17. R. J. Sturm and M. W. Guidry, Nucl. Instrum. Methods 138, 345 (1976).
18. F. James and M. Roos, Comput. Phys. Commun. 10, 343 (1975).

DEFORMATION EFFECTS IN ^{184}Pt

A. J. Larabee[1]
J. Nyberg[2]
M. P. Carpenter[1]
L. L. Riedinger[3]
C. R. Bingham[3]
L. H. Courtney[1]
S. Juutinen[1]
Z.-m. Liu[1]
Z.-y. Zhang[4]
C. Baktash
M. L. Halbert
N. R. Johnson
I. Y. Lee
Y. Schutz[5]
A. Johnson[2]
K. Honkanen[6]
D. G. Sarantites[6]
F. R. Haenni[7]

Data on ^{183}Pt were collected using a 163 MeV ^{34}S beam on a ^{154}Sm target. The experimental set-up is the same as that described in the contribution "Rotational Alignment Processes in ^{184}Pt" also included in this report. In the case of ^{183}Pt, selective gating on the total sum energy and γ-ray fold observed in the spin spectrometer was used to enhance the 5n reaction channel. Three different odd-neutron structures were observed: (1) the favored signature of the $p_{3/2}$ band, (2) both signatures of the $7/2^-[514]$ band and (3) both signatures of the $9/2^+[624]$ band. In this region of transitional nuclei, the configuration of the odd quasiparticle can directly influence the equilibrium deformation

of the core. These deformation effects are expected to differ for the $\nu f_{7/2}$ and $\nu i_{13/2}$ bands.

In Fig. 2.42, the experimental Routhians are plotted as a function of rotational frequency for the $\nu f_{7/2}$ (K = 7/2) and $\nu i_{13/2}$ (K = 9/2) bands. It is clearly shown that although no signature splitting is observed in the $f_{7/2}$ bands, a significant splitting is observed in the $\nu i_{13/2}$ bands. Both of these structures form high-K bands where essentially no signature splitting is expected to occur for a symmetrically deformed potential. However, it is well-known that in the N = 90 region signature splitting in high-K bands can occur due to the γ-driving influence of the odd quasiparticle on the core.[8]

In the N = 106 region, there is a further complication which arises from the very large hexadecapole (ε_4) deformations which can exist for these nuclei. Large ε_4 deformations appear to account for the large signature splitting observed in the $\nu i_{13/2}$ bands in odd-N $_{76}$Os nuclei.[9] A large ε_4 value has the effect of contracting the $i_{13/2}$ orbital, bringing the 1/2[660] configuration much closer to the high-K states. Therefore, even when the Fermi surface lies fairly high in the shell there can still be a significant mixing of the K = 1/2 configuration. In Cranked Shell Model (CSM) calculations, as ε_4 is increased, the signature splitting of the $i_{13/2}$ configurations also increases. Potential energy surface minimization calculations using a folded Yukawa potential give $\varepsilon_2/\varepsilon_4$ values of 0.225/0.04, 0.21/0.055 and 0.19/0.065 for ^{183}Pt, ^{185}Pt and ^{187}Pt, respectively. The decreasing ε_2 values and increasing ε_4 values should result in an increase in the signature splitting from ^{183}Pt to ^{187}Pt. However, recent data on ^{185}Pt (Ref. 10) indicate that the observed signature splitting in ^{185}Pt is only half of that observed in ^{183}Pt.

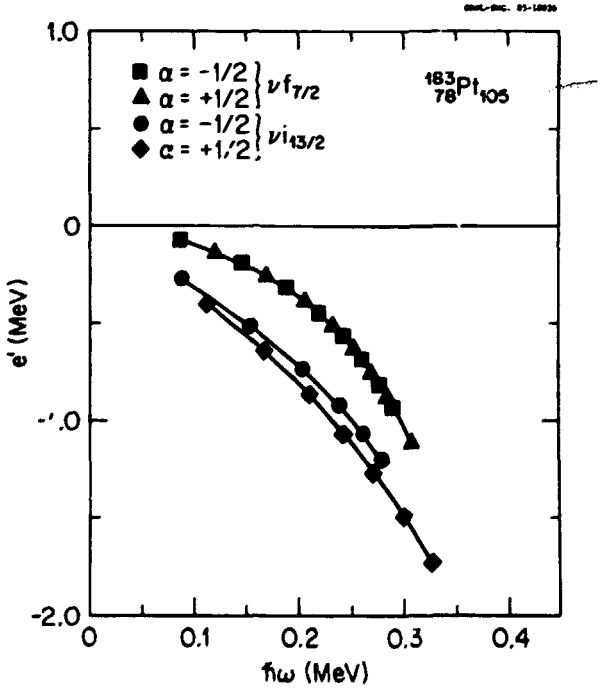

Fig. 2.42 Experimental Routhians (e') for ^{183}Pt as a function of rotational frequency. The reference parameters used were $\mathcal{I}_0$ = 22 ħ² MeV⁻¹ and $\mathcal{I}_1$ = 90 ħ⁴ MeV⁻³.

In the N = 106 region, the effects of both ε_4 and γ need to be considered in explaining the observed signature splitting. The magnitude of the γ-driving force of the quasiparticle on the core can be estimated roughly if the energy dependence of the quasiparticle Routhian as a function of γ is known. The quasiparticle Routhian can then be added to the core energy and the equilibrium shape can be determined.[8] The one-quasiparticle Routhians for the $\nu f_{7/2}$ and $\nu i_{13/2}$ configurations are shown in Fig. 2.43a. These have been calculated with a CSM code using the Nilsson potential. In order to be more self-consistent the ε_2 and ε_4 values used in the calculation were determined in a potential energy surface minimization calculation also using the Nilsson potential. The energy of the core was calculated using

$$E_{core} = \frac{1}{2}V_{po}\cos 3\gamma - \frac{1}{2}\omega^2(\mathcal{I}_0 + \frac{1}{2}\omega^2\mathcal{I}_1)x$$

$$\frac{4}{3}\cos^2(\gamma + 30°),$$

where the first term gives the deformation energy. The V_{po} factor is a fitted parameter representing the potential energy difference between the prolate and oblate shapes. The second term represents the contribution from the

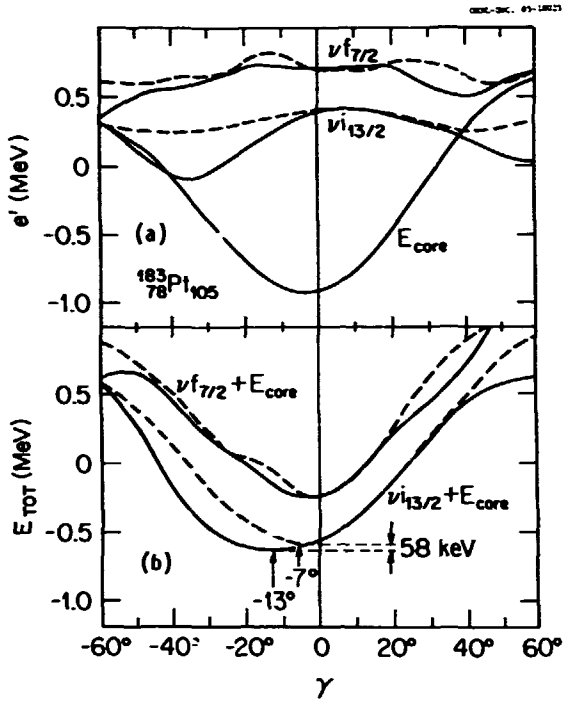

Fig. 2.43 (a). Calculated Routhians for the $\nu i_{13/2}$ and $\nu f_{7/2}$ one quasiparticle configurations in ^{183}Pt as a function of γ-deformation. The CSM calculation was done using $\varepsilon_2 = 0.229$, $\varepsilon_4 = 0.037$, $\Delta = 0.10\ \hbar\omega_0$ and $\hbar\omega = 0.023\ \hbar\omega_0$. Also shown is the calculated core energy, using reference parameters $\mathcal{I}_0 = 22\hbar^2$ MeV^{-1} and $\mathcal{I}_1 = 90\ \hbar^4$ MeV^{-3}. (b). Total energy curves for the $\nu i_{13/2}$ and $\nu f_{7/2}$ one quasiparticle configurations in ^{183}Pt as a function of γ-deformation. The V_{po} needed to fit the experimentally observed signature splitting in the $\nu i_{13/2}$ bands is -1.23 MeV.

rotational energy using the Harris expansion in terms of the moment-of-inertia parameters $\mathcal{I}_0$ and $\mathcal{I}_1$.[11] The total energy of the core is then given by

$$E_{tot} = \sum_{\mu} e'_{\mu} + E_{core}$$

when e'_{μ} is the quasiparticle Routhian for a given quasiparticle μ.

In Fig. 2.43a, the core energy is seen to minimize near $\gamma = 0°$. In this region the $\nu f_{7/2}$ Routhian is fairly flat as a function of γ and therefore is not expected to affect the equilibrium γ value. However, the $\nu i_{13/2}$ Routhians show a strong preference for negative γ values and will exert a driving force on the core in that direction. The resulting total energy curves as a function of γ are shown in Fig. 2.43b. The favored and unfavored signatures of the $\nu i_{13/2}$ configuration show minima at $\gamma = -13°$ and $\gamma = -7°$, respectively. The V_{po} for ^{183}Pt was fitted so that the energy difference between these two minima is equal to the observed signature splitting. The V_{po} so determined is -1.23 MeV, which is very close to the V_{po} predicted by the potential energy minimization calculation. The total energy curves for the $\nu f_{7/2}$ configuration show no significant change in their γ-deformation relative to the core and no signature splitting, as expected.

The above calculations indicate that γ-deformations also need to be considered in explaining the signature splitting in the odd-N Pt nuclei, although it is not clear just how the interplay of both ε_4 and γ affect the signature splitting. In order to get a better feel for the deformations in the N = 106 region it is necessary to do the potential energy surface minimization calculations as a function of ε_2, ε_4 and γ. Such calculations are currently underway.

---

1. University of Tennessee, Knoxville, TN.
2. Research Institute for Physics, Stockholm, Sweden.
3. Adjunct staff member from University of Tennessee, Knoxville, TN.
4. Joint Institute for Heavy Ion Research, Oak Ridge, TN. On leave from Institute of Modern Physics, Lanzhou, People's Republic of China.
5. On leave from CRN, Strasbourg, France. Present Address, GANIL, Caen, France.
6. Washington University, St. Louis, MO.
7. Texas A & M, College Station, TX.

8. S. Frauendorf and F. R. May, Phys. Lett. 125B 245 (1983).
9. J. D. Garrett and S. Frauendorf, Phys. Lett. 108B 77 (1982).
10. J. C. Waddington, S. Monaro et al., to be published.
11. S. M. Harris, Phys. Rev. B138 509 (1965).

ROTATIONAL ALIGNMENT PROCESSES IN ^{184}Pt

M. P. Carpenter[1], A. J. Larabee[1], L. L. Riedinger[2], C. R. Bingham[2], L. H. Courtney[1], S. Juutinen[1], Z.-m. Liu[1], C. Baktash, M. L. Halbert, N. R. Johnson, I. Y. Lee, Y. Schutz[3], A. Johnson[4], J. Nyberg[4], K. Honkanen[5], D. G. Sarantites[5], D. R. Haenni[6], Z.-y. Zhang[7]

The study of ^{184}Pt was carried out at the Holifield facility using a ^{154}Sm(^{34}S,4n) reaction at 163 MeV. Seven NaI counters in the Spin Spectrometer were replaced by Ge detectors, six of which were suppressed using NaI annuli. Selection of the 4n reaction channel was enhanced by setting selective gates on the total energy and total γ-ray fold observed in the Spin Spectrometer. The γ-γ coincidence data were analyzed and the yrastband was extended up to $I^{\pi} = 26^{+}$. A highly aligned side band which feeds into the yrast band at spins 14^{+} and 16^{+} was observed for the first time. The nature of this side band is not yet understood.

In Fig. 2.44, the alignment (i) is plotted versus the rotational frequency for the yrast structure of ^{184}Pt. A gentle upbend is observed starting at $\hbar\omega \approx 0.23$ MeV, with a total alignment gain of 9.7 $\hbar$. In $^{182}_{76}Os_{106}$, a sharp upbend occurring at $\hbar\omega \approx 0.25$ MeV has been attributed to the alignment of a pair of $i_{13/2}$ neutrons.[8] In $^{180}_{76}Os_{104}$, two distinct upbends are observed. The first upbend at $\hbar\omega \approx 0.26$ MeV is attributed to the alignment of a pair of $i_{13/2}$ quasineutrons and the second at $\hbar\omega \approx 0.38$ MeV to a pair of $h_{9/2}$ quasiprotons.[8] In ^{184}Pt, the upper limit of rotational frequencies observed is 0.4 MeV but only one upbend is observed.

Blocking experiments carried out on ^{185}Au (Ref. 9) and ^{185}Pt (Ref. 10) indicate that pairs of both $i_{13/2}$ quasineutrons and $h_{9/2}$ quasiprotons are involved in the upbend seen in ^{184}Pt. Alignment plots for the $\alpha = 1/2$ signatures of the $\pi h_{9/2}$ band in ^{185}Au and the $\nu i_{13/2}$ band in ^{185}Pt are also shown in Fig. 2.44. In ^{185}Pt, a sharp upbend at $\hbar\omega \approx 0.25$ MeV is seen with a total alignment gain $\Delta i = 5.1$ $\hbar$. Since the alignment of the $i_{13/2}$ quasineutrons will be blocked in ^{185}Pt, the upbend is most likely due to the alignment of a pair of $h_{9/2}$ quasiprotons. The gentle upbend observed in the $\pi h_{9/2}$ band in ^{185}Au occurs at $\hbar\omega \approx 0.32$ MeV with an alignment gain $\Delta i = 5.7$ $\hbar$. Blocking arguments, coupled with the results of Cranked Shell Model calculations, indicate that in the case of ^{185}Au, a pair of $i_{13/2}$ quasineutrons are aligning. Each of the alignment processes observed in ^{185}Pt and ^{185}Au occurs in the same frequency range as the upbend seen in ^{184}Pt and each has about half of the total alignment gain measured for ^{184}Pt. The upbend in ^{184}Pt thus appears to result from the alignment of four quasiparticles, two $h_{9/2}$ quasiprotons and two $i_{13/2}$ quasineutrons.

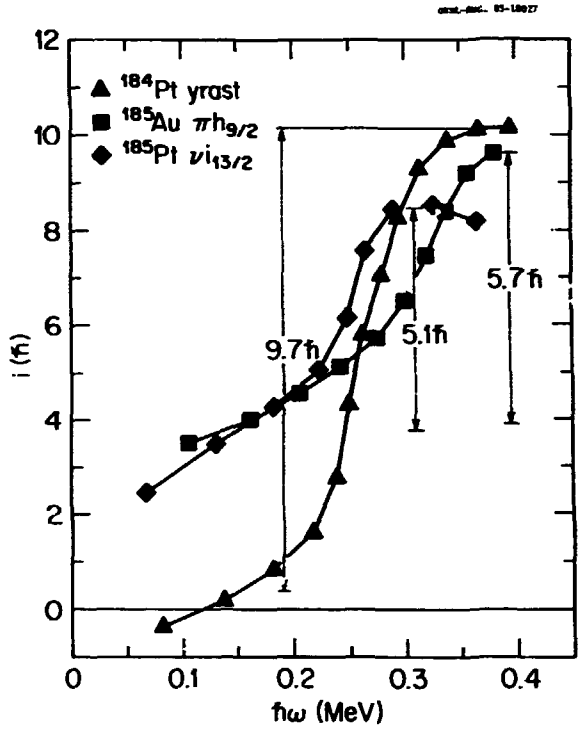

Fig. 2.44 The alignment (i) versus the rotational frequency for the yrast band in ^{184}Pt, the $\alpha = 1/2$ $\nu i_{13/2}$ band in ^{185}Pt and the $\alpha = 1/2$ $\pi h_{9/2}$ band in ^{185}Au. The reference parameters used were $\mathcal{J}_0 = 22$ $\hbar^2$ MeV^{-1} and $\mathcal{J}_1 = 110$ $\hbar^4$ MeV^{-3}.

In Fig. 2.45 a plot of the differences in crossing frequencies between the $h_{9/2}$ quasiprotons and the $i_{13/2}$ quasineutrons is shown from CSM calculations. The deformation parameters used in the CSM calculation were derived

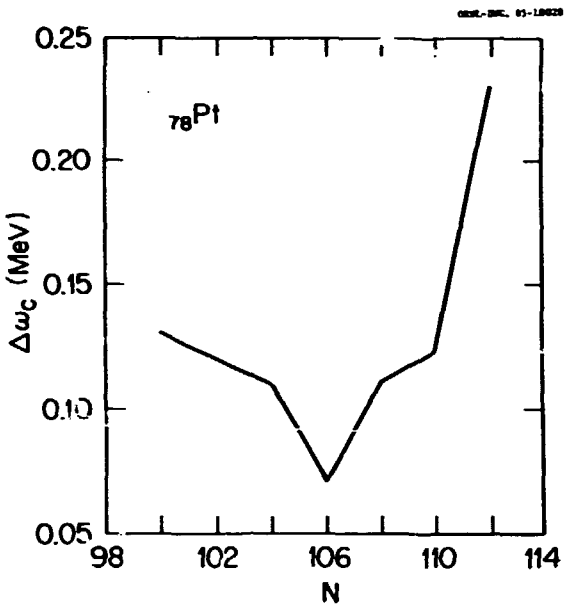

Fig. 2.45 *The difference in crossing frequencies for the proton and neutron crossings in the Pt isotopes is shown as a function of neutron number N, where* $\Delta\omega_c = \omega_c(\pi h_{9/2}$ *crossing)* $- \omega_c(\nu i_{13/2}$ *crossing). The crossing frequencies were calculated using a CSM Nilsson code with deformation parameters for each isotope taken from deformation energy minimization calculations in the* ϵ_2 *and* ϵ_4 *plane.*

from deformation energy minimization calculations using a Nilsson potential and carried out for each Pt isotope. In the CMS calculations, the $\nu i_{13/2}$ quasineutrons always align before the $\pi h_{9/2}$ quasiprotons. Even though the minimum difference in the proton and neutron crossing is calculated to be ~70 keV, it is significant that this minimum occurs for the N = 106 isotope. These calculations are therefore compatible with the experimental evidence that the proton and neutron crossings in ^{184}Pt are occurring at nearly simultaneous frequencies. Better calculations are currently being carried out which include the effect of γ-deformation on the potential energy surface minimization calculations.

---

1. University of Tennessee, Knoxville, TN.
2. Adjunct staff member from University of Tennessee, Knoxville, TN.
3. On leave from CRN, Strasbourg, France. Present address: GANIL, Caen, France.
4. Research Institute for Physics, Stockholm, Sweden.
5. Washington University, St. Louis, MO.
6. Texas A&M University, College Station, TX.
7. Joint Institute for Heavy Ion Research, Oak Ridge National Laboratory, Oak Ridge, TN 37831. On leave from Institute of Modern Physics, Lanzhou, People's Republic of China.
8. A. Neskakis, R. M. Lieder, G. Sletten and J. D. Garrett, Proceedings of the 1982 INS International Symposium on Dynamics of Nuclear Collective Motion, Pt. Fuji, 1982.
9. A. J. Larabee et al., submitted to Physics Letters B.
10. J. C. Waddington, S. Monaro et al., to be published.

A POSSIBLE NILSSON κ,μ PARAMETER SET IN THE Au-Pt REGION

Jing-ye Zhang[1] L. L. Riedinger[2]
A. J. Larabee[3]

The modified harmonic oscillator potential introduced by S. G. Nilsson et al.[4] has been extensively and successively employed in the interpretation of the single-particle motion in deformed nuclei.[5] There are two shell parameters, κ and μ, which appear in the potential

$$V = -\kappa\hbar\omega_o \{2\vec{l}_t\cdot\vec{S} + \mu (l_t^2 - \langle l_t^2\rangle_N)\}$$

where $\vec{l}_t$ is defined in stretched coordinates. As emphasized by the authors[4], the parameters κ and μ are optimized to reproduce the experimental level schemes for the rare-earth nuclei ($A \approx 165$) and the actinides ($A \approx 242$). For the other regions, the κ and μ are assumed to vary linearly with the mass number A. In order to better fit the experimental data in these regions, I. Ragnarsson et al.[6,7] assumed the parameters κ and μ to be dependent on the main oscillator quantum number N. However, such a $\kappa(N)$, $\mu(N)$ set does not fully reproduce single particle behavior in the $A \approx 187$ region as will be discussed below.

Recently, several new spectroscopic measurements for ^{185,186,187}Au and ^{183,184,185}Pt have been done, and these allow a more thorough examination of the validity of the latest set of κ and μ parameters by giving a more sensitive test of the relative positions of the different Nilsson single-particle orbits. A comparison of the data, with values calculated using the parameter set of Ref. 6, indicates that the $f_{7/2}$ orbital is too high and the $i_{13/2}$ orbital too

Table 2.9 A New Set of κ(N), μ(N) Parameters

N_{rot}	Protons		Neutrons*	
	κ	μ	κ	μ
0	.120	.00	.120	.00
1	.120	.00	.120	.00
2	.105	.00	.105	.00
3	.090	.30	.090	.25
4	.065	.57	.070	.39
5	.060	.54	.062	.43
6	.054	.52	.062	.34
7	.054	.52	.062	.26
8	.054	.52	.062	.26

* The same as described in Ref. 6.

low. On the other hand, use of the κ(N) and μ(N) values listed in Table 2.9 enables a reasonably good reproduction of the main features of the single-particle structure for nuclei in this region.

Figure 2.46 is the minimization calculation of the potential energy surface for different proton configurations in ^{185}Au (assuming γ = 0).

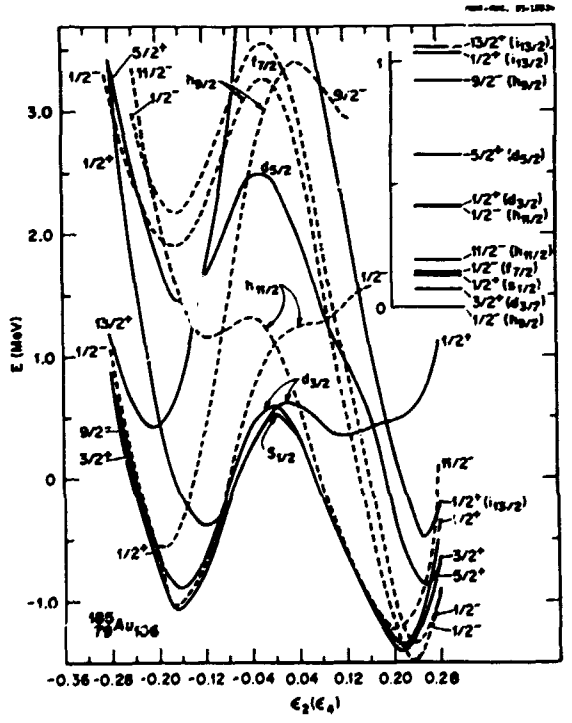

Fig. 2.46 Deformation energy curves as a function of ϵ_2 for various band heads in ^{185}Au. At every ϵ_2 the minimization was carried out for the ϵ_4 deformation parameter.

The $h_{9/2}$ [541]1/2 is found to be the ground configuration, while the $i_{13/2}$ [660]1/2 state lies ~1 MeV above the ground state. The $h_{9/2}$ proton crossing appears at $\hbar\omega_c \sim 0.255$ MeV. These are in agreement with the data.[8]

So far, ^{185}Au is the first nucleus where such a low-lying $f_{7/2}$ band structure is identified. Therefore a systematic search for the $f_{7/2}$ band in neighboring Au isotopes and Ir and Re isotopes will be critical for further testing of the single-particle model in this region. Fig. 2.47 shows the theoretical location of the $f_{7/2}$ band head in the Au isotopes using the κ(N) and μ(N) set in Table 2.9. Along with ^{185}Au, there are a few other candidates containing a low-lying $f_{7/2}$ band structure, such as ^{183}Au, ^{187}Au, ^{183}Ir (with $f_{7/2}$ band head ~ 0.257 MeV) and $^{181}_{75}$Re (with $f_{7/2}$ band head ~ 0.327 MeV). These band-head calculations are very sensitive to the κ(N) and μ(N) used. An alternative κ, μ parameter set is shown by the dashed lines in Fig. 2.47. This set also differs from the set given in Ref. 6 for the N = 5 parameters. This second set uses κ(5) = 0.065 and μ(5) = 0.52. A comparison

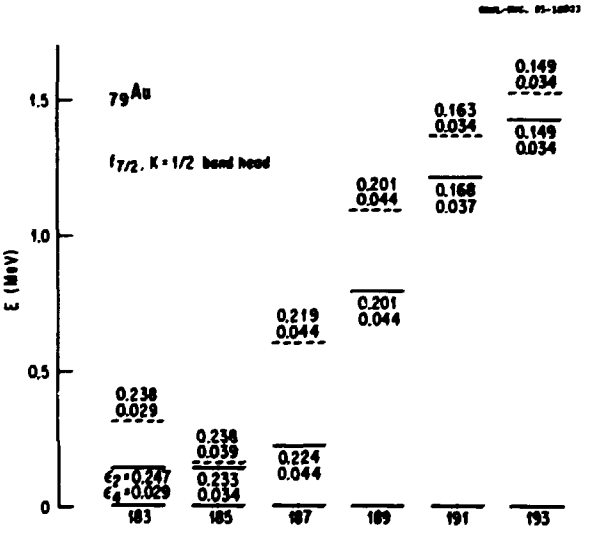

Fig. 2.47 Calculated band head energies from potential energy surface minimization calculations for the $\pi f_{7/2}$ configuration in the odd-N gold isotopes. Two different calculations are shown. The solid lines were determined using the κ(N), μ(N) Nilsson parameter set given in Table 2.7. The dashed lines use a slightly different set of parameters than those given in Table 2.9, i.e., κ(5) = 0.065 and μ(5) = 0.52.

of the results for this set compared to the set used in Table 2.9 shows very little difference in the $f_{7/2}$ band-head energy in ^{185}Au (the two results differ by only 20 keV). However, this second set results in much higher energies for the $f_{7/2}$ band-head in the neighboring odd-A gold isotopes. Information on the $f_{7/2}$ band-head in neighboring nuclei is therefore necessary in order to pin down the most valid set of κ and μ parameters. In order to get a universal κ, μ set over a wide region, it is clear one must systematically compare the theoretical and experimental results for components such as the band-head energies for different configurations and the single-particle structure of high-spin states.

The authors would like to thank R. Bengtsson, G. Leander, W. Nazarewicz, and I. Ragnarsson for helpful discussions.

1. Joint Institute for Heavy Ion Research, Oak Ridge National Laboratory, Oak Ridge, TN, 37831. On leave from Institute of Modern Physics, Lanzhou, People's Republic of China.
2. Adjunct staff member from University of Tennessee, Knoxville, TN.
3. University of Tennessee, Knoxville, TN.
4. S. G. Nilsson et al., Nucl. Phys. A131, 1 (1969).
5. A. Bohr and B. Mottelson, Nuclear Structure, Vol. II (1975), W. A. Benjamin, Inc., Reading, Massachusetts.
6. I. Ragnarsson, Future Directions in Studies of Nuclei far from Stability, Edited by J. Hamilton et al. (1980) p. 367.
7. T. Bengtsson and I. Ragnarsson, Nucl. Phys. A436 14 (1985).
8. A. J. Larabee et al., submitted to Physics Letters B.

SEARCH FOR ^{182}Tl

K. S. Toth, H. K. Carter[1], R. L. Mlekodaj[1], D. M. Moltz[2]

Levels in ^{184,186,188}Hg have been investigated[3,4] at the UNISOR facility via the decay of their thallium parents. These studies, coupled with in-beam data obtained at other laboratories, established in each of the three mercury nuclei the presence of an excited, strongly deformed band coexisting with levels built on the near spherical ground state. The 0^+ deformed band heads drop from 824 to 522 to 375 keV as one goes from ^{188}Hg to ^{184}Hg. Theoretical models predict that this deformed band should be lowest midway between N = 126 and N = 82 and that it should then go up in energy or else vanish as the neutron number decreases further. A crucial way to test these predictions is to locate the 0^+ deformed state in ^{182}Hg and ^{180}Hg.

Recent in-beam data[5] have shown the ^{182}Hg ground state to be near spherical. However, the 0^+ deformed level was not observed, indicating the necessity for an investigation of ^{182}Tl decay to levels in ^{182}Hg.

Early attempts[6] to identify ^{182}Tl by using beams from the Oak Ridge Isochronous Cyclotron, e.g., in the ^{180}W(^{14}N,12n) reaction, were unsuccessful presumably because the incident energies were too low. More recently, we bombarded ^{152}Gd with ^{35}Cl ions from the HHIRF tandem and focused on the nuclide's α-decay properties as a means of identification. A helium gas-jet system was used to transport products to a shielded area for assay with a Si(Au) surface barrier counter and a Ge(Li) detector. Mercury, gold, platinum, and other thallium nuclei were also made in reactions not only with ^{152}Gd (41.2%) but with heavier gadolinium isotopes as well. These other radioactivities were not expected to be a problem because ^{182}Tl, based on E_α systematics,[7] was anticipated to have the highest α-decay energy of any reaction product. Its α group would therefore not be obscured by other peaks.

Despite varying both the ^{35}Cl bombarding energy and the irradiation and counting time, ^{182}Tl was not seen. The explanation does not appear to be an unexpectedly low production cross section. Compound-nuclear calculations predict a peak cross section of ~ 30 mb, and the neighboring nuclide ^{184}Tl($T_{1/2}$ = 11 sec), produced in the (^{35}Cl,5n) reaction on ^{154}Gd was observed in both α-particle and γ-ray spectra. The answer seems to be that the ^{182}Tl half-life is much less than 0.5 sec, a limit set by the helium gas-jet transport time and the move time of the tape collector.

1. UNISOR, Oak Ridge Associated Universities, Oak Ridge, TN, 37830.

2. Present address: Lawrence Berkeley Laboratory, Berkeley, CA 94720.
3. J. H. Hamilton et al., Phys. Rev. Lett. 35, 562 (1975).
4. J. D. Cole et al., Phys. Rev. Lett. 37, 1185 (1976).
5. W. C. Ma et al., Phys. Lett. 139B, 276 (1984).
6. K. S. Toth et al., Phys. Div. Ann. Prog. Rept., June 1977 ORNL-5306, p. 83.
7. K. S. Toth et al., Phys. Lett. 63B, 150 (1976).

THE α-REDUCED WIDTH OF ^{194}Pb AND THE Z = 82 CLOSED SHELL

Y. A. Ellis-Akovali H. K. Carter[1]
K. S. Toth R. L. Mlekodaj[1]

We recently discussed[2] the s-wave α-reduced widths of ^{186,188,190,192}Pb. These widths were found to have a dependence on N similar to that observed for other neighboring elements, i.e., they decreased in value as the N = 126 shell was approached. However, contrary to the expectation of a shell effect on α-decay rates at Z = 82, they were larger than those of mercury isotopes with the same neutron numbers. We suggested[2] that this result could be related to a possible disappearance of the Z = 82 gap midway between N = 82 and N = 126. If correct, this suggestion implies that widths for lead nuclides with A > 192 should first come closer to and then, for larger neutron numbers, fall below mercury values.

A major difficulty in confirming this expectation arises because α-decay energies decrease with increasing N and the concomitant α branching ratios become extremely small. In fact, the α decay of ^{194}Pb has not been observed. We decided to search for the α decay of ^{194}Pb and to determine its α-branching ratio by examining its (E.C. + β^+) decay scheme in detail. Available data[3,4] list only a 204-keV transition in ^{194}Pb decay.

To this end we produced ^{194}Pb in bombardments of W with ^{16}O ions from the HHIRF tandem accelerator. Following mass separation, the isotope's decay properties were investigated. The α decay of ^{194}Pb was identified for the first time (E_α = 4.64 ± 0.02 MeV). In addition, a comprehensive β-decay scheme was constructed incorporating at least 40 γ-ray transitions. Based on this information the ^{194}Pb α-branching ratio was determined to be (1.0 ± 0.4) x 10^{-7}.

As in Ref. 2, we consider α-decay rates within the theoretical framework developed by Rasmussen.[5] A reduced width, δ^2, is defined in this formalism as $\lambda = \delta^2 P/h$ where λ is the decay constant, h is Planck's constant, and P is the penetrability factor for the α particle to tunnel through a barrier. Fig. 2.48 shows δ^2 values for ground state to ground state α transitions of even-even nuclei with Z from 78 to 100. One sees the regularity of these widths as a function of N, with the extremely sharp break at N = 126. This discontinuity has been shown to be a shell structure effect. A less pronounced minimum is seen at the N = 152 subshell. Note that while the δ^2 values for given neutron numbers decrease as Z approaches 82 those of ^{186,188,190,192}Pb are larger than neighboring Hg widths contrary to the expected shell effect at Z = 82. The ^{194}Pb width, however, is less than those of Pb, Hg, and Pt nuclei with A < 192 indicating that perhaps the Z = 82 gap is being restored for N > 112. We also show an estimated width for ^{184}Pb based on the data of Schrewe et al.[6] and on the assumption of a 100% α branch. It is appreciably smaller than those of ^{186,188,190}Pb; this may be an indication that the Z = 82 gap is also reappearing for N < 102.

1. UNISOR, Oak Ridge Associated Universities, Oak Ridge, TN, 37830.
2. K. S. Toth et al., Phys. Rev. Lett 53, 1623 (1984).
3. B. Jung and G. Anderssen, Nucl. Phys. 15, 108 (1960).
4. K. H. Hicks, et al., Phys. Rev. C 15, 2710 (1982).
5. J. O. Rasmussen, Phys. Rev. 113, 1593 (1959).
6. Schrewe et al., Phys. Lett 91B, 46 (1980).

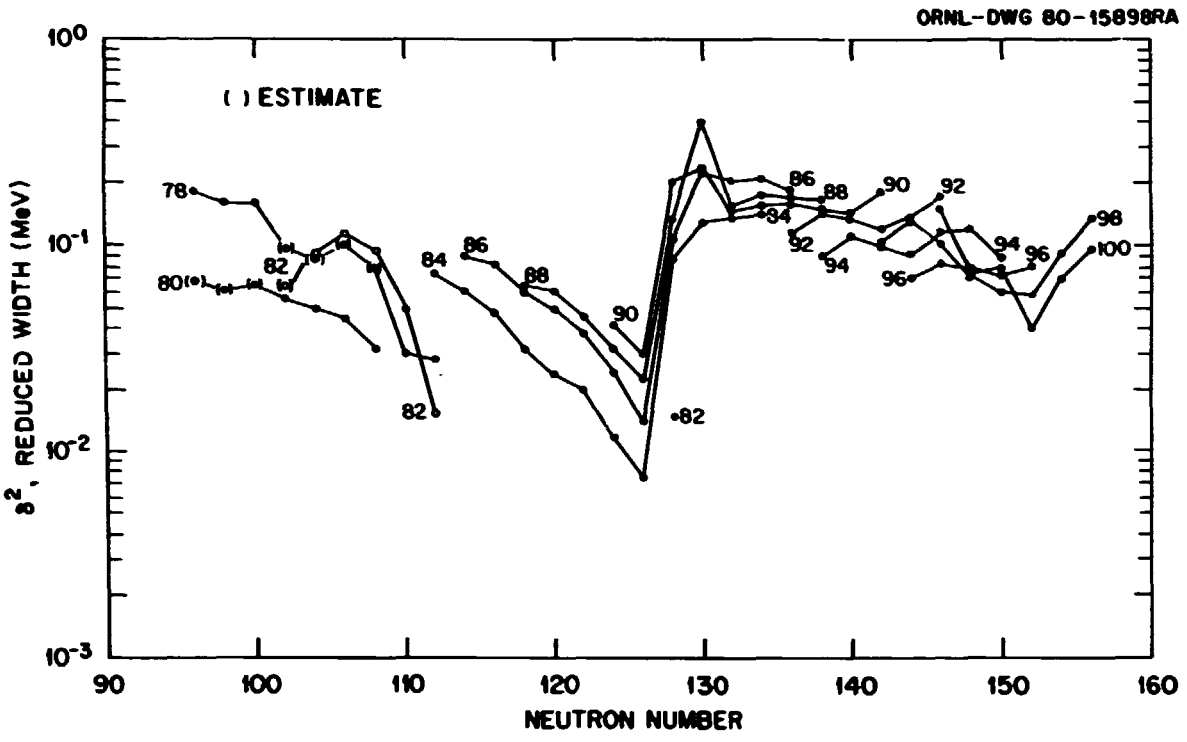

Fig. 2.48 Reduced widths for ℓ-wave α transitions plotted as a function of N for isotopes with Z from 78 to 100. Widths for Z = 82 are indicated by open points.

QUASI-ELASTIC HEAVY-ION REACTIONS

QUASIELASTIC SCATTERING OF ^{58}Ni + ^{208}Pb AT 15.7 MeV/NUCLEON

M. Beckerman[1]
E. E. Gross
R. L. Auble
F. E. Bertrand
J. L. Blankenship[2]
B. L. Burks
C. W. Glover
R. O. Sayer[3]
D. Shapira
Y. Sugiyama[4]

These measurements were undertaken to provide information on the quasielastic reactions between massive (A > 40) nuclei at energies above 10 MeV/nucleon, of which little is known. In our study, 913 MeV ^{58}Ni ions provided by coupled ORIC + tandem operation were used to bombard thin, isotopically enriched ^{208}Pb targets. Quasielastically scattered Ni^{25+}, Ni^{26+}, and Ni^{27+} ions were detected in small angular steps from far inside to well beyond the grazing angle, θ_{gr}. Unit Z and A separation and better than 1-MeV energy resolution were achieved using ΔE, TOF, $B\rho$, and E signals from the BRS focal plane detectors and a microchannel plate "start" detector.

Displayed in Fig. 2.49 are angular distributions of quasielastic events. Shown are the ratios of elastic to Rutherford cross sections, differential cross sections for the excitation of the 1.454-MeV 2^+ level in ^{58}Ni, the summed cross sections for higher-lying excitations of target and projectile, and differential cross sections for one- and two-nucleon transfer. We find considerable inelastic strength in the vicinity of 4 MeV. At angles near and beyond θ_{gr}, differential cross sections for the 1.454 MeV and higher-lying excitations are comparable. As can be seen in Fig. 2.49 the transfer yields are sharply focused near θ_{gr}. These processes have narrow angular ranges (2.9° to 3.2° FWHM) and large peak differential cross sections (~650 mb/sr for ^{59}Ni). The angle and energy integrated cross sections for neutron transfer are compared in Table 2.10 to values deduced by Rehm et al.[5] from measurements at 375 MeV. We see that the cross section for one neutron

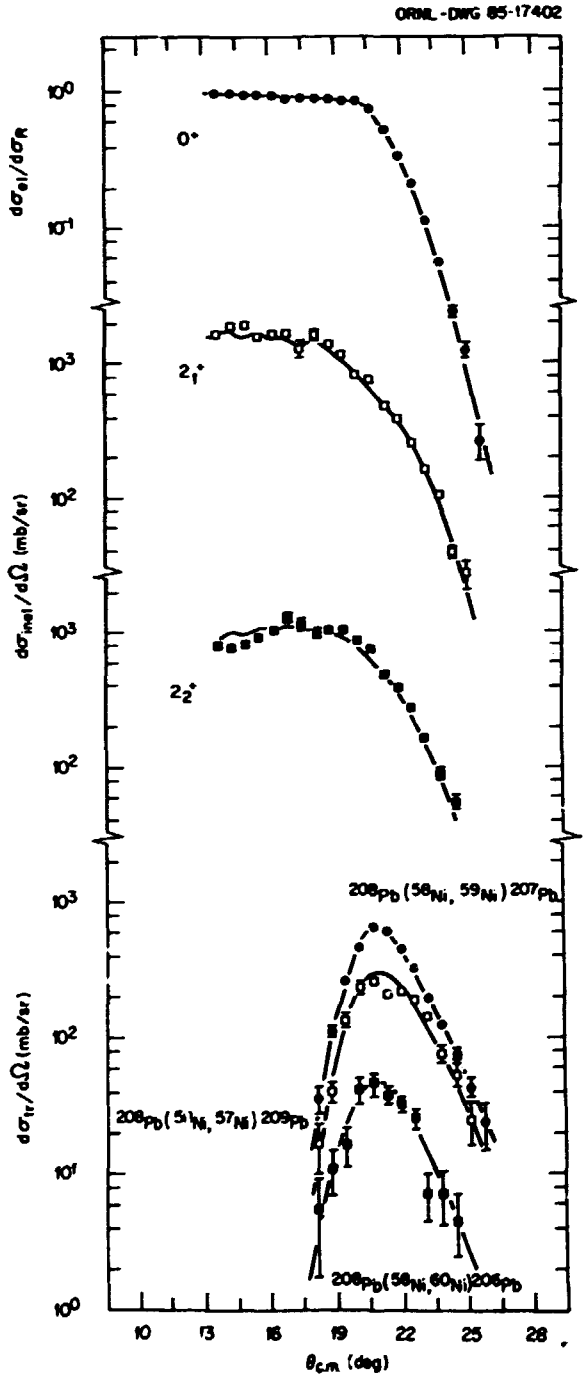

Fig. 2.49. Plots of quasielastic cross sections. Experimental results are preliminary. Final corrections to the data due to hit VDC wires have not been applied. The higher lying inelastic strength was treated in the coupled-channel calculations by placing an effective (fictitious) 2_2^+ level at an excitation of 3.0 MeV. Smooth curves through the transfer data are visual guides.

Table 2.10. Total cross sections for neutron transfer. The results at 913 MeV are for excitations from 0 to 15 MeV.

Reaction	$Q_{g.s.}$ (MeV)	σ_{tr} (mb) 913 MeV	375 MeV
$^{208}Pb(^{58}Ni,^{59}Ni)^{207}Pb$	+1.6	85	265
$^{208}Pb(^{58}Ni,^{60}Ni)^{206}Pb$	+6.3	6	61
$^{208}Pb(^{58}Ni,^{57}Ni)^{209}Pb$	-8.3	41	~10

pickup decreases by a factor of 3 in going from 375 to 913 MeV while the corresponding cross section for one neutron stripping increases by a factor of 4. The cross section for two-neutron pickup is only 6 mb at 913 MeV, declining by an order of magnitude from the value at 375 MeV.

DWBA and coupled-channel analyses of the transfer data are in progress. Results of a coupled-channel analysis of the elastic and inelastic data are presented in Fig. 2.49. The optical potential deduced in the analysis was $V = 27.7$ MeV, $W = 38.8$ MeV, $r_0 = 1.21$ fm, $r_{0I} = 1.16$ fm, $a = 0.934$ fm, and $a_I = 0.896$ fm. The deduced β_2 for the 1.454-MeV 2^+ level was $\beta_2 = 0.173$; the effective β_2 describing the higher-lying excitations was $\beta_2 = 0.170$. The total reaction cross section was found to be 5.56b. Upon subtracting inelastic scattering cross sections of 619 mb and 356 mb from the total reaction cross section we end up with a reaction cross section of 4.59b, in close agreement with the value of 4.48b deduced from a quarter-point analysis of the elastic data.

1. Joint Institute for Heavy Ion Research, ORNL, Oak Ridge, TN 37831.
2. Instrumentation and Controls Division, ORNL.
3. Computing and Telecommunications Division, ORNL.
4. Japan Atomic Energy Research Institute, Tokai Research Establishment, Tokai-mura, Naka-gun, Ibaraki-ken, Japan.
5. K. E. Rehm et al., Phys. Rev. Lett. 51, 1426 (1983).

HEAD-ON SCATTERING AT LOW ENERGIES

H. J. Kim
M. Beckerman[1]
B. A. Harmon[2]
D. Shapira
P. H. Stelson

Studies of fusion between Ti isotopes and Nb and Zr targets near and below the Coulomb barrier have shown marked differences in the magnitude and the energy dependence of the measured fusion cross sections.[3] Attempts at explaining these differences with the standard models which combine one-dimensional barrier penetration with inelastic scattering and nucleon transfer at long range have produced some success.[4]

As a step toward understanding the differences mentioned above, a survey study of other processes that occur at relatively large internuclear separation of colliding medium heavy ions was initiated. The study involves measurement of reaction products emitted at forward angles from nuclear collision at energies below and near the Coulomb barrier. The yield of target-like ejectiles resulting from the ^{46}Ti projectiles on ^{90}Zr and ^{93}Nb at energies ranging from 150 to 166 MeV was investigated in this initial study. We used the velocity filter to separate the ejectiles from the beam around 0°. Results from our initial measurement show that at subbarrier energies, nuclear collisions are complex. Long-range Coulomb excitations and nucleon-transfer reactions may not be the only significant processes besides the fusion at subbarrier energies. We observe target-like products emitted near 0° with energy losses as large as 35 MeV and also the transfer of substantial amounts of charge between the projectile and target.

---

1. Joint Institute for Heavy Ion Research, Oak Ridge, TN 37831.
2. University of Virginia, Charlottesville, VA 22901.
3. Phys. Div. Prog. Rep. for Period Ending Sept. 30, 1984, ORNL-6120, p. 69.
4. P. H. Stelson et al., "Fusion Cross Sections for Beams of ^{46,50}Ti on Targets ^{90}Zr and ^{93}Nb," this chapter.

NUCLEAR STRUCTURE AND BOMBARDING ENERGY DEPENDENCE OF QUASIELASTIC SCATTERING

M. Beckerman[1]
R. L. Auble
F. E. Bertrand
J. L. Blankenship[2]
B. L. Burks
C. W. Glover
R. O. Sayer[3]
D. Shapira
R. L. Varner

In order to probe the nuclear processes characteristic of two massive atomic nuclei in weak contact, quasielastic scattering yields were measured for the ^{58}Ni + ^{208}Pb system at several bombarding energies from 600 to 1011 MeV (10.3 to 17.4 MeV/nucleon). As in our previous study at 913 MeV, elastic, inelastic, and transfer components were completely resolved using the ORNL Broad Range Spectrograph plus a microchannel plate "start" detector.

Spectra for the one-neutron pickup reaction ^{208}Pb(^{58}Ni,^{59}Ni)^{207}Pb taken at bombarding energies of 600 and 1011 MeV are displayed in Fig. 2.50. The energy resolution achieved in the measurements was 600 to 700 keV. With this resolution we observe that there are two distinct structures in the spectra. First, there is a fairly narrow peak located at a low energy near the ground state. Second, there is a large, broad structure centered at an excitation of some 7 MeV. Previous studies of quasielastic transfer in the ^{58}Ni + ^{208}Pb system at 375 MeV[4] and in the ^{86}Kr + ^{208}Pb system at 695 MeV[5] carried out with lower energy resolution gave no indication for structure in the one-neutron pickup spectra. We observe in Fig. 2.50 that the spectral shape is remarkably stable as a function of bombarding energy. The main difference between 600- and 1011-MeV spectra is a mild shift in the relative population of the two structures.

A typical spectrum for the two-neutron pickup reaction ^{208}Pb(^{58}Ni,^{60}Ni)^{206}Pb at 1011 MeV is shown in Fig. 2.51. In contrast to the one-neutron pickup spectra, the two-neutron pickup spectrum does not exhibit evidence for substantial strength in the vicinity of the ground state. Instead, there is a single broad structure centered at an excitation energy of

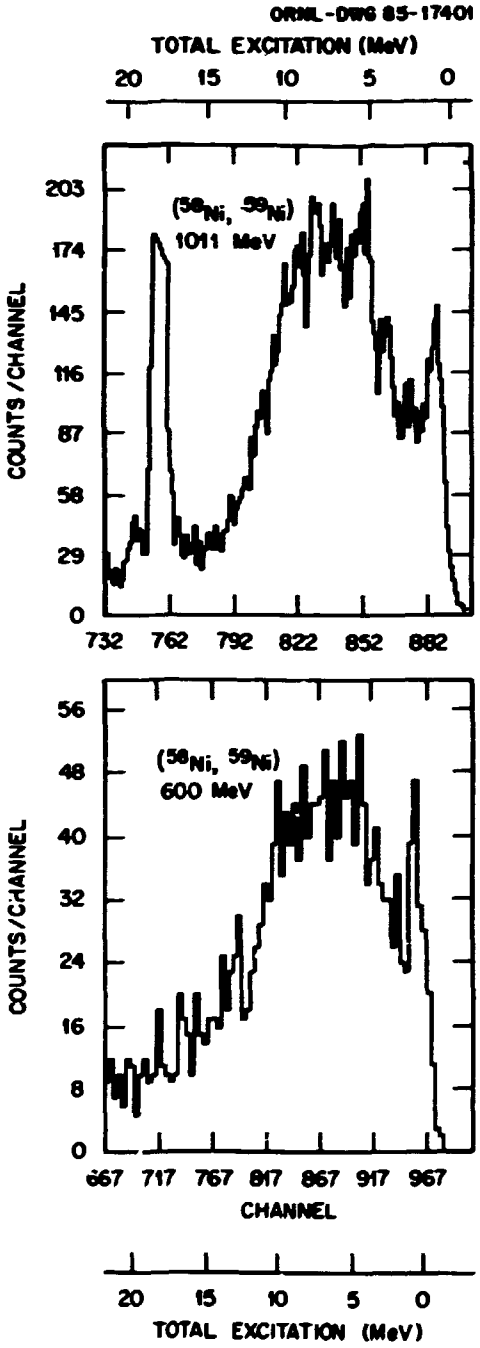

Fig. 2.50. Energy spectra for the one-neutron pickup reaction $^{208}Pb(^{58}Ni,^{59}Ni)^{207}Pb$. Upper portion: Spectrum at a bombarding energy of 1011 MeV for θ_{lab} = 14°. Lower portion: Spectrum at a bombarding energy of 600 MeV for θ_{lab} = 32°. The peak in the 1011-MeV spectrum near channel number 760 is due to elastic scattering.

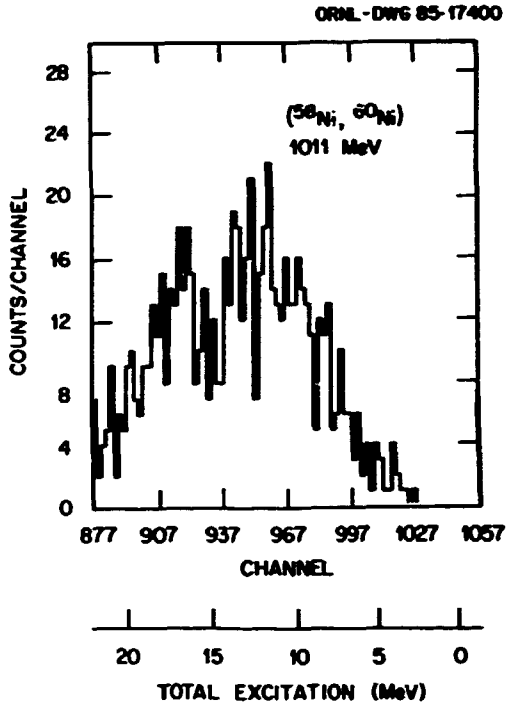

Fig. 2.51. Energy spectrum for the two-neutron pickup reaction $^{208}Pb(^{58}Ni,^{60}Ni)^{206}Pb$ for θ_{lab} = 14°.

approximately 12 MeV. We observe in all reaction channels that there is transfer to unbound levels. This process appears in the appropriate transfer spectra as broad structures at high (>30 MeV) excitation. In the two-neutron pickup reaction the strength seen in these channels is comparable to that observed at the lower excitations.

---

1. Joint Institute for Heavy Ion Research, ORNL, Oak Ridge, TN 37831.
2. Instrumentation and Controls Division, ORNL.
3. Computing and Telecommunications Division, ORNL.

4. K. E. Rehm et al., Phys. Rev. Lett. 51, 1426 (1983).
5. A. J. Baltz et al., Phys. Rev. C 29, 2392 (1984); H. Sohlbach et al., Phys. Lett. 153B, 386 (1985).

MULTIPARTICLE HEAVY-ION TRANSFER AND THE TRANSITION FROM QUASIELASTIC TO DEEP INELASTIC REACTIONS

S. Juutinen[1] D. Cline[2]
S. Sorensen[1] W. Kernan[2]
X. T. Liu[1] M. L. Halbert
M. W. Guidry[2] C. Baktash
I. Y. Lee

Rather little is known about the detailed evolution of the reaction mechanism from single nucleon transfer through multinucleon transfer to deep inelastic scattering (DIS), although both extremes, one or two neutron transfer and DIS, have been studied with heavy ions by many groups. Some aspects of multinucleon transfer have been illuminated by H. Sieckman et al.,[b] who studied reactions of ^{86}Sr with ^{88}Sr, ^{90}Zr and ^{92}Mo.

In the present work we have used particle particle - γ coincidence methods to study transfer reactions with a ^{58}Ni beam and ^{161,162}Dy targets with bombarding energies near (E_{LAB} = 270, 285 MeV) and above (345 MeV) the Coulomb barrier. The ORNL Spin Spectrometer was used to measure total γ-ray energies and multiplicities and to give approximate neutron multiplicities. Some of the Na(I) detectors in the ball were replaced by high resolution Compton-suppressed Ge-detectors. Scattered particles were observed with parallel plate avalanche detectors, which gave the scattering angles for the scattered ions and the time difference between beam-like and projectile-like ions in the counters.

From scattering angles measured in the experiment it was possible to calculate the momenta of the reaction fragments. Using the measured time difference ΔT we calculated low-resolution masses for the reaction fragments. Once the fragments were identified, A = 58 was assumed for the lighter fragment and A = 161 or 162 for heavier fragment because of the poor mass resolution. Scattering angle information and the calculated velocities of the reaction fragments were used to give Doppler shift corrections for the emitted γ-rays for discrete transitions in Ge-detectors and Na(I) detectors. Knowing masses and moments for the Dy-like and Ni-like fragment, one obtains approximate Q-value for the reaction. The full width half maximum of the Q-value spectrum for the inelastic excitation (Q = 0) is about 30 MeV, which gives an estimate for Q-resolution. The poor resolution is mostly due to poor (~2 degrees) resolution in particle counters. Good timing properties of the particle detectors allowed us to get a reliable T_0 for an event, which in turn gave a good neutron-gamma separation in the Spin Spectrometer.

At first glance ^{58}Ni + ^{161,162}Dy γ-ray spectra look very simple: strong inelastic scattering and somewhat weaker 1n and 2n transfer seem to be the only discrete-line reaction channels. Inelastic scattering is concentrated near the origin in the γ-ray fold (K) and total γ-ray energy (H) map, while 1n and 2n transfer reactions are associated with $\langle K \rangle$ = 5 and $\langle H \rangle$ = 3-5 MeV. However, we can find many other reaction channels from the data by setting gates on Q value, K, H, or neutron fold. As an example, an "ungated" Ge-spectrum and a spectrum which is optimized for these weak reaction channels integrated over the scattering angles from 40 to 62 degrees for the Dy-like fragment at E_{LAB} = 345 MeV is shown in Fig. 2.52. Comparing neutron energies and intensities in the latter spectrum with known level schemes of nuclei around the targets ^{161,162}Dy, we have found that γ-ray spectra can be explained by assuming reactions that populate high spin states in $^{156-158}$Dy and $^{158-164}$Er. Similar nuclei seem to be populated in ^{58}Ni + ^{162}Dy at E = 285 MeV and in ^{58}Ni+ ^{161}Dy at E = 270 MeV.

In the γ-ray spectrum of the ^{58}Ni+ ^{162}Dy reaction at E = 345 MeV, the background is much higher than at 285 MeV, a behavior which has an explanation in deep inelastic scattering. DIS is a weak reaction channel at bombarding energies near the Coulomb barrier, but becomes stronger at higher bombarding energies.

Based on potential energy surface calculations we would expect that, in reactions where charge is transfered, there would be a charge flow from Ni to Dy and a neutron flow in the opposite direction. Ground state Q-values favor

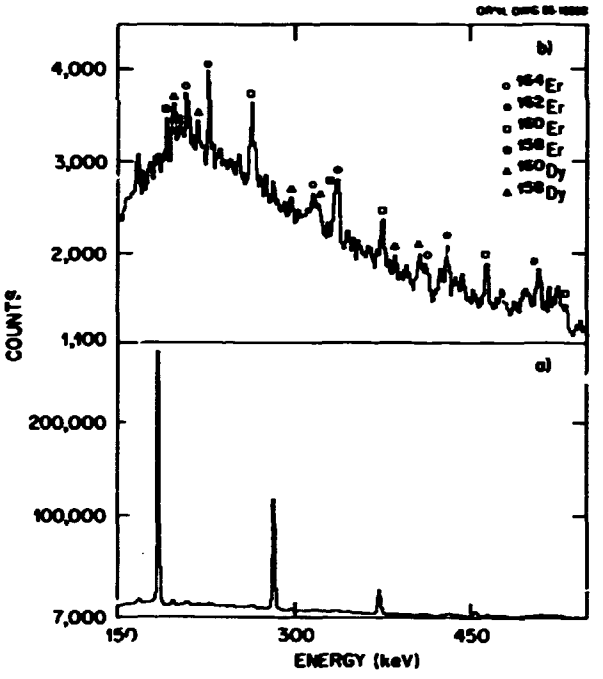

Fig. 2.52 Ungated (b) γ-ray spectrum and spectrum gated (a) to optimize multiparticle transfer in the ^{58}Ni + ^{162}Dy reaction at 345 MeV.

population several MeV above the yrast line in Er isotopes and reactions to nuclei that have larger neutron number than the target nuclei are unfavored, which is in good agreement with experiment.

Reaction channels that populate $^{156-158}$Dy and $^{158-164}$Er are, in general, weaker than 1n and 2n transfer channels in the ^{161}Dy and ^{162}Dy data. In the ^{58}Ni+ ^{162}Dy reaction at E = 285-MeV, the strongest transitions belonging to Er nuclei are about 20% of the intensity of the $4^+ \rightarrow 2^+$ transition in ^{160}Dy, while at 345-MeV bombarding energy Er transitions are only slightly weaker than the ^{160}Dy transition.

We have compared reactions populating $^{156-158}$Dy and $^{158-164}$Er with 1 or 2n-transfer and DIS. The results of the comparison are summarized in Table 2.11. A clear evolution from inelastic excitation to DIS is seen in the data. Reactions populating $^{156-158}$Dy and $^{158-164}$Er seem to have a different character at bombarding energies near the Coulomb barrier than somewhat above the Coulomb barrier. It is obvious that γ-ray fold, total γ-ray energy, and neutron fold increase when more and more nucleons are transferred, and that reactions at 345-MeV are hotter than at 285-MeV bombarding energy. At 285-MeV bombarding energy, reactions that populate $^{156-158}$Dy and $^{158-164}$Er seem to be mostly direct transfer with some neutron evaporation, while at 345-MeV, neutron evaporation is associated with almost every event.

A difference in the reaction mechanism for the multinucleon transfer between two bombarding energies is also seen in the scattering angle spectra of the Ni-like fragments, as presented in Fig. 2.53. At a bombarding energy near the Coulomb barrier the multinucleon transfer scattering angle distribution is similar to that of 2n transfer. At 345-MeV bombarding energy the

Table 2.11 Average Q Values $\langle Q \rangle$, neutron multiplicities $\langle K_N \rangle$, γ-ray folds $\langle K_G \rangle$ and total γ-ray energies $\langle H \rangle$ for different reaction channels in the ^{58}Ni+ ^{162}Dy reaction.

FINAL	^{58}Ni+ ^{162}Dy E=285 MeV				^{58}Ni+ ^{162}Dy E=345 MeV			
NUCLEUS	$\langle Q \rangle$/MeV	$\langle K_N \rangle$	$\langle K_G \rangle$	$\langle H \rangle$/MeV	$\langle Q \rangle$/MeV	$\langle K_N \rangle$	$\langle K_G \rangle$	$\langle H \rangle$
^{160}Dy	~0	0.2	6	5	~0	0.3	6	5
^{158}Dy	~0	0.4	6	5	-6	0.7	8	5
^{164}Er	-10	0.4	6	6	-30	1.3	8	8
^{162}Er	-20	0.7	8	7	-33	1.6	9	8
^{160}Er	-25	1.1	9	7	-50	2.2	11	10
^{158}Er	-	-	-	-	-60	3.9	12	13
DIS	-	-	-	-	<-40	3.8	13	11

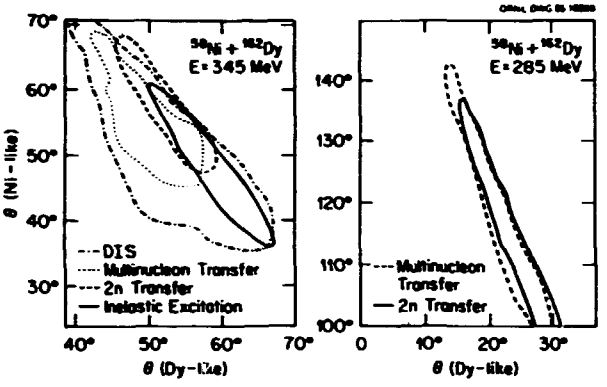

Fig. 2.53 Scattering angles of projectile-like vs target-like fragments in various reaction channels.

situation is rather different. The scattering angle of the Ni-like fragment moves forward when going from 2n-tranfer to multinucleon transfer and DIS, which represents a process where target and projectile begin to touch each other and rotate together more and more.

In conclusion, we have demonstrated the ability of particle-particle-γ coincidence methods to study multinucleon transfer reactions. For bombarding energies near the Coulomb barrier, multinucleon transfer seems to follow the Rutherford trajectory, while with bombarding energies about 20% above the Coulomb barrier multinucleon transfer resembles more DIS than 1 or 2n transfer reaction.

---

1. University of Tennessee, Knoxville, TN.
2. Adjunct staff member from University of Tennessee, Knoxville, TN.
3. University of Rochester, Rochester, NY.
4. H. Siekmann, et al., Z. Phys. A307, 113 1982).

COMPARISON OF PAIRING ENHANCEMENT FOR TWO-PARTICLE TRANSFER USING Sn AND Ni PROJECTILES

X. T. Liu[1] I. Y. Lee
M. W. Guidry[2] C. Baktash
S. Juutinen[1] M. L. Halbert
C. R. Bingham[2] D. Cline[3]
R. W. Kincaid[1] C. Y. Wu[3]
M. P. Carpenter[1] W. Kernan[3]
A. Larabee[1] E. Vogt[3]

Two-particle transfer reactions offer the possibility of studying pairing correlations. In the (t,p) or (p,t) reaction on "superfluid" nuclei the transfer rates are enhanced by ~ 50 over uncorrelated single particle rates, and the enhancement is ascribed to coherent pairing effects. In a heavy-ion collision it is possible for both collision partners to be superfluid, and considerably more dramatic effects may be expected.

Such effects are often discussed in terms of an "enhancement factor" which is generally of the form $F \sim P_2/(P_1)^2$, where P_2 is the probability for 2-particle transfer and P_1 is the probability for 1-particle transfer. Although appreciable enhancement has been observed in some experiments (e.g. Ref. 4), no experiment has demonstrated a definitive mechanism for that enhancement. In the absence of information about the spin and energy of states populated in transfer, it is difficult to decide whether a given enhancement occurs because of collective pair fields. Large 2-particle cross section might occur, not because of pairing, but because of enhanced tunneling of quasiparticles. This tunneling could be due to some combination of excitation before transfer and to a large density of 2QP states which satisfy kinematic constraints in the reaction. Inclusive cross-section measurements thus cannot distinguish the enhancement because of pairing from other sources. Von Oertzen has discussed this problem in some detail.[4]

We suggest that a minimal requirement is a measurement which distinguishes quasi-elastic from deep inelastic processes and which gives (1) the energy of states populated in the transfer, and (2) the angular momentum of states populated in the transfer. The measurement of total energy and multiplicity in transfer reactions is the key to resolving this problem.

A series of experiments of 2-neutron transfer reactions at near-barrier energies for deformed nuclei has been performed in the Spin Spectrometer for $^{162}Dy(^{58}Ni, ^{60}Ni)^{160}Dy$ E_{LAB} = 285 MeV, $^{162}Dy(^{58}Ni, ^{60}Ni)^{160}Dy$ E_{LAB} = 345 MeV, $^{162}Dy(^{116}Sn, ^{118}Sn)^{160}Dy$ E_{LAB} = 637 MeV, and $^{164}Dy(^{116}Sn, ^{118}Sn)^{160}Dy$ E_{LAB} = 637 MeV. The general experimental method is described in a separate contribution[5] to this progress report.

Figure 2.54 shows the total energy and multiplicity plots for the reaction ^{162}Dy(^{58}Ni, ^{60}Ni) ^{160}Dy, and ^{162}Dy(^{116}Sn, ^{118}Sn)^{160}Dy. An approximate ^{160}Dy yrast line that assumes no excitation of ^{58}Ni and ^{116}Sn is shown. The distributions of both cases are concentrated near the yrast line. This population pattern provides direct evidence for a cold mechanism giving large cross sections for transfer. This cold transfer mechanism is obviously significant for using these distributions as a tool to study pairing correlation. The transfer energy and multiplicity distributions appear to have two maxima. The lower part corresponds to the ground band of the Dy daughter and is the portion of the cross section which is most sensitive to pairing correlation. The upper part corresponds to population of the 2-quasiparticle (2QP) bands, and is much less dependent on the pairing. Thus, the ratio of the ground band and 2QP band populations contains information about pairing correlation.

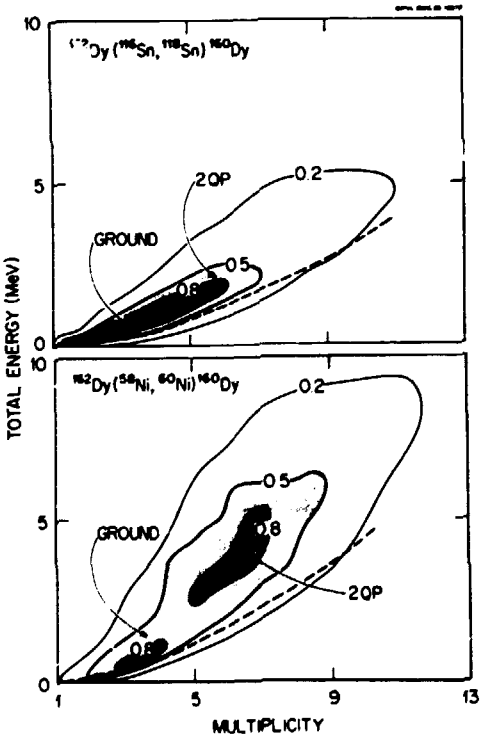

Fig. 2.54 Comparison of total energy vs multiplicity for the two-particle transfer reaction ^{162}Dy + ^{160}Dy induced by 285 MeV ^{58}Ni and 683-MeV ^{116}Sn projectiles. The results are based on a partial data analysis and are not yet fully corrected for Spin Spectrometer response.

In the Sn case the relative population of the region that we interpret as the ground band is considerably enhanced relative to the 2QP region when compared to the Ni case. In light of the preceding discussion, a possible interpretation presents itself. The Sn projectile is expected to have stronger pairing correlation than the Ni projectile. Thus, the enhancement of the ground band transition in the Sn reaction at the expense of 2QP transitions could be a measure of the pairing enhancement of the 2-Neutron transfer. However, kinematical factors also play important roles for these two reactions. These factors are at least partially responsible for the differences between the Ni and Sn data of Fig. 2.54. This is primarily because the ground-ground Q is 5.7 MeV for Ni reaction and 1.7 MeV for the Sn reaction. Preliminary estimates indicate that a factor of 2-3 for the 2QP-to-ground-band ratios could come from pure Q-window effects when comparing the Ni and Sn data. Thus, at this intermediate stage of analysis we believe that there is not much evidence for strong pairing enhancement in going from Ni to Sn projectiles. This estimate of relative pairing enhancement will be made more quantitative with completion of the energy window calculations such as those discussed in Ref. 6.

---

1. University of Tennessee, Knoxville, TN.
2. Adjunct staff member from University of Tennessee, Knoxville, TN.
3. University of Rochester, Rochester, NY.
4. W. Von Oertzen, et al., Z. Phys. A313, 189 (1983).
5. S. Juutinen, et al., this section.
6. R. W. Kincaid, et al., this section.

PARTICLE BOUND EXCITED STATE YIELDS PRODUCED IN THE REACTION: 181-MeV ^{19}F + ^{159}Tb

L. G. Sobotka[1]
H. Puchta[1]
M. Jääskeläinen[1]
M. L. Halbert
J. R. Beene
D. C. Hensley
D. G. Sarantites[1]
F. A. Dilmanian[1]
R. Woodward[1]
J. H. Barker
R. L. Ferguson
G. R. Young

The extent of sequential decay of projectile-like fragments in heavy ion reactions is a facet

of the more general question of the excitation energy imparted to the projectile-like fragment in the primary interaction. Recently, a great deal of effort has focused on the population of particle unbound levels. We have studied the complementary issue of the population of particle-bound levels. We have directly measured the bound excited state population for projectile-like fragments produced in the reaction 9.5-MeV/nucleon $^{19}F + ^{159}Tb$.

A 181-MeV ^{19}F beam was obtained from the HHIRF facility. The ^{159}Tb target was installed at the center of the Spin Spectrometer which served as the γ-ray detector. Inside the spectrometer were 11 silicon counter telescopes, positioned from 15° to 150°. The telescopes at 20°, 30°, 40°, and 50° provided data on heavy ions from Li to Mg. However, only the 20° and 30° telescopes yielded isotope resolution and therefore only these data will be presented here. A brief report of this experiment has appeared previously.[2]

The data analysis can be divided into two steps. In the first step neutron pulses in the NaIs are removed and the gamma ray pulse heights are corrected for the Doppler shift of the detected projectile-like fragment. The separation of neutrons from gamma-rays is done by setting a prompt gate on the time difference between a NaI pulse and the mean time of the gamma flash. These corrections are done on an event-by-event basis. The second step involves correcting the integrated intensity of a given transition for the detection efficiency. These efficiencies are determined by interpolation from the calibration response functions. These response functions were obtained from both γ-ray sources and proton inelastic scattering. Gamma-ray sources spanned the energy region from 136 keV to 2.75 MeV and additional points at 4.4, 6.1, and 15.1 MeV were obtained from proton inelastic scattering on C and mylar.

Figure 2.55 shows the observed gamma-ray structures in coincidence with carbon isotopes. This figure displays the difficulties in extracting yields of individual excited states for some isotopes. In the case of ^{12}C, with

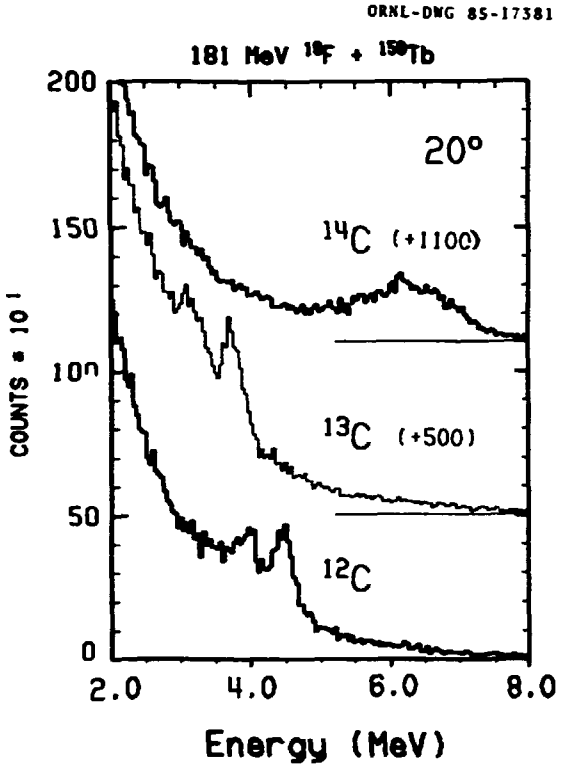

Fig. 2.55. Gamma-ray spectra in coincidence with carbon isotopes detected at 20°. A Doppler correction has been applied to the observed pulse heights, see text.

only one bound excited state, there is no difficulty in extracting the intensity of the 4.4-MeV transition. However, for ^{13}C the prominent structure at 3.8 MeV undoubtedly contains contributions from the decays of both the 3.68- and 3.85-MeV levels. Furthermore, the single escape peaks of the gamma rays from these levels are not resolved from the gamma transition from the first excited state in ^{13}C (3.09 MeV). In the case of ^{14}C a broad intense structure is observed at approximately 6 MeV. This structure can be explained by mixture of the deexcitations of all of the bound levels of ^{14}C (6 levels between 6.0 and 7.4 MeV). In our analysis we consider the population of unresolved transitions jointly. However, we use the response functions to extract the intensities of transitions which are unresolved from the single escape peak of another.

The energy spectra of selected isotopes are shown in Fig 2.56a (top). The dependence of the

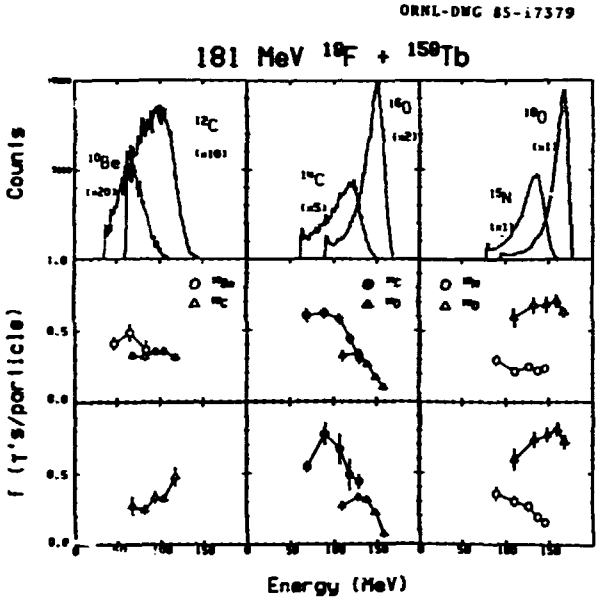

Fig. 2.56. Energy dependence of gamma ray yield. The particle energy spectra at $\theta_L = 20°$ are shown in (a). The gamma ray fractions (f = γ's/particle) for selected gamma ray structures are shown in (b) for k > 2. Bottom panel (c), requires $k > k_{avg}$.

number of gamma rays per particle (f) is shown in the bottom sections of this figure. Figure 2.56b includes all data with gamma-ray fold (k) greater than 2, while Fig. 2.56c selects $k > k_{avg}$. The magnitude of the fractions for all observed transitions range from a 2.5% to as much as 66%. The fractions for most of the γ rays do not exhibit any dependence on particle energy. On the other hand, the fractions from ^{14}C and ^{16}O (closed symbols) exhibit a strong dependence on particle energy. For these isotopes the population of excited states increases as the particle energy decreases. This trend continues to energies significantly lower than the most probable particle kinetic energy. However, for the smallest particle energies the excited state populations seem to level off.

The gamma ray fractions determined in this work are significantly larger than those determined for fragments in the reactions: 35-MeV/nucleon ^{14}N + Ag (Ref. 3) and 20-MeV/nucleon ^{14}N + ^{164}Dy (Ref. 4). This difference could be explained by a substantial increase of sequential particle decay, with preference for the ground state of the residual, with bombarding energy. This explanation is supported on one hand by the plastic box study of 11-MeV/nucleon Ne + Au (Ref. 5) which indicates a 90% survival of primary fragments, and on the other hand by the discrete gamma (target-like fragment) light fragment coincidence work for the system 20-MeV/nucleon ^{14}N + ^{164}Dy, which indicates that only 2% of the carbon isotopes originate in binary reactions.

Another difference between our results and those obtained from the higher energy experiments is our observation of a strong dependence of the excited state fraction with particle kinetic energy for certain isotopes (Fig. 2.56b, c).

This suggests that in our experiment ^{16}O and ^{14}C are predominant primary. In this case the sum of the excitation energies of the two exit channel fragments increases with decreasing kinetic energy of the detected fragment. Since the light fragment will get some fraction of the available excitation energy the excited state populations should increase with decreasing particle energy.

---

1. Washington University, Department of Chemistry, St. Louis, MO 63130.
2. M. L. Halbert et al., Physica Scripta T5, 91 (1983).
3. D. J. Morrissey et al., Phys. Rev. C 32, 877 (1985).
4. K. Siwek-Wilczynska et al., MSU Preprint, submitted to Physical Review C.
5. S. Wald et al., Phys. Rev. C 32, 894 (1985).

EXCITATION ENERGY DIVISION IN QUASI-ELASTIC TRANSFER REACTIONS

S. P. Sorensen[1]

The problem of how the total excitation energy created in a heavy-ion collision is shared between the two emerging fragments has recently received considerable attention. In strongly damped collisions it has been demonstrated that thermal equilibrium has been reached (excitation energy proportional to fragment mass),[2,3] but for partially damped collisions recent experiments[4,5] have shown that

the excitation energy is shared nearly equally, even for very asymmetric exit channels. In order to get a better understanding of this difference, the excitation energy division in quasi-elastic direct-transfer reactions has been studied.

In contrast to strongly damped collisions, where a neck has developed between the two fragments, the single-particle potential at the distance of closest approach will have a barrier between the two nuclei in the case of quasi-elastic collisions. In Fig. 2.57 are shown schematically two different transfer transitions between the donor nucleus and the acceptor nucleus. Both transitions have the same Q value so that the total excitation energy in the exit channel will be the same. In transition I the nucleon is picked up from the Fermi level in the donor and transferred to a highly excited state in the acceptor; whereas in transition II the nucleon is transferred to the Fermi level of the acceptor by creating a deep-lying hole state in the donor. In transition I all excitation energy will be deposited in the acceptor, while in transition II it will be deposited in the donor. If the transition probabilities I and II are identical, the excitation energy will, on the average, be shared equally.

However, since transition I is between states at higher single-particle energy than transition II, the barrier penetrability will be larger for I than for II. As a consequence, the acceptor nucleus will, on the average, receive most of the excitation energy. If several nucleons are exchanged in both directions, the excitation energy will be shared equally, but in situations where there is a net drift of nucleons in one direction the donor nucleus will remain "cold" while the acceptor will become "hot."

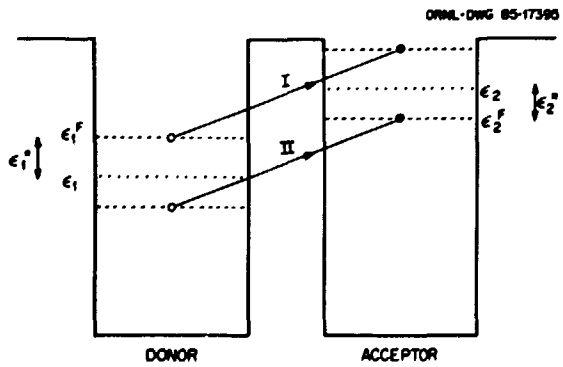

Fig. 2.57. Schematic drawing of the single-particle potential in a nucleus-nucleus grazing collision. ϵ_1 and ϵ_2 are the single-particle energies and ϵ_1^F and ϵ_2^F are the Fermi energies in the donor and the acceptor, respectively.

In order to estimate the magnitude of this effect, a recent semiclassical model for transfer probabilities by Lo Monaco and Brink[6] has been used to derive the following expression for the average excitation energy in the acceptor nucleus:

$$\frac{\langle\epsilon_2^*\rangle}{\epsilon^*} = \frac{1}{1 - e^{-\beta\epsilon^*}} - \frac{1}{\beta\epsilon^*} .$$

Here ϵ^* is the total excitation energy, and β is given by:

$$\beta = \frac{d}{\hbar}\sqrt{\frac{m}{2\epsilon_0}} ,$$

where

$$\epsilon_0 = \frac{1}{\epsilon_r}\,\frac{(Q - \epsilon_r)^2}{2} - \epsilon_2^F .$$

ϵ_r is the kinetic energy per nucleon at the barrier; d is the nucleus-nucleus distance at closest approach; and m is the mass of the transferred particle. Typically, between 60% and 70% of the total excitation energy will be deposited in the acceptor in one-nucleon transfer reactions.

This donor-acceptor asymmetry explains a main feature of the only published experimental data on excitation energy division in quasi-elastic transfer reactions.[7] In the one- and two-neutron transfer reactions induced by ^{86}Kr on ^{208}Pb, it was observed (by analyzing "bumps" in the energy spectra) that the excitation energy division was strongly exit-channel dependent. Especially, the pickup channels leading to ^{87}Kr and ^{88}Kr were found to have large excitation energies, and the reason was ascribed to nuclear structure effects. In contrast to this explanation, the model described above explains this as a consequence of the reaction mechanism.

DWBA calculations with the code ONEFF have also shown the donor-acceptor asymmetry in excitation energy sharing. Here the effect is further enhanced since, for reasonably large energy losses (>5-10 MeV), only transitions with large angular momentum transfer will be matched. These transitions can only take place between single-particle states with large spins, which are preferentially located at or above the Fermi level. This effect will again enhance transitions of type II relative to those of type I.

---

1. Adjunct research participant from the University of Tennessee, Knoxville, TN.
2. Y. Eyal et al., Phys. Rev. Lett. 4, 625 (1978).
3. D. Hilscher et al., Phys. Rev. C 20, 576 (1979).
4. T. Awes et al., Phys. Rev. Lett. 52, 251 (1984).
5. R. Vandenbosch et al., Phys. Rev. Lett. 52, 1964 (1984).
6. L. Lo Monaco and D. M. Brink, J. Phys. G11, 1935 (1985).
7. H. Solbach et al., Phys. Lett. 153B, 386 (1985).

Q-WINDOWS AND BINDING ENERGY EFFECTS FOR HEAVY ION TRANSFER IN THE PRESENCE OF STRONG COLLECTIVE EXCITATION

R. W. Kincaid[1] J. O. Rasmussen[3]
M. W. Guidry[2] L. F. Canto[4]
G. A. Leander[5]

The general structure observed in transfer total energy-multiplicity distributions can be understood in terms of a simple model. It is the result of an interplay between kinematic factors, i.e., the so-called energy window, which determines to what region of the E-M plane transfer is energetically possible, and to structure factors related to whether or not there actually are states of the proper form that can be populated by transfer within this region.

Figure 2.58a illustrates the proposed mechanism for the 1-neutron pickup reaction. In this explanation we will assume that the Ni-like ion remains in its ground state, or low-lying excited states. The data support this assumption. Shown are the experimental yrast lines for these systems with this assumption, plotted

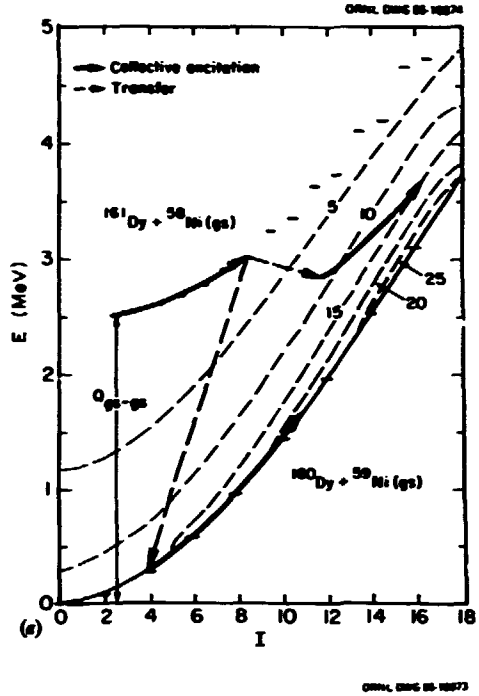

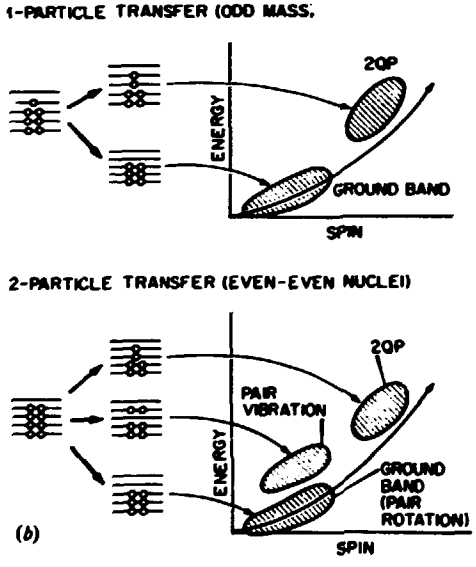

Fig. 2.58 (a) Evolution of a 1-neutron transfer reaction in the energy-angular momentum plane.

(b) A schematic picture of one- and two-particle transfer reactions populating even-even nuclei.

on a mass scale with the mass of ^{160}Dy(g.s.) + ^{58}Ni(g.s.) as the origin. In the entrance channel the ^{161}Dy is inelastically excited (predominantly by Coulomb excitation) to an average angular momentum ~ 17/2 at the turning point where particle transfer is assumed to take

place. The contours of the energy window are shown as dashed lines in Fig. 2.58a. Thus, kinematics and binding energies favor the population of ^{160}Dy states lying within this window. A cranked shell model calculation indicates that at I = 17/2 the core angular momentum in ^{161}Dy is ~ 4-6 ħ, with the remainder primarily carried by alignment of the unpaired particle. If the transfer operator is approximately one-body, the transfer cannot change the core angular momentum, so the transfer must proceed to states in ^{160}Dy with a core angular momentum R ~ 4-6 ħ. Analysis of the cranked shell model calculation shows that there are two general regions within the energy window which satisfy this condition: The ground band around I = 4-6, and the 2-quasiparticle bands near I ~ 10-12 (the average alignment in these bands is i ~ 6). Thus the transfer can proceed to the two regions indicated by the dashed arrows in Fig. 2.58a. Both regions are expected to involve states within collective bands, so exit channel inelastic excitation will further excite the ^{160}Dy nucleus as indicated by the heavy lines lying to the right in Fig. 2.58a. The flatter slope of the exit channel excitation in the 2QP bands reflects the structure given by the cranked shell model calculation.

Thus, at least schematically, two regions of the (E,M) plane should be populated in the 1-neutron transfer reaction as is illustrated in Fig. 2.58b (the ground band at an angular momentum comparable to that for inelastic excitation, and 2QP bands at higher angular momentum, with the difference in angular momentum between the two regions approximately given by the average aligned angular momentum in the 2QP bands). The data are qualitatively and quantitatively in agreement with this picture.

Figure 2.59 illustrates energy window contours for the 2-neutron transfer from ^{162}Dy with a ^{116}Sn beam. Analysis similar to that above again yields results in agreement with the data.

1. University of Tennessee, Knoxville, TN.
2. Adjunct staff member from University of Tennessee, Knoxville, TN.
3. Lawrence Berkeley Laboratory, Berkeley, CA and Joint Institute for Heavy Ion Research, ORNL, Oak Ridge, TN.
4. Federal University of Rio de Janeiro, Brazil and Joint Institute for Heavy Ion Research, ORNL, Oak Ridge, TN.
5. UNISOR, Oak Ridge Associated Universities, Oak Ridge, TN.

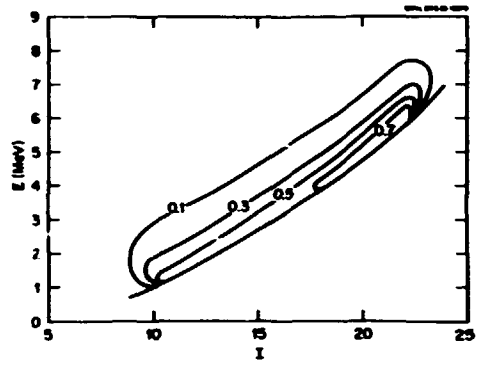

Fig. 2.59 The energy window contours for ^{162}Dy(^{116}Sn, ^{118}Sn)^{160}Dy in the region of the E-I plane accessible by transfer from ^{162}Dy at I ~ 8ħ followed by inelastic excitation in the exit channel.

STRONGLY DAMPED HEAVY-ION REACTIONS, FUSION, FISSION

ENERGY DISSIPATION IN BINARY REACTIONS-EJECTILE EXCITATION AND DECAY IN 12-MeV/NUCLEON ^{48}Ti + ^{150}Nd

T. M. Semkow[1] J. R. Beene
D. G. Sarantites[1] M. L. Halbert
K. Honkanen[1] D. C. Hensley
M. Ross[1]

In order to obtain some exclusive information on the energy and angular momentum dissipation in a moderately heavy, yet asymmetric, system we studied the binary reaction 12-MeV/nucleon ^{48}Ti on ^{150}Nd. An important quantity for the elucidation of the mechanism of binary reactions is the partition of the excitation energy between the primary fragments. Until recently, an equal-temperature assumption has been commonly applied.[2] This implies a partition of excitation energy proportional to the fragment mass and leads to a low excitation energy for the ejectile in very asymmetric systems. However, recent results[3] suggest an approximately equal sharing of the excitation energy between the two fragments.

We have detected the ejectiles (projectile-like fragments) using 7 Si (E,ΔE) telescopes

(4 at 20° and 3 at 50° relative to the beam). Figure 2.60 shows the (E,ΔE) map of the particles detected at 20°. The transition from the quasi-elastic and transfer component below the projectile to the fully damped component is clearly seen. In this way we measured the Z_L, A_L of the secondary light fragment and its kinetic energy. The particle telescopes were in coincidence with any of the 6 Compton-suppressed Ge detectors inserted in the Spin Spectrometer.

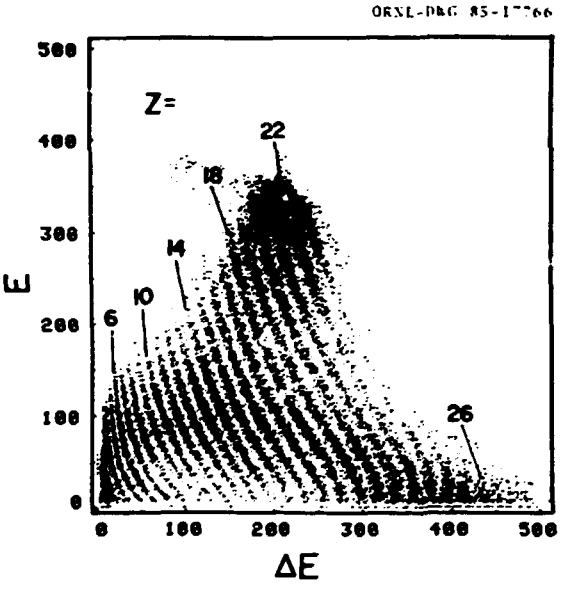

Fig. 2.60. (E,ΔE) map of the ejectiles at θ = 20° relative to the beam. A compression factor of 4 has been applied on both axes.

From the Ge spectra we can deduce the Z_H, A_H of the secondary heavy partner. In addition, the Spin Spectrometer supplies the total γ-ray multiplicity and energy, as well as neutron energy and multiplicity. The γ-rays from the Spin Spectrometer will be used for spin alignment studies and bound-state population studies of some of the ejectiles. The neutrons will be used for the excitation-energy partition studies. The neutrons and γ's were separated by time of flight. A modified version of the t_0 calculation[4] was done in which the most forward NaI detectors (A1-A5) were not included in the calculation. The NaI pulses were corrected for timing walk. As a result one can separate the neutrons from the γ's as illustrated in Fig. 2.61. In this figure an n-γ separation line is shown. We observe a strong kinematical focusing of the neutrons, resulting from preequilibrium and ejectile emissions.[5] The presence of some neutrons in the backward NaI's is due to emission from the heavy fragments. In order to

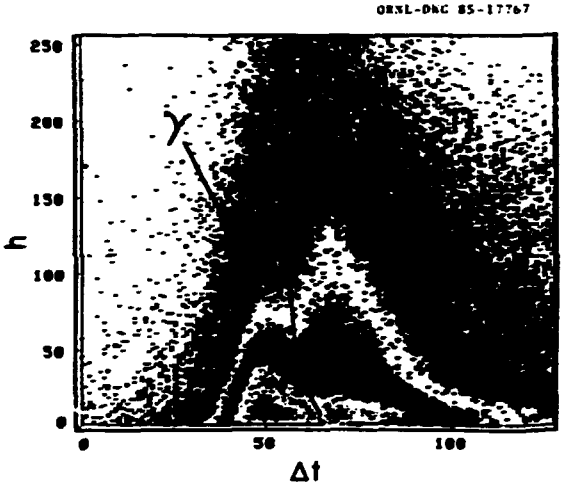

Fig. 2.61. (h,Δt) map of the pulse height vs time of flight for a NaI detector in the Spin Spectrometer at θ = 24°. The resolution on the x-axis is 0.25 ns/channel, and the gain on the y-axis is 40 keV/channel.

unfold the neutron spectra and get the energies and multiplicities, calibrations of the Spin Spectrometer for the neutron response are in progress. Although the light charged particles were not detected here (unless in coincidence with heavy ions), their multiplicities relative to those of neutrons can be estimated from statistical evaporation calculations for the heavier ejectiles. This will provide us with a reasonable estimate of the excitation energy imparted to the ejectile and will allow us to determine the excitation energy division.

---

1. Washington University, St. Louis, MO 63130.
2. J. Wilczynski et al., Nucl. Phys. A373, 109 (1982).
3. T. C. Awes et al., Phys. Rev. Lett. 52, 251 (1984).
4. M. Jaaskelainen et al., Nucl. Instrum. Methods 204, 385 (1983).
5. E. Holub et al., Phys. Rev. C 28, 252 (1983).

ANGULAR MOMENTUM TRANSFER IN Ni-INDUCED REACTIONS

S. P. Sorensen[1]
T. C. Awes
J. R. Beene
T. Dossing[2]
R. L. Ferguson
M. L. Halbert
D. C. Hensley
F. E. Obenshain
F. Plasil
M. Rajagopalan[3]
J. Randrup[4]
V. Rauch[5]
D. G. Sarantites[3]
Y. Schutz[5]
T. Semkow[3]
G. R. Young

The dynamics of the transfer of angular momentum from orbital angular momentum to intrinsic spin and the gradual excitation of the dinuclear spin modes are two aspects of heavy-ion reactions that still are not very well understood. Most of the experimental data have been discussed in terms of simple classical models (friction, sticking, etc.) combined with the excitation of the dinuclear modes in the thermal equilibrium limit. The aim of the present work is to provide a systematic set of gamma multiplicity data for several targets and bombarding energies in order to investigate whether the statistical model can account for the data or whether a more refined dynamic model has to be invoked.

The experiment was performed with the ORNL Spin Spectrometer. A ^{58}Ni beam at energies of 350 and 450 MeV was used to bombard ^{64}Ni, ^{118}Sn, and ^{174}Yb. The projectilelike fragments were detected with two solid state ΔE-E detectors. In order to minimize the uncertainties in the transformation from the raw gamma fold and NaI pulse height sum signal (k,H) to the gamma multiplicity and sum energy (M,E), a new iterative unfolding algorithm was developed, based on the method of decomposition of the Euclidian norm.[6] The algorithm has the virtue of being very fast for large systems (dimensions larger than 1000), robust for ill-conditioned systems, and has low sensitivity to the sampling noise in the experimental spectra.

The connection between the gamma multiplicity M_γ and the compound nucleus spin I, before the evaporation of particles and gammas, was studied in detail by combining the particle evaporation code ZPACE with the gamma-decay code GAMBLE. It was found that a major source of the large observed second moments of the M_γ distributions[7] is the summing over several exit channels with very different gamma-decay modes.

The first and second moments of the M_γ distributions were extracted from the data (Fig. 2.62), and as a new feature, it was also possible to calculate the skewness with reasonably small uncertainties (Fig. 2.63). The total-kinetic-energy-loss (TKEL) dependence of the first moments has been compared to calculations with the nucleon exchange transport model (NETM).[8] After corrections for particle evaporation effects, the model, in general, fits the

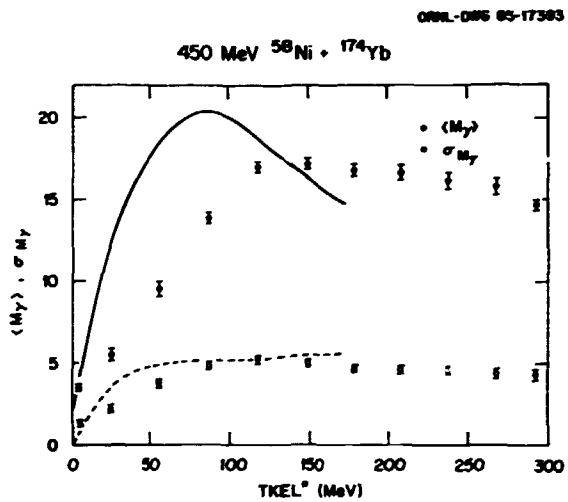

Fig. 2.62. The average and standard deviation of the M_γ distributions as a function of the TKEL*. The solid curve is the result of a NETM calculation corrected for particle evaporation.

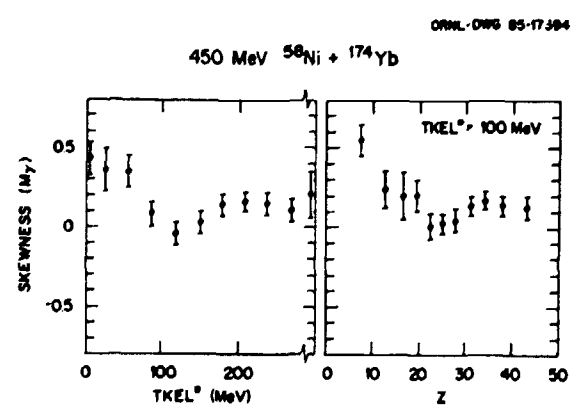

Fig. 2.63. The skewness of the M_γ distributions as a function of (a) the TKEL* and (b) the Z of the projectilelike fragment.

maximum value of <M>, but the tangential friction is too strong and results in a steep energy dependence at small energy losses. This problem has now been analyzed in more detail[9] and seems to be connected with the presence of a barrier in the single-particle potential of the dinuclear system at small energy losses. This barrier inhibits the transfer of nucleons with large tangential velocity components. As a consequence, the tangential friction is reduced by a factor of two in the partially damped energy region, which will give a much better fit to the data.

Another prediction from the NETM calculations[8] is that some of the dinuclear spin modes (bending and twisting) will have very long relaxation times and might not be strongly excited. In order to test whether such an effect could be observed, calculations within the statistical model[10] were carried out. The Monte Carlo calculations included the spin carried by each of the six orthogonal dinuclear modes, as well as the total orbital angular momentum L, and assumed that the sticking limit had been reached. Based on cross section systematics, it was estimated that a typical value of L is 135 for fully damped events. As can be seen in Fig. 2.64, the assumption of full thermal excitation of the dinuclear modes combined with the sticking picture results in gamma multiplicities that are much too large. Sticking or rolling only slightly underestimates M_γ at mass symmetry. This indicates that the dinuclear modes are not fully excited but have relaxation times that are longer than the relaxation time for the energy dissipation. Variations of L within reasonable limits does not change this conclusion qualitatively.

The NETM also predicts that the relaxation time for the rolling motion is shorter than for sticking. The flat Z dependence of M_γ as shown in Fig. 2.64 seems to indicate that only the rolling limit has been reached. It should be stressed, however, that by assuming a very strong orbital angular momentum fractionation,[10] a fit to the data with the sticking model can be obtained.

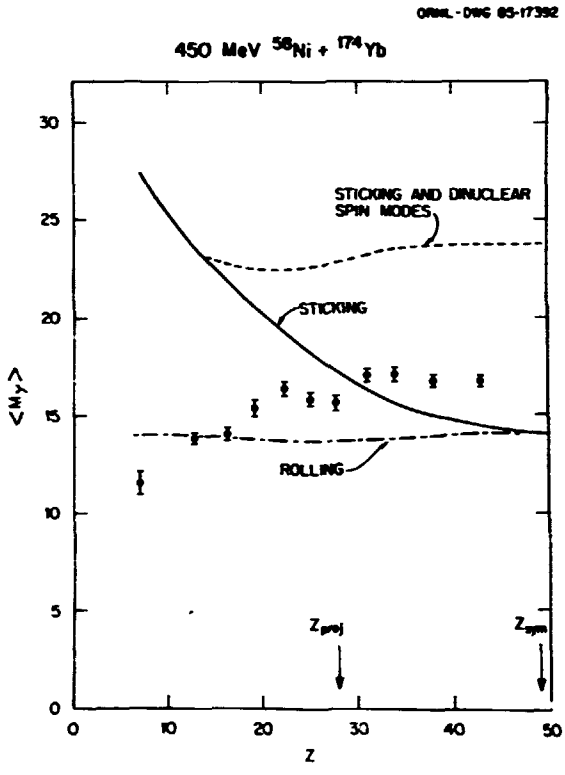

Fig. 2.64. The average M_γ as a function of the Z of the projectile fragment. The curves are the results of model calculations (see text for details).

The large second moments of the M_γ distributions can be understood within the NETM as a consequence of the strong excitation of the wriggling mode which, in contrast to bending and twisting, enhances spin fluctuations.

Even if the original skewness of the spin distribution will tend to be washed out by subsequent particle and gamma emission (a consequence of the central limit theorem), the general trend of the skewness of the M_γ distributions seems to reflect the original spin distribution. This distribution is expected to have a positive skewness in the partially damped region, where sliding is dominant, and a negative skewness in the completely damped region, where the distribution is proportional to $2*L + 1$ in the sticking limit. The gradual buildup of the dinuclear spin modes, which have a spin distribution with positive skewness, will

tend to change the skewness from negative to slightly positive values at the largest energy losses.

---

1. Adjunct research participant from the University of Tennessee, Knoxville, TN.
2. Niels Bohr Institute, Copenhagen, Denmark.
3. Washington University, St. Louis, MO.
4. Lawrence Berkeley Laboratory, Berkeley, CA.
5. Centre de Recherches Nucleaires, Strasbourg, France.
6. N. Gastinel, "Linear Numerical Analysis", Herman, Paris, 1970.
7. P. R. Christensen et al., Nucl. Phys. A349, 217 (1980).
8. T. Dossing and J. Randrup, Nucl. Phys. A433, 215 (1985) and private communication.
9. J. Randrup, NORDITA preprint 85/29, Copenhagen, Denmark.
10. L. G. Moretto and R. P. Schmitt, Phys. Rev. C 21, 204 (1980); R. P. Schmitt and A. J. Pacheco, Nucl. Phys. A379, 313 (1982).

FISSION DECAY OF REACTION PRODUCTS WITH A $\lesssim$ 150[1]

T. C. Awes — F. Plasil
R. L. Ferguson — V. Rauch[3]
R. Novotny[2] — G. R. Young
F. E. Obenshain — H. Sann[4]

The present experiment was performed with an 889-MeV beam of ^{58}Ni produced by coupled operation of the tandem electrostatic and cyclotron accelerators of the Holifield Heavy Ion Research Facility in Oak Ridge. Inclusive and two-fragment exclusive measurements of products resulting from interactions with a ^{58}Ni target (1.96 mg/cm^2) were made using two large solid-angle gas ionization chambers.

The experimental fission probabilities are shown in Fig. 2.65 for all fissionlike events with Z_1 and Z_2 > 3.5 and also for symmetric fission events only (Z_1 and Z_2 > 8.5). To extract the fission probabilities, a Monte Carlo simulation was made to determine the coincidence detection efficiency. The primary distribution of decaying fragments was taken from the measured inclusive distributions.[5] In the intrinsic frame, we have assumed the fission decay to be isotropic in the reaction plane with a Gaussian distribution out of the reaction plane. The calculated coincidence efficiencies are typically a few times 10^{-3} with an estimated uncertainty of 50%. The excitation energy of

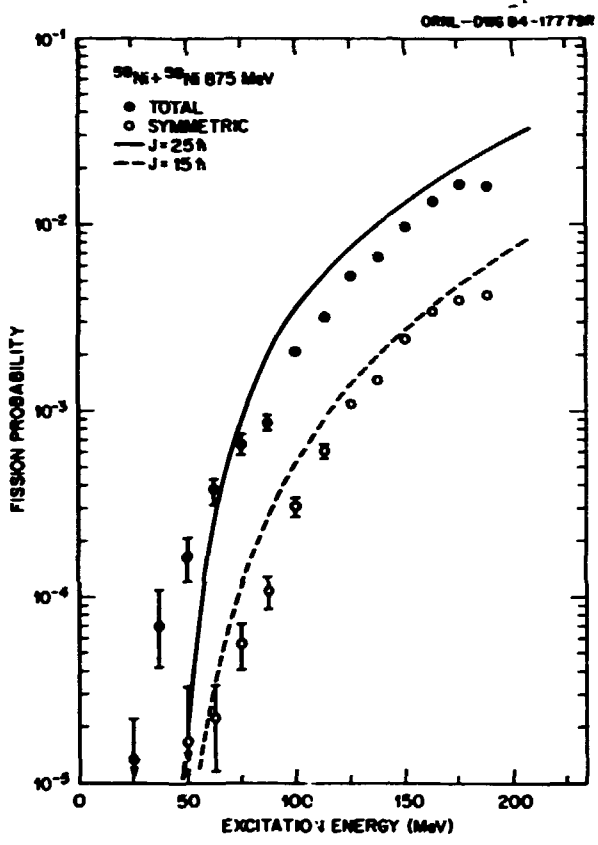

Fig. 2.65. Fission probability for all heavy fragment decays with 19.5 < $Z_1 + Z_2$ < 30.5 for (Z_1 and Z_2) > 3.5 (solid points) and symmetric decay only (Z_1 and Z_2) > 8.5 (open points). Fission evaporation calculations for ^{58}Ni are shown for a_f/a_n = 1.0, a = A/7.5, and J = 25 ħ (solid curve) or J = 15 ħ (dashed curve).

the decaying nickellike fragment was assumed to be half of the calculated energy loss. This neglects the effects of particle evaporation and Q values for mass transfer which, however, may be compensated by the width in the sharing of the excitation energy.

In order to determine whether the observed probabilities for fissionlike decay are consistent with an equilibrium process or instead indicate nonequilibrium effects, we have made statistical model calculations using the evaporation code PACE.[6] This code has recently been modified to include the fission barriers and moments of inertia calculated in the rotating-finite-range model (RFRM) of Sierk. These include the effects of the finite range of the nuclear force as well as the diffuseness of the

nuclear surface. There are two parameters of importance for the calculation, the ratio of saddle point to ground-state level densities, a_f/a_n, which we take to be 1.0, and the spin of the decaying nucleus. The calculated result is shown in Fig. 2.65 for the decay of ^{58}Ni with J = 25 ħ (solid curve), which corresponds to two-thirds of the grazing value and is probably a realistic estimate of the average. An additional result is shown for J = 15 ħ (dashed curve) to demonstrate the spin dependence. From these calculations we conclude that the observed decay is consistent with a statistical process.

This is in contrast to conclusions reached for the ^{129}Xe + ^{122}Sn reaction,[7] which suggested a nonequilibrium fission process, based in part on measured fission probabilities which were found to be one to two orders of magnitude larger than those estimated using the statistical model with reasonable parameter values.[7] However, we have used PACE with the same parameters of Ref. 7 (a_f/a_n = 1.09 and J = 40 ħ), and with RFRM barriers, and obtained adequate agreement with experiment, implying that, in this case, the measured fission probability is also consistent with a statistical process and not necessarily the result of a dynamical mechanism.

However, for the ^{129}Xe + ^{122}Sn reaction it has been shown[7] that the sequential fission decay is not a fully equilibrated process by the observation of a preference for asymmetric fission with the heavy fragment emitted opposite to the direction of the third body. These results indicated that the reaction products decay from an asymmetric deformation induced by the first step of the reaction. The fact that the observed decay probability is consistent with the statistical model, albeit assuming a symmetric saddle point, suggests that the dynamics of the first reaction step are not necessarily carrying the system over the conditional saddle point. As a consequence, the scission-to-scission time of 0.75-1. x 10^{-21} sec extracted[7] from the observation of proximity effects provides an upper bound on the saddle-to-scission time of the fissioning xenonlike nucleus.

The above limit, when compared to theoretical calculations of the saddle-to-scission time in fission, can provide unique information regarding the nuclear dissipation strength, γ. (For a definition of γ, see Ref. 8.) Within the framework of Kramer's stationary solution of the Fokker-Planck equation for an inverted oscillator,[8] a limit on the saddle-to-scission time of 0.75-1.0 x 10^{-21} sec for ^{129}Xe corresponds to an upper limit for the nuclear dissipation strength of γ = 1.0-1.4 (see Fig. 2.66), ruling out strongly overdamped dissipation strengths. Furthermore, if allowance is made

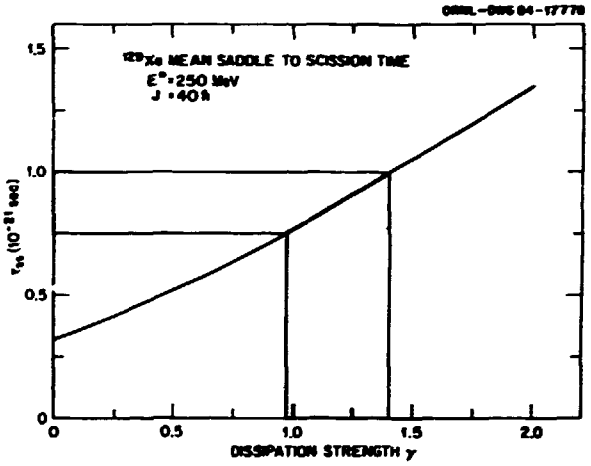

Fig. 2.66. Calculated saddle-to-scission time, τ_{ss}, for fission of ^{129}Xe as a function of the nuclear dissipation strength, γ (solid curve). The calculation was performed (Ref. 8) for an excitation energy E* = 250 MeV, spin J = 40 ħ, and level density parameter a = A/7.5. Also shown by the shaded region is the experimentally deduced (Ref. 7) scission-to-scission time of 0.75-1. x 10^{-21} sec, which provides an upper limit on the calculated saddle-to-scission time. Note: γ = 1.0 corresponds to critically damped motion.

for the time to reach the saddle point after the initial separation of the damped reaction products which, although highly uncertain, might be expected to be of the order of the lifetime of the xenonlike product nucleus at 250-MeV excitation, $\hbar/\Gamma_{tot}$ ≈ 5 x 10^{-22} sec, then dissipation strengths of the order of γ ≈ 0.5, corresponding to underdamped motion, are obtained.

1. Summary of published paper: Phys. Rev. Lett. 55, 1062 (1985).
2. Present address: University of Giessen, Giessen, F.R.G.
3. Present address: Centre de Recherches Nucleaires, Strasbourg, France.
4. GSI, Darmstadt, F.R.G.
5. T. C. Awes et al., Phys. Rev. Lett. 52, 251 (1984).
6. A. Gavron, Phys. Rev. C 21, 230 (1980).
7. D. v. Harrach et al., Phys. Rev. Lett. 48, 1093 (1982); P. Glassel et al., Z. Phys. A310, 189 (1983); P. Glassel et al., Phys. Rev. Lett. 48, 1089 (1982).
8. Helmut Hofmann and J. Rayford Nix, Phys. Lett. 122B, 117 (1983); J. R. Nix and A. J. Sierk, private communication.

TIME DELAYS OF 10^{-18} SEC MEASURED FOR THE PROJECTILE-LIKE FRAGMENTS OF 1760-MeV ^{40}Ar + [110] Ge[1]

J. Gomez del Campo[2] E. Pollacco[4]
J. Barrette[3] F. Saint-Laurent[5]
R. A. Dayras[3] M. Toulemonde[6]
J. P. Wieleczko[3] N. Neskovic[7]
R. Ostojec[7]

To achieve a better understanding of the reaction mechanisms in the peripheral collisions between heavy ions for intermediate bombarding energies (30-100 MeV/nucleon), it is necessary to know the amounts of mass and energy transferred to the primary fragments during the collision. These quantities can be obtained only through a detailed measurement of all the light particles and γ rays emitted in coincidence with the fragments and, hence, becomes an extremely difficult experimental problem. In this work a different approach was taken, namely, to measure, by the crystal blocking technique, the time of formation of secondary fragments that result from the light-particle decay of the excited primary fragments formed at the moment of interaction between target and projectile. The experiment was done by bombarding a mono-crystal of germanium with a 1760-MeV ^{40}Ar beam extracted from the GANIL (Caen, France) cyclotron facility. The reaction products were detected by a system consisting of a two-dimensional position-sensitive proportional counter and a solid-state telescope (300 μm, 5000 μm) to identify the nuclear charge of the fragments. The fragments of Z > 9 have been analyzed and their energy spectra and angular distributions show the same fragmentation features as those previously studied (Refs. 8, 9) with the same beam on targets of comparable mass. Figure 2.67 shows the two-dimensional blocking pattern obtained for all reaction products of Z > 9 emitted at a laboratory angle of 5.3 deg and along the direction of the [110] axis in the germanium crystal.

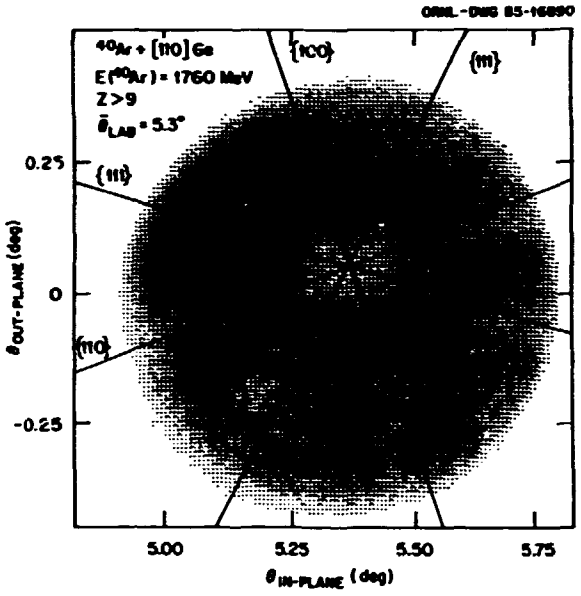

Fig. 2.67. Blocking pattern for all the projectile-like fragments of Z > 9 observed at θ_{lab} = 5.3 deg.

The typical crystallographic structure of the [110] axis can be seen, where also the major {110}, {100}, and {111} planes are observed. The blocking patterns can be obtained only after a very precise alignment of the beam and crystal has been achieved. For the present experiment, this was done by channeling the beam through the [110] axis observing the channeling pattern on a screen of zinc-sulfide placed at zero degrees. For the beam energy (1760 MeV) the channeling angle is approximately 0.08 deg and therefore channeling required the very high beam quality delivered by the GANIL facility. A stable beam of about 0.02-deg divergence and 2 mm x 2 mm size was used. In Fig. 2.67 it is important to point out that a reduction of the yield is seen in the center of the pattern, indicated by the intersection of the planes, and

it is precisely the amount of this reduction that is directly proportional to the lifetime of the fragment. For very short lifetimes, the primary fragments deexcite on a crystal lattice site and hence the secondary fragments are blocked by the lattice atoms and the reduction of the yield has its maximum. For longer lifetimes the deexcitation point is displaced towards the center of the channel between crystal planes, incrementing the yield along the channeling direction. This effect can be studied in a more quantitative way by integrating the area of the center hole in Fig. 2.67 normalized to the nonchanneled (random) yield. This procedure was done for the present data and the area is displayed in Fig. 2.68 as a function of scattering angle and Z of the fragments.

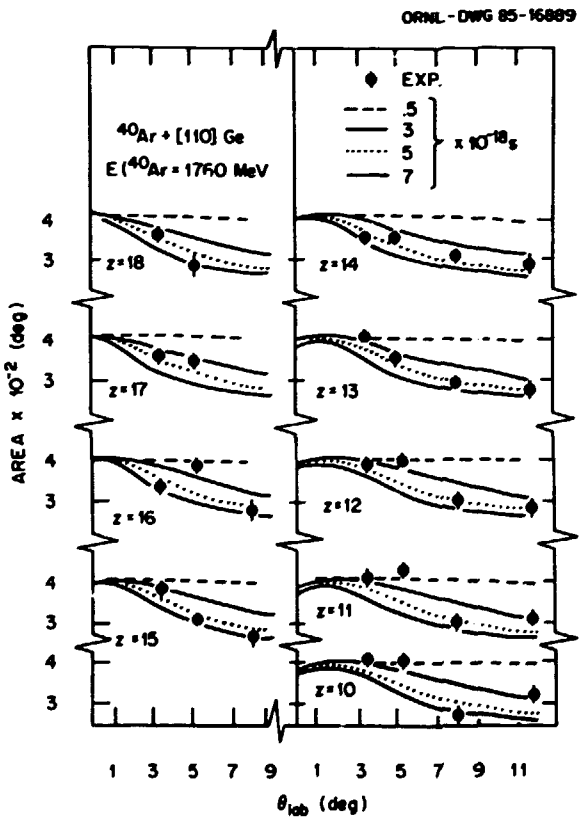

Fig. 2.68. Variation as a function of scattering angle of the area of the blocking dip measured along the [110] axis. The curves represent theoretical calculations for different decay t...es of the primary fragments.

Measurements were carried out for scattering angles of 3.5, 5.3, 8.0, and 11.8 degrees. The main observation to be drawn from Fig. 2.68 is that there is a reduction of the area as a function of the scattering angle for all the fragments — an indication of a time delay effect. To quantify this delay, four curves have been drawn (Fig. 2.68) representing theoretical calculations of the yields for different decay times ranging from 5 x 10^{-19} sec to 7 x 10^{-18} sec. This calculation takes into account dechanneling effects due to crystal thickness (10 μm), thermal motion, and static crystal imperfections. Also, the angular distribution of the primary fragments, used to compute the initial recoil velocities, was calculated with a simple abrasion model (Ref. 10). The dotted lines on Fig. 2.68 show the results for a decay time of 5 x 10^{-19} sec, corresponding to an average recoil distance of about 0.1 Å which is the lower limit of the present experiment. For this time the area should be essentially independent of the scattering angle, contrary to what is observed experimentally, namely, a 30% reduction from 3.5 deg to 11.8 deg. Decay times of 3, 5, and 7 x 10^{-18} sec are also given in Fig. 2.68 to indicate that for all the fragments their respective times are within these values and that no obvious dependence of the time as a function of the Z of the fragments is observed. A more detailed interpretation is in progress but already it is possible to note that the extracted times are similar to those measured for the decay of the ^{28}Si compound nucleus formed by the fusion of ^{16}O + ^{12}C (Ref. 11) at an excitation energy of 65 MeV, indicating that the process of secondary emission is very important in the production of projectile-like fragments in peripheral reactions. Preliminary calculations show that the measured decay times are consistent with a broad primary distribution of fragments at relatively low excitation energy (<60 MeV), and are not consistent with a highly excited primary fragment having a temperature of about 8 MeV (derived from the width

of the energy spectra) as suggested by simple fragmentation models (Ref. 10).

---

1. Summary of paper to be published.
2. Work done at DPh N/BE CEN Saclay, France, while on assignment from ORNL.
3. DPh N/BE CEN, Saclay, France.
4. I.S.N., Grenoble, France.
5. GANIL, Caen, France.
6. CIRIL, Caen, France.
7. Boris Kidric Institute, Belgrade, Yugoslavia.

8. V. Borrel et al., Z. Phys. A134, 191 (1983).
9. R. A. Dayras, Proceedings, 8th Symposium on Nuclear Physics, Oaxtepec, Mexico, January, 1985, Notas de Fisica 8-1, 68 (1985); J. Barrette el al., Proceedings, XXII International Meeting in Nuclear Physics, Bormio, Italy, 1984, p 561.
10. A. S. Goldhaber, Phys. Lett. 53B, 306 (1974).
11. J. Gomez del Campo et al., Phys. Rev. Lett. 51, 451 (1983)

HAUSER-FESHBACH CALCULATIONS FOR HEAVY FRAGMENT EMISSION[1]

J. Gomez del Campo[2]

The yield distribution, Y, of heavy fragments ($Z > 2$) in relativistic nucleon-nucleus collisions[3] follows a simple power law, $Y = CxA^{-t}$ ($t = 2.6$ for p + Kr and p + Xe reactions). Using the Fisher droplet model,[4] this power law can be interpreted as a manifestation of critical phenomena, namely, a liquid-gas phase transition at a critical temperature T_c of about 5 MeV.[3] In heavy-ion collisions a similar power law has been observed[5] in studies of the heavy fragment emission for 15- and 30-MeV/nucleon ^{12}C + Ag, and a possible correlation between the apparent exponent, t, and the critical temperature, T_c, has been pointed-out.[6] Theoretical calculations to explain the heavy fragment emission have been given in terms of statistical models. Recently Sobotka et al.,[7,8] using the theoretical framework given by Moretto,[9] have shown that the emission of heavy fragments can be interpreted as an asymmetric fission decay of the compound nucleus. Freedman and Lynch[10] have developed a multistep heavy fragment evaporation code from which they can follow the decay of the system as a function of time in a zero angular momen um approximation. In this work, an alterrative statistical model calculation is presented which uses the full angular momentum coupling in the framework of the Hauser-Feshbach formula. The study of cluster emissions (Li, Be, B, and C isotopes) has been the subject of intense studies using reactions of light heavy ion systems, and Hauser-Feshbach calculations with adequate values of the critical angular momentum (J_c) have been extremely useful in the understanding of compound nucleus decays. (A review on this subject is given in Ref. 11.)

The present calculations use the Hauser-Feshbach formula and level densities as given in Ref. 12 with statistical model parameters of Ref. 13 and optical model transmission coefficients — parametrized by a Fermi function — obtained from the optical potential parameters given in Ref. 14. A total of 175 heavy fragment decay channels have been included, in addition to neutron decay and the $Z = 1$ and $Z = 2$ channels. A decay channel in the present calculations is defined by its respective Z, A, excitation energy, and angular momentum; therefore, decays to excited states of the emitted fragments are included. Results of the calculations are shown for two systems: $^{3}He + ^{109}Ag$ (Fig. 2.69) at $E(^{3}He) = 90$ MeV and $^{12}C + ^{109}Ag$ at $E(^{12}C) = 180$ MeV (Fig. 2.70). The experimental cross sections (crosses) given on Fig. 2.69 have been obtained by integrating the differential cross sections (given in Ref. 7) from 90 to 180 deg and then multiplying by two. The calculations shown on Fig. 2.69 reproduce the data for a value of $J_c = 17\hbar$, corresponding to a fusion cross section of 827 mb. The angle integrated cross sections for the $^{12}C + ^{109}Ag$ system given on Fig. 2.70, solid dots, were obtained using the differential cross sections reported in Ref. 5 and assuming a $1/\sin(\theta)$ dependence on the angular distribution. The Hauser-Feshbach calculation (solid line) reproduces the experimental data for a value of $J_c = 35\hbar$, corresponding to a fusion cross section of 483 mb. Although experimental fusion cross sections do not exist for the systems studied, it is interesting to point out that

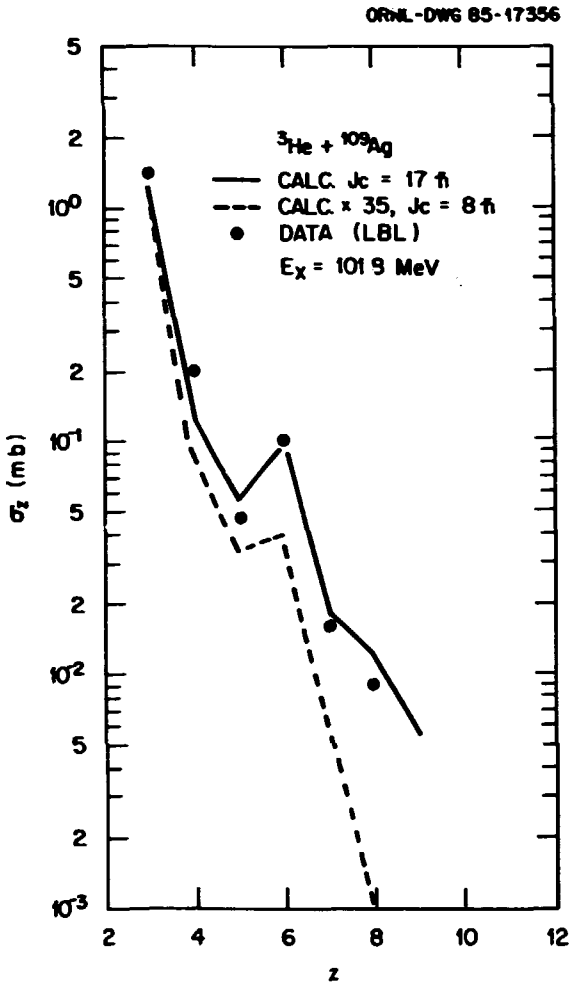

Fig. 2.69. Hauser-Feshbach calculations (solid and dashed lines) for the heavy fragment emission of $^3He + ^{109}Ag$ at $E(^3He)$ = 90 MeV.

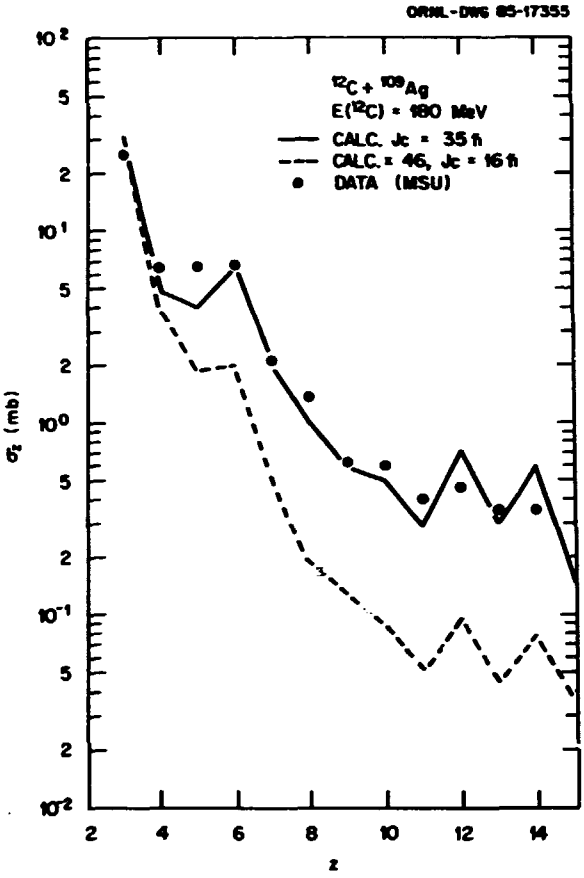

Fig. 2.70. Hauser-Feshbach calculations (solid and dashed lines) for the heavy fragment emission of $^{12}C + ^{109}Ag$ at $E(^{12}C)$ = 180 MeV.

from the systematic study of the Rochester group[15] a value of 827 mb of fusion is obtained for the $^3He + ^{109}Ag$ at $E(^3He)$ = 90 MeV and 940 mb for the $^{12}C + ^{109}Ag$ at $e(^{12}C)$ = 180 MeV. The agreement for the $^3He + ^{109}Ag$ is perfect but there is about a factor of two discrepancy for the $^{12}C + ^{109}Ag$ system. This discrepancy can be due partially to the fact that the total (backward c.m. angle) cross sections for heavy fragment emission have not been measured (only differential cross sections exist at a few angles), and that important amounts of incomplete fusion may be present.

To illustrate the importance of the critical angular momentum in the statistical emission of heavy fragments, Figs. 2.69 and 2.70 show the results obtained for substantially lower values of J_C of 8ħ for $^3He + ^{109}Ag$ and 16ħ for the $^{12}C + ^{109}Ag$ (dashed lines). Both calculations have been normalized, to the yield at Z = 3, by the indicated factors and, as can be seen, the predicted cross sections decrease more than an order of magnitude.

---

1. Summary of a paper to be published.
2. Work performed while on assignment at CEN Saclay DPh N/BE, France.
3. A. S. Hirsch et al., Phys. Rev. C 29, 508 (1984).
4. M. E. Fisher, Rep. Prog. Phys. 30, 615 (1967).
5. C. B. Chitwood et al., Phys. Lett. 131b, 289 (1983).
6. A. D. Panagiotou et al., Phys. Rev. Lett. 52, 496 (1984).
7. L. G. Sobotka et al., Phys. Rev. Lett. 51, 2187 (1983).
8. L. G. Sobotka et al., Phys. Rev. Lett. 53, 2004 (1984).

9. L. Moretto, Nucl. Phys. A247, 2111 (1975).
10. W. A. Friedman and W. G. Lynch, Phys. Rev. C 28, 16 (1983).
11. R. G. Stokstad, Treatise on Heavy Ion Science, Vol. III (1984), ed. D. A. Bromley (Plenum Press, New York).
12. J. Gomez del Campo et al., Phys. Rev. C 9, 1258 (1974).
13. G. Rohr, Z. Phys. A318, 299 (1984).
14. C. M. Perey and F. G. Perey, Atomic and Nuclear Data Tables 13, 293 (1974).
15. W. W. Wilcke et al., Atomic and Nuclear Data Tables 25, 389 (1980).

FUSION CROSS SECTIONS FOR BEAMS OF ^{46,50}Ti ON TARGETS ^{90}Zr AND ^{93}Nb

P. H. Stelson M. Beckerman[1]
H. J. Kim D. Shapira
R. L. Robinson

The collective properties of the first 2^+ states of the nuclei ^{46}Ti and ^{50}Ti are quite different (^{46}Ti: E_x = 0.89 MeV, β_2 = 0.314; ^{50}Ti: E_x = 1.55 MeV, β_2 = 0.173). For subbarrier fusion reactions involving these nuclei, the coupling of these inelastic channels to the elastic channels leads to the prediction that the subbarrier fusion cross sections for ^{46,50}Ti on ^{90}Zr should differ by a factor of ~20. We have used the velocity filter to measure these cross sections and also the cross sections for ^{46,50}Ti on the neighboring nucleus ^{93}Nb.

The measured fusion cross sections for these four systems are presented in Figs. 2.71 and 2.72. To facilitate the comparison of the different systems, we have plotted the cross sections vs the quantity $(E_{c.m.} - E_B)$(MeV), where $E_B = (1.44\, Z_1 Z_2)/r_0(A_1^{1/3} + A_2^{1/3})$. We have taken r_0 = 1.477 fm because this value gives good agreement with the barriers extracted from the measurements.

The results shown in Fig. 2.71 indicate progressively larger differences in fusion cross sections as we move farther below the barrier. We are now in the process of comparing these cross sections with different theoretical predictions.

The measurements show that all four systems have the same cross sections at and above the

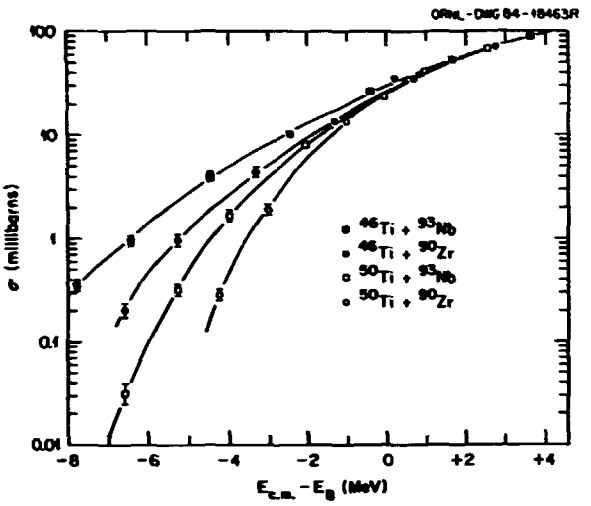

Fig. 2.71. Fusion cross sections for beams of ^{46,50}Ti on targets ^{90}Zr and ^{93}Nb in the region below the barrier.

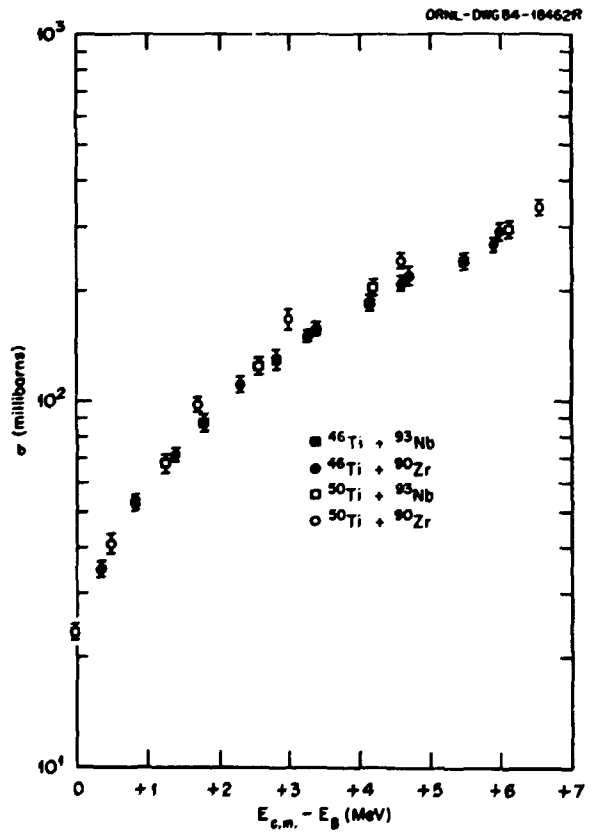

Fig. 2.72. Fusion cross sections for beams of ^{46,50}Ti on targets ^{90}Zr and ^{93}Nb in the region above the barrier.

barrier. However, the observed cross sections are rather uniformly about 30% less than the total calculated reaction cross section in the region above the barrier, which suggests that the evaporation residue fusion cross section must compete with other reaction mechanisms in the region of the barrier.

---

1. Joint Institute for Heavy Ion Research, ORNL, Oak Ridge, TN 37831.

AN ENTRANCE CHANNEL LIMIT ON THE FUSION OF ^{28}Si WITH ^{12}C AT HIGH ENERGY[1]

B. A. Harmon[2] D. Shapira
S. T. Thornton[2] J. Gomez del Campo
M. Beckerman[3]

The analysis of fusion data in the energy range 4.6 to 6.4 MeV/nucleon for the ^{28}Si + ^{12}C system (^{28}Si projectile) first reported last year[4] is now complete. The data in Fig. 2.73 show an entrance channel-imposed limit on the fusion cross section. The critical angular momentum extracted is considerably lower than those of other systems forming the same compound nucleus, ^{40}Ca [see part (b) of Fig. 2.73].

As the bombarding energy is increased, separation of products resulting from formation and evaporative decay of ^{40}Ca from those of other processes becomes difficult. Therefore, an extensive analysis was carried out comparing velocity and energy distributions for uniquely identified products (charge and mass) to kinematic calculations. The cross sections for each (Z,A) combination identified are shown in Fig. 2.74 for two bombarding energies along with the predictions of the Monte Carlo evaporation code PACE.[5] Fractions of the total yield for several products (indicated by upwardly extended crosses) were excluded from the fusion cross sections of Fig. 2.73. The velocity spectra for these isotopes, which contain contributions from other processes, show deviations from the calculated shapes of the velocity and energy spectra predicted for compound nucleus residues.

The critical angular momentum for the fusion of ^{28}Si and ^{12}C is in fact the same critical

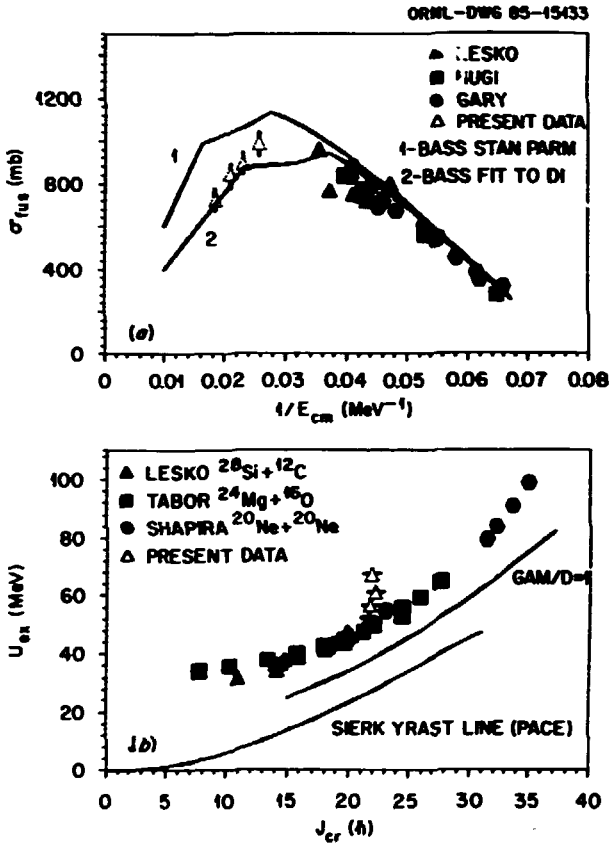

Fig. 2.73. (a) Fusion data for the ^{28}Si + ^{12}C system as a function of the reciprocal of the center of mass energy consisting of the present results and data from Refs. 8-10. Curves 1 and 2 are Bass model calculations[11] which incorporate the empirical nuclear potential used in the extraction of the critical angular angular momentum for the orbiting ^{28}Si + ^{12}C system.[6] Curve 2 represents a nucleus-nucleus potential strength yielding excitation functions in agreement with both the fusion and orbiting cross sections.[7] (b) Fusion data plotted as excitation energy versus critical angular momentum for systems which form the compound nucleus ^{40}Ca. The present results are shown along with data from Refs. 8, 12-13. The yrast line from the evaporation code PACE and the $\Gamma/D=1$ criterion for compound nucleus formation[14] are also shown.

angular momentum that was found to limit the formation of an orbiting dinuclear system.[6,7]

---

1. Summary of a paper to be submitted to Physical Review C.
2. University of Virginia, Charlottesville, VA 22901.
3. Joint Institute for Heavy Ion Research, Oak Ridge, TN 37831.

4. Phys. Div. Prog. Rep. for Period Ending Sept. 30, 1984, ORNL-6120, 59.
5. A. Gavron, Phys. Rev. C 21, 230 (1980).
6. D. Shapira et al., Phys. Rev. Lett. 53, 1634 (1984).
7. See also the following article, B. Shivakumar et al.
8. K. T. Lesko et al., Phys. Rev. C 25, 872 (1982).
9. S. Gary and C. Volant, Phys. Rev. C 25, 1877 (1982).
10. M. Hugi et al., Nucl. Phys. A368, 173 (1981).
11. R. Bass, Phys. Rev. Lett. 39, 265 (1977).
12. S. L. Tabor et al., Phys. Rev. C 17, 2136 (1978).
13. D. Shapira et al., Phys. Rev. C 28, 1148 (1983).
14. R. Vandenbosch and A. J. Lazzarini, Phys. Rev. C 23, 1074 (1981).

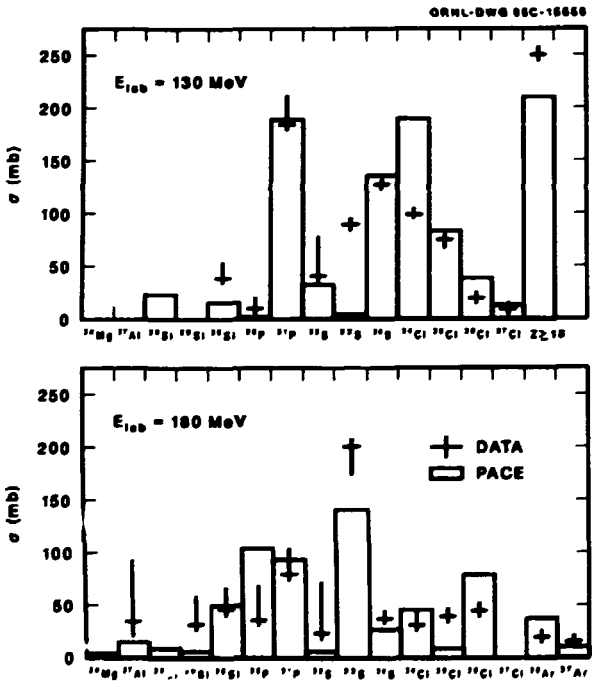

Fig. 2.74. Integrated partial yields for evaporation residues with the identified charge and mass of the reaction products. Upwardly extended crosses indicate the presence of non-fusion yields excluded from the fusion cross sections of Fig. 2.73 (see text). The bars are the result of the Monte Carlo evaporation code PACE.

BACKWARD ANGLE YIELDS IN THE ^{28}SI + ^{14}N REACTION; EVIDENCE FOR THE EQUILIBRATION OF MASS IN ORBITING REACTIONS

B. Shivakumar[1] B. A. Harmon[3]
D. Shapira P. H. Stelson
M. Beckerman[2] K. Teh[4]

We have measured the back angle yields of target-like products in a reaction between a ^{28}Si beam and a ^{14}N target at lab energies between 100 MeV and 170 MeV. The scientific motivation behind this measurement was to ascertain whether the orbiting process lasts long enough to allow for the equilibration of mass, and if the microscopic structure of the interacting nuclei has any effect on the nucleus-nucleus potentials and the yields in the different channels.

The existence of a long-lived dinuclear complex (DC) has already been established for the ^{28}Si + ^{14}N reaction (Ref. 5) as was done for the ^{28}Si + ^{12}C. Though both systems are similar in total mass, they are different in character, as shown in Fig. 2.75. This figure is a plot of the ground state Q-values of some of the channels open to the ^{28}Si + ^{12}C and ^{28}Si + ^{14}N reactions. It is obvious that the ^{12}C + ^{28}Si system has only two channels available at low Q for the DC to fragment into, whereas the

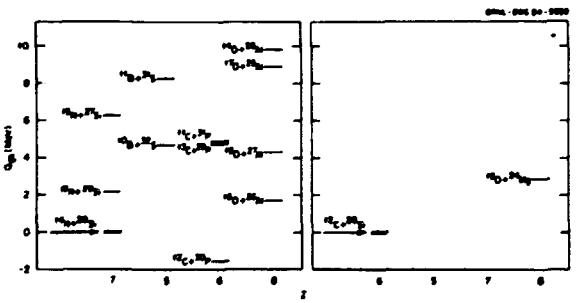

Fig. 2.75. 1. A plot of the ground state Q-values of channels resembling ^{12}C + ^{28}Si and ^{14}N + ^{28}Si. The vertical axis has been adjusted so that the entrance channel is at Q = 0.

$^{14}N + ^{28}Si$ has several. In the $^{12}C + ^{28}Si$ system, the strongest channels are carbon and oxygen respectively. This observation can be accounted for by either of two possible conclusions: (a) Orbiting is a fast process and the DC formed does not live long enough to change appreciably from the entrance channel, or (b) orbiting is a process slow enough to allow for the equilibration of mass, and the final yields in the different channels are determined by their respective Q- values. [The Q-value of a channel can be related in a simple way to the available phase space in that channel (Refs. 6 and 7).]

This ambiguity can be resolved by a study of the $^{28}Si + ^{14}N$ system. The backward angle (163 deg to 174 deg in c.m. frame) yields of reaction products ($10 < A < 21$) were measured at the ORNL HHIRF facility using a supersonic gas jet target (Ref. 8). Figure 2.76 shows a spectrum of the back angle yield of ^{12}C from the $^{28}Si + ^{12}C$ reaction. Since we are dealing here with continuum spectra, it becomes hard if not impossible to deconvolute yields coming from contaminants, especially carbon, in the target. Therefore, it is imperative that we have pure targets. The nitrogen gas target we used was free of impurities and contaminants. This unique feature of gas targets gives credibility to the conclusions we draw from our measurements. Figure 2.77 shows the orbiting cross sections measured for the $^{28}Si + ^{14}N$ system (Ref. 9). It is clear that at all the energies measured, the ^{12}C and ^{16}O yields are larger than the ^{14}N. This suggests to us that orbiting is a

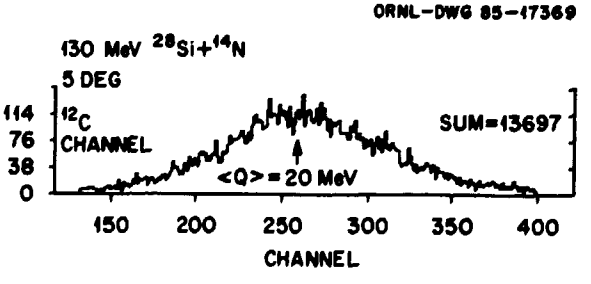

Fig. 2.76. A backangle spectrum of ^{12}C nuclei in the $^{28}Si + ^{14}N$ reaction. The data are from Ref. 9.

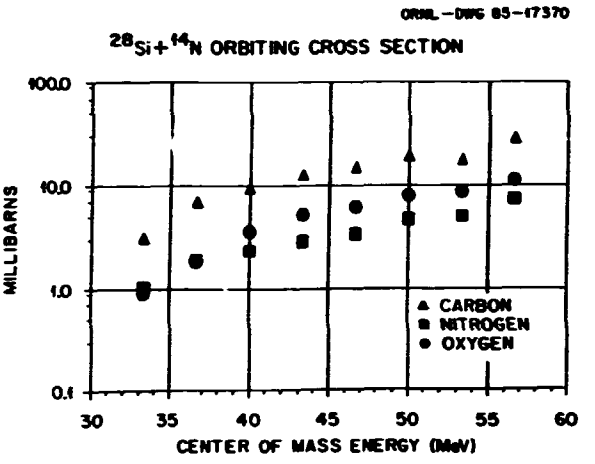

Fig. 2.77. Orbiting cross sections for the ^{12}C, ^{14}N, and ^{16}O channels in the $^{14}N + ^{28}Si$ reaction. The data are from Ref. 9.

process that is indeed sufficiently long-lived to allow for the equilibration of mass. The channel with the lowest Q-value is found to have the largest cross section.

How is it then that the ^{16}O channel has a higher yield than the ^{14}N? If we adjust the Q-values shown in Fig. 2.75 by the difference in Coulomb, nuclear and centrifugal energies between the different channels, the Q-differences between the three channels decrease with increasing angular momentum. However, the relative ordering still persists and hence fails to resolve why the ^{16}O yield exceeds the ^{14}N. We believe that the enhanced oxygen yield over that expected by simple Q-value arguments has its origin in the difference in the phase space available to the $^{14}N + ^{28}Si$ and the $^{16}O + ^{26}Al$ channels. This arises primarily from the difference in microscopic structure between the ^{28}Si and ^{26}Al nuclei.

We are now in the process of studying orbiting phenomena and their connection with fusion in the framework of compound nuclear (Ref. 10) and dinuclear models (Ref. 7).

---

1. Ph.D. thesis student, Yale University, A. W. Wright Nuclear Structure Laboratory, New Haven, CT 06511.
2. Joint Institute for Heavy Ion Research, ORNL, Oak Ridge, TN 37831.
3. Ph.D. thesis student, University of Virginia, Charlottesville, VA 22901.

4. Vanderbilt University, Nashville, TN 37235.
5. D. Shapira et al., Phys. Div. Ann. Prog. Rept. for Period Ending Sept. 30, 1984, ORNL-6120, p. 63.
6. V. Volkov, Sov. J. Part. Nucl. 6, No. 4, 331 (1979).
7. B. Shivakumar et al., this section and to be published. S. Ayik et al., to be published.
8. D. Shapira et al., Nucl. Instrum. Methods Phys. Res. 228, 259 (1985).
9. B. Shivakumar et al., to be published.
10. B. A. Harmon et al., to be published.

A MODEL FOR ORBITING AND FUSION

B. Shivakumar[1] B. A. Harmon[3]
S. Ayik[2] D. Shapira

Previous measurements at Oak Ridge and elsewhere have provided evidence for the formation of a long-lived dinuclear molecular complex (DMC) in the deep inelastic collisions between nuclei (Ref. 4). For the case of the $^{28}Si + ^{12}C$ system the maximum angular momentum that the DMC can sustain was inferred to be 18ħ (Ref. 5). The fusion cross section for the same system has been measured recently and found to be limited by the same maximum angular momentum (Ref. 6). We present here a model (Ref. 7) that provides a unified description of both these observations in terms of the formation, breakup (orbiting yield) and coalescing (fusion yield) of a DMC. Although attempts to describe fusion proceeding via a dinuclear configuration exist, none to our knowledge attempt to calculate the yield from the two phases of this process, i.e., products from the dinuclear and the fused system.

A schematic description of the transitions considered by this model appear in Fig. 2.78.

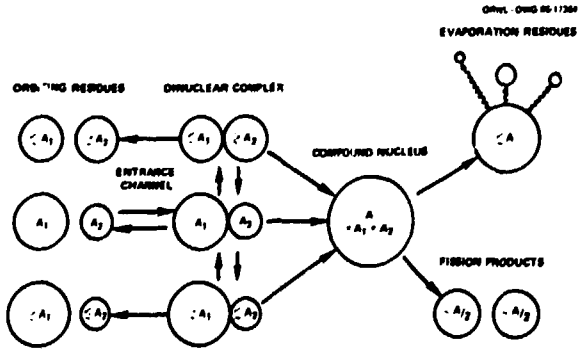

Fig. 2.78. Schematic diagram of the model.

As in other models describing deep inelastic scattering and fusion, a DMC is formed under the influence of conservative and dissipative forces in the collision between two ions. Once the DMC is formed it evolves through the exchange of particles to different dinuclear configurations. In our model each of these configurations has a probability to fragment into the outgoing channel it most resembles and results in the orbiting yield. What does not fragment is assumed to relax into a compound nuclear configuration and is identified as the fusion yield. In this way, the approximation used here circumvents the problem of dealing with the evolution of the dinuclear configuration into that of a compound nucleus.

The theoretical framework for this model is provided by taking the equilibrium limit of two coupled diffusion equations that describe the flow of mass, charge, and energy in an extension of the standard diffusion model (Refs. 8, 9). The evolution of the DMC between dinuclear configurations represented by a nucleus-nucleus potential energy surface (PES), defined in terms of the variables mass, charge, position, angular momentum, and energy, is described by a diffusion equation. A similar equation describes the fragmentation of each of the dinuclear configurations. In the equilibrium limit of such a formalism, the orbiting yields in each of the outgoing channels is determined by the density of states at the corresponding saddle point of the PES.

An additional ingredient of this model is the condition, in the initial stages of a collision, that determines whether a DMC can be formed at all. If the DMC cannot be formed, there can be no fusion. This condition is introduced, as in critical distance models (Ref. 10), by requiring that there be a pocket in the entrance channel PES. Trapping in such a pocket takes place with the dissipation of the energy of relative motion and angular momentum into the intrinsic excitation of the participant nuclei.

This model is expected to account for the fusion cross section, and the final kinetic energies and cross sections of the orbiting yields. Figure 2.79 shows the results of c

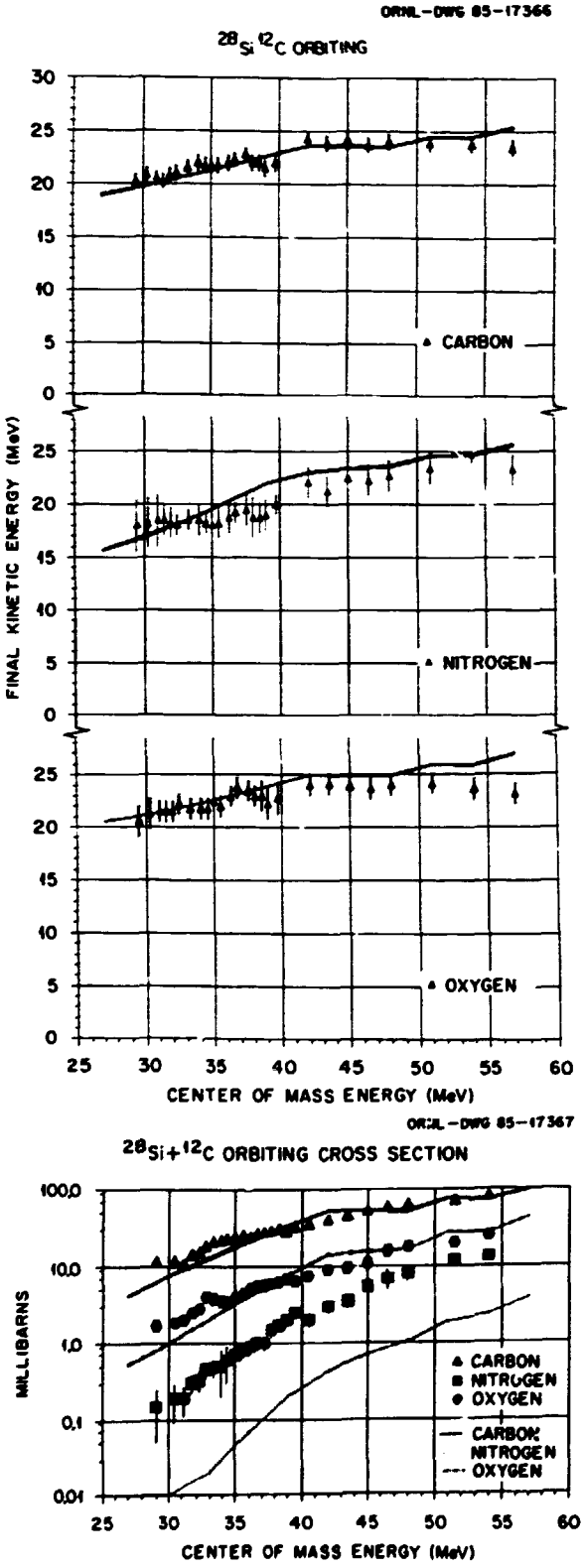

Fig. 2.79. Plot of the final kinetic energies and cross sections of the orbiting yield. The data are from Ref. 2. The continuous curves are the model predictions.

calculation for the orbiting yields of the carbon and oxygen channels in the $^{28}Si + ^{12}C$ reaction. Figure 2.80 shows a calculation of the fusion cross section for the same system. The agreement of our theory with the data in both these cases is very encouraging.

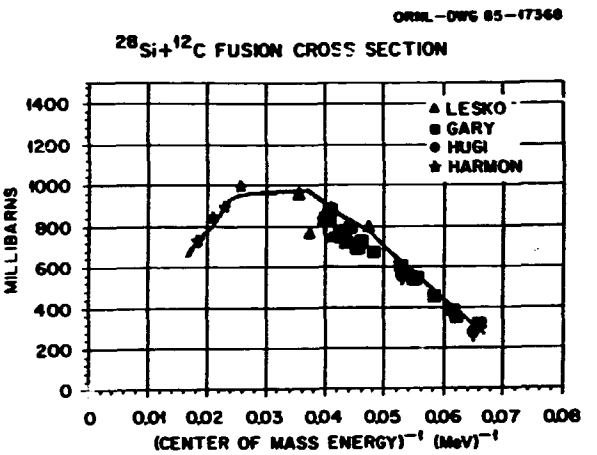

Fig. 2.80. Plot of the fusion cross section for the $^{28}Si + ^{12}C$ reaction. The data are from Refs. 6, 11, 12, and 13. The continuous curve is the model prediction.

The availability of both fusion and orbiting data imposes stringent restrictions on the range of potentials that can be used in the description of the processes under discussion. The final kinetic energies of the reaction products essentially determine the heights of the potential barriers at the saddle point, something that any parametrization of the process should be expected to reproduce. As of now, such data are available for only the $^{28}Si + ^{12}C$ system. The success of our model in describing the available data we hope will spur some interest in the measurement of complementary fusion and orbiting data for other systems.

---

1. Ph.D. thesis student, Yale University, A. W. Wright Nuclear Structure Laboratory, New Haven, CT 06511.
2. Joint Institute for Heavy Ion Research, ORNL, Oak Ridge, TN 37831, and Tennessee Technological University, Cookeville, TN 38505.
3. Ph.D. thesis student, University of Virginia, Charlottesville, VA 22901.

4. D. Shapira et al., Phys. Lett. 114B, 111 (1982).
5. D. Shapira et al., Phys. Rev. Lett. 53, 1634 (1984).
6. B. A. Harmon et al., to be published.
7. B. Shivakumar et al., to be published.
8. W. Norenberg, Phys. Lett. 53B, 289 (1974). S. Ayik et al., Z. Phys. A277, 299 (1976), Z. Phys. A279, 145 (1976), Z. Phys. A286, 271 (1978).
9. S. Ayik et al., to be published.
10. R. Bass, Phys. Rev. Lett. 39, 265 (1974).
11. M. Hugi et al., Nucl. Phys. A368, 173 (1981).
12. S. Gary and C. Volant, Phys. Rev. C 25, 1877 (1982).
13. K. T. Lesko et al., Phys. Rev. C 25, 872 (1982).

ZERO-POINT FLUCTUATIONS AND THE DIFFUSENESS OF THE NUCLEAR SURFACE

M. W. Guidry[1] J. O. Rasmussen[3]
R. Donangelo[2] M. S. Hussein[4]

For heavy ion reactions such as deep inelastic scattering or subbarrier fusion, the motion of classical nuclei of various static shapes on classical trajectories often provides a convenient starting point for the understanding of the reaction. In processes such as these, the distance between nuclear surfaces in the collisic plays a crucial role and zero-point surface fluctuations near the point of closest approach may have a significant effect on the reaction, as illustrated in Fig. 2.81. This point has been emphasized for deep inelastic processes in Ref. 5. In this report we will be concerned primarily with the effect of low-frequency, large-amplitude, zero-point modes on heavy-ion scattering, and will ignore the effect of high-frequency, small-amplitude motion connected with giant resonances. We will also restrict attention to spherical vibrators, even though similar arguments may apply to vibrations about deformed equilibrium shapes.

For the most collective of such modes the amplitude associated with the zero-point motion is large. If the Hamiltonian is assumed to be of the standard form

$$H = \frac{1}{2} \sum_{\lambda\mu} (B_\lambda |\dot{\alpha}_{\lambda\mu}|^2 + C_\lambda |\alpha_{\lambda\mu}|^2) ,$$

the zero-point amplitude for a quadrupole mode is[6]

$$\alpha_{20}^{o} = \left(\frac{\hbar^2}{4B_2C_2}\right)^{1/4} = (E_{2+}/2C_2)^{1/2} .$$

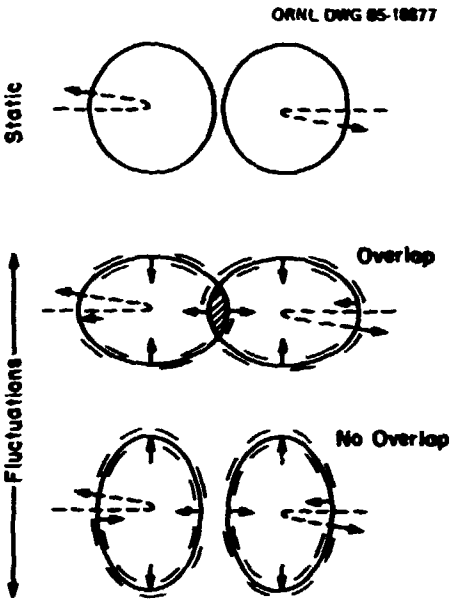

Fig. 2.81 Illustration of the effect of zero-point fluctuation on subbarrier fusion and deep inelastic reactions.

Parametrizing the radius as $R \sim r_0(1 + \alpha_{20}Y_{20}(\theta))$ and estimating B_2 and C_2 from the energies and B(E2) values associated with low-lying 2^+ states,[7] one finds that for the softest nuclei the zero-point fluctuations correspond to surface displacements of 0.5-1 fm. Thus in some cases these fluctuations are as large as the measured diffuseness in heavy-ion scattering.

In the classical limit of quantum mechanics, the cross sections for various processes result from a superposition of all initial phase angles for the zero-point fluctuations at the beginning of the classical trajectories. Thus, the collision of two sharp classical surfaces is replaced by a collision in which the surfaces are smeared by zero-point motion and the quantum-mechanical superposition principle. The question we pose is whether this phase information is irretrievably lost, or whether it is possible to recover it in such a fashion that the contribution to the nuclear diffuseness from collective zero-point motion can be determined.

It has been pointed out[8] that for the collective excitation of deformed rotors by spherical projectiles there is an uncertainty principle relation between the maximum classically allowed angular momentum I_{MAX} which can be excited in a heavy-ion collision and the uncertainty $\Delta\chi_0$ in

the initial orientation angle of the rotor in the collision $\Delta\chi_0 \sim 1/I_{MAX}$. Thus, in heavy-ion collisions where I_{MAX} can be large the orientation of the rotor in the collision can become highly localized, and the projectile "sees" different regions of the deformed nuclear surface when it excites different rotational states of the deformed nucleus.[8,9]

An analogous uncertainty principle argument may be applied in the case of vibrational excitation. For that case, the canonically conjugate variables are the phonon number N, and the phase angle q for the vibration, and we find $\Delta q_0 \sim 1/N_{MAX}$ where Δq_0 is the uncertainty in the initial phase angle for the zero-point fluctuation of a particular mode, and N_{MAX} is the maximum number of phonons of that mode which can be excited in a classical collision. Thus, in a heavy ion collision if N_{MAX} becomes large, a localization is possible in the phase angle of the vibrator.

These ideas are seen most clearly for the rotor if the problem is formulated in terms of the Classical Limit S-Matrix (CLSM).[8,9] An analogous formulation is possible for the collision of spherical vibrators. This has been discussed by Miller for the molecular scattering case[10] and the transcription to nuclear scattering is straightforward. We omit the details and discuss only the classical quantum-number function, which for the vibrator is the final phonon number N_f (considered as a continuous classical variable) vs the initial phase angle q_0 for the zero-point fluctuation. The general shape of this quantum number function is shown in Fig. 2.82 for several representative systems. There we see that if the phonon coupling is large, as might be expected in very heavy ion collisions, the excitation of particular phonon states occurs only for highly localized ranges of phase angles.

The experimental procedure to determine the optical potential could be as follows. Very heavy ions are used at energies in the Coulomb-nuclear interference region to excite multiphonon vibrational states. A detailed coupled-channel fit to the corresponding angular

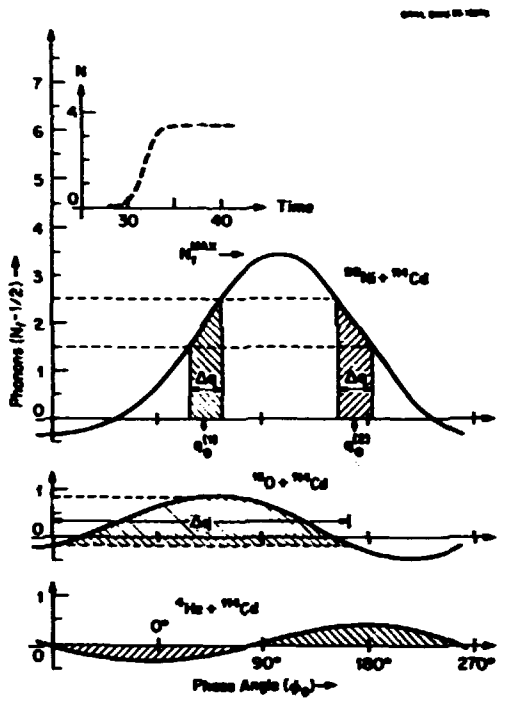

Fig. 2.82 The classical quantum number functions for vibrational excitation in light and very heavy ion reactions, assuming backward scattering of the projectile. In the calculations, monopole plus quadrupole Coulomb potentials and a real Woods-Saxon nuclear potential were included, with r_0 = 1.2 fm, a = 0.72 fm, V_0 = 50 MeV, E_{2+} (Cd) = 558.5 keV, and $B(E2, 0^+ \rightarrow 2^+)$ = 5640 fm^4. Projectile excitation was ignored, and the laboratory energies were 15 MeV (^{4}He), 50 MeV(^{16}O), and 230 MeV(^{58}Ni). High localization in q_0 is illustrated by hatching in the Ni Reaction. For example, excitation of the 2-phonon vibrational state occurs only if the phase angles lie in two narrow bands at $q_0^{(1)}$ and $q_0^{(2)}$. The larger N_{MAX}, the more narrow these bands. In contrast, for the ^{16}O and ^{4}He reactions there is almost no localization because N_{MAX} is small. The inset shows the classical time evolution of the phonon number for the Ni reaction for $q_0 = 100°$, with time in dimensionless units.

distributions (or excitation functions) is used to find an ion-ion potential which simultaneously fits all the inelastic scattering data (state by state). By the preceding arguments, such a potential should have most of the diffuseness due to zero-point fluctuation of the explicitly coupled modes removed. Conversely, a nuclear potential determined to fit only the total quasi-elastic cross section will include an average over all phase angles (cf. Fig. 2.82) and should exhibit a larger diffuseness.

lne implementation of such a study is possible, using particle-γ coincidence spectroscopy[9] and either classical-limit methods[8-10] or fast coupled-channels codes (e.g., Ref. 11).

Finally, we discuss the implications of these results, first with respect to reactions, and then with respect to structure. Potentials determined in the way suggested here provide a realistic starting point for the evaluation of zero-point fluctuations on more complicated heavy-ion reactions. By the present arguments, potentials determined in less restrictive fashion (e.g., from analysis of quasi-elastic scattering data) already contain appreciable effects due to zero-point motion, and it is inconsistent to use those potentials to govern trajectories to which zero-point motion effects are added by hand. A similar point has been made by Esbensen, et al.[5]

With respect to nuclear structurte, one may ask what is the physical meaning of the diffuseness associated with the zero-point fluctuation. We suggest a simple interpretation. The nuclear density diffuseness is composed of two parts, which we denote the mean-field and residual parts, respectively. The first is the diffuseness of the matter distribution of a pure shell model, without residual interactions. The second is the additional diffuseness due to the scattering of particles by the residual interaction, which manifests itself macroscopically in the zero-point fluctuations of the collective modes. These two contributions to the matter ribution diffuseness generate the ion-ion potential diffuseness when folded with effective nucleon-nucleon interactions. It will be interesting to see whether the experiments suggested here are sufficiently precise to separate these two components.

---

1. Adjunct staff member from University of Tennessee, Knoxville, TN.
2. Federal University of Rio de Janeiro, Brazil.
3. Lawrence Berkeley Laboratory, Berkeley, CA and Joint Institute for Heavy Ion Research, ORNL, Oak Ridge, TN.
4. University of Sao Paulo, Brazil.
5. H. Esbensen, A. Winther, R. A. Broglia, and C. H. Dasso, Phys. Rev. Lett. 41, 296 (1978).
6. A. Bohr and B. Mottelson, Nuclear Structure, vol. II, p. 683.
7. G. M. Temmer and N. P. Heydenburg, Phys. Rev. 104, 967 (1956).
8. R. E. Neese, M. W. Guidry, R. Donangelo, and J. O. Rasmussen, Phys. Lett. 85B, 201 (1979).
9. M. W. Guidry, et al., Nucl. Phys. A430, 485 (1984).
10. W. H. Miller, Advances in Chemical Physics 25, 69 (1974).
11. M. J. Rhoades-Brown, R. J. Donangelo, M. W. Guidry, and R. E. Neese, Phys. Rev. C24, 2747 (1981).

ENTRY STATES IN SUBBARRIER FUSION

M. L. Halbert K. Honkanen[1]
J. R. Beene T. Semkow[1]
D. C. Hensley V. Abenante[1]
D. G. Sarantites[1]

Over the past five years it has become clear that the cross section for fusion of heavy ions below the Coulomb barrier can be orders of magnitude larger than the predictions of models that are quite successful above the barrier.[2] More recently, studies of γ-ray multiplicity[3-6] have shown that the average ℓ of the partial waves participating in subbarrier fusion is much higher than expected. The discrepancies become larger as the mass asymmetry of the projectile and target decreases.

We have used the Spin Spectrometer, an ideal instrument for study of such angular-momentum effects, in coincidence with identified products from two reactions leading to the same compound nucleus, ^{164}Yb. The reactions were ^{64}Ni + ^{100}Mo and ^{16}O + ^{148}Sm; the conditions of bombardment are listed in Table 2.12. The two reactions cover similar ranges of excitation energy in the compound nucleus.

Exit channels were identified by known characteristic γ-ray lines observed in six Compton-suppressed Ge detectors which replaced a like number of pentagonal NaI units of the Spin Spectrometer. Recording of an event on tape was triggered by detection of a "clean" Ge pulse (i.e., no γ ray detected in its surrounding NaI shield). To reduce the recording of the many uninteresting events in the Ni + Mo bombardments due to Coulomb excitation (Coulex), the event trigger also required that at least one of the NaI detectors in the spectrometer had fired.

Table 2.12. Bombarding conditions. Energies are in MeV. E_{lab} is the bombarding energy halfway through the target. E_{cm} is the center-of-mass energy halfway through the target. E_{CN}^* is the excitation energy in the compound nucleus ^{164}Yb.

Projectile	Target	E_{beam}	E_{lab}	E_{cm}	E_{CN}^*
^{64}Ni	^{100}Mo	210.0	207.2	126.3	34.0
		215.0	212.2	129.4	37.1
		220.0	217.2	132.4	40.2
		225.0	222.2	135.5	43.2
		235.1	232.3	141.7	49.4
^{16}O	^{148}Sm	71.2	70.3	63.5	40.4
		81.3	80.4	72.6	49.5

Table 2.13. Cross sections (in mb) for the four dominant exit channels. Energies are in MeV. Uncertainties are about ±15%.

System	E_{beam}	2n	3n	4n	α2n	Sum
^{64}Ni + ^{100}Mo	210	0.26	-	-	-	0.26
	215	1.43	0.78	-	-	2.21
	220	3.26	4.19	-	-	7.46
	225	6.3	14.2	0.9	-	21.4
	235	11.0	39.3	18.1	2.3	70.7
^{16}O + ^{148}Sm	71	22.2	72.7	1.5	5.5	101.9
	81	6.4	208.9	166.3	35.7	417.2

This last requirement was removed for about 10% of the Ni + Mo data in order to measure the Coulex yields for normalization of the Ni + Mo cross sections.

An independent normalization of the absolute cross sections was obtained from the integrated beam current in the Faraday cup, measured target thicknesses, and calibrated efficiency-solid angle products of the Ge detectors. The two normalizations for the Ni + Mo agreed well within the estimated uncertainties. For the O + Sm reactions the Faraday cup provided the only normalization.

The cross sections listed in Table 2.13 are based on the observed yields of the $2^+ \rightarrow 0^+$ transition in ^{162}Yb (2n channel), ^{160}Yb (4n), and ^{158}Er (α2n), and the $17/2^+ \rightarrow 13/2^+$ plus the $9/2^- \rightarrow 5/2^-$ transitions in ^{161}Yb (3n). Corrections were made for internal conversion and angular distribution effects. No significant yield of ^{163}Yb (1n channel) was observed at any energy. Small amounts of ^{161}Tm (p2n), ^{157}Er (α3n), or other channels might have been present at the level of a few percent each of the total cross section. Fission is unlikely to contribute at these low bombarding energies. Thus the cross section for fusion may be estimated by adding 5-10% to the sum of the four cross sections shown in Table 2.13. This estimate of 5-10% is confirmed by the statistical model calculations described below.

The points in Fig. 2.83 show these estimated fusion cross sections (σ_{fus}) for both reactions as a function of ^{164}Yb excitation energy. The dashed line is the value of σ_{fus} for Ni + Mo given by the Bass model.[7] It is far from a satisfactory representation of the data. The full line represents a similar calculation[8] which incorporates effects of coupling to excited states in both projectile and target;[9] all inelastic couplings with the ground states were included with the appropriate β_λ taken from experiment. The calculated[8] barrier parameters for Ni + Mo (O + Sm), are as follows: barrier height = 141.6 (62.6) MeV, barrier radius = 10.92 (10.66) fm, and $\hbar\omega$ = 2.28 (4.37) MeV. These values were obtained with the choices ΔV = -20 (0) MeV, where ΔV allows adjustment of the nuclear potential well depth to fit the magnitude of the cross section. The shape of the excitation function is not sensitive to ΔV. The good agreement of the predicted and measured σ_{fus} as a function of energy is very encouraging.

The σ_ℓ distributions that the channel coupling model predicts, when used as input to

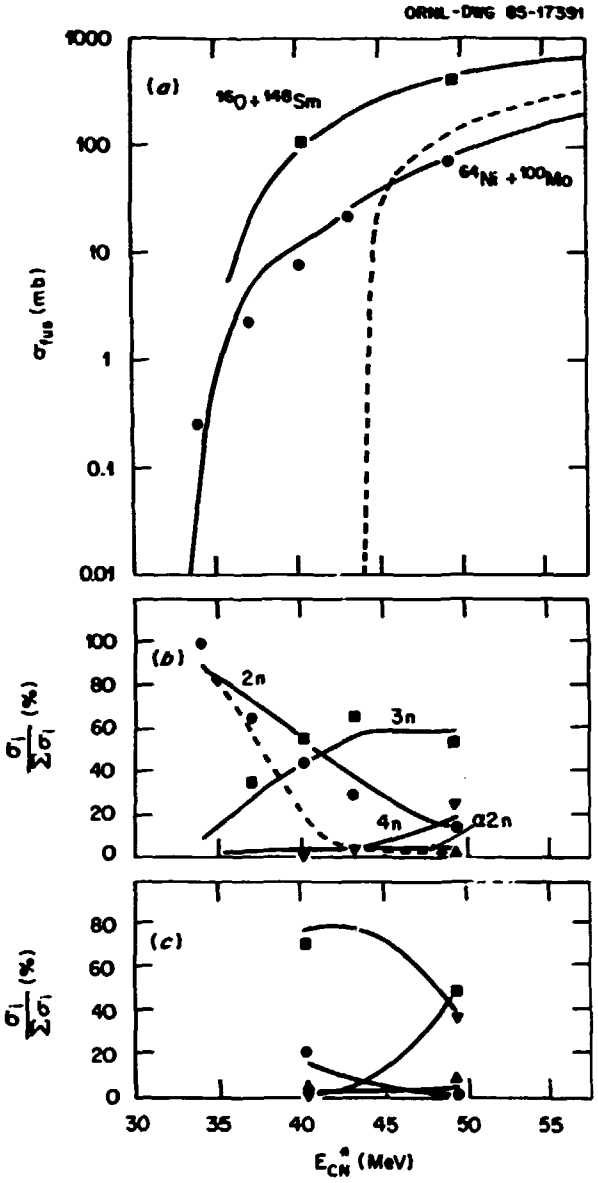

Fig. 2.83. (a). Fusion cross sections as a function of compound nucleus excitation energy. Experimental points (● = $^{64}Ni + ^{100}Mo$, ■ = $^{16}O + ^{148}Sm$) are sums of the measured 2n, 3n, 4n, and α2n cross sections plus a 5-10% allowance for all other channels. The full curves are predictions of the channel-coupling model (Refs. 8, 9). The dashed curve shows the prediction of the Bass model (Ref. 7). (b) and (c). Fractional yields, as a function of compound-nucleus excitation energy, of the four principal exit channels measured in the reactions $^{64}Ni + ^{100}Mo$ (b) and $^{16}O + ^{148}Sm$ (c). Experimental points: ● = 2n, ■ = 3n, ▼ = 4n, ▲ = α2n. Full curves: the statistical model with initial compound-nucleus ℓ distributions predicted by the channel-coupling model. Dashed curve: 2n fraction calculated with initial ℓ distributions from barrier-penetration calculations with the Bass potential (Ref. 12).

the statistical model, are quite successful in predicting the relative cross sections of the various exit channels. The results of these calculations are compared with experiment in Fig. 2.83b and c; the agreement is good for both reactions. The experimental lack of measurable ^{163}Yb (1n channel) is also well reproduced: in no case did the calculation predict a ^{163}Yb cross section larger than 0.6% of σ_{fus}. Similar calculations using σ_ℓ distributions obtained from barrier-penetration calculations with a parabolic approximation[11] to the Bass potential,[12] tend to underestimate the 2n fraction severely, as shown by the dashed curve in Fig. 2.83b. Likewise, the σ_ℓ distribution given by a rounded sharp-cutoff model requires an unusually large smoothing parameter (for example, $\Delta\ell \gtrsim 8$ for Fermi-function rounding) in order to give sufficient 2n yield. The channel-coupling model[8,9] naturally predicts ℓ distributions extending to higher ℓ values than those predicted without coupling.

These calculations were carried out with the statistical model program PACE2S[10] using the following conditions: (1) a = A/8.5, (2) giant-resonance E1 shape with strength = 100% of classical sum rule, (3) collective E2 strength = 100 W.u., (4) default values of other γ-ray strengths, and (5) yrast lines adjusted to provide a realistic representation of the known yrast lines of nuclei near A = 164. The calculations are rather insensitive to reasonable variations in (1), (3), and (4), but do show large discrepancies with experiment (insufficient 2n) when the default yrast-line option is taken instead of (5). Also, calculations in which the odd-even effect in the level density is ignored are noticeably less successful.

In summary, Fig. 2.83 shows that the statistical model reproduces our data excellently provided that (a) realistic nuclear properties are chosen (yrast line, γ-decay strength), and (b) high ℓ values are prominent in the entrance channel. We find no need to invoke superdeformation.[6]

The data from the Spin Spectrometer provide, of course, rather direct information on the ℓ

distributions. The analysis of these data is incomplete at this writing, but substantial progress has been made using standard procedures,[13] namely: (1) The raw NaI data have been corrected for energy response and pulses due to neutrons have been excluded. (2) (H,k) arrays in coincidence with each identified Ge peak (and background) have been generated [H = sum of corrected NaI pulse heights, k = number of responding detectors for each event]. (3) (E,M) arrays have been obtained for iterative unfolding for most of the (H,k) arrays by using the measured response function of each detector in the Spectrometer [E = entry-state excitation energy, M = γ-ray multiplicity].

Figure 2.84 presents samples of the k projections (peak-background) for the two reactions at nearly equal compound-nucleus energies. The entry states for Ni + Mo involve much higher k values than do those for O + Sm, showing clearly that higher angular momenta are involved in the more symmetric system. Further analysis is expected to quantify this salient feature.

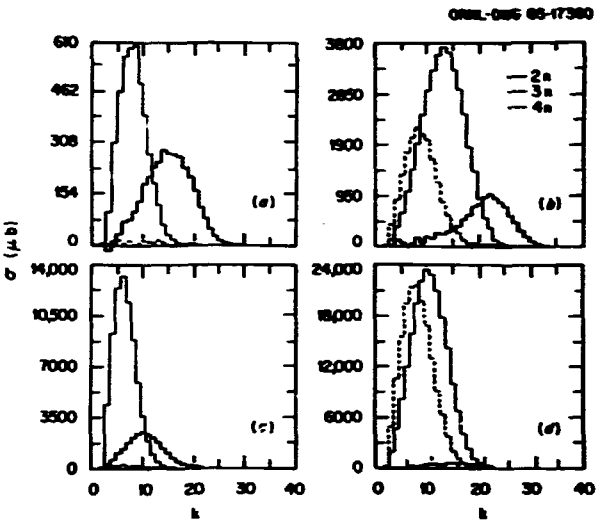

Fig. 2.84. Projected k distributions for xn channels from reactions of (a) 220-MeV and (b) 235-MeV ^{64}Ni on ^{100}Mo, and (c) 71-MeV and (d) 81-MeV ^{16}O on ^{148}Sm. Reaction pairs [(a), (c)] and [(b), (d)] lead to ^{164}Yb compound nuclei at nearly the same excitation energy.

SPINS AND SADDLE POINT SHAPES FROM LARGE FRAGMENT EMISSION STUDIES

D. G. Sarantites[1] M. L. Halbert
L. G. Sobotka[1] D. C. Hensley
E. L. Dines[1] H. C. Griffin[2]
L. A. Adler[1] R. Schmitt[3]
V. Abenante[1] G. Nebbia[3]
Li Ze[1] Z. Majka[3]
J. R Beene J. C. Lisle[4]

The object of studying heavy ion induced fission is to determine the magnitude and L-wave dependence of the fission barrier. The symmetric fission barrier can be considered as the central point in an ion-ion potential energy surface which extends into the mass asymmetry degree of freedom. It is this potential energy surface which determines the fate of a compound nucleus and will influence the pathway of non-compound heavy-ion reactions. Since reactions will not only proceed via a symmetric pathway, we must be concerned with the asymmetry dependence of the fission barrier.

1. Washington University, St. Louis, MO 63130.
2. M. Beckerman, Phys. Reports (in press).
3. S. Gil et al., Phys. Rev. C 31, 1752 (1985).
4. B. Haas et al., Phys. Rev. Lett. 54, 398 (1985).
5. P. J. Nolan et al., Phys. Rev. Lett. 54, 2211 (1985).
6. W. Kuhn et al., Phys. Rev. Lett. 51, 1858 (1983); A. Ruckelshaus et al., Legnaro Conference 27-31 May 1985.
7. R. Bass, Nucl. Phys. A231, 45 (1974).
8. Program CCFUS, by C. H. Dasso and S. Landowne (unpublished).
9. R. A. Broglia et al., Phys. Lett. 133B, 34 (1983).
10. Program PACE2S, written by A. Gavron, Phys. Rev. C 21, 230 (1980), with modifications by J. R. Beene.
11. C. Y. Wong, Phys. Rev. Lett. 31, 766 (1973).
12. R. Bass, Phys. Rev. Lett. 39, 265 (1977).
13. M. Jaaskelainen et al., Nucl. Instrum. Methods 204, 385 (1983).

Recently, the study of the emission of large fragments, intermediate in mass between alpha particles and fission fragments, from compound nuclear reactions has been used to determine the conditional saddle point masses, or barriers, as a function of asymmetry.[5-7] This work has confirmed the Businaro-Gallone transition[7] and verified the importance of a finite range correction to liquid drop models.[7,8]

The work mentioned above[5-8] does not, however, address the subject of the angular momentum dependence of these conditional saddles. In this report we present preliminary results of an experiment designed to address this issue.

We have recently studied the emission of large fragments from $^{110}Sn^*$ compound nuclei produced in the reaction 200-MeV ^{45}Sc + ^{65}Cu. In the Spin Spectrometer scattering chamber we positioned two large-area gas, solid-state telescopes near 90° or 60° in the center of mass (each telescope covered an angular span of 18° in the lab). By running with low- and high-gain amplifiers for the ΔE detectors we were able to achieve individual Z resolution for Z = 2 to 25.

The fact that the yield of the observed fragments with relaxed kinetic energies peaks near symmetry (Z_s = 25) and not at or below the projectile (Z_p = 21) is an indication that the fragments are emitted from the compound system. This is not surprising in view of the fact that approximately 65% of the reaction cross section is expected to fuse and that much of the remaining cross section involves transfer. Although there is likely to be a small deep inelastic contribution to the total reaction cross section, products from these reactions will be focused near the grazing angle and therefore well forward of our detectors.

The yield of large fragments detected near 45° in the laboratory is shown in Fig. 2.85. The prominent features seen in this figure are the minimum near Z = 8, where one observes a strong even-odd effect, and above Z = 12 a gradually increasing yield as symmetry is approached. The overall trend of these data can be reproduced quite nicely with a liquid drop

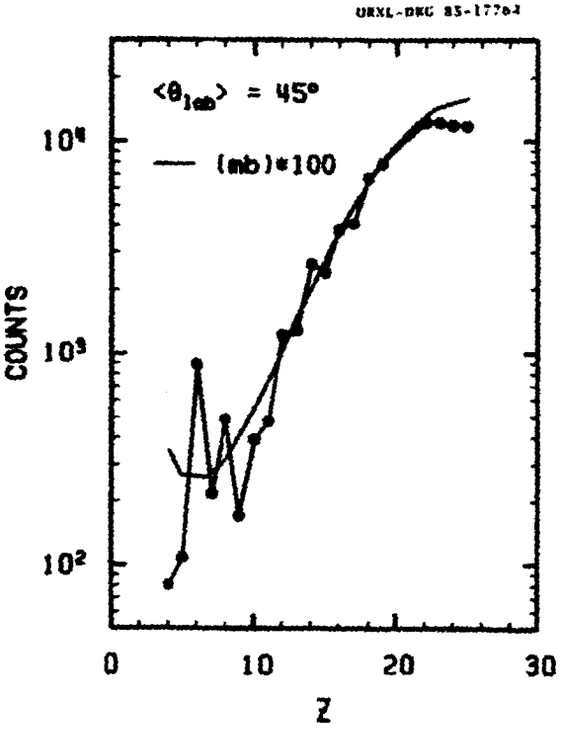

Fig. 2.85. Yields of heavy fragments emitted in the decay of $^{110}Sn^*$ compound nuclei from the reaction of 200-MeV ^{45}Sc with ^{65}Cu. The data points are connected with lines to guide the eye. The smooth solid line is from a liquid drop model calculation as described in the text.

calculation of the type described in Ref. 7 (solid line in Fig. 2.85). For this calculation, two rigidly rotating spheres separated by 2.5 fm are used to model the conditional saddle. We have however, scaled the barriers calculated from our simple sphere-sphere model such that for each L-wave the symmetric barrier agrees with finite range corrected liquid drop values.[8] Rigid body moments of inertia are used and L-waves less than 65 ħ are included.

The γ-ray fold (k_γ) distributions for fragments of each Z were determined from coincidences with the NaI detectors of the Spin Spectrometer. Distributions for selected Z values are shown in Fig. 2.86. It is seen that the mean $\langle k_\gamma \rangle$ values and the upper edges decrease rapidly with increasing Z of the detected fragment. This indicates a decreasing transfer of angular momentum to the fragments with increasing exit channel symmetry. This

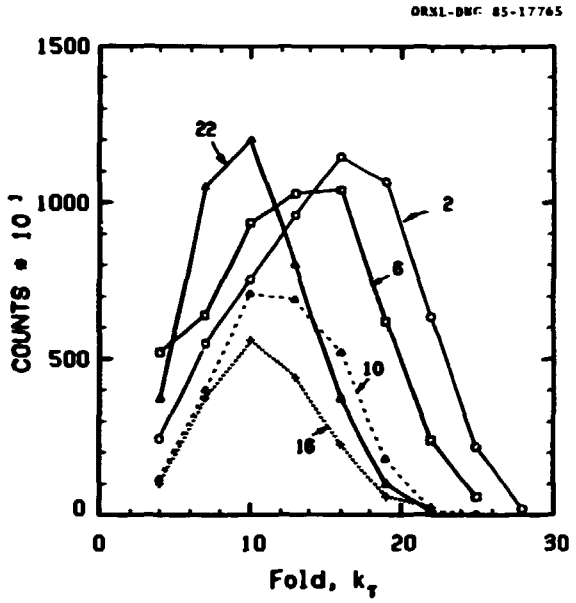

Fig. 2.86. Gamma ray fold distributions observed in coincidence with fragments observed at 55° with the Z values indicated. The yield for Z = 2 is in an arbitrary scale (due to scale-down during the experiment). The yields for Z = 6 and 10 and for Z = 16 and 22 have been multiplied by factors of 50 and 10, respectively.

trend is observed in the liquid drop calculation of Fig. 2.85. The calculation indicates that even though the symmetric divisions are biased towards the larger L-waves, the fraction of this angular momentum transferred dramatically decreases as symmetry is approached. This produces an overall trend of the calculated $(I_L + I_H)$ Z-dependence similar to the experimental Z-dependence of $\langle k_\gamma \rangle$.

Although the Z-dependence of the calculated $\langle I_L + I_H \rangle$ and experimental $\langle k_\gamma \rangle$ have the same trend the slopes and second moments differ considerably. Improved calculations, including fluctuations in the transferred spin[9] and consideration of the $I_L + I_H$ to k_γ transformation, are in progress.

---

1. Washington University, Department of Chemistry, St. Louis, MO 63130.
2. University of Michigan, Department of Chemistry, Ann Arbor, MI 48109.
3. Texas A&M University, Cyclotron Institute, College Station, TX 77843.
4. University of Manchester, Manchester, England.

5. L. G. Sobotka et al., Phys Rev Lett. 51, 2187 (1983).
6. M. A. McMahan et al., Phys Rev Lett. 59, 1995 (1985).
7. L. G. Sobotka et al., Phys Rev Lett. 53, 2004 (1984).
8. A. J. Sierk, Phys Rev Lett. 55, 582 (1985).
9. R. P. Schmitt and A. J. Pacheco, Nucl. Phys. A379, 313 (1982).

FISSION CROSS SECTIONS UP TO 20 MeV/NUCLEON[1]

A. Gavron[2]
J. Boissevain[2]
H. C. Britt[2]
K. Eskola[2,3]
P. Eskola[2,3]
M. M. Fowler[2]
H. Ohm[2,4]
J. B. Wilhelmy[2]
T. C. Awes
R. L. Ferguson
F. E. Obenshain
F. Plasil
G. R. Young
S. Wald[5]

Fission cross sections have been measured for the following reactions: ^{12}C (at E_b = 95, 122, 186, 245, and 291 MeV) on ^{174}Yb, ^{198}Pt, and ^{238}U; ^{16}O (at E_b = 140, 175, 216, 250, and 315 MeV) on ^{142}Nd, ^{170}Er, ^{192}Os, and ^{238}U; ^{32}S (at E_b = 350, 500, and 700 MeV) on ^{126}Te, ^{144}Nd, and ^{238}U; and ^{58}Ni (at E_b = 352 and 875 MeV) on ^{96}Zr, ^{116}Cd, and ^{238}U. We find that use of statistical model calculations with the bass heavy-ion potential, which fit the data below 10 MeV/nucleon, do not fit fission cross sections at higher energies. Invoking dynamical limitations to fusion, such as "extra-push" model calculations, improves the fit to most of the data. For ^{12}C and ^{16}O projectiles on lighter targets, the fission cross section at higher energies is significantly below the value obtained from the rotating liquid drop angular momentum limit, indicating that incomplete fusion reactions may be limiting the fusion process. For S and Ni projectiles, the cross section implies the existence of a composite system sustaining angular momenta far above the limit beyond which, on the basis of liquid drop model predictions, compound nuclei are not expected to have a finite fission barrier. The angular distribution of fission fragments in ^{12}C- and ^{16}O-induced reactions has been measured and compared to calculated values. Discrepancies between the measurements and calculated values imply conditions for the breakdown of the transition state model.

1. Abstract of published paper: Phys. Rev. C 30, 1550 (1984).
2. Los Alamos National Laboratory, Los Alamos, NM.
3. Present address: University of Helsinki, Helsinki, Finland.
4. Present address: Mainz University, Mainz, F.R.G.
5. Lawrence Berkeley Laboratory, Berkeley, CA.

EMISSION OF LIGHT IONS, NEUTRONS, PIONS, AND PHOTONS IN HEAVY-ION REACTIONS

STATISTICAL EMISSION OF ^{2}He FROM HIGHLY EXCITED NUCLEAR SYSTEMS[1]

M. A. Bernstein[2], M. B. Tsang[3], W. A. Friedman[2], T. C. Awes, W. G. Lynch[3], R. L. Ferguson, C. B. Chitwood[3], F. E. Obenshain, D. J. Fields[3], F. Plasil, C. K. Gelbke[3], R. L. Robinson, G. R. Young

Correlations between two protons at small relative momenta are presented for ^{16}O-induced reactions on ^{12}C and ^{27}Al at 400 MeV. These data are well described by a statistical calculation which incorporates the thermal emission of the particle-unstable nucleus, ^{2}He, from the compound nucleus. The good agreement suggests that the emission of particle-unstable light nuclei can be an important decay channel for highly excited nuclear systems and can strongly influence two-particle correlations.

1. Abstract of published paper: Phys. Rev. Lett. 54, 402 (1985).
2. University of Wisconsin, Madison, WI.
3. National Superconducting Cyclotron Laboratory, Michigan State University, East Lansing, MI.

FINAL-STATE INTERACTIONS BETWEEN NONCOMPOUND LIGHT PARTICLES FOR ^{16}O-INDUCED REACTIONS ON ^{197}Au AT E/A = 25 MeV[1]

C. B. Chitwood[2], M. B. Tsang[2], J. Aichelin[2], J. C. Shillcock[3], D. H. Boal[2], T. C. Awes, G. Bertsch[2], R. L. Ferguson, D. J. Fields[2], F. E. Obenshain, C. K. Gelbke[2], F. Plasil, W. G. Lynch[2], R. L. Robinson, G. R. Young

Correlations between protons, deuterons, and tritons at small relative momenta were measured for ^{16}O-induced reactions on ^{197}Au. Final-state interactions are observed for all measured correlations. Analysis of the measured two-deuteron correlations favors the d-d phase shifts extracted by R-matrix techniques over those found from the resonating-group approach. The two-deuteron correlations, which cannot be explained by the decay of unbound resonances, yield source radii which are considerably larger than those extracted from two-proton correlations.

1. Abstract of published paper: Phys. Rev. Lett. 54, 302 (1985).
2. National Superconducting Cyclotron Laboratory, Michigan State University, East Lansing, MI.
3. Simon Fraser University, Burnaby, B.C., Canada.

AZIMUTHAL CORRELATIONS BETWEEN LIGHT PARTICLES EMITTED IN ^{16}O-INDUCED REACTIONS ON ^{12}C AND ^{197}Au AT 400 MeV[1]

M. B. Tsang[2], G. R. Young, W. G. Lynch[2], T. C. Awes, C. B. Chitwood[2], R. L. Ferguson, D. J. Fields[2], F. E. Obenshain, D. R. Klesch[2], F. Plasil, C. K. Gelbke[2], R. L. Robinson

Azimuthal correlations between light particles emitted to polar angles of 40° and 70° with respect to the beam axis were measured for ^{16}O-induced reactions on ^{12}C and ^{197}Au at 400 MeV. Coincident light particles are preferentially emitted in a plane which contains the beam axis. For reactions of ^{12}C, coincident light particles are preferentially emitted to opposite sides of the beam axis. These correlations may be understood in terms of the phase-space constraints imposed by momentum conservation on systems with finite number of nucleons. For reactions on ^{197}Au, on the other hand, preferential emission of coincident deuterons and tritons to the same side of the beam axis may be caused by the shadowing of preequilibrium particles by the adjacent cold spectator nuclear matter.

1. Abstract of published paper: Phys. Lett. 148B, 265 (1984).
2. National Superconducting Cyclotron Laboratory, Michigan State University, East Lansing, MI.

NEUTRON EMISSION PRIOR TO SCISSION

J. R. Beene
J. Boissevain[1]
H. C. Britt[1]
C. Butler[2]
B. Cheynis[3]
D. Drain[3]
R. L. Ferguson
A. Gavron[1]
A. Gayer[1]
P. Grangé[4]
S. Hassani[4]
J. R. Nix[1]
F. E. Obenshain
G. A. Petitt[2]
F. Plasil
A. J. Sierk[1]
H. A. Weidenmüller[5]
G. R. Young

The determination of nuclear dissipation, a fundamental nuclear property, has proved to be elusive, largely because of the difficulty of distinguishing the final effects of dissipation from those resulting from the excitation of specific collective degrees of freedom. In this work, we have approached this problem from both the experimental side and the theoretical side by investigating the average number of neutrons emitted during the fission process, prior to scission. In previous experiments carried out at relatively high excitation energies, a significant enhancement has been found in the number of neutrons emitted prior to scission relative to the number calculated from a standard statistical model. Proposed explanations have included neutron emission during the descent from saddle to scission, as well as during the acceleration of the fission fragments.

From theoretical considerations, nuclear dissipation is expected to affect the number of neutrons emitted prior to scission in three significant ways. First, according to Kramers,[6] when fission is viewed as a quasi-stationary diffusion process over the barrier, dissipation increases the fission lifetime relative to that calculated with the standard Bohr-Wheeler statistical model. Second, dissipation affects the transient time needed for the system to build up the quasi-stationary probability flow over the barrier,[7] which further increases the time available for neutron emission before it passes over the barrier. Third, dissipation increases the mean time required for the system to descend from the saddle point to scission, during which time additional neutrons can be emitted.[8]

Neutron emission measurements were made for the ^{158}Er composite system, for which the fission barrier and statistical model parameters had been studied earlier.[9] Neutrons in coincidence with either fission fragments or evaporation residues were measured at a number of angles. The number of neutrons preceding fission was inferred by comparing our experimental spectra to simulated results obtained by assuming that three sources of neutrons are responsible for the measured neutron spectra. In each case the c.m. spectrum was taken to be isotropic and of the form $\epsilon \exp(-\epsilon/T_i)$, where ϵ is the c.m. neutron energy and T_i is the nuclear temperature of the particle source. The three sources are (1) nonequilibrium neutrons emitted from a moving source of velocity V_{NE} (1.4 cm/ns) and temperature T_{NE} (5.5 MeV); (2) neutrons evaporated from the composite system; and (3) neutrons evaporated from fission fragments. A Monte Carlo technique was used in performing a five-parameter fit. Corrections for various experimental and kinematic effects were included. The results are 0.8 ± 0.1 nonequilibrium neutrons, 2.7 ± 0.4 neutrons evaporated prior to scission, 1.9 ± 0.2 neutrons evaporated from each fission fragment, 2.2 ± 0.1 MeV for the effective temperature of the composite system, and 1.4 ± 0.1 MeV for the temperature of the fission fragments. The above value of 2.7 ± 0.4 neutrons evaporated prior to scission is to be contrasted with 1.6 neutrons obtained from a standard statistical model using parameters determined earlier.[9]

To interpret our experimental results, we take into account the three effects of nuclear dissipation on neutron emission listed above. This is done by first relating various times associated with the fission process to β, the reduced dissipation coefficient obtained by dividing the dissipation coefficient by the inertia. In the next step, the time-dependent fission rate is related to the neutron multiplicity by following in time the competition between neutron emission and fission. This calculation is also performed as a function of β.

First, we modify the statistical model expression for the fission lifetime by including

the effect of dissipation, as discussed by Kramers.[6] Second, we take into account the transient time τ needed for the system to build up the quasi-stationary probability flow over the barrier.[7] The result describes the gradual spreading of the initial probability distribution which arises physically from the coupling of the collective degree of freedom with the internal degrees of freedom. Since the probability current over the barrier rises smoothly from zero to the quasi-stationary value calculated by Kramers, this determines a time-dependent fission rate $\lambda_f(t)$. We denote by τ the time required for $\lambda_f(t)$ to reach 90% of Kramers' value, and refer to τ as the transient time.

The transient time τ is shown in Fig. 2.87 (solid curve) as a function of the reduced dissipation coefficient β for angular momentum $J = 65\ \hbar$, which is the beginning of the angular momentum window that contributes to fission.

The third effect taken into account is the mean time required for the system to move from the saddle point to the scission point.[8] For angular momentum $J = 65\ \hbar$, the dot-dashed curve in Fig. 2.88 shows the dependence of the mean saddle-to-scission time $\bar{t}$ on β.

In the next step, the time-dependent fission rate $\lambda_f(t)$ was used to calculate the neutron multiplicity by following in time the competition between neutron emission and fission. This was done by solving a set of coupled differential equations, with a gain term describing the feeding of a given nucleus by neutron decay of the preceding nucleus and a loss term accounting for both neutron decay and fission.[10]

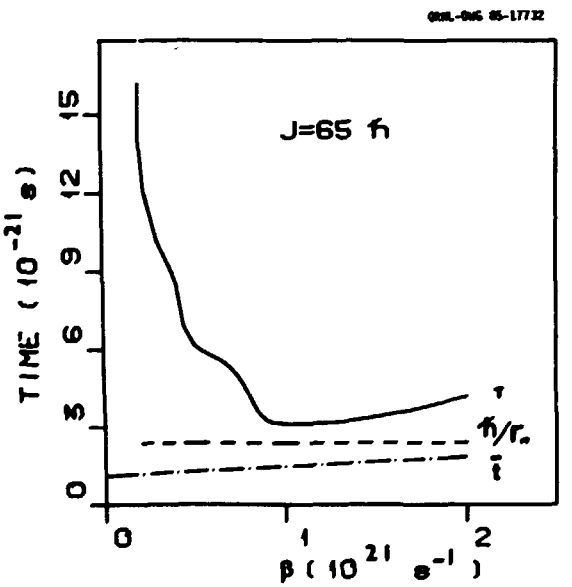

Fig. 2.87. Dependences of the transient time τ (solid curve) and the mean saddle-to-scission time $\bar{t}$ (dot-dashed curve) upon the reduced dissipation coefficient β for angular momentum $J = 65\ \hbar$. The constant dashed curve gives the corresponding lifetime τ_n for the first neutron emitted; this lifetime increases substantially for the emission of subsequent neutrons.

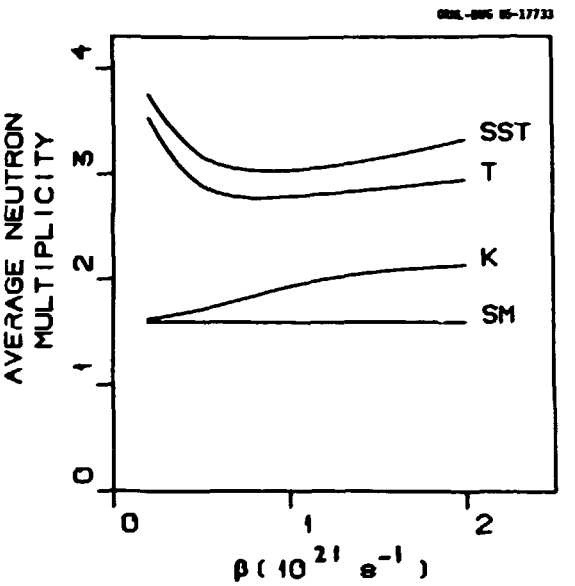

Fig. 2.88. Dependence of the average neutron multiplicity upon the reduced dissipation coefficient β as three modifications to the constant statistical model result, labeled SM, are successively taken into account. The curves labeled K, T, and SST refer to the inclusion of Kramers' formula, transients, and the saddle-to-scission time, respectively.

Figure 2.88 shows how each of the three effects of dissipation that we are considering successively modifies the average neutron multiplicity $\bar{\nu}$. Compared to the constant statistical model value of $\bar{\nu} = 1.6$, the inclusion of Kramers' result leads to a monotonic increase of $\bar{\nu}$ with increasing dissipation. The further inclusion of the transient time required to

build up the quasi-stationary probability current over the barrier leads to an initial decrease of $\bar{\nu}$ with increasing dissipation, followed by a gradual rise after passing through a minimum value. This results from the behavior of the transient time in Fig. 2.87. Finally, inclusion of the saddle-to-scission time causes a monotonical increase in this curve with increasing dissipation, but the final result is qualitatively similar and still contains a minimum.

By comparing the upper limit of our experimental result of 2.7 ± 0.4 neutrons prior to scission with the top curve of Fig. 2.88, we obtain the range $0.5 < \beta < 1.4$ for the reduced nuclear dissipation coefficient, in units of 10^{21} s^{-1}. The corresponding sum of the transient and mean saddle-to-scission times, averaged over angular momentum, ranges from 5.7 to 7.6 x 10^{-21} s.

The above result for the range of β is to be regarded as preliminary, since it may be modified by the following considerations. It appears likely that the effect of dissipation on the fission width, discussed by Kramers, has been taken into account implicitly in previous analyses of experimental fission excitation functions, such as those of Ref. 9, through an adjustment of the ratio a_f/a_n of the level density parameter for fission to that for neutron emission. The much smaller effect of transients on fission excitation functions seems to have been similarly taken into account implicitly through the adjustment of a_f/a_n. Thus, it appears that a_f/a_n values, consistent with experimental results, should be determined as a function of β, and Fig. 2.88 should be recalculated with the dependence of a_f/a_n on β taken into account. These new calculations will probably be closer to the experimental multiplicity of 2.7 ± 0.4 neutrons prior to scission, and the upper limit on the extracted range of β is likely to be significantly larger.

1. Los Alamos National Laboratory, Los Alamos, NM.
2. Georgia State University, Atlanta, GA.
3. Present address: Institut de Physique Nucleaire, Universite Claude Bernard, Lyon, France.
4. Centre de Recherches Nucleaires and Universite Louis Pasteur, Strasbourg, France.
5. Max-Planck Institut fur Kernphysik, Heidelberg, F.R.G.
6. H. A. Kramers, Physica 7, 284 (1940).
7. P. Grange et al., Phys. Rev. C 27, 2063 (1983).
8. J. R. Nix et al., Nucl. Phys. A424, 239 (1984).
9. J. van der Plicht et al., Phys. Rev. C 28, 2022 (1983).
10. S. Hassani and P. Grange, Phys. Lett. 137B, 281 (1984).

NEUTRON EMISSION IN INELASTIC REACTIONS OF ^{12}C + ^{158}Gd AND ^{20}Ne + ^{150}Nd[1]

G. A. Petitt[2] F. E. Obenshain
A. Gavron[3] F. Plasil
J. R. Beene G. R. Young
B. Cheynis[4] M. Jääskeläinen[5]
R. L. Ferguson D. G. Sarantites[5]
C. F. Maguire[6]

Energy spectra and angular distributions of neutrons emitted in coincidence with projectile-like fragments produced in inelastic collisions of ^{12}C with ^{158}Gd at 192 MeV and ^{20}Ne with ^{150}Nd at 176 and 239 MeV have been measured. No evidence for nonequilibrium neutron emission is found for the Ne + Nd reaction at either energy. For the C + Gd reaction a small fraction (~9%) of the neutrons emitted is due to nonequilibrium emission. The multiplicity of neutrons emitted from the targetlike fragment is, in all cases, approximately six times that of neutrons emitted from the projectilelike fragment.

1. Abstract of paper to be published: Physical Review C.
2. Georgia State University, Atlanta, GA.
3. Los Alamos National Laboratory, Los Alamos, NM.
4. Present address: Institut de Physique Nucleaire, Universite Claude Bernard, Lyon, France.
5. Washington University, St. Louis, MO.
6. Vanderbilt University, Nashville, TN.

NEUTRAL PION EMISSION IN 25-MeV/NUCLEON ^{16}O + Al,Ni REACTIONS[1]

P. Braun-Munzinger[2] P. Paul[2]
R. Freifelder[2] F. Plasil
F. E. Obenshain J. Stachel[2]
G. R. Young

Significant pion production cross sections have been observed recently in nucleus-nucleus collisions at energies $35 < E_{lab}/A < 100$ MeV.[3-6] While models based on production from independent nucleon-nucleon collisions generally fail to reproduce the observed cross sections and spectral distributions by several orders of magnitude,[7-10] the data above 50 MeV/nucleon admit an interpretation in terms of various statistical descriptions based on local equilibrium and/or cooperative action of several of the target and projectile nucleons along with cluster formation in the final channel.[11-14] However, at 35 MeV/nucleon there are already significant discrepancies between the data and the predictions of such models.[15]

The measurements were performed using an E/A = 25 MeV beam of ^{16}O provided by the Holifield Heavy Ion Research Facility at ORNL. Beams with an average current of 16 particle nA were used to bombard natural Al and Ni targets which had areal densities of 41 and 45 mg/cm^2, respectively. Neutral pions produced were detected by measuring the two γ rays emitted in their main (98.8%) decay mode, with the use of an array of 20 Pb-glass Cerenkov-detector telescopes. More details of the setup and analysis procedure can be found in Refs. 4 and 16. To tag cosmic-ray events occurring during the experiment, the front of each telescope was covered by a 2.5-cm-thick plastic Cerenkov veto detector,[17] 12.5 x 12.5 cm^2 in area.

Energy and angular distributions of the pions and the corresponding total cross section were obtained with the method described in Ref. 4, except that Monte Carlo simulations[18] were used to determine the energy dependence of the photon detection efficiency of the converters.

The resulting pion production cross sections for ^{16}O + ^{27}Al are shown as a function of π^0 polar angle in Fig. 2.89. The kinetic energy spectra exhibit a peak near T_π = 10 MeV with an exponential falloff towards higher energies.

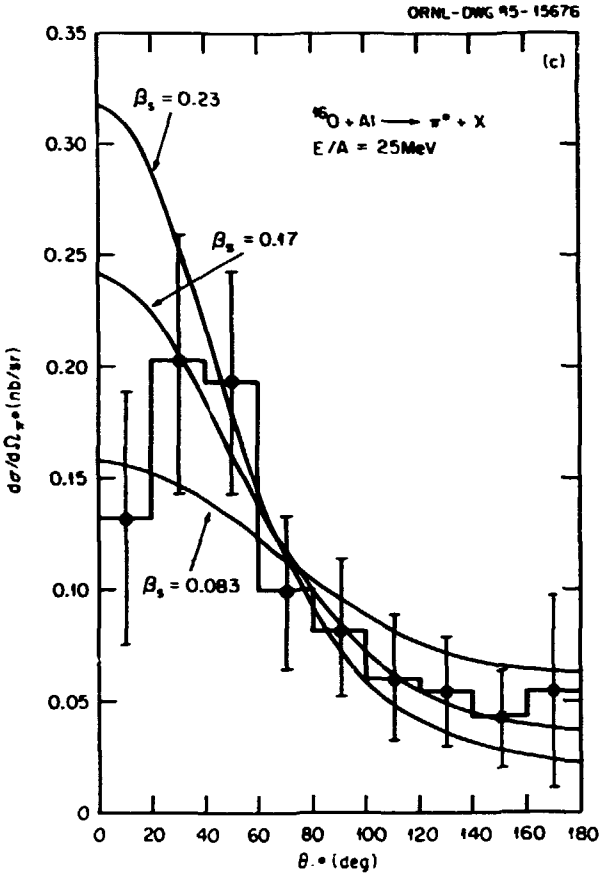

Fig. 2.89. Laboratory angular distribution for neutral pions observed in the reaction E_{lab}/A = 25 MeV ^{16}O + Al → π^0 + X. The solid lines are the predictions of the simple thermal model discussed in the text, with T = 11.6 MeV and source speeds β_s = 0.083, 0.17, and 0.23.

The spectra can be examined to determine whether they are consistent with emission from a common source, as would be expected in present thermal models. For a single thermal source, Hagedorn[19] has derived an expression for $d\sigma/dp_\perp$, which depends only on the temperature of the moving source and is not distorted by source motion along the beam axis. The expression is (for bosons):

$$\frac{d\sigma}{dp_\perp} = \text{const} \cdot p_\perp \cdot \int_0^\infty \frac{dp_z}{\exp\left[\left(m_\pi^2 + p_\perp^2 + p_z^2\right)^{1/2}/T\right] - 1} \qquad (1)$$

The best fit result using this expression yields a temperature of T = 11.6 ± 0.8 MeV (the error

corresponds to a 10% increase in χ^2). Since eq. (1) implies isotropic emission with $d^3\sigma/dp^3 \propto e^{-E_\pi/T}$ in the frame in which the source is at rest, the value of $d^3\sigma/dT_\pi d\Omega$ in the laboratory frame can be computed for various values of the source velocity, β_S, and the results integrated and compared with the measured $d\sigma/dT_\pi$ and $d\sigma/d\Omega_\pi$ spectra. The solid curves drawn in Fig. 2.89 correspond to emission from the center-of-momentum frame ($\beta_S = 0.083$), emission from a frame having the average rapidity of the observed pions ($\beta_S = 0.17$), and emission from the projectile frame ($\beta_S = 0.23$), all for T = 11.6 MeV. The calculated values have been normalized to give the measured total cross section. The results for the calculated angular distribution indicate that values $\beta_S \gtrsim 0.15$ are clearly favored. Although these results indicate that the data are not incompatible with isotropic emission by a single "source," they are at variance with the predictions of the models in Refs. 11-14, which predict $\beta_S < 0.11$. From the shape of the angular distribution at forward angles, it appears that reabsorption of the pions[15,20] in the surrounding nuclear matter may be an important consideration.

The measured inclusive π^0 cross section for the system $^{16}O + ^{27}Al$ is $\sigma_{\pi^0} = 1.22 \pm 0.11 \pm 0.16$ nb, where the first error is systematic as a result of the finite opening angle of the converters and the second is statistical. The measured inclusive π^0 production cross section for the system $^{16}O + Ni$ is $\sigma_{\pi^0} = 2.31 \pm 0.26 \pm 0.45$ nb, which is again more than two orders of magnitude larger than predicted by Ref. 11 or 14. Models based on a nucleon-nucleon single collision production mechanism[9,10] underestimate the measured total cross sections at $E_{lab}/A = 25$ MeV by more than four orders of magnitude and are, therefore, inadequate to describe these data. All theoretical estimates are upper limits as they do not account for the possible reabsorption of the pions after their creation. Estimates[15,20] of this reabsorption probability indicate that the theoretical cross sections will be reduced by factors of two to five depending on pion mean-free path and source geometry.

An idea of the restricted phase space available for π^0 production in the $^{16}O + Al$ reaction can be had from the fact that already at $T_\pi = 40$ MeV, two-thirds of the c.m. energy is taken by the single π^0.

Yasak et al.[21] propose that the pions are produced in a process called pionic bremsstrahlung. In this process pions are radiated as a result of the rapid deceleration of the projectile as it plunges into the target. This model assumes a collective deceleration of target and projectile. For the symmetric system $^{12}C + ^{12}C$, excitation functions have been calculated[21] which fall much less steeply with decreasing beam energy than those predicted in Refs. 10-14. Since at 25 MeV/nucleon the reaction $^{12}C + ^{12}C \rightarrow \pi^0 + X$ is only ~17.7 MeV above the absolute threshold determined by $^{12}C + ^{12}C \rightarrow ^{24}Mg$ (T = 1) + π^0, such calculations cannot be compared to our data. The extension of such bremsstrahlung calculations to asymmetric systems would therefore be interesting as it would also allow comparison of the calculations with the measured energy and angular dependences of the π^0 production cross section.

Brown and Deutchmann[22] have proposed a model in which pions are produced by coherent excitation of a $\Delta(3,3)$ isobar in one nucleus while the other is excited to an S = 1, T = 1 state. Although the original model would not apply at the low bombarding energies studied here due to rapidly decreasing form factors, recent work[23] indicates it can be extended by using closure and thus including all possible excitations of the projectile and target nuclei.

---

1. Summary of paper to be published: Physical Review C.
2. State University of New York, Stony Brook, NY.
3. T. Johannson et al., Phys. Rev. Lett. 48, 732 (1982).
4. P. Braun-Munzinger et al., Phys. Rev. Lett. 52, 255 (1984).
5. H. Noll et al., Phys. Rev. Lett. 52, 1284 (1984); E. Grosse, Proc. Int. Workshop on Gross Properties of Nuclei and Nuclear Excitations XIII, Hirschegg, Austria, January 1985, p. 65.

6. H. Heckwolf et al., Z. Phys. A315, 243 (1984).
7. G. Bertsch, Phys. Rev. C 15, 713 (1977).
8. B. Jakobsson, Phys. Scr. T5, 207 (1983).
9. R. Shyam and J. Knoll, Phys. Lett. 136B, 221 (1984).
10. C. Guet and M. Prakash, Nucl. Phys. A428, 119c (1984).
11. R. Shyam and J. Knoll, Nucl. Phys. A426, 606 (1984).
12. J. Aichelin and G. Bertsch, Phys. Lett. 138B, 350 (1984).
13. J. Aichelin, Phys. Rev. Lett. 52, 2340 (1984).
14. M. Prakash, P. Braun-Munzinger, and J. Stachel, to be published.
15. J. Stachel et al., Proc. INS RIKEN Int. Symp. on Heavy Ion Physics, Mt. Fuji, 1984, Suppl. J. Phys. Soc. (Japan) 54, 400 (1985) and Proc. 7th High Energy Heavy Ion Study, GSI, Darmstadt, 1984, GSI Report 85-10.
16. J. Stachel et al., to be published.
17. Cerenkov plastic SCINTIPLEX I, manufactured by National Diagnostics, Somerville, N.J.
18. C. Michel, submitted to Nuclear Instruments and Methods in Physics Research.
19. R. Hagedorn, Suppl. Nuovo Cimento III, 147 (1965).
20. J. Aichelin, private communication.
21. D. Vasak, B. Müller, and W. Greiner, Phys. Scr. 22, 25 (1980); D. Vasak et al., Phys. Lett. 93B, 243 (1980); D. Vasak et al., Nucl. Phys. A428, 291c (1984).
22. G. E. Brown and P. A. Deutchmann, Proc. Workshop on High Resolution Heavy Ion Physics, Saclay, France, May 1978, p. 212.
23. M. Prakash, C. Guet, and G. E. Brown, to be published.

22-MeV/NUCLEON ^{32}S + Al,Ni π^0 PRODUCTION

T. C. Awes
P. Braun-Munzinger[1]
J. L. Chance[2]
R. L. Ferguson
F. E. Obenshain
P. Paul[1]
F. Plasil
J. Stachel[1]
G. R. Young

We have continued the measurements of subthreshold π^0 production described in the preceding write-up and the references therein to lower bombarding energies and more massive projectiles. The measurements were performed using an E/A = 22 MeV beam of ^{32}S provided by the Holifield Heavy Ion Research Facility at ORNL. Beams with an average current of 10 particle nA were used to bombard natural Al and Ni targets which had areal densities of 13.7 and 19.3 mg/cm^2, respectively. The beam lost less than 70 MeV passing through these targets. Neutral pions produced were detected by measuring the two γ rays emitted in their main (98.8%) decay mode using an array of 20 Pb-glass Cerenkov-detector telescopes. Each telescope consisted of a 5-cm-deep active converter, 9 x 9 cm^2 in area, backed by a 35-cm-deep absorber, 15 x 15 cm^2 in area. More details of the setup can be found in Refs. 3-5. The telescopes were placed on two symmetric conical surfaces centered above and below a horizontal plane containing the beam axis and target. Telescopes were located at intervals corresponding to 30° in the horizontal plane. Each telescope had its front face at 35.9 cm from the target and subtended a solid angle of 60 msr. An energy calibration was obtained from cosmic-ray muons whose pulse height relative to that of 123-MeV electrons had been measured earlier. To tag cosmic-ray events occurring during the experiment, the front of each telescope was covered by a 2.5-cm-thick plastic Cerenkov veto detector,[6] 12.5 x 12.5 cm^2 in area. As their radiation length is quite long (~48 cm), these paddles have less than a 10% chance of rejecting a valid two-photon event if the rejection criterion is that neither veto may fire in a good candidate event. During the experiment, energy thresholds of ~8 MeV were set separately for the converter and absorber in each telescope. Events of twofold or higher coincidence between any valid telescopes (defined as converter and absorber, both exceeding threshold within 35 ns of one another) were recorded on magnetic tape, together with paddle information, for off-line analysis.

Candidate events were selected by requiring a prompt (FWHM < 2 ns) coincidence between absorbers of candidate telescopes and a second prompt (FWHM < 3.3 ns) coincidence between converter and absorber of each telescope. These events were then sorted into a two-dimensional array of invariant mass $M_{inv} = 2(E_{\gamma_1} E_{\gamma_2})^{1/2}\sin(\phi/2)$ (where $c \equiv 1$) versus the opening angle ϕ between the two telescopes. Neutral pions are clustered about $M_{inv} = 135$ MeV independent of ϕ on such a plot. A loose gate on candidate pions of 50 MeV < M_{inv} < 200 MeV and $\phi > 80°$ then indicated that a threshold could be placed on total photon energy in each telescope of 31 MeV with less than 2% loss of efficiency. A candidate event was rejected if any veto paddle fired in the

spectrometer. Lastly, an event was required to occur within ±1.1 ns of the cyclotron rf pulse in order to reduce the cosmic-ray background by an additional factor of 35.

Energy and angular distributions of the pions and the corresponding total cross section were obtained with the method described in Ref. 3, except that Monte Carlo simulations[7] were used to determine the energy dependence of the photon detection efficiency of the converters.

The preliminary total cross section determined for ^{32}S + Al is 0.3 ± 0.1 nb. This value is included in Fig. 2.90 as the open diamond. Plotted there as a function of projectile energy per nucleon in the laboratory is the inclusive cross section for π^0 production divided by the product $A_p^{2/3}$ $A_T^{2/3}$, where A_p and A_T are projectile and target mass numbers, respectively. The curves shown in Fig. 2.90 give the predictions of the models in Refs. 8–12 for the total π^0 cross section as a function of bombarding energy. All theoretical estimates are upper limits as they do not account for the possible reabsorption of the pions after their creation. Estimates[5,13] of this reabsorption probability indicate that the theoretical cross sections will be reduced by factors of 2 to 5 depending on pion mean-free path and source geometry. We therefore conclude that at very low bombarding energies (E_{lab} < 35 MeV/nucleon), the major part of the observed pion production cross section can be understood neither in models based on nucleon-nucleon collisions[8,14] nor in models using statistical phase-space approaches.[9-12] A more collective mechanism must be found.

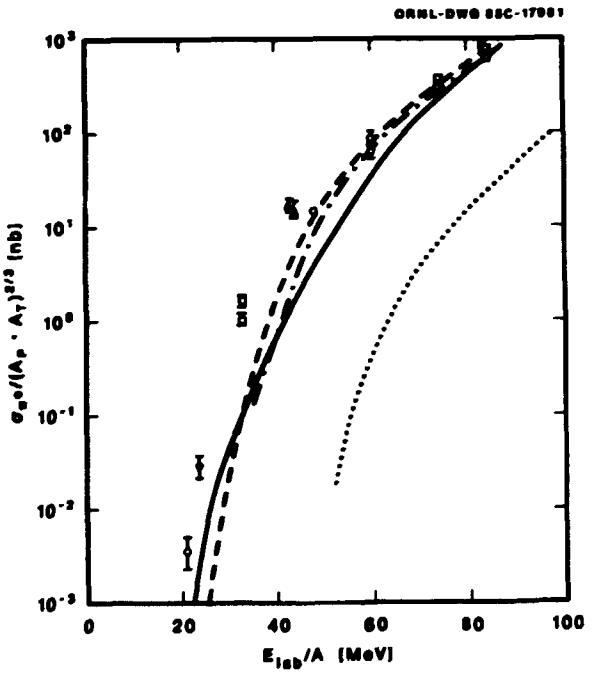

Fig. 2.90. Inclusive cross section for π^0 production, divided by $(A_p^{2/3} \cdot A_T^{2/3})$, where A_p and A_T are the projectile and target mass numbers, respectively, as a function of laboratory bombarding energy. (Open circles: Ref. 15; open triangles: Ref. 16; open squares: Ref. 3; closed diamond: previous write-up; open diamond: present work. The theoretical curves are from Ref. 8 (dotted line), Ref. 9 (long dashed line), Ref. 11 (dash-dot line), and Ref. 12 (solid line).

---

1. State University of New York, Stony Brook, NY.
2. ORAU Student Research Participant from New College, Sarasota, FL.

3. P. Braun-Munzinger et al., Phys. Rev. Lett. 52, 255 (1984).
4. J. Stachel et al., to be published.
5. J. Stachel et al., Proc. INS RIKEN Int. Symp. on Heavy Ion Physics, Mt. Fuji, 1984, Suppl. J. Phys. Soc. (Japan) 54, 400 (1985) and Proc. 7th High Energy Heavy Ion Study, GSI, Darmstadt, 1984, GSI Report 85-10.
6. Cerenkov plastic SCINTIPLEX I, manufactured by National Diagnostics, Somerville, NJ.
7. C. Michel, submitted to Nuclear Instruments and Methods in Physics Research.
8. C. Guet and M. Prakash, Nucl. Phys. A428, 119c (1984).
9. R. Shyam and J. Knoll, Nucl. Phys. A426, 60((1984).
10. J. Aichelin and G. Bertsch, Phys. Lett. 1388, 350 (1984).
11. J. Aichelin, Phys. Rev. Lett. 52, 2340 (1984).
12. M. Prakash, P. Braun-Munzinger, and J. Stachel, to be published.
13. J. Aichelin, private communication.
14. R. Shyam and J. Knoll, Phys. Lett. 1368, 221 (1984).
15. H. Noll et al., Phys. Rev. Lett. 52, 1284 (1984); E. Grosse, Proc. Int. Workshop on Gross Properties of Nuclei and Nuclear Excitations XIII, Hirschegg, Austria, January 1985, p. 65.
16. H. Heckwolf et al., Z. Phys. A315, 243 (1984).

STUDY OF HEAVY-ION BREMSSTRAHLUNG VIA HIGH-ENERGY PHOTON EMISSION

N. Alamanos[1] F. Plasil
T. C. Awes K. Smith[2]
P. Braun-Munzinger[1] J. Stachel[1]
F. E. Obenshain L. Waters[1]
G. R. Young

In recent experiments to measure subthreshold π^0 production[3] and attempts to measure subthreshold π^+ production[4] below 65 MeV/nucleon, it has been noticed that there is a much larger yield of energetic single photons. Whereas the production cross sections for π^0 emission range from μbarns at 60 MeV/nucleon to less than a nanobarn at 22 MeV/nucleon, the inclusive single photon production cross sections exceed 100 μbarns, even at 17 MeV/nucleon as discussed below.

Theoretical models advanced to account for the large yield have investigated production via coherent bremsstrahlung by the two colliding nuclei[5] and both coherent and incoherent bremsstrahlung originating from nucleon-nucleon pairs whose relative motion has been modeled in an intranuclear cascade model.[6] A general theoretical presentation is given in Ref. 7.

We have made measurements of the inclusive single photon yield in a variety of reacting systems. Beams of 25.2-MeV/nucleon ^{16}O, 22.7-MeV/nucleon ^{32}S, and 15.8-MeV/nucleon ^{58}Ni were each used to bombard targets of Al, Ni, and Au. Target thicknesses were chosen to cause a projectile to lose less than 10% of its kinetic energy while passing through the target. The targets were placed at the center of an 80-cm-diameter spherical chamber, which has a 3-mm-thick Al wall.

Photons were detected using the 6" x 6" x 15" lead-glass absorber blocks from the π^0 spectrometer. These are made of type SF5 lead glass which has a critical energy of 15.2 MeV. The resolution has been measured, using the tagged photon beam at Mainz, to be $\sigma/E = 300\%/\sqrt{E}$, E measured in MeV. Four of the absorber blocks were placed at polar angles of 20°, 60°, 100°, and 140° for all bombardments. Four of the remaining 16 absorbers were placed on the tops and sides of each of these "primary" absorbers in order to tag cosmic-ray events and to reject showers from single photons which hit too near the edge of the primary absorber, thus producing a shower that was not contained in the primary absorber. The plastic veto paddles from the π^0 spectrometer were placed in front of the primary absorber in order to tag cosmic rays entering from that direction and to tag electrons or positrons coming from the target. Such electrons or positrons could arise either from prompt production in a reaction or from conversion of outgoing energetic photons in the 3-mm (=1/29.7 X_0) aluminum wall of the vacuum chamber. The number of such events seen in this experiment is consistent with their all being produced by photon conversion in the chamber wall.

After rejecting events hitting the veto paddles and absorbers, a correction was made for background events and nonrejected cosmic rays by subtracting spectra gated off the cyclotron rf peak from those gated in prompt coincidence with that peak. Some of the resulting photon energy spectra are shown in Fig. 2.91.

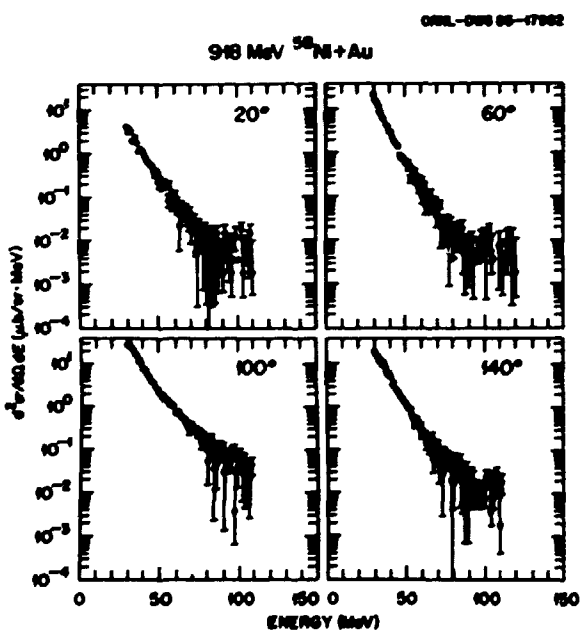

Fig. 2.91. Representative energy spectra of single photons produced in heavy-ion collisions at E/A = 16-25 MeV. The abscissa is in MeV. The production angle is noted on the figure.

It is seen that they extend to energies in excess of 100 MeV, even for bombarding energies of 15.8 MeV/nucleon. The falloff below 25 MeV is due to electronic thresholds.

Table 2.14 gives energy-integrated yields of single photons for photon energies from 25 to 125 MeV at each of the 4 angles measured for the 12 projectile-target combinations. Figure 2.92 shows the yields plotted as a function of polar angle for a few representative cases. It is expected that dipole radiation from incoherent neutron-proton collisions will peak at $\theta = 90°$ and that quadrupolar radiation from coherent emission in proton-proton collisions will peak near 45° and 135°. The degree of coherent production is expected to increase markedly with the Z's of the colliding partners.

The similarity of the production cross sections for the different targets for a given incident projectile does not appear to favor coherent emission from deceleration of the two colliding nuclei as a whole. The lack of a measurable (<3% contribution) direct yield of positrons or electrons also does not favor models predicting an appreciable yield of leptons relative to photons.

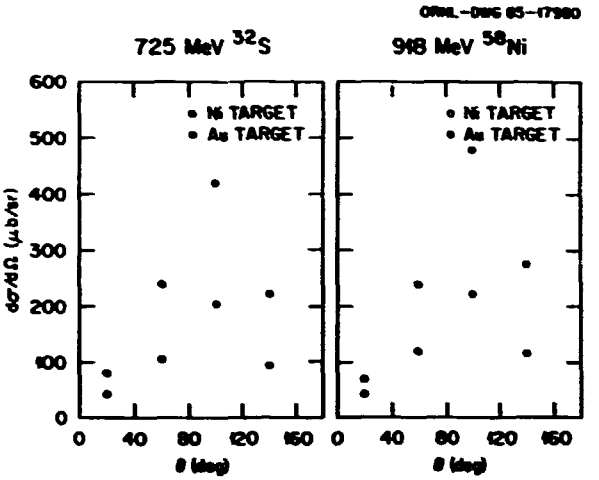

Fig. 2.92. Angular distributions of energy-integrated (25-125 MeV) photon yield for various projectile-target combinations.

1. State University of New York, Stony Brook, NY.

2. GLCA Science Semester Student from Rollins College, Winter Park, FL.

3. See previous two articles on subthreshold π^0 production in this section and references therein.

4. K. B. Beard et al., Phys. Rev. C 32, 1111 (1985).

5. T. de Reus and W. Greiner, to be published; D. Vasak et al., Nucl. Phys. A428, 291c (1984).

6. Che Ming Ko, G. Bertsch, and J. Aichelin, Phys. Rev. C 31, 2324 (1985).

7. H. Nifenecker and J. P. Bondorf, Nucl. Phys. A442, 478 (1985).

Table 2.14. Energy-integrated (from 25 to 125 MeV) inclusive yield of photons for the projectile-target systems indicated. $d\sigma_\gamma/d\Omega_\gamma$ is given in units of microbarn/steradian.

Projectile	E/nucleon	Target	20°	60°	100°	140°
^{16}O	25.2	Al	34.6	63.6	53.4	142.3
		Ni	29.5	69.0	96.4	67.9
		Au	48.8	123.8	163.0	156.1
^{32}S	22.7	Al	33.8	74.3	161.6	70.9
		Ni	44.6	108.6	203.9	96.1
		Au	81.0	241.1	421.5	217.9
^{58}Ni	15.8	Al	32.0	76.7	151.4	77.1
		Ni	45.5	122.6	222.8	116.5
		Au	68.4	243.0	479.0	276.7

MISCELLANEOUS TOPICS

E2 AND E4 DEFORMATIONS IN ^{232}Th AND ^{239,240,242}Pu[1]

J. D. Zumbro[2,3] W. Reuter[4,5]
R. A. Naumann[2] E. B. Shera[4]
M. V. Hoehn[4] C. E. Bemis, Jr.
Y. Tanaka[4,6]

High-resolution muonic K, L, and M X-ray spectra from ^{232}Th and ^{239,240,242}Pu have been measured using a stopping μ^- beam at the biomedical channel of LAMPF in a manner previously described for the isotopes of uranium (Ref. 7). Precise intrinsic quadrupole (Q_0) and hexadecapole (H_0) moments have been determined for these nuclides from analyses of the spectra. The resultant parameters of the deformed Fermi charge distribution (c, a, β_2, and β_4), the rms radii ($\langle r^2 \rangle^{1/2}$) and the intrinsic moments are listed in Table 2.15.

For the odd-A case studied here, ^{239}Pu (K = 1/2), the large amount of information contained in the muonic hyperfine structure enabled us to independently determine nine E2 intraground-state-band matrix elements as listed in Table 2.16. These matrix elements are completely specified in zero order by the single parameter, Q_0, and the rotational quantum numbers. Small deviations may be expected for odd-A nuclides due to Coriolis coupling ($\Delta K = 1$). The adiabatic rotational model agrees with experiment to within ±3% for all nine matrix elements, and a slight improvement is obtained when the first order ($\Delta K = 1$) band mixing correction is included and when the band mixing coefficient, ζ, is adjusted to best fit the experimental values. A comparison of the experimental and model matrix elements for ^{239}Pu is given in Table 2.16. The band mixing coefficient, $\zeta = -(1.8 \pm 0.5) \times 10^{-3}$, is consistent with values observed by us for the odd-A uranium isotopes, ^{233}U and ^{235}U.

---

1. Summary of paper in press: Physics Letters B.
2. Princeton University, Princeton, NJ.
3. Present address: Physics Department, University of Pennsylvania, Philadelphia, PA.
4. Los Alamos National Laboratory, Los Alamos, NM.
5. Present address: University of Tubingen, Tubingen, F.R.G.
6. Present address: The Chukyo College, Gifu-ken, Japan.
7. J. D. Zumbro et al., Phys. Rev. Lett. 53, 1888 (1984).

Table 2.15 ^{232}Th and ^{239,240,242}Pu charge parameters. The parameters c, a, and $\langle r^2 \rangle^{1/2}$ are given in units of fm, Q_0 in units of eb, and H_0 in units of eb^2.

Nucleus	^{232}Th	^{239}Pu	^{240}Pu	^{242}Pu
c*	6.9445 (16)	7.0366 (17)	7.0369 (15)	7.0632 (14)
a*	0.5110 (12)	0.4985 (13)	0.5055 (11)	0.4988 (11)
Q_0†	9.645 (53)	11.563 (61)	11.860 (65)	11.901 (63)
H_0†	2.48 (19)	2.84 (6)	2.47 (13)	2.08 (12)
β_2*	0.2331 ( )	0.2607 (7)	0.2718 (17)	0.2766 (15)
β_4*	0.0946 (94)	0.0896 (18)	0.0700 (57)	0.0498 (52)
$\langle r^2 \rangle^{1/2}$*	5.8024 (43)	5.8765 (22)	5.8867 (30)	5.8973 (25)

*Model-dependent analysis (statistical uncertainties only).
†Q_0 and H_0 include 0.5% and 2.0% model uncertainty, respectively.

Table 2.16. Spectroscopic quadrupole moments and B(E2) values for ^{239}Pu. Spectroscopic and intrinsic moments (q and Q, respectively) are given in units of eb, and the B(E2) values are given in $(eb)^2$. Errors, enclosed in parentheses, do not include model uncertainties. The value listed in [ ] is the change in the given quantity corresponding to a 0.06 eb^2 change in the intrinsic hexadecapole moment (i.e., the uncertainty in H_0 listed in Table 2.15).

	Present experiment	Theory	
		Adiabatic rotation	Rotation $+\Delta K = 1$ mixing
B(E2; 1/2 → 3/2)	5.313 (22) [2]	5.347	5.314
B(E2; 1/2 → 5/2)	7.951 (35) [1]	8.020	8.031
q(3/2)	-2.319 (7) [1]	-2.319	2.327
B(E2; 3/2 → 5/2)	1.097 (26) [3]	1.146	1.111
B(E2; 3/2 → 7/2)	6.999 (38) [4]	6.875	6.884
q(5/2)	-3.345 (13) [1]	-3.312	-3.324
B(E2; 5/2 → 7/2)	0.476 (13) [0]	0.509	0.476
B(E2; 5/2 → 9/2)	6.428 (34) [1]	6.365	6.374
q(7/2)	-3.826 (26) [4]	-3.864	-3.878
Q_{20}		11.592 (13)	11.583 (13)
ζ		0.0	$-1.8\ (5) \times 10^{-3}$
χ^2/DF		4.61	3.41

SEARCH FOR SUPERHEAVY ELEMENTS IN DAMPED COLLISIONS BETWEEN ^{238}U AND ^{248}Cm[1]

J. V. Kratz[2] G. Herrmann[3]
W. Brüchle[2] U. Hickmann[3]
H. Folger[2] P. Peuser[3]
H. Gäggeler[2] N. Trautmann[3]
M. Schädel[2] E. K. Hulet[4]
K. Sümmerer[2] R. W. Lougheed[4]
G. Wirth[2] J. M. Nitschke[5]
N. Greulich[3] R. L. Ferguson
R. L. Hahn[6]

Upper limits for the production of superheavy elements (SHE's) in damped collisions between ^{238}U projectiles and ^{248}Cm targets were measured. This reaction is believed to permit a closer and more generally applicable approach to the predicted island of stability near Z = 114 and N = 184 than any practical fusion reaction. Aqueous and gas-phase chemistry techniques were used to isolate SHE fractions. The fractions were counted for spontaneous fission activity; fragment kinetic energies and neutron multiplicity were measured. Cross section limits for half-lives from hours to several years are $< 4 \times 10^{-35}$ cm^2.

1. Abstract of paper to be published: Physical Review C.
2. GSI, Darmstadt, F.R.G.
3. Institut fur Kernchemie, Universitat Mainz, Mainz, F.R.G.
4. Lawrence Livermore National Laboratory, Livermore, CA.
5. Lawrence Berkeley Laboratory, Berkeley, CA.
6. Chemistry Division, ORNL.

MEASUREMENTS OF MOELLER AND BHABHA SCATTERING NEAR E = 1.6 MeV

K. A. Erb W. T. Milner
I. Y. Lee D. Shapira

The narrow peaks observed in positron spectra from collisions of very heavy nuclei have

spurred [illegible] explanations. The Frankfurt [illegible]ying initially predicted spontaneous [illegible] emission in superheavy quasi-atomic [illegible]tly showed that the formation of [illegible] $>10^{-20}$ sec) nuclear molecules could [illegible] peaks in the positron energy spectra.

More recently, [illegible]idates for the long-lived intermediate [illegible]ich is required to account for the [illegible] have been put forward. Wong[1] [illegible] positronium ions were formed [illegible] collision, their e^+-γ two-body [illegible] could produce monoenergetic positrons [illegible] the energy of the observed peaks. [illegible]tcher, Strayer, and Lee[2] [illegible] the possibility that the [illegible] of an axion-like object having [illegible] MeV could account for the positron [illegible] the latter mechanism, in particular, existence of a resonance in the [illegible] positron interaction at a relati[illegible]y.

We are measuring electron-ele[illegible] electron-positron elastic scattering [illegible] functions over the relevant range of [illegible] order to probe this possibility. The el[illegible] and positron beams are obtained from radi[illegible] sources. Various metallic targets are being studied. The scattered leptons are detected [illegible] mini orange spectrometers constructed from perm[illegible] manent rare earth magnets, following a design of J. Saladin.[3] Preliminary electron-electron data have been measured and we are now beginning the electron-positron measurements.

1. C. Y. Wong, ORNL Preprint, 1985.
2. A. B. Balantekin, C. Bottcher, M. R. Strayer, and S. J. Lee, Phys. Rev. Lett. 55, 461 (1985).
3. J. X. Saladin, private communication.

PHYSICS WITH ONE-ELECTRON, HIGH-Z IONS: PREPARATIONS FOR EXPERIMENTS AT THE BEVALAC

C. E. Bemis, Jr.
J. R. Beene
J. Gomez del Campo
C. R. Vane
H. Gould[1]
C. Munger[1]
J. Alonso[1]
R. McDonald[1]
G. Drake[2]

Exciting new research opportunities in the interface area of atomic-nuclear physics are opened when fully stripped (bare) and single-electron (hydrogenlike) ions of high Z ($Z > 80$) are available for experimentation. The next generation of proposed higher energy heavy-ion accelerators will allow such opportunities to be fully exploited, but at present, the Bevalac at Lawrence Berkeley Laboratory is the only accelerator capable of providing such ions. Most atomic-physics-oriented experiments at the Bevalac, to date, for ions with $Z > 50$ have dealt with charge-changing phenomena, such as electron capture and loss, and with energy loss and stopping processes. The remainder have dealt with tests of quantum electrodynamics (QED) in one- and two-electron ions.

We have an approved Bevalac experiment[3] to explore the selective preparation and detection of electron-spin-polarized one-electron ions of high Z. Such state-selected one-electron ions can then be used in other experiments, such as determination of the QED contributions to the magnetic moment of bound electrons in the high Coulomb field limit and unique determinations of hyperfine structure and hyperfine structure anomalies which, in turn, can provide unique information on higher order QED terms. Hyperfine structure anomalies in single-electron $1s\ 1/2$ ions may be related to the distribution of nuclear magnetism in the nucleus in an unambiguous fashion.

Our initial experimental investigations will involve axial channeling phenomena [illegible] electron-pickup and electron-l[illegible] expected to have become greatly [illegible] those present in an amorphous solid [illegible] an example, for well-channeled [illegible] fully stripped ^{238}U ions, the predominant electron-capture mechanism is expected to be direct K-shell radiative capture (KREC) since the nonradiative capture processes, which require small impact parameter collisions, are greatly suppressed. The KREC cross section may be calculated exactly and is 40 barns/electron for $^{238}U(+92)$ at 400 MeV/nucleon. Similarly, the electron-loss mechanisms in axial channeling have also become simplified. We expect that electron-impact ionization would be the dominant electron removal process for the single K-shell

electron in 400-MeV/nucleon $^{238}U(+91)$, again since hard ion-atom collisions are suppressed for well-channeled ions.

Demonstration of channeling for ^{238}U ions at 400 MeV/nucleon requires a beam emittance that must be achieved by brute collimation at the Bevalac. Axial channeling half-angles in the <110> axis of Si are 0.02°. Channeling may be detected by an analysis of the emergent charge-state spectrum and by the beam energy loss, both of which are provided by magnetic analysis. The simplification of capture and loss processes in channeling at these energies make the channeling process itself interesting for study, but the goal of our efforts is to produce spin-state-selected one-electron ions which might be achievable by channeling in ferromagnetic single crystals. Pickup of polarized electrons by KREC might provide this selection.

1. Lawrence Berkeley Laboratory, Berkeley, CA.
2. University of Windsor, Windsor, Ontario, Canada.
3. H. Gould and C. E. Bemis, Jr., Bevalac Proposal #719M, "Polarized Hydrogenlike Uranium" (unpublished).

STUDY OF NUCLEUS-NUCLEUS COLLISIONS AT RELATIVISTIC ENERGIES: CERN-SPS WA80 EXPERIMENT

R. Albrecht[1]
T. C. Awes
C. Baktash
P. Beckmann[2]
J. R. Beene
F. Berger[2]
R. Bock[1]
G. Claesson[1]
M. Doss[3]
L. Dragon[2]
R. L. Ferguson
S. Garpman[4]
R. Glasow[2]
E. E. Gross
H. A. Gustafsson[4]
H. H. Gutbrod[1,5]
J. W. Johnson
K. H. Kampert[2]
B. Kolb[1]
P. Kristiansson[3]
I. Y. Lee
M. Löhner[2]
F. E. Obenshain
A. Oskarsson[4]
I. Otterlund[4]
T. Peitzmann[2]
S. Persson[4]
F. Plasil
A. M. Poskanzer[3]
M. Purschke[2]
H. G. Ritter[3]
R. Santo[2]
R. Schmidt[1]
R. Schulze[1]
T. Siemiarczuk[6]
K. Soderstrom[4]
S. P. Sorensen[7]
E. Stenlund[4]
Y. Stepaniak[6]
R. Wienke[2]
G. R. Young
I. Zielinski[6]

WA80 is an approved experiment to be carried out at CERN in 1986 and 1987. It originated from experiment PS190 (Ref. 8), which was proposed in 1981 and approved in 1982 as a three-part activity. PS190 consisted of the installation of an injector-preaccelerator for ^{16}O ions at CERN by GSI and LBL, together with the simultaneous operation of two experiments referred to as "streamer chamber" and "plastic ball," in accordance with their respective 4π vertex detectors. In a subsequent development, the scope of the plastic ball experiment of PS190 was expanded, and was then independently approved by the CERN SPS committee in 1984. It was assigned the name WA80.

The primary physics goals of WA80 are:

1. survey of high energy nucleus-nucleus collisions (i.e., ^{4}He, ^{16}O, and ^{32}S projectiles of 60 and 225 GeV/nucleon incident on Al, Ag, and Au targets) and comparisons with pion and proton-nucleus collisions;
2. search for indications of the formation of the quark-gluon plasma (QGP) or similar phase transitions;
3. determination of nuclear stopping power and thus the maximum baryon density limit.

The survey part of WA80 follows from the experience of the LBL and GSI groups at the Bevalac. It is evident that global observables of these collisions have to be established to differentiate between the various classes of reactions. There is no simple way to distinguish, in a single event, between a few hard nucleon-nucleon collisions and many soft nucleon-nucleon collisions. WA80, therefore, aims at differentiating a collision by impact parameter, by the entropy produced, and by the transverse energy content. (The mean transverse energy per particle can be related to the temperature in a thermalized system.) Below we indicate the studies that we intend to perform as a function of projectile and target masses.

In the baryon-rich fragmentation region, which coincides mostly with the target region due to the kinematics involved in collisions of light ions with heavy target nuclei, we plan to:

1. Determine matter flow from a global analysis approach.[9] If finite flow angles are observed, then the reaction plane is defined, and together with multiplicity measurements, the impact parameters can be deduced. The

observation of flow will allow us to investigate shock phenomena in the collision.

2. Measure the extent of spectator drag from determinations of the average value of $p_{\parallel}$ in this rapidity region.
3. Determine pertinent temperatures from inclusive energy spectra.[10]
4. Determine the entropy from d/p ratios.[11]
5. Determine the size of emitting sources from two-particle correlations, such as π^+-π^+ or p-p correlations.[12]
6. Search for high-energy nuclear states through two- and three-particle correlations.

The above set of studies is, in effect, an extension of the current GSI/LBL plastic ball program from Bevalac energies of 1 GeV/nucleon to high energies.

It is difficult to predict what might be observed in the mid-rapidity region in the collisions of ^{16}O nuclei with heavy target nuclei. From nuclear emulsion studies[13] it is evident that from the charged-particle multiplicity distribution, it is possible to extract the effective target size involved in the collision and thus to define the collisions kinematics. Furthermore, assuming all charged particles to be pions, or having originated from pions, their number M_c can be related directly to the entropy produced in the participant region, which, in turn, can reflect possible phase transitions. Strong fluctuations of M_c with pseudorapidity could be attributed to deflagration phenomena of the QGP.[14] It is, therefore, the goal of WA80 to measure carefully, in geometrical detail, all charged particles in θ and ϕ so that all possible fluctuations in $dM_c/d\theta d\phi$ can be spotted.

Along with the matter- or energy-flow data from the fragmentation region, it is very important to study the transverse energy distribution ($dE_{\perp}/d\eta$) in the mid-rapidity region as a function of the number of participants. If multiple collisions of constituents dominate the reaction, then the transverse energy increases with increasing number of participants.[10] Furthermore, azimuthal asymmetries in the $E_{\perp}$ distribution, if detected, could yield information on the reaction mechanism. We intend to measure $dE_{\perp}/d\eta$ in the forward part of the mid-rapidity region, together with the full coverage of $E_{\perp}$ in the target-fragmentation region.

Complementary to global observables, such as $E_{\perp}$, there are single-particle observables of great importance, such as $p_{\perp}$. For studying intermediate to large $p_{\perp}$ phenomena as seen in ^4He-^4He collisions at the ISR,[15] we have chosen to study π^0 and single photons at intermediate to large $p_{\perp}$ near 90° in the nucleon-nucleon center of mass. In this region, "temperatures" beyond the Hagedorn limit can be studied. The use of Pb-glass Cerenkov detectors in a finely segmented array helps to suppress the low-energy soft particles and allows the identification of π^0. The observation of direct gamma production may be one of the signatures of a QGP.[16]

Finally, the projectile rapidity region needs to be addressed primarily for the purpose of providing a trigger for other components of the experiment. Thus, it needs to be determined whether or not the projectile has undergone any type of interaction with a target nucleus. Furthermore, the study of nuclear stopping will involve the measurement of leading particles as a function of target thickness. Also, bremsstrahlung photons are predicted to be produced at projectile rapidity in reactions where the projectile has been stopped by the target, and an effort may be made to detect them.

The experimental arrangement is shown in Figs. 2.93 and 2.94. It consists of five major pieces of equipment: the plastic ball,[17] SAPHIR (single arm photodetector for heavy-ion reactions),[18] the wall calorimeter,[19] the multiplicity array,[20] and the zero-degree calorimeter.[19] In addition, there is a vacuum pipe containing a beam counter upstream of the target and a bull's eye detector downstream.

The plastic ball,[17] presently in operation at the Bevalac, consists of 655 ΔE-E telescopes and will detect target rapidity fragments from protons through alphas and π^+. It will be modified, opening it up at forward angles, so as not to shadow the downstream detectors. A time-of-flight wall of 60 pairs of 8-cm-wide by 72-cm-long and 4.5-cm-thick scintillators will

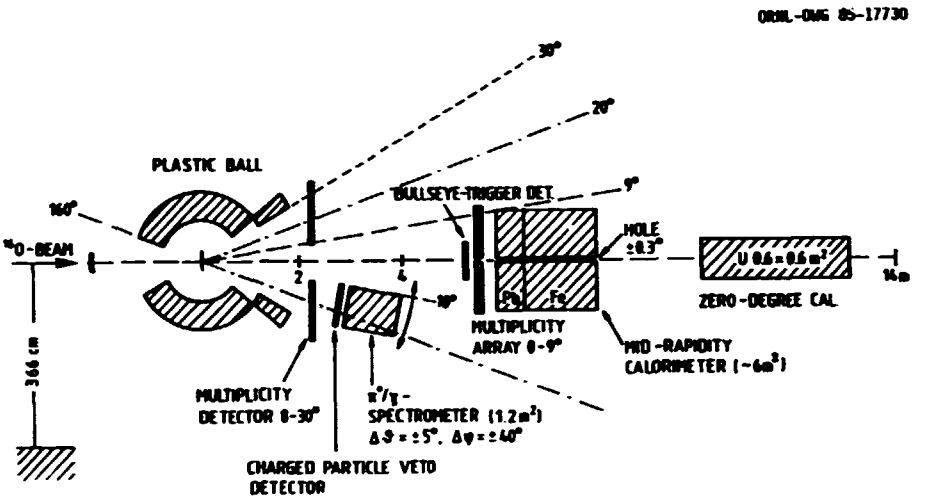

Fig. 2.93. WA80 experimental configuration.

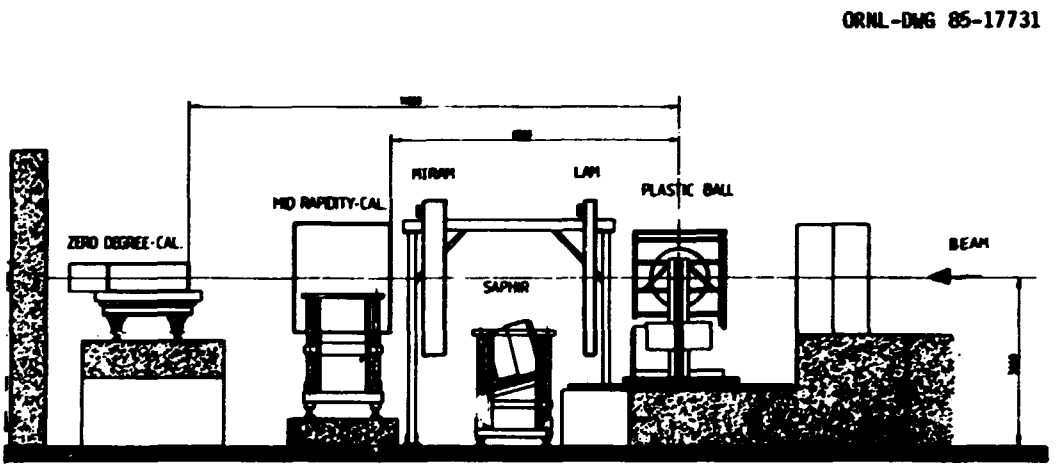

Fig. 2.94. Side view of the WA80 experimental arrangement. The distances indicated are in mm.

cover the angles of $10° < \theta < 30°$ on both sides. The double layer allows a good discrimination against neutral particles. Of special interest is the detection of $Z > 2$ fragments of energies below 1 GeV/nucleon.

SAPHIR[18] is a lead-glass calorimeter for π^0 and direct gamma identification, consisting of 1350 modules. The modules of SF5 lead glass are 48 cm long and 3.5 x 3.5 cm at the front face. It will be placed under the beam line at $8° < \theta < 18°$ and cover approximately 40° in azimuthal angle. A streamer-tube multiplicity detector will serve for charged-particle discrimination.

The 6-m^2 wall calorimeter[19] at a distance of 6.5 m from the target will detect mid-rapidity baryons and pions. It is a modified version of the Fabjan-Willis sampling calorimeters used at CERN. It consists of 150 towers with a lead-scintillator electromagnetic section (15 radiation lengths) and a stainless steel-scintillator hadronic section (6.2 nuclear interaction lengths).

Multiplicity arrays[20] will determine the pseudorapidity of all charged particles. LAM (the large-angle multiplicity detector) will cover the angles from 9° to 30°. Just behind

LAM and covering the area of SAPHIR will be SAM, the small-angle multiplicity detector. MIRAM (mid-rapidity multiplicity detector), consisting of a double layer (for 100% efficiency), will be placed in front of the wall calorimeter. The multiplicity arrays will be made of streamer tubes of the Iarocci type with pad readout setting of a bit for each of the 25,000 cells.

The zero-degree calorimeter[19] will measure the total kinetic energy of the projectile fragments for use in the trigger. It contains both electromagnetic and hadronic sections, each consisting of interleaved uranium-scintillator plates.

The upstream beam counter will identify the Z of the projectile (from protons to ^{40}Ca) and generate the timing signal which will be used as a trigger. The bull's eye detector at the exit of the vacuum pipe downstream of the target will measure the sum of the square of the nuclear charges of the projectile fragments for use in the trigger. Both detectors will probably be Cerenkov counters made of thin sheets of quartz; these are being developed.

The survey part of the experiment requires the choice of at least three targets, spread in mass. Due to the high multiplicity of secondaries and due to the detection of photons and of relatively slow fragments, the target thickness cannot be more than 200 mg/cm^2, or about 0.5% of the interaction length. We have chosen our targets to be Al, Ag, and Au. The first beam period of about two weeks is expected to occur in December 1986. It is to be followed by a second beam period of about equal length in the first part of 1987.

---

1. GSI, Darmstadt, F.R.G.
2. Munster University, Munster, F.R.G.
3. Lawrence Berkeley Laboratory, Berkeley, CA.
4. Lund University, Lund, Sweden.
5. Spokesman for WA80 experiment.
6. Warsaw University, Warsaw, Poland.
7. Adjunct research participant from the University of Tennessee, Knoxville, TN.
8. A. Angert et al., "PS190 Proposal," p. 557 in Quark Matter Formation and Heavy-Ion Collisions, World Science Publishers, Singapore, 1982.
9. H. A. Gustafsson et al., Phys. Rev. Lett. 52, 1590 (1984).
10. H. A. Gustafsson et al., Phys. Lett. 142B, 141 (1984).
11. K.G.R. Doss et al., Phys. Rev. C 32, 116 (1985).
12. H. A. Gustafsson et al., Phys. Rev. Lett. 53, 544 (1984).
13. S. Garpman et al., Z. Phys. C20, 281 (1983).
14. M. Gyulassy, Nucl. Phys. A418, 59 (1984).
15. A.L.S. Angelis et al., Phys. Lett. 116B, 379 (1982); A.L.S. Angelis et al., Nucl. Phys. A418, 321c (1984).
16. W. Willis, Proc. Physics Opportunities at Isabelle Summer Workshop, Brookhaven National Laboratory, BNL Report 51443, Vol. 2, p. 652 (1981).
17. A. Baden et al., Nucl. Instrum. Methods Phys. Res. 203, 189 (1982).
18. SAPHIR is the responsibility of Münster University.
19. ORNL has the responsibility for the wall and the zero-degree calorimeters.
20. GSI is responsible for the multiplicity arrays.

INSTRUMENTATION

MID-RAPIDITY AND ZERO-DEGREE CALORIMETERS FOR THE CERN WA80 EXPERIMENT

T. C. Awes
C. Baktash
J. R. Beene
R. L. Ferguson
T. A. Gabriel[1]
E. E. Gross
J. W. Johnson
I. Y. Lee
F. E. Obenshain
F. Plasil
S. P. Sorensen[2]
G. R. Young

The CERN WA80 experiment is described in the preceding article. Two calorimeters are being built for this experiment. Both are the responsibility of ORNL. The wall calorimeter is one of the main detector systems of the experiment. It is a joint venture with LBL, Lund University, and GSI, Darmstadt. The zero-degree calorimeter is primarily a trigger calorimeter, and only ORNL is involved in its design and construction.

Wall Calorimeter

The wall calorimeter covers an area of 6 m^2 and will be located 6 m downstream from the target. It has been designed to study the participant mid-rapidity region (rapidity $\gtrsim$ 2). In addition to providing results of intrinsic interest, it is also to be used as a specialized trigger, capable of selecting events with a high

associated transverse energy, E_T. When combined with the multiplicity array located just in front of it, it is an excellent tool for the study of global energy flow, of energy fluctuations, and of the relative contributions of hadronic and electromagnetic components. The extremely large multiplicities anticipated from central events make the use of calorimeters particularly desirable. Aside from the obvious advantage of circumventing the measurement of a large number of individual particles, calorimeters have the advantage that effects of fluctuations in the number of particles emitted from a quasi-thermal distribution are relatively small, even in the case of single events. This fact, together with the tendency to average-out instrumental fluctuations, results in an accurate determination of the energy flow on an event-by-event basis. Thus, any observed structure (as a function of rapidity or azimuthal angle) may be attributed to the physical process involved. For example, in the case of a deconfinement transition involving large latent heat, structure in the energy flow is predicted. During the expansion and cooling stages, the latent heat may manifest itself in the form of a deflagration shock wave,[3] resulting in observable structure that is expected to be quite different from that associated with jets.

The choice of calorimeter was determined by the requirements of granularity, of separate electromagnetic and hadronic readouts, and of adequate energy resolution. The design chosen, after extensive Monte Carlo simulation studies,[4] is a modified version of the modular uranium calorimeter stacks of the AFS collaboration at CERN.[5] The constituent towers of this calorimeter each cover an area of 20 x 20 cm^2. The primary modifications to the AFS design are as follows:

1. Instead of uranium and copper, lead is used in the electromagnetic section, and stainless steel in the hadronic section.
2. The length of the electromagnetic section was increased from 6 to 15 radiation lengths, corresponding to 97.4% containment for 1-GeV γ's and 91% containment for 30-GeV γ's.
3. The length of the hadronic section was increased to contain 96% of the energy of a 50-GeV proton.
4. The mechanical rigidity of the stacks was increased by the replacement of corner washers in the scintillator sheets with rods and washers.
5. The center rod was replaced by a tube to permit the insertion of a calibration source.
6. An optical laser light fiber system was added for stability checking and calibration procedures.
7. Grooves have been cut into the plastic sheets along the boundaries of individual towers in order to increase the position sensitivity.

From the Monte Carlo calculations, the optimum thickness of the steel plates was found to be 8 mm. The overall composition of each stack is as follows. The electromagnetic section consists of 27 lead sandwiches (consisting of 0.8-mm Al + 3-mm Pb + 0.8-mm Al), interleaved with 27 scintillator sheets (3 mm thick). The length of the section is 21.6 cm, and the weight is 280 kg. The nominal size of all plates is 20 cm x 120 cm, as in the case of the AFS calorimeters. The 122 8-mm-thick steel plates of the hadronic section are interleaved with 122 scintillator plates of 3-mm thickness. The length of the hadronic section is 134 cm, and the weight is 1947 kg. The overall length is 156 cm, and the overall weight is 2227 kg. A stack of the wall calorimeter is illustrated in Fig. 2.95. For this design, the following calculated results were obtained by T. A. Gabriel:

	1 GeV	5 GeV
Resolution for protons $\sigma/E(\%)$	37 (45)	22 (22)
e/p ratio	1.50 (1.15)	1.86 (1.24)

The numbers in parentheses are balanced numbers. They result from multiplying the signal from the hadronic section by 1.86, which is the ratio of the energy loss in a unit cell of the hadronic section to that in a unit cell of the electromagnetic section.

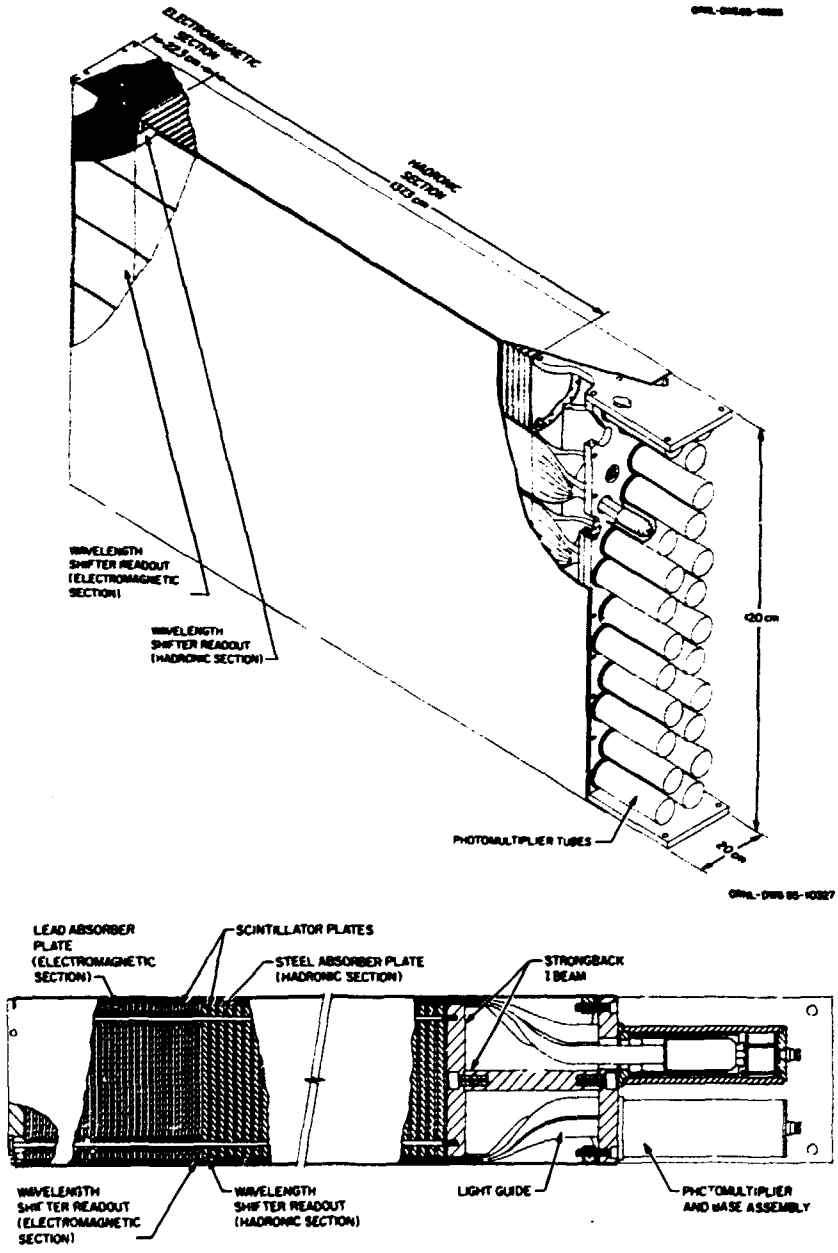

Fig. 2.95. One of the stacks of the wall calorimeter.

Extensive simulation calculations have been performed by S. P. Sorensen[6] in order to anticipate the response of the wall calorimeter to likely events. The event generator used is the Lund model, as applied to nucleus-nucleus collisions.[7] The results are very encouraging and show that the wall calorimeter will detect a large fraction of the particles produced in central collisions.

Zero-Degree Calorimeter

The primary considerations in the case of this trigger calorimeter were: (1) near-total containment for protons of 225 GeV; (2) excellent energy resolution; and (3) fast count rate capability. Monte Carlo calculations[4] were used to optimize the design. The calorimeter was designed to have good energy resolution so that

the difference of one nucleon could be distinguished; i.e., 14 or 15 nucleons could be distinguished from the oxygen projectile having 16 nucleons. It was determined that a uranium-plastic sampling calorimeter would provide the required resolution. The optimum area turned out to be 0.6 x 0.6 m. The device has an electromagnetic section consisting of 32 uranium sheets (2 mm thick) interleaved with 3-mm-thick scintillator sheets. The hadronic section contains 275 uranium sheets (3 mm thick) interleaved with 275 3-mm-thick scintillator sheets.

For this design, the following results were obtained:[b]

	5 GeV	50 GeV
Resolution for protons σ/E'(%)	17 (18)	10 (11)
e/p ratio	1.3 (1.1)	1.3 (1.1)

The numbers in parentheses are the balanced numbers.

The zero-degree calorimeter consists of only one stack. Thus, close packing of stacks is not required, and the plates are enclosed in a frame, with two dual readout systems on all four sides. Corner rods are also used to stabilize the assembly. The calorimeter is illustrated in Fig. 2.96.

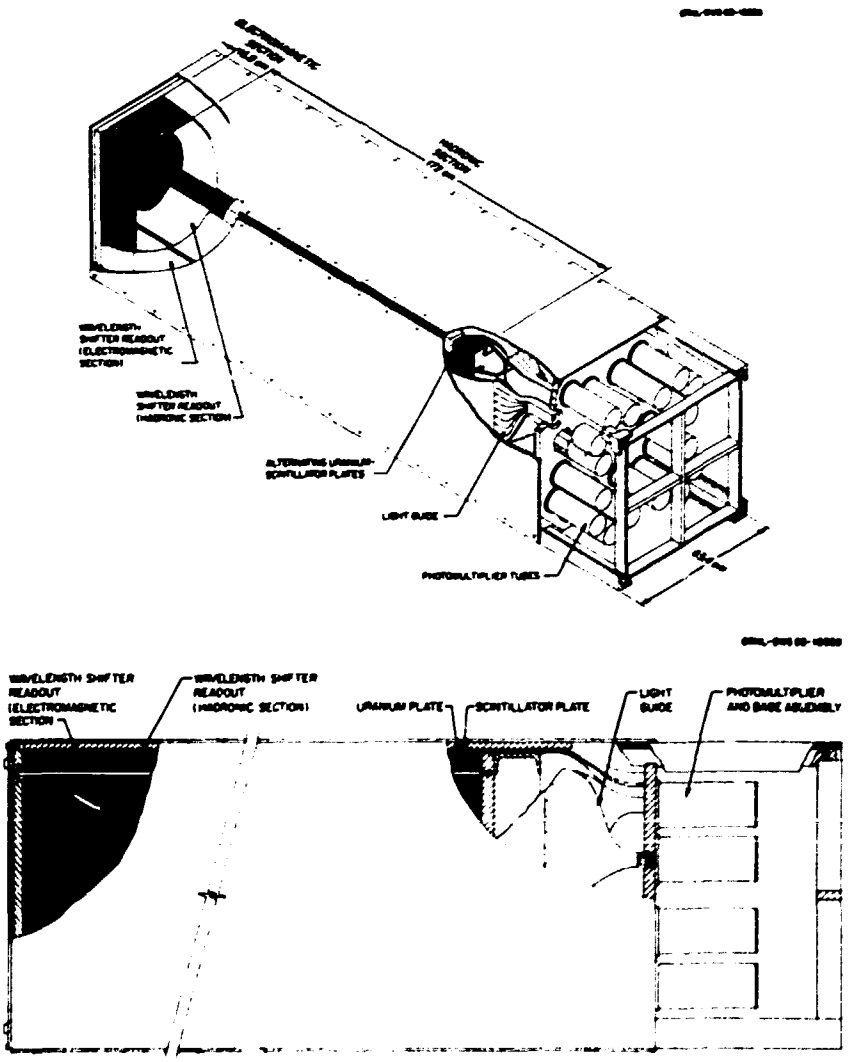

Fig. 2.96. Zero-degree calorimeter.

1. Engineering Physics and Mathematics Division, ORNL.
2. Adjunct research participant from the University of Tennessee, Knoxville, TN.
3. M. Gyulassy, Nucl. Phys. A418, 59c (1984).
4. T. A. Gabriel, Oak Ridge National Laboratory, private communication.
5. H. Gordon et al., Nucl. Instrum. Methods 196, 303 (1982); T. Akesson, Report CERN-EP/85-80, submitted to Nuclear Instruments and Methods in Physics Research, 1985.
6. S. P. Sorensen, "Simulations of the Reponse of the WA80 Wall Calorimeter," in this report.
7. B. Andersson, in Proceedings of the Second International Conference on Nucleus-Nucleus Collisions, Visby, Sweden, June 10-14, 1985, to be published in Nuclear Physics A.

SIMULATIONS OF THE RESPONSE OF THE WA80 WALL CALORIMETER

S. P. Sorensen[1]

As part of the preparations for the WA80 experiment,[2] the response of the wall calorimeter has been simulated. The two major ingredients in the calculations are (a) the LUND event generator which calculates particle species, multiplicities, and four-momentum distributions in high-energy nucleus-nucleus collisions and (b) the response of the wall calorimeter to each of the impinging particles.

For the calculation of this response, there exist several Monte Carlo programs, which in great detail simulate the development of both electromagnetic and hadronic showers. They are, however, extremely time-consuming and costly to run, so we have chosen to find an analytical parametrization of the energy deposition for both types of showers. Based partly on Monte Carlo calculations by T. Gabriel with the code HETC[3] and partly on results from the UA1 group,[4] the following parametrization for the average energy deposition has been chosen:

$$\left\langle \frac{d^3E}{dxdydz} \right\rangle = N \; F(z) \; G(r) \; ;$$

$$F(Z) = \frac{\eta}{\Gamma(\alpha_1)} t_1^{\alpha_1 - 1} e^{-t_1} + \frac{1-\eta}{\Gamma(\alpha_2)} t_2^{\alpha_2 - 1} e^{-t_2} \; ;$$

$$t_1 = \beta_1 \frac{z}{X_0}; \; t_2 = \beta_2 \frac{z}{\lambda} \; ;$$

$$G(r) = \frac{\omega}{2\pi\lambda_1^2} e^{-r/\lambda_1} + \frac{1-\omega}{2\pi\lambda_2^2} e^{-r/\lambda_2} \; .$$

The normalization factor N depends on the type and energy of the incoming particle. F(z) describes the longitudinal shape of a shower measured from the start of the shower. The first term, which scales with the radiation length X_0, represents the electromagnetic part (neutral pions) of the shower, and the second term represents the pure hadronic interactions and scales with the absorption length λ. For an electromagnetic shower the second term is not used. G(r) describes the transverse profile of the shower. For hadronic showers it contains two exponential components: a long-range term (λ_1 = 6 cm) originating from neutrons and a short-range term (λ_2 = 1-4 cm) caused by the rest of the hadronic particles. For hadronic showers the free parameters were determined by a least-squares fit to the HETC results; for electromagnetic showers, values from the literature were used.[4]

Only the energy deposited in the plastic scintillators results in emission of light. This energy can be estimated from the ratio between the energy loss of minimum ionizing particles in the scintillator and the passive absorber. The light collection is simulated by taking the absorption in both the scintillator and the wavelength shifter into account. For the electromagnetic section also, the reduced cross-talk due to slotting the scintillator is included.

Due to the stochastic nature of a shower, the energy deposited in the calorimeter will have very large fluctuations, both in total magnitude and in spatial position. These fluctuations have been approximated by randomly varying the origin of the shower, the total deposited energy, the length of the shower, and the radial size of the shower. The magnitude and probability distributions for the variations were again determined from the HETC calculations.

Ultrarelativistic nucleus-nucleus collisions will produce extremely high particle multiplicities. Our calculations have shown that, for $^{16}O + ^{197}Au$ at 225A GeV, a typical central event will produce 600-800 particles and that half of them will hit the wall calorimeter. The towers

at the smallest angles will each be hit by up to 40 particles, and the total deposited energy can go up to 400-500 GeV. These high multiplicities have a positive effect on the energy resolution of the calorimeter, since the individual shower fluctuations are averaged out. As can be seen from Fig. 2.97, the total transverse energy impinging on the calorimeter can be estimated to within 4-5%. Since the calorimeter samples a large fraction of all particles produced in each event, the total transverse energy of all particles emitted in an event can be determined with an uncertainty of between 10% and 15%.

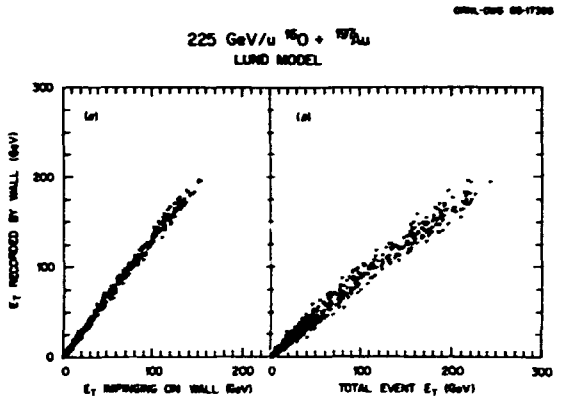

Fig. 2.97. Transverse energy deposited in the wall calorimeter as function of (a) the incident E_T, and (b) the total event E_T for 500 LUND model events.

An important feature of the WA80 experiment is the measurement of the energy flow on an event-by-event basis. It is therefore essential to know to what extent the original spatial energy distribution in an event will be distorted by the calorimeter response and how well the off-line analysis will be able to restore this distribution. Figure 2.98 shows that most of the energy is deposited in a few towers at the smallest angles and that the gross features of the energy distribution are preserved by the calorimeter response. A closer inspection reveals that a substantial fraction of the energy of the hadrons is deposited in the electromagnetic section and that many of the finer details in each section are washed out.

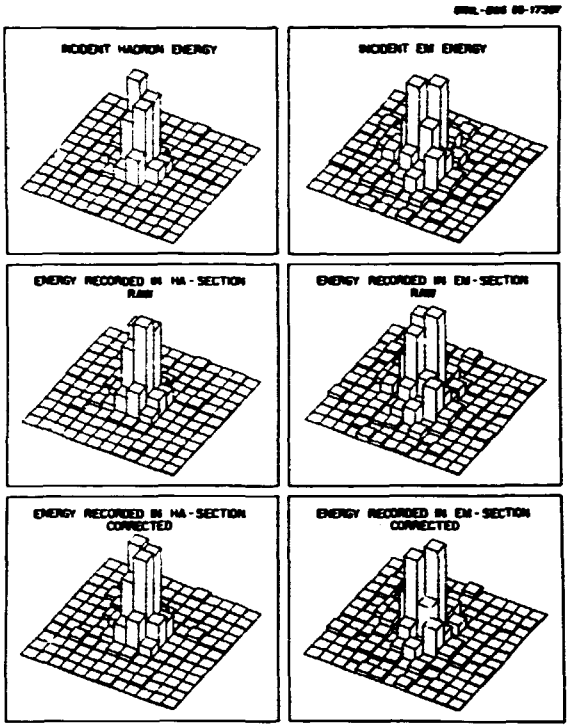

Fig. 2.98. The simulated energy deposition in each tower of both the electromagnetic and hadronic sections for a "typical" high multiplicity LUND model event. The upper row shows the incident energy; the middle row shows the uncorrected deposited energy; and the lower row shows the energy deposition corrected with the off-line analysis algorithms.

Based on the same algorithm that is used to unfold the detector response in the Spin Spectrometer, we have found that the off-line analysis, to a large extent, can restore both the original electromagnetic to hadron balance and many of the finer details in the energy distribution.

The simulation code has also been used to (a) determine the multiplicity and energy distributions in each tower, (b) investigate whether rapid fluctuations in the pseudorapidity distributions can be detected, (c) estimate the effects of "dead" photomultipliers on the E_T trigger and the energy-flow measurements, and (d) test a variety of off-line correction algorithms.

---

1. Adjunct research participant from the University of Tennessee, Knoxville, TN.

2. R. Albrecht et al., "Study of Nucleus-Nucleus Collisions at Relativistic Energies: CERN-SPS WA80 Experiment," in this report.
3. T. A. Gabriel, Nucl. Instrum. Methods 150, 145 (1978) and private communication.
4. M. Della Negra, Phys. Scr. 23, 469 (1981).

DEVELOPMENT OF THE OAK RIDGE COMPTON SUPPRESSION SPECTROMETER SYSTEM

N. R. Johnson, I. Y. Lee, C. Baktash, F. K. McGowan, J. W. Johnson, R. P. Cumby, D. C. Hensley, M. L. Halbert, L. L. Riedinger[1], D. G. Sarantites[2], J. W. McConnell, M. E. Whitley

In recent years there has been an intense interest in understanding the behavior of nuclei when excited into states of very high energy and very high angular momentum. At present there exists at the Holifield Heavy Ion Facility of ORNL an outstanding device, the Spin Spectrometer, for studying nuclei under these extreme conditions. However, this device, consisting of a 4π array of sodium iodide (NaI) detectors, does not have the resolution necessary for the study of properties of the many closely spaced γ-ray lines found in the spectra of highly excited nuclei formed in compound nucleus reactions. Replacement of some of the NaI elements with solid-state germanium (Ge) detectors provides the high resolution needed for these experiments, but has the shortcoming of having a large unusable background component arising from Compton-scattered photons. The result is that many weak transitions are simply masked in the spectra. A far more favorable situation can be achieved if the Ge detector is surrounded by a high stopping power medium which senses the Compton scattered photons and provides a veto signal to reject the residual energy left in the Ge detector. In so doing, much of the background in a γ-ray spectrum is eliminated, offering exceptional capabilities for the study of these highly excited nuclear systems. Consequently, we have begun a project to develop a Compton suppression spectrometer system whose units can either be inserted into the Spin Spectrometer or can be arranged in stand-alone configurations.

After a considerable effort in formulating the design concept, we purchased a prototype suppression unit to fit into the Spin Spectrometer. The unit was comprised primarily of the scintillator bismuth germanate (BGO) because of its large absorption coefficient for γ rays (more than twice that of NaI). However, since BGO has a much smaller light output than does NaI, we decided to make the front 0.40-inch-thick lip of the prototype from NaI for effective detection of the low-energy photons backscattered from the Ge detector. Monte Carlo calculations were performed for the prototype design and these indicated that, for a 1-MeV photon incident on the Ge detector, an average Compton-suppression factor of about 6 should be obtained.

Once received, the prototype system was tested extensively, and the results were very gratifying. The test data revealed that for ^{60}Co γ rays the suppression below the full-energy peaks averages almost a factor of five. This result is in good agreement with the value obtained in the Monte Carlo calculations.

From these tests we concluded that our design concept could provide the improved γ-ray detection capability needed at the HHIRF and that we could enhance the performance by reducing the diameter of the opening in the front face of the detector, by increasing the thickness of this front lip to 0.78 inches, and by making the lip of BGO also. These modifications should yield further suppression, particularly in the region of 700-1000 keV in the spectrum of ^{60}Co. Based on the excellent performance of this prototype unit, we placed orders for five more pentagonal BGO suppression units and for six hexagonal units and returned the prototype for modifications to the front lip.

The final design of the Compton suppression unit is illustrated in Fig. 2.99. To each of the five optically isolated segments of this pentagonal unit there is attached a 1.5-inch-diameter photomultiplier tube to collect the light output. The Ge detector is inserted down the 2.5-inch-diameter well in the BGO unit to a point near the front lip. Just behind the Ge

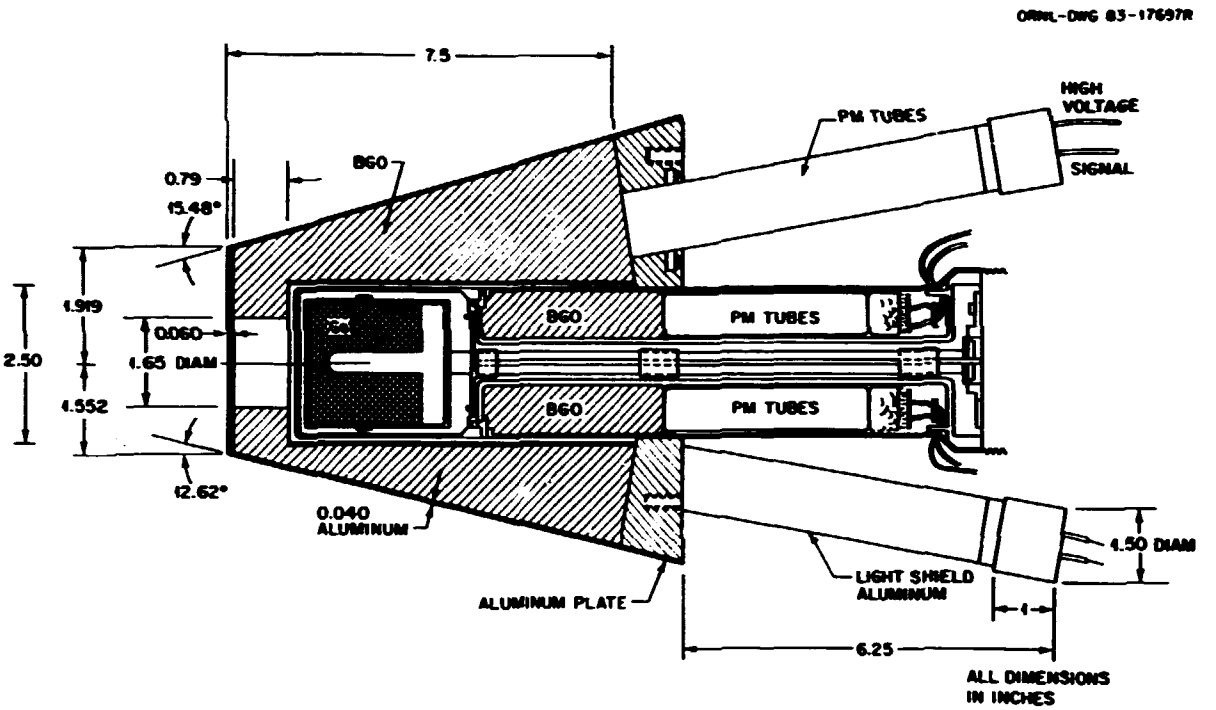

Fig. 2.99 Illustration of a full Compton-suppressed Ge detector unit.

detector, and around its 0.75-inch cooling arm, are attached the two halves of an additional small BGO cylinder which intercepts the photons scattered in the forward direction.

Recently we received the first three BGO suppression shields. The power of this Compton suppression device is obvious from an examination of the test data shown in Fig. 2.100. The top spectrum contains the unaltered results (normal spectrum) from a ^{60}Co source as seen by the Ge detector. This detector is a large volume ORTEC "γ-x" type germanium diode. The middle spectrum shows that portion of the normal spectrum which is rejected by the suppression shield. (Note that the heights of the full-energy peaks at 1173 and 1333 keV are off scale but are normalized in these data.) Finally, the bottom spectrum shows the net results that are recorded and used from such a Compton-suppression system. As we had anticipated after the prototype tests, our design modifications provided substantial improvement in the detection of large-angle scattered photons, resulting in better quality suppression at high energies.

Because of predicted slow delivery times on BGO suppression units and of the time to be consumed in testing the prototype, we elected to purchase several NaI suppression shields which could be delivered more rapidly. At the present time a total of nine NaI suppressors is available. These units provide modest suppression factors of from 2.5 to 3. In this interim period, more than a dozen experiments have been carried out with whatever components of the Compton suppression system were available at that given time. These involved mostly nuclear structure studies of high-spin states, but also have included several reaction mechanism studies. The large central cavity (35 cm diameter) of the Spin Spectrometer provides exceptional capability for experiments on reaction mechanisms because it can accommodate large and complex arrays of particle detectors.

In the fall of 1985, high efficiency γ-γ coincidence measurements will be carried out with from 12 to 15 Compton suppressed Ge detectors in the Spin Spectrometer. In the spring of 1986, we expect to have 17 units operational

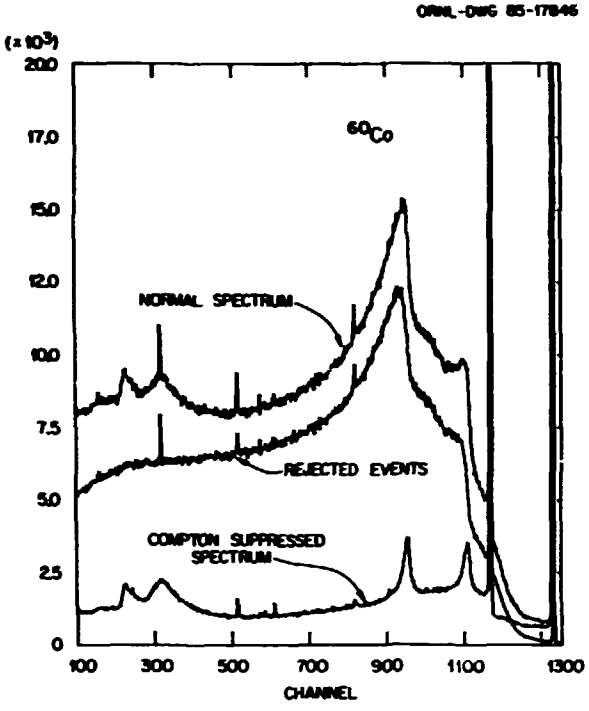

Fig. 2.100. ^{60}Co spectra taken with the Compton-suppression unit shown in Fig. 2.99. The top spectrum contains the unaltered results (normal spectrum) from a ^{60}Co source as seen by the Ge detector. The middle spectrum shows that portion of the normal spectrum which is rejected by the suppression shield. Note that the heights of the full-energy peaks at 1173 and 1333 keV are off scale, but have been normalized in these data. The bottom spectrum shows the net results that are recorded and used from such a Compton-suppression system.

(with 12 BGO and 5 NaI suppressors). This system will include dedicated electronics and an automated liquid nitrogen filling system.

---

1. Adjunct staff member from the University of Tennessee, Knoxville, TN.
2. Washington University, St. Louis, MO.

PROGRESS ON HILI -- HEAVY-ION LIGHT-ION DETECTOR

D. Shapira J. L. Blankenship[2]
B. L. Burks C. A. Reed[3]
K. Teh[1] J. W. McConnell

Detailed design of the proposed counter system[4] is complete and actual construction is underway. Two test runs were performed with a coupled 15-MeV/nucleon Ni beam.

The first test run in November 1984 was to study beam transmission and beam quality for coupled operation into the 76-cm chamber site, the actual site intended for HILI. Particular attention has been paid to ascertain that the beam can be transferred down a 2-cm-diameter tube placed at a distance further than 60 cm from the target. Test results have shown that this can be done provided the beam can be tuned to a 4 x 3 mm or larger spot on the target with a focus (or waist) past the target position.

The second test was performed in February 1985 to study the performance of a phoswich detector. Several types of plastic scintillators were studied and the performance of different phototubes evaluated. The results showed that the intended separation of protons and α particles is easily obtained over the whole dynamic range desired. The signal processing scheme that was used and the quality of ΔE-E map identifying various products are shown in Figs. 2.101 and 2.102.

The event-by-event output from the evaporation code PACE[5] is used to simulate the coincident yield of light and heavy particles emitted by different heavy ion reactions. The program has just been brought on line and will be used to evaluate and predict the response of the counter system.

In a subsequent test run[6] an alternate scheme of processing phoswich signals was tested. It is similar to the scheme shown in Fig. 2.102 but has a fast linear gate for the current signal. This is the actual scheme adopted for processing the signals from the HILI hodoscope.

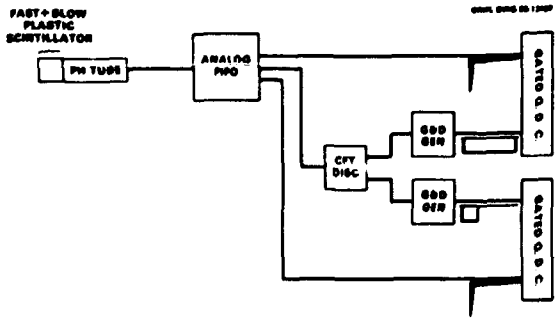

Fig. 2.101. A block diagram of signal processing for the phoswich detector signals.

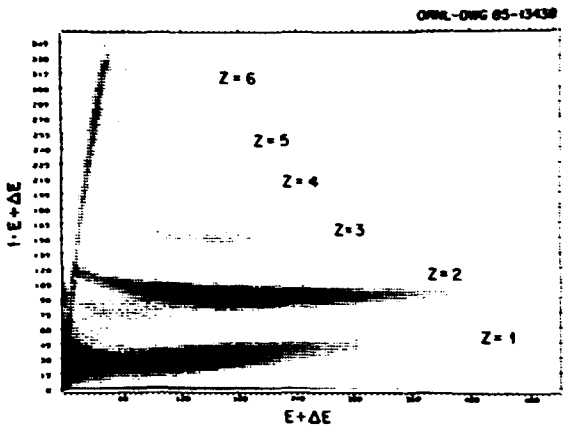

Fig. 2.102. Total energy vs energy loss map note that a small fraction f << 1 of the slow plastic signal is included in the ΔE signal.

Procurement of most of the parts for the HILI is complete. Pending still are the detailed design work and construction of a position-sensitive parallel-plate avalanche counter that will provide trigger signals for the HILI, and the necessary modification to the existing scattering chamber.

---

1. Vanderbilt University, Nashville, TN 37235 and Joint Institute for Heavy Ion Research, ORNL, Oak Ridge, TN 37831.
2. Instrumentation and Controls Division, ORNL.
3. Oak Ridge Associated Universities, Oak Ridge, TN 37831.
4. D. Shapira, J. L. Blankenship, and B. L. Burks, Phys. Div. Prog. Rept. Sept. 30, 1984, ORNL-6120, p. 114.
5. J. R. Beene, private communication.
6. K. Teh et al., following article in this section.

DECAY TIMES OF SLOW PLASTIC SCINTILLATORS

K. Teh[1] R. L. Varner
C. F. Maguire[1] J. L. Blankenship[2]
D. Shapira E. J. Ludwig[3]
B. L. Burks R. E. Fauber[3]

The recent introduction of plastic scintillators with relatively long decay times has enabled the phoswich technique to be used for charged particle detection and identification. This technique involves the optical coupling of two plastic scintillators with different thicknesses and decay times. In our application a thin, fast scintillator and a thick, slow scintillator were used. Light produced when radiation is incident on this particle telescope is viewed with a single photomultiplier tube. Contributions from the two scintillators in the combined light signal can be easily differentiated by their characteristic decay constants. By integrating appropriate portions of the light signal one is able to essentially measure (1) the energy loss in the thin piece and (2) the total energy deposited by the incident radiation. The feasibility of such a scheme was tested earlier this year at the Holifield Heavy Ion Research Facility.[4] A ^{58}Ni beam was used to bombard a ^{12}C target and the reaction products were detected with the phoswich telescope. From a two-dimensional plot of the light yield in the thin plastic versus the total light yield in the telescope, products ranging from protons and deuterons to carbon nuclei were easily identified.

The effective use of the phoswich technique for particle identification requires (1) establishing the time structure of the light signal, (2) calibrating the light yield as a function of energy deposited, and (3) determining the scintillator's response to specific ionization. Since such information is not yet available for slow plastic scintillators, measurements were made to determine the above characteristics. This was done at the Triangle Universities Nuclear Laboratory, where monoenergetic protons and alpha particles were used to bombard a gold target. Beams of 8-, 12-, 16-MeV protons and 12-, 18-, 24-MeV alpha particles were elastically scattered from the target and detected with a single piece of the slow scintillator.

Two different slow scintillators were examined: NE115 (Nuclear Enterprises) and BC444 (Bicron). Each piece, 10-cm-long and 2.5 cm in diameter, was coupled to a single photomultiplier tube and mounted approximately 10 inches from the target at a scattering angle of 30° on either side of the beam direction. The signal from the PMT was analyzed with a charge integrating ADC (see Fig. 2.103). The gate signal was varied in width to determine the

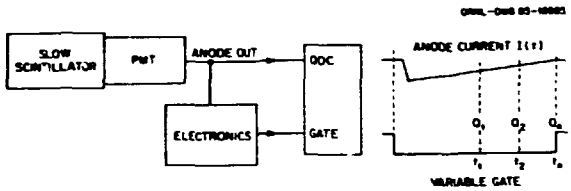

Fig. 2.103. The integrated charge (Q_1, Q_2, ... Q_n) as a function of integration time is obtained by varying the gate signal width (t_1, t_2, ... t_n). The decay time is deduced by assuming $dq/dt \sim \exp(pt/t_d)$.

integrated charge as a function of integration time. By assuming the following functional form of the current pulse

$$I(t) = dQ/dt = A*\exp[-(t-t_0)/t_D]$$

the decay time t_D can be deduced by performing a least-squares fit to the derivative of the data points. The central difference formula was used to approximate the time derivative of the charge. Figure 2.104 shows a sample fit using this method.

The results are tabulated in Table 2.17. Both plastics have long decay times — on the order of 300-350 nsec. The NE115 has on the average, a 50 nsec longer decay time than the BC444. There is no indication of any systematic dependence on the incident energy. The estimated accuracy of the method used to extract the

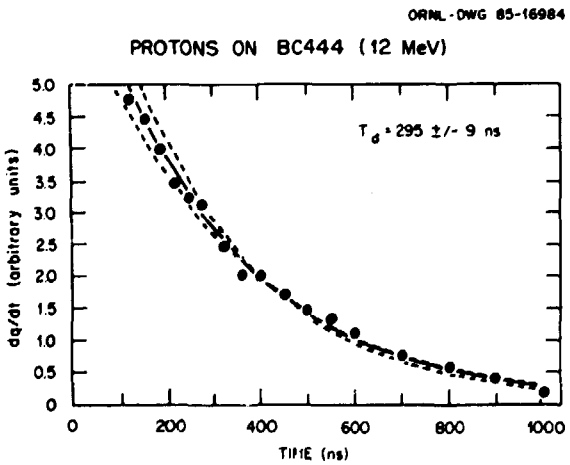

Fig. 2.104. Shown here is a fit to data which were extracted using the procedure shown in Fig. 2.103. The dotted lines are calculations for decay constants that differ from the fitted value by ±25 ns.

Table 2.17. Decay times from TUNL data. The uncertainties in the least-squares fit are given in parentheses. This value does not include statistical errors from the determination of peak centroids or other uncertainties from the experimental technique. The overall uncertainty in these measurements is about ±20 nanoseconds.

Bicron BC444		
Alphas	24 MeV	317 (8) ns
	18 MeV	280 (5) ns
	12 MeV	292 (8) ns
Avg. decay time	296.3 ns	
Protons	16 MeV	263 (11) ns
	12 MeV	295 (9) ns
	8 MeV	299 (8) ns
Avg. decay time	285.6 ns	
Nuclear Enterprises NE115		
Alphas	24 MeV	339 (8) ns
	18 MeV	334 (6) ns
	12 MeV	336 (8) ns
Avg. decay time	336.6 ns	
Protons	16 MeV	330 (5) ns
	12 MeV	378 (6) ns
	8 MeV	345 (10) ns
Avg. decay time	351.0 ns	

decay times is approximately ±20 nsec. Noting this, the data also indicates that the time structure of the light signal is independent of specific ionization.

The application of the phoswich technique is a recent development in nuclear detection methods. The lack of a decay time dependence on specific ionization implies that this method of identification can be extended to heavy ions as well. Besides understanding the time structure of the light signal from these new scintillators, the light yield as a function of energy has to be examined. Analysis of the calibration data is now underway.

---

1. Vanderbilt University, Nashville, TN 37235, and Joint Institute for Heavy Ion Research. ORNL, Oak Ridge, TN 37831.
2. Instrumentation and Controls Division, ORNL.

3. University of North Carolina, Chapel Hill, NC 27514.
4. D. Shapira et al., preceding article, this report.

MAJORITY-LOGIC NE-110 DETECTOR FOR keV NEUTRONS[1]

N. W. Hill[2] D. J. Horen
J. A. Harvey[2] G. L. Morgan[3]
R. R. Winters[4]

An NE-110 proton-recoil scintillation counter whose efficiency is reproducible and stable has been developed for neutrons in the energy range from 5 keV to 1 MeV. Majority-of-two logic at below the single photoelectron level is used between two or more phototubes viewing the same scintillator. Pulse height distributions as a function of neutron energy have been measured between 5 and 350 keV with two different detector configurations: a thin square slab of NE-110 and a cylinder of NE-110. The absolute efficiency of the slab detector has also been determined. The measured results are in good agreement with results from Monte Carlo calculations.

---

1. Abstract of published paper: IEEE Trans. Nucl. Sci. NS-32, 367 (1985).
2. Engineering Physics and Mathematics Division, ORNL.
3. Denison University, Granville, OH 43023.
4. Los Alamos National Laboratory, Los Alamos, NM 87545.

A NEUTRON POLARIMETER FOR (p,n) MEASUREMENTS AT INTERMEDIATE ENERGIES

T. N. Taddeucci[2,3] T. A. Carey[4]
C. D. Goodman[3] D. J. Horen
R. C. Byrd[3] J. Rapaport[2]
E. Sugarbaker[5]

A large-volume large-acceptance neutron polarimeter consisting of two parallel planes of plastic scintillators has been used to measure transverse polarization transfer in (p,n) reactions in the energy range 80 MeV < E_p < 160 MeV. The effective analyzing power obtained from $^1H(\vec{n},n)^1H$ reactions in the plastic scintillator has been measured by observing neutrons from the $^{14}C(\vec{p},\vec{n})^{14}N$ (2.31 MeV) reaction at $\theta = 0°$. Neutron energies are determined by time-of-flight with a resolution of about 1 MeV for 160-MeV neutrons. At this same energy the effective left-right analyzing power is 0.34 ± 0.02 and the effective area is 1.9 ± 0.3 cm^2.

---

1. Abstract of paper to be published in Nuclear Instruments and Methods in Physics Research.
2. Ohio University, Athens, OH 45701.
3. Indiana University Cyclotron Facility, Bloomington, IN 47405.
4. Los Alamos National Laboratory, Los Alamos, NM 87545.
5. Ohio State University, Columbus, OH 43214.

A COMPACT AND RELIABLE 200-kV POWER SUPPLY FOR THE RECOIL MASS SEPARATOR (RMS)

J. L. Blankenship[1]

A 200-kV power supply was designed to provide reliable operation under repeated vacuum spark discharges and to fit into a cavity 4.75 in. (12.1 cm) diameter by 10.25 in. (26.0 cm) deep. Four of the supplies, two negative and two positive, are used in the Recoil Mass Separator (RMS). The power supply is comprised of a 20-stage, half-wave multiplier housed in a PVC cylinder filled with mineral oil and sealed with an aluminum flange. All capacitors and rectifiers are conservatively rated, and all capacitors have resistors in series to limit peak currents during discharge.

The power supply has been tested in mineral oil to 230 kV without internal breakdown or failures, and has been subjected to repeated breakdown in air and in vacuum without component failure in the multiplier stack. The only observed failure mode has been in the coaxial cable and connectors between the 7-kV ac flyback transformer and the multiplier housing. A design change will incorporate the flyback transformer in a box on top of the flange of the multiplier stack, and will eliminate the coaxial cable and connectors.

---

1. Instrumentation and Controls Division, ORNL.

IMPROVEMENTS IN TIMING AND DETECTION EFFICIENCY OF THE TIME ZERO, MICROCHANNEL PLATE DETECTOR USED IN THE BROAD RANGE MAGNETIC SPECTROGRAPH MULTIPARAMETER DETECTION SYSTEM

J. L. Blankenship[1] R. L. Auble

A time zero detector is used in the Broad Range Spectrograph (BRS), along with a Parallel Plate Avalanche Counter (PPAC) as a stop detector, to measure time of flight of the heavy ion being analyzed. The time zero detector originally used was comprised of a thin carbon foil in the particle path, and a microchannel plate assembly located coaxial to the foil at a spacing of 0.7 cm to detect electrons knocked out of the foil. In this detector design, the microchannel plates have a 1.08-cm hole in the center for the passage of heavy ions, and an annular, sensitive region. The detection efficiency for ^{58}Ni ions at 913 MeV was initially about 30 per cent.

The electron optics in the foil-MCP region were redesigned to improve electron collection and to allow higher MCP gain without ion feedback. A radial field gradient was produced by placing a wire cross made of tungsten of diameter 20 μm at a point about two-thirds of the distance between the foil and the suppressor electrode, and biased at a voltage which repels the electrons. The wire cross introduces a radial velocity component to the electron motion and directs electrons into the sensitive region of the MCP. A suppressor electrode in the shape of a "top hat" was placed in front of the MCP and was biased at a potential such that ions created in the first third of the MCP would be repelled, thus preventing multiple pulsing at high bias and gain. Both of the changes in the detector design increased the pulse height for a heavy ion. The detection efficiency for 1011-MeV ^{58}Ni ions has improved to almost 100 per cent, and a better than 10 to 1 peak-to-valley ratio was achieved between "mass" spectra for A = 58 and A = 59.

1. Instrumentation and Controls Division, ORNL.

BRS FOCAL PLANE DETECTOR PERFORMANCE

R. L. Auble R. O. Sayer[1]

Hardware Development

Several modifications have been made to the beam line and focal plane detectors which have improved the performance of the BRS. These are summarized below.

(a) A viewer has been installed on the beam line between the BRS and the 153-degree analyzing magnet. This allows precise positioning of the intermediate focus required for dispersion matching and optimum position resolution at the focal plane.

(b) A 4-jaw collimator installed 4.4 m upstream of the target allows one to control the angular divergence of the incident beam, which is particularly important for small-angle measurements. It also provides for limiting of the beam intensity and emittance for zero-degree beam measurements allowing more rapid optimization of the focal plane detector system. Using this technique, we have studied the characteristics of the detector system with 1-GeV ^{58}Ni projectiles. The position and angular resolution obtained with the VDC are illustrated in Fig. 2.105. The 0.26-mm FWHM spatial resolution, which includes contributions from the analyzing magnet entrance slit, magnet aberrations, etc., is believed to be the limit on the achievable experimental resolution even though the intrinsic resolution of the VDC is probably much better than this. The angular resolution of 0.3-deg FWHM implies an uncertainty of only 0.08 deg in the scattering angle (due to the angular magnification of the BRS).

(c) The micro-channel-plate detector, used for time-of-flight measurements with heavier projectiles (e.g., A > 32), was modified to provide larger signals and

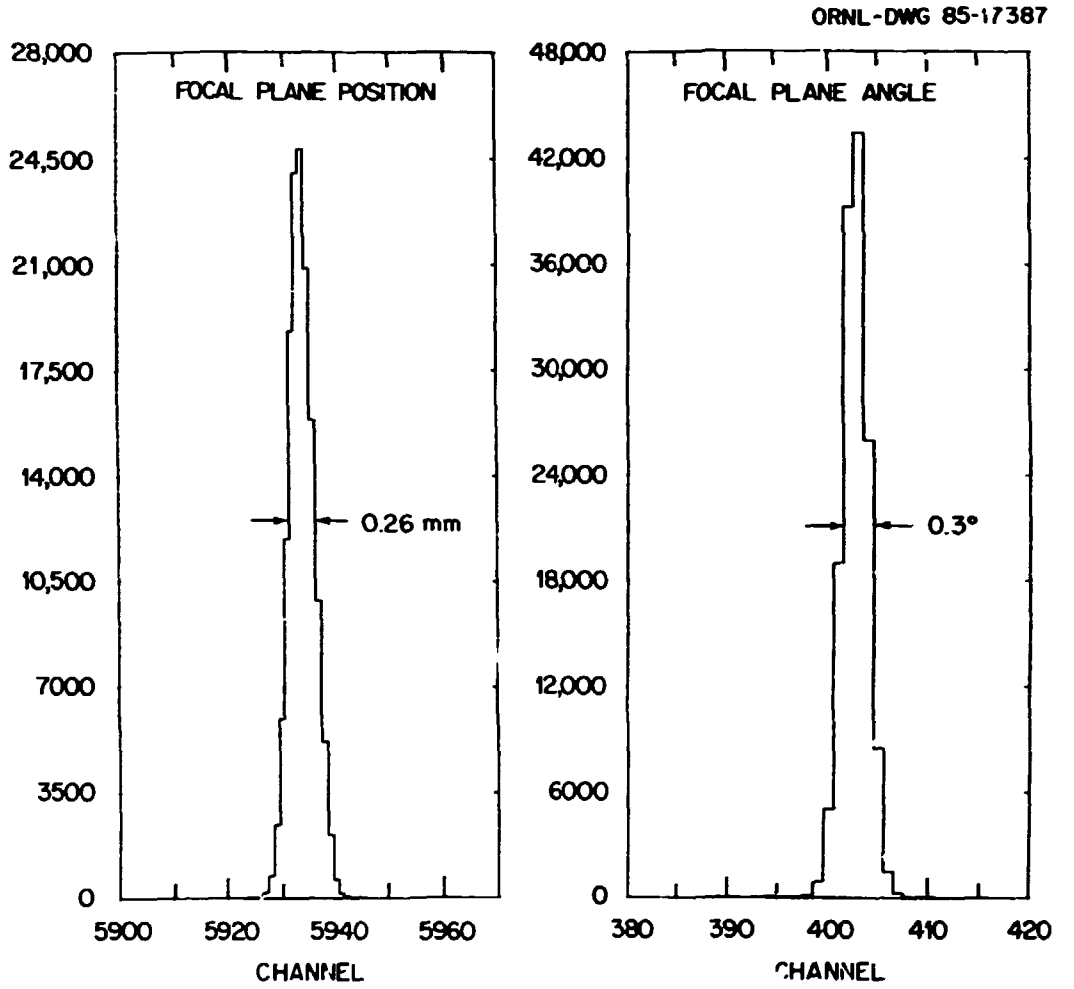

Fig. 2.105. Position and angle resolution obtained with the VDC using a 1-GeV ^{58}Ni beam at 0°.

lower background counting rates. These modifications are discussed in the detector development section of this report.

(d) The cathode planes in the vertical drift chamber have been decoupled from the outer framework. This has eliminated the wrinkling which had occurred due to stresses induced during assembly and improved the uniformity of the drift field.

(e) Improved time-of-flight resolution and position independence of the "start" signal were achieved by a redesign of the 5 x 40 cm^2 avalanche counter used to trigger the focal plane detector system. In the original design, the signal was obtained from a contact located at the center of the anode. This introduced a ~1 ns variation in the time of arrival of the start signal, depending on the position of the incident particle. The anode was modified to provide signals from both ends of the detector which are then sent to a "mean timer" (LeCroy 624) to give a position independent time signal. The time resolution was checked by using ^{244}Cm alpha particles traversing this detector and a small PPAC positioned back-to-back. A time spectrum is shown in Fig. 2.106. The two peaks were obtained by inserting a 1.0 ns delay in the stop signal. Spectra were obtained at several positions along the detector and shifts due to particle position were less than 40 ps.

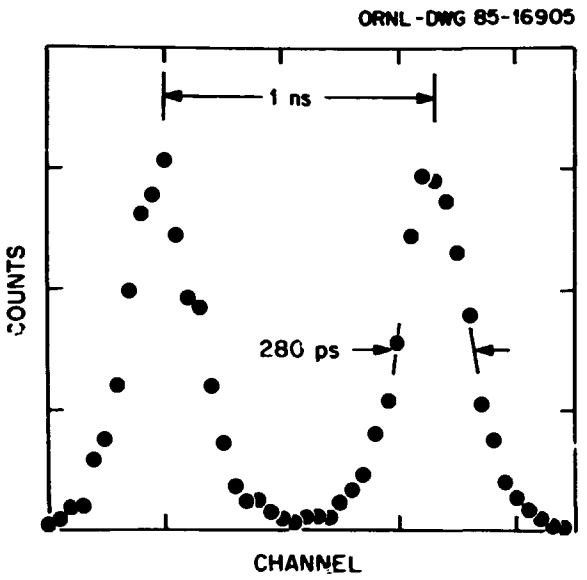

Fig. 2.106. TAC spectrum from 5 x 40 cm² "start" detector and 2.5 x 2.5 cm² "stop" detector using ^{244}Cm α-particles. A 1.0-ns delay was inserted to obtain the two peaks.

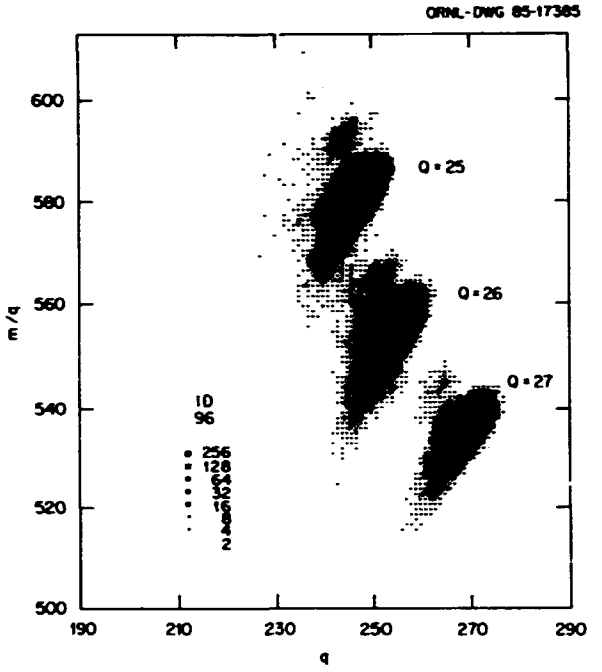

Fig. 2.107. Plot of m/Q vs. Q used to determine the charge state of a particle entering the BRS focal plane detector system.

Software Enhancements

For heavy ions such as Ni at 17 MeV/nucleon, several charge states are detected simultaneously, and therefore there is an ambiguity in mass as determined from time-of-flight (TOF) through the system. This ambiguity is removed by specification of "Q-contours" on a map of m/Q vs Q as shown in Fig. 2.107 for $(^{58}Ni)^{+25,+26,+27}$. The charge state Q is calculated from the total energy deposited in the ion chamber, Bρ, and velocity from TOF. For each specified combination of Z- and Q-contours, a "mass contour" may be drawn on a map of mass vs focal plane position. This technique has been applied to separate individual nickel isotopes ($\Delta A/A < 1/60$).

Variation in energy loss with angle occurs because projectiles traverse varying thicknesses of window and gas. The resulting degradation in E and dE resolution may be particularly severe for heavier ions and/or lower energies. A procedure was developed to optimize E and ΔE resolution by empirical first- and second-order corrections for variation in energy loss. Corrected and uncorrected E-spectra from the ion chamber are shown in Fig. 2.108.

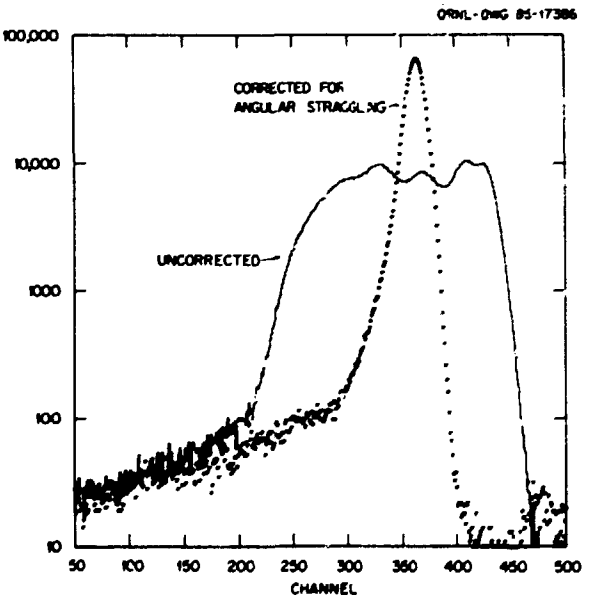

Fig. 2.108. Energy spectra obtained with the ΔE-E ion chamber before and after empirical correction for energy loss in detector windows.

Enhanced standard software modules for setup, calibration, and diagnostic procedures were developed to further automate the process of optimization of the BRS focal plane detector system. TDCAL automatically fits centroids

generated by a pulser and determines TDC slope values. CELLTOFF searches on TDC offset values to minimize the VDC cell precision. LOGSCA monitors experimental conditions such as target deterioration by displaying and recording scaler rates and ratios of rates.

---

1. Computing and Telecommunications Division, ORNL.

PREPARATION OF TARGETS FOR NUCLEAR PHYSICS RESEARCH

D. M. Galbraith F. K. McGowan

The preparation of thin targets for particle spectroscopy in nuclear physics research by the focused ion-beam sputtering system has continued to be extremely useful. Self-supporting targets of ^{58}Ni as thin as 100 $\mu g/cm^2$ have been produced. An annealing system utilizing a projector lamp was developed for use in the focused ion-beam sputtering system. The purpose of this is to anneal the material deposited on the substrate during the sputtering process. Table 2.18 contains examples of the targets prepared by ion-beam sputtering and by evaporation.

Many evaporations of Al for production of detector windows and planes for avalanche counters were done. Production runs of slackened carbon stripper foils for the tandem and ORIC accelerators were completed.

Table 2.18 Targets for nuclear physics research

Element	Weight	Backing	Method	Remarks
^{27}Al	100 $\mu g/cm^2$	none	evaporation	
^{58}Ni	100 $\mu g/cm^2$	none	sputtering	
^{58}Ni	100 $\mu g/cm^2$	30 $\mu g/cm^2$ C	sputtering	
^{90}Zr	200 $\mu g/cm^2$	30 $\mu g/cm^2$ C	sputtering	
^{90}Zr	50 $\mu g/cm^2$	30 $\mu g/cm^2$ C	sputtering	Recoil mass spectrometer
^{90}Zr	100 $\mu g/cm^2$	30 $\mu g/cm^2$ C	sputtering	Recoil mass spectrometer
In	1 mg/cm^2	none	evaporation	
^{124}Sn	1 mg/cm^2	none	evaporation	Recoil distance device
^{182}W	50 $\mu g/cm^2$	30 $\mu g/cm^2$ C	sputtering	Broad range spectrometer
^{184}W	50 $\mu g/cm^2$	30 $\mu g/cm^2$ C	sputtering	Broad range spectrometer
^{184}W	50 $\mu g/cm^2$	30 $\mu g/cm^2$ C	sputtering	Broad range spectrometer
^{182}W	33 $\mu g/cm^2$	10 $\mu g/cm^2$ C	sputtering	Broad range spectrometer
^{184}W	33 $\mu g/cm^2$	10 $\mu g/cm^2$ C	sputtering	Broad range spectrometer
^{197}Au	1 $\mu g/cm^2$	100 $\mu g/cm^2$ C	evaporation	
^{197}Au	2 $\mu g/cm^2$	20 $\mu g/cm^2$ C	evaporation	
^{197}Au	50 $\mu g/cm^2$	30 $\mu g/cm^2$ C	evaporation	
^{208}Pb	300 $\mu g/cm^2$	none	evaporation	
^{208}Pb	500 $\mu g/cm^2$	none	evaporation	
^{208}Pb	200 $\mu g/cm^2$	30 $\mu g/cm^2$ C	evaporation	Recoil mass spectrometer
^{208}Pb	50-200 $\mu g/cm^2$	20 $\mu g/cm^2$ C	evaporation	Broad range spectrometer

3. THE UNISOR PROGRAM

The University Isotope Separator - Oak Ridge is a cooperative venture of ten universities, Oak Ridge Associated Universities, Oak Ridge National Laboratory, the U.S. Department of Energy, and the State of Tennessee. The primary purpose of the UNISOR consortium is to investigate the structures and decay mechanisms of rare, short-lived atomic nuclei which are prepared by means of a magnetic isotope separator coupled to the accelerators in the Holifield Heavy-Ion Research Facility. The accounts which follow describe work at the UNISOR facility or work associated with UNISOR research performed principally by investigators outside of the Physics Division. Theoretical research performed by UNISOR staff and collaborators is included in the Theoretical Physics section of this report. Research and development performed at UNISOR by Physics Division staff members are included in the Nuclear Physics section.

THE UNISOR EXPERIMENTAL FACILITY

R. L. Mlekodaj[1] R. W. Fink[3]
C. R. Bingham[2] J. C. Griffin[3]
J. A. Bounds[2] W. T. Milner
R. A. Braga[3,4] C. A. Reed[1]
H. K. Carter[1] C. N. Thomas[1]
V. Carmichael[5] E. H. Spejewski[1]
W. M. Fairbank[6] E. V. Weber[7]

A new thermal-ionization source with internal temperatures up to 3000°K has been brought into routine service. This source, shown in Fig. 3.1, is being used for the production of isotopes in the neutron-deficient light rare earth region. Good results with Eu, Sm, and Pm isotopes have been obtained in the mass range A = 135-140.

A new, very high temperature ion source based on the FEBIAD concept and similar to the GSI[8] model F has been designed, constructed, and tested on-line. This source is depicted in Fig. 3.2. The main thrust of this source is to give high yields of isotopes for collinear laser studies. In initial tests, yields of Pb

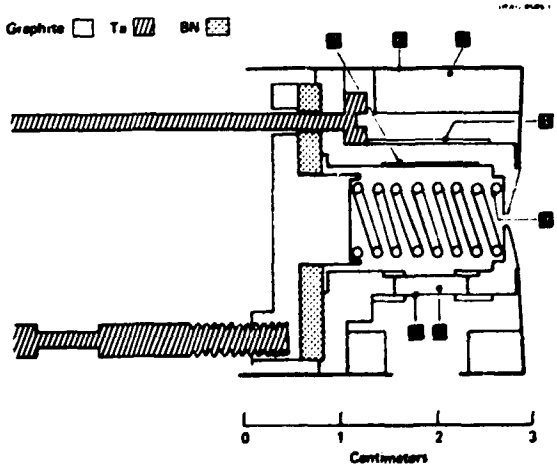

Fig. 3.1. UNISOR thermal-ionization source. (1) target/window, (2) graphite felt catcher, (3) tungsten filament, (4) target retainer, (5) graphite felt heat shielding, (6) Ta heat shield, (7) Ta support for graphite felt.

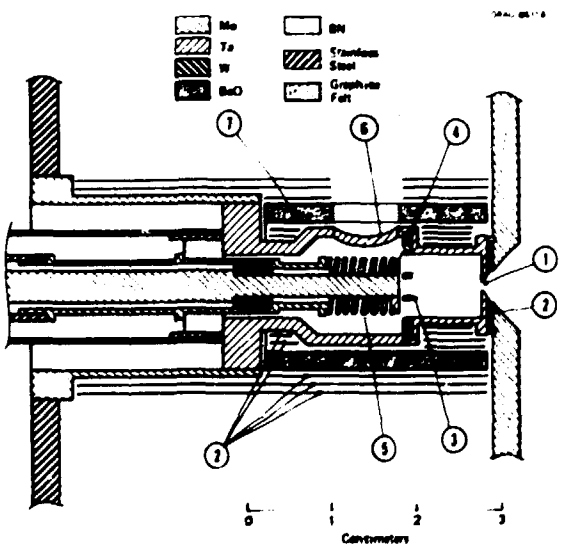

Fig. 3.2. UNISOR-FEBIAD ion source. (1) exit hole, (2) heat shields, (3) extraction electrode, (4) electron-emitting surface, (5) tungsten filament, (6) target mounting hole, (7) graphite felt insulation.

and Tl isotopes up to 4.5×10^6 atoms sec^{-1} particle-μA^{-1} have been obtained.

The HHIRF data acquistion system has been integrated into UNISOR experiments. Special acquisition software was written to enable "UNISOR-style" experiments to be run on the Perkin-Elmer. Simultaneous coincidence and spectrum multiscaling data can be acquired on up to 10 separate experiments.

A short-lived conversion electron and alpha-particle standard energy and relative intensity calibration source has been developed and is now in use. The source consists of 500 μg of ^{232}U (73 yr) in secular equilibrium with its daughters. A conical glass sleeve is inserted into the container which allows only the ^{220}Rn gas daughters to be deposited onto the source holder. The resulting source is virtually mass-free and decays with a 10.6-hour half-life and gives conversion lines from 24 keV to 2526 keV.

Design details for the UNISOR on-line $^3He/^4He$ dilution refrigerator for low-temperature nuclear orientation have been finalized and site preparations are under way. The system is expected to be operational in early FY 1987.

Current work at the UNISOR laser facility includes the conclusion of experiments on Tl isotopes and the development of new techniques for the study of other nuclei of interest. A scheme using resonance ionization spectroscopy to study Kr and other nuclei has undergone initial testing. A detection scheme was developed and apparatus built and tested. Due to collisional ionization in the residual gas, the background was too high to enable a signal to be observed. A much improved vacuum in the detection region should solve the problem. A method to measure nuclear spins by observing atomic hyperfine splitting in a magnetic field also had some developmental work. A code was written to predict the Zeeman spectra at any magnetic field for the special case of I or J = 1/2. The predicted spectra compared quite favorably with data obtained on the UNISOR laser system. At the conclusion of the laser experiments on Tl, the next nuclei to be studied will be the neutron-deficient lead isotopes. The detection scheme for Pb has been worked out. The change-over from Tl experiments has been accomplished by changing the dye and optics in the dye laser and the colored glass filter for the photomultiplier. A signal from stable Pb has been observed with a measured efficiency close to that observed for Tl.

---

1. UNISOR, Oak Ridge Associated Universities, Oak Ridge, Tennessee.
2. University of Tennessee, Knoxville, Tennessee.
3. Georgia Institute of Technology, Atlanta, Georgia.
4. Joint Institute for Heavy Ion Research, Oak Ridge, Tennessee.
5. Francis Marion College, Florence, South Carolina.
6. Colorado State University, Fort Collins, Colorado.
7. Grinnell College, Ames, Iowa.
8. R. Kirchner, G.S.I. Darmstadt, Annual Report, 1984.

THE DECAY OF MASS-SEPARATED ^{203}At

P. B. Semmes[1] J. L. Wood[2]
R. A. Braga[2] R. W. Fink[2]
J. D. Cole[3]

The neutron-deficient Po isotopes lie in a little-explored region of the nuclear mass surface. The nuclei $^{209,210}Po$ are only a few particles beyond the doubly magic ^{208}Pb and, consequently, their structures are dominated by single-particle effects. The Po isotopes become more collective with decreasing neutron number, and their properties reflect the competition between collective and single-particle effects.[4]

The isotope ^{203}Po is at the limit of present detailed experimental data for low-spin excited states and, therefore, a study of the $^{203}At \rightarrow ^{203}Po$ decay scheme was undertaken to extend the systematics of the low-spin states in odd-A Po nuclei. Time-sequenced spectra of gamma rays, X rays, and conversion electrons were obtained, together with γ-γ-t and e$^-$-γ-t coincidence data. From this information a decay scheme has been constructed consisting of 30 excited states and 45 transitions that incorporate approximately 90% of the decay intensity assigned to ^{203}At. Prior to this only three excited states were known in ^{203}Po. All excited states below 1 MeV

have been assigned unique spin-parity values, and the observed level scheme can be understood qualitatively in terms of a particle-core weak coupling description. For example, a multiplet of negative parity states observed near 700 keV (9/2⁻: 803 keV; 7/2⁻:719, 639 keV; 5/2⁻: 686, 532 keV) correspond to the low-lying negative parity shell model orbitals ($f_{5/2}$, $p_{3/2}$ and $p_{1/2}$) coupling to the 2^+ core state. Additional negative parity states which belong to this multiplet are expected with spins of 3/2 and 1/2, but are not populated strongly in the ^{203}At decay (ground state spin-parity 9/2⁻). Furthermore, a number of positive parity states built on the 13/2+ isomer ($i_{13/2}$ shell model orbital) were identified. Unique spin and parity assignments were made for the states at 1129 keV (9/2+) and 1671 keV (11/2+).

---

1. Georgia Institute of Technology, Atlanta, Georgia; present address: Joint Institute for Heavy Ion Research, Oak Ridge National Laboratory, Oak Ridge, Tennessee.
2. Georgia Institute of Technology, Atlanta, Georgia.
3. Idaho National Engineering Laboratory, Idaho Falls, Idaho.
4. A. Zemel and J. Dobes, Phys. Rev. C27, 2311 (1983).

DECAY OF ^{137}Sm AND DEFORMATION IN THE LIGHT Pm REGION

R. A. Braga[1] B. D. Kern[3]
R. W. Fink[1] G. A. Leander[4]
B. E. Gnade[2] R. L. Mlekodaj[4]
K. S. Toth

The ongoing investigation of the predicted[5] new region of deformation in the Z > 50, N < 82 rare earth nuclei has involved detailed spectroscopic studies of the transitional nuclei ^{137}Sm and ^{137}Pm populated from the decay of 9-sec ^{137}Eu and 45-sec ^{137}Sm, respectively. The activities were produced by the bombardment of natural Ag targets with 160 MeV ^{35}Cl and ^{92}Mo targets with 220-MeV ^{48}Ti beams.

The γ rays associated with the A = 137 mass chain have been identified and, for the first time, a partial decay scheme for ^{137}Pm has been constructed. Of particular interest in the level structure of ^{137}Pm is the position of the 11/2⁻ state observed in the heavier odd mass Pm isotopes. This $h_{11/2}$ odd proton state comes lower in energy as nuclei become more neutron-deficient. If this trend continues, the 11/2⁻ state should eventually become the ground state This has been recently shown[6] to occur in the odd mass Eu isotopes at ^{139}Eu.

---

1. Georgia Institute of Technology, Atlanta, Georgia.
2. Texas Instruments Inc., Dallas, Texas.
3. University of Kentucky, Lexington, Kentucky.
4. UNISOR, Oak Ridge Associated Universities, Oak Ridge, Tennessee.
5. G. A. Leander et al., Phys. Lett. B110, 17 (1982).
6. S. Lunardi et al. Z. for Physik A321, 177 (1985).

SHAPE COEXISTENCE IN ^{185}Au

E. F. Zganjar[1] C. D. Papanicolopoulos[2]
J. L. Wood[2] R. A. Braga[3]
R. W. Fink[3] A. J. Larabee[4]
M. Carpenter[4] D. Lo[illegible]e[4]
C. R. Bingham[4] L. L. Riedinger[4]
J. C. Waddington[5]

Shape coexistence appears to be a general feature of nuclei in the neutron-deficient region near Z = 82. The coexistence observed in the odd-mass Au isotopes can be understood as arising from the coupling of the proton particle ($h_{9/2}$) and the proton hole ($h_{11/2}$) to the different core shapes in the even-even Pt and Hg isotopes, respectively. These ideas were stimulated by the study[6,7] of the low-energy structure of ^{187}Au following the decay of isomeric and ground state ^{187}Hg. In that case, the $h_{9/2}$ particle couples to the ^{186}Pt core to form two bands with states of the same spin connected by transitions of E0+M1+E2 multipolarity.[7]

We initiated a careful and detailed study at UNISOR of the decay of the isomeric and ground state of ^{185}Hg to explore further the shape coexistence phenomenon, to resolve the disagreement between our earlier[7] data on this decay and that of the Orsay[8] group, and to provide complementary information for an in-beam study[9] of ^{185}Au. The decay of isomeric (28s, 13/2+) and ground state (55s, 1/2⁻) ^{185}Hg to excited states

in ^{185}Au were studied by γ-ray and conversion-electron singles, time-sequence spectroscopy, and coincidence measurements. An important feature of the coexisting bands are the E0+M1+E2 transitions which connect them. Preliminary analysis of our results on ^{185}Au supports our earlier[7] interpretation of such transitions as E0+M1+E2 in ^{187}Au and contradicts the interpretation[8] that these transitions in ^{185}Au have anomalous M1 components. The Orsay group[8] were forced to conclude that anomalous M1 components were involved since they obtained conversion coefficients larger than M1 or E2 for a number of transitions between levels of different spin. Our coincidence data were of sufficient statistical quality that we could quantitatively distinguish unresolved doublets. In essentially all cases, we were able to account for the anomalous internal conversion by locating another transition of nearly the same energy which connected states of the same spin and could thus contain an E0 component.

As in the ^{187}Au study, transitions in ^{185}Au with strong E0 components were observed to feed the $h_{9/2}$ and $h_{11/2}$ bands. These results are summarized in Fig. 3.3.

1. Department of Physics, Louisiana State University, Baton Rouge, Louisiana.

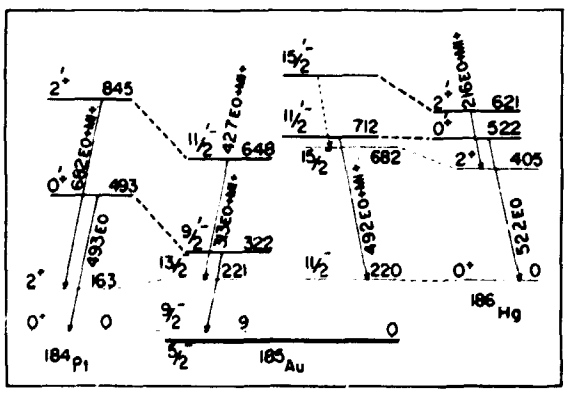

Fig. 3.3. Portions of the $h_{9/2}$, $h_{11/2}$, $h'_{9/2}$, and $h'_{11/2}$ bands in ^{185}Au compared to the 0^+, 2^+, and $0^{+\prime}$, $2^{+\prime}$ levels in ^{184}Pt and ^{186}Hg. The corresponding core-particle couplings are noted with dashed lines. Only transitions with E0 components are shown.

2. School of Physics, Georgia Institute of Technology, Atlanta, Georgia.
3. School of Chemistry, Georgia Institute of Technology, Atlanta, Georgia.
4 Department of Physics, University of Tennessee, Knoxville, Tennessee.
5. Department of Physics, McMaster University, Hamilton, Ontario, Canada.
6. M. A. Grimm, Thesis, Georgia Institute of Technology, 1978; unpublished.
7. E. F. Zganjar et al., Proc. 4th Int. Conf. on Nuclei Far From Stability, Helsingor, June 1981, CERN 81-09, p. 631.
8. C. Bourgeois et al., Nucl. Phys. A386, 308 (1982).
9. A. J. Larabee et al., preprint, Oct 1985, submitted to Physics Letters.

DECAY OF ^{138}Eu, ^{136}Eu AND DEFORMATION IN THE Sm REGION

R. L. Mlekodaj[1] B. D. Kern[3]
G. A. Leander[1] K. S. Toth[4]
R. A. Braga[2] B. Gnade[5]

It has long been recognized[6] that a region of permanently deformed nuclei exists in the region where Z and A are both between 50 and 82. This region, however, is located well away from the line of β-stability with the centroid lying beyond the proton drip line. The recently developed UNISOR on-line thermal-ionization ion source[7] capable of efficiently ionizing the elements in this region has been coupled with the favorable targets with Z from 40 to 47 (Zr to Ag). This target/ion source system, together with good beams of ^{32}S, ^{35}Cl, ^{48}Ti, and ^{46}Ti from the HHIRF, has led to the initiation of a program to study the unknown or little known nuclei in this region. The specific experiments described here are the production of ^{136}Eu and ^{138}Eu and the first observation of gamma rays from their decays.

The 12 s half-life obtained for ^{138}Eu from gamma rays agrees with a value obtained in an earlier reported analysis of X rays and attributed to ^{138}Eu.[8] The level scheme derived for ^{138}Sm based on a complete analysis of the gamma-gamma coincidence relationships is given in Fig. 3.4. In addition, the ^{136}Eu decay was investigated for a brief time. Although no gamma lines could be discerned in the singles data, the

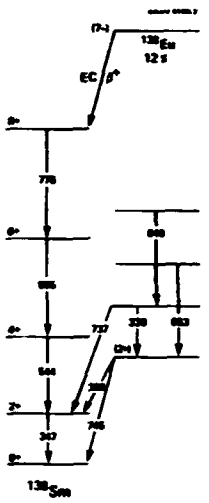

Fig. 3.4. Derived level scheme for ^{138}Sm.

256 keV (2+ → 0+ transition[9] in ^{136}Sm) line was observed in the total coincidence spectrum.

In Fig. 3.5 the 2+ energies from this work, along with other known 2+ energies for even-even Sm isotopes, are plotted along with the results of some theoretical predictions. The IBM2 calculations were carried out as described by Scholten[10] using parameters for the light Sm isotopes derived from Puddu et al.[11] The cranking calculations were made with the modified oscillator (Nilsson) single-particle model at the Strutinsky equilibrium deformations. BCS pairing was treated by the average gap method. The average gap was obtained by scaling the global formula of Jensen et al.[12] The present cranking calculations are slight extensions and modifications of calculations by Ragnarsson et al.[13]

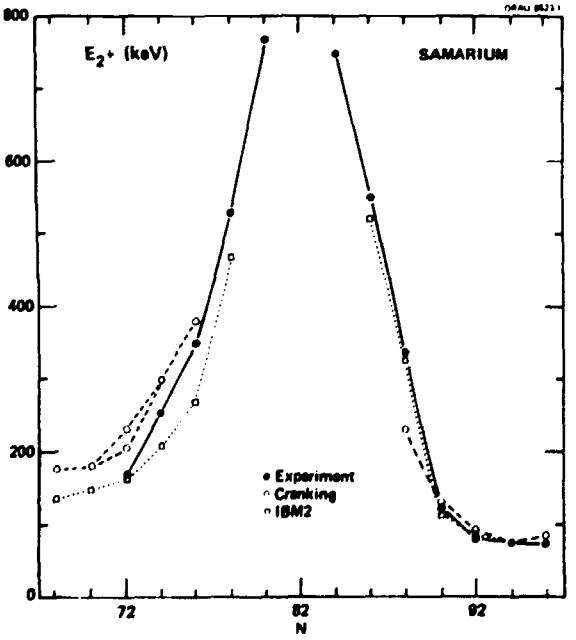

Fig. 3.5. Comparison of experimental data with cranking and IBM2 models.

The experimental points for ^{138}Sm (N = 76) and ^{136}Sm (N = 74) fall between the predictions of the two calculations. The trend of the 2+ energies shows a smooth rapid decrease out to N = 74. The 2+ energy at N = 72 as determined by Lister et al.[9] is 163 keV, again within the range of the calculations, and continues the rapid decrease. The trend from N = 76 to 72 appears more compatible with the recently predicted[14] large increase in deformation between these neutron numbers (lower branch of the dashed curve in Fig. 3.5) than with the smooth evolution of deformation obtained earlier[13] (upper branch) and also suggested by the IBM2 results. Finally, we note that the theoretical 2+ energies are higher for N < 82 than for N > 82, and this prediction is borne out by the data.

---

1. UNISOR, Oak Ridge Associated Universities, Oak Ridge, Tennessee.
2. School of Chemistry, Georgia Institute of Technology, Atlanta, Georgia.
3. University of Kentucky, Lexington, Kentucky.
4. Oak Ridge National Laboratory, Oak Ridge, Tennessee.
5. Texas Instruments Corporation, Dallas, Texas.

6. R. K. Sheline, et al., Phys. Rev. Lett. 7, 446 (1961).
7. R. L. Mlekodaj et al., "The UNISOR Experimental Facility," this report.
8. M. Nowicki, et al., Act. Phys. Pol. B12, 879 (1982).
9. C. J. Lister, et al., Phys. Rev. Lett. 55, 810 (1985).
10. O. Scholten, in Interacting Bosons in Nuclear Physics, ed. F. Iachello, Plenum Press, NY, 1979, p. 17.
11. G. Puddu et al., Nucl. Phys. A348, 109 (1980).
12. A. S. Jensen, et al., Nucl. Phys. A431, 393 (1984).
13. I. Ragnarsson, et al., Nucl. Phys. A223, 329 (1974).
14. G. A. Leander, et al., Phys. Lett. 110B, 17 (1982).

MEASUREMENT OF THE ISOTOPE SHIFTS AND HYPERFINE STRUCTURES OF 189-194Tl AT THE UNISOR LASER FACILITY

J. A. Bounds[1] J. C. Griffin[4]
C. R. Bingham[1] P. Juncar[5]
H. K. Carter[2] G. A. Leander[2]
W. M. Fairbank, Jr.[3] R. L. Mlekodaj[2]
E. H. Spejewski[2]

The laser facility on-line to the UNISOR separator was utilized to measure the atomic hyperfine structures and isotope shifts in a series of on-line produced light Tl isotopes in the range A = 189-194. For each mass, the isomeric nuclear state was produced; in addition, the A = 193 ground state was populated sufficiently to be observed. Mass separated beam rates for the various isotopes ranged from 7×10^4 to 3×10^5 atoms per second. The atomic spectra were measured using the laser facility essentially as described earlier.[6]

From the hyperfine structure, the magnetic dipole moments were determined and, in several cases, the electric quadrupole moments were also deduced. In addition, the isotope shift of each mass was measured. An atomic isotope shift is composed of a mass shift related to the mass change of the nucleus, and a field shift which is nearly proportional to the change in charge radius, $\delta\langle r^2\rangle$, of a nucleus. We have interpreted the Tl atomic isotope shift data in terms of nuclear deformation by fitting droplet model[7] predictions to the deduced field shifts. We normalized the $\beta = 0$ droplet model $\delta\langle r^2\rangle$ prediction to ^{207}Tl, which, due to its proximity to a doubly closed shell nucleus should have near-zero deformation, and to ^{200}Tl, which from the data has the greatest field shift per change in mass number relative to ^{207}Tl. This done, deformations for the other isotopes may be deduced (see Fig. 3.6). If ^{200}Tl in fact has a nonzero deformation, the droplet model lines would have steeper slopes and, thus, the deformation taken from Fig. 3.6 would represent minimum possible values. Regardless of absolute values, it is clear that for each nuclear spin the deformation is increasing in going away from the closed neutron shell at N = 126. Furthermore, there is a large isomer shift observed for A = 193, reflecting a considerable change in deformation in the isomeric $9/2^-$ nuclei relative to the $1/2^+$ ground state nuclei.

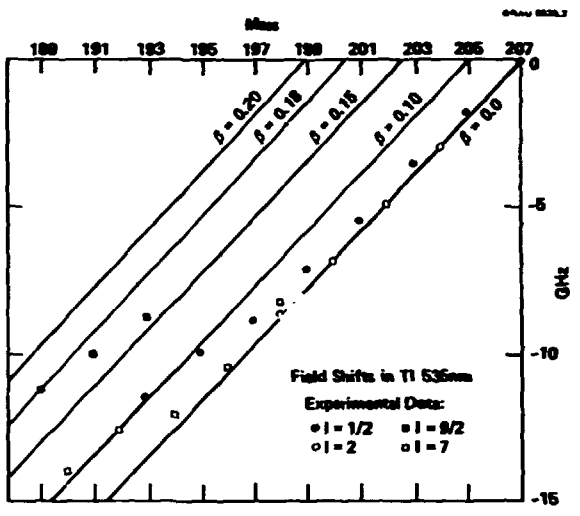

Fig. 3.6. Field shifts in Tl with droplet model predictions. All errors are ± (< 120 MHz). Data for A < 193 are from the present work; results for A > are cited in Ref. 8.

A theoretical calculation was carried out to see if all of the observed features of the Tl isotopes would emerge from the deformed shell model. Information on these calculations are reported by G. A. Leander in section 5 of this report. Briefly, the microscopic calculation has reproduced the minimum observed in the energy of the $h_{9/2}$-levels and the nearly constant band spacings built on the $h_{9/2}$ states. Earlier, changing deformation could explain the minimum, but seemed to be ruled out by the nearly constant band spacings. The laser experimental results now show that deformation is indeed increasing in going away from stability. The theoretical calculations reproduced all of the observed features by letting the neutron superfluid correlations also increase with decreasing neutron number, which compensates for the increasing deformation's effect on the collective excitation energy.

---

1. University of Tennessee, Knoxville, Tennessee.

2. UNISOR, Oak Ridge Associated Universities, Oak Ridge, Tennessee.
3. Colorado State University, Ft. Collins, Colorado.
4. Georgia Institute of Technology, Atlanta, Georgia.
5. Laboratoire Aimé Cotton, Orsay, France.
6. H. K. Carter et al., Physics Division Progress Report, ORNL-6004 (1983), p. 169.
7. W. D. Myer and H.-K. Schmidt, Nucl. Phys. A410, 61 (1983).
8. R. C. Thompson, et al., J. Phys. G9, 443 (1983).

SYSTEMATICS OF THE VERY NEUTRON DEFICIENT Au ISOTOPES

J. L. Wood[1] E. F. Zganjar[2]

The neutron deficient odd-mass Hg → Au decay schemes have been a major focal point of our effort to find new degrees of freedom in the low-energy spectra of nuclei. These studies, which extend from A = 185 to 195, have been done systematically in order to reveal the dependence of excitation modes on changing neutron number. Such systematic studies provide[3] a bridge between nuclei near the β-stability line, where detailed spectroscopic information is available, and nuclei far from β-stability.

Two features make these decay schemes particularly attractive: First, all of the odd-mass Hg isotopes have β-decaying high-spin isomers (13/2) and low-spin ground states (1/2 or 3/2). Second, the spins of these states and of the corresponding Au ground states are known from atomic spectroscopic measurements. Consequently, an extensive range of spin states (J = 1/2 to 15/2) are populated and multipolarity information can be used to fix their spin values, thus providing an essentially complete picture of the low-energy structure of the odd-mass Au isotopes. Additionally, because of the extensive high-spin population, it is possible to have a large overlap of states seen in decay with those seen in-beam. In addition to early in-beam experiments,[4] recent[5] in-beam work on ^{185}Au has confirmed the assignments made in the radioactive decay studies.

The recent extension of these systematics for mass numbers 185 → 189 are shown in Figs. 3.7-3.10. These are a product of the unpublished

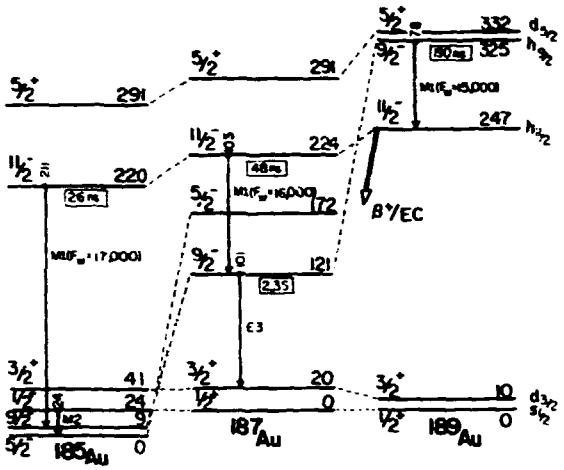

Fig. 3.7. Shell Model States. The isotopes are joined together at the $s_{1/2}$ state.

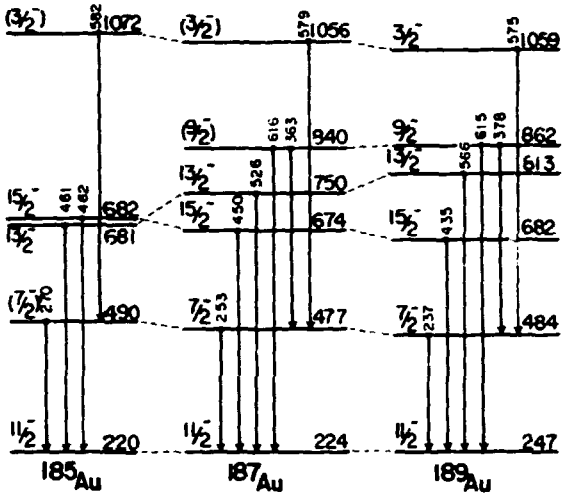

Fig. 3.8 Systematics of levels associated with the $h_{11/2}$ hole state.

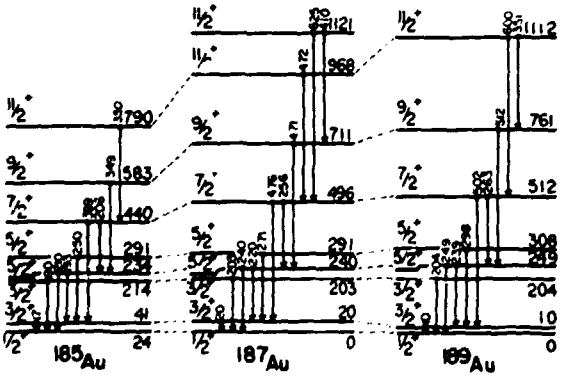

Fig. 3.9. Systematics of the positive parity states associated with $s_{1/2}$, $d_{3/2}$, and $d_{5/2}$.

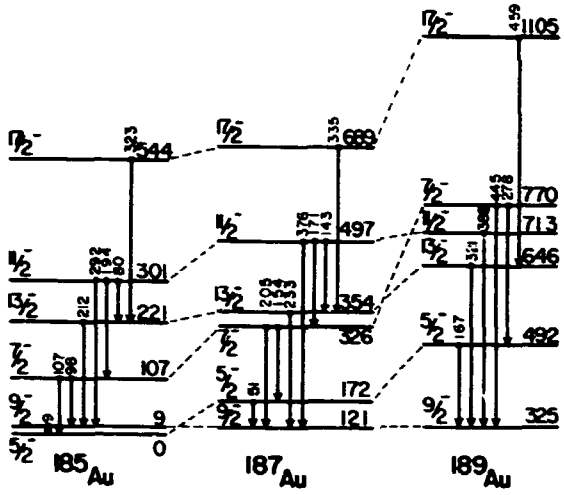

Fig. 3.10. Systematics of high-spin states associated with the $h_{9/2}$ intruder state.

data, a thesis,[6] and the available published[7-11] information.

---

1. School of Physics, Georgia Institute of Technology, Atlanta, Georgia.
2. Department of Physics, Louisiana State University, Baton Rouge, Louisiana.
3. J. L. Wood, in Future Directions in Studies of Nuclei Far From Stability, J. H. Hamilton et al., ed. (North Holland Pub. Co., Amsterdam, 1980) p. 37; and E. F. Zganjar, ibid., p. 49.
4. P. O. Tjom et al., Nucl. Phys. A231, 397 (1974).
5. A. J. Larabee et al., preprint, October 1985, submitted to Physics Letters.
6. M. A. Grimm, Thesis, Georgia Tech., 1978; unpublished.
7. E. F. Zganjar et al., Phys. Lett. 58B, 159 (1975).
8. V. Berg et al., Nucl. Phys. A244, 462 (1975).
9. C. Bourgeois et al., Nucl. Phys. A295, 424 (1978).
10. C. Bourgeois et al., Nucl. Phys. A388, 308 (1982).
11. V. Berg et al., Nucl. Phys. A410, 445 (1983).

A NEW CLASS OF LOW-ENERGY STRUCTURE AT CLOSED SHELLS: LEVELS IN $^{185-187}$Au

E. F. Zganjar[1] J. L. Wood[2]

The mechanism of pair excitation across a shell gap to produce shape coexistence appears to be fairly well established near closed shells.[3] The results of our studies[4,5] on the neutron deficient $^{185-187}$Au isotopes support this view. We believe that we have observed four families of states which arise from the couplings associated with the $h_{9/2}$ intruder

$$^{184,186}\text{Pt}\ [0_1^+ \otimes (2p\text{-}6h)] + \nu h_{9/2}^{+1}$$

and

$$^{184,186}\text{Pt}\ [0_2^+ \otimes (4h)] + \nu h_{9/2}^{+1},$$

depicted in Fig. 3.11, and the couplings associated with the $h^{11/2}$ hole states

$$^{186,188}\text{Hg}\ [0_1 \otimes (2h)] + \nu h_{11/2}$$

and

$$^{186,188}\text{Hg}\ [0_2 \otimes (2p\text{-}4h)] + \nu h_{11/2},$$

depicted in Fig. 3.12.

Transitions with strong E0 components feeding the $h_{9/2}$ and $h_{11/2}$ bands are interpreted as decays out of the $h'_{9/2}$ and $h'_{11/2}$ bands which result from the coupling of the $h_{9/2}$ and $h_{11/2}$ single proton configurations in the ^{184,186}Pt and ^{186,188}Hg cores, respectively.

These Au isotopes lie in a most interesting region of shape coexistence where many different shapes are observed at low energies. Recent in-beam work[6] on ^{185}Au suggests that these various

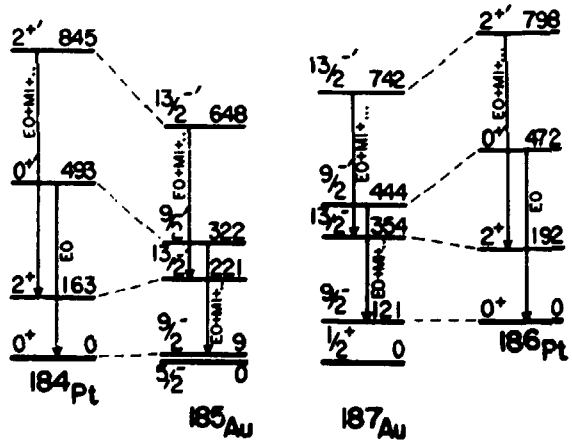

Fig. 3.11. Portions of the $h_{9/2}$ and $h'_{9/2}$ bands in ^{185,187}Au compared to the 0_1^+ and 0_2^+ (0^{+1}) bands in ^{184,186}Pt. The corresponding core-particle couplings are noted with dashed lines. Only transitons w.th E0 components are shown.

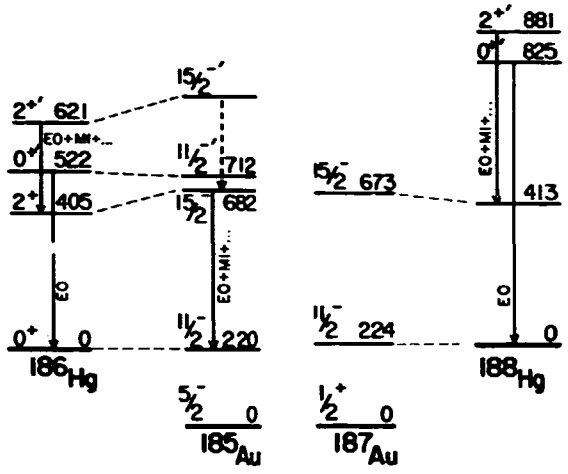

Fig. 3.12. Portions of the $h_{11/2}$ and $h'_{11/2}$ bands in ^{185,187}Au compared to the 0_1 and 0_2 (0^{+1}) bands in ^{186,188}Hg. The corresponding core-particle couplings are noted with dashed lines. Only transitons with E0 components are shown.

shapes are made up of both oblate and prolate structures which can be understood as arising from competition between close-lying K = 1/2 (oblate) and K = 11/2 (prolate) states for $h_{11/2}$; and K = 1/2 (prolate) and K = 9/2 (oblate for $h_{9/2}$). While the results of these studies are consistent with the explanation of shape coexistence based on the promotion of a pair of particles into an intruder orbital, additional experimental and theoretical work is needed to fully determine which mechanism gives rise to shape coexistence in the Z = 82 region.

SEARCH FOR BARELY BOUND MULTINEUTRON SYSTEMS

R. L. Kozub[1]

A preliminary search for bound clusters of four or five neutrons which may be produced in heavy-ion reactions at low center-of-mass energies was conducted using the off-line counting facilities of UNISOR. A beam of 200-MeV ^{50}Ti bombarded a ^{9}Be target. The "reverse" kinematics of this combination is such as to force most of the light reaction products to be emitted in the forward hemisphere. Adjacent to and downstream from the target were sufficient combined thicknesses of Ta and Al (~ 3 mm each) to stop the beam and the most energetic tritons which could be created in the target. A large quantity (500 g) of 99.999%-pure MgO was placed outside the vacuum system just downstream from the target. If clusters of neutrons were produced and lived long enough (at least a few ns), some of them should have initiated reactions of the type ^{26}Mg(A_n,A-2n)^{28}Mg(21 hr).

After bombardment, activities from the MgO sample were recorded as a function of time using the TENNECOMP system at UNISOR and five Ge detectors. One of the detectors was Compton-suppressed, but the sacrifice in overall counting statistics owing to the small solid angle proved to be greater than the gain in sensitivity with lower background. Thus, the most useful data were acquired with the four unsuppressed detectors. A key γ-ray line is the one from decay of the first excited state of ^{28}Si at 1779 keV, which would be populated eventually by all ^{28}Mg β decays. Although the Compton background from ^{24}Na activity in the sample is large at the 1779-keV position in the spectra, the spectra are quite clean in this region. No evidence for a peak was observed. A detection threshold (one standard deviation) on the product of the cross sections for production of neutron clusters in the ^{9}Be target and for the production of ^{28}Mg is conservatively estimated to be ~ 100 mb[2], which would probably correspond to a bound multineutron production cross section of a few mb. It is anticipated

1. Department of Physics, Louisiana State University, Baton Rouge, Louisiana.
2. School of Physics, Georgia Institute of Technology, Atlanta, Georgia.
3. K. Heyde et al., Phys. Repts. 102, 291 (1983).
4. E. F. Zganjar et al., in Proc. 4th Int. Conf. on Nuclei Far From Stability, CERN 81-09, p. 630.
5. E. F. Zganjar et al., in Proc. of the Symposium on Nuclei Far From Stability, Chicago meeting of the American Chemical Society, September 1985.
6. A. J. Larabee et al., preprint, October 1985, submitted to Physics Letters.

that the sensitivity can be improved by about two orders of magnitude by making several changes in the experiment. These include longer bombardment times, thicker targets to degrade the beam energy, different detection materials, and more (at least six) Ge detectors for off-line counting. An experiment incorporating such improvements is planned.

The author appreciates contributions by TTU undergraduate students M. G. Prahovic, T. R. Campbell, and R. W. Tramel.

---

1. Tennessee Technological University, Cookeville, Tennessee.

4. EXPERIMENTAL ATOMIC PHYSICS

The experimental atomic physics program within the Physics Division is carried out by two groups, whose reports are given in this section. Work of the accelerator atomic physics group is centered around the 6.5-MV EN tandem accelerator; consequently, most of its research is concerned with atomic processes occurring to, or initiated by, few MeV/nucleon heavy ions. Additional activities of this group concerns itself with lower energy atomic collision physics in support of the Fusion Energy Program. A new electron cyclotron resonance source of low-energy multiply charged ions is central to this activity, and some recent results obtained using this facility will be presented here. In addition to these two activities in experimental atomic physics, other chapters of this report describe the progress in related activities of these groups in theoretical atomic physics experimental plasma diagnostic development, and atomic data center compilation.

ATOMIC PHYSICS FOR FUSION PROGRAM

THE ECR MULTICHARGED ION SOURCE

F. W. Meyer J. W. Hale

During the past year, performance of the ECR multicharged ion source has been optimized. The first stage of the ion source was redesigned to operate at 10.6 GHz in the electron cyclotron resonance mode. Microwave power to the first stage is obtained from the main 10.6 GHz supply providing power to the second stage by means of a low reflectivity variable power divider. Addition of this improved first stage has been found to significantly enhance stability of very-high-charge-state ion beams, and of ion beams of the lighter elements. In order to compensate for the lower magnetic field in the first stage relative to earlier over-dense operation, an auxiliary coil was added to the middle second-stage coil.

In order to maximize axial field tuning capability, a third axial field coil supply was installed. In this new configuration, the currents in all three axial field coils can be varied independently over a sufficiently wide range to find the optimum axial magnetic field profile.

The capabilities of the ECR source were extended to metallic ion production by use of a solid sample feed technique. Using this technique, a metallic vapor is created from a thin foil sample heated by insertion into the second stage plasma edge. The foil is clamped to the end of a lever arm that can be rotated about a pivot. Rotation of the sample into the plasma edge is achieved via a mechanical linkage to a linear motion feedthrough located on the microwave feedthrough flange. A 0.2-mm-thick sample of type 302 stainless steel sheet was used in this manner to obtain beams of Fe, Cr, and Ni ions. Charge states of iron up to 15+ were produced with sufficient beam intensity for use in crossed beams experiments.

Table 4.1 summarizes ion currents presently attainable with the ECR source for beams produced from three representative permanent gases, as well as for iron beams produced by the solid feed technique described above.

ION-ATOM MERGED BEAM EXPERIMENT

C. C. Havener[1] R. A. Phaneuf
P. A. Schulz[2]

Our objective is to measure the total electron capture cross section for collisions of multicharged ions with H (or D) in the energy range of 1-500 eV/nucleon. At such low energies, theoretical models remain essentially untested. In some multiply ionized systems, an orbiting mechanism is predicted to give very

Table 4.1. Representative ORNL ECR source beam currents (el. μA). O beam currents for 10 kV source voltage; Ar and Kr beam currents for 12 kV source voltage (15 × 15 mm charge analyzer slits)

	O	Ar	Fe	Kr
+1	105	110	10	
+2	95	120	*	
+3	80	90	20	
+4	*	75	*	
+5	83	*	23	20
+6	50	65	25	25
+7	2.5	73	*	26
+8	0.1	105	*	27
+9		45	20	33
+10		*	10	31
+11		3.0	5	33
+12		0.7	*	40
+13			2	23
+14			*	21
+15			0.5	10
+16				
+17				1.0
+18				*
+19				0.25

*Indicates m/q degeneracy with contaminant beam.

large electron capture cross sections with a 1/v velocity dependence.

Details of the apparatus can be found elsewhere.[3] 5-7 keV beams of D^0 have been successfully merged with 30-40 keV beams of N^{3+} in a 76-cm-long ultrahigh vacuum merge path yielding center-of-mass energies of 4-70 eV/nucleon. A D^- beam from a duoplasmatron ion source is photodetached using a 1.06-μm Nd:YAG laser producing a highly collimated beam of D^0. A N^{3+} beam was produced by the ORNL-PIG ion source. Significant improvements in beam-line optics, vacuum, and noise reduction have led to the operating parameters presented in Table 4.2. The secondary electron emission coefficient, λ, needed to calibrate the neutral Faraday cup can be experimentally determined in situ to a few percent. Signals in the D^+ detector (channel electron multiplier) resulting from beam-beam interaction are measured above the background from beam-gas interactions by using a standard beam-modulation scheme to chop both the multicharged ion and neutral beams, and to gate dual counters to record both signal-plus-background

Table 4.2. Typical operating parameters

D^- beam:	$E = 4.00$ keV, $I(D^-) = 1.5$ μA $I(D^0) = 13$ nA, $\gamma = 0.59 \pm 0.02$
N^{3+} beam:	$E = 36.0$ keV, $I(N^{3+}) = 1.0$ μA
Center of mass energy:	35.9 eV/nucleon
Merge path pressure:	2×10^{-10} Torr (base) 7×10^{-10} Torr (w/beams)
D^+ background rate due to D^0 stripping:	3 kHz
Noise from N^{3+} beam:	50 Hz
Beam-beam signal:	120 Hz
Average two-dimensional form factor:	2.5 cm^{-2}
Time for s.d. of 10% on signal:	3 minutes

and background events. The form-factor is a measure of the two-dimensional beam-beam overlap and is measured at four positions along the merge path by two mechanical knife edge scanners and two commercial rotating wire scanners. The two rotating wire scanners provide a real time two-dimensional profile of the beams that has proved essential in tuning the D^0 and N^{3+} beams to achieve a good overlap throughout the merge path.

Extensive diagnostics have been performed on the beam-beam signal observed in the N^{3+} + H system. Horizontal and vertical scans of the signal indicate that all the signal is being collected. The signal was observed to be independent of the beam chopping frequency above 500 Hz, indicating that beam-produced gas-pressure modulation effects were being correctly subtracted from the background. However, since the N^{3+} beam was obtained from the ORNL-PIG ion source, measurements of the beam-beam overlap, signal, and diagnostics on the signal were not possible before the characteristics of the N^{3+} beam changed. This instability and the presence of an unknown admixture of metastables in the N^{3+} beam made meaningful measurements of a cross section impossible.

The merged-beams experiment is presently being installed on the new ORNL-ECR ion source. This source has produced ion beams significantly more intense and stable than the ORNL-PIG ion

source and in considerably higher charge states. This will allow measurements of more interesting systems, e.g., O^{5+} and C^{3+}, which are Li-like and contain no metastables to complicate comparisons between theory and experiment.

---

1. ORAU Postdoctoral Research Associate.
2. ORAU Summer Faculty Research Participant, Georgia Institute of Technology, Atlanta.
3. Abstracts of Contributed Papers of XIV International Conference on the Physics of Electronic and Atomic Collisions, p. 662, July 1985, Palo Alto, California.

ELECTRON-IMPACT IONIZATION OF MULTICHARGED IRON IONS[1]

D. C. Gregory
F. W. Meyer
A. Müller[2]
P. Defrance[3]

Electron-impact ionization cross section measurements have been made for a number of multicharged iron ions as part of our continuing work in support of the fusion energy program. In addition to its astrophysical significance, iron is expected to be a contaminant in any laboratory plasma contained in a stainless steel vessel, so it is one of the critical elements for which atomic collision cross sections are needed in order to model plasmas and to interpret diagnostics. The only data available for ionization of iron ions are crossed-beams measurements for Fe^{+} (ref. 4), Fe^{2+} (measured at ORNL[5]), and rate coefficient measurements[6] for Fe^{8+}-Fe^{10+} (which are considered to have rather large absolute uncertainties). The development of the new ORNL ECR ion source and recent improvements in our experimental apparatus have made it possible to extend ionization measurements to higher charge states.

The experimental apparatus is shown in Fig. 4.1. After entering the ultrahigh vacuum chamber, the incident ion beam is electrostatically analyzed in the charge purifier. The beam then passes through the interaction region where it is crossed at 90° by a magnetically-confined electron beam of variable energy. The ions are separated by charge state in the post-collision analyzing magnet, and the ionized signal ions are counted in a channeltron detector while the parent ion beam current is measured in one of

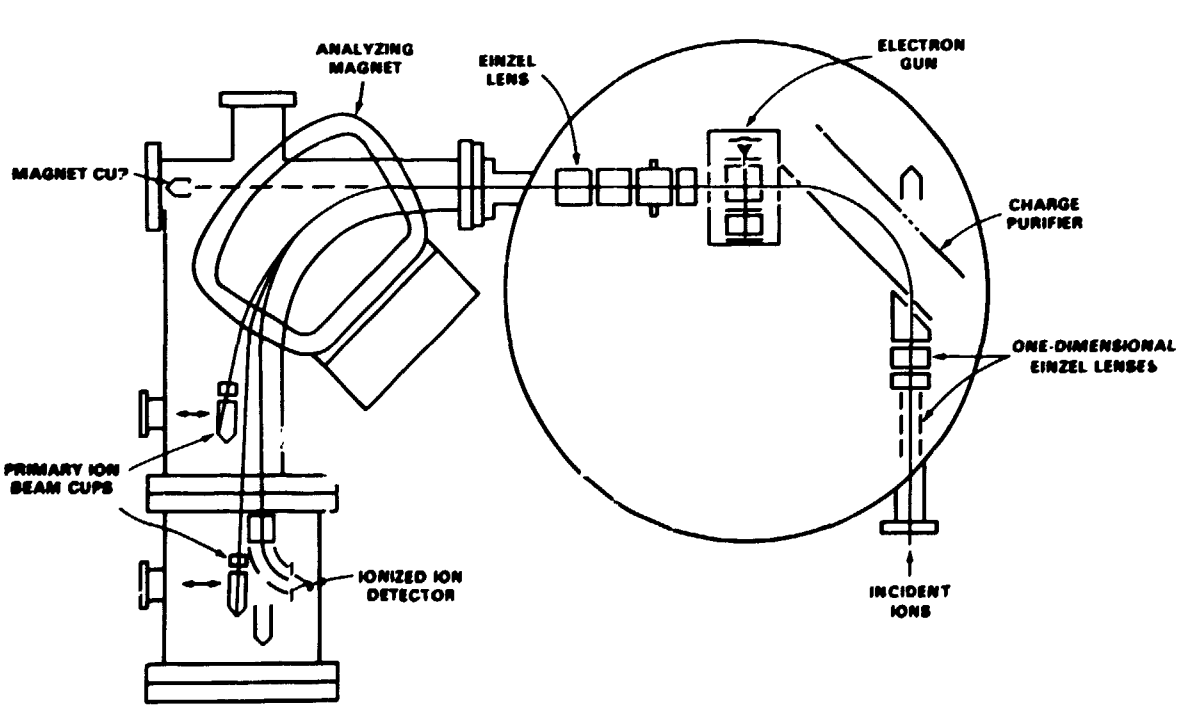

Fig. 4.1. The ORNL electron-ion crossed beams apparatus.

two movable cups. The apparatus is capable of resolving parent/product ion charge ratios in the range 5/6 to 15/16.

In the present study, absolute cross sections for electron-impact ionization of Fe^{5+}, Fe^{6+}, and Fe^{9+} were measured as a function of electron energy. Fe^{5+} and Fe^{6+} cross sections are about twice that predicted for direct ionization by distorted-wave theory.[7] Concurrent work on indirect ionization theory for these ions[8] attributes the difference to the process of electron-impact excitation of the target ions to autoionizing levels, and good agreement is found between theory and experiment when these excitation-autoionization contributions are included. The outstanding feature of the Fe^{9+} cross section curve is that the ionization onset is observed 50 eV below the energy expected for the ground state ion, indicating a large metastable component in the target ion beam coming from the ECR ion source. The presence of a large number of highly excited metastables in Fe^{9+} is therefore predicted to be found in many plasmas containing Fe contaminants.

The rate coefficients for ionization of all iron ions for which crossed beams data exist are summarized in Fig. 4.2. It is clear that the earlier rate-coefficient measurements for Fe^{9+} were correct in slope but a factor of three low in magnitude. We expect to extend our studies of iron ions to even higher charge states and to include other metal ions of interest to the fusion community.

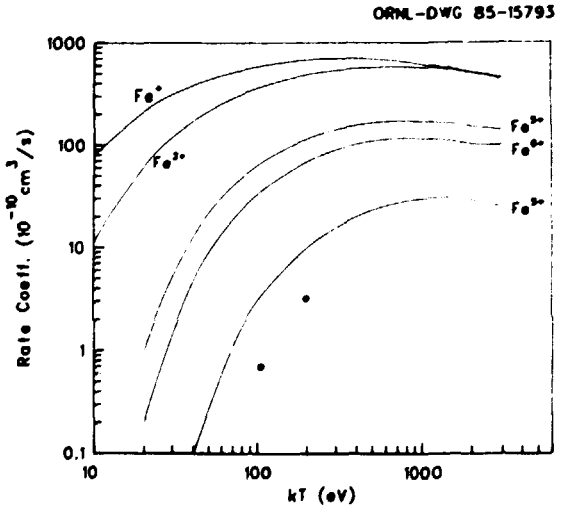

Fig. 4.2. Rate coefficients for electron impact ionization of Fe ions. The curves are calculated from cross section measurements (referenced in the text), and the two points are rate measurements for Fe^{9+} (ref. 6).

---

1. Summary of paper to be submitted for publication.
2. Joint Institute for Laboratory Astrophysics, Boulder, Colorado, on leave from Justus-Liebig Universitat, Giessen, West Germany.
3. Universite Catholique, Louvain-la-Neuve, Belgium.
4. R. G. Montague, M. J. Diserens, and M.F.A. Harrison, J. Phys. B 17, 2085 (1984).
5. D. W. Mueller et al., Phys. Rev. A 31, 2905 (1985).
6. R. L. Brooks, R. U. Datla, A. D. Krumbein, and Hans R. Griem, Phys. Rev. A 21, 1387 (1980).
7. S. M. Younger, Atomic Data for Fusion (Bulletin of the Controlled Fusion Atomic Data Center - ORNL) 7, 190 (1981).
8. See C. Bottcher, M. S. Pindzola, and D. C. Griffin, Chapter 5 of this report.

ELECTRON-IMPACT DISSOCIATION OF H_3O^+[1]

P. A. Schulz[2] F. W. Meyer
D. C. Gregory R. A. Phaneuf

Electron-impact dissociative recombination ($e^- + AB^+ \rightarrow A + B$) has long been recognized as an important process at electron energies of a few eV and below in astrophysical plasmas and in other areas of research such as excimer laser development. The competing process of electron-impact dissociation ($e^- + AB^+ \rightarrow A^+ + B + e^-$), however, generally has a larger cross section at energies above 5 eV and has received relatively little attention. The present study of dissociation of H_3O^+ was undertaken to determine the absolute cross sections for the various dissociation channels and to determine, if possible, the mechanisms leading to dissociation. The cross sections for dissociation of H_3O^+ due to collisions with background gas have also been determined.

The apparatus used in this experiment is exactly the same as that described in the previous section. The post-collision magnetic charge analyzer can also serve as a mass analyzer so that no modifications were necessary.

H_3O^+ (and D_3O^+) ions were produced in the first stage of the ORNL ECR ion source, then were allowed to drift through the second stage of the ion source before being accelerated. For this application, the second stage was used only as a drift section to transport the H_3O^+ ions to the extraction region (i.e., no microwave power was applied). Since the transit time through the second stage (~ msec) was long compared to the excited vibrational-state lifetimes of the ions, the target ion beam was probably quite "cold" in the collision region. This important feature of the ECR ion source may make it an unexpectedly valuable source for experiments involving molecular ions.

Cross sections for the process of dissociation of the 5-kV H_3O^+ ions in collision with residual gas in the target region were estimated from the background count rate in the signal detector. The cross sections for the possible dissociation products are 3×10^{-18} cm^2 for O^+, 4×10^{-17} cm^2 for OH^+, and 7×10^{-16} cm^2 for D_2O^+. The exact composition of the residual gas is not known, but is most likely a combination of N_2, H_2, and CO. These effective cross sections are based on a number of assumptions, but are almost certainly accurate within a factor of 4. The relative magnitudes of the cross sections are more accurate, and it is somewhat surprising that roughly an order of magnitude separates the relative probabilities of dissociation into each of the channels.

Electron-impact dissociation of H_3O^+ yields O^+, OH^+, and H_2O^+ products. Since the apparatus was not able to adequately separate H_2O^+ from H_3O^+, the production of D_2O^+ from target D_3O^+ ions was studied in its place. This reaction is assumed to have the same cross section as that producing H_2O^+.

The cross sections for electron-impact dissociation of H_3O^+ to produce O^+ as a function of energy are shown in Fig. 4.3. The threshold is observed near 18 eV, which is consistent with the estimated onset of this dissociation channel from the ground vibrational state of H_3O^+. The cross section rises sharply at the threshold, then continues to rise gradually to a peak of

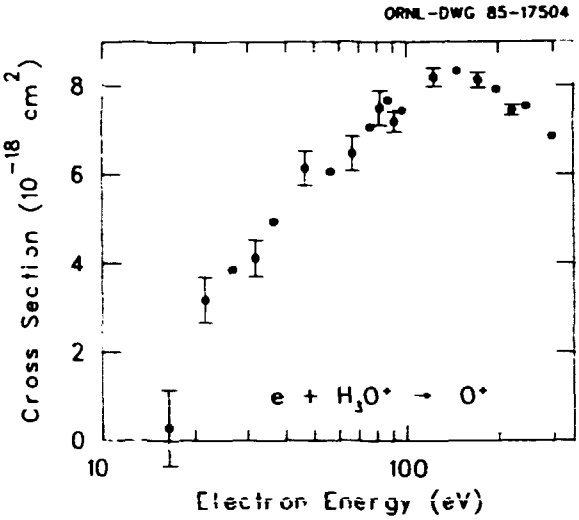

Fig. 4.3. Cross sections for electron impact dissociation of H_3O^+ to O^+.

8×10^{-18} cm^2 at about 150 eV. The gradual rise is characteristic of an ionization process, and we conclude that this dissociation channel is fed predominantly by ionization of H_3O^+. The cross section curve for production of OH^+ from H_3O^+ is shown in Fig. 4.4. The threshold is between 14 and 17 eV and, in contrast to O^+, the maximum cross section of 45×10^{-18} cm^2 is observed at threshold. This energy dependence (maximum cross section at threshold) is characteristic of excitation of ions, and we conclude

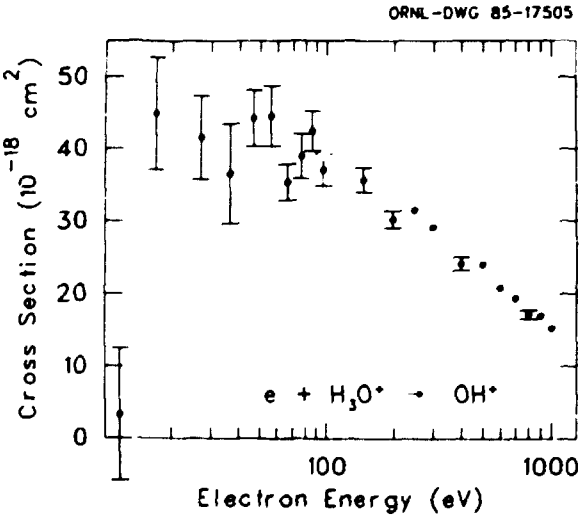

Fig. 4.4. Cross sections for electron impact dissociation of H_3O^+ to OH^+.

that the dominant channel for production of OH^+ is through excitation of H_3O^+. The cross section for production of D_2O^+ from D_3O^+ is not shown here. Due to the high rate of D_2O^+ production through collisions of the target ions with residual gas, high background count rates made the accumulation of signal statistics difficult at low energies, and normal diagnostic measurements even more difficult. The peak cross section for this dissociation channel is about 70×10^{-18} cm^2, but we were unable to extend measurements to low energies with sufficient accuracy to determine if the dissociation is produced through excitation or ionization of the parent D_3O^+ ion.

This initial study of electron impact dissociation of molecular ions has opened a new field of research for our laboratory. Future studies will include ionization or dissociation of ions of interest in laser development or astrophysical studies.

---

1. Summary of paper to be submitted for publication.
2. ORAU Summer Faculty Research Participant, Georgia Institute of Technology, Atlanta.

ELECTRON-IMPACT IONIZATION OF Li-LIKE MULTICHARGED IONS[1]

D. H. Crandall[2] D. W. Mueller[4]
R. A. Phaneuf T. J. Morgan[5]
D. C. Gregory G. H. Dunn[4]
A. M. Howald[3] R.J.W. Henry[6]

Measurements of electron-impact ionization of ions are of general interest because of the uncertain state of basic collision theory as applied to ionization and because of the important role of ionization in laboratory and astrophysical plasmas. In recent years, we have provided accurate experimental data from crossed-beams experiments along a number of isoelectronic sequences in order to test theoretical approaches in a consistent manner, and to establish a database of results for ionization of multicharged ions.[7,8] The present results for B^{2+} and O^{5+} complete a series of experiments on ionization of Li-like ions for the first five ions of the isoelectronic sequence. Because of the absence of metastable ions in the beams, simple electronic structure, and prominence of emission lines from plasmas, the lithium sequence is a prime candidate for extensive study by experiment and theory. These measurements also provide a reasonable basis for extrapolation of the predicted magnitude of indirect ionization effects to higher members of this sequence.

The first measurements[9] on ionization of Li-like ions C^{3+}, N^{4+}, and O^{5+} provided a mild surprise in that inner-shell excitation followed by autoionization produced a measurable contribution to the ionization cross section. Subsequent calculations[10] showed that almost all of the inner-shell excited states of these ions would decay by autoionization rather than by radiative stabilization and that the calculated inner-shell excitation cross sections were roughly appropriate for the observed structure in the ionization cross sections. However, trends in the experimental data indicated that the relative importance of excitation-autoionization increased more rapidly with ionic charge than predicted by theory.[11] In addition to the basic questions raised about collision physics, this discrepancy implied significant uncertainty for even the most refined predictions of ionization and excitation rates for other, more highly charged ions of this sequence (e.g., Fe^{23+}, which is important in analyzing high temperature plasmas of fusion and astrophysical interest).

The present studies were undertaken in an attempt to clarify the scaling of excitation-autoionization effects in multiply charged Li-like ions. In the six years since the publication of the original data, a number of improved calculations of both excitation and direct ionization have been published, as well as experimental data[12] for Be^+. We have added measurements for ionization of B^{2+} (previously unmeasured) and have remeasured the O^{5+} system which was significantly larger than theory in the previous analysis. Sophisticated distorted-wave calculations[13] for direct ionization have been taken as a basis for extraction of the

excitation cross sections from the total ionization measurements for each member of the isoelectronic sequence from Be^{+} through O^{5+}.

The experimental technique and apparatus have been described.[14] The B^{2+} measurements used the ORNL-PIG ion source, while the latest O^{5+} results were obtained with the new ORNL ECR ion source. In both cases the experiments were pursued with the highest level of precision in the energy regions where the excitation threshold occurs. Absolute uncertainty in the overall magnitude of the cross section curve was about ±8% of the peak cross section at good confidence level, while the relative uncertainty in the excitation threshold region is considerably less. The B^{2+} measurements are in reasonably good agreement with distorted-wave calculations of Younger,[13] both in shape and in magnitude (experimental results are consistently 10% higher than theory). O^{5+} measurements are in excellent agreement with the distorted-wave results up to about 400 eV, where the cross section suddenly increases by about 7%. Independent measurements[15] corroborate the existence of this feature, although the physical process causing it is still unidentified.

The extracted total excitation cross sections (obtained by subtracting Younger's direct ionization prediction — scaled where appropriate — from the total measurements) for each of the Li-like ions studied to date are presented in Table 4.3. The ratios of these deduced excitation cross sections to six-state close-coupling calculations of total excitation are also included in the table, and the agreement is seen to be excellent for all members of the isoelectronic sequence except Be^{+}. The reason for this agreement, as opposed to the marked disagreement of previous analyses, is twofold. First, an error in the distorted-wave ionization calculations used as a basis for obtaining the excitation cross sections has recently been corrected, producing much more accurate estimates of the direct ionization component for each of the ions. Second, the new O^{5+} results indicate a smaller indirect ionization component than the previous measurements. It is felt that the new data are more accurate and precise than the previous results due to the improved beam intensity and stability obtained with the new ion source. The only remaining discrepancy between theory and experiment for excitation in this isoelectronic sequence is found in the lowest charge-state ion of the sequence. Additional comparisons between theory and experiment for selected highly charged Li-like ions will be necessary, however, to assure the accuracy of scaled cross sections many charge states further along the isoelectronic sequence.

Table 4.3. Excitation cross sections for Li-like ions (10^{-19} cm^2)

Ion	Six-State Close-Coupling Theory	Presently Deduced Experiment	Ratio (Expt./Theory)
Be^{+}	9.3	20 + 8	2.1
B^{2+}	4.1	4.0 + 1.0	1.0
C^{3+}	2.24	2.3 + 0.7	1.0
N^{4+}	1.27	1.6 + 0.4	1.3
O^{5+}	0.74	0.9 + 0.3	1.2

---

1. Summary of paper to be published in Physical Review A.
2. Present address: ER-542, Office of Fusion Energy, U.S. Department of Energy, Washington, D.C. 20545.
3. Appointed through the postgraduate research training program administered by Oak Ridge Associated Universities; present address: GA Technologies, Inc., San Diego, CA 92138.
4. Joint Institute for Laboratory Astrophysics, Boulder, CO 80309.
5. Wesleyan University, Middletown, CT 06457.
6. Louisiana State University, Baton Rouge, LA 70803.
7. D. H. Crandall, R. A. Phaneuf, and D. C. Gregory, Electron Impact Ionization of Multicharged Ions, Oak Ridge National Laboratory Report ORNL/TM-7020, September 1979.
8. D. C. Gregory et al., Electron Impact Ionization of Multicharged Ions at ORNL: 1980-1984, Oak Ridge National Laboratory Report ORNL/TM-9501, May 1985.
9. D. H. Crandall et al., J. Phys. B 12, L249 (1979).
10. R.J.W. Henry, J. Phys. B 12, L309 (1979).
11. D. H. Crandall, p. 595 in Physics of Electronic and Atomic Collisions, ed. S. Datz (North Holland, 1982).
12. R. A Falk and G. H. Dunn, Phys. Rev. A 27, 754 (1983).
13. S. M. Younger, J. Quant. Spectrosc. Radiat. Transfer 26, 329 (1981); corrected parameters, private communication (1984).

14. D. C. Gregory, P. F. Dittner, and D. H. Crandall, Phys. Rev. A 27, 724 (1983).
15. P. Defrance et al., submitted to Journal of Physics B, 1985.

ELECTRON-IMPACT IONIZATION OF Mg-LIKE IONS[1]

A. M. Howald[2] R. A. Phaneuf
D. C. Gregory A. Müller[3]
F. W. Meyer N. Djuric[3]
G. H. Dunn[3]

The implementation of the ECR multicharged ion source provided an opportunity to extend our systematic studies of collision processes along ionic sequences. The first intersecting-beams experiments involved cross-section measurements for electron-impact ionization of three ions in the Mg-isoelectronic sequence: S^{4+}, Cl^{5+}, and Ar^{6+}. These experiments were performed in collaboration with the JILA group led by G. H. Dunn, which had previously made measurements for Al^{+}, the first member of the sequence.

The electron-ion crossed-beams apparatus and experimental technique have been described in detail in previous reports.[4] The experimental total single-ionization cross section measurements are compared in Fig. 4.5 to scaled Coulomb-Born calculations[5] for direct ionization, and also to the predictions of the Lotz semiempirical formula.[6] The changes in slope of the cross sections at electron energies near 170, 190, and 220 eV for S^{4+}, Cl^{5+}, and Ar^{6+}, respectively, are signatures of the onset of 2p-nl inner-shell excitation, followed by autoionization. This indirect excitation-autoionization mechanism (EA) contributes a relatively larger fraction to the total ionization cross section as the ionic charge increases along the sequence. Detailed distorted-wave theoretical calculations of this process have been performed for these ions by Pindzola, Griffin, and Bottcher, and are summarized in Chapter 5 of this report.

A number of interesting features emerge from a detailed analysis of the data. First, the experimental ionization onsets are lower than the ionization potentials of the $2p^6 3s^2$ ground state, indicating that a significant fraction of the incident Mg-like ions are in metastable

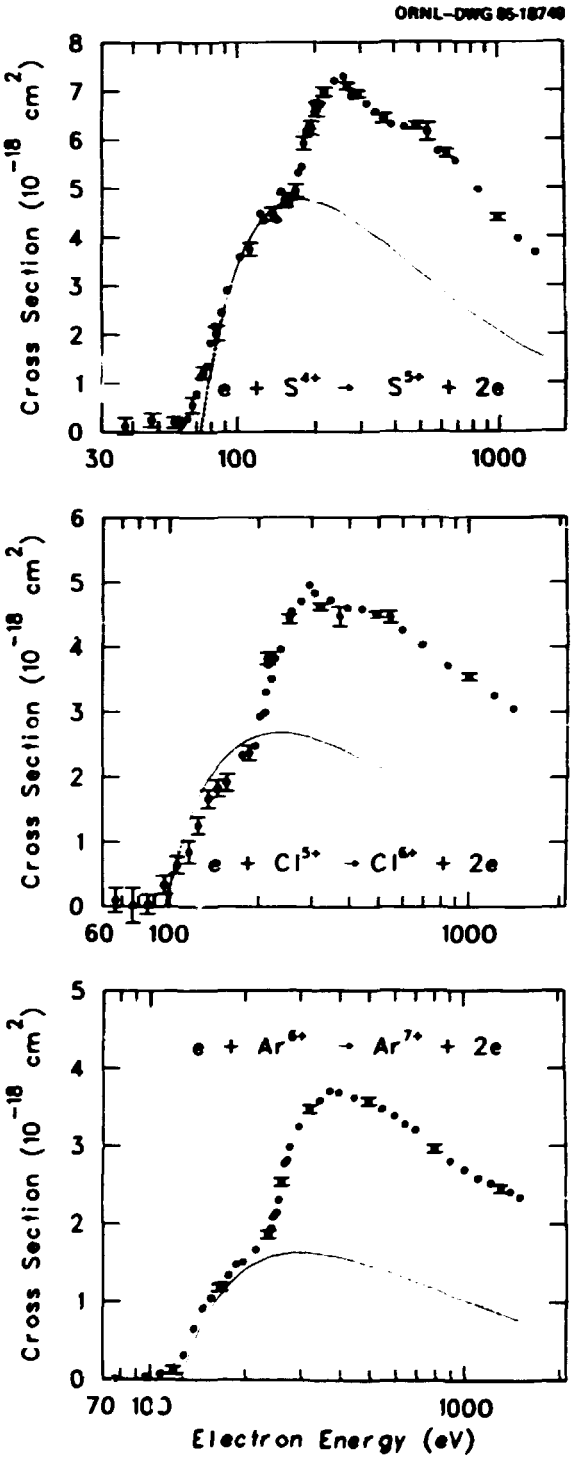

Fig. 4.5. Experimental cross sections for electron-impact single ionization of S^{4+}, Cl^{5+}, and Ar^{6+}. Dashed curves are Lotz semiempirical predictions for direct ionization, and solid curve for Ar^{6+} is distorted-wave calculation of Younger. For S^{4+} and Cl^{5+}, the solid curves are scaled from that for Ar^{6+} by the inverse squares of their respective ionization potentials.

levels of the $2p^63s3p$ configuration. Second, the single-ionization cross sections show contributions due to direct 2p inner-shell ionization. The 2p-vacancy state is predicted to decay almost completely by autoionization, in which case 2p ionization would contribute to double rather than single ionization. This was perplexing, until it was realized that removal of a 2p electron from a metastable $2p^63s3p$ Mg-like ion produces a Na-like ion in the $2p^53s3p$ configuration, in which many of the levels are also metastable with lifetimes against both radiative and Auger decay of tens of microseconds or longer.[7] Such times are longer than flight times in the apparatus. This realization also has allowed us to resolve some outstanding issues relative to earlier experiments on Na-like ions, which were characterized by large autoionizing backgrounds. The apparently missing contribution of the 2p-3p EA contribution to single ionization of Na-like Al^{2+} (ref. 8) may be attributed to metastability of the $2p^53s3p$ levels.

Low-lying metastable levels clearly play important roles in the state dynamics of many high-temperature plasmas. Such levels may well account for unresolved discrepancies between predictions and recent measurements on Ne-like ions in X-ray laser plasmas.[9]

---

1. Summary of a paper to be submitted for publication to Physical Review A.
2. Appointed through the postgraduate research training program administered by Oak Ridge Associated Universities; present address: GA Technologies, Inc., San Diego, CA 92138.
3. Joint Institute for Laboratory Astrophysics, University of Colorado and National Bureau of Standards, Boulder, Colorado.
4. D. C. Gregory, P. F. Dittner and D. H. Crandall, Phys. Rev. A 27, 724 (1983).
5. S. M. Younger, Atomic Data for Fusion 7, 190 (ORNL, 1981).
6. W. Lotz, Z. Physik 216, 241 (1968).
7. S. E. Harris, D. J. Walker, R. G. Caro, A. J. Mendelsohn and R. D. Cowan, Opt. Lett. 9, 168 (1984).
8. D. H. Crandall, R. A. Phaneuf, R. A. Falk, D. S. Belic, and G. H. Dunn, Phys. Rev. A 25, 143 (1982).
9. D. L. Matthews et al., Phys. Rev. Lett. 54, 110 (1985).

MULTICHARGED ION - SURFACE SCATTERING AT GRAZING INCIDENCE

F. W. Meyer[1]
C. C. Havener[1]
W. Heiland[2]
S. Overbury[3]
D. Zehner[3]

In an experiment designed to investigate the feasibility of studying the ion-surface interactions using the ORNL ECR multicharged ion source, we have measured the energy distributions of secondary electrons produced during collisions of H-like and He-like light ions with a gold surface at grazing incidence. The study of multicharged ion-surface interactions is of considerable current interest, in large part due to the significant neutralization potential energy that the multicharged projectiles carry into the collision. Experiments studying the reflected ion charge state distributions and the secondary electron emission coefficients for collisions with W surfaces have been reported.[5,6] The present experiment is the first to our knowledge to investigate the energy distributions of secondary electrons produced during multicharged ion-surface collisions.

Beams of N^{5+}, N^{6+}, O^{6+}, and O^{7+} were produced by the ORNL ECR ion source at 10 kV source potential. After charge selection and beam collimation, the ions were made incident at 5° on the (110) surface of a gold single crystal mounted in an ultrahigh vacuum chamber equipped with a 4-grid low energy electron diffraction (LEED) system. The condition of the surface of the Au crystal was determined by the use of electron-induced Auger spectroscopy and the observation of LEED patterns. In addition, the energy distributions of the multicharged-ion-induced secondary electrons were obtained by using the LEED grids in the retarding field mode and numerically differentiating the transmitted secondary electron current vs retarding voltage curves.

Figures 4.6 and 4.7 show the secondary electron spectra observed for N^{6+} and O^{7+} incident projectiles. Both spectra show two peaks superimposed on a "kinetic emission" background having a monotonic energy dependence. The higher energy peaks at ≈350 eV and ≈480 eV in

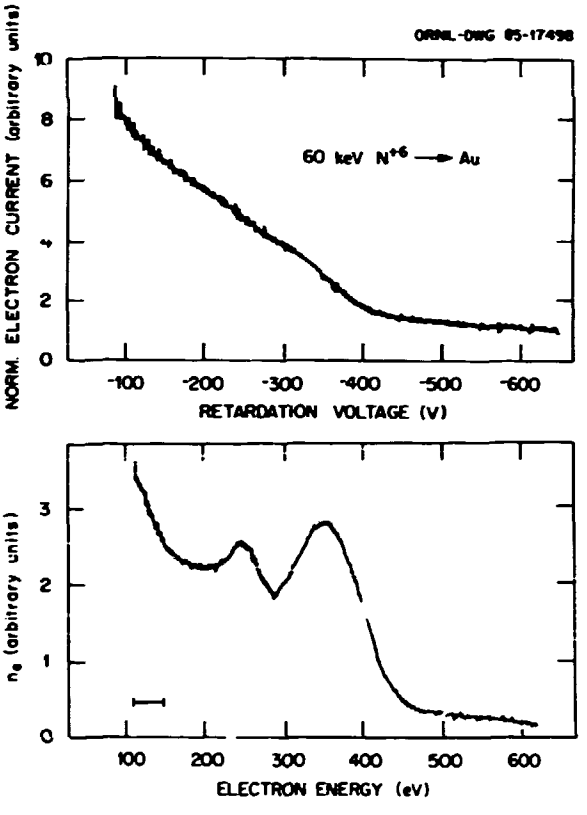

Fig. 4.6. N^{6+} incident on Au at 5°: top — transmitted secondary electron current vs retarding voltage; bottom — secondary electron energy distribution (bar indicates "instrumental" width introduced by numerical differentiation).

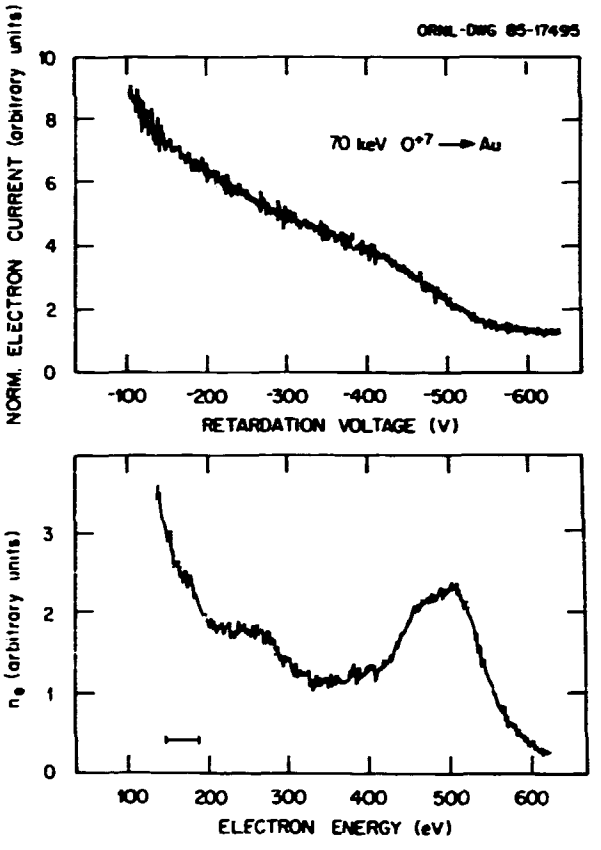

Fig. 4.7. O^{7+} incident on Au at 5°: description of curves same as Fig. 4.6.

the case of the N^{6+} and O^{7+} induced spectra, respectively, are believed to be associated with Auger decay of the K-shell vacancy in the H-like projectile via electrons in highly excited states. These high-lying states are populated during the collision by resonance neutralization from the valence band of the solid. The lower energy peaks at ~250 eV occur at the same energy in both spectra and are believed to be associated with Auger decay of a target-atom inner-shell vacancy created during the collision.

Secondary-electron spectra were obtained both for the case of a "clean" surface that was etched by a 10-keV Ar^{1+} beam and subsequently annealed, and for the case of a "dirty" surface that had just previously been exposed to atmosphere. The "clean" surface was characterized as having less than 20% of a monolayer of C surface contamination. The spectra acquired under the two surface conditions were indistinguishable.

Secondary-electron spectra were also measured for N^{5+} and O^{6+} incident projectiles, whose ground-state configurations have filled K-shells. Although the latter spectra were dominated by the "kinetic emission" background, the same peaks as were observed for the H-like incident ions could be discerned, albeit greatly reduced in size. These spectra indicate that a small fraction of the He-like ions extracted from the ECR source are created in 1s2s metastable states. Since these metastable ions necessarily have K-shell vacancies, the secondary electrons they produce during surface collisions manifest the same Auger peaks as were observed for the H-like ions.

Further work is planned to determine the extent to which ion-induced secondary electron spectroscopy may be used as a quantitative tool for studying the metastable content of ion beams, as well as to study in greater detail the mechanisms underlying ion neutralization and secondary electron emission during multicharged ion-surface interactions.

---

1. ORAU Postdoctoral Research Associate.
2. Vanderbilt University, permanent address: Osnabrück Universität, Osnabrück, Federal Republic of Germany.
3. Chemistry Division, ORNL.
4. Solid State Division, ORNL.
5. S. T. de Zwart, T. Fried, U. Jellen, A. L. Boers, and A. G. Drentje, J. Phys. B 18, 1623 (1985).
6. M. Delaunay, S. Dousson, and R. Geller, Proc. XIV ICPEAC, Palo Alto, July 23-31, 1985, p. 477.

ACCELERATOR-BASED ATOMIC PHYSICS

RESONANT COHERENT EXCITATION OF O^{7+}, F^{8+}, AND C^{5+} IN THE <100> AXIAL CHANNEL IN GOLD

P. D. Miller, J. A. Biggerstaff, S. Datz, J. Gomez del Campo, N. Neskovic[1], H. F. Krause, O. H. Crawford[2], P. F. Dittner, C. D. Moak, M. D. Brown[3], P. L. Pepmiller

When an ion moves along an axial channel in a crystal it interacts with the static periodic potential arising from the lattice, and it interacts dynamically with the valence and conduction electrons in the channel. An ion with several MeV/nucleon energy has sufficient momentum that its motion within the channel can be treated classically. For a thin enough crystal, the impulse approximation may be used. The dynamic interaction results in a primarily longitudinal force acting on the ion, and this braking force we call the electronic stopping power in the channel. This interaction is dependent on both velocity and electron density, and through this density dependence it varies with impact parameter. The static periodic potential may be Fourier analyzed, in the frame of the moving ion, into an average value and a series of harmonics of the fundamental string frequency v/d, where v is the velocity of the projectile, and d is the spacing of the atoms within the strings bounding the channel. The negative gradient of the average value of this static potential gives the transverse force acting on the ion. The action of this impact parameter dependent force is responsible for the rainbow scattering reported in the previous contribution.[4]

The Hamiltonian of an electron bound to the projectile ion can be written as[5]

$$H = H_0 + V_S(x,y) + V_{OSC}(x,y,t). \qquad (1)$$

H_0 is the hydrogenic Hamiltonian; $V_S(x,y)$ is the time average of the crystal static potential plus a potential equivalent to the dynamic stopping field; and $V_{OSC}(x,y,t)$ can be represented as a Fourier series of potentials having frequencies Kv/d. Resonant coherent excitation (RCE) of the ions may occur when the frequency of one of these components of $V_{OSC}(x,y,t)$ is close to a transition energy in the ion divided by Planck's constant. For the case where a one-electron ion may be excited to the n = 2 excited states, electric fields derived from $V_S(x,y)$ act on the projectile electron to remove the degeneracy and Stark shift and split the n = 2 manifold into four states.

RCE has been observed for a number of one- and two-electron light ions in several axial and planar channels in gold and silver crystals.[6-8] Many of these resonances exhibited complex shapes, but the theoretical interpretation of the details of these splittings and asymmetries were not entirely clear.[5] The origins of these features of the resonances might be clarified by higher energy experiments since the energy losses in the crystal would be smaller.

Beams of the one-electron ions C^{5+}, O^{7+}, and F^{8+} were furnished by the Holifield Heavy Ion Research Facility (HHIRF) tandem accelerator. Collimation in front of the crystal assured a maximum beam divergence of $<<10^{-4}$ rad. The gold crystal was 1600 Å thick along the <100> axial channel. Charge states of the ions leaving the crystal were electrostatically analyzed. The acceptance of the analyzer was 0.3 mrad. Each

resonance was scanned twice, with the crystal alignment being renavigated between the scans. In all three cases the two scans were indistinguishable.

The fundamental (K = 1) resonance for C^{5+} would occur at an energy, E_r, of 81.634 MeV in the absence of any Stark shift of the n = 2 states. Figure 4.8 shows the observed surviving fraction of C^{5+} ions as a function of projectile velocity divided by the velocity at $E = E_r$. The resonance is extremely broad and very deep compared to resonances previously observed at lower energies.[6-8] This large strength indicates that power broadening should be considered in any theoretical attempt to calculate transition probabilities. Statistical errors are comparable to the sizes of the circles.

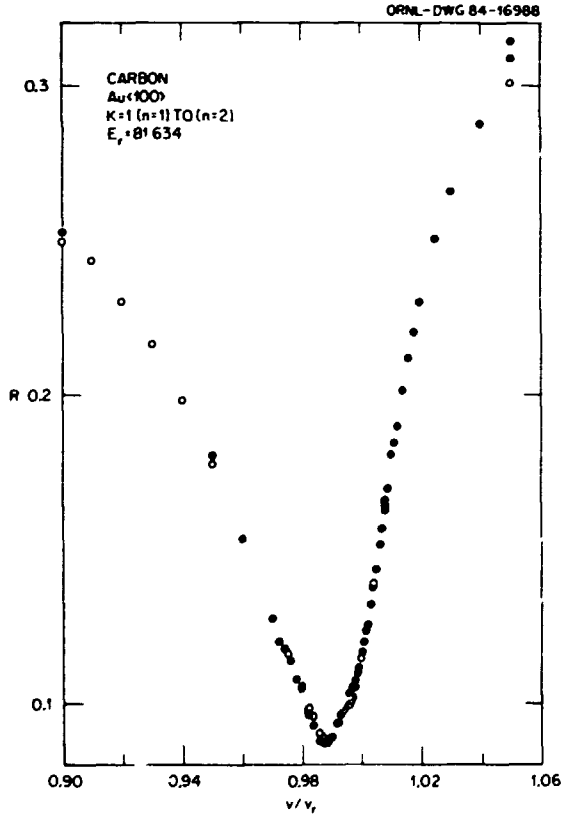

Fig. 4.8. Surviving fraction of C^{5+} ions transmitted through a 1600 Å gold crystal in the <100> axial channel. The 1s → 2p unperturbed transition energy is 13.506 Hartrees, corresponding to a projectile energy of 81.634 MeV for a K = 1 resonance. The fraction is given versus the velocity of the projectile divided by the velocity at resonance for the unperturbed state. The results of two different velocity scans are indicated by the closed and open circles.

The K = 2 resonance for F^{8+} is shown in Fig. 4.9. The data are characterized by a very narrow dip (FWHM = .0037 v/v_r) located at $v/v_r = 0.9985$ superimposed on a much broader asymmetric structure centered at about $v/v_r = 0.98$. The K = 2 resonance for O^{7+} is not shown, but it is very similar to Fig. 4.9 except that the narrow dip is about 60% wider. These resonances are qualitatively different from the K 2 resonances reported for C^{5+} and N^{6+}.[7]

The experimental data were compared to Monte Carlo calculations using a procedure developed by Neskovic[9] which utilizes the following approximations: For the calculation of the ion trajectory and the energy levels of the n = 2 states of the ion, we consider only the time average of the perturbing potentials $V_s(x,y)$. To determine the ion trajectory, an impact parameter is chosen, and the scattering angles θx

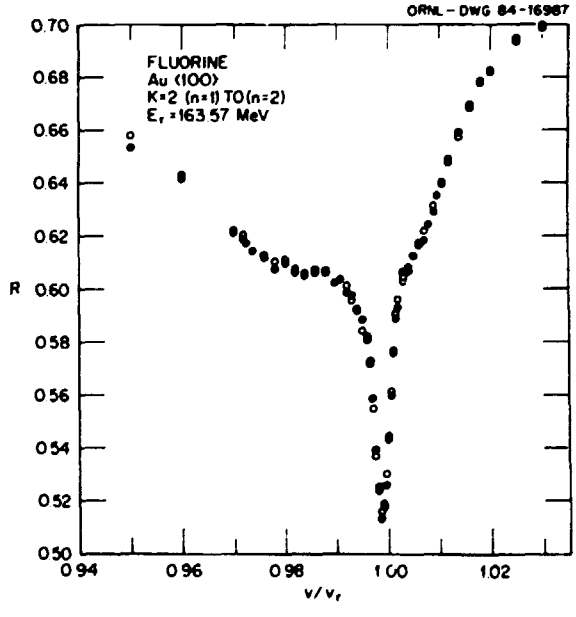

Fig. 4.9. Surviving fraction of F^{8+} ions transmitted through a 1600 Å gold crystal under the same conditions as Fig. 4.8. The symbols and axes have the same definitions as given in the caption of Fig. 4.8. The 1s → 2p unperturbed transition energy is 30.40 Hartrees, corresponding to a projectile energy of 163.6 MeV.

and θ_y are calculated in the impulse approximation using the Lindhard potential.[10] The acceptability of the impact parameter was tested by requiring that the nearest approach of the ion to a string be greater than a screening length, and by requiring that the scattering angles lie within the acceptance of the charge state analyzer. For trajectories passing these tests, the electronic energy levels for the n = 2 states were calculated using the entire time-independent part of the perturbation $V_s(x,y)$. The dynamic part of the perturbation was treated according to the formalism of Neufeld and Ritchie.[11] The positions of each of the four n = 2 states were then histogrammed for all acceptable impact parameters.

Figures 4.10 and 4.11 show the results of the Monte Carlo calculations and a qualitative comparison with experiment for two K = 2 resonances. The experimental data in Fig. 4.10a, N^{6+}, are taken from Moak et al.[7] For comparison with the calculations, the bare ion fraction is shown instead of the surviving one-electron fraction. The Monte Carlo calculations are shown only at a projectile energy E_r since there is very little change in the histogrammed state energies in scanning the projectile energy across the resonances. The four calculated transition energies correspond to the four Stark shifted members of the n = 2 manifold.

Several features of Figs. 4.10 and 4.11 should be noted: (1) In both cases the low-energy tail of the resonance is given by state 1, and the low-energy part of state 2. (2) The low-energy peak in the nitrogen data and the sharp peak in the fluorine data result from the

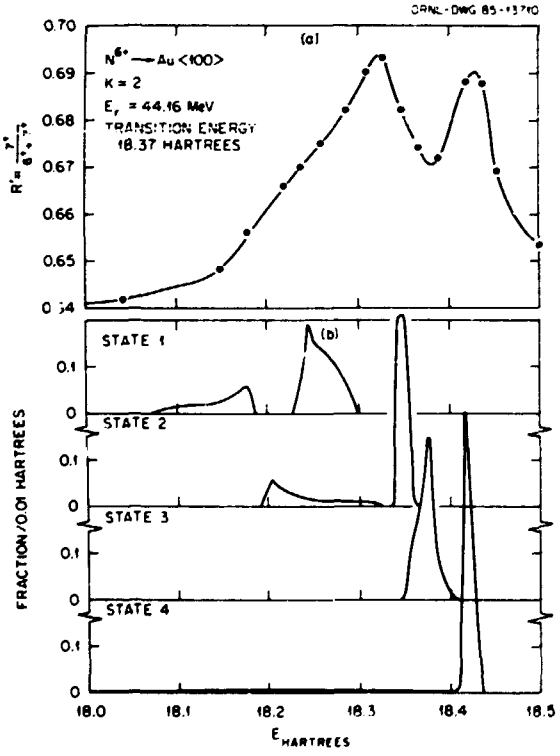

Fig. 4.10(a). Bare ion fraction leaving a 1450 Å gold crystal for N^{6+} ions incident in the <100> direction. The excitation energy is given by E = hKv/d. The harmonic number is K = 2. (b) Monte Carlo calculations of the four trajectory-dependent, Stark shifted transition energies of the projectile electronic states. 1000 trajectories were followed and the results were histogrammed in 0.01 Hartree bins.

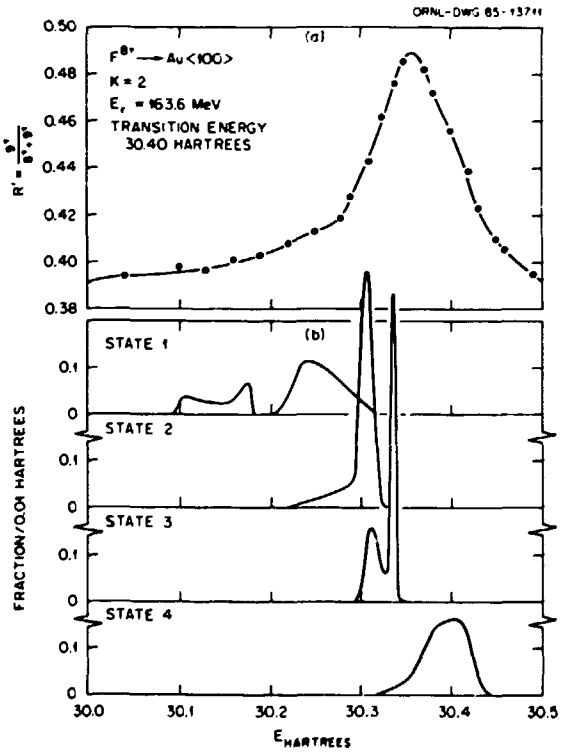

Fig. 4.11(a). Bare ion fraction leaving a 1600 Å gold crystal for F^{8+} ions incident in the <100> direction. The excitation energy is given by E = hKv/d. The harmonic number is K=2. (b) Monte Carlo calculations of the four trajectory-dependent, Stark shifted transition energies of the projectile electronic states. 1000 trajectories were followed and the results were histogrammed in 0.01 Hartree bins.

nearly degenerate states 2 and 3. (3) It is particularly interesting to note that state 4 is quite sharp for the 44.16-MeV N^{6+} ions, but it is broader for the 163.6-MeV F^{8+} ions. This phenomenon is quite reasonable, considering the behavior of the energy of the highest energy member of the n = 1 to n = 2 manifold as a function of the Stark field [e.g., ref.12]. The energy of this state versus electric field goes through a maximum. The Stark field acting on 44.16-MeV N^{6+} ions is much larger due to their lower projectile velocity; the transition energy of the uppermost state is near the maximum, and hence nearly constant as a function of electric field. In contrast, the energy of the uppermost state of the 163.6-MeV F^{8+} ions varies rapidly with the weaker Stark fields corresponding to different trajectories in the channel leading to a broader distribution of histogrammed state energies. One may speculate that this difference might account for the absence of the second peak in the flourine data, but a definite conclusion can be reached only by comparing with calculations of the transition probabilities using the time dependent part of the perturbation $V_{osc}(x,y,t)$. (4) The origin of the splitting of states 1 and 2 into a high-energy group and a low-energy group in the Monte Carlo calculations was investigated. For our acceptance solid angle of 0.3 mrad, the acceptable region of impact parameter space was mapped. Seventy percent of the acceptable trajectories originate near the center of the channel where the electron density is low and deflections are small. The second region producing small deflections lies near the bisector of a line connecting two adjacent strings. Since the electron density is much higher in this region, larger Stark shifts are produced, and projectiles having these impact parameters are in the lower energy group of state 1. The oscillating fields in this second region are stronger, since the ions are nearer to strings, so we might expect that the transition probabilities would be larger than for those ions near the center of the channel.[5] Similar calculations and comparisons have been made for the case of the K = 1 resonance of C^{5+}.[13]

In order to quantitatively understand RCE, it will certainly be necessary to calculate the transition probabilities as a function of projectile velocity using the time dependent portion of the interaction Hamiltonian. It will also be necessary to include trajectory dependent multiple scattering. Fitting the strength of the experimentally observed resonances and the background shape of the charge state fractions on each side of the resonances will require the use of the electron impact ionization cross sections for both the ground state and the n = 2 states of the projectile. For example, if the electron density calculated from the Lindhard potential[10] is used with the electron impact ionization theory of Golden and Sampson[14] to calculate the mean free paths (MFP's) of 163.6-Mev F^{8+} ions in the gold <100> channel, the 1s ground state varies from 4500 to 14,000 Å, depending on impact parameter, while the MFP for ionization of the n = 2 states varies from 800 to 2400 Å. These distances are comparable to the thickness of our channeling crystal. It would be particularly interesting to investigate experimentally and theoretically how the different regions of scattering angle space, corresponding to different regions of impact parameter space, contribute to RCE.

---

1. Present address: Boris Kidric Institute of Nuclear Sciences, Belgrade, Yugoslavia.
2. Chemistry Division, Oak Ridge National Laboratory.
3. Naval Surface Weapons Center, Silver Springs, MD 20910.

4. H. F. Krause et al., accepted for publication in Phys. Rev. B.
5. Oakley H. Crawford and R. H. Ritchie, Phys. Rev. A20, 1848 (1979).
6. S. Datz et al., Phys. Rev. Lett. 40, 843 (1978).
7. C. D. Moak et al., Phys. Rev. A19, 977 (1979).
8. S. Datz et al., in Nucl. Inst. and Meth. 170, (1980) 15-20 (Proceedings of the Eighth International Conference on Atomic Collisions in Solids).
9. N. Neskovic, p. 289 in Proceedings of the Second Workshop on High Energy Ion-Atom Collision Processes, Debrecen, Hungary, 1984, ed. D. Berenyi and G. Hock (Akademiai Kiado, Budapest, 1984).
10. J. Lindhard, Mat. Fys. Medd. Dan. Vid. Selsk. 34, No. 14 (1965).
11. J. Neufeld and R. H. Ritchie, Phys. Rev. 98, 1632 (1955).

12. E. U. Condon and G. H. Shortley, The Theory of Atomic Spectra, Cambridge of the University Press, Cambridge, UK (1953).
13. P. D. Miller, accepted for publication in Nuclear Instruments and Methods in Physics Research, Section B: Beam Interactions with Materials and Atoms.
14. L. B. Golden and D. H. Sampson, J. Phys. B10, 2229 (1977).

THE RAINBOW EFFECT IN AXIAL ION-CHANNELING

H. F. Krause
S. Datz
P. F. Dittner
J. Gomez del Campo
P. D. Miller
C. D. Moak
N. Neskovic[1]
P. L. Pepmiller

In a previous report,[2] we discussed a study of the angular scattering distributions produced in axial channeling when incident protons (7 MeV) are well aligned to the axial direction of a thin silicon crystal (1400 Å). Measured angular distributions obtained in the <100> and <110> directions using a two-dimensional (2-D) position-sensitive detector (resolution <0.015°) were interpreted by comparison with Monte Carlo trajectory calculations for these channels in the momentum approximation. The measured angular distributions showed patterns in two dimensions which were in good agreement with the calculations. The patterns depend on the location of atomic strings and the nature of the interatomic interactions. We believed that the general shape and structure in the angular contour maps for each channel might be a consequence of extrema in the 2-D classical deflection functions via a rainbow effect (analogous to the peaking of light flux scattered from water droplets at certain angles in optical rainbows). However, a study of the 2-D deflection function versus the channeling impact parameter (that could support this hypothesis) had not been performed. By performing these studies we have now firmly established that (1) the rainbow effect can occur for ions axially channeled in very thin crystals and (2) the 2-D deflection function for 7-MeV protons channeled in Silicon has extrema at the observed angular locations. The work discussed previously[2] is the first observation of a rainbow in transmitted channeling angular distributions. In this report we will show that the rainbow arises when a projectile interacts simultaneously with the atomic strings surrounding an axial channel.

The origin of the rainbow in scattering processes is an extremum in the classical deflection function that gives rise to an infinite differential cross section at certain scattering angles. In order to show that the rainbow can occur in axial channeling, we will examine the deflection function for the case of 7-MeV protons axially channeled in silicon and show that the extremum is a consequence of the geometrical arrangement of atomic strings. Consider the <100> axial channel defined by the four atomic strings shown in Fig. 4.12a. Let the 2-D cartesian scattering angles in the laboratory frame be

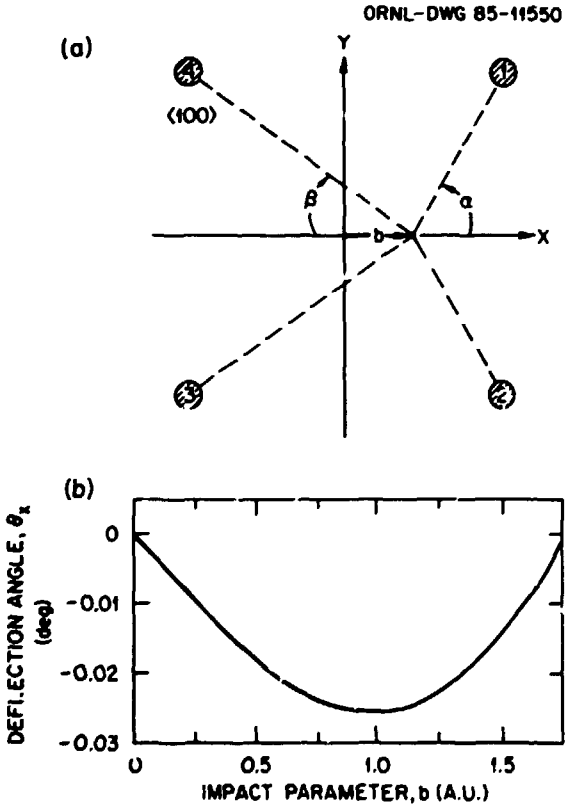

Fig. 4.12. (a) Atomic string positions for the <100> axis of silicon. An impact parameter, b, lying along the X-axis (and measured from the center of the channel) is shown. (b) Deflection function, θx(b), for a very thin crystal generated for y = 0. The deflection function has an extremum which gives rise to the rainbow (see text).

denoted by θ_x, and θ_y for the small-angle scattering problem at hand. A projectile entering at the center of the channel (x = o, y = o) will experience a symmetrical repulsion from each string that imparts no net transverse momentum to the projectile in a simultaneous interaction with all strings and therefore the projectile suffers no angular deflection. A particle entering the crystal at ($x = x_o$, y = o) will experience no deflection in the θ_y direction but it will be increasingly deflected toward increasing negative θ_x as x_o is increased positively. The deflection function for θ_x, calculated for such a sequence of impact parameters, x_o, is shown in Fig. 4.12b. Referring to Fig. 4.12b, we see that the deflection angle decreases until it reaches a minimum (a turning point) at the rainbow angle corresponding to θ_x = -0.0257 deg (corresponding to an impact parameter of x_o = 0.98 a.u.) and then increases until it reaches a turning point in the channel located to the right of that shown in Fig. 4.12a. The physical reason for the extremum in the deflection function (i.e., the rainbow) is readily explained on the basis of geometrical considerations. As x_o increases from the center of the channel, the repulsive force from strings 1 and 2 increases as the distance from each string decreases, but the component of these forces in the negative x direction eventually weakens when the angle denoted by α becomes large. Even though the repulsive interaction with strings 3 and 4 is weakening when the projectile moves closer to strings 1 and 2, the angle denoted by β is decreasing and strings 3 and 4 direct more of the repulsive force in the positive x-direction.

Thus, we see that the vector sum of monotonically decreasing repulsive forces simultaneously acting on the projectile, in combination with the geometrical location of atomic strings, produces the rainbow effect in axial channeling. Rainbow scattering in axial channeling therefore gives rise to a transverse correlation effect.

A Monte Carlo angular distribution for 7-Mev protons scattered in the <100> axial channel that illustrates the full 2-D consequences of the rainbow and simulates the angular broadening effects (produced by electron multiple scattering) is shown in Fig. 4.13. An experimental angular distribution[3] is similar to Fig. 4.13. Intensity maxima occur in the angular distribution where the 2-D deflection function has extrema. The maxima lying along the <110> axial directions correspond to the extrema in the deflection function illustrated in Fig. 4.12. The 2-D rainbow (i.e., the maximum that lies between the 60% level contours was resolved only in the measurements where peaks are shown at the 90% contour levels. These peaks are the consequence of two overlapping branches of the rainbow. Finite detector resolution prevented complete resolution of the rainbow.

We have established the connections between the unusual focal properties of very thin crystals and individual particle trajectories. The unusual channeling patterns, which depend on the geometrical locations of atomic strings in a

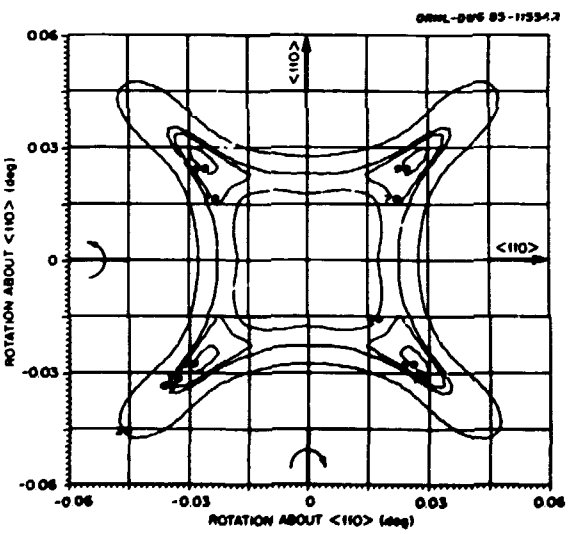

Fig. 4.13. A calculated angular distribution for 7-Mev protons axially channeled in the <100> direction of silicon which illustrates the rainbow ridge. An effective angular dispersion of 0.006° (FWHM) was used to simulate angular broadening in the crystal due to electron multiple scattering. Intensity cuts through the distribution at a fraction of the peak intensity (percentage) are plotted as contours at the 20, 60, 70, and 90 percent levels. The rainbow ridge lies between the 60 percent level contours.

given channel, are explained by the rainbow effect. We hope that the low angular dispersion Monte Carlo calculation (Fig. 4.13) will challenge channeling experimentalists to perform better experiments since there is a wealth of scattering-potential information that may be extractable by studying structures lying on the rainbow ridge.

---

1. Boris Kidric Institute of Nuclear Sciences, Belgrade, Yugoslavia.
2. H. F. Krause et al., pp. 135-137 in Physics Division Progress Report, ORNL-6120 (1984).
3. H. F. Krause et al, submitted to Physical Review B (1985).

DOUBLE- AND SINGLE-ELECTRON CAPTURE IN 1-2 MeV/Nucleon O^{8}-He COLLISIONS[1]

R. Hippler[2] S. Datz
P. D. Miller P. L. Pepmiller

We report results of an experimental study of charge changing collisions of bare nuclei with He atoms, with particular emphasis on the double-capture process. In Fig. 4.14, we present the results for 16- to 32-MeV O^{8+}-He collisions. Our measured single-capture cross sections agree with measurements of MacDonald and Martin[3] within the quoted accuracy (±10% for the present measurements). Our measured double capture cross sections are typically more than two orders of magnitude smaller than single-capture cross sections (Fig. 4.14). At 1 MeV/nucleon, the double-capture to single-capture ratio is ~6 x 10^{-3}. At 2 MeV/nucleon the ratio drops to 4 x 10^{-3}. These numbers are consistent with a ratio of ~10^{-2} estimated by Tawara et al.[4] for 15-MeV F^{9+}-He collisions. However, our measurements for double-capture cross sections are a factor of ~10 smaller than those reported by MacDonald and Martin[3] for the same system. The discrepancy may be due to the small ratio of double- to single-capture events. This separation was achieved, in the present investigation, by performing measurements at different gas pressures and by a careful analysis of this pressure dependence.

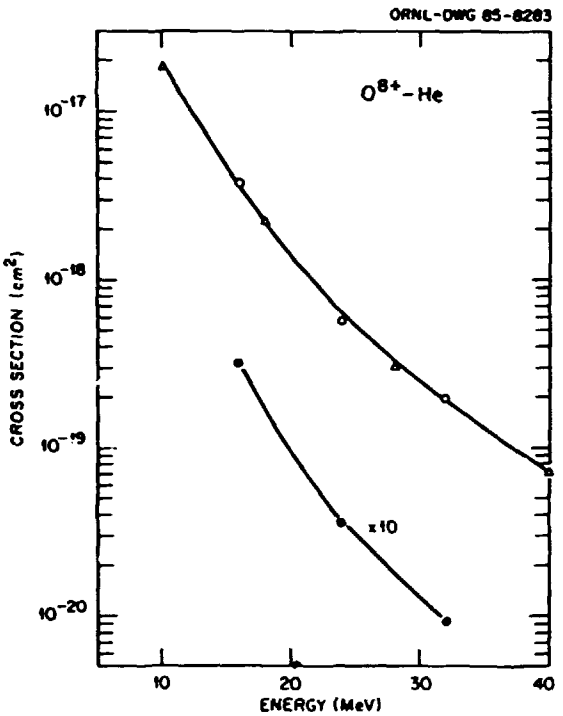

Fig. 4.14. Present data for single (o) and double (•) electron capture cross section for O^{8+}-He collisions. Δ, data of Ref. 1 for single capture.

The present double- to single-capture cross section ratios are also considerably smaller than first-order theoretical estimates. Using, for example, a classical Bohr-Linhard model, the probability P_c for electron capture may be expressed as[5]

$$P_c = (v/a)\ (R_c/v_i)$$

with v and a the target electron velocity and radius, respectively, and v_i the projectile velocity. The distance R_c below which capture occurs is given as

$$R_c = 2\ q\ a_0\ (v_0/v_i)^2$$

with a_0 and v_0 Bohr radius and velocity, respectively, and q the projectile charge. In an independent electron model, the double- to single-capture cross-section ratio is ~$P_c/2$, amounting to 0.22 and 0.08 at 1 and 2 MeV/nucleon, respectively. These numbers are larger than the experimental values by factors of about 36 and 20, respectively.

At the velocities under consideration here, a large fraction of electrons is expected to be captured into excited projectile states. For two-electron capture, these states can autoionize and escape detection as double-capture events.[6] To be detected as a double capture event, either one or both of the two electrons must be captured into a 1s state (about 0 and 5% probability at 1 and 2 MeV/nucleon) or the doubly excited states must be radiatively stabilized (estimated fluorescence yield ~10%). With these considerations, the present data are qualitatively understandable. Data which will be presented on other bare nucleus-He atom collisions show similar tendencies.

---

1. Summary of this paper published in Electronic and Atomic Collisions, ed. M. J. Coggiola, D. L. Huestis, and R. P. Saxon, Palo Alto, 1985, p. 505.
2. Permanent address: Fakultat fur Physik, Universitat Bielefeld, Bielefeld, F.R.G.
3. J. F. MacDonald, F. W. Martin, Phys. Rev. A4, 1965 (1971).
4. H. Tawara, P. Richard, K. A. Jamison, T. J. Gray, J. Newcomb, C. Schmiedekamp, Phys. Rev. A19, 1960 (1979).
5. H. Knudsen, H. K. Haugen, P. Hvelplund, Phys. Rev. A23, 597 (1981).
6. J. Newcomb, T. R. Dillingham, J. Hall, S. L. Varghese, P. L. Pepmiller, P. Richard, Phys. Rev. A30, 106 (1984).

ON THE DEPENDENCE OF ELECTRON PLANAR CHANNELING RADIATION ON LATTICE VIBRATION AMPLITUDE

S. Datz, B. A. Dahling[1], H. Park[2], R. K. Klein[2], J. O. Kephart[2], R. H. Pantell[2], B. L. Berman[3], M. V. Hynes[4]

At this writing, the observation of channeling radiation from a considerable number of monatomic and binary crystals has been reported.[5] The application of channeling radiation as a tool to understanding crystal properties requires first that simple parameters such as temperature dependence be understood quantitatively. Some measurements have been noted[6] for 54-MeV electrons in Si at elevated temperatures and Andersen et al.[7] reported some temperature dependent measurements on 2p → 1s and 3p → 1s transitions for 3.5 MeV electrons in the Si <111> axis. Here, we report on electron planar channeling in Si and compare results with those obtained with other diamond structure crystals (C, Ge, and GaAs).

Channeling radiation (CR) arises from transitions between eigenstates of electrons bound to a continuum potential; two-dimensional (axial) or one-dimensional (planar), as the case may be. This continuum potential is made up in a coherent way from the individual potentials of the atoms making up the row or plane. In practice, it is more convenient to use the many-beam method for calculating eigenstates, in which case one can use Doyle-Turner scattering factors derived from Hartree-Fock atomic wave functions.

A static lattice potential may be constructed in this manner in which one assumes that the atoms are at rest in their lattice positions. A more realistic potential must take into account the thermal vibrations of atoms at their lattice sites. Since the velocity of channeled particles is rapid compared to lattice vibrational motion, the particles see a frozen lattice and the continuum potential experienced is obtained by averaging over the thermal displacements from individual lattice sites. Assuming that the atomic displacement, x, is independent of its neighbors' motion, that it is isotropic, and that it has a Gaussian distribution. The probability

$$P(x) = (2\pi u^2)^{-1/2} \exp[-x^2/(2u^2)]$$

where u is the rms displacement obtained from the Debye theory.

The principal effect of the thermal vibrations is upon the bottom of the potential well, larger vibrations rounding it more and making it more shallow (Fig. 4.15). The level of the lowest eigenstate is most affected and, hence, the highest energy (n = 1 → 0) spectral line. The dependence on vibrational amplitude should also be evident in room temperature (T = 300 K) measurements. Shown in Table 4.4 is a sampling of our room temperature data. Excellent agreement is shown between theory and experiment for diamond,[8] Ge,[9] and GaAs.[10] The exception is Si where there is a significant discrepancy.

Turning things around, one might ask if the CR spectra can be used to measure lattice vibration amplitudes and hence Debye temperatures.

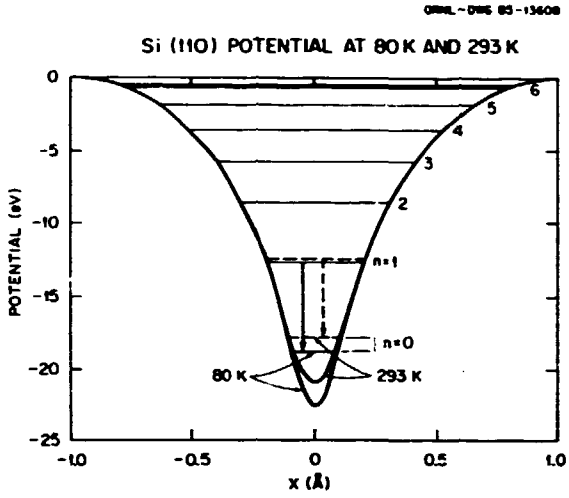

Fig. 4.15. Potentials and eigenvalues for the 110 plane in Si for two different temperatures, 80°K and 293°K. The eigenvalues are calculated for 54.4-MeV (γ = 107.5) electrons. A Debye temperature of 495°K was used in the potential calculation.

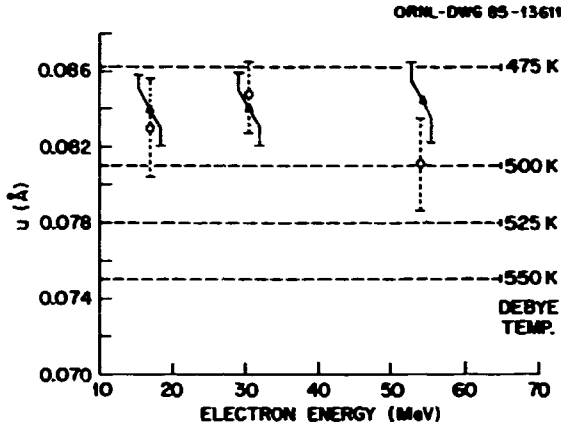

Fig. 4.16. Lattice displacement amplitude u in Å obtained from measurements of n = 1 → n = 0 channeling radiation transition energies in the (100) plane (o) and (110) (Δ) plane of Si as a function of electron energy.

To do this, we calculated the expected energies for the 1 → 0 transitions in (100) and (110) Si as a function of u at three different electron beam energies (16.7, 30.5, and 54.4 MeV) where we have made measurements. We then plotted photon energy versus u and from the experimental peak position we determine u. Since the eigenstates move down with increasing electron energy, checking on the energy dependence is another way to sense the bottom of the well. The results are shown in Fig. 4.16 together with an associated Debye temperature (θ_D) scale from which it is seen that a $\theta_D \cong 490$ K fits all the data quite well. The data are clearly in disagreement with the X-ray results,[11] θ_D = 543 K and the calculations Nielsen and Webber[12] θ_D = 526 K.

A possible source of error in our determining the Debye temperature in this way may be inherent in the use of an average crystal potential. In calculating peak energies in planar channeling radiation, one starts with the planar-averaged potential. Assuming a Gaussian distribution of atoms, one can get a final form of the potential. From the potential, one then can calculate the radiation peak energies easily

Table 4.4 Several properties of channeling radiation from diamond structure crystals.

Z	Crystal	Electron Energy (MeV)	θ_D	u(Å)	n = 1 → n = 0 energy (keV) (110) plane Calc.	(110) plane Meas.	(100) plane Calc.	(100) plane Meas.
6	C(Diamond)[a]	54.4	2000	0.040	163.7	161 ± 0.5	120.6	119.8 ± 0.7
14	Si	54.4	543	0.075	128.5	122.2 ± 1.0	100.0	97.5 ± 1
32	Ge	16.9	290	0.085	26.94	27.6 ± 0.5		
31-33	GaAs	16.9	260	0.088	26.6	26.6 ± 0.4	~20.5[a]	20.6 ± 0.5

[a]Mean value between 20.0 for Ga plane and 21.0 for As plane.

and conveniently. However, the rigorous approach is to solve the Schrödinger equation for the frozen lattice sites at different times and to average the peak energies subsequently. This rigorous method is quite complicated and very involved, but should be looked into to see whether it yields a different value.

Be that as it may, it is difficult to see why Si should be the only crystal to exhibit this difficulty. It should be expected that in the case of diamond with such a high θ_D the line energies would not be much affected by the particular choice of θ_D. But for the Ge and GaAs lattices, with even lower θ_D than Si, even greater sensitivity is obtained and the agreement with experiment is excellent.

To test the temperature dependence, we measured planar CR spectra for 54.4-MeV electrons in (110) and (100) Si over a range from -190°C to room temperature. Peak energies in the (110) spectra taken at seven different temperatures are shown in Fig. 4.17. The solid lines are calculated energies using θ_D = 495 K; the dashed line is for n = 1 → 0, using θ_D = 543 K

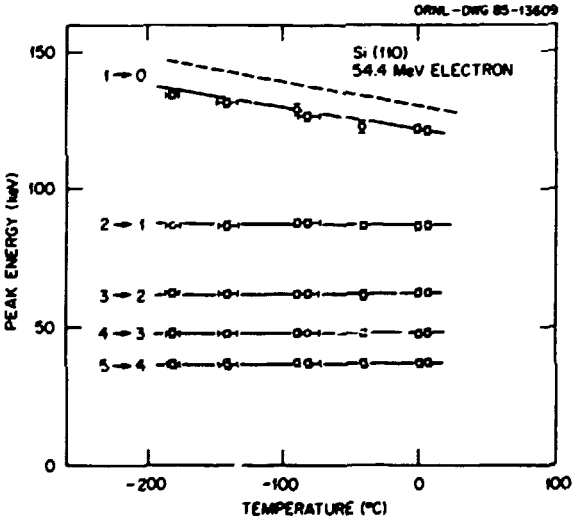

Fig. 4.17. Channeling radiation peak energies for 54.4-MeV electrons in (110) Si as a function of temperature. Solid lines are calculations using θ_D = 495 K dashed line is for n = 1 → n = 0 transition using θ_D = 549 K.

From this data it is evident that the thermal vibration amplitudes derived from the quoted Debye temperatures do not predict the peak positions for Si accurately. If this were the case for other members of the C, Ge, and GaAs group, one would be tempted to suspect the efficacy of the calculational method or of the assumptions implicit in the use of a Debye-Waller factor to represent thermal lattice displacements. Since this is not the case, one is led to question the accuracy of the previously reported Debye temperature for Si and more significantly, to propose the possibility of determining lattice vibration amplitudes from measurements of channeling radiation spectra.

---

1. Lawrence Livermore National Laboratory, University of California, Livermore, California.
2. Department of Electrical Engineering, Stanford University, Stanford, California.
3. George Washington University, Washington, DC.
4. Los Alamos National Laboratory, Physics Division, Los Alamos, New Mexico.

5. B. L. Berman and S. Datz, "Channeling Radiation Experiments" in Topics in Current Physics: Coherent Radiation Sources, (Saenz and Uberall, Eds.) Springer-Verlag, in press.
6. R. L. Swent, R. H. Pantell, S. Datz, and R. Alvarez, Nucl. Instr. Meth. 194, 235 (1982).
7. J. U. Andersen, E. Laegsgaard, and A. H. Sorensen, Nucl. Instr. Meth. B2, 63 (1984).
8. R. K. Klein et al., Phys. Rev. B31, 68 (1985).
9. H. Park et al., Phys. Lett. 96A, 45 (1983).
10. H. Park et al., to be published.
11. B. W. Batterman and D. R. Chipman, Phys. Rev. 127, 690 (1962).
12. O. H. Nielsen and W. Weber, J. Phys. C: Solid State Physics 13, 2449 (1980).

L X-RAY EMISSION FROM HIGH-Z ELEMENTS AFTER IONIZATION BY 1 MeV u^{-1} Ag IONS[1]

W. Uchai[2] W. T. Milner
G. Lapicki S. Raman
C. R. Vane

L X-ray spectra from even elements (Yb, Ta, W, Pt, Au, Pb and Th) bombarded by 1-MeV u^{-1} silver ions were studied with a Si(Li) detector. The observed intensity ratios are consistent with theory if the rates calculated for a single vacancy are multiplied by a statistical scaling factor. Conversely, the measured ratios imply a

high degree of multiple ionization in the outer shell. An L_1-$O_{4,5}$ transition is discovered in ion-atom collisions.

---

1. Abstract of published paper: J. Phys. B: At. Mol. Phys. 18, L389 (1985).
2. Guest graduate student from Emory University, Atlanta, CA. Portions of this paper were submitted as part of a Ph.D thesis.
3. Emory University, Atlanta, GA 30322.

ATOM CAPTURE AND LOSS IN ION MOLECULE COLLISIONS

M. Breinig[1]

We report progress in measuring the energy and angular distribution of protons emerging with velocity close to the beam velocity from the target region when Ar^+ beams collide with a CH_4 target and ArH^+ beams collide with a He target at asymptotically high speeds, much greater than the characteristic vibrational speeds of atoms in molecules. The protons result from the transfer of a target constituent to the projectile (atom capture) or from the dissociation of the projectile molecule in the collision (atom loss). For atom capture processes the Thomas peak is clearly observed.

In 1927, Thomas[2] gave a classical treatment of the transfer of a light target constituent to a heavy projectile valid in the asymptotic regime. Thomas scattering is a two-step process. The light particle is first scattered by the projectile and then by a heavy target constituent in such a manner that projectile and captured particle emerge with almost the same velocity at a critical angle θ_c with respect to the incident beam direction. For atom capture at asymptotically high velocities we have observed the Thomas peak at $\theta_c = 1.3°$ with Ar^+ projectiles and a CH_4 target.[3]

In our early measurements we recorded the number of protons emerging into a cone of half angle θ_0 about the forward direction as a function of proton energy for 100-300 eV/u Ar^+ and Kr^+ projectiles incident on CH_4. States in the vibrational continuum of ArH^+ and KrH^+ dissociate into $Ar + H^+$ and $Kr + H^+$, respectively.[4] After a continuum capture event the electron follows the projectile ion and the proton emerges with velocity $v_p \cong v$. If atom capture proceeds via the double scattering mechanism, then the projectile and the captured atom emerge at a critical angle θ_c. For Ar^+ on CH_4, $\theta_c = 1.3°$ and for Kr^+ on CH_4, $\theta_c = 0.6°$. For Ar^+ projectiles we have varied θ_0 from being smaller to being larger than the critical angle. while still collecting protons emerging at all azimuthal angles. For acceptance angles $\theta_c > \theta_c$ we observe a central peak in the proton spectra centered at a proton velocity $v_p = v'$, where v' is close to but slightly less than the beam velocity v. This peak vanishes for $\theta_0 < \theta_c$. We interpret this central peak as the atom capture to the continuum peak, produced via the double scattering mechanism. For 100-300 eV/u Ar^+ and Kr^+ projectiles on the CH_4, measured integrated cross sections are small - they lie between 5 and 100 barn.

Differential measurements in proton scattering angle and energy are now being made using a two-dimensional position-sensitive particle detection system.

Our beams pass through a 1-cm-long target gas cell located at the entrance focus of a doubly focussing, spherical sector, electrostatic analyzer accepting protons emitted into a cone of half angle $\theta < 6°$ about the beam direction. A 1-mm aperture in the exit focus of the analyzer sets the energy resolution to $\Delta E/E = 1\%$ FWHM. The position-sensitive detector system is mounted 15 cm away from the exit aperture. We record an atom capture to the continuum or atom loss event by detecting a proton emerging from the collision with velocity v_p close to the beam velocity v. We measure the angular and energy distribution of the protons emerging from the collision, i.e., we measured $d^2\sigma/d\Omega_p dE_p$. The angular distribution of the protons with v_p close to v in the scattering region is imaged one to one into the detection region. The entire distribution in polar angle θ and azimuthal angle ϕ can be acquired simultaneously. A microchannel electron multiplier array of 25-mm-diameter active area is the primary event detector. Output pulses are collected on a

resistive anode, and position decoding utilizes the charge division method. Computer assisted data acquisition is implemented using the modular CAMAC standard and a multitasking control program.

Figure 4.18 shows the angular distribution of protons emerging from the target region with speed equal to the projectile speed v, for 7 keV Ar^+ projectiles on CH_4. It can be seen that the protons emerge preferentially at a nonzero angle $\theta \cong 1.4°$ relative to the beam direction. This measured angle agrees well with $\theta_c = 1.3°$ predicted for atom capture via Thomas double scattering. Figure 4.18 shows raw data, not yet corrected for slight distortions due to the imperfect focussing properties of the 160° spherical sector proton energy analyzer. Because atom capture cross sections are so small (on the order of barn) great care must be taken to eliminate background. Here we have not been completely successful and the ring structure in the angular distribution, which is the Thomas peak, does not have perfect symmetry. Background problems are being corrected. The results presented in Figure 4.18 show that atom capture to the continuum at asymptotically high speeds proceeds via the Thomas double scattering mechanism. To investigate the detailed shape of the Thomas peak, measurements are now being made of the angular distribution of the protons emerging from the target region as a function of proton energy. We will then be able to map the complete velocity distribution of the captured particles. The velocity of a detected proton along the beam direction is determined by the analyzer field and the velocity transverse to the beam direction from the measured position of arrival on the channel plate.

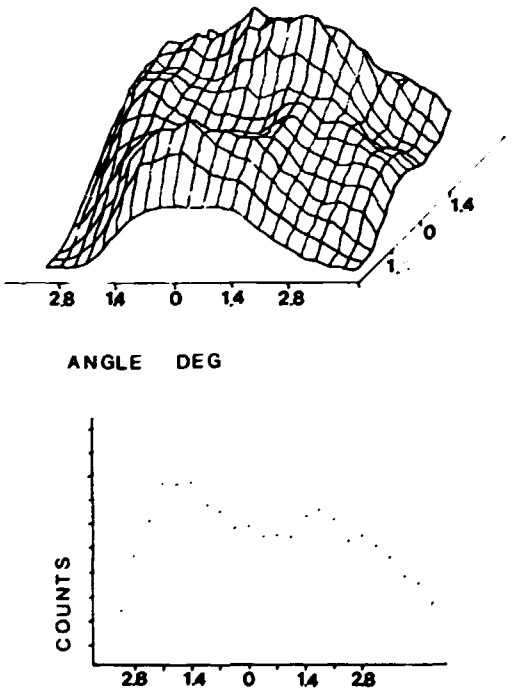

Fig. 4.18. Angular distribution of protons emerging from the target region with speed equal to the projectile speed v for 7-keV Ar^+ projectiles on CH_4. The protons emerge preferentially at a nonzero angle $\theta \cong 1.4°$ relative to the beam direction as predicted for continuum capture proceeding via the Thomas double scattering mechanism. The lower graph shows a cut through the channel plate image shown in the upper graph.

For atom loss processes complete velocity distributions will also be obtained from measurement of proton spectra differential in proton energy and scattering angle.

---

1. Adjunct staff member from the University of Tennessee, Knoxville, TN.
2. L. H. Thomas, Proc. R. Soc. London 114, 561, (1927).
3. M. Breinig et al., Phys. Rev. Lett. 51, 1751 (1979).
4. P. Rosmus and E. A. Reinsch, Z. Naturforsch. 35a, 1066 (1980).

ION-ION COLLIDER EXPERIMENT

H. J. Kim

As the result of a major effort, the folded beam ion-ion collision apparatus was improved in reliability, and simplified in operation. With these improvements, and using the more stable beams provided by the newly commissioned electron cyclotron resonance (ECR) source, more reliable electron loss cross sections can now be measured. Absolute values of the electron-loss cross

sections $\sigma(3^+ \rightarrow 4^+)$ for the head-on (collinear) interactions of colliding beams of 30-keV isotopically separated ^{40}Ar and $^{82,84,86}Kr$ ions in the 3^+ charge state were measured. Table 4.5 summarizes the results. Due to the difficulty of determining the beam overlap in the interaction region, the uncertainties of the absolute cross sections are rather large. As shown in the table, however, the ratios of the cross sections are considerably more precise. A measurement of the energy dependence of these cross sections is being planned.

Table 4.5. Summary of σ $(3^+ \rightarrow 4^+)$ for $X^{3+} + X^{3+} \rightarrow X^{4+} + ?$

Ion (X^{3+})	α Relative	$\sigma(10^{-16}$ cm$^2)$
^{40}Ar		6.01 ± 2.90
^{82}Kr	1.02 ± 0.06	2.92 ± 1.90
^{84}Kr	1 (reference)	2.86 ± 1.40
^{86}Kr	1.01 ± 0.07	2.89 ± 1.80

CORRELATED ELECTRON TRANSFER IN HIGHLY CHARGED ION ATOM COLLISIONS: CHARGE CHANGING COLLISIONS OF $^{238}U^{q+}$ (0.25 - 1 MeV/NUCLEON) WITH He

S. Datz
P. F. Dittner
H. Knudsen[1]
P. L. Pepmiller
L. H. Andersen[1]
R. Hippler[2]
P. D. Miller
N. Stolterfoht

Last years's annual report[3] described a transfer ionization (TI) experiment in which 20-MeV Au^{15+} ions were used to bombard He gas. In TI the projectile captures one electron and the target loses two. For the case in question, a very large TI cross section $\sim 6 \times 10^{-16}$ cm^2 is observed. A rather remarkable result of these experiments was to find that >85% of the cross section for producing He^{++} was accounted for by the following single mechanism: $Au^{15+} + He^0 \rightarrow Au^{14+} + He^{++} + e_{pc}$, where e_{pc} signifies an electron moving at a very small velocity with respect to the projectile, hence, projectile centered. The shape of the energy spectrum of the projectile centered electrons was measured and found to be cusp-shaped and symmetric with the velocity peaked at the projectile velocity. The mechanism for TI in this case was hypothesized to involve a process in which two electrons are transferred as a correlated pair to the rest frame of the moving ion whereupon one is lost to the continuum and the other is left in a bound state.

At sufficiently high velocity or low charge state, q, a breakdown in correlation should occur and the independent particle model may become valid. To test this hypothesis we collided HHIRF tandem beams of ^{238}U at 0.25 MeV/nucleon with q = 17 → 30, 0.5 MeV/nucleon with q = 23 → 37, and at 1.0 MeV/nucleon with q = 26 → 45 with a He target and measured the recoiling He ion charge state in coincidence with the emergent uranium ion charge state. From these measurements we could determine the partial cross sections for the various charge changing processes.

We found a drastic change in behavior between 0.25 and 0.5 MeV/nucleon and a reasonable extrapolation of the results between 0.5 MeV/nucleon to 1.0 MeV/nucleon. At 0.25 MeV/nucleon and for a typical charge state, say q = 30+, the process can be ranked in decreasing order of importance as follows. Single ionization was dominant at $\sim 6 \times 10^{-15}$ cm^2, followed by single capture (5×10^{-15}), "transfer ionization" (3×10^{-15} cm^2), double capture (6×10^{-16} cm^2) and double ionization (2×10^{-16}). For the same charge state (30+), single ionization remained approximately constant at 0.5 and 1.0 MeV/nucleon while double ionization rose a factor of 5 from 0.25 to 0.5 MeV/nucleon; single capture and transfer ionization dropped by a factor of 50 from 0.25 to 1 MeV/nucleon. With the exception of single ionization, the data seem consistent with our previous 0.1 MeV/nucleon data and the higher energy data. Further investigation on these systems will include the measurements on cusps in coincidence with TI.

---

1. University of Aarhus, Denmark.
2. Permanent address: Fakultat fur Physik, Universitat Bielefeld, Bielefeld, F.R.G.
3. C. Bottcher et al., Phys. Div. Prog. Rep., Sept. 1984, ORNL-6120, p. 126.

ENERGY SHIFTS OF L X RAYS FROM 70 < Z < 90 ELEMENTS DUE TO MULTIPLE M-VACANCIES[1]

W. Uchai[2] S. Raman
C. W. Nestor, Jr.[3] C. R. Vane

The transition energies of L x-ray for states with 1-11 M-shell spectator vacancies are calculated by using a Dirac-Fock computer program. The calculations are done for 7 elements with atomic numbers in the 70 < Z < 90 range. In each of these elements, the transition energies of 10 L x-rays (L_ℓ, $L_{\alpha 2}$, $L_{\alpha 1}$, L_η, $L_{\beta 1}$, $L_{\gamma 1}$, $L_{\gamma 2}$, $L_{\gamma 3}$, $L_{\gamma 4,}$, $L_{\gamma 4}$) are calculated as differences of average-of-configuration energies. The energy shifts of these X rays for various multiple M-vacancy states are deduced from the transition energies and plotted as a function of atomic number.

---

1. Abstract of a paper to be published in the Atomic Data and Nuclear Data Tables.
2. Guest graduate student from Emory University, Atlanta, GA. Portions of this compilation were submitted as part of a Ph.D thesis. Authors's permanent address: Chulachomkloa Royal Military Academy, Bangkok, Thailand.
3. Computing and Telecommunications Division, ORNL.

COHERENT EXCITATION IN ELECTRON CAPTURE COLLISIONS

J. Burgdorfer[1] L. J. Dube[2]

We have calculated the complete axial symmetric n = 3 density matrix produced during the capture process, $H^+ + He \rightarrow H(n = 3) + He^+$. The study of this particular system is motivated by the corresponding experimental investigation[3] which reveals a large positive dipole moment for the excited electron, $\langle d_z \rangle > 0$, in contrast to the first Born (OBK) approximation which predicts a vanishing value.

For the capture amplitude, we have used (a) a multiple scattering approach, namely, the Continuum Distorted Wave (CDW) approximation,[4] and, as a standard for comparison, (b) the OBK approximation, which includes single scattering contribution only. Moreover, an improvement of the primary capture amplitude has been achieved by including the final-state mixing of the nearly degenerate hydrogenic levels due to the Coulomb field of the residual target ion. This process can be treated analytically using the Post Collision Interaction (PCI)[5] model leading to (c) the CDW-PCI and (d) the OBK-PCI approximations.

We have utilized the multipoles of the angular momentum, L, and of the Runge-Lenz vector, A, to classify the ten (6 real diagonal and 4 complex off-diagonal) elements of the n = 3 density matrix. For example, Fig. 4.19 displays the z-component of A of the perihelion vector, LxA, i.e., $\langle A_z \rangle$ ($\propto \langle d_z \rangle$) and $\langle (LxA)_z \rangle$, both multipoles of rank 1, with available experimental data. This comparison exhibits clearly the sensitivity of the coherence parameters upon the details of the underlying approximations.

The finite value of $\langle A_z \rangle$ is a direct measure of the existence of second and higher order contributions to the capture amplitude. Furthermore, the superiority of the CDW-PCI calculation (Fig. 4.19b, indicates the importance of including the PCI effect in a perturbative treatment of electron capture.

We have also used the expectation values of A and LxA to construct a classical orbit description of the coherently excited manifold. In

ORNL-DWG. 85-18507

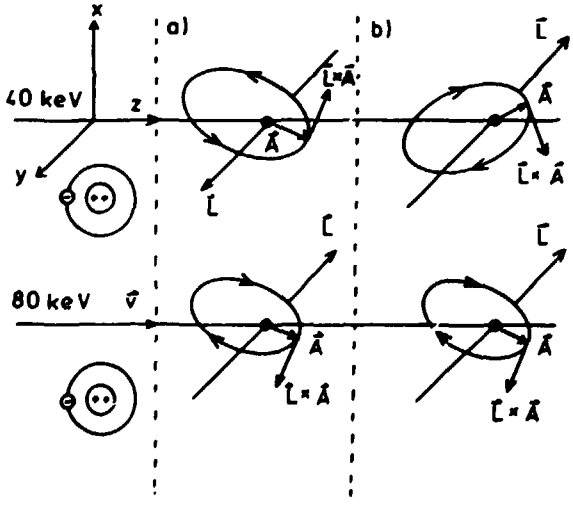

Fig. 4.19. (a) $\langle A_z \rangle$ and (b) $\langle (L \times A)_z \rangle$ as a function of the projectile velocity. ♦ experimental data of Ref. 1.

the CDW-PCI model, we have obtained the following picture: A stays inclined with respect to the beam direction, while the rotational sense changes with increasing energies. Furthermore since $\langle A_z \rangle > 0$, one expects the electron to lag behind the center of attraction (Fig. 4.20a). An alternative interpretation can

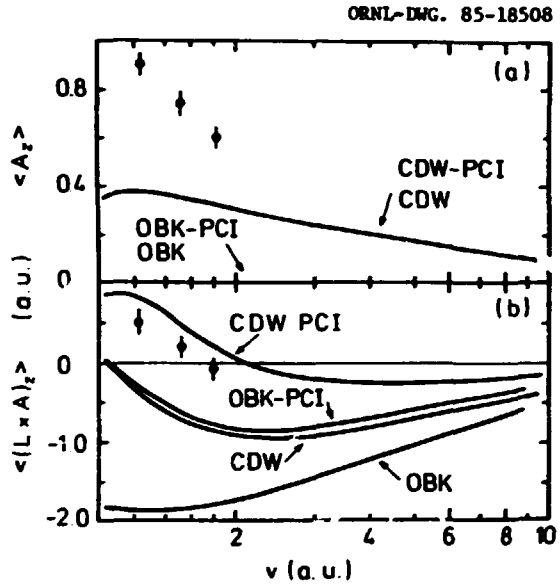

Fig. 4.20. "Classical" orbits of the coherently excited electron. (a) model suggested by the CDW-PCI approximation; (b) possible alternative also consistent with the data of Ref. 1.

be formulated however where the sense of rotation remains fixed while A rotates (Fig. 4.20b). Further work is needed to distinguish between these two (consistent) possibilities.

---

1. Department of Physics and Astronomy, University of Tennessee, Knoxville, TN 37996.
2. Fakultat fur Physik, Universitat Freiburg, 7800 Freiburg, FRG.
3. C. Havener et al., Phys. Rev. Lett. 48, 926 (1982).
4. I. M. Cheshire, Proc. Phys. Soc. 84, 89 (1964).
5. J. Burgdorfer, Phys. Rev. A24, 1756 (1981).

MULTIPOLE MOMENTS OF FORWARD ELECTRON EMISSION IN HIGH VELOCITY ION-ATOM AND ION SOLID COLLISIONS[1]

S. B. Elston[2]
M. Breinig[2]
R. DeSerio[3]
K.-O. Groeneveld[4]
P. Koschar[4]
I. B. E. Nemirovsky[5]
S. D. Berry[3]
J. Burgdorfer[3]
C. E. Gonzalez-Lepera[3]
D. Hofmann[4]
L. Liljeby[6]
I. A. Sellin[2]

The spectrum of electrons emitted near zero degrees in ion-atom and ion-solid collisions is dominated by a strong 'cusp'-shaped peak corresponding to electrons nearly matched in vector velocity to that of the projectile ion. Two fundamental processes contribute to the forward peak: projectile capture of target electrons into low continuum states in the projectile rest frame, often referred to as Electron Capture to the Continuum (ECC), and loss of projectile electrons due to collisions with the target, or Electron Loss to the Continuum (ELC). Production of electrons in the forward peak in ion-solid collisions is more complex, and must involve some combination of at least these two processes and may involve others as well. In solid collisions, the forward peak electrons are named convoy electrons. The generic phenomenon is frequently called Electron Transfer to the Continuum (ETC).

Advances in experimental technique and theory permit simplification of the description of the spectrum of cusp electrons and suggest new approaches to long-standing questions about the importance of excited states of ions traversing condensed matter. In short, the asymmetric spectral signature of cusp electrons produced by capture processes is now seen as the result of a strong dipole moment in the emitted charge distribution, explainable in second Born approximation. That produced by projectile ionization processes is a transversely emitted charge distribution characterized by even-order multipole moments (monopole, quadrupole, hexadecapole, etc.) and maximum multipolarity $\kappa = 2n$ determined by the principal quantum number n of the contributing projectile orbital. The cusp produced by swift charged particles passing through solid materials possesses the transverse

signature of the projectile loss mechanism and becomes enriched in high-order multipoles with increasing projectile speed, suggesting steady-state excitation of high n-states during passage through the bulk material.

The theoretical basis of this work stems from the development by Burgdorfer[7] of a density matrix description of the ELC process which exploits smooth continuation of projectile excitation across the ionization limit to show that a set of dynamical multipoles originally introduced to describe bound-state coherences are suited for the description of continuum-state coherences as well. Consequently, the anisotropies in the doubly differential cross section (DDCS) for ETC can be expressed as expectation values of the dynamical multipoles, which contain the orientation and alignment parameters introduced by Fano and Macek[8] as a subset.

In this method, the DDCS for ETC processes is expanded in the zero-velocity limit as

$$\frac{d\sigma}{dv} = \left[\frac{a}{v}\right] \sum_{\kappa=0}^{\infty} P_\kappa(\cos\theta)\beta_\kappa$$

where $\vec{v}$ is the electron PRF emission velocity, P_κ are the Legendre polynomials, and β_κ are asymmetry parameters derivable from the theory.

Experimental results are obtained with a novel apparatus which permits rapid and efficient data acquisition by employing position-sensitive electron detection to combine emission angle definition with conventional electrostatic spectrometry.

The resulting doubly differential distributions, corresponding least-squares fits using the previous expansion, and theoretical predictions are shown in summary form in Figure 4.21. The data shown are contours of equal intensity of electron emission in the emission-energy and polar-emission-angle plane for single collisions of v_p = 10.1, 14.3, and 16.2 au O^{5+} ions with He and Ar targets. The longitudinal (emission energy) and transverse (emission angle) axes are scaled so that equal intervals in either direction represent approximately equal intervals in longitudinal projectile-frame emission velocity

ORNL-DWG. 85-18506

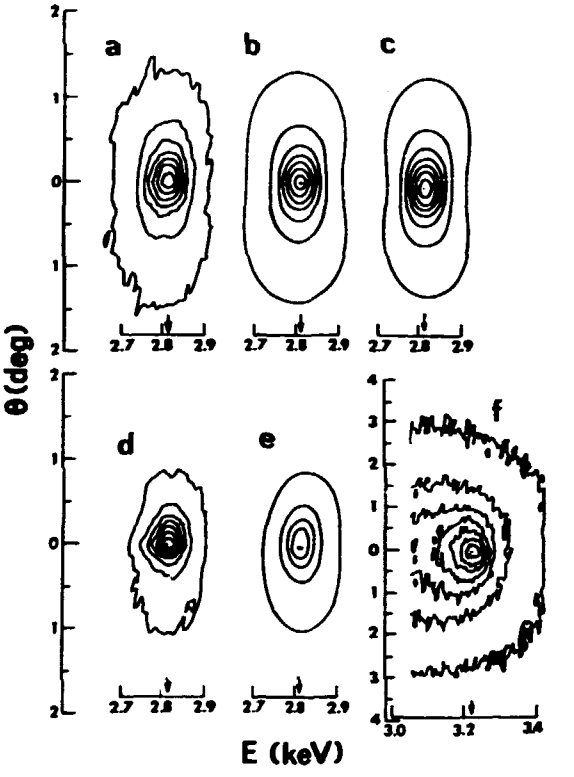

Fig. 4.21. Contour plots for ELC by O^{5+} in Ar and He at v_p = 14.3 atomic unit, and ECC by O^{8+} in Ne at 15.4 atomic unit. Contours shown represent multiples of 12.5% of peak height. Horizontal scale represents lab frame electron energy; vertical scale represents polar electron ejection angle. Scaling is chosen so that isotropic emission would produce essentially circular contours. (a) Measured distribution for Ar target. (b) Corresponding best fit to (a), normalized to peak height of data. (c) Theoretical distribution after convolution with spectrometer acceptance, also normalized to peak of (a). (d) Measured distribution for He target. (e) Corresponding He target fit, normalized to peak of (d). (f) Measured ECC distribution for 15.4 au O^{8+} in Ne.

v_ℓ and transverse projectile-frame emission velocity v_t. As might be expected, the O^{5+} distributions are dominated by ELC from the loosely bound n = 2 levels by an order of magnitude over ECC and ELC from n = 1. The immediate appearance of these data are of strongly transverse emission, as predicted by Burgdorfer's calculation[7], and in striking contrast to the strong dipole character of the ECC distribution obtained from a v_p = 15.4 atomic unit collision

in Ne, shown in part f of the same figure. Also shown is the theoretical angular distribution calculated by Burgdorfer, convoluted with the spectrometer acceptance function.

Comparison of ELC cusp moment distributions with those for cusps produced by passage of ions through solids implies a dominant role for bulk ELC processes in the formation of the convoy peak. Attempts to fit multipole moments to the convoy distributions in the same manner as was done with the ELC data produced poor results until multipoles of the order up to $\kappa \sim 10$ were included in the fitting procedure. A close examination of the β_κ values shows the multipolarity of convoy emission skewing toward higher multipoles with increasing projectile velocity. Since the maximum multipolarity P_κ of ELC from a given n level is $\kappa = 2n$, the data then suggests convoy production via loss from highly excited states formed by capture or capture plus excitation within the bulk plus excitation within the bulk material of the target. While it is expected that elastic and inelastic electron scattering processes which occur after convoy production and prior to or during exit from the foil surface (including the effect of the exit potential 'step') must be taken into account in any detailed examination of convoy multipole distributions, the strong Coulomb 'focusing'[9] provided by the nearby projectile ion may make these effects smaller than they would appear to free electrons of the same speed, at least for the highly charged ions studied here.

---

1. Summary of paper published in Phys. Rev. Lett. 55, 2281 (1985).
2. Adjunct staff member from the University of Tennessee, Knoxville, TN 37996.
3. University of Tennessee, Knoxville, TN 37996.
4. Institut fur Kernphysik, Universitat Frankfurt, August-Euler-Strasse, D 6 Frankfurt am Main, Federal Republic of Germany.
5. Centro Atomico Bariloche, Argentina.
6. Atomfysik, Research Institute for Physics, Stockholm, Sweden.
7. J. Burgdorfer, Phys. Rev. Lett. 51, 374 (1983); J. Burgdorfer, M. Breinig, S. B. Elston, and I. A. Sellin, Phys. Rev. A28, 3277 (1983).
8. U. Fano and J. Macek, Rev. Mod. Phys. 43, 553 (1973).
9. C. Bottcher, J. Phys. B. 11, 3887 (1978).

AUTODETACHMENT STUDIES OF THE He_2^- METASTABLE MOLECULAR NEGATIVE ION

G. D. Alton
R. N. Compton[1]
T. J. Kvale[2]
D. J. Pegg[1]
J. S. Thompson[3]

During the fiscal year, the structure and decay processes of the recently discovered He_2^- dimer[4] were investigated for the first time by the negative ion physics research group at the modified Negative Ion Source Test Facility[5] using electron energy spectroscopy techniques and the experimental apparatus described previously.[6] The negative ion is formed by electron capture to the metastable $He_2(a^3\Sigma_u^+)$ state to form either $He_2^-(a^4\pi_g)$ or $He_2^-(a^4\Sigma_u^+)$.[7] The data indicate that only one long-lived state with a lifetime of the order of microseconds exists below the $a^3\Sigma_g^+$ threshold with the more likely state being a $^4\pi_g$ state. This state decays by two different processes. Two distinct autodetachment channels are observed in the electron energy spectra of He_2^- formed by double-charge exchange of energetic He_2^+ (30-65 keV) in Li vapor. A single narrow peak, present in the spectra, has a center-of-mass energy of 11.4 MeV; the decay mechanism which produces this peak is attributed to vibrational autodetachment [e.g., $He_2^-(^4\pi_g)_{v=1} \rightarrow He_2(a^3\Sigma_u^+)_{v=0} + e$]. A second broad peak is observed which has a center-of-mass energy of 15.85 eV. The peak results from autodetachment of He_2^- into the $x^1\Sigma_g^+$ He_2 + e repulsive continuum. The dominant decay mechanism appears to be vibrational autodetachment, where the $(a^4\pi_g)_{v=1}$ state decays into the $(a^3\Sigma_u^+)_{v=0}$ state plus an electron. This identification is supported by recent theoretical calculations.[7] Figure 4.22 shows measured electron energy spectra for the low-energy decay processes for 50 keV $^3He_2^-$ and 40 keV $^4He_2^-$. The second decay process is "eximer" autodetachment where the $(a^4\pi_g)_{v=0}$ state decays to the repulsive $x^1\Sigma_g^+$ state to form 2 $He(1^1s)$ + e. The high electron energy peak, shown in Fig. 4.23, is an indication of this process. The $x^1\Sigma_g^+$

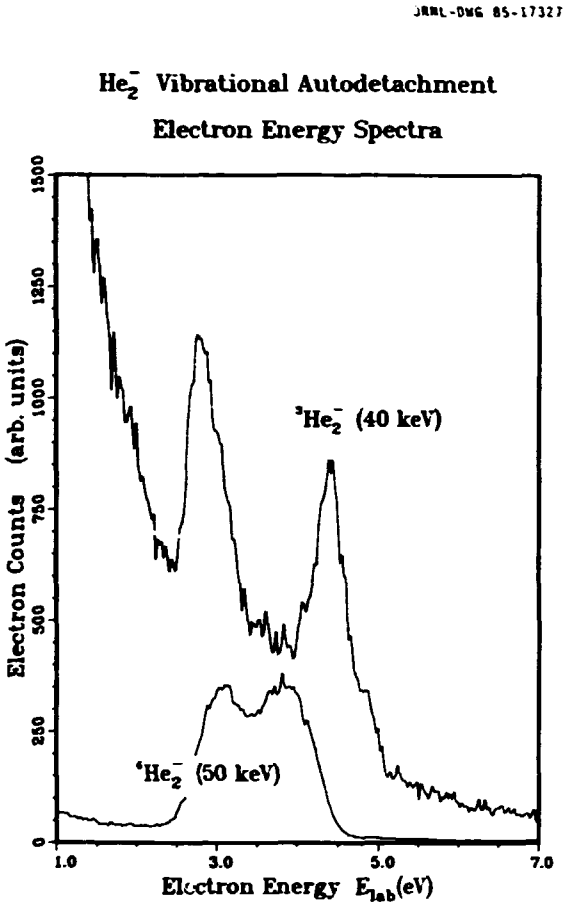

Fig. 4.22. Low energy vibrational autodetachment electron spectra for 50 keV $^3He_2^-$ and 40 keV $^4He_2^-$.

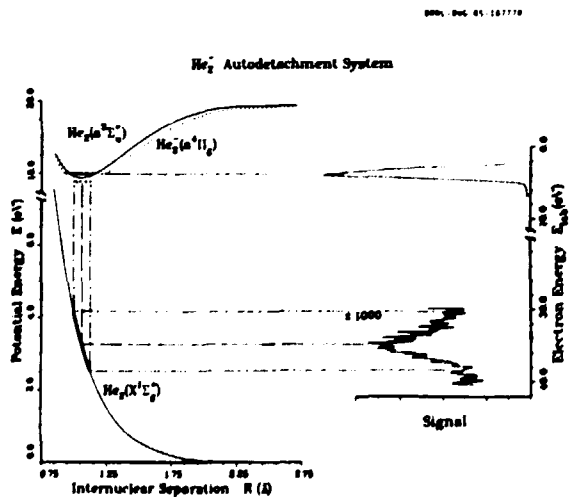

Fig. 4.23. Autodetachment electron energy spectra and potential energy curves for He_2^-.

potential energy curve was reconstructed by deconvoluting the apparatus resolution function from the measured high-energy electron distribution. The electron affinity E_A for the $He_2^-(^4\Sigma_g)$ state, with value E_A = 0.172 eV, was also determined by comparing the autodetachment spectra from $^4He_2^-$, and $^3He_2^-$. This procedure constitutes a new method for solving the classic quantum chemistry problem, i.e., the interaction between two ground state helium atoms. The He_2^- → $He^-(^4P^0)$ + He decay mode is not observed.

---

1. University of Tennessee, Knoxville, TN and Oak Ridge National Laboratory, Oak Ridge, TN.
2. Postdoctoral Fellow in the Postgraduate Training Program administered by Oak Ridge Associated Universities, Oak Ridge, TN.
3. Graduate student at the University of Tennessee, Knoxville, TN.
4. Y. K. Bae, M. J. Coggiola, and J. R. Peterson, Phys. Rev. Lett. 52, 747 (1984).
5. G. D. Alton and T. J. Kvale, Physics Division Progress Report for Period Ending September 30, 1984, ORNL-6120 (1985), p. 138.
6. G. D. Alton, R. N. Compton, and D. J. Pegg, Phys. Rev. A29, 1405 (1983).
7. H. H. Michels, Phys. Rev. Lett. 52, 1413 (1984).

ENERGY LEVEL MEASUREMENTS OF $Be^-(1s^22s2p^2)^4P$

G. D. Alton T. J. Kvale[2]
R. N. Compton[1] D. J. Pegg[1]
J. S. Thompson[3]

During the fiscal year, first measurements were made of the energy level for metastably bound $(1s^22s2p^2)^4P$ state of Be^- (Ref. 4) by the negative ion research group. The measurements were made at the modified Negative Ion Source Test Facility[5] using the electron spectroscopy apparatus and techniques described previously.[6] The energy level of the negative ion state was determined by measuring the energy distribution of electrons autodetached from energetic (50 - 60 keV) Be^- formed by double-charge exchange of Be^+ in Li vapor. This negative ion species is formed in a ^4P state much like the extensively studied $^4P^0$ state of He^- (Ref. 6) and is of considerable importance from a theoretical as well as a practical viewpoint. The

efficiency at which the ion can be formed[7] (~5%), makes it a viable candidate for tandem accelerator applications.

The metastability of the species has long been speculated due to the fact that production can be efficiently effected only through double-charge exchange of Be^+. This speculation has been born out by recent theoretical predictions of a long-lived ^4P state[8,9] and by observation of its decay.[10] The results of the present investigation support theoretical predictions that there is only one state of the beryllium negative ion which lies below the $Be(1s^2 2s2p)^3P^0$ threshold and is metastable against both autodetachment and radiative decay. Figure 4.24 displays a high resolution electron energy spectrum taken with and without argon target gas which was introduced into a gas cell preceding the electron spectrometer. The electron peak centered at a laboratory energy of ~3.3 eV is produced by electron detachment which occurs during collisions between the Be^- beam and the argon target. The peak centered at 11.71 eV is attributable to autodetaching electrons from the ^4P state of Be^-. The center-of-mass energy of this state was found to be 2.53 eV with respect to the ground state of neutral beryllium. From this result and the experimental value from Bashkin and Stoner[11] for the $Be(1s^2 2s2p)^3P$ state, an electron affinity of 195 MeV ± 90 for the $Be^-(1s^2 2s2p^2)^4P$ state is deduced.

Experiments designed to measure the lifetimes of the decaying fine structure components of $Be^-(1s^2 2s2p^2)^4P_J$ will be performed in the near future.

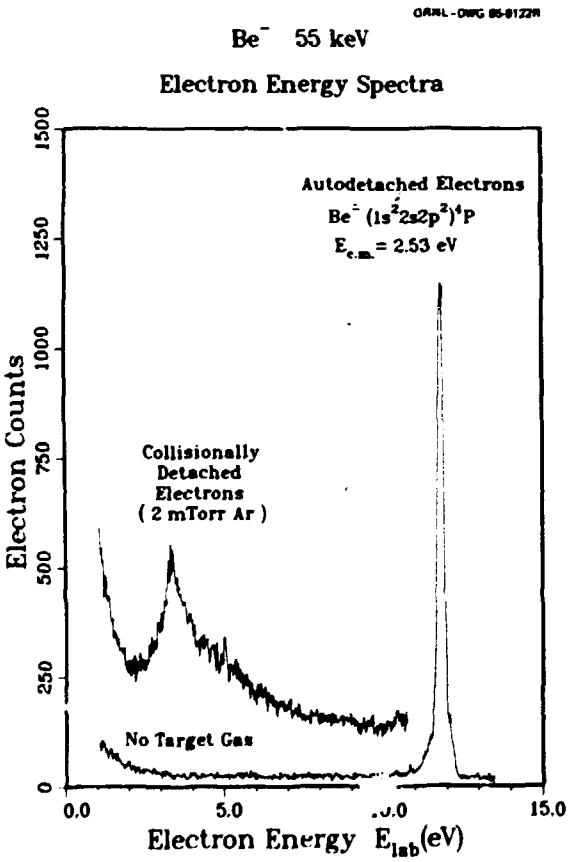

Fig. 4.24. Autodetachment electron energy spectra from the decay of $Be^-(^4P)$.

---

1. University of Tennessee, Knoxville, TN and Oak Ridge National Laboratory, Oak Ridge, TN.
2. Postdoctoral Fellow in the Postgraduate Training Program administered by Oak Ridge Associated Universities, Oak Ridge, TN.
3. Graduate student at the University of Tennessee, Knoxville, TN.
4. T. J. Kvale, G. D. Alton, R. N. Compton, D. J. Pegg, and J. S. Thompson, Phys. Rev. Lett. 55, 484 (1985).
5. G. D. Alton and T. J. Kvale, Physics Division Progress Report for Period Ending September 30, 1984, ORNL-6120 (1985), p. 138.
6. G. D. Alton, R. N. Compton, and D. J. Pegg, Phys. Rev. A28, 1405 (1983).
7. J. Heinemeier and P. Hvelplund, Nucl. Instrum. Methods 148, 65 (1978); J. Heinemeier and P. Hvelplund, Nucl. Instrum. Methods 148, 425 (1978).
8. C. F. Bunge, M. Galán, R. Jáuregui, and A. V. Bunge, Nucl Instrum. Methods 202, 299 (1983).
9. D. R. Beck and C. A. Nicolaides, Int. J. Quantum Chem. Quantum Chem. Symp. 18, 467 (1984).
10. Y. K. Bae and J. R. Peterson, Phys. Rev. A30, 2145 (1984).
11. Atomic Energy Levels and Grotian Diagrams I; Hydrogen I-Phosphorus XV, edited by Stanley Bashkin and John O. Stoner (North-Holland, Amsterdam, 1975).

FURTHER PROGRESS IN THE MEASUREMENT OF DIELECTRONIC RECOMBINATION

S. Datz C. M. Fou[1]
P. F. Dittner P. D. Miller
P. L. Pepmiller

The apparatus and technique for the measurement of dielectronic recombination (DR) was described in the previous progress report.[2] We have concluded our measurements and analysis of the data for the Na-like ions, P^{4+}, S^{5+}, and Cl^{6+} undergoing DR via the 3s-3p transition. From our measurements we have now deduced a relative velocity distribution, $f(v_r)$, of our electron beam which has a component parallel to the ion beam, $f_\parallel$, given by,

$$f_\parallel = \alpha/\sqrt{\pi}\ \exp[-\alpha^2(v_\parallel - v_o)^2]$$

and a component transverse to the ion beam, $f_\perp$, given by,

$$f_\perp = 2\ \beta\ v_\perp \exp(-\beta^2 v_\perp^2)$$

where $v_\parallel$ and $v_\perp$ are the relative velocity components parallel and transverse to the ion beam respectively, α and β are constants, and v_o is given by

$$v_o = E_e/m + E_i/M - 2(E_e E_i/mM)^{1/2},$$

where E_e and m are the energy and mass of the electron, and E_i and M are the energy and mass of the ion, respectively. We have convoluted the calculated cross section,[3] σ, with the velocity distributions above and deduced the values of $\alpha = 6.89 \times 10^{-8}$ sec/cm and $\beta = 7.55 \times 10^{-9}$ sec/cm from our Cl^{6+} data. Using these values, we convolute the theoretical σ with the relative velocity, v_r, and $f(v_r)$ to get the calculated DR rate, $\langle v_r\sigma\rangle$, given by,

$$\langle v_r\sigma\rangle = \int f(v_r) v_r \sigma dv_r.$$

Since σ depends on the field in the interaction region, the $\langle v_r\sigma\rangle$ is calculated for each value of the field for which σ is calculated.* The comparison of our measurements of the DR rate with the rates calculated from theory for Cl^{6+} is shown in Fig. 4.25.

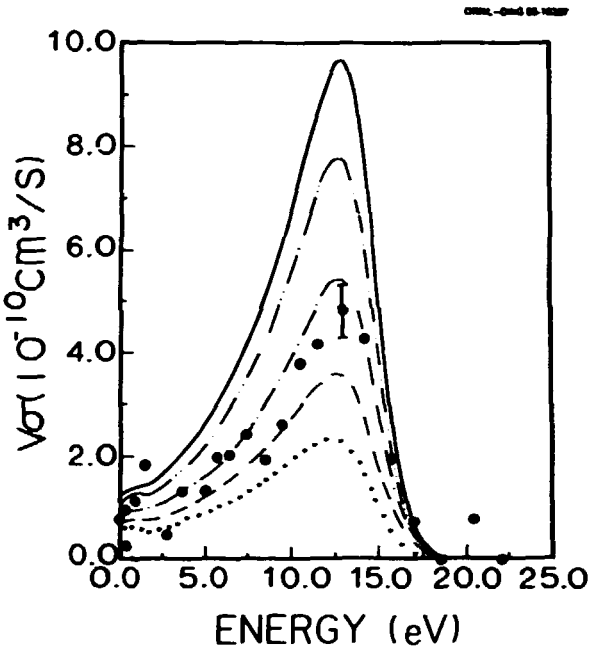

Fig. 4.25. The DR rate, $\langle v_r\ \sigma\rangle$, vs. the relative energy, E_r, for Cl^{6+}. Solid circles are the experimental data, the curves are calculated from the σ of Ref. 3 for a field (in V/cm) in the interaction region = 0 (....), 5 (---), 25 (-.-), 125 (-..-) and 625 (—).

The agreement with theory is excellent if the effective field in the interaction region is 25 V/cm (a value which roughly agrees with what one would calculate from the experimental parameters). The agreement of the P^{4+} and S^{5+} data with theory (for 25 V/cm) is equally good.

In another series of experiments[5], we investigated the DR of the Li-like ions, B^{2+}, C^{3+} and O^{5+}. Here we find that the measured rates are much larger than the rates calculated from theory for a field of 25 V/cm (see Fig. 4.26) for all three ions. Even for extremely large and physically unlikely fields in the interaction region, the measured rates are larger than or equal to the calculated rate. It is not known why agreement between theory and experiment occurs in the DR via 3s-2p of Na-like ions but not for the DR via 2s-2p of Li-like ions.

We have also measured DR rates in other ionic systems for which no theoretical values have been calculated. The first of these is DR

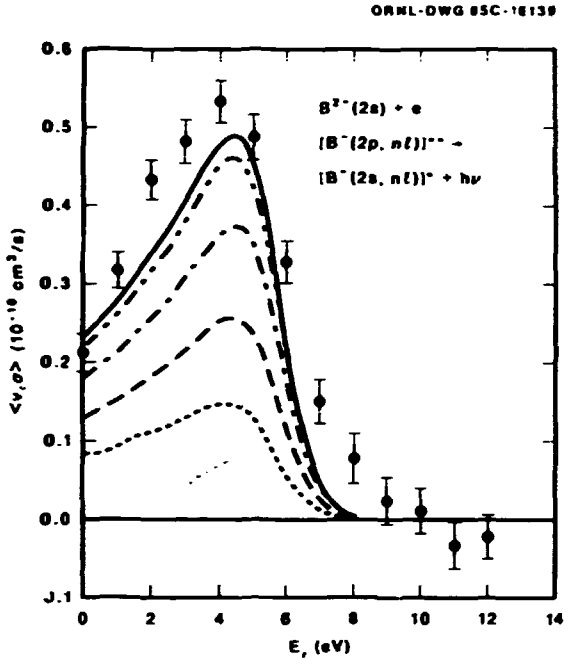

Fig. 4.26. Same as Fig. 4.25 for B^{2+}.

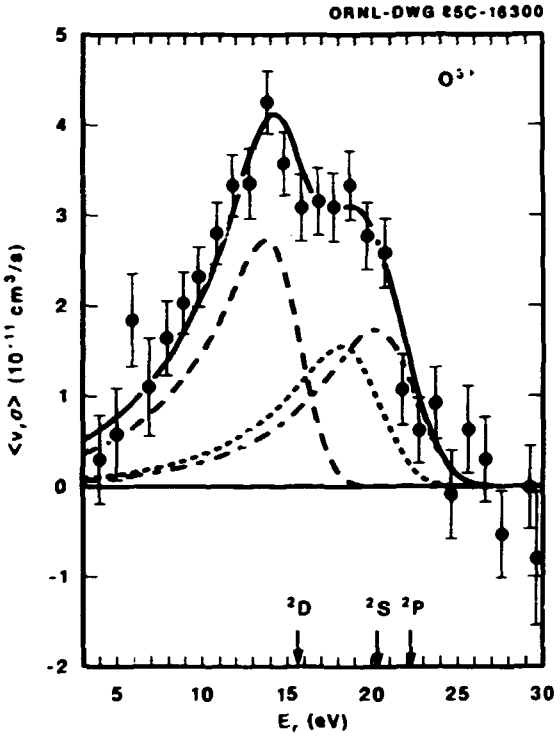

Fig. 4.27. The DR rate, $\langle v_r\sigma \rangle$ vs. E_r for O^{3+} where the solid circles are the experimental data. The curves are calculated for the ^2D (— — —), ^2S (---) and ^2P (- — -) resonances and the solid curve is the sum of the three components.

via 2s-2p in B-like O^{3+} and F^{4+}, which is interesting because three final recombined states, ^2D, ^2S, and ^2P result. The relative energies at which the ^2D, ^2S, and ^2P resonances occur are 15.707, 20.347 and 22.365 eV in O^{3+} and 18.894, 24.434 and 26.619 eV in F^{4+}, respectively. The DR σ versus n for O^{3+} and F^{4+} is similar[6] to the calculated case of C^+ and this and the relative energies of the resonances allowed us to model the DR σ for O^{3+} and F^{4+}. We then convoluted the σ with our velocity distribution to get a DR rate and did a least squares fit with our measured DR rate to extract the magnitude of σ for each resonance. The comparison of our data with the rate calculated as above is shown in Fig. 4.27. Another ionic system we investigated is the Be-like ions C^{2+} and O^{4+} which again undergo DR via 2s-2p. However, the ion beam coming from the EN-tandem contains an appreciable unknown fraction, f, of metastable ions in the ^3P state and a fraction (1-f) in the ^1S ground state, both of which undergo DR. The resultant DR signal clearly reflects the presence of the two initial states but until we can determine the fraction of metastables in the beam, we cannot determine the individual DR rates.

We have also attempted to measure DR via 2s-3p in B^{2+} for which calculations without such complicating factors as the field effect exist. We did not observe any signal above our background and further analysis to determine an upper limit for the DR rate and comparison with theory is under way.

---

1. Department of Physics, University of Delaware, Newark, DE 19711.

2. For the experimental apparatus and procedure, see pp. 134-135 in Physics Division Progress Report, Sept. 30, 1984, ORNL-6120.

3. D. C. Griffin, M. S. Pindzola and C. Bottcher, submitted to Physical Review A.

4. P. F. Dittner, S. Datz, P. D. Miller, P. L. Pepmiller and C. M. Fou, Physical Review A, to be published.

5. P. F. Dittner, S. Datz, P. D. Miller, P. L. Pepmiller and C. M. Fou, submitted to Physical Review A.

6. K. LaGatutta, private communication.

EN TANDEM OPERATIONS AND VAX-BASED DATA ACQUISITION SYSTEM

P. L. Pepmiller H. F. Krause
P. D. Miller

The EN tandem accelerator has operated quite reliably during the reporting period, requiring only two short tank openings while providing about 2000 hours of beam on target for research. The accelerator has been used for a variety of experiments in basic atomic physics. These have included the in-house groups, and groups from the University of Tennessee, North Texas State University, ORAU, and the Chemistry Division of ORNL. The major down times were the result of source development. During the year we installed two new ion sources, replaced many of the ion source power supplies, and developed new lower emittance beams. Problems with the reliability of these power supplies are gradually being resolved. The new lower emittance sources have resulted in greatly improved transmission through the EN-tandem. We have now supplied beams of H, B C, N, O, F, Si, P, S, Cl, Ni, and Au, with good intensities. We are confident that other beams will follow. Major improvements have been made in operator training, safety guidelines, and documentation.

The computer/data acquisition system for the EN Tandem Facility was upgraded by the purchase and installation of a VAX 11/750 computer, CAMAC data acquisition hardware and numerous supporting peripherals. The computer, operating under the VAX/VMS operating system, presently supports the FORTRAN language and numerous numerical utilities (such as the NAG library and the ORNL-generated CORLIB and GRAFIX libraries) for data processing, graphics, and computation by up to 17 interactive users. The CAMAC hardware was configured to run under the XSYS data acquisition software that was developed and provided by the Triangle Universities Nuclear Laboratory (TUNL) at Duke University. Data acquisition using one CAMAC crate was debugged and operating in less than three man-months after receipt of the computer by a person previously unfamiliar with VAX/VMS and the X-SYSTEM. Five data acquisition programs, tailored to EN-Tandem user needs (different from TUNL), are now running. Users are presently becoming familiar with the computer and the X-SYSTEM, and their reactions to the system have been overwhelmingly favorable. Users have logged more than three months of CPU usage in six months of operation.

5. THEORETICAL PHYSICS

INTRODUCTION AND OVERVIEW

Theoretical research programs in both nuclear and atomic physics are carried out within the Physics Division. Many of the projects in nuclear physics are stimulated by the current research program on the Holifield Heavy Ion Research Facility or by future experiments planned by Physics Division staff. The atomic theory program benefits from and contributes to the experimental atomic physics program on the EN tandem accelerator at ORNL and the experimental program to support the plasma physics projects.

In nuclear theory, major efforts continued in the areas of direct nuclear reactions, the structure of nuclei at low and high temperatures and in regions of strong deformation, time-dependent Hartree-Fock calculations of heavy-ion reactions, and ultrarelativistic heavy-ion collisions. The study of relativistic nuclear models continues to increase. There was major activity this year to find new models for the production of discrete-energy positrons in low-energy collisions between highly charged systems.

In atomic physics, the development of quantitatively accurate models to describe L-shell vacancy production in heavy-ion collisions continues. Various ionization and dielectronic recombination processes have been studied in detail.

This year, the theory program was significantly enhanced by the presence of an ORNL-UT Distinguished Scientist in nuclear theory, and by the generous funding of the Joint Institute for Heavy Ion Research Facility through, in large part, the University of Tennessee Centers of Excellence grant from the State of Tennessee. As a direct result of the Distinguished Scientist program, there were two post-doc positions filled jointly at ORNL and UT. Through the Joint Institute, a number of theory visitors were at ORNL for periods of two weeks to one year, with a total of two man-years. The presence of these visitors and post-docs created an intellectually stimulating atmosphere. Much of the effort of these new researchers was in the area of intermediate heavy-ion physics which is relevant to the physics of a possible booster to HHIRF. The Distinguished Scientist position in nuclear theory was vacated in August, 1985. In addition to these new programs, the nuclear theory effort was also enhanced by a Laboratory-funded Wigner post-doctoral appointment in nuclear theory.

Most of the theory computing was done on the Physics Division VAX/FPS-164 array processor system. Towards the end of this reporting period, the VAX 11/780 was upgraded to a VAX 11/785, and a matrix accelerator capability was added to the FPS-164. The system was heavily utilized and proved to be reliable and highly satisfactory.

LOW-ENERGY HEAVY-ION PHYSICS

DISPERSION RELATION AND THE LOW-ENERGY BEHAVIOR OF THE HEAVY-ION OPTICAL POTENTIAL[1]

M. A. Nagarajan[2] C. C. Mahaux[3]
G. R. Satchler

A dispersion relation is used to show that the "anomalous" behavior of the real part of the optical potential for $^{16}O + ^{208}Pb$ scattering at low energies is an example of a general property of heavy-ion optical potentials at energies approaching the top of the Coulomb barrier, where the flux into nonelastic channels is drastically reduced.

---

1. Abstract of paper: Phys. Rev. Letts. 54, 1136 (1985).
2. Daresbury Laboratory, Daresbury, Warrington, England.
3. Université de Liège, Liège, Belgium.

CAUSALITY AND THRESHOLD ANOMALY OF THE NUCLEUS-NUCLEUS POTENTIAL[1]

C. C. Mahaux[2] H. Ngô[3]
G. R. Satchler

According to the causality principle, a scattered wave cannot be emitted before the arrival

of the incident wave. This principle implies the existence of a dispersion relation between the real and the imaginary parts of the optical potential. We discuss the difference between the dispersion relations which hold for nucleus-nucleus scattering on the one hand and for nucleon-nucleus scattering on the other hand. In the case of nucleus-nucleus scattering, the dispersion relation predicts that the modulus of the real part of the optical potential has a bell-shaped maximum, as a function of energy, when the imaginary part approaches zero, i.e., for energies near the top of the Coulomb barrier. The shape of this apparent anomaly is investigated in the framework of several models. It is shown that there exists an algebraic model which is at the same time simple and sufficiently accurate in the sense that the difference between its outcome and that of more realistic models is smaller than the uncertainties introduced by the assumptions which have to be made. Various systems are discussed, in particular $^{16}O + {}^{208}Pb$ and $\alpha + {}^{40}Ca$. Several implications of the anomaly are pointed out, including its effect on the sub-barrier fusion of two heavy ions.

---

1. Abstract of paper accepted for publication in Nuclear Physics A.
2. Université de Liège, Liège, Belgium.
3. Institut de Physique Nucléaire, Orsay, France.

RADIAL DEPENDENCE OF THE DISPERSIVE CONTRIBUTION TO A NUCLEUS-NUCLEUS POTENTIAL NEAR THE THRESHOLD ANOMALY

C. Mahaux[1] H. Ngô[2]
G. R. Satchler

Previous work (see preceding abstract) on the application of a dispersion relation to the energy dependence of the strength of the nucleus-nucleus potential near the threshold anomaly has been extended to consideration of the radial shape, and its energy dependence, expected for the dispersive correction to the real potential, $\Delta V(r;E)$. The shape has been studied both explicitly and in terms of certain weighted samples, such as radial moments. Detailed applications have been made to the optical potentials for the scattering of $\alpha + {}^{16}O$ and $\alpha + {}^{40}Ca$.

---

1. Université de Liège, Liège, Belgium.
2. Institut de Physique Nucléaire, Orsay, France.

ABSORPTION CROSS SECTIONS AND THE USE OF COMPLEX POTENTIALS IN COUPLED-CHANNELS MODELS[1]

G. R. Satchler

We give a simple and transparent derivation of a result obtained recently by Kim, Udagawa, and Tamura for the loss of flux occurring in the coupled-channels scattering problem when a complex potential is used. The loss of flux, or absorption cross section, consists of three components: absorption from the elastic channel, absorption from the nonelastic channels, and absorption occurring during the elastic-nonelastic transitions. Some discussion is given of these results and their application to fusion reactions.

---

1. Abstract of paper accepted for publication in Physical Review C Comments.

ASYMMETRIC DEFLECTION FUNCTIONS AND THE EXTINCTION OF RAINBOWS: A COMPARISON OF α-PARTICLE SCATTERING FROM ^{40}Ca AND ^{44}Ca[1]

K. W. McVoy[2] M. M. Shalaby[3]
H. M. Khalil[3] G. R. Satchler

A decomposition of elastic scattering amplitudes into their nearside and farside components is employed to exhibit the presence of a spectacular farside ("nuclear") rainbow in the angular distributions for $\alpha + {}^{40}Ca$ scattering at energies from 30 to 60 MeV. The rainbow is identified by a deep "Airy minimum" which is present in the farside components of the angular distributions throughout this energy region. Over the same energy range, the angular distributions for the more absorptive $\alpha + {}^{44}Ca$ scattering exhibit no Airy minima, and in this sense, show no nuclear rainbow. However, a steepening of the slope of their smooth farside

component, which appears at energies above that (~60 MeV) for which the rainbow angle for α + ^{40}Ca becomes less than 180°, may serve to identify a residual rainbow effect, even in α + ^{44}Ca, at energies above 60 MeV. The manner in which the Airy minima of this and other nuclear rainbows are extinguished by absorption is examined in detail and is found to depend critically on the asymmetry in the shape of their low-energy deflection functions.

---

1. Abstract of paper to be submitted for publication in Nuclear Physics A.
2. University of Wisconsin, Madison, WI 53706.
3. Ain Shams University, Abbassia, Cairo, Egypt.

OPTICAL-POTENTIAL AMBIGUITIES AND FUSION CROSS SECTIONS FOR HEAVY IONS[1]

M. M. Shalaby[2] G. R. Satchler

We explore some of the effects of optical-potential ambiguities on the fusion cross sections for heavy-ion collisions, especially at energies below the top of the Coulomb barrier when the barrier-penetration model is used. Ambiguities of the Igo type in the real potential are found to have little effect except when the potential is very shallow. The cross sections are seen to be very sensitive to the imaginary potential adopted if this allows for some absorption within the barrier; both the magnitude and shape of the excitation function may be changed.

---

1. Abstract of paper: Nucl. Phys. A442, 469 (1985).
2. Ain Shams University, Abbassia, Cairo, Egypt.

FOLDING-MODEL POTENTIALS AND COUPLED-CHANNELS EFFECTS IN THE FUSION OF Ti + Zr

G. R. Satchler

Potential-model calculations are being made for comparison with fusion cross sections recently measured[1] for ^{46,50}Ti + ^{90}Zr at energies near and below the top of the Coulomb barrier. Comparison of the two systems is of interest because the two Ti isotopes have very different quadrupole deformation parameters, hence coupled-channels calculations including this degree of freedom are being studied.

Initially, the real parts of the optical potentials were constructed using the folding model with the M3Y interaction.[2] Fermi-shaped density distributions were assumed, with radii and diffusenesses of 4.9, 0.515 (^{90}Zr); 3.85, 0.5 (^{46}Ti); 3.95, 0.5 (^{50}Ti), all in fm. These resulted in Coulomb barriers for ^{46}Ti and ^{50}Ti with peak heights of 108.3 and 107.0 MeV at radii 10.9 and 11.05 fm, respectively. These folded potentials may be compared with other, "standard," potentials. That of Christensen and Winther[3] is appreciably steeper and stronger in the vicinity of the barrier top (-11.7 MeV at 10.9 fm, compared to -7.9 MeV for the folded one). The later prescription of Akyuz and Winther[4] is also somewhat steeper and stronger (-9.1 MeV). The Woods-Saxon proposed by Broglia and Winther[5] has a slope very similar to the folded one, but is 5% stronger. The usual proximity potential[6] (with b = 1 fm) has the same slope in the barrier region, but is considerably weaker (-4.4 MeV at 10.9 fm).

For convenience in the coupled-channels calculations, the folded potentials were replaced by Woods-Saxon potentials, with radius parameters of 1.15 fm, fitted to the folded ones over the important radial range of ~9.5 to 13 fm. A diffuseness of 0.67 fm, with depths of 97.7 MeV (^{46}Ti) and 100 MeV (^{50}Ti), were found to be satisfactory and give essentially the same barrier heights, positions, and curvatures. These real potentials were used in conjunction with short-ranged imaginary potentials chosen to ensure complete absorption after the real potential barrier had been penetrated.[7] A Woods-Saxon shape was used with depth 10 MeV, radius parameter 1.0 fm, and diffuseness 0.25 fm. The fusion cross section is identified with the absorption cross section calculated with this model.[7]

The one-channel version of the model corresponds to the simple barrier penetration model.[8] This reproduces quite well the fusion cross sections measured at the highest energies ($E_{cm} \gtrsim$ 113 MeV) when the potentials just described are

used, but completely fails to reproduce those at energies close to, and below, the barrier. One way of representing this failure is to ask by what factors do the real, attractive nuclear potentials have to be enhanced in order to yield the observed fusion cross sections. As shown in Fig. 5.1, these factors steadily increase above unity as the energy is reduced, reaching about 2.2 for ^{46}Ti and 1.7 for ^{50}Ti at the lowest energies (E_{CM} = 100 MeV). This behavior is very much like that typically found[9] for the dispersive correction to the real optical potential in the vicinity of the Coulomb barrier (the so-called "threshold anomaly"). These renormalizations correspond to lowering the height of the barrier by 6 MeV (^{46}Ti) or 4 MeV (^{50}Ti), at the same time moving its peak to larger radii by 0.8 fm (^{46}Ti) or 0.5 fm (^{50}Ti).

Initially, coupled-channels calculations (performed with the program PTOLEMY[10]) were made including only coupling to the lowest 2^+ states of the Ti nuclei, assuming a harmonic vibration with deformation parameters β_2 = 0.314 (^{46}Ti), 0.173 (^{50}Ti). Although this provides considerable increase of the fusion cross section at subbarrier energies (by a factor of 3 for ^{50}Ti, and more than an order of magnitude for ^{46}Ti, at E_{CM} = 105 MeV), it is still far short of the observed enhancement. Adding the lowest 3^- states of the ^{46}Ti and Zr nuclei, or adding the (0^+,2^+,4^+) two-phonon triplet in ^{46}Ti, each produce further enhancement at E_{CM} = 105 by nearly a factor of 3. Including both sets of states nearly doubles the cross section again at this energy, to about 6 mb, still appreciably less than the measured 14 mb. Further, the slope of the cross section curve with respect to energy is too steep compared to the measured one, differing little from the slope of the uncoupled optical model curve.

This analysis is being continued.

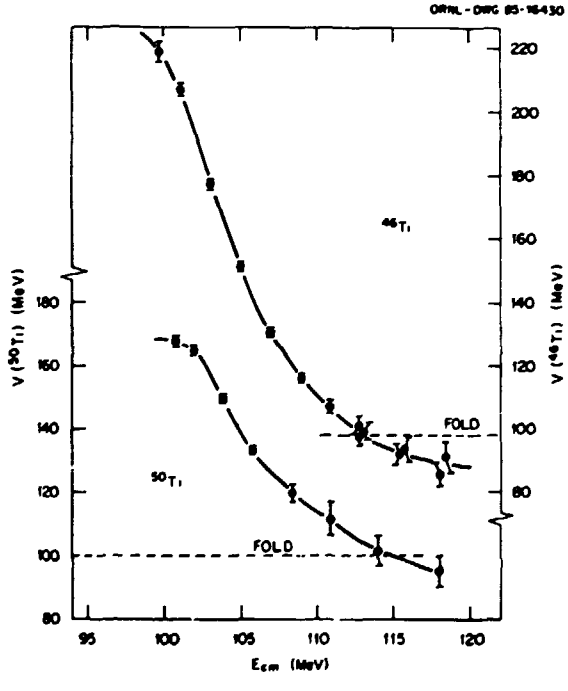

Fig. 5.1. Depth V of the Woods-Saxon nuclear potential required to reproduce the measured fusion cross sections for ^{46,50}Ti + ^{90}Zr at various energies. The dashed lines indicate the values that are equivalent to the folding-model potentials. The solid curves are drawn to guide the eye. The lefthand ordinate scale is for ^{50}Ti, the righthand one is for ^{46}Ti.

1. P. H. Stelson et al., this report.
2. W. G. Love and G. R. Satchler, Phys. Reports 55, 183 (1979).
3. P. R. Christensen and A. Winther, Phys. Lett. 65B, 19 (1976).
4. O. Akyuz and A. Winther, Proc. E. Fermi Int. School of Physics, 1979 (North-Holland Press, Amsterdam (1981).
5. R. A. Broglia and A. Winther, Heavy-Ion Reactions, Vol. 1 (Benjamin/Cummings, Reading, Mass., 1981), p. 114.
6. J. Blocki et al., Ann. Phys. (N.Y.) 105, 427 (1977).
7. M. J. Rhoades-Brown and P. Braun-Munzinger, Phys. Lett. B136, 19 (1984).
8. L. C. Vaz, J. M. Alexander, and G. R. Satchler, Phys. Reports 69, 373 (1981).
9. M. A. Nagarajan, C. Mahaux, and G. R. Satchler, Phys. Rev. Lett. 54, 1136 (1985); C. Mahaux, H. Ngô, and G. R. Satchler, Nucl. Phys. (1985) in press.
10. M. J. Rhoades-Brown, M. H. Macfarlane, and S. C. Pieper, Phys. Rev. C 21, 2417, 2436 (1980).

TIME-DEPENDENT HARTREE-FOCK STUDIES OF THE SENSITIVITY OF DYNAMICAL FUSION THRESHOLDS TO THE EFFECTIVE TWO-BODY INTERACTION[1]

J. A. Maruhn[2] K.T.R. Davies
M. R. Strayer

Results are presented for time-dependent Hartree-Fock calculations of mostly head-on collisions of ^{86}Kr + ^{139}La and ^{16}O + ^{16}O. These

studies demonstrate the sensitivity of the time-dependent Hartree-Fock dynamical fusion thresholds to the effective two-body interaction used in the calculations. The main thrust of this paper is to investigate the dynamical threshold which is the microscopic analog of the macroscopic extra-push threshold. We find that, for head-on collisions at bombarding energies above the interaction barrier, the onset of fusion is extremely sensitive to the interaction used. The thresholds calculated with different Skyrme forces differ by several hundreds of MeV or more, and are related to the effective mass of the interaction. We also show that the high-energy angular momentum window threshold has a pronounced force dependence, a feature which must be properly taken into account in comparing time-dependent Hartree-Fock window predictions with experimental data. Finally, it is shown that the fusion behavior can be sensitive both to the numerical time step used and to the precision of the calculation, a problem which may have implications regarding the validity of the time-dependent Hartree-Fock results after time scales of the order of 10^{-20} s.

---

1. Abstract of paper: Phys. Rev. C 31, 1289 (1985).
2. University of Frankfurt, Frankfurt, West Germany.

TIME-DEPENDENT HARTREE-FOCK CALCULATIONS OF ^{4}He + ^{14}C, ^{12}C + ^{12}C(0^{+}), AND ^{4}He + ^{20}Ne MOLECULAR FORMATIONS[1]

A. S. Umar[2] R. Y. Cusson[3]
M. R. Strayer P.-G. Reinhard[4]
D. A. Bromley[5]

Time-dependent Hartree-Fock calculations for head-on collisions of ^{4}He + ^{14}C, ^{12}C + ^{12}C(0^{+}), and ^{4}He + ^{20}Ne have been performed at bombarding energies near the Coulomb barrier. The results are interpreted in terms of their classical quasiperiodic and chaotic behavior. The position of the time-dependent Hartree-Fock collective path with respect to the multidimensional energy surface of the compound nuclear system is shown. Dynamical collective degrees of freedom are identified and classical frequencies associated with each degree of freedom are calculated. For ^{24}Mg we calculate molecular frequencies of about 0.8 and 1.0 MeV and a characteristic moment of inertia of 15 MeV^{-1}.

---

1. Abstract of paper: Phys. Rev. C 32, 172 (1985).
2. University of Pennsylvania, Philadelphia, PA 19104.
3. Consultant from Duke University, Durham, NC 27706.
4. University of Erlangen, Erlangen, West Germany.
5. Yale University, New Haven, CT 06510.

DENSITY AS A CONSTRAINT AND THE SEPARATION OF INTERNAL EXCITATION ENERGY IN TDHF[1]

R. Y. Cusson[2] M. R. Strayer
P.-G. Reinhard[3] J. A. Maruhn[4]
W. Greiner[4]

We present a fast and efficient constrained Hartree-Fock iteration scheme which constrains the complete density distribution to remain constant. The scheme is particularly suited to a coordinate- or momentum-space representation. The technique is applied to separate the collective and the internal energy in a propagating TDHF state. We study the behavior of these two energies in an ^{16}O+^{16}O collision.

---

1. Abstract of paper: Z. Phys. A320, 475 (1985).
2. Consultant from Duke University, Durham, NC 27706.
3. University of Erlangen, Erlangen, West Germany.
4. Consultant from University of Frankfurt, Frankfurt, West Germany.

DYNAMICAL SPIN-ORBIT CURRENTS IN HEAVY-ION COLLISIONS

P.-G. Reinhard[1] M. R. Strayer
A. S. Umar[2]

It is generally acknowledged that the time-dependent Hartree-Fock (TDHF) method provides a useful foundation for a fully microscopic many-body theory of low-energy heavy-ion reactions.[3] This assumption is predicated in part on the results of fusion excitation function calculations for light mass systems and particular energy angle correlation function calculations for

strongly damped heavy mass collisions.[4] The details of these calculations suggest that the Pauli principle plays an important role in simultaneously building up a time-dependent mean field and suppressing the propagation of the strong N-N interaction terms. These calculations exhibit an unusual degree of transparency for the very central collisions which affects the interplay between fusion and inelastic scattering and which seems to disagree with experiment.[4,5]

However, all of the TDHF calculations which have addressed this question have been carried out with approximations which impose symmetries on the TDHF wavefunctions and thereby reduce the number of degrees of freedom carried by the system. It is argued that the restoration of symmetries to the TDHF wavefunction reduce the amount of dissipation and hence the amount of fusion.

To this end, we consider the addition of spin-orbit current interaction terms to the TDHF Hamiltonian. Thus far, all TDHF calculations have ignored these terms by assuming completely spin-degenerate and spin-saturated states. Including the spin-orbit coupling terms in Skyrme forces provides an additional term to the TDHF Hamiltonian density,[6]

$$H(\vec{r}) = -t_4 \left[\rho\vec{\nabla}\cdot\vec{J} + \sum_q \rho_q \vec{\nabla}\cdot\vec{J}_q\right]\Big/2 \qquad (1)$$

In (1) t_4 is the strength of the spin-orbit force, ρ_q is the nuclear density for isospin $q = \pm 1/2$, and the divergence of the current in state q is given in terms of single-particle states $\psi_{\alpha q}$,

$$\vec{\nabla}\cdot\vec{J}_q = i \sum_\alpha [(\vec{\nabla}\psi_{\alpha q})^* \cdot \vec{\sigma}\times(\vec{\nabla}\psi_{\alpha q})] \qquad (2)$$

We have solved the TDHF equations to head-on collisions of $^{16}O + ^{16}O$ at a variety of bombarding energies using the Skyrme II force with the spin-orbit interaction as given above. We find a threshold for the onset of inelastic scattering occurring at a bombarding energy per particle of about 9 MeV. In contrast, calculations without spin-orbit forces give an inelastic threshold occurring at about 3.5 MeV for this system. Thus, we note that the dynamical breaking of the spin degeneracy substantially modifies the amount of dissipation observed in TDHF calculations.

---

1. University of Erlangen, Erlangen, West Germany.
2. University of Pennsylvania, Philadelphia, PA 19104.

3. J. W. Negele, Revs. Mod. Phys. 54, 913 (1982).
4. K.T.R. Davies et al., in "Treatise on Heavy-Ion Science," Vol. 3, ed. by D. A. Bromley (Plenum, New York, 1985).
5. A. Lazzarini et al., Phys. Rev. C 24, 309 (1981).
6. Y. M. Engel et al., Nucl. Phys. A249, 215 (1975).

NUCLEAR SHAPE-ISOMERIC VIBRATIONS

A. S. Umar[1] M. R. Strayer

It has been suggested that states built on shape-isomeric configurations could represent the underlying physics of the observed correlated resonances in the collisions of light heavy ions.[2] In calculating these states, we face the difficulty of performing nuclear structure calculations for triaxially deformed nuclei. However, for a variety of reasons, it is physically reasonable to consider vibrational states having a particular symmetry. Thus, we calculate the low-lying vibrational states built on the axially symmetric shape-isomer of ^{24}Mg.

The density vibrations of the isomer are calculated using the linear response formalism.[3] We study the response of the nucleus to a time-dependent one-body external perturbation coupled to the nuclear density

$$H_x(t) = \int d^3r\, \rho(\vec{r},t)F(\vec{r},t) \qquad (1)$$

where ρ is the nuclear density, and F represents an arbitrary external field. Under general assumptions, the equations of motion for the density matrix, $\hat{\rho}$ can be written as

$$i\, d\hat{\rho}/dt = [(h(\rho) + f(t)),\hat{\rho}] \qquad (2)$$

where $h(\rho)$ is the single-particle Hartree-Fock Hamiltonian, and f is

$$f(\vec{r},t) = \lambda\, \delta(t) \begin{cases} r^L\, Y_{L0}(\hat{r}) & L \neq 0 \\ r^2 & L = 0 \end{cases} \quad (3)$$

In coordinate space, the response function, $\delta\rho$, is defined to be the change in the density with respect to the equilibrium density and the strength function which measures the transition strength from excited states to the ground state is

$$S_L(\omega) = \int d^3r\, dt\, e^{-i\omega t}\, f(\vec{r},t)\delta\rho(\vec{r},t) \quad (4)$$

We have computed the response $\delta\rho$, and the strength function for vibrations about the axially symmetric isomer of ^{24}Mg using the Skyrme I force. The time dependence of the second moment of the response function and the energy dependence of the strength function are shown in Fig. 5.2. In Fig. 5.2(a) we see that the time evolution is nearly periodic over a range of very long times and has a frequency of about 1 MeV, as can be seen from the strength function in Fig. 5.2(b). The energy spacings observed in Fig. 5.2(b) are in agreement with those of the U(4) model and the experimental data.

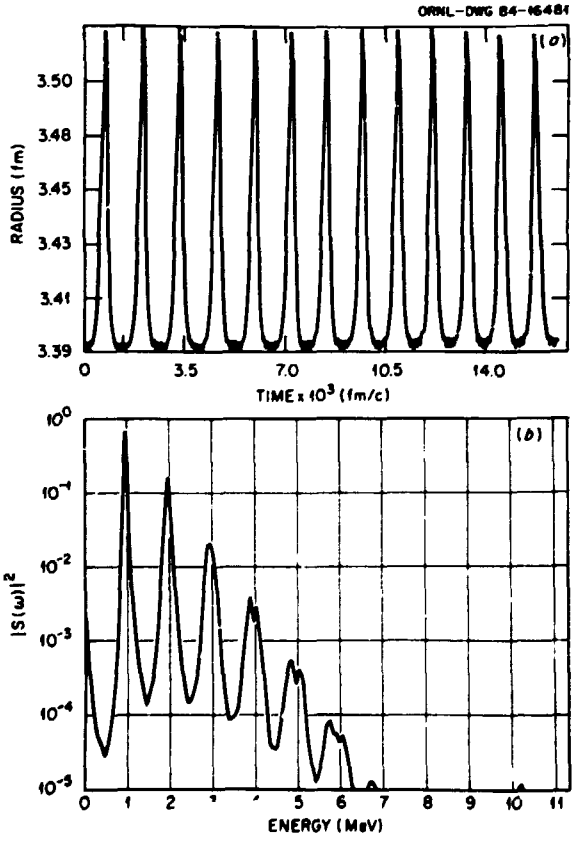

Fig. 5.2. a) The time of the nuclear radius for the oscillating ^{24}Mg isomer with the Skyrme I force. (b) The strength function $S_0(\omega)$ computed for the oscillations shown in (a).

---

1. University of Pennsylvania, Philadelphia, PA 19104.
2. K. A. Erb and D. A. Bromley, in "Treatise on Heavy-Ion Science," Vol. 3, ed. D. A. Bromley (Plenum, New York, 1985).
3. G. F. Bertsch and S. F. Tsai, Phys. Rep. 18, 125 (1975).

CHANNEL COUPLING EFFECTS IN THE SUBBARRIER FUSION OF ^{16}O ON ^{16}O AND ^{18}O[1]

J. Q. Wu[2] G. F. Bertsch[3]
A. B. Balantekin[4]

Isotopic differences in the fusion cross section for oxygen on oxygen, observed by Thomas et al.,[5] are interpreted with a coupled-channel model. We find that most of the subbarrier enhancement of ^{18}O + ^{16}O over ^{16}O + ^{16}O is attributable to the excitation of the low 2^+ state in ^{18}O. However, our model predicts the enhancement to persist above the barrier contrary to the experimental findings.

---

1. Abstract of paper: Phys. Rev. C 32, 1432 (1985).
2. Guest assignee from University of Tennessee, Knoxville, TN 37916.
3. Michigan State University, East Lansing, MI 48824.
4. Eugene P. Wigner Fellow.
5. J. Thomas et al., Phys. Rev. C 31, 1980 (1985).

PATH INTEGRAL APPROACH TO THE MULTI-DIMENSIONAL QUANTUM TUNNELING IN THE FINITE TEMPERATURE CASE

A. B. Balantekin[1] N. Takigawa[2]

Recently, we formulated the path integral approach to the coupled channels problem and worked out transmission probabilities for some simple cases.[3] We extended this work to include the effects of the finite temperatures in the tunneling process. Starting from the Hamiltonian

$$H = T(\hat{R}) + V(R) + H_0(q) + H_{int}(q,R)$$

where R is a translational degree of freedom and $H_0(q)$ is the Hamiltonian of the internal system coupled to this degree of freedom, the finite temperature influence functional can be written as

$$\rho_\beta = \sum_n \langle n | e^{-\beta H_0} \hat{U}^\dagger(\bar{R},\bar{T})\hat{U}(R,T) | n\rangle$$

where the operator $\hat{U}$ satisfies the equation

$$i\hbar \frac{\partial \hat{U}}{\partial t} = [H_0 + H_{int}]\hat{U}.$$

The path integral expression for the penetrability is calculated using the above temperature-dependent influence functional for the simple cases where the influence functional reduces to a group character.

---

1. Eugene P. Wigner Fellow.
2. Tohoku University, Sendai, Japan.
3. A. B. Balantekin and N. Takigawa, Ann. Phys. (N.Y.) 160, 441 (1985).

EFFECTIVE RADIUS DETERMINATION FROM γ-RAY MULTIPLICITIES IN FUSION REACTIONS[1]

A. B. Balantekin[2] P. E. Reimer[3]

The angular momentum quantum number dependence of the transmission probability in fusion reactions is usually approximated as

$$T_L(E) = T_0\left[E - \frac{L(L+1)\hbar^2}{2mR^2(E)}\right] \qquad (1)$$

where the effective moment of inertia $mR^2(E)$ is not explicitly known. The energy dependence of R(E) is approximated in various ways. We have shown that using the integral equation

$$\langle L\rangle = \frac{m}{\hbar^2}\frac{R^4(E)}{E\sigma(E)}\int_{-\infty}^{E} dE' \frac{E'\sigma(E')}{R^2(E')}\left[\frac{mR^2(E)}{\hbar^2}(E-E') + \frac{1}{4}\right]^{-1/2}, \qquad (2)$$

simultaneous measuremerts of the fusion cross section and the gamma ray multiplicities can be used to determine R(E). Results obtained using model potentials is shown in Fig. 5.3. The

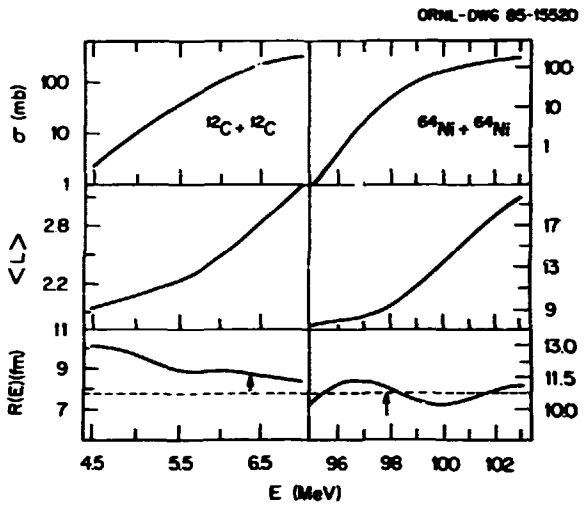

Fig. 5.3. Results obtained using the Woods-Saxon potential for ^{12}C-^{12}C and the Krappe, Nix, and Sierk potential for ^{64}Ni-^{64}Ni. Upper and middle portions are the cross section and average angular momenta determined using the WKB formalism. The lower portion shows the effective radius R(E) (solid line) obtained using σ(E) and <L>(E) given above. The dashed line is the actual position of the barrier maximum, and the arrow identifies the position of the barrier.

average angular momentum quantum number <L> is usually related to the gamma-ray multiplicity as

$$\langle L\rangle = \alpha M_\gamma - \beta. \qquad (3)$$

Since the information to be obtained from R(E) (position, height, and the thickness of the barrier) can also be accurately determined from other experiments, the consistency between the two sets of information indicates that the values of the parameters α and β used to determine <L> are correct. We have used our results to study the data[4] for the systems ^{12}C-^{154}Sm and ^{16}O-^{154}Sm. The result for the latter system is shown in Fig. 5.4.

---

1. Summary of paper: Phys. Rev. C 33, 379 (1986).
2. Eugene P. Wigner Fellow.
3. Student Research Participant from Bethel College, North Newton, KS, summer, 1985.
4. R. Vandenbosch et al., Phys. Rev. C 28, 1161 (1983).

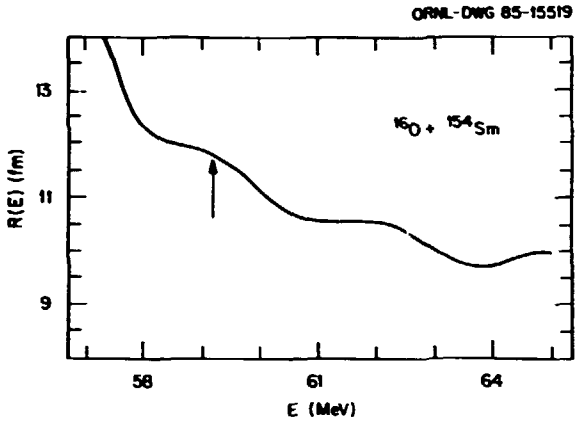

Fig. 5.4. The effective radius for the ^{16}O-^{154}Sm system.

CORRELATIONS BETWEEN PRE-EQUILIBRIUM NUCLEONS[1]

D. J. Ernst[2] M. R. Strayer
A. S. Umar[3]

A quantum-mechanical model for the emission of fast nucleons in low-energy nucleus collisions is presented. The role of a classical emission function is shown to be played by the time derivative of an impact-parameter-integrated, time-dependent, distorted-wave Wigner function. Correlations between the emitted particles are shown to be caused by the Pauli principle, by the impact-parameter dependence of the emission process, and by two-body collisions including the final-state interactions, as well as those due to the size of the emitting source.

---

1. Abstract of paper: Phys. Rev. Letts. 55, 584 (1985).
2. Texas A & M University, College Station, TX 77843.
3. University of Pennsylvania, Philadelphia, PA 19104.

SUBTHRESHOLD π^0-PRODUCTION IN THE BOLTZMANN-UEHLING-UHLENBECK THEORY[1]

J. Aichelin[2]

π^0-production in medium-energy heavy-ion reactions is studied via the Boltzmann-Uehling-Uhlenbeck approach. The mass dependence and bombarding energy dependence of the calculated absolute pion cross sections agree remarkably well with the recent data of Noll et al. for ^{12}C(60,75,85 MeV/N)+C, Ni, Au. Pion reabsorption occurs in ≥50% of the events. Shadowing is important for the angular distributions of pions produced in heavy systems and also changes the apparent velocity of the "pion emitting source."

---

1. Abstract of paper submitted to Physical Review Letters.
2. Max-Planck Institut für Kernphysik, Heidelberg, West Germany.

CONDITIONAL SADDLE POINT CONFIGURATIONS[1]

K.T.R. Davies A. J. Sierk[2]

A general method is presented for determining an equilibrium point on a potential energy surface subject to an arbitrary number of constraints. The method is then specialized to the calculation of a conditional saddle point in the liquid-drop model for which the constraint is the mass-asymmetry degree of freedom. This approach is useful for cases in which the mass asymmetry is not one of the chosen coordinates but instead is a function of these coordinates. Conditional saddle points are calculated for the liquid-drop and Yukawa-plus-exponential nuclear energy models, with the nuclear shape parametrized using both a three-quadratic-surface model and a Legendre polynomial expansion of the nuclear surface function. We show how the conditional saddle-point shapes and energies change as the fissility x and the mass asymmetry value α are varied. As α increases for fixed x, the saddle point configurations effectively behave like lighter (less fissile) nuclei. For fissilities less than the Businaro-Gallone value (x_{BG}), the conditional saddle point energy always decreases with increasing α. For $x > x_{BG}$, with increasing α the conditional saddle point energy increases until it reaches the limit of the Businaro-Gallone peak, after which the energy decreases.

---

1. Abstract of paper: Phys. Rev. C 31, 915 (1985).
2. Los Alamos National Laboratory, Los Alamos, NM 87545.

SIMPLE OPERATORS FOR OBTAINING SEMI-INCLUSIVE TRANSITION PROBABILITIES IN TIME-DEPENDENT PROBLEMS

J. E. Purcell[1] M. R. Strayer
C. Bottcher

In mean-field theories, it is presently not known how to calculate directly the particle emission energy spectrum associated with the low-energy collision of two heavy ions. To this end, we need the collision-induced probability of a transition from the initial single-particle bound state to a final continuum state. We have found two operators which, when used together with the final wavefunction, produce the desired transition probability. They are:

$$\lim_{N\to\infty} \left(\exp\left(-(E-H)^2/\Gamma^2\right)^N\right)$$

and

$$\lim_{N\to\infty} \left((E-H)^{-1}\right)^N,$$

where H is the final (i.e., $t\to\infty$) Hamiltonian.

We use these operators on a grid in coordinate space and require that the wavefunctions go to zero on the boundaries. The effect of the above operators is to project out of an arbitrary wavefunction that the eigenfunction of H whose energy is nearest to E. From this we get the exact eigenvalue, E_i, and, given the final time evolved wavefunction, ψ_f, we can obtain the particle emission probability at the energy E_i from the overlap $\langle\psi_f | O_p | \psi_f\rangle$ where O_p is either of the above operators.

We have tested the method in several one-dimensional models where exact probabilities can be obtained for comparison. More realistic cases are currently being studied in which both energy and angular distributions are to be obtained.

1. Consultant from Georgia State University, Atlanta, GA 30303.

NUCLEAR STRUCTURE

THE UNISOR NUCLEAR STRUCTURE THEORY PROGRAM

Introduction

G. A. Leander[1]

A structure theory program is supported by UNISOR, the university isotope separator at ORNL. It has been greatly strengthened, especially in the area of high spins, by the new visitor program at JIHIR. The aim is to conduct and stimulate theoretical research on nuclear structure, particularly in areas where experiments at the Holifield facility have or potentially could have an impact. The main areas of current interest are: the low-energy structure of nuclei far from stability, the intrinsically cold states at high angular momentum that are observed in discrete-line spectroscopy, and the warmer states that are studied by quasicontinuum spectroscopy. The theoretical approaches focus on nuclear collectivity, its basic principles, microscopic origin, and physical consequences.

The major development during the past year is a theory of static isovector E1 deformations in nuclei. This theory accounts for the low-energy collective E1 mode that has been discovered recently in certain nuclei. Other highlights have been the first charting of reflection asymmetric equilibrium shapes at high angular momentum, and an evaluation of UNISOR laser data which sheds light on the collectivity in semi-magic nuclei. These and other results are summarized below under four topical headings with reference to the respective publications.

Low-Energy Structure

A. F. Barfield[2]
F. Dönau[3]
J. Dudek[4]
B. E. Gnade[5]
W. M. Howard[6]
G. A. Leander[1]
D. Lewellen[1,7]
P. Möller[8,9]
W. Nazarewicz[10,11]
J. R. Nix[9]
Ph. Quentin[10,12]
P. B. Semmes[10,13]
O. Scholten[14]
J. L. Wood[13]
L. Zamick[15]
J.-y. Zhang[10,16]

The ability to describe the onset of collectivity is a stringent test of nuclear models,

and a part of the theoretical and experimental work at UNISOR is geared to this problem.

A long-standing puzzle regarding the onset of deformation in the $_{81}$Tl isotopes has been resolved.[17,18] Early UNISOR experiments had shown that the $h_{9/2}$ proton orbit, located above the Z=82 spherical shell gap, comes down in energy with decreasing neutron number below N = 126 and reaches a minimum at N = 108 (A = 189 in Fig. 5.5, top frame). One of several theories

ORNL-DWG 85-18083

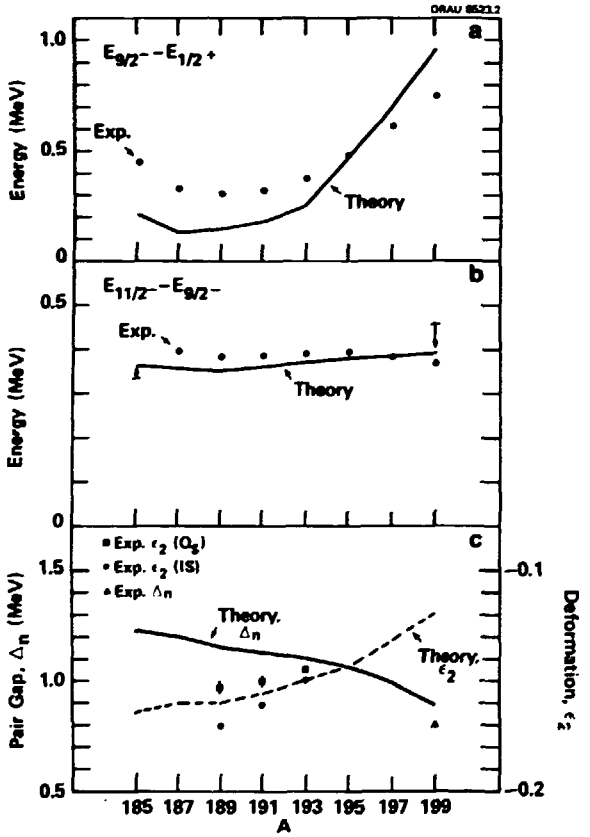

Fig. 5.5. Theory vs. experiment for $^{185-199}$Tl. (a) Energy of the 9/2$^-$ isomer with respect to the 1/2$^+$ ground state. (b) Energy of the first state in the band based on the 9/2$^-$ isomer. (c) Deformation, ϵ_2, of the 9/2$^-$ isomer from theory (dashed line) and from the experimental Q_s (▬) and isotope shifts (●) obtained in this work. The odd-even energy difference, Δ_n, from BCS theory (solid line) and from experimental masses (▲). Note that both Δ_n and $|\epsilon_2|$ increase for an increasing number of neutron holes below N = 126, with compensating effects on the moment of inertia. The arrows in (b) indicate the effect of a self-consistent instead of fixed Δ_n.

attributed the changing $h_{9/2}$ energy to the onset of oblate deformation, despite the proximity to the Z=82 shell closure. Rotational-like bands built on the 9/2$^-$ levels were in fact observed. However, the energy spacings within these bands are almost identical along the isotopic chain (Fig. 5.5, middle frame), and this was interpreted as evidence against a changing deformation. A UNISOR laser measurement has now established that the deformation does change (Fig. 5.5, bottom frame), and a theoretical calculation based on the Nilsson model has explained the seemingly contradictory aspects of the data. The minimum in the $h_{9/2}$ energy was reproduced for the first time (Fig. 5.5, top frame), the key being, as is so often the case in nuclear structure, a better parametrization of the single-particle potential. The energy of collective excitations based on the 9/2$^-$ bandheads was obtained by a method we developed a few years ago for K-bands. This rotational energy was indeed found to be nearly constant (Fig. 5.5, middle frame) despite the changing quadrupole deformation, ϵ_2 (Fig. 5.5, bottom frame). The reason is that with an increasing number of neutron holes there is an increase of both the deformation and the neutron superfluid correlations (Fig. 5.5, bottom frame), with offsetting effects on the collective excitation energy. It is interesting to speculate that this mechanism is responsible for the near-constant collective energy spacings that seem to be a rather general feature in sequences of semimagic nuclei.

In the $_{62}$Sm isotopes, it is well known that ground-state deformation sets in via a sharp phase transition for N > 82. Most models predict a smoother transition for N < 82, but a few years ago it was found that a relatively sudden transition is predicted by the folded Yukawa single-particle model specifically for Pm and Sm. Measurements of 2$^+$ energies in the light Sm isotopes, partly done at UNISOR, are consistent with the sudden transition,[19] c.f. the lower branch of the dashed curve in Fig. 5.6.

The interacting boson model (IBM) is a model designed to describe the onset of quadrupole collectivity in nuclear spectra, and it is being

ORNL-DWG 85-18084

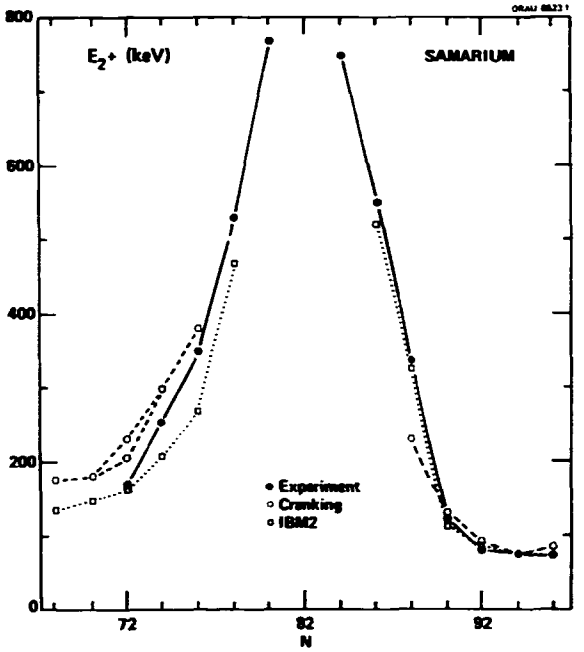

Fig. 5.6. Theory vs. experiment for the energy of the first 2^+ level in the Sm isotopes. The experimental points for N = 72, 74, and 76 are new. They lie on a line which slopes even more steeply than the lower branch of the dashed curve, which latter corresponds to a rapid shape change.

studied and tested. Calculations have been made for the phase transition in the light Sm isotopes[19] (c.f. Fig. 5.6). Work is under way[20] to describe octupole vibrational bands by the inclusion of a f-boson in IBM. A form of the IBM Hamiltonian has been found which incorporates the equivalent of Coriolis coupling between the K-bands, and which gives rise to appropriate splittings of the octupole K-bandheads. An appropriate form of the exchange interaction is essential to describe cases where $K^\pi = 1^-$ or 2^- comes lowest. The same form of the octupole operator is used for the Hamiltonian and the E3 transition rates. The systematic trends of the parameters are currently being studied by fitting the spectra of twelve rare-earth nuclei. Another region of interest is the light Pt, Au, Hg, Tl, and perhaps Pb and Bi isotopes, where well-deformed states coexist at low energy with less deformed or spherical states. The stability of IBM predictions for this region is being examined.[21] Also, the validity of the IBM parametrizations for even-even nuclei is being tested by coupling on an odd particle and comparing with experimental data for odd-mass nuclei.[22] Previously published parametrizations are shown to be unsatisfactory in some respects. The odd-particle coupling calculations are carried out by the dynamical core-quasiparticle coupling method, rather than the interacting boson-fermion model (IBFM). These two methods have been compared systematically.[23,24] One conclusion is that 'Coriolis attenuation' can be engineered in IBFM with the parameter A_0 (Fig. 5.7). However, there are several other spectroscopic consequences of changing A_0 which would show up in a sufficiently extensive experimental spectrum or spectra for a sequence of nuclei. Phenomenologically based conclusions regarding IBFM and Coriolis attenuation in the present literature can therefore be deemed inconclusive.

ORNL-DWG 85-18101

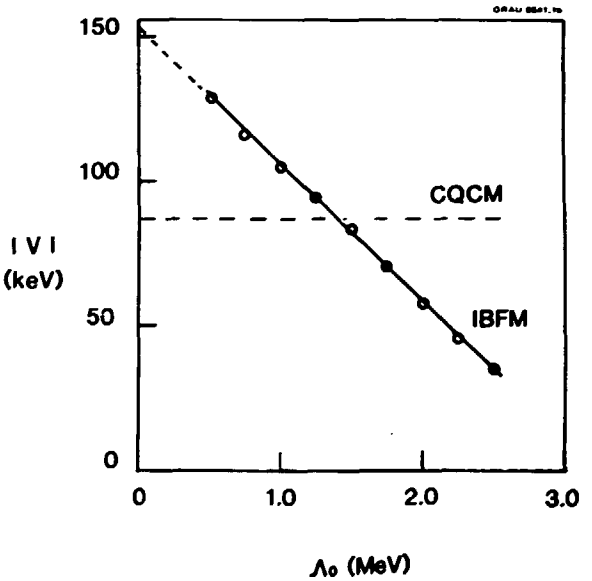

Fig. 5.7. The effective Coriolis matrix element extracted from the E2 transition rate between the first and second 9/2 states in the IBFM spectrum for j = 9/2, $v^2 = 0.8$, and an SU(3) core. The IBFM results are shown as a function of the exchange term parameter A_0. The horizontal dashed line shows the result from core-quasiparticle coupling using the same j, v^2, and SU(3) core, with the BCS gap parameter $\Delta = 1$ MeV.

The odd-mass nuclei ^{107,109}Ag were studied following a measurement of excited-state magnetic moments at Rutgers.[25] These moments contradict the old interpretation of the low-lying levels as basically spherical single-particle states. The moments had been reproduced previously by an IBFM calculation. Now it was shown that a simpler even-even core, the triaxial rotor, is sufficient to describe even more extensively the electromagnetic properties of these transitional nuclei.

The onset of pairing, or "deformation in gauge space," is poorly described by standard BCS theory. Many years ago, Lipkin proposed a slight modification of BCS, which improves the solutions in the transition region. A numerical method of solution which converges in the general case was previously lacking but has now been developed.[26] Lipkin's scheme is useful in near-magic nuclei like Au and Tl, where BCS correlations break down for some configurations. Following up on Lipkin's idea, equations have also been derived for rotating nuclei. These equations may provide the most viable solution to the problem of pairing reduction at high spins.

Microscopic theories of nuclear structure are often based on single-particle orbits in a mean field, and an important activity is to follow up the results of spectroscopy in order to test and improve models for calculating such orbits. The analysis of ORNL-McMaster data on ^{185}Au showed that the proton orbits in this region are adequately described by the Warsaw Woods-Saxon potential but not by any previous set of Nilsson model parameters.[27] A new set of Nilsson proton parameters has been proposed.[28] The 1981 parametrization of the folded Yukawa model, featuring a linearly A-dependent spin-orbit strength, has been explored in the region of very heavy and superheavy nuclei.[29,30] The shell energy is minimized at N = 178 rather than 184. There is also a new local minimum around Z = 110 and N = 162, which should enhance the stability of these elements relative to systematics. These predictions might be tested within the framework of the proposed LEAP project.

Intrinsic Reflection Asymmetry

G. F. Bertsch[31,32]
Y.-s. Chen[10,33]
J. Dudek[4]
G. A. Leander[1]
P. Möller[8,9]
W. Nazarewicz[10,11]
P. Olanders[8]
I. Ragnarsson[8]

A few years ago we found that reflection asymmetric equilibrium shapes occur in certain nuclei according to mean-field theory. The asymmetric intrinsic shapes are an "exotic" state of nuclear matter, where phenomena can be observed which do not occur elsewhere. An ongoing effort is now being made to understand the consequences of this asymmetry, and to relate it to a body of relevant experimental data that has begun to emerge largely during the past few years. A review is provided in Ref. 34.

Two significant theoretical advances have been made during the past year. One is the initiation of calculations to map out the evolution of reflection asymmetric shapes at high angular momentum.[35,36] This is described below under the heading 'High Spins.' The other advance is a theory for the isovector E1 moments that accompany isoscalar reflection asymmetric deformations.[34,37,38] The idea is to calculate the static E1 deformation of the equilibrium shape using the Strutinsky method. The semiclassical dependence of the E1 moment on isoscalar deformation is obtained from the liquid-drop model. A quantal shell correction is obtained from the deformed shell model taking into account the residual dipole-dipole interaction, which latter is not included in the one-body field and strongly affects the E1 moments. Experimentally, collective E1 transitions have been observed at both high and low spins. An example from in-beam work is the alternating parity ground band of ^{222}Th, where the E1 transition intensities are about as strong as the collective E2 intensities. The E1 transitions in ^{226}Ra are also fast, nevertheless the B(E1)/B(E2) ratios in ^{226}Ra are an order of magnitude smaller than in ^{222}Th (Fig. 5.8). The theory explains this as a shell effect. For ^{222}Th the shell correction and the liquid-drop term have the same sign, but for ^{226}Ra they have opposite signs and tend to cancel (Fig. 5.9). A quantitative comparison

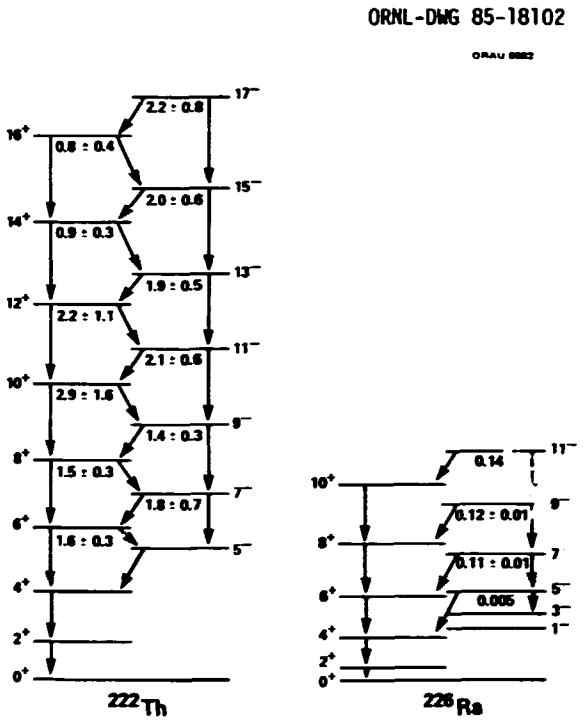

Fig. 5.8. The experimental yrast bands of ^{222}Th and ^{226}Ra, which exhibit the characteristic features of soft intrinsically reflection asymmetric rotors. The numbers below the levels are the B(E1)/B(E2) branching ratios in 10^{-6} fm^{-2}.

between theory and experiment in the Ra-Th region is shown in Table 5.1. Experimental data are more scarce in the rare earth region. Fast E1 transitions within alternating parity bands are, however, observed in nuclei around ^{148}Sm, and a large E1 shell correction with the same sign as the liquid-drop contribution is indeed predicted for these nuclei.

An interesting problem has arisen[39] from the measurement of three E1 transition rates between low-lying states of ^{225}Ra. The E1 rates are fast and support our previous interpretation of these states as $K^{\pi} = 1/2^{+}$, $1/2^{-}$ parity doublet bands based on a single reflection asymmetric Nilsson orbital. All three E1 rates can be fitted with two parameters, the E1 moment and the electric decoupling factor. This first empirical electric decoupling factor turns out to be nonzero, although zero would be required by symmetry in the limit of strong coupling.

There are many other deviations from the reflection asymmetric strong-coupling limit in the spectra of relevant odd-mass nuclei. These deviations are sometimes cited as evidence against the usefulness of reflection asymmetric mean fields. However, significant deviations are expected to arise from nonadiabatic decoupling of the odd particle, both Coriolis decoupling and decoupling from the reflection asymmetry. In order to investigate the role of decoupling more quantitatively, numerical applications of the rigid reflection asymmetric rotor plus particle model are in progress.[40] The Ra, Ac, light Th, and heavy Ba nuclei are the most likely candidates for reflection asymmetry at low spins.[41,42] Experimental items of prime interest, in addition to the K=1/2 bands of ^{225}Ra, are some spectroscopic factors in ^{227}Ac that were measured at Livermore, and a spectrum for ^{145}Ba from TRISTAN.

High Spins

R. Bengtsson[8,10] G. A. Leander[1]
T. Bengtsson[8] W. Nazarewicz[10,11]
Y.-s. Chen[10,33] P. Olanders[8]
J. Dudek[4] I. Ragnarsson[8]
S. Frauendorf[3] P. B. Semmes[10,13]
J.-y. Zhang[10,16]

Nuclear rotation was found to be strongly influenced by intrinsic reflection asymmetry in our previous studies with the cranked Woods-Saxon-Bogoliubov model. The collective aspect of rotation is enhanced, single-particle aspects are suppressed, and the surprisingly smooth level sequence in ^{222}Th could be reproduced, assuming that the reflection asymmetric shape calculated for the ground state is also valid at high spins. The same model has now been applied to calculating the equilibrium shapes at high spins for ^{222}Th and several other nuclei.[35] The results for the Th isotopes are summarized in Fig. 5.10. Similar results were obtained for the Ra isotopes with A = 218-226. Constant deformation is seen to be a good approximation for ^{222}Th at I < 20, but is by no means the universal rule. In the heavier isotopes, a reflection symmetric band with both $\pi i_{13/2}$ and $\nu j_{15/2}$

ORNL-DWG 85-18103
ORAU 854L1a

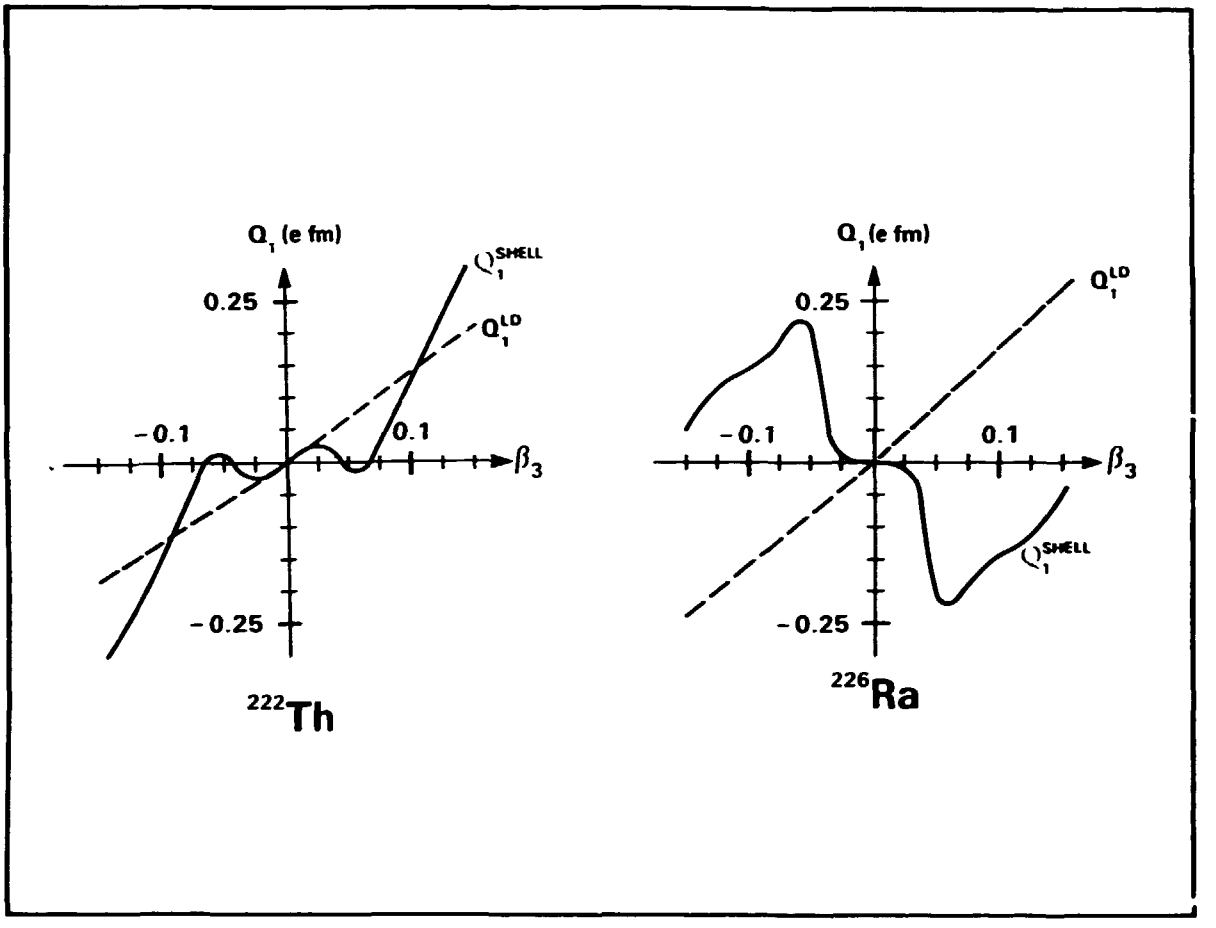

Fig. 5.9. The shell-correction and liquid-drop contributions to the intrinsic electric dipole moment, plotted vs. octupole deformation β_3 for ^{222}Th and ^{226}Ra. The calculated equilibrium shapes occur at $|\beta_3| \approx 0.1$. Note at these equilibrium shapes the coherent sign of the two contributions in ^{222}Th and the cancellation in ^{226}Ra, which explains the order of magnitude difference in the B(E1)/B(E2) ratios for these two nuclei (c.f. Fig. 5.8).

rotation-aligned quasiparticles crosses the reflection asymmetric ground band at high spin ($I \approx 26$ in ^{222}Th). The lighter isotopes, ^{218,220}Ra and ^{220}Th, have spherical ground states, but under rotation they acquire reflection asymmetric shapes which persist up to very high spins.

Experimentally, alternating parity yrast sequences and an absence of quasiparticle alignment phenomena have been observed at very high spins, $I > 30$, for some rare-earth nuclei. Initial cranking model calculations[36] have provided examples, such as ^{168}Yb, where reflection asymmetric equilibrium shapes occur at the appropriate spins in the appropriate nuclei and help to explain the data.

In order to better understand the systematic effects of reflection asymmetric deformation on rotation and backbending, a schematic cranked two-j-shell model was considered.[42] The contribution of the two j-shells to the collective ground-band moment of inertia is increased by reflection asymmetry. Backbending may still occur but is less likely, because the admixture of the lower-j shell decreases the number of zeros in the interband interaction matrix element $V(\lambda_F)$, increases the average amplitude of

Table 5.1. Theory vs experiment for the B(E1)/B(E2) branching ratios in doubly even Ra-Th nuclei. Column 1 indicates the approximate region of angular momentum, column 2 gives the rotational model branching ratio obtained from the E1 and E2 moments at the equilibrium shape, and column 3 gives the experimental branching ratios, which may have sizeable uncertainties.

Nucleus	<I> (ħ)	B(E1)/B(E2) (fm^{-2}) TH.	EXP.
^{218}Ra	12	$5.0\ 10^{-6}$	$3\ 10^{-6}$
^{220}Ra	9	$1.1\ 10^{-6}$	$1\ 10^{-6}$
	17	$2.3\ 10^{-7}$	
^{222}Ra	5-12	$3\ 10^{-7}$	
	21	$8\ 10^{-8}$	
^{224}Ra	8	$2\ 10^{-7}$	$1\ 10^{-7}$
	23	0	
^{226}Ra	3-11	$3\ 10^{-8}$	$< 2\ 10^{-7}$
	24	$3\ 10^{-8}$	
^{220}Th	13	$2.5\ 10^{-6}$	$1.9\ 10^{-6}$
^{222}Th	0-12	$2.0\ 10^{-6}$	$2\ 10^{-6}$
	26	0	
^{224}Th	5-14	$1.6\ 10^{-6}$	
^{226}Th	6	$9.6\ 10^{-7}$	$4\ 10^{-7}$
	20	0	
^{228}Th	8	$9\ 10^{-8}$	$8\ 10^{-8}$
	15	0	

$V(\lambda_F)$, and reduces the quasiparticle alignment.

The effect that 'spectator' quasiparticles have on backbending due to angular momentum coupling is being investigated.[43] In the cranking model, quasiparticles have little effect unless they polarize the self-consistent fields, as is further discussed below. In core-particle coupling to good angular momentum, however, each state contains a superposition of several core states and therefore the core backbends are smoothed in the coupled system.

Widespread experimental progress is being made in charting out bands and band crossings, and theoretical cranking calculations can be helpful in characterizing the observed structures. Thus, alignment phenomena observed in experiments on ^{185}Au and ^{184,186}Hg could be ascribed to the alignment of $i_{13/2}$ neutrons and

ORNL-DWG 85-18104

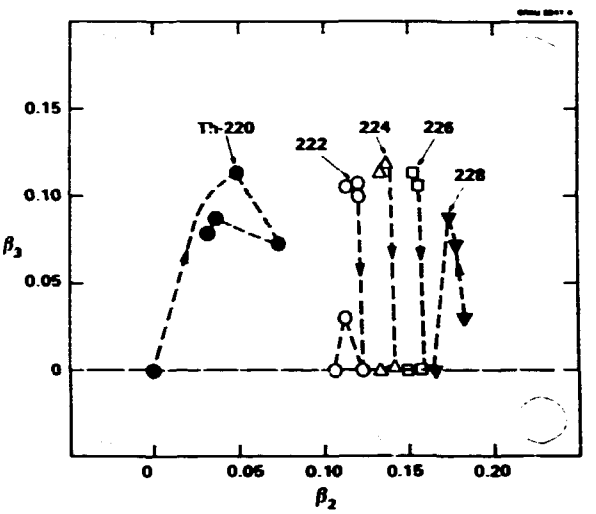

Fig. 5.10. Calculated evolution of the equilibrium shape with rotation for the nuclei $^{220-228}$Th, in terms of the quadrupole (β_2) and octupole (β_3) deformation coordinates.

$h_{9/2}$ protons at similar rotational frequencies and for prolate shape.[30,44] An unexpected band observed in ^{185}Au was identified as predominantly $f_{7/2}$. The yrast band of ^{163}Lu could be identified as $h_{11/2}$ on the basis of signature splitting and M1 rates.[45] Many bands have been observed in ^{133,135}Pr; the present status of interpretation[45] is that negative γ-deformations and neutron band-crossings are not observed, contrary to expectations based on ^{134}Ce data and on theory.

A simple method to calculate the gamma deformation-driving effect of rotating quasiparticles is to minimize the total Routhian of a semiclassical core plus rotating quasiparticles with respect to γ. Such calculations have now been repeated for the N=88 and 90 nuclei,[46] using microscopic moments of inertia for the core instead of phenomenological expressions. Transitions to $\gamma = +60°$, where the rotation is noncollective, are obtained at spins which agree with experiment. On the basis of a more fully microscopic calculation, the observed yrast levels of ^{158}Yb had previously been proposed to exhibit band termination due to such a transition to the noncollective regime.[47] A mechanism

has also been found to explain why the negative-parity sideband in this nucleus, ^{158}Yb, is collective up to much higher rotational frequency than the yrast band.[45] The excited neutron $i_{13/2}$ Routhian, denoted C in cranking model terminology, is found to be strongly γ deformation driving away from +60°. The sideband is obtained by occupying this Routhian instead of an $h_{9/2}$ Routhian which drives towards +60°.

Cranked Woods-Saxon-Bogoliubov calculations for the Pt-Au-Hg region are in progress, in order to determine the equilibrium shapes in β, γ, and β_4 for different configurations as a function of spin.[48] The goal is a consistent description of all the bands in this region. The I=0 potential-energy surfaces are available at this stage. They support prolate-oblate shape coexistence in the A<190 Pt as well as Hg isotopes.

When sufficiently systematic measurements of high-spin states are available, it becomes possible to obtain 'double' Routhians, meaning that the collective energy of rotations in both configuration space and gauge space are subtracted out.[49] Double Routhians have been constructed for $^{159-170}$Yb and used to compare the correlations at high and low spins in different configurations.

The M1 transition rates at high spin can be valuable probes of nuclear structure. They have previously been calculated by methods with a limited range of applicability. A method based on the cranking model which could be applied to very high spins and the quasicontinuum is now being examined.[50] The nucleus is divided into one active quasiparticle and a rotor core. The g-factor of the core is obtained by projecting the magnetic moment and angular momentum of its microscopic cranking wave function on the cranking axis. Experimental data for 1- and 3-quasiparticle bands of ^{159}Tm are reproduced. Further tests of this method versus models and experiments are in progress.

The merit of the triaxial rotor plus particle model in connection with the signature dependence of M1 properties has previously been expounded in the literature. This model was applied[51] to new data on branching and mixing ratios in ^{75}Kr. An 'effective' value of $(g_K-g_R)^2/Q_0^2$ can be extracted from either of these ratios using the strong-coupled rotational model formulas. In Fig. 5.11 the rotational model formulas have been applied to the experimental and triaxial rotor branching and mixing ratios in the 5/2[422] band of ^{75}Kr. Experiment and theory agree on a substantial reduction of the effective $(g_K-g_R)^2/Q_0^2$ below the strong-coupling value, and on the staggering between the signatures obtained from the branching ratios. However, conflicting signature splitting is obtained from the mixing ratios. The domain of validity of the model remains to be established.

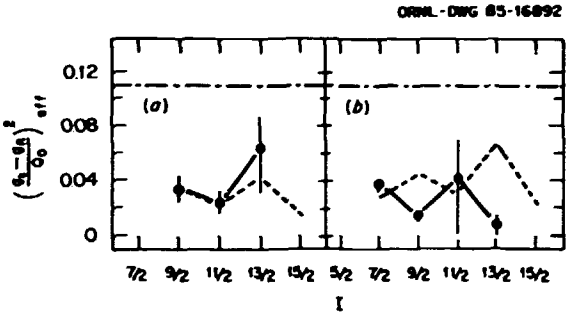

Fig. 5.11. The ratio $(g_K-g_R)^2/Q_0^2$ in the 5/2[422] band of ^{75}Kr obtained by a rotational model interpretation of inband branching ratios (left) and mixing ratios (right) from experiment (points and solid lines) and from a triaxial rotor plus Nilsson quasiparticle coupling calculation (dashed lines). Note the anomalous signature splitting from the mixing ratios.

Quasicontinuum Spectroscopy

T. Bengtsson[8] Y.-s. Chen[10,33]
G. A. Leander[1]

The experimental study of nuclei at high spin and finite temperature by quasicontinuum gamma-ray spectroscopy is undergoing rapid development. The design of both the experiments and the multidetector arrays with which they are carried out is becoming more sophisticated. On

the theory side, two approaches are being followed. One is to explore microscopic models in search of spectral features that might also show up in experimental quasicontinuum spectra. The other is to carry out Monte Carlo cascade calculations that simulate the experiments.

The microscopic model is usually some form of the cranking model. For example, the so-called dynamical or second rotational moment of inertia can be calculated for a number of bands, if the average field is adjusted self-consistently within each band separately, and the results may be compared with E_γ-E_γ correlations in the quasicontinuum spectrum.[52-54] Another approach is to look for many strong M1 transitions of about the same energy in the cranked single-particle spectrum, which might give rise to a bump at that transition energy in the quasicontinuum spectrum. For example, the quasicontinuum data on ^{158}Yb exhibit a bump around E_γ = 2.5 MeV which emerges from the spin region I = 40-50. Theory predicts triaxial structures with ε = 0.4 and γ = 20° in precisely this spin region, with a bunching of strong M1 transitions near the energy of the observed bump.[45]

The Monte Carlo code GAMBLE for gamma cascade calculations underwent significant development during the past year.[55] In order to simulate the bias toward higher gamma-ray energies caused by competition from particle emission, without a full-blown evaporation calculation in GAMBLE itself, the effective level density for gamma transitions is defined as $\rho_{eff} = \rho\, f_e/f_p$, where f_e is the entry distribution and f_p the total pass-through distribution for the final nucleus under consideration. Spreading of the collective E2 strength in the quasicontinuum plays a role in the pathway problem and for E_γ-E_γ correlations, and some alternative phenomenologies for the spreading were developed. Notably, if the B(E2) distribution is Gaussian, $N(\omega,\sigma)$, around the inband transition energy, ω, then the T(E2) distribution is to a very good approximation Gaussian, $N(\bar{\omega},\bar{\sigma})$, with

$$\bar{\omega} = \tfrac{1}{2}\left(\omega + \sqrt{\omega^2 + 20\sigma^2}\right);\quad \bar{\sigma} = \sigma\bar{\omega}\sqrt{\omega^2 + 5\sigma^2}$$

Selection of gamma-ray cascades on the basis of the spin spectrometer observables H and K, as opposed to E and I or M, was implemented. The evaluation of H,K-gated experimental spectra is in progress.[56,57] Yrast feeding patterns, E_γ-E_γ correlations and difference spectra for different H,K are being studied as functions of the nuclear structure input.

---

1. UNISOR, Oak Ridge Associated Universities.
2. University of Arizona, Tucson, AZ 85721.
3. ZfK Rossendorf, Dresden, GDR.
4. Centre de Recherches Nucléaires, Strasbourg, France.
5. Texas Instruments Corp., Dallas, TX 75265.
6. Lawrence Livermore National Laboratory, Livermore, CA 94550.
7. Cornell University, Ithaca, NY 14853.
8. Lund University, Lund, Sweden.
9. Los Alamos National Laboratory, Los Alamos, NM 87545.
10. Joint Institute for Heavy Ion Research, Oak Ridge.
11. Warsaw Technical Institute, Warsaw, Poland.
12. Université de Bordeaux, Gradignan, France.
13. Georgia Institute of Technology, Atlanta, GA 30332.
14. National Superconducting Cyclotron Laboratory, Michigan State University, East Lansing, MI 48824.
15. Rutgers University, New Brunswick, NJ 08903.
16. Institute of Modern Physics, Lanzhou, People's Republic of China.
17. J. A. Bounds et al., BAPS 30, 777 (1985); Phys. Rev. Lett., in press.
18. H. K. Carter et al., Proc. ACS Symp. on Recent Advances in the Study of Nuclei Off the Line of Stability, Chicago, 1985, ed. R. A. Meyer, in press.
19. R. L. Mlekodaj et al., ibid.
20. A. F. Barfield and O. Scholten, Phys. Lett. B, submitted; A. F. Barfield, J. L. Wood, and B. R. Barrett, current work.
21. A. F. Barfield and B. R. Barrett, Phys. Lett. 149B, 277 (1984) and current work.
22. P. B. Semmes, G. A. Leander, and J. L. Wood, in Interacting Boson-Boson and Boson-Fermion Systems, ed. O. Scholten (World Scientific, Singapore, 1985), p. 208; A. F. Barfield and P. B. Semmes, current work.
23. G. A. Leander, P. B. Semmes, and F. Dönau, ibid., p. 167.
24. P. B. Semmes et al., Phys. Rev. C, submitted.
25. O. Ballon et al., Phys. Rev. C, submitted.
26. W. Nazarewicz et al., Proceedings Contributions Niels Bohr Centennial Conference on Nuclear Structure, Copenhagen, 1985, p. 91; current work.

27. A. J. Larabee et al., Phys. Lett. B, submitted.
28. J.-y. Zhang, L. L. Riedinger, and A. J. Larabee, Phys. Lett. B, to be submitted.
29. G. A. Leander et al., in Atomic Masses and Fundamental Constants, ed. O. Klepper (GSI, Darmstadt, 1984) p. 466.
30. P. Möller, G. A. Leander, and J. R. Nix, Z. Physik, submitted.
31. University of Tennessee, Knoxville, TN 37916.
32. Oak Ridge National Laboratory.
33. Institute of Nuclear Energy, Beijing, People's Republic of China.
34. G. A. Leander, in "Nuclear Structure 1985," ed. by R. A. Broglia, G. B. Hagemann, and B. Herskind, Copenhagen, 1985 (Elsevier Science, Amsterdam, 1985) p. 249.
35. W. Nazarewicz, G. A. Leander, and J. Dudek, Proceedings Contributions Symposium on Electromagnetic Properties of High-Spin States, Stockholm, 1985; Nucl. Phys. A, to be submitted.
36. J. Dudek, W. Nazarewicz, and G. A. Leander, Proceedings Contributions Niels Bohr Centennial Conference on Nuclear Structure, Copenhagen, 1985, p. 40; Phys. Lett. B, to be submitted.
37. G. A. Leander, AIP Conf. Series 125 (American Institute of Physics, New York, 1985) 125.
38. G. A. Leander et al., Nucl. Phys. A, submitted.
39. C. W. Reich, I, Ahmad, and G. A. Leander, "E1 Transition Probabilities Within the $K^{\pi}=1/2^{\pm}$ Parity-Doublet Bands in ^{225}Ra," Physics Letters B, submitted for publication (1985).
40. G. A. Leander, Y.-s. Chen, and W. Nazarewicz, current work.
41. W. Nazarewicz et al., Nucl. Phys. A429, 269 (1984).
42. W. Nazarewicz and P. Olanders, Phys. Rev. C 32, 602 (1985).
43. P. B. Semmes, Y.-s. Chen, and G. A. Leander, current work.
44. W. C. Ma et al., Phys. Lett. B, submitted.
45. Y.-s. Chen et al., current work.
46. Y.-s. Chen, S. Frauendorf, and L. L. Riedinger, to be published.
47. I. Ragnarsson et al., Phys. Rev. Lett. 54, 978 (1985).
48. J.-y. Zhang et al., current work.
49. J.-y. Zhang et al., Nucl. Phys. A, submitted.
50. Y.-s. Chen, G. A. Leander, and P. B. Semmes, current work.
51. M. A. Herath-Banda et al., J. Phys. G, in press.
52. H. El-Samman et al., Nucl. Phys. A427, 397 (1984).
53. H. El-Samman et al., Proc. Int. Symp. on In-Beam Nuclear Spectroscopy, Debrecen, Hungary (Akademiai Kiado, Budapest, 1984) p. 177.
54. J. Gizon et al., Contr. Niels Bohr Cent. Conf. on Nuclear Structure, Copenhagen, 1985, p. 91.
55. G. A. Leander, current work.
56. A. J. Larabee et al., BAPS 30, 761 (1985); current work.
57. G. A. Leander and I.-Y. Lee, current work.

COLLECTIVE M1 STATES IN THE CLASSICAL LIMIT OF THE NEUTRON-PROTON INTERACTING BOSON MODEL[1]

A. B. Balantekin[2] B. R. Barrett[3]

The recent discovery[4] of the collective magnetic-dipole excitation mode in ^{156}Gd has renewed interest in such modes. Although such a mode had been predicted and discussed in earlier work,[5] the motivation for the ^{156}Gd experiment was provided by the neutron-proton Interacting Boson Model[6] (IBM-2). In earlier work[7] we looked at potential energy surfaces in the classical limit of IBM-2. We expanded our previous work by including the appropriate kinetic energy terms in the IBM-2 Hamiltonian to study the properties of collective 1^+ states. By writing the Hamiltonian in the form

$$H = \frac{1}{2}\mu\dot{\chi}^2 + V(\beta_{\pi_0}, \beta_{\nu_0}, \gamma_\pi = \gamma_\nu = 0, \chi)$$

where χ is the angle between the static deformed valence neutron (β_{ν_0}) and proton (β_{π_0}) distributions, we obtain the energy of the collective M1 mode as $\sqrt{2D/\mu}$ where

$$D = \frac{\partial^2 V}{\partial \chi^2}$$

and

$$\mu = \frac{m_\pi m_\nu}{m_\pi + m_\nu}$$

with

$$\frac{1}{m_\rho} = \left(\frac{\partial^2 H}{\partial \rho_\rho{}^2}\right)\Bigg|_{\text{all } \rho = 0}$$

This result can be used to determine the excitation energy in the classical limit as a first-order approximation.

---

1. Summary of paper: Phys. Rev. C 32, 288 (1985).
2. Eugene P. Wigner Fellow.
3. University of Arizona, Tucson, AZ 85721.
4. D. Böhle et al., Phys. Lett. 137B, 27 (1984).
5. N. Lo Iudice and F. Palumbo, Phys. Rev. Lett. 41, 1532 (1978).
6. F. Iachello, Nucl. Phys. A358, 89c (1981).
7. A. B. Balantekin, B. R. Barrett, and S. Levit, Phys. Lett. 129B, 153 (1983).

A NEW SUPERSYMMETRY CHAIN FOR THE DESCRIPTION OF ODD-ODD Au NUCLEI[1]

A. B. Balantekin[2] V. Paar[3]

Recent dynamical supersymmetry schemes[4] have been very successful in studying correlations between the energy spectra and the electromagnetic transition probabilities of even-even, odd-even, and odd-odd nuclei. A new possibility arises when the dimension of the unpaired proton subspace is equal to the dimension of the unpaired neutron subspace in which case it is possible to construct the dynamical supersymmetry chain starting with the decomposition

$$U(6/2m) \supset U_B(6) \times U_F(2m) \supset U_B(6) \times Sp_F(2m)$$

The most appealing aspects of this chain are that (a) it emphasizes the residual interaction between the unpaired fermions, and (b) it distinguishes the unpaired fermions which are particle-like from those which are hole-like. A typical spectrum predicted by this scheme for the odd-odd gold isotopes is shown in Fig. 5.12. Contrary to the previous attempts,[4] a comparison of the predictions of this new scheme with the experimental spectra for ^{196}Au and ^{198}Au is very encouraging.

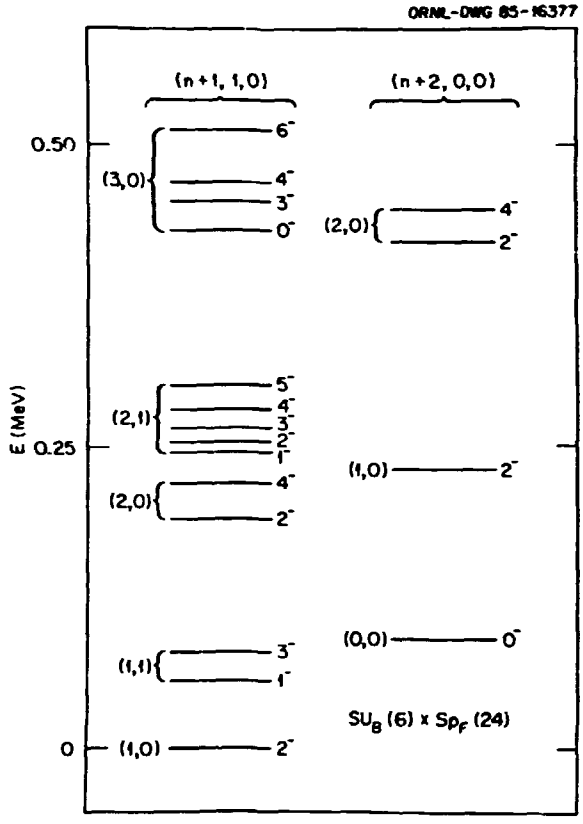

Fig. 5.12. A typical spectrum predicted by the $U_B(6) \times Sp_F(2m)$ scheme for the odd-odd Au isotopes.

1. Summary of paper submitted to Physical Review Letters.
2. Eugene P. Wigner Fellow.
3. University of Zagreb, Zagreb, Yugoslavia.
4. P. Van Isacker et al., Phys. Rev. Lett. 54, 653 (1985).

EXACTLY SOLVABLE BOSON-FERMION HAMILTONIANS AS A GENERALIZATION OF THE PAIRING HAMILTONIAN

A. B. Balantekin[1]

The general form of the boson-fermion interaction in the Interacting Boson-Fermion Model (IBFM) Hamiltonian contains many different parameters. Consequently, it is not practical to analyze the spectra of odd-even nuclei using this general form. However, using a microscopic approach in the context of the shell model, one can simplify the boson-fermion interaction considerably. In this simplified form, there is an exchange interaction which takes into account the fact that bosons are correlated fermion pairs. It is given by[2]

$$V = \sum_{jj'j''} \left[A^{j''}_{jj'} \, (a^\dagger_j \tilde{d})^{(j'')} \cdot (d^\dagger a_{j'})^{(j'')} \right]^{(0)} .$$

where $A^{j''}_{jj'}$ can be related to the single-particle occupation properties.

We have studied an extremely simplified version of the IBFM Hamiltonian for the case of bosons with angular momenta 0 and 1 and fermions occupying the j=1/2 orbital. It turns out that a Hamiltonian which includes a pairing term for the bosons in addition to the exchange interaction given above, can be exactly solved using the noncompact orthosymplectic supergroup Osp(2/2). An extension of this work to more realistic cases is currently under investigation.

1. Eugene P. Wigner Fellow.
2. O. Scholten, Ph.D. thesis, University of Groningen, 1980.

CLASSICAL DESCRIPTION, CLASSIFICATION, AND QUANTIZATION OF COMPLICATED NUCLEAR COLLECTIVE MOTION

M. Baranger[1] K.T.R. Davies

Complicated nuclear collective motion may be bound or unbound. Bound collective motion leads to families of collective energy levels connected by collective transitions. Unbound collective motion leads to elastic or inelastic scattering of heavy nuclei and nuclear fragments. In both cases, a manageable description exists in terms of a time-dependent Hartree-Fock (TDHF) approximation or some similar mean-field approach. In this approach, the nuclear wavefunction is essentially a wavepacket in the space of the collective coordinates, or of the one-body density, and therefore the approximation contains a large classical element. Hence, it is not capable of describing the features of individual energy levels and transitions, or the finer features of the scattering. If one wants it to do these things, it has to be requantized.

Our work is concerned with this requantization both for the bound and for the unbound case. Up to this point, however, we have put most of our emphasis on the bound case, and we shall restrict ourselves to it for the remainder of this report. We do have several new ideas on how to deal with the unbound case, i.e., the scattering of heavy ions, and we are considering developing them in the future.

Let us start by discarding two obvious ideas. (1) If the collective motion can be linearized, then the well-known random phase approximation can be used. Unfortunately, most nuclear collective motion is not linear. (2) One could adopt some kind of ad hoc quantization procedure, for instance Pauli quantization, as was done in the old work of Baranger and Kumar.[2] This idea is deficient for many reasons: it is arbitrary; it assumes the existence of a quadratic kinetic energy, which can be a bad approximation; and generally its accuracy is outdated for modern experiments and theory. Something better must be done.

The solution that we know, the TDHF solution, is classical in appearance; therefore the problem is similar to that faced originally by the founders of quantum mechanics: how to go from classical trajectories to stationary state wavefunctions and energy levels. The complete, correct way to do this is the Schroedinger equation, of course. However, the TDHF method does not present us with a simple, low-dimensional Hamiltonian, from which some reasonably solvable Schroedinger equation could be obtained. Rather, TDHF is a multidimensional formalism, in which the collective and the single-particle degrees of freedom are inextricably mixed up. The only relatively simple thing that one knows how to do with TDHF is to calculate the multidimensional, classical trajectories. Hence the problem is more like the Bohr-Sommerfeld quantization problem, i.e., going directly from trajectories to energy levels. Do we know an exact way of doing this?

This is a very famous, unsolved problem, to which an enormous amount of literature has been devoted in the last 15 years.[3] Much interest has been directed to the distinction between regular and chaotic classical trajectories, and how this affects quantization.[4] Of course, WKB provides an immediate approximate solution for a one-dimensional system, and the so-called "integrable" multidimensional systems can be quantized in the same way, but this is the trivial case: such systems are exceedingly rare. The classical dynamics of nonintegrable systems is very complicated and still badly understood. We see that anyone seeking to quantize TDHF trajectories gets drawn into it unavoidably.

One of us has shown[5] that exact energy levels can be obtained from classical trajectories in the form of series expansions. This is a fully quantal treatment in which the zeroth-order wavefunction consists of a moving wavepacket (for a one-body problem) or a TDHF wavefunction (for a many-fermion problem). The series involves an infinite set of diagrams, requiring a complete time-dependent basis. It turns out that this expansion is possible only when the zeroth-order wavefunction is periodic. This is the motivation for the study of <u>periodic classical trajectories</u>. However, even in the simplest

two-dimensional nonintegrable problems, the classification and the topology of periodic trajectories can be very complicated. Their study rejoins the studies of chaos,[6] which have been so popular recently for quite different reasons.

We have found that periodic trajectories occur in one-parameter families, which can be plotted as continuous lines in the plane of τ (the period) and E (the energy). No line ever ends; rather, the various families branch into each other in a variety of ways, and the resulting plot looks like an infinite tree. We have a systematic method for finding all of the branches of this tree. Moreover, each branch can be either stable or unstable, and our methods work equally well for both kinds. This is important, because people who work on chaos are used to following one stable family, with the consequence that they miss the unstable branches, but these unstable branches could lead them to discover some previously unknown stable branches.

The distinction between stable and unstable trajectories is crucial, because we have reasons to believe that the series expansion mentioned earlier, which is formally equal to an exact energy level, will be convergent when the trajectory is stable and divergent when it is unstable. If this is so, we shall have a quantization method yielding exact energy levels from the regular regions of classical phase space, but not from the chaotic regions.

To return to nuclear physics, the main conclusion of our work so far is that it should be possible to identify collective coordinates by looking for periodic solutions of the TDHF equations, which is something that we know now how to do in a systematic way. We should not be so naive as to expect a totally clean separation between collective and other coordinates. Even in the simplest cases[7] there will be branches, resonances, and other interactive phenomena. We can confidently expect, however, that the main collective branches will be stable (as they are in Ref. 7), and therefore quantization should be straightforward.

---

1. Massachusetts Institute of Technology, Cambridge, MA 02139.
2. M. Baranger and K. Kumar, Nucl. Phys. A122, 241 (1968).
3. For a review, see for instance M. Berry, "Semiclassical Mechanics of Regular and Irregular Motion," Lectures given at the Nordita School on Chaos, June 1982.
4. See Ref. 3 or, as an illustrative example, E. J. Heller, Phys. Rev. Letts. 53, 1515 (1984).
5. I. Zahed and M. Baranger, Phys. Rev. C 29, 1010 (1984); M. Baranger, to be published.
6. See, for instance, J. M. Greene et al., Physica 3D, 468 (1981).
7. Such as potential V_1 in K.T.R. Davies et al., "Exploring the Tree of Periodic Trajectories for Two Non-Integrable Two-Dimensional Potentials," this report.

HOT BUBBLE AND ROTATING TOROIDAL NUCLEI[1]

Jing-Ye Zhang[2] Cheuk-Yin Wong

As nuclear temperature increases, the surface tension coefficient decreases and the Coulomb repulsion is effective in pushing the nuclear matter outward, leading to the formation of toroidal and bubble nuclei. We obtain the threshold temperatures, above which these nuclei are stable against symmetry-preserving distortions. They are found to decrease with the mass number. We further examine the effect of nuclear rotation for which the centrifugal force is also effective in pushing the nuclear matter outward. For a given angular momentum, we calculate the temperature threshold above which a toroidal nucleus is stable against symmetry-preserving distortions. The temperature threshold for a hot and rotating toroidal nucleus is lower than that for a nonrotating nucleus.

---

1. Summary of paper: Phys. Rev. Lett. 55, 1973 (1985) and paper to be published.
2. Guest assignee from Institute of Modern Physics, Lanzhou, People's Republic of China.

THE SYMPLECTIC SHELL-MODEL THEORY OF COLLECTIVE STATES[1]

J. Carvalho[2] M. Vassanji[2]
R. Le Blanc[2] D. J. Rowe[2]
J. B. McGrory

The implications of the microscopic structure of collective Lie algebras and their hydrodynamic (contraction) limits are explored. A decomposition of the nuclear Hilbert space into collective subspaces and symplectic shells is proposed. The resultant symplectic shell model is shown to provide a basis for microscopic calculations which are immediately interpretable in collective model terms.

---

1. Abstract of paper submitted to Nuclear Physics A.
2. University of Toronto, Toronto, Ontario M5S 1A7, Canada.

POSITRON PRODUCTION IN STRONG ELECTROMAGNETIC FIELDS

NEW PARTICLE PRODUCTION IN HEAVY-ION COLLISIONS[1]

A. B. Balantekin[2] M. R. Strayer
C. Bottcher S. J. Lee[3]

It was suggested some time ago that positrons would be emitted nonperturbatively[4] from the vacuum in low-energy collisions of heavy ions with a combined charge greater than 173 as a result of the diving of the 1s state into the negative energy continuum. The spectra of positrons emitted from the center of mass of the heavy-ion system have been studied experimentally; in particular, some sharp lines were identitified.[5] The existence of such peaks were attributed to the possible existence of nuclear reactions with a very long time delay. Formation of quasimolecular nuclear configurations with a lifetime of 10^{-20} sec or more has been proposed[6] as a possible mechanism to obtain such a delay time. However, our present understanding of such systems requires that the energy of the peak change considerably from system to system. For systems studied experimentally so far, the sharp lines in the positron emission spectra occur at approximately the same positron kinetic energy of 300 keV, with integrated cross sections of about 200 μb and with widths less than approximately 70 keV.[7]

We have shown that the production and subsequent decay of a new neutral, pseudoscalar particle is a viable alternative explanation of the sharp peaks in the positron emission spectra to the formation of a long-lived superheavy nuclear complex. The mass of this particle is about 1.6 ~ 1.7 MeV and its lifetime is approximately 10^{-13} sec. The existence of such a particle is demonstrated to be consistent with all presently known experimental, observational, and theoretical limits. It is further shown that if this particle exists, it is not the standard axion, and it must be produced by nuclear and/or nonperturbative electromagnetic processes.

There are two experimental tests to confirm the validity of our interpretation of the heavy-ion data. First, in the heavy-ion reactions it is desirable to measure the yield versus invariant mass by detecting electrons and positrons in coincidence. Second, it would be possible to observe such particles directly in electron-positron collisions in the appropriate energy range.

---

1. Summary of paper: Phys. Rev. Lett. 55, 461 (1985).
2. Eugene P. Wigner Fellow.
3. Predoctoral guest assignee from Yale University.
4. W. Greiner, ed. Quantum Electrodynamics of Strong Fields (Plenum, N.Y., 1983).
5. J. Schweppe et al., Phys. Rev. Lett. 51, 2261 (1983); M. Clemente et al., Phys. Lett. 137B, 41 (1984).
6. U. Heinz et al., Ann. Phys. (N.Y.) 151, 227 (1983).
7. T. Cowan et al., Phys. Rev. Lett. 54, 1761 (1985).

POLYELECTRON P^{++-} PRODUCTION IN HEAVY-ION COLLISIONS[1]

Cheuk-Yin Wong

We explore the possibility of whether the anomalous positron peak observed recently in heavy-ion experiments may be due to the polyelectron[2] P^{++-}. The decay of P^{++-} with the emission of a photon leads to a positron with a kinetic energy of 340.66 keV which coincides

with the recently observed anomalous positron peak to within the experimental error.

---

1. Abstract of paper submitted for publication in Physical Review Letters.
2. J. A. Wheeler, Ann. N.Y. Acad. Sci. 48, 219 (1946).

PAIR PRODUCTION AT GeV/u ENERGIES[1]

C. Bottcher M. R. Strayer

Electron and positron production in relativistic ion-atom collisions is discussed within the context of the time-dependent Dirac-Hartree approximation to a fully relativistic field theory of the collision. The time-dependent fields are treated classically, and the numerical methods employing basic splines are discussed in detail and contrasted with results obtained from the case of nonrelativistic velocities. The results of a one-dimensional model are presented and show a moderately large probability for pair production followed by electron capture.

---

1. Abstract of paper to be published in Proceedings of the Atomic Theory Workshop on Relativistic and QED Effects in Heavy Atoms, Washington, DC, May, 1985.

RELATIVISTIC NUCLEAR MODELS

THE TIME-DEPENDENT DIRAC EQUATION (TDDE) WITH RELATIVISTIC MEAN-FIELD DYNAMICS APPLIED TO HEAVY-ION SCATTERING[1]

R. Y. Cusson[2] H. Stöcker[4]
P.-G. Reinhard[3] M. R. Strayer
J. J. Molitoris[4] W. Greiner[5]

We treat the relativistic propagation of nucleons coupled to scalar and vector meson fields in a mean-field approximation. The time-dependent Dirac (TDDE) and mean meson field equations are solved numerically in three dimensions. Collisions of ^{16}O(300, 600, and 1200 MeV/nucleon) + ^{16}O are studied for various impact parameters. The TDDE results are compared to other recent theoretical approaches. The TDDE calculations predict spallation, large transverse momentum transfer and positive angle sidewards flow, in qualitative agreement with the data in this energy regime.

---

1. Abstract of paper submitted to Physical Review Letters.
2. Consultant from Duke University, Durham, NC 27706.
3. University of Erlangen, Erlangen, West Germany.
4. Michigan State University, East Lansing, MI 48824.
5. Consultant from University of Frankfurt, Frankfurt, West Germany.

RELATIVISTIC HARTREE CALCULATIONS FOR AXIALLY SYMMETRIC NUCLEI

S. J. Lee[1] M. R. Strayer
P.-G. Reinhard[2] A. B. Balantekin[3]
A. S. Umar[4]

Most of the relativistic calculations for finite nuclei have been carried out for spherical systems.[5,6] Such calculations test only the relativistic propagation of nucleons in nuclei indirectly via their density and momentum dependence induced by the small components of the Dirac wavefunctions. However, the detailed shell structure of deformed nuclei provide a much wider range of experimental data to test relativistic nuclear shell models. Axially symmetric deformed nuclei require a representation in at least two spatial dimensions. We have derived the relativistic expressions for the axially symmetric nuclei starting from the Lagrangian density which is constituted of nucleon, scalar meson, and vector meson fields. The coupling of the nucleon fields is through a vector meson field and a nonlinear scalar field.[7]

For axial symmetry, we can eliminate the azimuthal angle dependence in the field equations and therefore need only to consider r and z variables in a cylindrical coordinate system. We first discretized the action of the system with $r = (i-1/2)Dr$ and $z = (j-1)Dz$, where Dr is the step size in r direction and Dz in z direction. We apply the variational method on this discretized action to obtain the equations of motion for each of the fields. To eliminate the

fermion doubling problem,[8] we have used different mesh points for each component of the nucleon field, i.e., (r,z) = ((i-1/2)Dr, (j-1)Dz) for spin-up of large components of the nucleon field, (iDR, (j-1/2)Dz) for spin-down of large components, ((i-1/2)Dr, (j-1/2)Dz) for spin-up of small components, and (iDR, (j-1)Dz) for spin-down of small components. The one-dimensional dispersion relation for free Dirac particles on this lattice is E**2-m**2 = [2sin(kDz/2)/Dz]**2 where k is the wavenumber instead of the usual result [2sin(kDz)/Dz]**2. The latter result, as shown in Fig. 5.13, has the doubling of the spectrum.

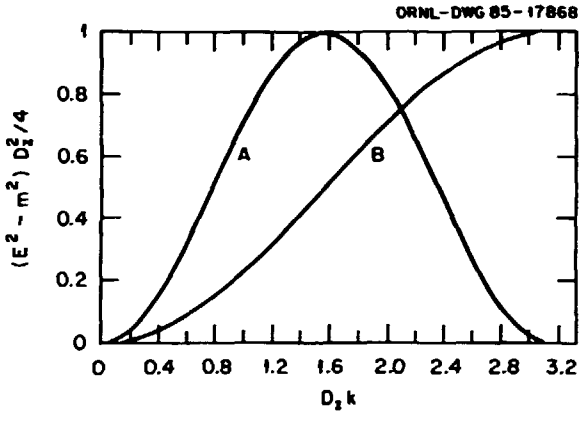

Fig. 5.13. (a) normal spectrum, (b) fermion doubled spectrum.

To solve these equations numerically for finite nuclei, we have used the damped gradient iteration method for the discretized Dirac equation and Gaussian elimination methods for the discretized Helmholtz equations. To check the validity of this method, we are applying this method to the structure of spherical nuclei such as ^{16}O.

---

1. Predoctoral guest assignee from Yale University, New Haven, CT 06510.
2. University of Erlangen, Erlangen, West Germany.
3. Eugene P. Wigner Fellow.
4. University of Pennsylvania, Philadelphia, PA 19104.
5. C. J. Horowitz and B. D. Serot, Nucl. Phys. A368, 503 (1981).
6. L. D. Miller, Phys. Rev. C 9, 537 (1974).
7. J. D. Walecka, Ann. Phys. (N.Y.) 83, 491 (1974).
8. C. M. Bender, K. A. Milton, and D. H. Sharp, Phys. Rev. Lett. 51, 1815 (1983).

ONE-DIMENSIONAL HARTREE MEAN-FIELD MODEL OF RELATIVISTIC HEAVY-ION COLLISIONS

M. R. Strayer C. Bottcher

Walecka and his associates[1] have proposed a covariant description of nuclear processes at intermediate and high energies, in which all strong interactions are mediated by classical massive boson fields. They refer to this approach as Quantum Hadro-Dynamics (QHD). If a single scalar field ϕ and a single vector field V_μ are introduced, the equations describing the baryon spino· field ψ as it evolves along with the meson fields, have the form

$$i\frac{\partial\psi}{\partial t} = [-i\gamma_0\vec{\gamma}\cdot\vec{\nabla} + M_B\gamma_0 + g_S\gamma_0\phi + g_V\gamma_0\gamma_\mu V^\mu]\psi \quad (1)$$

$$(\partial_t^2 - \nabla^2 + M_S^2)\phi = g_S\langle\bar{\psi}\psi\rangle \quad (2)$$

$$(\partial_t^2 - \nabla^2 + M_V^2)V_\mu = g_V\langle\bar{\psi}\gamma_\mu\psi\rangle \quad (3)$$

The meson couplings and masses are adjusted to fit nuclear structure data.

Most of the literature on this model to date is concerned with static solutions. Time-dependent solutions of (1)-(3) describing heavy-ion collisions have indeed been carried out for a limited number of velocities, but the numerical techniques used were cumbersome and failed to resolve questions associated with current and gauge conservation. We believe that our new basic-spline collocation methods (described elsewhere in this report) represent a great improvement, and they are being applied in a pilot study of the 1D form of (1)-(3). If the numerical problems are resolved, it will be possible to obtain from the model a fully covariant description of ultrarelativistic heavy-ion collisions.

---

1. J. D. Walecka, Ann. Phys. (N.Y.) 83, 491 (1974).
2. R. Y. Cusson et al., ORNL Ann. Rept., p. 171 (1984).

INTERMEDIATE-ENERGY HEAVY-ION PHYSICS

NUMERICAL SIMULATION OF MEDIUM-ENERGY HEAVY-ION REACTIONS[1]

J. Aichelin[2] G. Bertsch[3]

Reactions between heavy ions at medium energy are calculated using the Boltzmann-Uehling-Uhlenbeck equation. This equation incorporates the effects of a mean field as well as Pauli blocking of the nucleon-nucleon collisions. The numerical solution for two light systems, ^{16}O + ^{12}C at 25 AMeV bombarding energy and ^{12}C + ^{12}C at 84 AMeV bombarding energy, is presented and discussed in detail. In the absence of nucleon-nucleon collisions, the theory reduces to classical mean-field physics and agrees well with the quantal time-dependent Hartree-Fock theory. With collisions, the system is driven toward equilibrium even at the lower bombarding energy. The final-state nucleon distribution is compared to single-particle spectra and is found to agree quite well in shape.

---

1. Abstract of paper: Phys. Rev. C 31, 1730 (1985).
2. Max-Planck Institut für Kernphysik, Heidelberg, West Germany.
3. Michigan State University, East Lansing, MI 48824.

PROBING HEAVY-ION COLLISIONS WITH BREMSSTRAHLUNG[1]

Che-Ming Ko[2] G. Bertsch[3]
J. Aichelin[4]

We calculate bremsstrahlung spectra for intermediate-energy heavy-ion collisions to see the sensitivity of photon cross sections to reaction dynamics. Modeling the collisions with the intranuclear cascade, we find a clear collective quadrupole bremsstrahlung signal only for heavier nuclei, A > 40. Maximum sensitivity to dynamics is likely to be for photons in the range of 10-30 MeV. For higher-energy photons or lighter nuclei, there is a large background coming from the incoherent dipole component of the bremsstrahlung.

---

1. Abstract of paper: Phys. Rev. C 31, 2324 (1985).
2. Texas A & M University, College Station, TX 77843.
3. Michigan State University, East Lansing, MI 48824.
4. Max-Planck Institut für Kernphysik, Heidelberg, West Germany.

LAMBDA PRODUCTION FROM ANTI-PROTON ANNIHILATION IN NUCLEI[1]

Che-Ming Ko[2] G. F. Bertsch[3]
J. Aichelin[4]

The lambda particle production in $\bar{p}$-nucleus annihilation is estimated due to multiple interactions of $\bar{p}$ and interactions of the secondary pions produced in the annihilation. We find an enhancement over the $\bar{p}$-p production of a factor of ~100, compared with the experimentally measured value of ~400.

---

1. Abstract of paper submitted to Physical Review C.
2. Texas A & M University, College Station, TX 77843.
3. Michigan State University, East Lansing, MI 48824.
4. Max-Planck Institut für Kernphysik, Heidelberg, West Germany.

HYPERNUCLEUS PRODUCTION IN HEAVY-ION COLLISIONS[1]

Che-Ming Ko[2]

In terms of the participant-spectator model for high-energy heavy-ion collisions, the probability that a hyperon is created from the participants directly in the nuclear single-particle states of the spectator fragment is evaluated. It is found that the magnitude of the cross section for producing a hypernucleus depends on both the lifetime of the hyperon source and the impact parameter of the reaction.

---

1. Abstract of paper: Phys. Rev. C 32, 326 (1985).
2. Texas A & M University, College Station, TX 77843.

KAON AS A PROBE TO THE NUCLEAR EQUATION OF STATE[1]

J. Aichelin[2] Che-Ming Ko[3]

The production of kaons from heavy-ion collisions is sensitive to the nuclear equation of

state. In the Boltzmann-Uehling-Uhlenbeck model, the number of produced kaons from central collisions between heavy nuclei at incident energies around 700 MeV/nucleon can differ by a factor 2-3, depending on the equation of state.

---

1. Abstract of paper submitted to Physical Review Letters.
2. Max-Planck Institut für Kernphysik, Heidelberg, West Germany.
3. Texas A & M University, College Station, TX 77843.

ULTRA-RELATIVISTIC HEAVY-ION COLLISIONS

STOPPING OF HEAVY NUCLEI IN RELATIVISTIC HEAVY-ION COLLISIONS[1]

Cheuk-Yin Wong

We examine the space-time dynamics of the baryons in nucleus-nucleus collisions and estimate the energy density reached in the central rapidity region. It is found that with an incident laboratory energy of 15 GeV per projectile nucleon, a head-on collision of Au on Au will leave a substantial spatial region with an energy density of 1.5-3 GeV/fm^3 which may exceed the energy density for a quark-gluon plasma formation.

---

1. Abstract of paper submitted for publication in Physical Review.

TRANSVERSE-MOMENTUM DISTRIBUTION OF PRODUCED PARTICLES IN ULTRA-RELATIVISTIC NUCLEUS-NUCLEUS COLLISIONS[1]

Ban-Hao Sa[2] Cheuk-Yin Wong

In order to discern coherent or collective processes from incoherent processes in nucleus-nucleus reactions at high energies, we study the transverse-momentum distribution of the produced particles with an incoherent-multiple-collision model. In this model, the projectile nucleon makes successive inelastic collisions with nucleons in the target nucleus, the probability of such collisions being given by the thickness functin and the nucleon-nucleon inelastic cross section. It is assumed that each baryon-baryon collision produces particles and degrades momenta just as a baryon-baryon collision in free space, and that there are no secondary collisions between the produced particles and the nucleons. We found that the average transverse momentum and the charged-multiplicity data at Fermilab and CERN ISR energies can be well explained by such a model. However, the average transverse momentum for some events observed by the Japanese-American Cooperative Emulsion Experiment (JACEE) associated with large energy density in the central rapidity region differ markedly from the model results. Such a deviation indicates the presence of coherent or collective effects for these collisions and may indicate the possibility of a formation of quark-gluon plasma.

---

1. Abstract of paper: Phys. Rev. D 32, 1706 (1985).
2. Institute of Atomic Energy, Beijing, People's Republic of China.

TRANSVERSE MOMENTUM DISTRIBUTIONS OF π^0 AND ITS PRODUCT GAMMA RAYS[1]

Cheuk-Yin Wong

We study the relationship between the transverse momentum distribution of the π^0 and that of its product gamma rays. A new relationship between the average transverse momenta is obtained by taking into account the mass of the pion. The correlation between the average transverse momentum and energy density as observed in the Japanese-American Cooperative Emulsion Experiment is discussed.

---

1. Abstract of paper to be published in Physical Review D (in press).

RAPIDITY DISTRIBUTION OF PRODUCED PARTICLES IN NUCLEON-NUCLEON COLLISIONS[1]

Cheuk-Yin Wong

We parametrize the rapidity distribution of the produced charged particles in nucleon-nucleon collisions in terms of simple functions of the light-cone variables. The unknown constants in the parametrization are fixed by using

the data of average multiplicities, the rapidity densities at the central rapidity region and the rapidity distribution at $\sqrt{s}$ = 540 GeV. Energy losses due to particle production are inferred from the parametrized distribution.

---

1. Abstract of paper to be submitted for publication in Physical Review D.

PHOTON BREMSSTRAHLUNG FROM ULTRA-RELATIVISTIC NUCLEAR COLLISIONS[1]

Che-Ming Ko[2] Cheuk-Yin Wong

The photon bremsstrahlung spectra from nucleus-nucleus collisions at ultrarelativistic energies are calculated using the proton spectra obtained in a multiple scattering model. At small laboratory angles they are sensitive to the law of stopping when nucleons of one nucleus pass through the other nucleus.

---

1. Abstract of paper: Phys. Rev. C 33, 153 (1986).
2. Cyclotron Institute, Texas A & M University, College Station, TX 77843.

ATOMIC PHYSICS

MULTIPLE VACANCY PRODUCTION BY HIGH-ENERGY HEAVY IONS[1]

R. L. Becker A. L. Ford[2]
J. F. Reading[2]

Multiple vacancy production (MVP) is a signature for and probe of strong interactions between an ionic projectile and the target electrons. Its theoretical description requires a unitary, nonperturbative treatment, now available in the coupled-channels theory of atomic collisions.[3,4] For special problems, analytically tractable models have been devised. For example, a simple, unitary, "geometrical encounter probability" model for the calculation of $p_L(o)$, the inclusive L-shell vacancy probability per electron in collisions with impact parameter B = 0, has been introduced.[5] Along with earlier coupled-channels calculations[6,7] and first Magnus calculations,[7] this model is able to describe the "saturation" of $p_L(o)$ with projectile charge, Z_p, whereas all first-order theories predict $p_L \propto Z_p^2$, which eventually exceeds unity. We have previously reviewed[7] some of the new measurements and calculations of MVP in close collisions detected through K_α X-ray or Auger satellites (K^1L^v holes) and hypersatellites (K^2L^v), especially those comparing satellites and hypersatellites for the same collision systems, and those for rather highly charged ions. In the last two years, there have been exciting new measurements of MVP in primarily distant collisions, with experimental separation of those reactions involving, or not involving, electron transfer to the projectile (e.g., DuBois[8]). The distributions for the number of (primarily outer shell) vacancies in coincidence with charge transfer are distinctly nonbinomial in character; they lack the v=0 component of a binomial distribution.

Aside from our work, the atomic structure theory used for MVP has always ignored correlations between the vacancies. We have termed[9] the conventional model a single-particle model (SPM) because it uses quantum mechanics only for single-electron transitions and obtains the cross sections for multiple vacancy production by combining single-electron probabilities, not complex-valued quantal amplitudes. The SPM distribution of multiple vacancies is binomial. Our work has involved generalizing from the SPM to the independent Fermi particle model (IFPM), which is obtained by working at all stages with an antisymmetrized many-electron wavefunction.[9] In the case of multiple outer-shell vacancies in coincidence with one or two electron transfers to the K-shell of the projectile, we report here for the first time that the IFPM gives strongly nonbinomial distributions in which for single charge transfer the v=0 component, and for double transfer the v=0 and v=1 components, are negligible. There is a Pauli correlation between the transferred electron and the electron vacated from the outer shell. This result is in agreement with our earlier finding[3] that there

is a large effect of Pauli correlations on the cross section for electron transfer in coincidence with a vacancy in the target K-shell.

---

1. Summary of paper: Proceedings of Second Workshop on High-Energy Ion-Atom Collisions, Debrecen, Hungary, August 1984, ed. D. Berényi and G. Hock (Akademiai Kiado, Budapest, 1985), pp. 141-154.
2. Consultant from Texas A & M University, College Station, TX 77843.
3. R. L. Becker, A. L. Ford, and J. F. Reading, J. Phys. B: Atom. Mol. Phys. 13, 4059 (1980).
4. J. F. Reading, A. L. Ford, and R. L. Becker, J. Phys. B: Atom. Mol. Phys. 14, 1995 (1981).
5. B. Sulik, G. Hock, and D. Berényi, J. Phys. B: Atom. Mol. Phys. 17, 3239 (1984).
6. R. L. Becker, A. L. Ford, and J. F. Reading, Nucl. Instr. Meth. B3, 43 (1984).
7. R. L. Becker, A. L. Ford, and J. F. Reading, Nucl. Instr. Meth. B4, 271 (1984).
8. R. D. DuBois, Phys. Rev. Lett. 52, 2348 (1984).
9. R. L. Becker, A. L. Ford, and J. F. Reading, Phys. Rev. A29, 3111 (1984).

THEORY OF K^nL^v MULTIPLE VACANCY PRODUCTION BY HEAVY IONS[1]

R. L. Becker A. L. Ford[2]
J. F. Reading[2]

Observation of intensities of K_α X-ray or Auger satellites and hypersatellites together with fluorescence yields provides knowledge of KL^v and K^2L^v vacancy distributions produced by ion-atom collisions. The traditional theory used since about 1972 employs a single-particle model and a weak-coupling ionization approximation. We review our recent extensions of the theory to include Pauli correlations in the independent-Fermi-particle model, a unitary collision theory in the first Magnus and coupled-channels approximations, electron transfer to the projectile, and contributions from shakeoff which interfere with the collision-induced amplitudes.

---

1. Abstract of invited paper presented at the Eighth International Conference on the Application of Accelerators in Research and Industry, published in Nucl. Instrum. and Meth. B10/11, 1 (1985).
2. Consultant from Texas A & M University, College Station, TX 77843.

MULTIPLE-ELECTRON PROCESSES IN H^+ + (He,Ne) COLLISIONS AT 300 keV[1]

R. L. Becker

Pauli exchange terms (PET's) play an important role in the Hartree-Fock independent-Fermi-particle model (IFPM) of atomic structure, but are usually neglected in ion-atom collisions. We have developed the IFPM formulation of collision theory over the past few years.[2] It was applied first to close collisions: (a) K-vacancy production in coincidence with charge transfer,[3] in which the PET's strongly correct the single-particle-model (SPM),[2,4] leading to a cross section close to that of the single-electron-transition (SET) model;[5,4] and (b) K^mL^v multiple-vacancy distributions for K_α satellites ($m = 1$) and hypersatellites ($m = 2$), where the sum of PET's is small because of a tendency toward random phases in the transition amplitudes[6] so that the distributions are determined by the mean L-shell vacancy per electron, $\bar{p}_L^{(m)}$. More recently, we have applied the IFPM to more distant collisions, corresponding to coincidence measurements (summarized in Ref. 7) of the final projectile and target charges, in which target K-shell vacancies are not detected. The calculations were done with the coupled-channels method in the single-center-expansion approximation (see Ref. 3) or with our "one-and-a-half center" expansion (OHCE).[8] The cross sections will be denoted[7] by $\sigma_{qq'v}$ where q and q' are the initial and final ionic charges of the projectile and v is the final number of vacancies in the target. We also define cross sections for inclusive electron ejection,

$$\sigma_{11}^{e^-} = \Sigma\, v\, \sigma_{11v},\ \sigma_{10}^{e^-} = \Sigma\, (v-1)\sigma_{10v},\ \sigma^{e^-} = \sigma_{11}^{e^-} + \sigma_{10}^{e^-},$$

single-electron capture,

$$\sigma_{10} = \sum_{v=1}^{N} \sigma_{10v},$$

and noncapture ("direct") ionization,

$$\sigma_{11} = \sum_{v=1}^{N} \sigma_{11v}$$

(N = 2 for He and 8 for Ne).

Hippler et al.[9] have measured the energy and angle of an ejected energetic ("δ") electron in H^+ + (He,Ne,Ar) at 300 keV, together with the final charge v of the recoiling target, obtaining values of

$$\frac{d^2\sigma_v^{e^-}}{d\Omega_\delta dE_\delta} = v\,\frac{d^2\sigma_{11v}}{d\Omega_\delta dE_\delta} + (v-1)\,\frac{d^2\sigma_{10v}}{d\Omega_\delta dE_\delta}$$

for v = 2 and 3(Ne) relative to v = 1. Additional unpublished work in which q' instead of v is measured gives the ratio of ejection plus transfer to total ejection,

$$\frac{d^2\sigma_{10}^{e^-}}{d\Omega_\delta dE_\delta}\Big/\frac{d^2\sigma^{e^-}}{d\Omega_\delta dE_\delta}.$$

They have suggested that the cross sections differential in E_δ could give information on the impact-parameter dependence of the transition probabilities, and proposed that ejection at energy E_δ comes predominantly from b = $hv_p/(I+E_\delta)$, where I is the ionization potential.

We have calculated the impact-parameter dependent IFPM probabilities for all of the above processes. The PET terms are important for all transitions involving charge transfer. Integration over b gives good agreement with measured σ_{10}, σ^{e^-}, and the cross section for non-v-weighted vacancy production, $\sigma_{11} + \sigma_{10}$. In neon our K_α-satellite $\bar{p}_L$ value, 0.100, is close to the experimental 0.105.[10] The impact-parameter dependence suggests that electrons of high energy E_δ correspond to values of b larger than those of the equation above by factors of two or more. Calculations for argon are in progress.

---

1. Summary of paper presented at the 14th International Conference on the Physics of Electronic and Atomic Collisions published in Electronic and Atomic Collisions, ed. by M. J. Coggiola, D. L. Huestis, and R. P. Saxon (Palo Alto, 1985) p. 454.

2. R. L. Becker, J. F. Reading, and A. L. Ford, IEEE Trans. Nucl. Sci. NS-28, 1092 (1981); R. L. Becker, A. L. Ford, and J. F. Reading, Phys. Rev. A 29, 3111 (1984).

3. R. L. Becker, A. L. Ford, and J. F. Reading, J. Phys. B 13, 4059 (1980).

4. R. L. Becker, A. L. Ford, and J. F. Reading, Proceedings Eighth Conference on the Application of Accelerators in Research and Industry, Nucl. Instrum. and Meth. B10/11, 1 (1985).

5. R. L. Becker, A. L. Ford, and J. F. Reading, Proceedings Second International Seminar on High Energy Ion-Atom Collisions, ed. by G. Hock and D. Berényi (Akadémiai Kiadó, Budapest, 1985), p. 141.

6. R. L. Becker, A. L. Ford, and J. F. Reading, Nucl. Instrum. and Meth. B4, 271 (1984).

7. D. Dubois, Phys. Rev. Lett. 52, 2348 (1984).

8. J. F. Reading, A. L. Ford, and R. L. Becker, J. Phys. B 14, 1995 (1981).

9. R. Hippler, J. Bossler, and H. O. Lutz, J. Phys. B 17, 2453 (1984).

10. J. O. Christensen and Finn Folkmann, International Symposium on Production and Physics of Highly Charged Ions (Stockholm, 1982), contrib. papers, p. 55.

IFPM THEORY AND OHCE CALCULATIONS OF SINGLE AND DOUBLE K-VACANCY PRODUCTION BY $Cl^{(15-17)+}$ IN Ti

R. L. Becker

In 1981 James Hall, Pat Richard, and collaborators presented the first systematic study[1] of double K-shell to K-shell electron transfer in heavy-ion-atom collisions. K_α X rays were detected with resolution sufficient to distinguish hypersatellites (K^2L^v holes) from satellites (KL^v). This separated the inclusive K-vacancy production cross section (σ_K) into double (σ_{K^2}) and single ($\sigma_{K^1} = \sigma_K - 2\sigma_{K^2}$) vacancy components. The vacancies can be produced by excitation, direct ionization, transfer to the projectile K-shell ($\bar{K}$), or transfer to higher shells of the projectile. To isolate the contribution of transfer to $\bar{K}$, they varied the ionic charge of the projectile. As the initial number of electrons on the projectile is decreased, the cross sections σ_{K1} and σ_{K2} jump upward for hydrogenic and again for bare projectiles. The jumps are attributed to single and double transfer, respectively, to the projectile $\bar{K}$ shell. Additional experiments followed.[2] Recently, new work involving six collaborators from ORNL (Pepmiller, Gregory, Miller, Moak, C. Jones, and Alton) has appeared.[3] In all of these works the K-to-K transfer cross sections have been inferred only indirectly. In particular, a number

of assumptions have been made, e.g., that the direct ionization cross section is independent of the ionic charge of the projectile. Moreover, in the calculations employed, different methods were used for the direct ionization and for the electron transfer, and the transfer calculations were done with a simple two-state model which allows only K-to-$\bar{K}$ and 2K-to-2$\bar{K}$, but not transfer and ionization from the K-shell nor double transfer to $\bar{K}$ from K and L or from L^2.

To put the theoretical analysis on a better footing, we have made coupled-channels calculations with our one-and-a-half center (OHCE) method and have included Pauli exchange terms with our independent-Fermi-particle model (IFPM). The direct ionization and electron transfer are calculated, thereby, in the same framework and transfers from shells above the K-shell and combined transfer and direct ionization are included. We find that when the projectile has an initial hole in its $\bar{K}$ shell, the opening of the channel for electron transfer to the $\bar{K}$ shell can affect the direct ionization channel, either reducing or enhancing it (depending on the impact speed). We also find significant contributions from $\sigma_{K1}^{\bar{K}2}$ (double capture into the $\bar{K}$ shell and a single K-vacancy) and $\sigma_{K2}^{\bar{K}1}$ (single capture into the K shell and two K vacancies). It is suggestd that measurement of the ionization cross sections for these collisions, as a function of the ionic charge of the projectile, would provide valuable additional information.

---

1. J. Hall et al., Phys. Rev. A 24, 2416 (1981).
2. J. Hall et al., Phys. Lett. 90A, 129 (1982); J. Hall et al., Phys. Rev. A 28, 99 (1983).
3. J. Hall et al., Bull. Am. Phys. Soc. 30, 885 (1985) and paper submitted to Physical Review A.

CALCULATIONS OF K_α X-RAY, IONIZATION, AND EXCITATION-IONIZATION COINCIDENCE CROSS SECTIONS IN $He^{2+} + {}_{14}Si^{11+}$ COLLISIONS

R. L. Becker

In connection with their research program at the Triangle Universities Nuclear Laboratory on resonant and non-resonant electron transfer to the projectile accompanied by excitation of the projectile, S. Schafroth, J. Anthony, and collaborators have made complementary measurements of the coincidence cross section for combined excitation and ionization of the projectile unaccompanied by capture of an electron from the target. Their first experiments[1] were for lithium-like silicon incident on He for E/A = 0.5 to 3.4 MeV. Our interest in electron-electron correlations, which sometimes show up in coincidence measurements, has led us to perform coupled-channels calculations for these experiments. We neglect the electrons on the helium atom target and consider $He^{2+} + Si^{11+}$, regarding Si as the target. Heretofore, our independent-Fermi-particle model (IFPM) formalism had been used only for targets with all shells closed. Si^{11+} provided an initial, simple case for the generalization to an open shell.

Our inclusive ionization cross section is in good agreement with the singles data. It is mostly from ionization of the L-shell (2s) electron and shows the expected peak near E/A = 0.6 MeV corresponding to the matching of the projectile and 2s-electron speeds. Our inclusive K_α X-ray cross section is slightly lower than experimental singles data at all energies when we assume a fluorescence yield of one. A fluorescence yield of ~0.3 (Ref. 2) would appear to be too low. A reinvestigation of the fluorescence yield is called for. The coincidence cross section data and calculation (again assuming unit fluorescence yield) are shown in Fig. 5.14. The full curve lies below the data by about the same ratio as for the K_α cross section. With the convention that the 2s electron initially has its spin up, the dashed curve is the contribution in which a 2p↑ state is excited (either from the 2s or the 1s) and the dotted (lowest) curve is the contribution in which a 2p↓ state is excited from the 1s shell. The 2p↑ contribution contains the effect of Pauli correlations between the two spin-up electrons. Further work on this calculation will separate the contributions of all the important transitions and

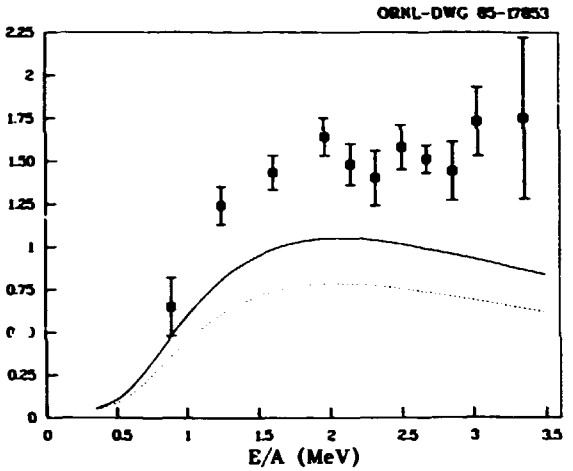

Fig. 5.14. Cross section for a projectile K_α X ray in coincidence with single-ionization of the projectile in Si^{11+} + He collisions. The data are from Ref. 1. The theoretical curves are described in the text.

exhibit the Pauli exchange terms. Experiments and calculations for Ne and Ar targets are in progress. We hope these will sharpen the results concerning both the fluorescence yield and the Pauli correlations.

---

1. M. Clark et al., in Electronic and Atomic Collisions, ed. by M. J. Coggiola, D. L. Huestis, and R. P. Saxon (Palo Alto, 1985), p. 398.

2. B. L. Doyle et al., Phys. Rev. A 17, 523 (1978).

IONIZATION PROCESSES IN TRANSITION METAL IONS[1]

M. S. Pindzola[2] D. C. Griffin[3]
C. Bottcher

In the last decade, experiment and theory have shown[4] that indirect resonance processes may make substantial contributions to the electron-impact ionization of transition metal ions in low stages of ionization. Contributions to the electron-impact single-ionization cross section can be made by the following processes,

$$e^- + A^{q+} \rightarrow A^{(q+1)+} + e^- + e^-, \qquad (1)$$

$$e^- + A^{q+} \rightarrow (A^{q+})^* + e^- \qquad (2)$$
$$\hookrightarrow A^{(q+1)+} + e^-,$$

and

$$e^- + A^{q+} \rightarrow (A^{(q-1)+})^* \qquad (3)$$
$$\hookrightarrow (A^{q+})^* + e^-$$
$$\hookrightarrow A^{(q+1)+} + e^-,$$

where A represents an arbitrary ion with charge q. The first process is called direct ionization, the second excitation-autoionization, and the third resonant-recombination double autoionization. Contributions to the electron-impact double-ionization cross section can also be made by the following processes,

$$e^- + A^{q+} \rightarrow (A^{(q+1)+})^* + e^- + e^- \qquad (4)$$
$$\hookrightarrow A^{(q+2)+} + e^-,$$

and

$$e^- + A^{q+} \rightarrow (A^{q+})^* + e^- \qquad (5)$$
$$\hookrightarrow (A^{(q+1)+})^* + e^-$$
$$\hookrightarrow A^{(q+2)+} + e^-.$$

The first process is called ionization-autoionization and the second excitation-double autoionization.

Though other processes are possible, these are of most interest in fusion plasmas. We are engaged in a survey of (1)-(5) for all stages of ionization of the stainless steel impurities present in such plasmas, notably iron. Our approach is to make an initial survey using configuration average approximations, e.g., if the initial state belongs to the complex $3p^5 3d^2$, we average over all LS terms in this complex. If some case shows interesting features or anomalies, or the average approximation is dubious for any reason, we carry out calculations with full allowance for intermediate coupling in the final state. Recently we have developed the ability to include configuration interactions as well, e.g., the mixing of $3p^5 3d^2$ with $3p^3 3d^4$. For systems with several d-electrons, considerable optimization of algorithms is needed to

make these calculations feasible at all. A single case may still take several hours to run on a Cray-XMP.

We began with low stages of ionization as described in Ref. 5, and have now reached Fe^{13+} in the iron sequence. The single ionization cross section is plotted as a function of electron impact energy in Fig. 5.15. The enhancement due to the indirect process (2) is about a factor of 3 over a wide range.

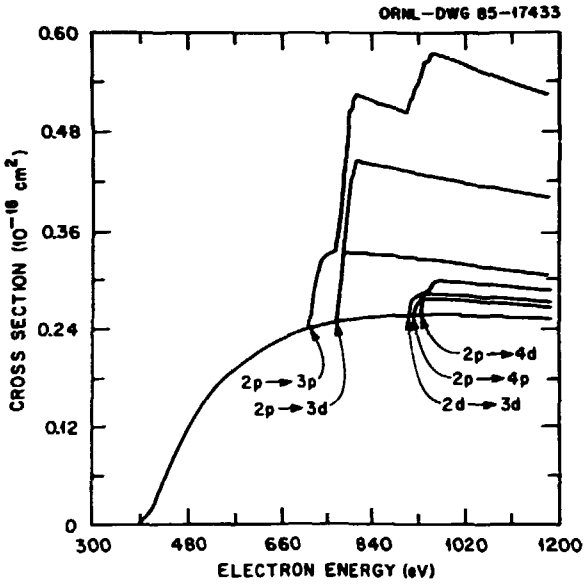

Fig. 5.15. Electron-impact, single-ionization cross section of Fe^{13+}. Thresholds for various excitation-ionization processes are indicated by arrows.

Much interesting physics is contained in these cross sections. We cite two examples. In low stages of ionization, double ionization can be comparable with single due to process (3). This is the case[5] in Fe^{2+}. In higher stages, low-lying metastable states (living longer than 1 μs) can dominate ionization both in plasmas and beam experiments, which appears to be the case in Fe^{9+}. Metastable states are discussed further elsewhere in this section and in the Experimental Atomic Physics section of this report.

---

1. Summary of paper submitted for publication in Nuclear Fusion.

2. Consultant from Auburn University, Auburn, AL 36849.

3. Consultant from Rollins College, Winter Park, FL 32789.

4. D. H. Crandall, in "Physics of Electron and Atomic Collisions; Invited Papers of the XII ICPEAC," ed. S. Datz (North-Holland, Amsterdam, 1982), p. 595.

5. M. S. Pindzola et al., ORNL/TM-9436 (1985).

DIELECTRONIC RECOMBINATION IN EXTERNAL ELECTRIC FIELDS[1]

D. C. Griffin[2] M. S. Pindzola[3]
C. Bottcher

Dielectronic recombination (DR) can be thought of as a two-step process. In the first step, a free electron collisionally excites an N-electron ion and is simultaneously captured into a doubly excited autoionizing state of the (N+1)-electron ion:

$$e^- + X_i(Z,N) \rightarrow X_j^{**}(Z,N+1). \qquad (1)$$

It can then autoionize back to the initial state i, or to an excited state k of the N-electron ion:

$$X_j^{**}(Z,N+1) \rightarrow X_k^{*}(Z,N) + e^-. \qquad (2)$$

However, it can also emit a photon and decay to an excited state f of the (N+1)-electron ion:

$$X_j^{**}(Z,N+1) \rightarrow X_f^{*}(Z,N+1) + h\nu. \qquad (3)$$

If this state is below the first ionization limit of the (N+1)-electron ion, it will be stable, and the DR process will be complete.

We have considered DR transitions associated with $\Delta n=0$ excitations. For such transitions within high temperature plasmas, recombination through the multitude of doubly excited Rydberg states with very high-principal quantum numbers will normally dominate the total DR process. Therefore, the cross section will be very sensitive to the existence of external electric fields, which surely are present in plasmas and electron-ion beam experiments. First of all, such fields can ionize electrons in high-Rydberg states and thereby decrease the DR rate. Secondly, electric fields redistribute the angular momentum among the doubly excited Rydberg

states which tends to open up more recombination channels and enhance the rate of dielectronic recombination.

In an earlier study[4,5] we examined the systematics of field mixing in dielectronic recombination in the Li and Na isoelectronic sequences by employing the configuration-average and linear-Stark approximations. This provided physical insight into field-mixing effects and enabled us to determine the maximum field enhancement of DR cross sections as a function of ionization stage. More recently, we have performed extensive distorted-wave calculations of dielectronic recombination as a function of electric field strength. The intermediate-coupled, field-mixed eigenvectors used to represent the doubly excited Rydberg states were determined by diagonalizing a Hamiltonian which includes the spin-orbit, internal electrostatic, and Stark matrix elements. These calculations then properly take into account the mixing between individual doubly excited states with the same value of n but different values of ℓ due to the presence of an external electric field. However, as in earlier studies, we do not include mixing between Rydberg states with different values of n, and we ignore the effect that the electric field may have on the incoming continuum electron.

Studies are complete on the alkali-like ions extensively investigated by means of the merged-beam experiment at ORNL (described in the Experimental Atomic Physics section of this report).[6] A typical comparison of theory and experiment is shown in Fig. 5.16. The data are fit by the calculation corresponding to the mean field in the collision region of the apparatus (25 V/cm).

These calculations are very expensive and, unfortunately, they have not so far suggested any simple model for the variation of cross section with field, especially at very low field values (< 10 V/cm).

---

1. Summary of paper submitted for publication in Physical Review A.
2. Consultant from Rollins College, Winter Park, FL 32789.
3. Consultant from Auburn University, Auburn, AL 36849.
4. D. C. Griffin, M. S. Pindzola, and C. Bottcher, Atomic Excitation and Recombination in External Fields, eds. M. H. Nayfeh and C. W. Clark, Harwood Academic Publishers, New York, 1985.
5. D. C. Griffin, M. S. Pindzola, and C. Bottcher, Oak Ridge National Laboratory Report ORNL/TM-9478.
6. P. F. Dittner et al., Physical Review A, submitted for publication.

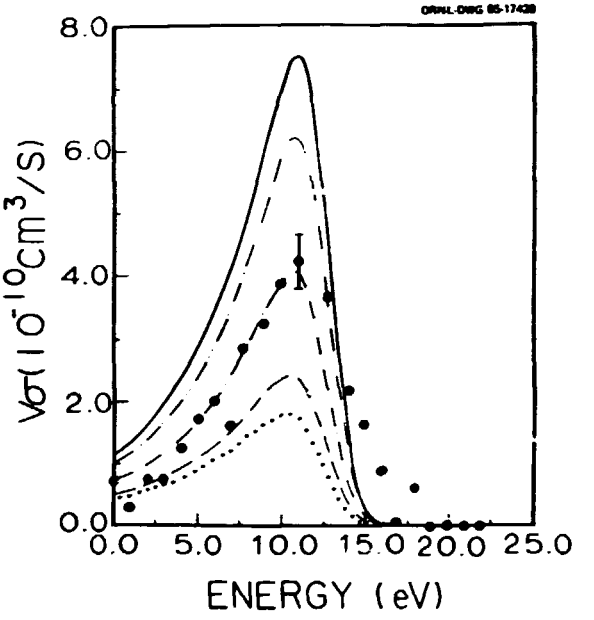

Fig. 5.16. Theoretical values of the dielectronic recombination rate coefficients for S^{5+} (as measured in the electron-ion merged-beam experiment) as a function of electron energy for five different electric fields in the interaction region. .... F=0 V/cm; —— F=5 V/cm; -.-.- F=25 V/cm; -..-..- F=125 V/cm; —— F=625 V/cm. The calculations include all resonances up to $n_{max} = 63$. The circles are the experimental data from Ref. 6.

ROLE OF METASTABLE STATES OF COMPLEX IONS IN CROSSED-BEAM EXPERIMENTS[1]

M. S. Pindzola[2] D. C. Griffin[3]
C. Bottcher

We have studied the contributions of excitation-autoionization to the electron-impact ionization of several multiply charged ions in the magnesium isoelectronic sequence. The largest contributions are due to 2p→3p monopole and 2p→3d dipole excitations which are of current

interest in short wavelength laser research.[4] The recent experimental crossed-beams measurements of Howald et al.[5] for S^{4+}, Cl^{5+}, and Ar^{6+} show a clean separation between sizable excitation-autoionization features and the background direct ionization process at incident electron energies around twice the ionization threshold. These measurements present a clear challenge to theoretical interpretation and calculation.

Electron-impact ionization of an atomic ion labeled A can follow two paths:

$$e^- + A^{n+} \rightarrow A^{(n+1)+} + e^- + e^-, \qquad (1)$$

or

$$e^- + A^{n+} \rightarrow (A^{n+})^* + e^-, \quad \lfloor \rightarrow A^{(n+1)+} + e^-. \qquad (2)$$

The first process is direct ionization, while the second is excitation-autoionization. It is assumed that these processes are independent and that radiative stabilization of the autoionization states is negligible for low stages of ionization along the Mg isoelectronic sequence. This latter assumption was tested by explicit calculation of branching ratios for several of the doubly excited configurations considered in this paper.

Most of the calculations were performed using the average-configuration distorted-wave approximation. The energy spread within configurations was then established by a procedure we call the average-statistical model (ASM), in which the total cross section is divided among the levels of the final complex according to the statistical weights of the various terms. For S^{4+} in the threshold energy region, we compared the ASM with a detailed intermediate-coupled level-to-level calculation. Except for some refined details, the ASM is acceptable.

Results for S^{4+} are shown in Fig. 5.17 and compared with experimental crossed-beams measurements of Howald et al.[5] over a wide energy range. Although the overall agreement is quite good, three discrepancies were noted: (a) The ionization threshold is too low. (b) The experimental excitation-autoionization features are spread over a wider energy interval than predicted by theory. (c) Experiment and theory diverge increasingly above 240 eV. The same discrepancies were repeated in Cl^{5+} and Ar^{6+}.

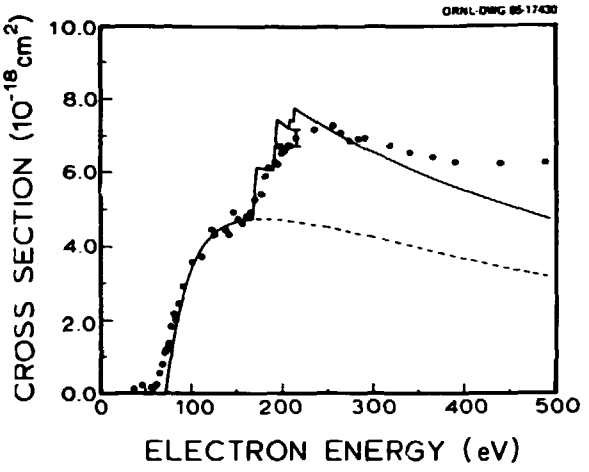

Fig. 5.17. Electron impact ionization of S^{4+}. Solid curve: total cross section from the $2p^63s^2$ ground configuration in the average statistical model; dashed curve: direct cross section only; solid circles: experimental measurements (Ref. 5).

The puzzle was resolved by repeating the calculations for ions initially in the metastable $2p^63s3p^3P$ state, which lives longer than the transit time through the apparatus. These results are compared with the same data in Fig. 5.18; the discrepancies are seen to be resolved. The data are consistent with between 50% and 100% metastables in the beam for all the ions studied.

We believe that low-lying metastable states will dominate the measured cross sections for many highly ionized species. They may also dominate the physics of the same species in plasmas, including X-ray laser plasmas, where they may help to resolve the longstanding disagreement between observations and computer simulations.

---

1. Abstract of paper submitted for publication in Physical Review A.
2. Consultant from Auburn University, Auburn, AL 36849.

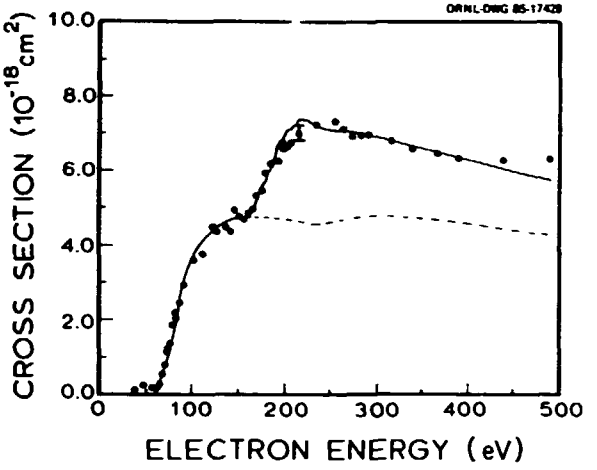

Fig. 5.18. Electron impact ionization of S^{4+}. Solid curve: total cross section from the $2p^6 3s3p$ excited configuration in the average statistical model; dashed curve: direct cross section only; solid circles: experimental measurements (Ref. 5).

3. Consultant from Rollins College, Winter Park, FL 32789.

4. P. Hagelstein, in Atomic Physics 9, eds. R. S. Van Dyck, Jr. and E. N. Fortson (World Scientific, Singapore, 1984).

5. A. M. Howald et al., submitted to Physical Review A. C.f. also the Experimental Atomic Physics section of this report.

THEORY OF ELECTRON-IMPACT IONIZATION NEAR THRESHOLD[1]

C. Bottcher

We have continued to study the Peterkop model of low-energy ionization, based on the Schroedinger equation

$$\left\{-\frac{1}{2}\left(\frac{\partial^2}{\partial r_1^2}+\frac{\partial^2}{\partial r_2^2}\right)+\left(\frac{1}{r_1+r_2}-\frac{1}{r_1}-\frac{1}{r_2}\right)\right\}\psi = \left(E+\frac{1}{2}\right)\psi \tag{1}$$

The calculation of ionization cross sections is hindered by a lack of understanding of the asymptotic solutions of (1). We have made progress in two directions.

The first direction is to obtain asymptotic solutions of (1) with uniform error on the hyperspherical arc $0 < \alpha < \pi/4$ where $(r_1,r_2) = (\rho\cos\alpha, \rho\sin\alpha)$. These solutions are obtained by joining exact semiclassical wavefunctions valid in $\alpha_1 < \alpha < \pi/4$, to a "near-axis expansion" valid in $0 < \alpha < \alpha_2$ where $\alpha_2 > \alpha_1$.

The exact semiclassical wavefunction has the form

$$\psi(\xi,\eta) = [P(\xi,\eta)\omega(\xi,\eta)]^{-1/2}\exp\left[-i\int_{\xi_0}^{\xi} ds\, P(\xi,\eta)\right] \tag{2}$$

where (ξ,η) refer to a bundle of classical trajectories emanating from a single "condensation point" (ρ_0,α_0). The initial condition, apart from energy, is η and the distance along the trajectory is ξ; two adjacent trajectories η and $\eta+\Delta\eta$ are separated by a distance $\omega(\xi,\eta)\Delta\eta$ at later times. Thus ω is the cross section of a tube of flux. As usual, P is the momentum along ξ. When the trajectories have been computed, (ξ,η) have to be mapped numerically onto (ρ,α).

The near axis expansion is obtained by making the ansatz (for $r_1 >> r_2$)

$$\psi(r_1,r_2) = r_2^{1/2} H_1^{\pm}[(8r_2)^{1/2}]\exp\left[ikr_1 + \sum_{\lambda=2}^{\infty}\frac{f_\lambda(r_2)}{r_1^\lambda}\right] \tag{3}$$

in (1), where $H_n^{\pm}$ are Hankel functions and $\kappa^2 = 2E$. The functions $f_\lambda(x)$ satisfy a hierarchy of nonlinear ordinary differential equations which are readily integrated numerically.

To compare (2) and (3), we calculate $\Delta S = \mathrm{Re}S(\rho,\alpha) - \kappa\rho$ both ways, where $\psi = \exp(iS)$. Typical results are shown in Fig. 5.19. The two expressions have a common interval of validity around 30° (this number depends on ρ) and so may be patched together to span the whole range of α. The arbitrary constant which may be added to one or the other expression for ΔS is independent of ρ, so that we have a uniform solution of (1), valid in this example for all $\rho \geq 40\, a_0$. Our hope is that this solution can be extended to smaller values of ρ by numerical integration.

The second direction is the application of (2) to obtain exact threshold laws numerically. The ionization probability for producing two particles of energies ε and $E-\varepsilon$ can be written, for small E, as

$$P(E,\varepsilon) = CE^{1+\alpha} f(\varepsilon/E) \tag{4}$$

Analytic treatments[2] valid near $\varepsilon = E/2$ suggest that $\alpha = 0.1269$ and $f = 1$. The function P/E

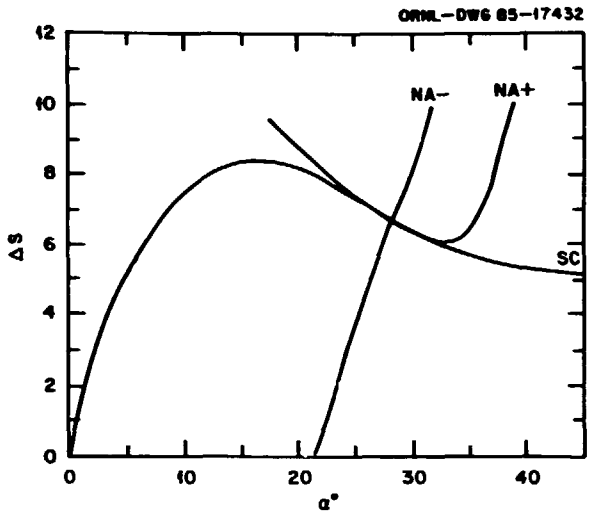

Fig. 5.19. $\Delta S = \mathrm{Re}S - \kappa\rho$ vs α for $\kappa = 1$, $\rho = 90a_0$. SC is the exact semiclassical result, (2) and NA+, NA- are the solutions defined by (3).

turns out to be simply proportional to the ω appearing in (2). Our calculations reproduce $\alpha = 0.127 \pm 0.001$, but show deviations of f from unity as shown in Fig. 5.20. Indeed, f has a bonafide singularity, albeit a weak one, $f \sim \epsilon^{-1/4}$ near $\epsilon = 0$. These results agree fairly well with purely classical calculations[3] of f, except for the singularity; either behavior of f

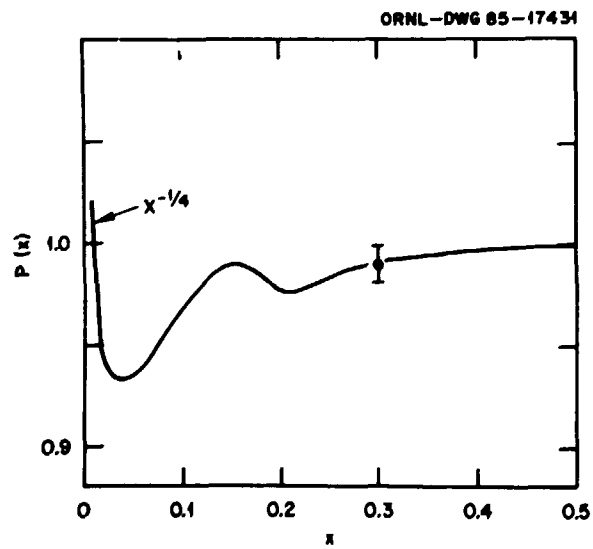

Fig. 5.20. The function $f(x)$ defined in (4), calculated from (2). The error bar indicates residual numerical uncertainty.

is consistent with experimental data. The singularity is, of course, a semiclassical pathology which emphasizes the need for a fully quantal solution of the problem.

---

1. Summary of contributed paper at 13th ICPEAC meeting.
2. R. Peterkop, J. Phys. B: Atom. Molec. Phys. 4, 513 (1971).
3. F. H. Read, J. Phys. B: Atom. Molec. Phys. 17, 3965 (1984).

MATHEMATICAL PHYSICS

BASIS SPLINE AND COLLOCATION METHODS FOR NUCLEAR AND ATOMIC COLLISION PROBLEMS

C. Bottcher M. R. Strayer

The use of numerical techniques for solving the Schroedinger and Dirac equations in atomic and nuclear physics is now well established. In the realm of complicated many-body systems, especially at relativistic velocities, the power of numerical approaches is unrivaled. Since the subject has acquired some maturity, it is now timely to develop methods more sophisticated and accurate than the early finite difference and finite-element algorithms. It is also timely to address problems such as fermion doubling, conservation laws and gauge conditions in a systematic way. We have thus turned to the use of basis splines (or B-splines) of arbitrary order, combined with the method of collocation.[1]

Basis splines are simply localized, piecewise continuous and differentiable polynomials, erected on a grid of points, called knots. A simple example is shown in Fig. 5.21. An arbitrary function is written as a linear superposition of these functions,

$$\psi(x) = \sum_{k=1}^{n} u_k(x)\psi^k. \qquad (1)$$

Between the knots, we choose collocation points $\{\xi_\alpha\}$ at which the equation to be solved, say $L\psi = 0$, is identically satisfied. The coefficients $\{\psi^k\}$ are eliminated in favor of $\{\psi_\alpha\}$, the values of ψ at the collocation points. Thus we arrive at a matrix equation

$$\underline{L}\,\underline{\psi} = 0 \qquad (2)$$

ORNL-DWG 85-13531

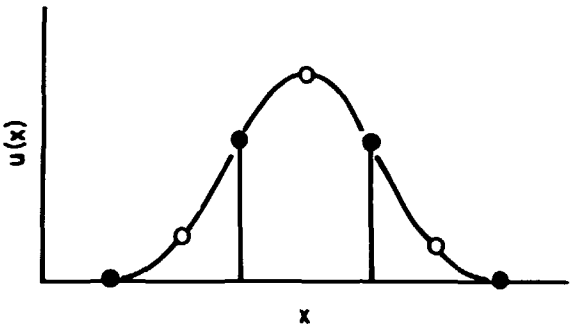

Fig. 5.21. Quadratic (third-order) basis spline. The knots are indicated by the filled circles and the collocation points by the open circles.

for the vector of $\{\psi_\alpha\}$. This technique is accurate, stable, efficient, and easy to code, particularly in more than one dimension. A slight drawback is that (2) is not, in general, self-adjoint.

The doubling of the fermion spectrum when the Dirac equation is discretized[2] can be traced to a pathology of most numerical methods; the matrix $\underline{\Delta}$ representing d^2/dx^2 is not, in general, the square of $\underline{D}$ representing d/dx. Our prescription is to replace first derivatives in the Dirac Hamiltonian by the matrices which provide an LU decomposition of $\underline{\Delta}$,

$$\underline{\Delta} = \underline{D}_-\underline{D}_+. \qquad (3)$$

The use of $\underline{D}_\pm$ to represent d/dx can be justified in a fairly rigorous way. If certain auxiliary conditions are satisfied, $\underline{D}_\pm$ satisfy identities pertaining to vectors of moments of the collocation points $\omega_\mu = \{\xi_\mu^\alpha/\mu!\}$

$$\underline{\omega}_{\mu+1}^T \underline{D} = \underline{\omega}_\mu^T \underline{D}. \qquad (4)$$

Thus $\underline{D}_\pm$ and their powers and inverses behave intuitively as operators of differentiation and integration should.

Using (3) and (4), we can define current operators which satisfy finite analogues of all desirable conservation laws in both differential and integral forms. This program has now been carried through for Dirac and Maxwell fields in three dimensions. Applications of our methods are described elsewhere in this section.

---

1. C. de Boor, A Practical Guide to Splines, Springer-Verlag, New York, 1978.
2. C. M. Bender and D. H. Sharp, Phys. Rev. Lett. 50, 1535 (1983).

ACCIDENTAL DEGENERACIES AND SUPERSYMMETRIC QUANTUM MECHANICS[1]

A. B. Balantekin[2]

We consider two Hamiltonians motivated by the nuclear shell model

$$H = \frac{1}{2}\left(\vec{p}^2 + \vec{r}^2\right) + \lambda(\vec{\sigma}\cdot\vec{L} + 3/2)$$

and

$$H = \frac{1}{2}\left(\vec{p}^2 + \vec{r}^2\right) + \frac{1}{2r^2} + \lambda\,\vec{\sigma}\cdot\vec{L} + \frac{3}{8r^2}\,.$$

For the first Hamiltonian when we fix j, there is a degeneracy for the two cases $\lambda = +1$, $\ell = j + 1/2$, and $\lambda = -1$, $\ell = j - 1/2$. For the second Hamiltonian, the degeneracy is between $\lambda = +1$, $j = \ell + 1/2$, and $\lambda = -1$, $j = \ell - 1/2$ with fixed ℓ. It is shown that the degeneracy of such Hamiltonians is due to an underlying supersymmetric quantum-mechanical structure, i.e., H can be written as

$$H = \frac{1}{2}\{\theta,\theta^\dagger\}.$$

To study such systems, spectrum-generating superalgebras are introduced and developed. In this context, one-parameter realization of the relevant noncompact superalgebras Osp(1/2) and Osp(2/2) are worked out. In both cases, the anticommuting charges are identified with the fermionic generators of the superalgebra Osp(2/2). The Hamiltonians (1) and (2) with $\lambda = +1$ and $\lambda = -1$ can be written together as

$$H = 2(K_0 + Y),$$

where K_0 is the diagonal element of the subalgebra Sp(2) which acts on the bosonic subspace, and Y is the element of the subalgebra SO(2) which acts on the fermionic subspace.

---

1. Summary of paper: Ann. Phys. (N.Y.) 164, 277 (1985).
2. Eugene P. Wigner Fellow.

COHERENT STATES FOR ORTHOSYMPLECTIC SUPERGROUPS

A. B. Balantekin[1] H. Schmitt[2]

Aside from their mathematical significance in relation to the geometry of the group manifolds, coherent states have been very useful in studying classical (geometrical) limits of quantum-mechanical Hamiltonians with specific symmetry properties. In particular, SU(6) coherent states have been successfully used[3] in studying the geometry associated with three limits of the Interacting Boson Hamiltonian of the low-lying quadrupole collective states in even-even nuclei. Although this approach to nuclear spectra has been generalized to describe odd-even nuclei by including fermionic, in addition to the bosonic degrees of freedom, the geometry of the nuclear models obtained in this way has not been studied. In a parallel development, supersymmetric quantum mechanics have been associated[4] with superalgebras and supergroups. Time development of states of such supersymmetric quantum-mechanical Hamiltonians is also coherent.

To facilitate the study of supergroup coherent states, we examined the coherent states associated with the simplest orthosymplectic supergroups, namely Osp(1/2) and Osp(2/2) ~ SU(1,1/1). The resolution of identity for these coherent states has been derived and expectation values of the group generators have been calculated. At the present, we are extending our analysis to the higher rank orthosymplectic supergroups.

---

1. Eugene P. Wigner Fellow.
2. ORAU Student Research participant from University of Arizona, Tucson, AZ 85721.
3. R. Gilmore, J. Math. Phys. 20, 891 (1979).
4. E. D'Hoker and L. Vinet, Phys. Lett. 137B, 72 (1984); A. B. Balantekin, Ann. Phys. (N.Y.) 164, 277 (1985).

NUMERICAL METHODS FOR FINDING PERIODIC TRAJECTORIES OF NON-INTEGRABLE CLASSICAL PROBLEMS

K.T.R. Davies M. Baranger[1]
M. Saraceno[2]

The classical equations of motion for a two-dimensional periodic trajectory can be expressed as

$$\ddot{x} + \frac{\partial V(x,y)}{\partial x} = 0, \tag{1a}$$

$$\ddot{y} + \frac{\partial V(x,y)}{\partial y} = 0, \tag{1b}$$

with the boundary conditions

$$\begin{aligned} x(t+\tau) &= x(t),\ y(t+\tau) = y(t), \\ \dot{x}(t+\tau) &= \dot{x}(t),\ \dot{y}(t+\tau) = \dot{y}(t). \end{aligned} \tag{2}$$

The dot refers to a time derivative, τ is the period of the motion, V is the potential energy, and we chose a position-independent inertia, $m \equiv 1$. If we discretize these equations on a time mesh ($\tau = N\varepsilon$), we obtain

$$g_{xn}(x,y) \equiv \varepsilon^{-2}\left(x_{n+1} - 2x_n + x_{n-1}\right) + \frac{\partial V}{\partial x}(x_n,y_n) = 0, \tag{3a}$$

$$g_{yn}(x,y) \equiv \varepsilon^{-2}\left(y_{n+1} - 2y_n + y_{n-1}\right) + \frac{\partial V}{\partial y}(x_n,y_n) = 0, \tag{3b}$$

$$n = 0,1,2,\ldots N-1,$$

with

$$(x_N,y_N) = (x_0,y_0),\ (x_{N+1},y_{N+1}) = (x_1,y_1). \tag{4}$$

A variety of methods have been used to solve Eqs. (3) and (4). Here we discuss two methods which we have found to be especially efficient for calculating periodic trajectories. Both of these methods assume that one can linearize in the vicinity of an approximate solution, namely

$$x_n = x_n^{(o)} + x_n', \tag{5a}$$

$$y_n = y_n^{(o)} + y_n', \tag{5b}$$

and x_n' and y_n' are taken to be small corrections.

A. The Vector Newton's Method

Using Eqs. (5), Eqs. (3) can be rewritten as

$$G(x,y) = G(x^{(o)},y^{(o)}) + D(x^{(o)},y^{(o)})Z' = 0, \quad (6)$$

where

$$G \equiv \begin{bmatrix} g_{x0} \\ g_{x1} \\ \vdots \\ g_{x,N-1} \\ \hline g_{y0} \\ g_{y1} \\ \vdots \\ g_{y,N-1} \end{bmatrix} \quad \text{and} \quad Z \equiv \begin{bmatrix} x_0 \\ x_1 \\ \vdots \\ x_{N-1} \\ \hline y_0 \\ y_1 \\ \vdots \\ y_{N-1} \end{bmatrix} \quad (7)$$

are 2N component column vectors and D is a 2N×2N derivative matrix

$$[D(x,y)]_{i,j} \equiv \partial g_i/\partial z_j. \quad (8)$$

These equations can be solved by using a vector version of Newton's method,[3] which gives

$$Z = Z^{(o)} - [D(x^{(o)},y^{(o)})]^{-1} G(x^{(o)},y^{(o)}). \quad (9)$$

The derivative matrix can be separated into N×N submatrices, which for many potentials simplify into diagonal and tridiagonal form. However, the usual methods of Gaussian elimination[4] are not applicable here because of the periodic boundary conditions. One solves Eq. (3) by iteration, picking an initial set of $x_n^{(o)}$ and $y_n^{(o)}$ which generates a new set of x_n and y_n to be used in the next iteration. How fast this procedure converges depends upon how close one is initially to the true solution. The vector Newton's method is moderately fast for dimensionalities of $N \lesssim 100$, with convergence usually taking place in 3-8 iterations.

B. The Monodromy Matrix Method

There is another way of expanding Eqs. (3) using Eqs. (5), namely

$$x'_{n+1} - 2x'_n + x'_{n-1} + \epsilon^2 \frac{\partial^2 V}{\partial x^2}(x_n^{(o)},y_n^{(o)})x'_n + \epsilon^2 \frac{\partial^2 V}{\partial x \partial y}(x_n^{(o)},y_n^{(o)})y'_n = a_n, \quad (10a)$$

$$y'_{n+1} - 2y'_n + y'_{n-1} + \epsilon^2 \frac{\partial^2 V}{\partial y \partial x}(x_n^{(o)},y_n^{(o)})x'_n + \epsilon^2 \frac{\partial^2 V}{\partial y^2}(x_n^{(o)},y_n^{(o)})y'_n = b_n; \quad (10b)$$

where

$$-a_n = x_{n+1}^{(o)} - 2x_n^{(o)} + x_{n-1}^{(o)} + \epsilon^2 \frac{\partial V}{\partial x}(x_n^{(o)},y_n^{(o)}) \quad (11a)$$

$$-b_n = y_{n+1}^{(o)} - 2y_n^{(o)} + y_{n-1}^{(o)} + \epsilon^2 \frac{\partial V}{\partial y}(x_n^{(o)},y_n^{(o)}). \quad (11b)$$

We now define a four-component column vector

$$Z_n = \begin{bmatrix} x'_n \\ y'_n \\ x'_{n-1} \\ y'_{n-1} \end{bmatrix}, \quad (12)$$

and one obtains the recursive relation

$$Z_{n+1} = U_n Z_n + C_n, \quad (13)$$

where

$$C_n = \begin{pmatrix} a_n \\ b_n \\ 0 \\ 0 \end{pmatrix} \quad (14)$$

is a four-component vector, and

$$U_n = \begin{pmatrix} P_n & -1 \\ 1 & 0 \end{pmatrix} \quad (15)$$

is a 4×4 matrix. Each block in Eq. (15) is a 2×2 matrix and P_n is given by

$$P_n = \begin{pmatrix} 2-\epsilon^2 \frac{\partial^2 V}{\partial x^2}(x_n^{(o)},y_n^{(o)}) & -\epsilon^2 \frac{\partial^2 V}{\partial x \partial y}(x_n^{(o)},y_n^{(o)}) \\ -\epsilon^2 \frac{\partial^2 V}{\partial y \partial x}(x_n^{(o)},y_n^{(o)}) & 2-\epsilon^2 \frac{\partial^2 V}{\partial y^2}(x_n^{(o)},y_n^{(o)}) \end{pmatrix} \quad (16)$$

From Eq. (13) we obtain

$$Z_{N+1} = M_1 Z_1 + B_1, \quad (17)$$

where

$$B_1 = \sum_{n=1}^{N} U_N U_{N-1} \cdots U_{n+1} C_n, \quad (18)$$

and

$$M_1 = U_N U_{N-1} \cdots U_2 U_1 \qquad (19)$$

is the monodromy matrix. If we now impose the boundary conditions, Eq. (4), we find

$$Z_{N+1} = Z_1 = (1-M_1)^{-1} B_1, \qquad (20)$$

which gives us explicit values for x_1', y_1', x_0', y_0' provided we solve a system of 4×4 linear equations. The other x_n', y_n' follow from Eq. (13). Then from Eqs. (5) we compute a new set of x_n, y_n to be used in the next iteration.

This method is completely equivalent to that described in part A since, in each iteration, the values of x_n and y_n are identical for the two methods. Clearly, the two methods are equivalent because they are based on the same expansion, namely Eq. (5). However, the monodromy matrix method is many times faster than the Newton's method, as we show in Table 5.2. This

Table 5.2. Comparison of typical CPU times on the VAX computer for the vector Newton's method and the monodromy matrix method.

N	No. of iterations	CPU time in minutes using the vector Newton's method	CPU time in min. using the monodromy matrix method
96	3	3.89	0.038
192	7	71.98	0.082

behavior arises from the difference in the order of the system of equations which must be solved: in Eq. (9) the matrix is 2N × 2N (which in most cases can be reduced to N × N), whereas in Eq. (20), the matrix is 4 × 4, which is considerably smaller.

1. Massachusetts Institute of Technology, Cambridge, MA 02139.
2. Departamento de Fisica, Comision National de Energia Atomica, Av. del Libertador 8250, 1429 Buenos Aires, Argentina.
3. S. Trentalange, S. E. Koonin, and A. J. Sierk, Phys. Rev. C 22, 1159 (1980).
4. S. E. Koonin et al., Phys. Rev. C 15, 1359 (1977).

EXPLORING THE TREE OF PERIODIC TRAJECTORIES FOR TWO NON-INTEGRABLE TWO-DIMENSIONAL POTENTIALS

K.T.R. Davies[1] M.A.M. de Aguiar[2]
M. Baranger[1] C. P. Malta[2]
E.J.V. de Passos[2]

We are now calculating classical periodic motion in two nonintegrable, two-dimensional potentials:

$$V_1(x,y) = .05\,x^2 + (y - \tfrac{1}{2}x^2)^2, \qquad (1)$$

and

$$V_2(x,y) = \tfrac{1}{2}x^2 + \tfrac{3}{2}y^2 - x^2 y + \tfrac{1}{12}x^4. \qquad (2)$$

For a given potential there are many families of periodic trajectories. It is of interest to plot these families in a (τ,E) or (period, energy) plane. Such a plot, portions of which are shown in Figs. 5.22 and 5.23, displays an infinite "tree" of the various families.

Our central purpose has been to study this tree, and we have developed several new, efficient numerical methods for calculating the periodic trajectories.[3] As we show in Figs. 5.22 and 5.23, within one family the trajectories often switch back and forth between being stable and unstable, and our methods allow us to find the unstable ones as easily as the stable ones. In Figs. 5.24 and 5.25 we plot in the x,y plane various families from Figs. 5.22 and 5.23, respectively. The potential V_1 was chosen because it has a deep narrow curved valley (see its contours in Fig. 5.24). We can think of this valley as the locus of the collective configurations of a nucleus. We would expect collective motion to correspond to trajectories which remain near the bottom of this valley, but the valley is not straight and therefore this motion does not uncouple. We see from Figs. 5.23 and 5.25 that there are indeed periodic trajectories of varying amplitude which follow the valley floor approximately. But these trajectories do not form a single family; as the amplitude is varied, the trajectories of one family will suddenly begin to climb the walls and leave the valley (see Fig. 5.25); then, there is usually a small gap in the amplitudes, after which another family comes down from the mountains and takes

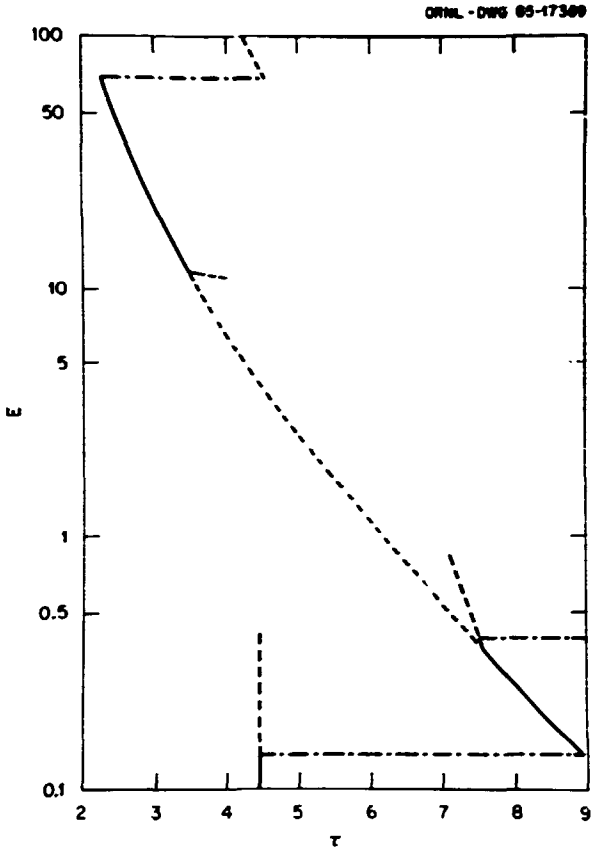

Fig. 5.22. Energy vs period for the "boomerang" family obtained using potential V_1. Branchings are also included in the plot. The full lines are for stable periodic trajectories while the dashed lines are for unstable ones. The dot-dashed lines indicate branchings to period doubling trajectories.

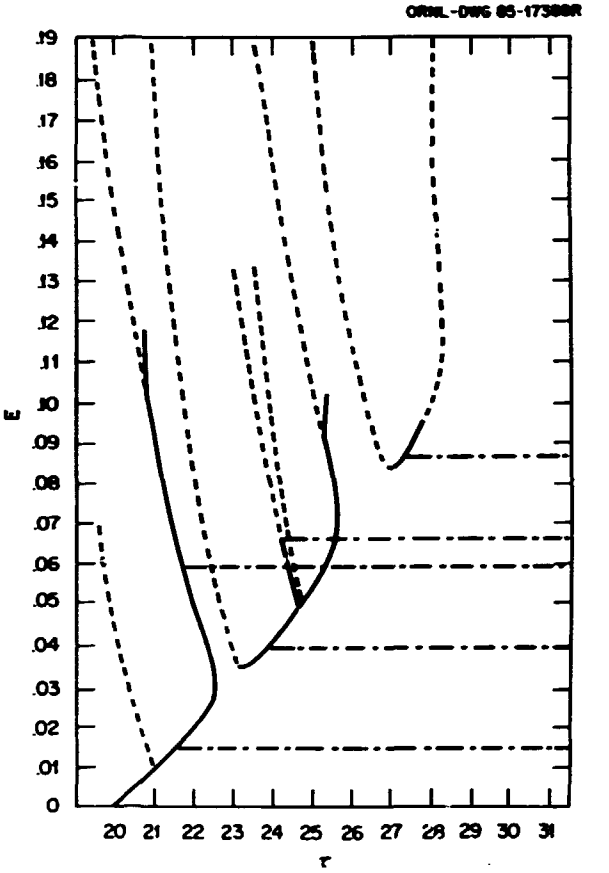

Fig. 5.23. Energy vs period for the horizontal family and other families obtained using potential V_1. See the caption to Fig. 5.22 for further details.

over the valley. Presumably the gap which occurs between two adjacent families in the valley is due to some kind of resonance, in the sense of the KAM theorem.[4]

Also, our methods are especially useful for calculating new members or shapes of the family where "branching" occurs. Branching behavior is determined by the eigenvalues of the monodromy matrix, M.[3] This matrix describes the shape of a new trajectory when a small perturbation is propagated once around a periodic trajectory, and the trace of M tells you where the branchings occur. For example, if Trace(M) = 4, there is a branching to a new shape with no change of period, and if Trace(M) = 0, there is a branching to a new type of trajectory whose period is

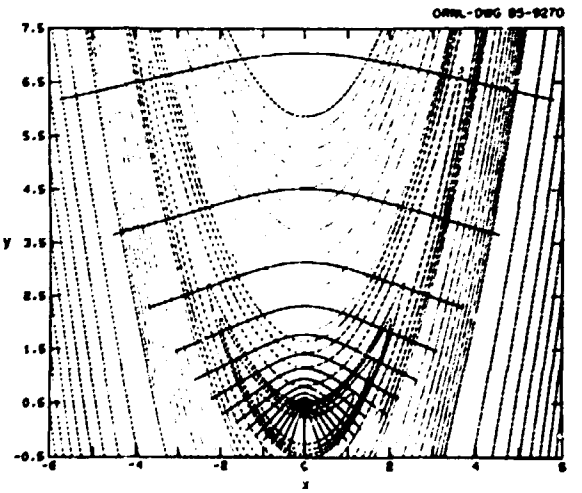

Fig. 5.24. "Roomerang" family in the x,y plane for the potential V_1. The full curves are the periodic trajectories for different values of the period, while the dotted and dashed curves are the equipotential contours.

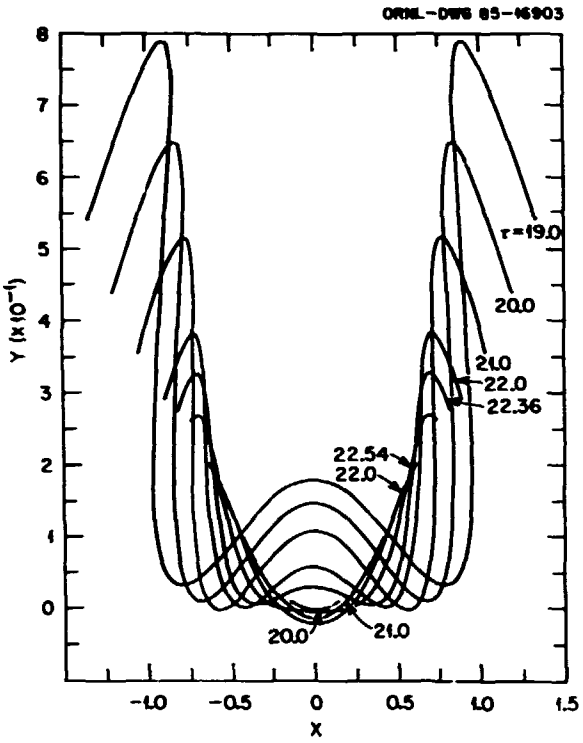

Fig. 5.25. Horizontal family of periodic trajectories in the x,y plane for potential V_1. For small amplitudes, the curves form the family of small horizontal oscillations.

twice that of the original trajectory (period-doubling branch). There are also branchings giving period tripling, period quadrupling, etc. Typical branchings are shown in Figs. 5.26 and 5.27. In Fig. 5.26, the double open symmetric boomerang and the double mushroom-shaped trajectories are examples of period doubling; the other two shapes in Fig. 5.26 and the one shown in Fig. 5.27 are examples of isochronous branchings (Trace(M) = 4). Figure 5.27 shows the transition from one family to anotner at a branching. Finally, in Fig. 5.24 we see that the boomerang family starts out as a period doubling branching from the vertical family of oscillations. In general, the tree displays a rich variety of shapes, with many examples of both librational and rotational periodic motion.

---

1. Massachusetts Institute of Technology, Cambridge, MA 02139.
2. Instituto de Fisica, Universidade de São Paulo, CP 20516, 01000 São Paulo SP, Brazil.
3. "Numerical Methods for Finding Periodic Trajectories of Non-Integrable Classical Problems" by K.T.R. Davies, M. Baranger, and M. Saraceno, this report.
4. V. I. Arnol'd, Russ. Math Survey 18, No. 5, 13-39, No. 6, 61-196 (1963).

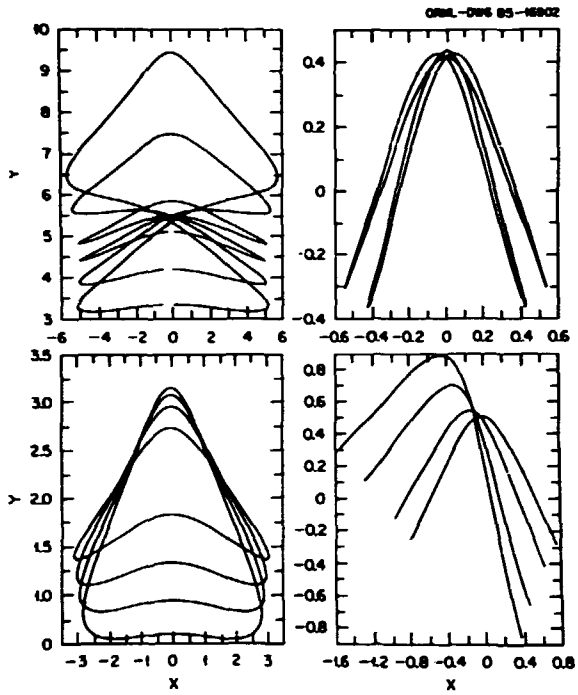

Fig. 5.26. Four branchings from the "boomerang" family in the x,y plane obtained using potential V_1. Clockwise from top right, we have the following: double open symmetric boomerang (rotation), asymmetric boomerang (libration), open symmetric boomerang (rotation), and double mushroom-shaped trajectories (rotation).

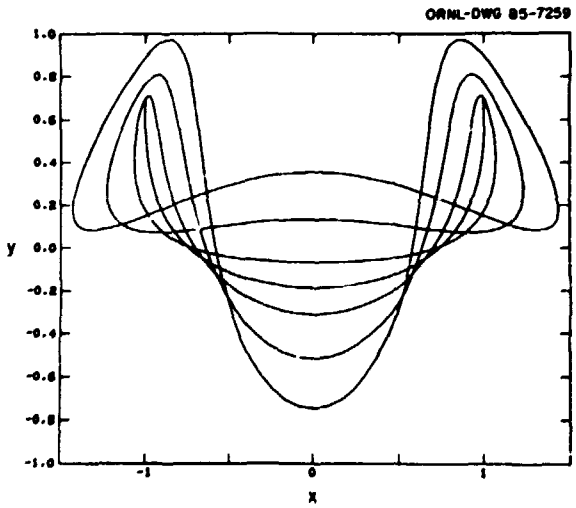

Fig. 5.27. Example of branching for potential V_2. The three outermost curves are "cloverleaf"- or "cowboy hat"-shaped trajectories. These trajectories branch off of the innermost curve, which is U-shaped.

RELATIONSHIP OF TDHF TO QUANTUM-FLUID DYNAMICS

C. Bottcher V. Protopopescu[1]

We have begun to investigate the relationship of time-dependent Hartree-Fock (TDHF) theory to classical nonlinear phenomenologies such as kinetic theory and fluid dynamics. As a focus, we have chosen the finite one-dimensional electron gas with a screened Coulomb interaction. In particular, we want to explore how plasmons emerge from the single-particle spectrum. This problem is addressed by studying how collective descriptions, e.g., fluid mechanics, can be derived from independent-particle descriptions, e.g., TDHF.

We are developing two approaches. The first is to make numerical experiments on the long-time behavior of the TDHF equations, of which little is known. Standard nonlinear diagnostics such as Poincaré sections and time spectra are beginning to show evidence of interacting resonances and some degree of "thermalization." While the problem is too complicated to expect rapid simple answers, almost any information would be of widespread interest.

Our second approach is to derive quantum fluid mechanics by expanding the density matrix of a many-electron system in a ring of operators O_I such that $\mathrm{Tr}(O_I O_J) = \delta_{IJ}$.

We circumvent the difficulties of earlier discussions by working entirely with discrete representations of the system. Then we can derive from TDHF operator equations with a familiar form, e.g., densities ρ and currents J satisfy

$$\dot{\rho} = -\frac{\Delta}{\Delta q} J, \tag{1}$$

$$\dot{J} = F\rho - \frac{\Delta}{\Delta q}\left(J\rho^{-1}J + \Pi\right). \tag{2}$$

As operator or matrix equations, these are equivalent to infinite systems of linear equations. However, if the operators are replaced by average values, they become finite systems of nonlinear equations. This paradigm occurs in several branches of physics under various disguises, but it has never been formalized nor its validity explored. This we propose to do with numerical experiments, particularly on the same electron gas model which can be investigated by TDHF.

---

1. Engineering Physics and and Mathematics Division.

6. NUCLEAR SCIENCE APPLICATIONS

Nuclear science has common frontiers with other basic sciences. The current program concentrates on three areas: (1) In cooperation with the Engineering Physics and Mathematics, Analytical Chemistry, and Computing and Telecommunications Divisions, a program is currently underway to obtain verification of the neutronic and irradiation performance of higher actinides in fast spectrum reactors. This program utilizes the Dounreay Prototype Fast Reactor in Scotland and will be completed by 1988. (2) In association with the Analytical Chemistry Division, the technique of studying the heavy-ion-induced X-ray satellite spectra has been advanced to the point that it can be applied to metal alloys and other materials of interest to the Metals and Ceramics Division. This program utilizes the EN Tandem and the HHIRF. Significant advances in this area are expected with the implementation by early 1986 of an ultrahigh resolution Von Hamos spectrometer. (3) Working with personnel from outside agencies, a program to study single event upsets in integrated circuits has been started. Plans are being drawn up to build a beam line at HHIRF dedicated to this program.

CONTINUED ACTIVITIES IN SUPPORT OF THE US/UK JOINT EXPERIMENT IN THE DOUNREAY PROTOTYPE FAST REACTOR

S. Raman
H. L. Adair[1]
J. L. Botts[2]
B. L. Broadhead[3]
D. A. Costanzo[2]
J. K. Dickens[4]
J. F. Emery[2]
R. L. Walker[2]

The United States and the United Kingdom are engaged in a joint research program in which samples of the higher actinides are irradiated in the Dounreay Prototype fast reactor in Scotland. The purpose of the program is (1) to study the materials behavior of selected higher actinide "fuels" and (2) to determine the integral cross sections of a wide variety of the higher isotopes. Samples of the actinides are incorporated in fuel pins inserted in the core. For the fuel study, the actinides selected are ^{241}Am and ^{244}Cm in the form of Am_2O_3, Cm_2O_3, and $Am_6Cm(RE)_7O_{21}$, where (RE) represents a mixture of lanthanides. For the cross-section determinations, the samples are milligram quantities of actinide oxides of ^{248}Cm, ^{246}Cm, ^{244}Cm, ^{243}Cm, ^{243}Am, ^{244}Pu, ^{242}Pu, ^{241}Pu, ^{240}Pu, ^{239}Pu, ^{238}U, ^{236}U, ^{235}U, ^{234}U, ^{233}U, ^{232}Th, ^{230}Th, and ^{231}Pa encapsulated in vanadium. The development and application of the technology for preparing the actinide samples have been described in a report by Quinby, et al.[5] The characterization of the starting materials used in the samples for the cross-section determinations (denoted as physics specimens) and in the dosimeters has been described in a report by Walker, et al.[6] Preanalysis calculations were carried out[7] concerning actinide buildup and burnup in order to aid the experimentalists in the planning and preparation of their respective measurements.

Following the removal of the first fuel pin (FP1) experiment in late 1983 and subsequent shipping to ORNL, three separate series of measurements were performed beginning in May 1984 and ending in mid-1985. These measurements are herein compared to the final calculations to provide an indication of the reliability of the results.

The initial set of experimental investigations provided measurements of the fission product activities for several of the dosimeters. The

experimental-to-calculational (E/C) ratios are presented in Table 6.1 for four dosimeters, ^{235}U, ^{238}U, ^{239}Pu and ^{237}Np at three locations each in the fuel pin. The calculated values are in general 5 to 10% higher than the measured values and, with the exception of ^{238}U, show only slight sensitivity to the axial position in the fuel pin. The variation in the ^{238}U E/C values as a function of axial position is probably attributable to the variation in the high energy flux in the axial direction, because the ^{238}U fission cross section has a high energy threshold. From the overall E/C values it appears that 5% and 7% increases in the total flux at the first two locations (i.e., positions #1, #2 and #17, #18), respectively, are indicated.

The next series of experiments involved a similar set of measurements, this time including most of the remaining actinides. The experiment involved a gamma-ray characterization of some 19 different actinides. Table 6.2 gives the results for the fission product yield of ^{137}Cs from each of these actinides. With the exception of the results for ^{230}Th, ^{238}Pu, ^{239}Pu and ^{244}Cm, the agreement between the calculated and measured values is quite good, particularly since ENDF/B-V contains evaluated yields only for ^{232}Th, ^{233}U, ^{236}U, ^{238}U, ^{239}Pu, ^{240}Pu, ^{241}Pu and ^{242}Pu of the actinides shown in Table 6.2. The four actinides with less than desirable E/C ratios are all either known or suspected damaged capsules. Thus the results for ^{137}Cs are also very encouraging.

The third set of experiments consisted of examining the final concentrations and isotopic determinations for each of the actinide samples contained in the fuel pin FP1. The results from the analysis of the ^{233}U sample are shown in Table 6.3, where both the measured uranium

Table 6.1. E/C Values for Dosimetry Material Activities in Fuel Pin FP1

	^{238}U Pos. #1	^{238}U Pos. #17	^{238}U Pos. #33
^{95}Zr	0.94	0.84	1.02
^{103}Ru	0.98	0.87	1.09
^{106}Ru	0.96	0.88	1.07
^{137}Cs	0.92	0.79	1.05
^{144}Ce	0.98	0.92	1.29
Average	0.96	0.86	1.10
	^{235}U Pos. #1	^{235}U Pos. #17	^{235}U Pos. #33
^{95}Zr	0.97	0.97	1.02
^{103}Ru	0.94	0.89	0.96
^{106}Ru	0.88	0.88	0.91
^{137}Cs	0.93	0.93	0.98
^{144}Ce	0.97	1.00	0.98
Average	0.94	0.93	0.97
	^{239}Pu Pos. #2	^{239}Pu Pos. #18	^{239}Pu Pos. #34
^{95}Zr	0.85	0.87	0.95
^{103}Ru	0.87	0.87	0.86
^{106}Ru	0.89	0.91	0.95
^{137}Cs	0.85	0.87	0.94
^{144}Ce	0.84	0.87	0.94
Average	0.86	0.88	0.93
	^{237}Np Pos. #2	^{237}Np Pos. #18	^{237}Np Pos. #34
^{95}Zr	0.95	0.93	0.93
^{103}Ru	1.00	0.97	0.98
^{106}Ru	0.91	0.92	0.86
^{137}Cs	0.97	0.94	0.93
^{144}Ce	0.93	0.91	0.89
Average	0.95	0.93	0.92

Table 6.2. E/C Values for Fission Yields (atoms) of ^{137}Cs in Fuel Pin FP1

Actinide	E/C	Actinide	E/C
^{230}Th	0.32	^{240}Pu - #2	0.90
^{232}Th	0.92	^{241}Pu	0.65
^{231}Pa	0.88	^{244}Pu	0.85
^{233}U	1.02	^{241}Am - #1	0.85
^{234}U	1.01	^{241}Am - #2	0.89
^{235}U	0.89	^{243}Am	0.79
^{236}U	0.91	^{243}Cm	1.29
^{238}U	0.89	^{244}Cm - #1	0.72
^{238}Pu	0.14	^{244}Cm - #2	0.38
^{239}Pu	0.04	^{246}Cm	0.86
^{240}Pu - #1	0.98	^{248}Cm	0.75

Table 6.3. Isotopic and Concentration Analysis Results for ^{233}U Sample in Fuel Pin FP1

	Initial	Predicted	Measured
	Isotopic Analysis, At. %		
^{233}U	99.89	99.38	99.41
^{234}U	0.052	0.55	0.55
^{235}U	0.003	0.007	0.005
^{236}U	0.002	0.002	0.001
^{238}U	0.056	0.059	0.031
	Concentration Analysis, mg		
^{233}U	7.92	7.52	7.45

isotopic compositions and the mass of the principal isotope, ^{233}U, are compared to the "predicted" values obtained by the ORIGEN depletion analysis code. These comparisons are not meant to be typical of the remaining samples. The comparisons for the isotopics are, in general, good; however, there are problems in the concentration results which are continuing to be investigated and should be resolved at a later date.

1. Operations Division, ORNL.
2. Analytical Chemistry Division, ORNL.
3. Computing and Telecommunications Division, ORNL.
4. Engineering Physics and Mathematics Division, ORNL.
5. T. C. Quinby et al., Preparation of Actinide Specimens for the US/UK Joint Experiment in the Dounreay Prototype Fast Rector, ORNL-5858 (1982).
6. R. L. Walker et al., Characterization of Actinide Physics Specimens for the US/UK Joint Experiment in the Dounreay Prototype Fast Reactor, ORNL-5986 (1983).
7. B. L. Broadhead, N. B. Gove, and S. Raman, Preanalysis Calculations in Support of the US/UK Joint Experiment in the Dounreay Prototype Fast Reactor, ORNL-6058 (1984).

FISSION-PRODUCT YIELD DATA FROM THE US/UK JOINT EXPERIMENT IN THE DOUNREAY PROTOTYPE FAST REACTOR

J. K. Dickens[1] S. Raman

The heavy actinide experiment discussed in the previous section was extended to determine fission-product activitation following the irradiation. In this experiment aliquots of the samples were prepared for γ-ray assay, which used high-resolution γ-ray and X-ray detectors. Two sets of γ-ray and X-ray counting measurements were performed, one set at approximately nine months following the end of the irradiation and the second set approximately six months later. The resulting spectral data were analyzed to obtain absolute values of activities for several long-lived fission products, namely ^{91}Y, ^{95}Zr, ^{95}Nb, ^{103}Ru, ^{106}Rh (following decay of ^{106}Ru), ^{110m}Ag, ^{125}Sb, ^{134}Cs, ^{137}Cs, ^{141}Ce, $^{144}Ce + ^{144}Pr$, and ^{155}Eu.

Because of uncertainties associated with the experiment, it was found that the experimental data could not be reported on an absolute basis. Instead, the yield data for the fission product ^{137}Cs were designated as monitor data for the yield data of the other fission products. The fission product ^{137}Cs was so chosen because (a) its yield per fission is near the peak of the heavy-mass distribution for fast-neutron fission of all of the actinides in this study, (b) the half-life of ^{137}Cs ($T_{1/2}$ = 30 yr) is sufficiently long that details of the PFR irradiation during the 1-yr irradiation are not important in deducing the yield of this fission product, and (c) the decay of ^{137}Cs is characterized by a dominant single γ-ray having E_γ = 662 keV and the yield determinations have essentially no uncertainties other than counting statistics which were small for all samples studied.

The deduced fission-product yields for ^{91}Y to ^{134}Cs and ^{141}Ce to ^{155}Eu (from the list above) have been prepared as ratios to the yield for ^{137}Cs. A correction factor as a function of the half life of a given fission product vis-a-vis the PFR irradiation history was deduced so that the experimental ratio data could be corrected to represent similar ratio data that would have been measured at the end of a short irradiation. Then these corrected ratios can be compared with ratios deduced from evaluated[2] fission-product yields from fast-neutron fission. In addition, the variation of yields for a given fission product as a function of the mass of the fissioning actinide can be represented. One such trend,

for the fission product ^{95}Zr, is exhibited in Fig. 6.1; another, for the fission product ^{141}Ce, is shown in Fig. 6.2. The experimental ratios (solid dots in the figures) agree quite well with the ratios deduced from the evaluation (shown as open circles in the figure) for fast-neutron fission of ^{231}Pa, $^{233-236}U$, ^{238}U, $^{238-242}Pu$, and $^{241,243}Am$. Disagreements are observed only for fast-neutron fission of ^{232}Th, disagreements which we have not yet resolved. For the other actinides of the experiment which do not yet have evaluations, namely ^{230}Th, ^{244}Pu and $^{243,244,246,248}Cm$, the ratio results appear to be consistent with apparent trends as a function of principal actinide mass in these two figures.

A report is being prepared describing this portion of the experimental program in some detail. The deduced experimental ratio data will be completely reported, both graphically and tabulated. Needed are experimentally determined absolute values for the yields of ^{137}Cs and these may be forthcoming from the next fuel pin. However, even as ratios the current results may provide a stringent test of the capabilities and data bases for computational programs designed to calculate fission-product inventories in a real fast-neutron reactor environment.

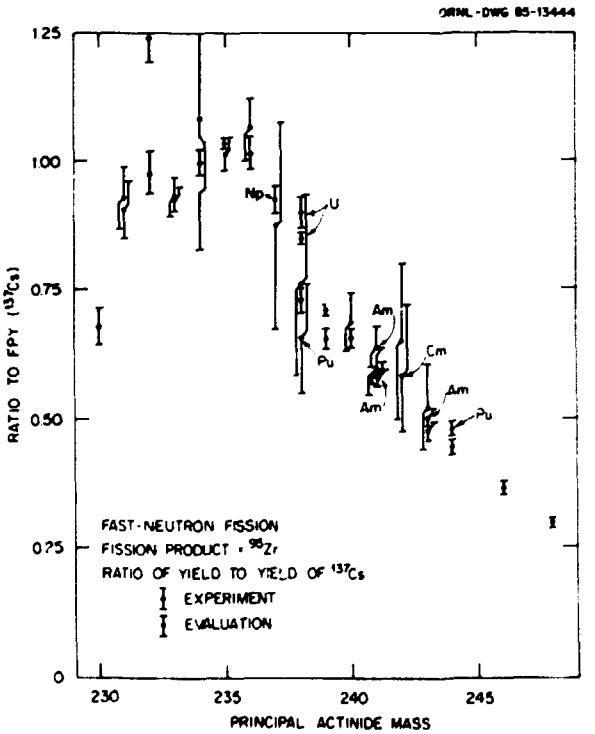

Fig. 6.1. Relative yields of ^{95}Zr following fast-neutron fission of actinides between ^{230}Th and ^{248}Cm. The present measurements are plotted as ratios to the experimental ^{137}Cs-fission-product yields. The data agree well with equivalent ratios deduced from the evaluation.

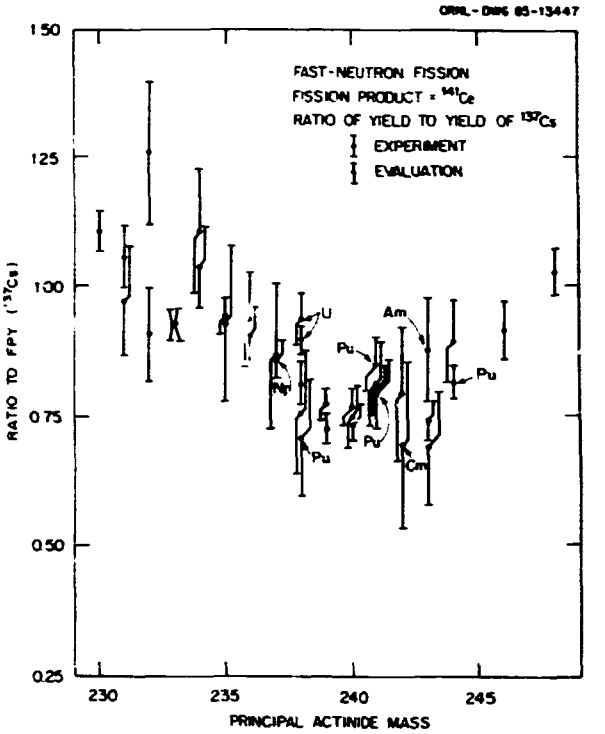

Fig. 6.2. Relative yields of ^{141}Ce following fast-neutron fission of actinides between ^{230}Th and ^{248}Cm. The present measurements are plotted as ratios to the experimental ^{137}Cs-fission-product yields. The experimental data agree quite well with equivalent ratios deduced from the evaluation.

---

1. Engineering Physics and Mathematics Division.
2. R. F. Rider, Compilation of Fission Product Yields, NEDO-12154-3(C), ENDF-322, General Electric Company, 1981; T. R. England (private communication, 1985).

VON HAMOS CRYSTAL SPECTROMETER FOR STUDIES OF HEAVY-ION INDUCED X RAYS

C. R. Vane
G. Morford[1]
D. Nagel[2]
S. Raman
B. Sales[3]
M. S. Smith[4]

Studies of X rays emitted after collisional excitation offer a direct pathway to quantitative description of many properties of excited atomic systems as well as a method of elucidating the excitation process itself. Heavy-ion impact at MeV energies produces large X-ray yields compared to other excitation methods allowing detailed studies of what are normally low probability (hence low signal) processes, such as environmental effects on higher X-ray satellites, which have been relatively neglected in past research.

As noted previously,[5] systematic measurements of X-ray satellite fine structures found in heavy-ion induced fluorescence of chemically complex targets require a dispersive instrument having both high energy resolution and yet good collection efficiency. Based on a narrow-band instrument borrowed from plasma diagnostic work,[6] we have designed, constructed, and tested a new Von Hamos geometry[7] crystal spectrometer which meets the above requirements by employing large curved crystals and a position-sensitive detector.

We have successfully used this instrument to measure ion-impact generated X-ray spectra in the 1.5-8.5 keV region from the following targets: Al and Si alloys (K X rays); Fe, Ni, and Cu (K X rays); and Tm and Ta (M X rays). Figure 6.3 shows a comparison of Aluminum K X-ray spectra produced by electron impact and by 64-MeV S^{4+} ions from the HHIRF tandem accelerator. Drastic enhancements of multiply-ionized target states are clearly displayed in the ion-inouced spectrum. The data were taken with a small ADP(101) crystal designed for erstwhile use in a commercial X-ray spectrometer based on a Rowland Circle geometry. The measured line width of $K_{\alpha_{1,2}}$ is ~1.5 eV. Detailed characterization studies of this particular crystal have shown that it contains serious flaws which limit the validity of measurements made from these raw data.

ORNL-DWG 85-18092

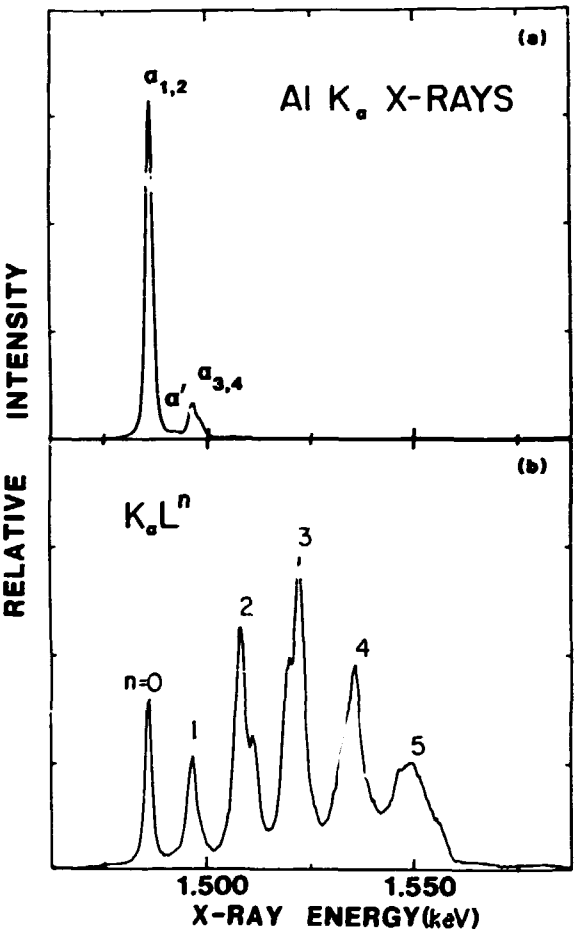

Fig. 6.3. Comparison of target Al K X rays generated by (a) 7 keV electrons and (b) 64 MeV S^{5+} ions. Extra peaks in ion-impact spectrum result from multiple Al L-Shell ionization.

Fig. 6.4 shows a target Fe K X-ray spectrum produced by 126 MeV Cu^{5+} ions from the HHIRF tandem accelerator. The diffracting crystal used was a large, flat Si(100), 2d = 2.715 A crystal. Characterization (especially spatial uniformity of the reflectivity) of the Si(100) crystal was also carried out during these measurements and it has been returned to the Naval Research Laboratory for preparation and curved-mounting at the design radius. The entire spectrum (taken at one positioning of the crystal and detector required 5000 seconds at ~8 pnA beam current on target. With this crystal bent to a 25.4-cm radius of curvature we

expect an improvement in collection efficiency of ~20–30.

In Fig. 6.4 the two sharp lines near 6.40 keV are Fe K_{α_1} and K_{α_2}, which are separated by 13 eV. The major satellite structure labelled $K_\alpha L^n$ is due to Fe K_α emission while the atom

ORNL-DWG 85-18093

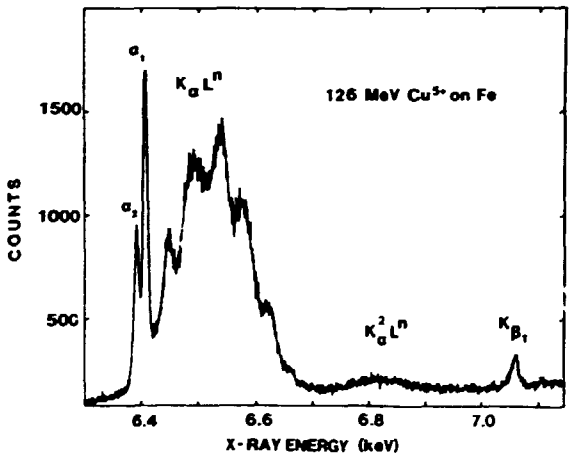

Fig. 6.4. Fe K X rays generated by 126 MeV Cu^{5+} ions on a thick Fe target.

has varying degrees of L-shell ionization. (Each additional L-vacancy shifts the energy by ~40 eV.) The resolved high energy peak is Fe K_{β_1} at 7.06 keV. Both $K_{\alpha_{1,2}}$ and K_{β_1} are enhanced in intensity compared to their satellites because of the normally singly-ionizing process of photo-fluorescence of the iron target by Cu projectile K X rays. The broad, low-intensity feature labelled $K^2{}_\alpha L^n$ is due to Fe hypersatellite X rays emitted from iron atoms initially having two K vacancies and n L vacancies. The higher efficiency afforded by large curved crystals currently on order will allow us to study such features in much greater detail. The entire instrument, attached to a tandem beam line, is displayed in Fig. 6.5.

1. Now a graduate student at Michigan State University, East Lansing, MI 48823.
2. Naval Research Laboratory, Washington, D.C. 20375.
3. Solid State Division, ORNL.
4. Now a graduate student at Yale University, New Haven, CT 06511.
5. Physics Division Progress Report for Period Ending September 30, 1984, ORNL-6120, (1984).
6. E. Kallne and J. Kallne, Physica Scripta T3, 185 (1983).
7. C. R. Vane, M. S. Smith and S. Raman, ORNL report, in preparation.

ORNL-PHOTO 2061-85

Fig. 6.5. Photo of Von Hamos Spectrometer as attached to HHIRF Tandem beam line.

DEDICATED BEAMLINE FOR SINGLE EVENT UPSET MEASUREMENTS

S. Raman
L. P. Clark[1] E. G. Stassinopoulos[4]
S. C. McGuire[2] C. R. Vane
R. W. Miles O. Van Gunten[5]
E. Petersen[3] T. A. Walkiewicz[6]

Single event upset (SEU), the change of a logic state of a bit in memories and related semiconductor charge-storage devices, is due to the energy loss by ionization of a single energetic particle passing through a sensitive

region of the semiconductor device. As the physical dimensions and the associated total charge specifying a particular logic state decreases, computer failure due to SEU by heavy ions becomes of particular concern since this can lead to catastrophic results for space missions. Energetic ions with a stopping power, or linear energy transfer (LET), capable of inducing upsets include the Fe or C-N-O peaks in the cosmic ray flux.

Two different physical mechanisms are basically reponsible for single-event phenomena in space. Heavy-ion cosmic rays produce upsets directly by ionization energy loss. However, the cosmic ray intensity can vary appreciably with changes in the solar wind and solar activity. In the second mechanism, the populous cosmic ray protons produce upsets by way of ionization energy loss by particles produced in proton-induced nuclear reactions in silicon, primarily by the recoiling heavy ion. In either case, SEU requires deposition of a threshold amount of energy or critical charge near a sensitive region, and this critical charge depends primarily on circuit parameters. Although circuit modeling can yield reasonable results in some cases for critical charge and sensitive volume, from which upset rates can be predicted, it is still necessary to measure these quantities directly with heavy-ion beams for the numerous families of ICs susceptible to SEU and for all varieties of IC technologies and manufacturing processes.

SEU testing of devices by accelerator beams consists basically of measuring the upset cross-section (number of upsets per incident particle fluence) as a function of LET. The saturation cross-section yields the effective total area of charge collection regions, and the threshold LET yields the critical charge collected if the effective collection length is known. A predicted upset rate for the device can then be made for a particular radiation environment using an appropriate physical device model.

The advantages of using the 25 MV tandem accelerator for SEU testing include the relative ease of obtaining a wide range of energies of various ion species in order to obtain the necessary range of LET. Initial testing of several types of devices with beams of C, Ag, and Au has already demonstrated the usefulness of this machine (see next section of this report). Typical SEU cross-sections measurements demand very low ion flux ($\sim 10^3$-10^5 ions/cm^{2}sec) spread uniformly over large areas (many cm^2). A DC beam is also the best simulator of conditions in space. To efficiently provide these conditions a new beamline at the HHIRF tandem accelerator is being designed specifically for SEU testing. A schematic is shown in Fig. 6.6. It will include equipment necessary for ion beam preparation, transport, and

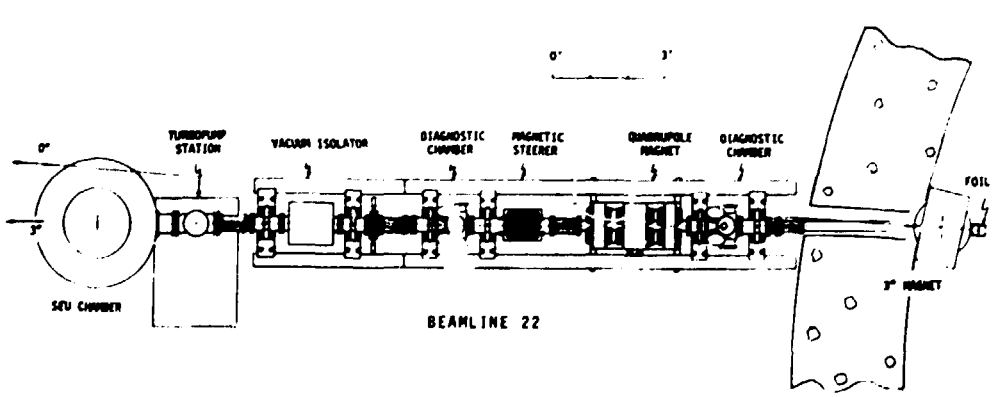

Fig. 6.6. Top-view schematic diagram of beamline designed for integrated circuit testing.

monitoring, as well as a large vacuum chamber instrumented for precise positioning of printed circuit boards containing many ICs under test. The beamline and chamber are expected to be completed in late 1986. This facility will allow detailed studies of upset cross-section versus energy, from which distinct critical charges may be determined for specific sensitive regions of the device, and a microbeam can be used to directly characterize single junctions of an integrated circuit.

1. NASA Headquarters, Washington DC 20546.
2. Alabama A & M University, Huntsville, AL 35762.
3. Naval Research Laboratory, Washington DC 20375.
4. NASA, Goddard Space Flight Center, Greenbelt, MD 20771.
5. NSA, Physical Sciences Laboratory, College Park, MD 20740.
6. Edinboro University, Edinboro, PA 16444.

SIMULATION OF COSMIC RAY EFFECTS ON INTEGRATED CIRCUIT LOGIC DEVICES

W. A. Kolasinski[1] J. Olsen[3]
G. J. Brucker[2] S. Raman
R. Koga[1] C. R. Vane

Upset of digital electronic circuits by cosmic rays in space (termed "Single Event Upset" or SEU) was predicted more than two decades ago[4]. However, it is only during the late seventies, with the greatly increased use of microcircuits in space vehicles, that the phenomenon of SEU became of wide concern in the space community, and so to speak, "fashionable" as a topic of investigation.

Recently, we have performed an experiment on the HHIRF tandem accelerator to evaluate its suitability for future SEU investigations and to assess the vulnerability of several microcircuits to SEU in the process. Table 6.4 summarizes the tests performed and their results. The experiment has demonstrated conclusively that the HHIRF tandem can be a very valuable tool in the SEU area of applied research. Some of the results listed in Table 6.4 are discussed in more detail in what follows.

Many descriptions of test procedures for SEU have been published in the literature[5] and they will not be reiterated here. Suffice it to say that in all cases involving circuits where information is stored, we enter the information into the device just before or during the bombardment with beam. The information contents of the device could be checked for errors and corrected during the bombardment (dynamic test) or left undisturbed till the conclusion of bombardment (static test). At the end of each irradiation all the errors and total beam fluence were recorded. Figure 6.7 shows the experimental hardware in schematic form.

Table 6.4. Summary of Results of the Cosmic-Ray-Simulation Experiment

Devices		Beams		
ID No.	Description	126 MeV ^{12}C dE/dx = 1.3 MeV-cm^2 mg	374 MeV ^{108}Ag dE/dx = 54 MeV-cm^2/mg	591 MeV ^{197}Au dE/dx = 88 MeV-cm^2/mg
SA 2999	16 Kx1 EAROM	Read: No effect Write: No effect	Read: No effect Write: Permanent Damage	Read: No effect Write: Permanent Damage
TA 12702	16 Kx1 RAM	Not tested	Not tested	Some upsets seen
SA 3240	16 Kx1 RAM	Not tested	Some upsets	Some upsets
93L422	256 x4 RAM	Many upsets	Not tested	Not tested
93422	256 x4 RAM	Many upsets	Not tested	Not tested

ORNL-DWG 85-17776

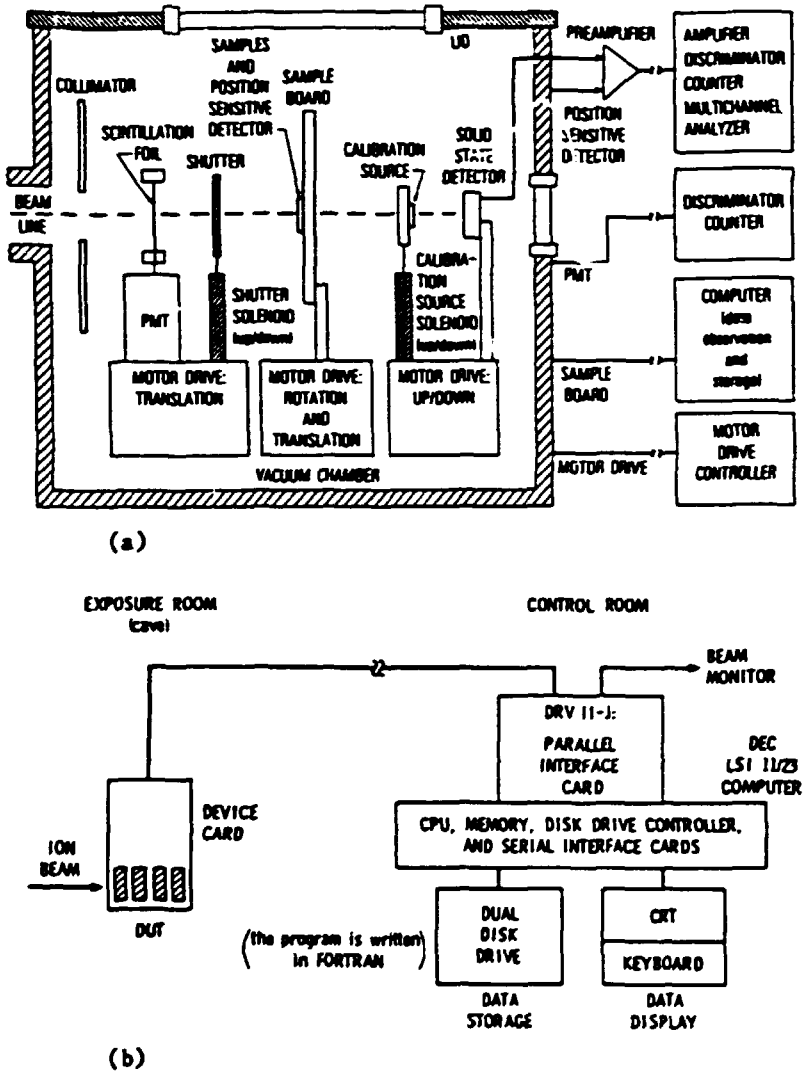

Fig. 6.7. Schematic representation of test hardware. (a) Beam-control and exposure apparatus, and (b) Computer hardware for test-drive operation and data recording.

The ratio of the total number of errors to the particle fluence was calculated and, in analogy with nuclear physics terminology, defined as the upset cross-section. An example of upset cross-sections plotted as functions of the incident particle energy transfer (LET or dE/dx) appears in Fig. 6.8. The experiment for which the results are given in this figure was performed to assess the effect of feature size in CMOS/SOS RAMs on critical charge for SEU. The results, together with data taken at the Lawrence Berkeley Laboratory 88-Inch Cyclotron, have been published by Brucker, et al[6].

In the case of the SA2999 EAROM, a completely unexpected result was obtained. Irradiation of the device with gold or silver ions, even at zero bias, resulted in permanent damage to individual memory cells. No damage

ORNL-DWG 85-17777

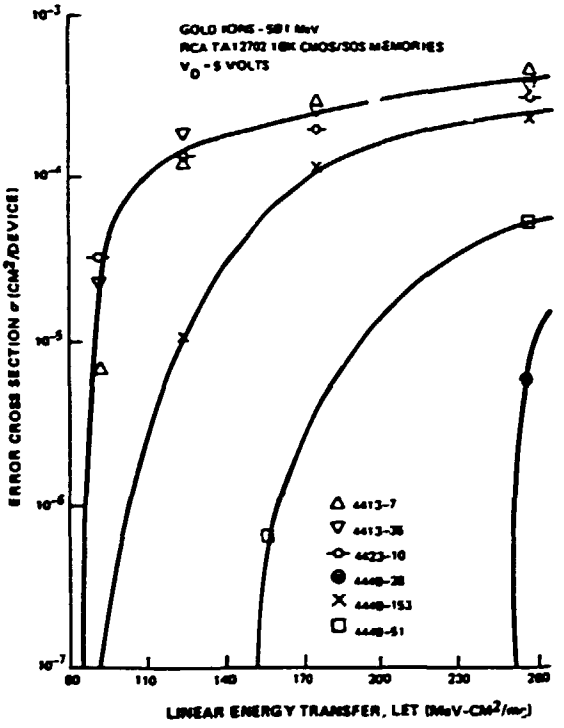

Fig. 6.8. Error cross section versus linear energy transfer (LET) for test memories exposed to 591-MeV Au ions.

of any kind was observed, with or without bias, when the device was bombarded with carbon. Subsequent tests at Berkeley showed the onset of permanent damage occurs at an LET or dE/dx value somewhere between 17 and 40 MeV-cm^2/mg. Clearly an experiment to pin down the value more accurately would be worthwhile.

The tests on the SA3240 RAMs were performed to evaluate the effect of resistors of various sizes used to decouple the inverter-pair gates in the RAM cells and thus increase the critical charge required for upset. The experiment showed that 200K resistors were required to make the cell completely impervious to SEU - a very useful result!

In the case of the fourth and fifth devices in Table 6.4, we wanted to measure and compare the threshold LETs for upset which were already known to be quite low. Unfortunately, we overestimated the threshold LET and were able to establish only an upper bound of 1.3 MeV-cm^2/mg for the threshold, before running out of allocated machine time.

---

1. Aerospace Corporation, Los Angeles, CA 92957.
2. RCA Astro-Electronics, Princeton, NJ 08540.
3. Sandia National Laboratories, Albuquerque, NM 87185.
4. J. T. Wallmark and S. M. Marcus, "Minimum Size and Maximum Packing Density of Non-Redundant Semiconductor Devices," Proc. IRE 286-298 (1962).
5. R. Koga and W. A. Kolasinski, "Heavy Ion Induced Single Event Upsets of Microcircuits: A Summary of The Aerospace Corporation Test Data," IEEE Trans. Nucl. Sci. NS-31, 1190-1191 (1984).
6. G. J. Brucker, R. Smeltzer, W. A. Kolasinski and R. Koga, "Soft Error Dependence on Feature Size," IEEE Trans. Nucl. Sci. NS-31, 1562-1563 (1984).

PRODUCTION OF UNIFORM, VERY-LOW INTENSITY ION BEAMS THROUGH RUTHERFORD SCATTERING

L. Maliner[1] . C. R. Vane
S. Raman O. Van Gunten[2]

There is a need in several areas of applications of heavy ions (for example, in upset testing of integrated circuits and in production of distributed, micron-size holes in insulating foils) for very-low intensity (<10^4 ions/cm^2 sec) beams spread uniformly over areas of many cm^2. Because typical ion beam currents, under stable, slit-controlled accelerator operation, are >1 enA, the primary beam must be attenuated by ~10^5 to reach the required levels. Several methods of attenuation have been considered including:

(1) passage of primary beam through a small aperture (where most ions are lost) with subsequent defocusing to achieve large beam spot size on target,
(2) passage of primary beam through a thick foil producing significant angular spread followed by downstream apertured selection of a small fraction of transmitted beam,
(3) magnetic selection of charge states far from equilibrium to achieve attenuation, with subsequent beam defocusing, and

(4) Rutherford scattering of primary beam from a thin target foil and subsequent apertured selection of a small transmitted solid angle to maintain beam uniformity.

We have studied the last of these in some detail because of certain advantages it has over the others, namely that the experimenter can, by choosing scattering foils and angles, vary the intensity, uniformity, and energy of the secondary ion beam on target rapidly and predictably.

We considered two cases for study in a computer model. In the first case, shown schematically in Fig. 6.9(a), a primary ion beam of intensity I_0 is scattered (assumed totally Rutherford) from a single foil, and a small solid angle element is allowed to pass downstream to the target. With heavy (e.g., Au) foils of thickness ~300 μg/cm^2, the fraction (f) of primary beam reaching the (2.5 x 2.5)cm^2 target area can be selected by choosing the appropriate scattering angles θ_1 and θ_2. Unfortunately, the beam intensity usually varies significantly over the target area, as expected since $d\sigma_R \sim \sin^{-4}\theta$. Simultaneously achieving the required beam intensity and uniformity can be accomplished only with small angles θ_1 and θ_2 and distant targets. For example, with 10 enA of 2 MeV/nucleon Cu^{5+} ions scattering from a 300 μg/cm^2 Au foil (from θ_1 = 3.0° to θ_2 = 3.3°) located 5 m upstream of the target area, f = 1 x 10^{-5}, and the beam intensity on target varies by ±16%.

The second method for achieving uniform low-intensity involves double Rutherford scattering as shown in Fig. 6.9(b). Again assuming pure Rutherford scattering, a computer model was used to calculate the scattered beam intensity at a given target location. The results are shown in Fig. 6.10 for a 10 enA, 2 MeV/nucleon Cu^{5+} beam scattering from two 200 μg/cm^2 Au foils, with θ_1 = 1.2° and θ_2 = 1.8°. The mean intensity on target is 2 x 10^3 ions/cm^2 sec (f = 3 x 10^{-6}). Angular straggling effects have not been included in the calculations. Experimental tests of the model results will be carried out soon.

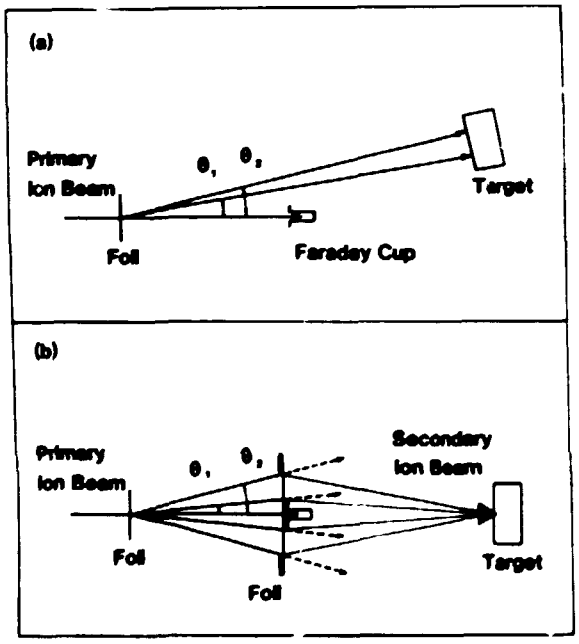

Fig. 6.9. Schematics of Rutherford scattering techniques for production of uniform, low-intensity ion beams. (a) Single scattering, and (b) Double scattering.

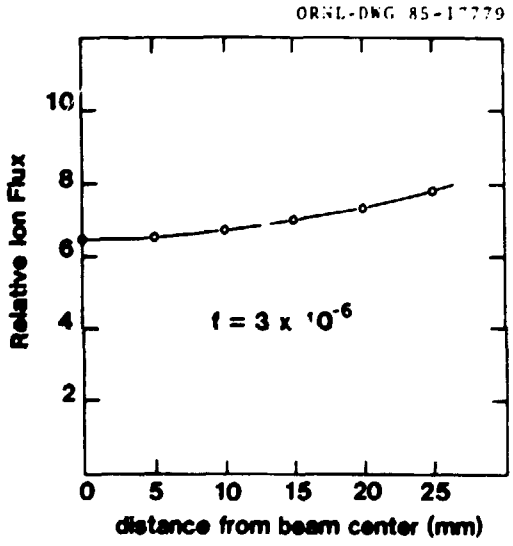

Fig. 6.10. Radial ion intensity distribution at target position for 2 MeV/nucleon Cu ions subjected to double Rutherford scattering.

---

1. ORAU summer student from Union College, Schenectady, NY.
2. Physical Sciences Laboratory, NSA, College Park, MD. 20740.

7. PLASMA DIAGNOSTICS FOR FUSION PROGRAM

ALPHA PARTICLE DIAGNOSTICS

D. P. Hutchinson
K. L. Vander Sluis
R. K. Richards[1]
C. H. Ma

In an ignited D-T fusion reactor, the 3.5 MeV fusion-product alpha particles will provide the energy required to sustain ignition. Techniques for monitoring these products as they thermalize and give up their energy to the plasma will be crucial to the development and operation of a successful reactor. During the past year we have concentrated our efforts on development of the necessary technology to perform laser Thomson scattering from alpha particles in a burning plasma. With this technique, information about the velocity distribution of these products is obtained from the Doppler shift of the laser radiation which is scattered at small angles.

One feature which is essential to the success of this diagnostic is an optical-heterodyne scheme for detection of the scattered radiation. A test stand has been constructed to analyze and optimize the noise figure of the multichannel heterodyne receiver for the experiment. The primary components of this facility are a 5-watt waveguide, single-mode CO_2 laser, a 500-K blackbody source, and the associated electronics to heterodyne-detect the blackbody signal from the detector. The test stand will also be used to measure the absorption coefficient of a CO_2 hot cell. This cell will be used in the receiver optics assembly to attenuate any stray laser light entering the detection system. A low-power sequence-band CO_2 laser has also been developed and tested for use as a local oscillator in this system.

A resonator design has been chosen for the high-power pulsed CO_2 laser that will restrict operation to a single fundamental mode, an essential feature for the small scattering angles required by the experiment. The pulsed laser source for the scattering experiment will be a 100-J Lumonics Model 602 laser. The laser cavity is being modified to include a 1-meter-long low-pressure transverse discharge cell and unstable-resonator optics. The low-pressure cell, containing a $He-CO_2-N_2$ laser mixture will be fired by a thyratron approximately 90 μsec before the main discharge of the pulsed laser is initiated. The population of the upper laser level in the low-pressure cell will be a maximum after the 90-μsec delay resulting in a slower rise time and longer duration of the 100-J pulse. The unstable resonator optics configuration will restrict operation of the laser to a single fundamental mode. The intra-cavity low-pressure cell and unstable resonator should produce a pulse length of approximately 1 μsec with a beam divergence compatible with the requirements of the scattering experiment.

We have defined an experiment on a nonburning plasma which we believe will demonstrate the feasibility of the alpha-particle scattering diagnostic. In our original feasibility study,[2] we predicted that the scattered signal from the alpha-particles would be three to five times the signal from background plasma electrons over a particular range of frequency shifts from line center (5 to 20 GHz). Therefore, we plan to perform a small-angle scattering experiment from electrons in a non-burning plasma. If we are able to measure the scattered signal from the background electrons, then we may proceed with further development with some confidence that the diagnostic system will have the sensitivity to measure the alpha-particle density and velocity distribution in an ignited plasma. In addition, the detection of scattered radiation from the electrons at larger frequency shifts (40 to 60 GHz) would permit a study of the high energy tail of the electron distribution in a region inaccessible to standard Thomson scattering diagnostics.

1. Fusion Energy Division.
2. D. P. Hutchinson, K. L. Vander Sluis, J. Sheffield and D. J. Sigmar, Feasibility of Alpha Particle Measurement by CO_2 Laser Thomson Scattering, ORNL/TM-9090, Oak Ridge National Laboratory, December 1984.

MULTICHANNEL INTERFEROMETRY

W. H. Casson[1] H. T. Hunter
C. H. Ma D. P. Hutchinson
R. K. Richards[2] K. L. Vander Sluis
C. A. Bennett[3]

The ISX interferometer system was moved from the Y-12 plant to the development laboratory at X-10 for modifications necessary for installation on the Advanced Toroidal Facility (ATF) in late 1986. Observation of laser stability and noise indicated that changes to the basic laser design were necessary in order to improve resolution and reliability. The interferometer system consists of two independent laser systems operated at a constant frequency difference of about 1 MHz. Each laser system is comprised of a carbon dioxide pump laser and a far-infrared (FIR) optically pumped laser cavity. Figure 7.1 shows the five-channel system in place on the ISX-B tokamak. The output wavelength can be chosen from a very large number of known laser lines by changing the molecular gas and the pump frequency. An analysis of the required spatial resolution and refractive effects on ATF dictate a shorter wavelength than was used on ISX. The most attractive candidate is the 119-micron line of methyl alcohol which is one of the strongest emission lines in the FIR. For accurate Abel inversion of chordal data from the highly elliptical cross section of the ATF plasma, a 15-channel system is necessary. In order to operate this number of channels, each with an individual system of optics, the amount of alignment work necessary and the required design complexity becomes prohibitive. The alternative that has been chosen is a single optical beam, highly elliptical in cross section, which will be focused onto a detector array after passing through the plasma. Each element of the detector array will consist of a Schottky diode mounted in a corner cube reflector. The total number of optical elements necessary can thus be reduced from about 225 to around 30.

ORNL-Photo 8655-82

Fig. 7.1. Photograph of the five-channel FIR interferometer/polarimeter system installed on the ORNL ISX-B tokamak. The optical waveguides and Schottky-diode detectors are visible in the foreground. The optically pumped laser systems are located beneath the detector array.

Modifications made to the carbon dioxide pump laser include elimination of the internal Brewster windows, redesign of the electrodes, and a slightly different set of cavity optics. The Brewster windows, which were mounted between the electrical discharge tube and the internal optical elements, were a known source of beam distortion and thermal noise. They have been eliminated by installing the optics within the vacuum of the discharge but physically separated from the discharge by a reasonable distance. Distortion of the discharge itself was reduced by designing electrodes which are symmetric about the discharge axis. Further improvement

of the pump laser was made by replacing the plane grating, used for selection of the carbon dioxide emission line, with a spherical curved grating and replacing the curved output coupler with a plane coupler. This effectively decreases the power density on the grating surface, optimizes use of the discharge volume, and places the output beam waist at the output coupler. One further improvement in the pump source was made by replacing the ZnSe lens used to focus the beam into the FIR cavity with a curved reflector, thereby further reducing beam distortion.

Most laser control functions are being automated by a complex feedback arrangement overseen by a small computer control system. The carbon dioxide laser will be tuned for optimum power and frequency by an acousto-optic cell monitoring device. FIR output will be monitored for output power and the frequency difference between the two laser systems. The operator will have a continuously updated readout of all laser functions and will have override control at all times. The resulting improvements in the interferometer will give a single operator the ability to start up and operate the laser system, as well as monitor the data output and analysis.

---

1. ORAU Postdoctoral Research Associate.
2. Fusion Energy Division.
3. ORAU Summer Faculty Research Participant, University of North Carolina, Asheville.

FAR-INFRARED SOURCE DEVELOPMENT

D. P. Hutchinson J.-N. Juang[1]
C. H. Ma

The availability of a suitable directly excited laser source of far-infrared (FIR) radiation would be of significant benefit in plasma diagnostics, both in simplicity of operation and cost. We have begun the development of a directly excited HCN laser which we intend to use to study density fluctuations in the ATF device currently under construction in the Fusion Energy Division. In the past, HCN lasers were very large and required long down times for maintenance. Recently, work by several experimenters in Japan and the Soviet Union has pointed to the possibility of the construction of a reliable, high-power rf-driven HCN laser operating at a wavelength of 337 microns. We have undertaken the construction of a small rf-driven HCN laser to evaluate its performance as a source of FIR power for plasma diagnostic applications. Our initial tests have been very encouraging and we are proceeding with the design of an HCN laser with an integral radio frequency power oscillator.

---

1. Graduate student, Tennessee Technological University.

CALIBRATION OF THE FIR POLARIMETER ON TFTR TOKAMAK

C. H. Ma D. K. Mansfield[1]
D. P. Hutchinson H. Park[1]
K. L. Vander Sluis L. C. Johnson[1]

We have been engaged in the development of a multichord far-infrared (FIR) polarimeter for the TFTR tokamak at Princeton Plasma Physics Laboratory. During the past year, simultaneous measurements of electron density and Faraday rotation in TFTR tokamak plasmas have been achieved. Density measurements have been made successfully on all five channels of the FIR interferometer/polarimeter system. However, due to limited resources, both budgetary and time, a decision was made by PPPL to delay the multichord measurements of the Faraday rotation. The system has been routinely employed to study the ohmic- as well as neutral-beam-heated plasmas including multiple solid hydrogen pellet injections. It is believed that this is the first successful simultaneous measurement of electron density and Faraday rotation in multiple pellet-injected plasmas. Apparatus for expansion to ten-channel operation has been designed, constructed, and tested. The installation of the ten-channel system on TFTR is under way.

A schematic diagram of the interferometer/polarimeter system on TFTR is shown in Fig. 7.2.

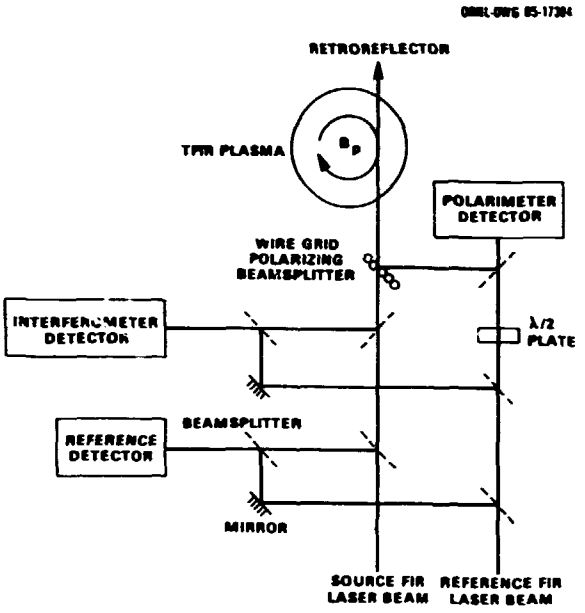

Fig. 7.2. Schematic of the FIR interferometer/polarimeter system on TFTR.

The system consists of a Michelson-type interferometer made from two cw 119-μm methanol lasers, optically pumped by a CO_2 laser. The beat frequency of the FIR lasers is usually adjusted to approximately 1 MHz by tuning the cavity length. The probing and reference beams are divided into ten channels (only five channels were in operation by April 1985) by metallic meshes. The probing beams go through the plasma from bottom to top and are returned by the retro-reflectors. All optical components are mounted on a diagnostic support structure totally isolated from the TFTR machine and supported on seismic isolators. The FIR laser beams are initially linearly polarized. A wire-grid polarizer is used as an analyzer to provide the Faraday rotation signal. The analyzer is adjusted such that it passes the outgoing probing beam and reflects any rotated component of the return beam. This component is mixed with a portion of the reference beam, and is directed onto the polarimeter detector. Schottky diodes are utilized for all detectors. The output of the polarimeter detector is filtered, amplified, and fed into an envelope detection circuit. If the ellipticity of the polarization of the return beam is negligible, the output of the detection circuit is proportional to $\sin(\theta_F)$, where θ_F is the Faraday rotation angle of the polarization vector, and is proportional to the line integral of electron density times the poloidal magnetic field along the double-path of the probing beam. Part of the beam from the reference laser is mixed first in the reference detector with a portion of the source laser, which is split off before passage through the plasma, and the remainder is guided to the signal detector to mix with part of the return beam. The outputs of both detectors are also filtered, amplified, and fed into a digital phase detection circuit to extract the phase shift produced by the electron density. Due to limited resources, only the outputs of the phase detectors are digitized for computer storage and processing (April 1985). The output of the envelope detection circuit is displayed on oscilloscopes for photographic recording (only one channel). The interferometer/polarimeter system was routinely employed to study the ohmic- as well as neutral-beam-heated plasma discharges in the TFTR tokamak for more than four months. Figure 7.3 shows the time-resolved traces of (a) line electron density and (b) rotation of a neutral-beam-heated plasma discharge. During this discharge, three solid hydrogen pellets were injected into the plasma at intervals of approximately one-half second. The abrupt changes of density and Faraday rotation occur during a period of approximately 400 μs.

An algorithm for the solution of the wave-propagation equation has been developed and has been used to determine the polarization evolution on the Poincaré sphere. Computer codes have been utilized to calculate the ellipticity, ϵ, and the rotation angle of the vibrational ellipse, ϕ, of the polarization.

The parameters for TFTR are major radius, $R = 265$ cm; minor radius, $a = 85$ cm; central electron density, $n_0 = 10^{14}/cm^3$; plasma current, $I_p = 2.5$ MA; toroidal field, $B_T = 5.2$ T; wavelength, $\lambda = 119$ μm. In this case, the maximum ϕ is approximately 15° with a maximum ellipticity

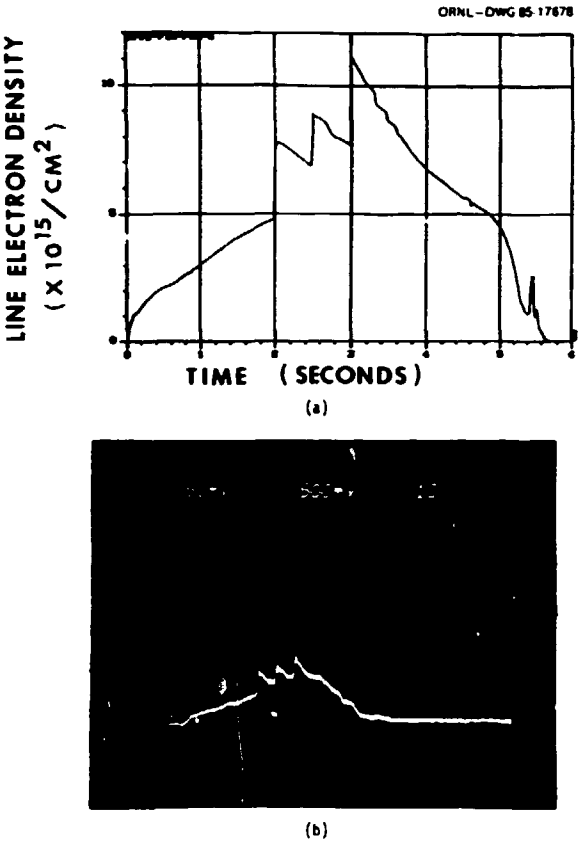

Fig. 7.3. Time variation of (a) line electron density and (b) Faraday rotation measured by the multichord FIR interferometer/polarimeter system on TFTR tokamak. The abrupt changes of the line density and Faraday rotation are caused by the injections of solid hydrogen pellets.

of 0.045 for double path of the beam. The output signals of the interferometer detector, V_i, and polarimeter detector, V_p, can be expressed by the following relations:

$$V_i = V_{io}\cos(\phi)[1 + \varepsilon^2\tan^2(\phi)]^{1/2} \cos(\Delta\omega t + \phi + \phi_i)$$

$$V_p = V_{po}\sin(\phi)[1 + \varepsilon^2\cot^2(\phi)]^{1/2} \cos(\Delta\omega t + \phi + \phi_p)$$

where V_{io} and V_{po} are the calibration constants for the interferometer and polarimeter, respectively, ϕ is the phase shift due to electron density, and ϕ_i and ϕ_p are given by

$$\phi_i = \tan^{-1}[\varepsilon \tan(\phi)]$$

$$\phi_p = \tan^{-1}[\varepsilon \cot(\phi)]$$

It can be seen in the equations that both the amplitude and the phase of the signals depend on the ellipticity of the polarization which cannot be measured easily due to limitations on the experimental techniques. The error in density measurement due to neglecting the ellipticity is very small (0.024 percent), and the error in the Faraday rotation measurement is approximately 1.7 percent.

During the period of operation, sinusoidal oscillation of the Faraday rotation signal due to the cross-coupling of the laser beams was observed. A modified theory for the polarimeter including the cross-coupling was developed. A comparison between the theory and the experiments gave excellent agreement. Experiments for calibration of the polarimeter were also carried out to determine the effects on the sensitivity of the system and the rotation angle due to the cross-coupled beams.

---

1. Princeton Plasma Physics Laboratory, Princeton, New Jersey.

8. HIGH ENERGY PHYSICS

H. O. Cohn W. M. Bugg[1]
G. T. Condo[1]

PHOTOPRODUCTION AT 20 GeV

The primary purpose of this experiment by the SLAC Hybrid Facility Photon collaboration was to study charmed particles, however, the vast size of the experiment has permitted photoproduction studies of vector meson and charge exchange processes which have heretofore proved impervious to analysis. We describe briefly studies which have been completed in the past year.

The first study utilizes data from the reaction, $\gamma p \to n\pi^+\pi^+\pi^-$. It was initiated to study s-channel helicity conservation in much the same way as was studied in the reaction $\gamma p \to \rho^0 N^* \to (\pi^+\pi^-)(p\pi^+\pi^-)$. The unusual occurrence in this channel was the observation of a signal in the neutral dipion spectrum in the f^0 mass region. The f^0 is not produced in the reaction, $\gamma p \to \pi^+\pi^- p$, which is dominated by pomeron exchange. Nor can it be produced by one-pion exchange since $f^0 \to \pi^0\gamma$ is forbidden by C-parity conservation. The enhancement in the 3π spectra of events in the A_3 and A_3' mass region strongly indicates that this is the source of these f^0 mesons. Thus, this became the first observation of the A_3 in a charge exchange process, and, being free of Deck-type backgrounds, verifies the existence of the A_3 in a totally model independent fashion.

The second study is devoted to the photoproduction of charged A_1 mesons in the reaction $\gamma p \to \Delta^{++}\pi^-\pi^-\pi^+$. The radiative widths, using Coulomb production, of the A_1, A_2 and B mesons have recently been measured at Fermilab. The $\pi\gamma$ width of the charged A_1 was found to be about twice that of the A_2 or B. This is reasonably consistent with theoretical estimates. Thus the isolation of a pion exchange process in photoproduction should result in the photoproduction of all of these states.

In the $p\pi^+\pi^+\pi^-\pi^-$ final state, the restriction to Δ^{++} events effectively eliminates diffractive ρ' (1600) production. After elimination of diffractive $\rho^0 N^* \to (\pi^+\pi^-)(p\pi^+\pi^-)$ events, the $\rho^0\pi^-$ spectrum at low t' contained a (relatively) enormous signal around 1300 MeV ($\sigma(\gamma p \to A_2\,\Delta^{++}) = 0.17 \pm 0.2$ μb at $|t'_{\gamma,3\pi}| < 0.15$ GeV^2). This signal also was far too broad to be consistent with an A_2 alone ($\Gamma = 211 \pm 29$ MeV). Our resolution in this mass region is about 10 MeV. Under the assumption that this enhancement represents both A_1 and A_2 production, we find that the A_1 mass and width are 1316 ± 30 MeV and 310^{+100}_{-60} MeV, respectively.

The study of s-channel helicity conservation in inelastic rho diffraction produced by the SLAC Hybrid Facility Photon collaboration shows that the ρ^0 produced in the reaction $\gamma p \to \rho^0_{fast} p\pi^+\pi^-$ has angular distributions and spin density matrix elements consistent with s-channel helicity conservation. Other features of elastic ρ^0 photoproduction and π-induced diffraction, such as the $\pi^+\pi^-$ mass shape skewing and $p\pi^+\pi^-$ mass distributions, are also similar.

NEUTRINO INTERACTION

During the past year we have worked on a high energy muon neutrino experiment (E745) at Fermilab, utilizing the Tohoku University holographic one-meter bubble chamber. Set-up for the experiment started in November 1984 and the first phase of data taking was completed in September 1985. Ten planes of 1.2-meter square drift chambers were designed and constructed by us as part of the counter bubble chamber hybrid system. We obtained about 200,000 untriggered conventional pictures (316 rolls) and 63,500 triggered holograms. The trigger was an interaction trigger with an efficiency of about 0.85 and false trigger rates of about 10/1. The

conventional film contains about 3,500 events, most of which are neutrino interactions. The quality of the conventional film is good, but since E745 is the first major holographic exposure in a large bubble chamber, the technique had to be perfected over the course of the run. At the start, only one-third of the events had holograms in which the vertex could be found, although tracks were generally present. By the end of the run the efficiency had increased to better than 2/3.

Scanning and measuring the film was begun while the experiment was still in progress. A digitized holographic scanning machine, using light from an argon laser is now operational to scan the holograms for abnormalities at the interaction vertex which could signal charm production. Three such candidates have so far been identified in our scanning effort. Preliminary data on prong distribution, measurement of quasi elastic neutrino interaction and other data useful for implementing improvements for the next stage of the experiment are being evaluated.

---

1. Adjunct staff member from the University of Tennessee, Knoxville, TN 37996.

9. COMPILATIONS AND EVALUATIONS

CONTROLLED-FUSION ATOMIC DATA CENTER

C. F. Barnett[1]
H. B. Gilbody[2]
D. C. Gregory
P. M. Griffin
C. C. Havener
A. M. Howald
H. T. Hunter
R. K. Janev[3]
M. I. Kirkpatrick
C. R. Mahon[4]
E. W. McDaniel[5]
F. W. Meyer
T. J. Morgan[6]
R. A. Phaneuf
M. S. Pindzola[7]
E. W. Thomas[5]

The Controlled-Fusion Atomic Data Center (CFADC) was established at ORNL in 1959, with a primary task to collect, review, evaluate, and recommend numerical atomic collision data of interest in controlled thermonuclear fusion research. The CFADC operates with an equivalent of two full-time staff members, as well as a number of expert consultants from the research community, upon which it depends heavily. The major activities of the data center are threefold:

- -the production of up-to-date bibliographies of fusion-related publications on atomic collision processes in computer files for on-line searching and publication.
- -the preparation and publication of compilations of recommended atomic collision data for fusion research.
- -the handling of user requests for specific data or information about relevant atomic processes.

The data center actively participates in cooperative agreements with the Atomic Data Center for Fusion at the Institute for Plasma Physics (IPP) of Nagoya University, Japan, the Atomic and Nuclear Data Center of the Japan Atomic Energy Research Institute (JAERI), and the Atomic and Molecular Data Unit of the International Atomic Energy Agency (IAEA) in Vienna. Our staff continues to participate in the IAEA International Atomic and Molecular Data Center Network and to advise the IAEA data center on their activities. Our bibliographic computer tapes are sent to these centers every three months and form the basis for the quarterly IAEA International Bulletin on Atomic and Molecular Data for Fusion.

Our data center also maintains a close cooperation with the Atomic and Molecular Processes Information Center at the Joint Institute for Laboratory Astrophysics in Boulder, Colorado, and with the NBS Data Center on Atomic Spectral Lines and Transition Probabilities in Washington.

During this reporting period, a major effort has been directed toward the preparation of an updated and expanded version of the 1977 two-volume compilation of recommended tabular and graphical data, entitled Atomic Data for Controlled Fusion Research, and published as ORNL-5206 and -5207 (commonly referred to as the "Redbooks"). The new multiple-volume series is entitled Atomic Data for Fusion, and will consist initially of five volumes (ORNL-6086 through ORNL-6090). These volumes, with their (expected) publication dates, are as follows:

- -Volume 1: Collisions of H, H_2, He and Li Atoms and Ions with Atoms and Molecules (10/86).
- -Volume 2: Collisions of Electrons with Atoms and Molecules (3/87).
- -Volume 3: Particle Interactions with Surfaces (published 2/85).
- -Volume 4: Spectroscopic Data for Iron (published 2/85).
- -Volume 5: Collisions of Carbon and Oxygen Ions with Electrons, H, H_2 and He (5/86).

All tabular and graphical data for the new "Redbook" series are computer-generated in publication-ready format. To make the recommended data more compatible with the needs of fusion-plasma modelers, a computer code has been

implemented to calculate Maxwellian rate coefficients from the cross sections, and to produce Chebychev polynomial fits to both the cross sections and rate coefficients. This will facilitate our plan to eventually place these recommended collision data in user-accessible files on the National Magnetic Fusion Energy Computer Center (NMFECC) network.

---

1. Consultant, ORNL.
2. Consultant, Queen's University, Belfast, Northern Ireland.
3. Consultant, Institute of Physics, Belgrade, Yugoslavia.
4. Consultant, University of Virginia, Charlottesville, Virginia.
5. Consultant, Georgia Institute of Technology, Atlanta, Georgia.
6. Consultant, Wesleyan University, Middletown, Connecticut.
7. Consultant, Auburn University, Auburn, Alabama.

NUCLEAR DATA PROJECT

Y. A. Ellis-Akovali M. R. McGinnis
M. J. Martin M. R. Schmorak

The Nuclear Data Project (NDP) is one of five data evaluation centers comprising the U.S. Nuclear Data Network (USNDN). The Project is responsible for the evaluation of nuclear structure information in the mass region A > 190. The NDP maintains a complete computer-indexed library of reports and published articles in experimental nuclear structure physics as well as copies of the Evaluated Nuclear Structure Data and Nuclear Structure Reference files (ENSDF, NSR).

The Project houses the position of Editor-in-Chief of the Nuclear Data Sheets. All mass chains from the 14 centers in the International Nuclear Data Network are edited here, and the Editor-in-Chief has the ultimate responsibility for the quality of the mass chains entered into ENSDF and, thus, for what is published in the Nuclear Data Sheets.

Activities

Data Evaluation. During this report period, NDP staff members prepared revised evaluations for 9 mass chains. References to the publications based on these evaluations are given in the publications section of this report.

Mass Chain Editing and Review. NDP staff members edited and/or reviewed 19 mass chains.

Information Services. NDP staff members responded to requests by researchers outside the evaluation center for specific information. Responses took the form of searches of the ENDSF and NSR files and personal consultation. A list of reports and preprints received by the NDP is prepared and distributed monthly to division staff members.

Research. NDP staff members have participated in research with other groups in the division. References to these activities are given in the publications section of this report.

10. BOOSTER ACCELERATOR STUDIES

G. D. Alton
R. M. Beckers[1]
J. B. Ball
J. A. Biggerstaff
S. Datz
P. F. Dittner
D. T. Dowling
D. L. Haynes
E. O. Hudson
J. W. Johnson
C. M. Jones
I. Y. Lee
R. S. Lord[2]
C. A. Ludemann
J. E. Mann[2]
J. A. Martin
J. B. McGrory
F. W. Meyer
P. D. Miller
W. T. Milner
S. W. Mosko
J. A. Murray[1]
D. K. Olsen
P. L. Pepmiller
G. R. Young
N. F. Ziegler

During the past year the division has investigated two possibilities for adding booster accelerators to the HHIRF. The collider study described in last year's report was completed and issued as ORNL report ORNL/CF-84/319. Because opportunities for obtaining funding for a booster for the present tandem accelerator seemed more likely, a group of division staff members evaluated the best energy range to pursue for a booster for nuclear physics research. It was decided to study a synchrotron ring that would have a bending strength of 8 tesla meters and to adjoin a storage ring of equal bending strength, which would contain an electron gun for phase-space cooling. In the same period of time, new developments in the atomic physics program raised interest in a smaller synchrotron ring designed especially for the study of the atomic physics of highly ionized heavy atoms. It was decided to investigate the design of a synchrotron/storage ring with a bending strength of 2 tesla meters for this program.

NUCLEAR PHYSICS 8-Tm RINGS

The existing tandem accelerator is proposed as the injector for these accelerators. Using foil stripping in the tandem terminal and at the tandem exit means that ions ranging from $^{12}C^{6+}$ to $^{238}U^{+3+}$ will be available. For a bending strength of 8 tesla meters, these charge-to-mass ratios correspond to 587 and 96 MeV/nucleon, respectively. To increase the duty factor for extracted beams and provide a separate area for cooling and internal target experiments, a separate storage ring is included. This ring would also have a bending strength of 8 tesla meters. It would be injected by fast transfer from the synchrotron and would contain a 250-keV electron gun for cooling heavy ions up to 500 MeV/nucleon. It would also contain an internal target area which would be used in conjunction with detectors, such as a magnetic spectrograph or the spin spectrometer. Since this ring operates in a storage mode, its magnets and power supplies would not have to be built for pulsed operation.

The tandem has been tested for macro-pulsed-beam operation. The results of these tests show that injected currents of 200 μA of negative ions with a duty factor of 10^{-3} cause no discernible change in performance of the tandem. A factor of 5 increase in this beam current would not fill the booster synchrotron to its incoherent space-charge limit and could be accommodated by the tandem. Since it was also demonstrated that the tandem could handle several pulses per second (eight/second were injected in the tests), we have decided to take advantage of this by making the booster a fast cycling machine with a repetition rate of 20 Hz.

The booster was designed with a simple gradient-magnet lattice with 16 cells and a superperiodicity of 8. The structure is $O_1QFFDO_2QFFDO_1$, where the drift O_1 is kept as short as possible and O_2 is stretched to 4 meters to accommodate special hardware such as injection and rf. Since the machine is fast cycling, the peak magnetic field is kept to about 8 kG, while the peak voltage delivered is $V\sin\phi_S$ = 38 kV.

The transfer line to the stretcher/cooler ring includes a pair of quadrupole doublets soon after ejection to provide a low β point for stripping foils, followed by an achromatic bend with a momentum-dispersed crossover at the center to allow charge-state selection, followed by an emittance-matching section for injection into the stretcher ring. The stretcher ring has a FODO type lattice set up to allow variable dispersion in both long straights. Modifications to provide a dispersion-free straight at the electron gun are being investigated. The circumference of the storage ring matches that of the booster. Since the dipoles are operated in dc mode, their peak fields are chosen to be 16 kG. This frees much of the circumference of this ring for specialized optics in the straight insertions. The ejection line from the stretcher leads through a splitter magnet and then either back to the booster (e.g., for reacceleration after stripping for a very heavy ion) or to the existing target caves at HHIRF. The reinjection capability is attractive, either to provide a second acceleration for very heavy ions at a bette charge-to-mass ratio than the one they had upon initial injection into the booster, or to provide for deceleration of either highly ionized, very heavy beams for atomic physics studies or secondary radioactive beams for [e.g., (HI,xnγ)] experiments.

A layout of the booster and storage ring on the HHIRF site is shown in Fig. 10.1. A detailed layout is presented in Fig. 10.2, illustrating transfer lines to and from the present facility and transfer lines between

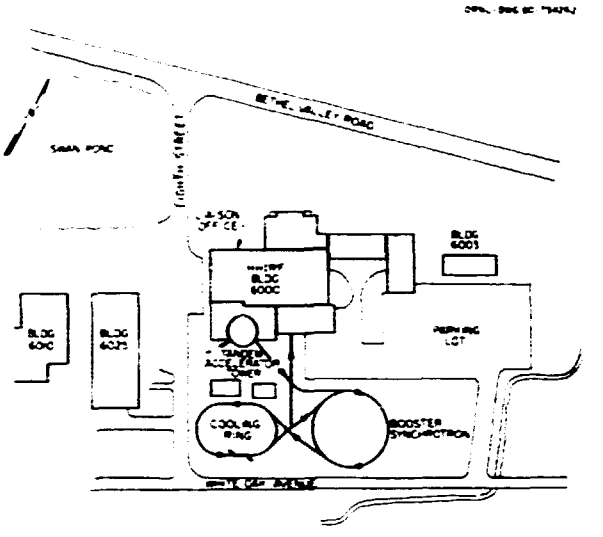

Fig. 10.1. Site plan for the 8-Tm booster.

the rings. The expected energy per nucleon for beams, both with and without stripping after exiting the tandem, is given in Fig. 10.3. The corresponding beam currents, given in units of particle nanoamperes, are shown in Fig. 10.4.

To explore the physics potential of such a complex, a workshop was held on September 23-25, 1985. From the ensuing discussions, a reexamination of the maximum energy from the accelerator is being made, with a view to increasing the top energy to provide a facility which can produce a good yield of fully ionized uranium ions.

ATOMIC PHYSICS 2-1m RING

Many types of atomic physics collision studies could be carried out if stored beams of cooled, highly charged heavy ions were available. These include both experiments of interest to basic research and experiments of interest to, for example, the fusion confinement program. Some of the possible experiments are listed here.

A. In-Ring Experiments

1. Electron-ion interactions: These experiments are a natural consequence of having the electron beam cooling section in place; i.e.,

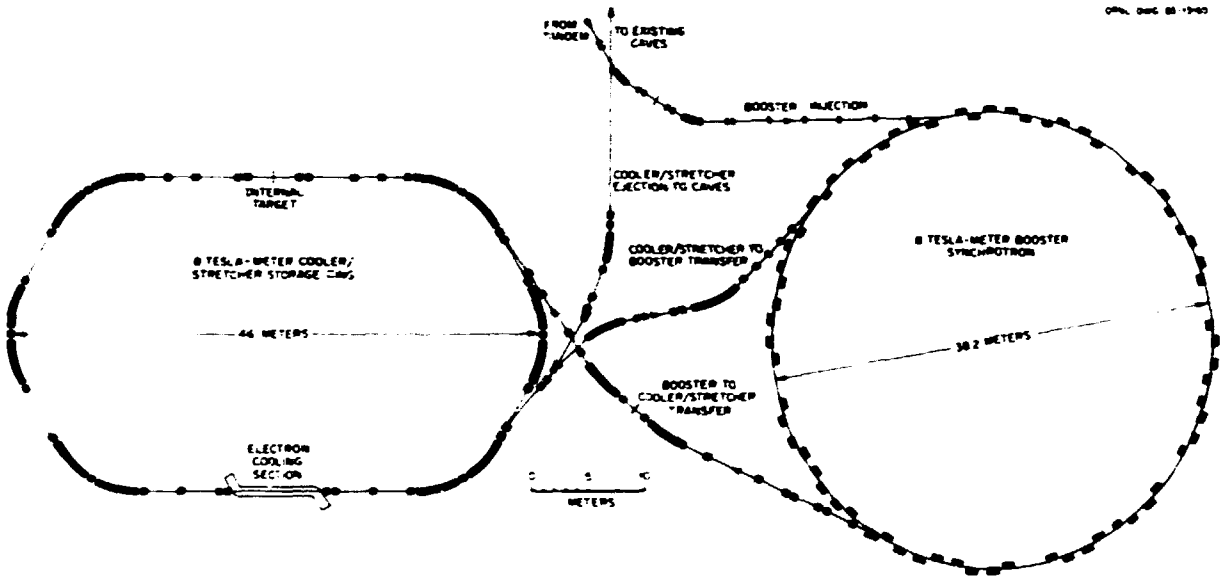

Fig. 10.2. Machine laycut of the 8-Tm booster and stretcher rings.

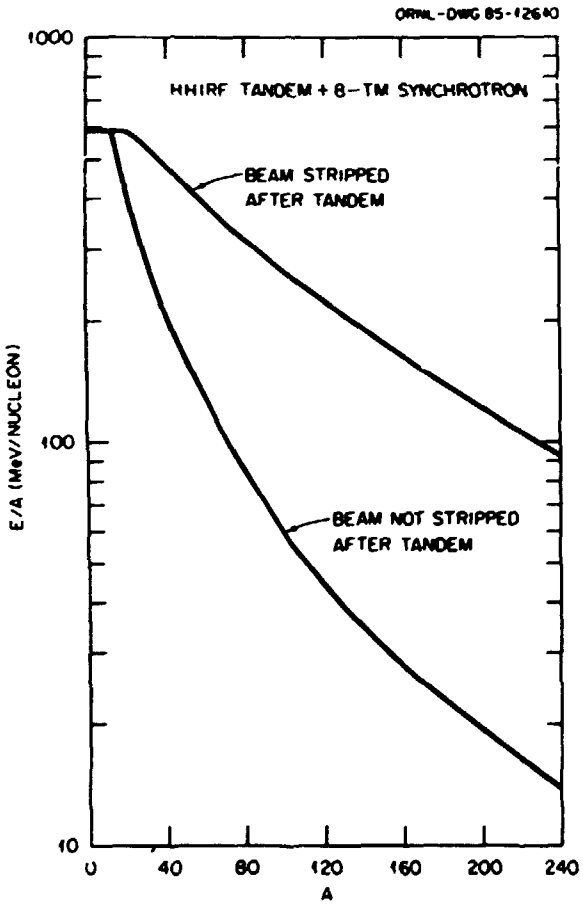

Fig. 10.3. Energy/nucleon as a function of mass number for the 8-Tm booster, with and without stripping at the tandem exit.

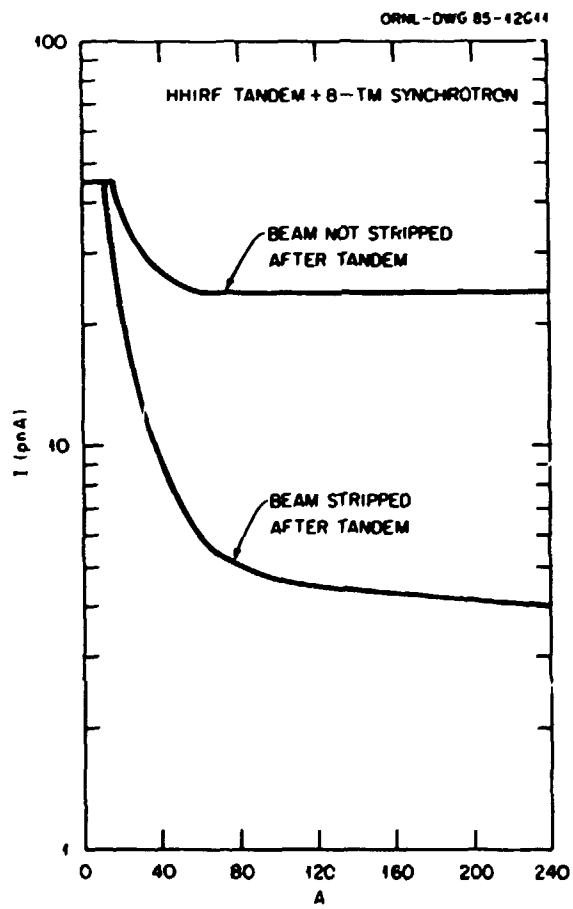

Fig. 10.4. Current in particle nanoamperes as a function of mass number for the 8-Tm booster, with and without stripping at the tandem exit.

this section is a merged-beam system in which low-energy interactions can be studied with very high resolution.

2. Photon-ion reactions: If a laser beam is directed down a straight. the same ions are exposed to the beam at every pass. If the lifetime of the state being excited is greater than 1 μs (the ring transit time), the effective exposure time is continuous, and extremely narrow lines may be obtained.
3. Photon-electron-ion interactions: In these experiments a laser beam is directed down the "cooling" straight which contains the merged-electron-ion beam. Possible experiments include laser-enhanced dielectronic recombination and laser-enhanced radiative recombination.
4. Ion-atom collisions: Because of the stringent vacuum conditions, an in-ring gas target will have to be very dilute. However, the in-ring current is extremely large, which will provide large signals with very dilute targets.
5. Ion-ion interactions: All types of merged-beam experiments at low energies are possible. Cooling the primary heavy-ion beam makes possible decelerating it, greatly relaxing energy requirements for the injector of the second ion beam. Crossed-beam experiments of ions with ions can be studied by crossing a second beam with the stored ion beam.
6. Precision spectroscopic studies: Transitions in highly charged ions can be studied by taking advantage of the very small Doppler shift and broadening for a decelerated cooled beam.
7. Electron capture, plasma impurities, radiative capture, and loss processes can be studied for different charge states and at variable energies, particularly at very low energies characteristic of impurity ions in a confined plasma.

B. Extracted Beams

Beams can be extracted either as a single pulse or by gradual draw-down of the stored beam. External experiments are as with other systems. One advantage of this ring is that decelerated beams can be produced with excellent emittance, so that low-energy differential scattering experiments are made possible.

Sources of highly charged ions, such as an electron cyclotron resonance source (ECR) or an electron beam ionization source (EBIS), produce modest currents with a low duty factor in the latter case; whereas a stored highly charged beam can have 100% duty factor and an effective increase in current of 10^6 by recirculation of the beam.

The production of highly charged ions for atomic physics research usually requires first accelerating them and then passing them through a thin foil. This means experiments must be done with beams having kinetic energies of several MeV/nucleon; whereas, frequently, the energies of interest are one to three orders of magnitude lower. These beams must usually strike targets of neutral atoms. Many interesting experiments could be done if it were possible to study collisions between charged ions.

The following considerations summarize the utility of a heavy-ion cooling ring (HICR) as described above.

a. A HICR would provide variable energy beams of highly charged ions with 100% duty factor and an effective current of more than 1 particle microampere.
b. A HICR would provide cooled beams with very small transverse momentum spread and size for precision spectroscopy and very low center-of-mass energy studies.
c. A HICR would allow experiments with crossed or merged beams. The following classes of collisions are possible: ion-electron, ion-photon, ion-ion, and ion-atom.
d. A HICR would allow studies of long-lived states of highly charged ions by virtue of its ability to store ions for extended periods of 1 second up to 1 hour.
e. Some nuclear physics needs could be filled by HICR beams. An example here would be the use of extracted beams of, for example, 50-MeV/nucleon ^{16}O with very good emittance

and delta-p/p for precision studies of giant resonances.

The HICR will consist of a small synchrotron cooling ring of approximately 47-m circumference, which will form an addition to the heavy-ion accelerators existing at the HHIRF. The project will include a special electron gun for producing low temperature, intense beams of electrons, which will be used to cool heavy ions circulating in the synchrotron ring. The project will also include special equipment for injecting heavy-ion beams either from the tandem electrostatic accelerator at HHIRF or from an electron cyclotron resonance ion source (ECRIS) from which the beam has been accelerated by a radio-frequency quadrupole (RFQ) preaccelerator. Capability will be provided for accelerating or decelerating these beams and for either using them for experiments in the ring or extracting them to bombard an external target. The ring will be able to accommodate beams of very heavy ions, such as gold nuclei, at kinetic energies from 20 keV/nucleon up to 8 MeV/nucleon. The ring will have a bending limit of 2.0 tesla meters $EA/q^2 = 192$ MeV.

The cooling ring will be housed in an addition to the present HHIRF building. The cooling ring will consist of 8 dipole magnets, 12 quadrupole magnets, and a number of correction and steering magnets arranged in a four-sided pattern. The electron gun and associated beam-merging and capture equipment will occupy a straight section of the ring free of magnets. A tuned radio-frequency cavity will occupy another straight section. Injection and extraction equipment will occupy a third straight section, and the fourth straight section will be kept free for insertion of various devices as part of the experimental program. A vacuum of approximately 10^{-12} torr will be required in the vacuum chamber due to the large charge-changing probabilities for very heavy ions. Figure 10.5 shows a layout of the ring, injection lines, and the ECR and RFQ.

This ring will be used to accelerate, decelerate, cool, and perform experiments with cooled, stored beams of several charge states. The arrangement of the quadrupole magnets should produce beta functions which are small in the dipole magnets. However, in the cooling section the minimum value of β is limited by the desired upper limit of the cooling time, because a small β gives a large angular divergence which requires more time to cool to a given final emittance. On the other hand, the minimum angular divergence of the beam attainable by cooling is limited by the angular divergence of the electron beam due to thermal motion. The minimum angular divergence of the electron beam is thus given by the electron gun design. Since the emittance $\epsilon = \theta^2\beta$, a smaller emittance can be reached if the cooling section has a small β function. A value of $\beta \sim 10$ m gives optimal cooling rates for a beam with an energy of 50 MeV/nucleon, emittance $\epsilon = 40\pi$ mm-mrad, and an electron thermal temperature of 0.1 eV.

It is desirable to have the beam nondispersive in the straight sections for cooling, rf, and experiment. The requirement of holding several charge states simultaneously means the maximum value of the dispersion function has to be small. Also, it is important that quadrupoles be placed in dispersive sections so that the sextupoles for chromaticity correction can be placed nearby. In addition, the horizontal and vertical β functions should be different at the sextupoles.

The values of tune of the synchrotron have to be chosen to avoid resonances, especially the structure resonances. We plan to use one-third integer resonance extraction horizontally, meaning the horizontal tune has to be near a one-third integer not corresponding to a structure resonance. Also, it is preferable to have the horizontal and vertical tune differ by an integer amount in order to have a large resonance-free space around the working point.

In addition to long straight sections, additional space for correction magnets, bump magnets for injection, vacuum equipment, and beam monitoring devices has to be provided in the ring. Since space is at a premium, the trade-off between circumference and aperture is an important consideration.

Finally, the lattice has to be reasonably tolerant to magnet strength and alignment errors, so that only a small aperture allowance will be needed for closed orbit distortion and beta function variations.

The lattice as shown in Fig. 10.5 has fourfold symmetry. Each quadrant consists of a quadrupole triplet between two dipole magnets. In addition, each quadrant has reflection symmetry about its mid-point. The straight sections are 4 meters long. Three of the straights are used for cooling, extraction, and experiments, respectively. The fourth one is used for both injection and the rf cavity.

The nondispersiveness in the straight sections is achieved by making the three-quadrupole and two-dipole section a 90° achromatic bend. The quadrupole triplet consists of focusing (F)-defocusing (D)-focusing (F) quadrupoles in the horizontal plane. This arrangement minimizes the dispersion in the quadrupole magnets. The horizontal and vertical tunes of the ring are chosen to be near 7/3, i.e., $\nu_x = 2.3088$ and $\nu_y = 2.2744$, which avoids structure resonances at $\nu = 8/3$ and facilitates extraction by excitation of the third integer resonance. The parameters of the synchrotron are given in Table 10.1; lattice functions are shown in Fig. 10.6.

In order to hold several charge states of the same beam in storage mode, the chromaticity has to be cancelled by using higher multipole magnets (i.e., sextupole, octupole, etc.). Since all the quadrupoles are in dispersive regions, this cancellation can be achieved locally by placing a multipole magnet next to each quadrupole. A 12-pole magnet will be used for this chromaticity correction. Its primary excitation will be sextupolar, while small correcting multipole components will also be applied.

---

1. Engineering Division.
2. Consultant.

ORNL-DWG 85-15677

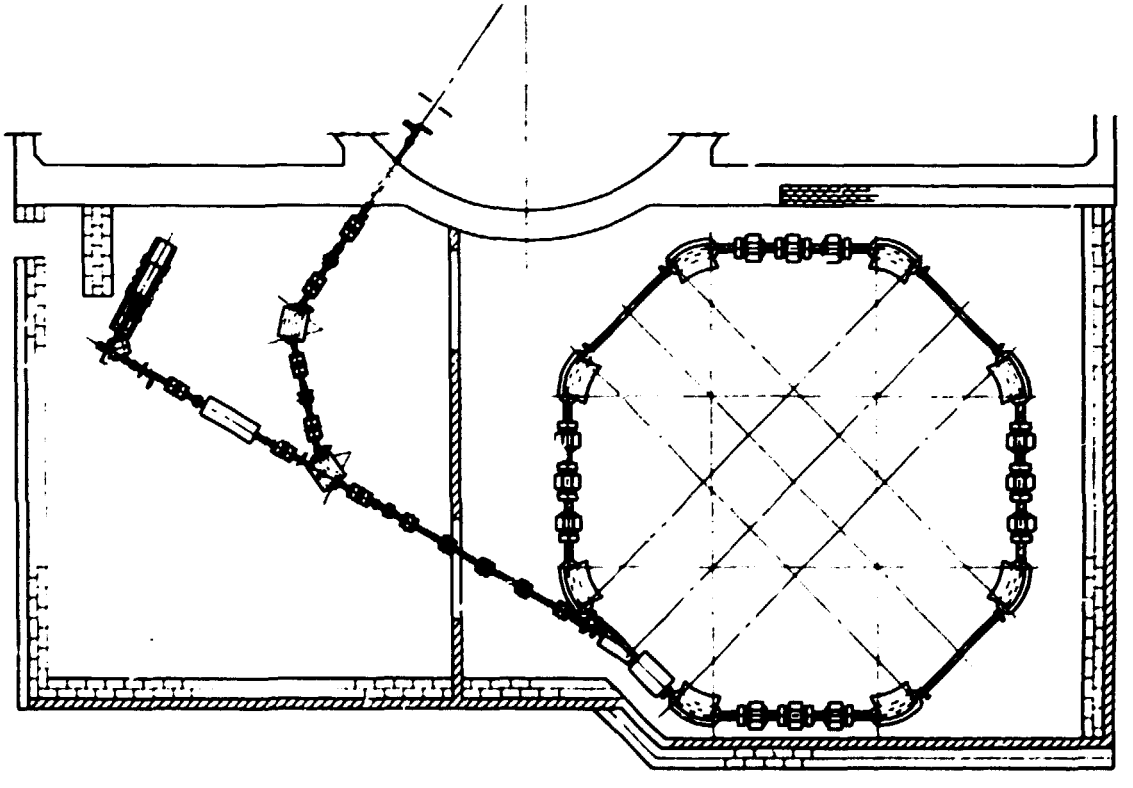

Fig. 10.5. Plan view of the proposed 2-Tm atomic physics ring.

Table 10.1. Parameters of the synchrotron

Magnetic rigidity	$B\rho$ = 2.0 Tm
Circumference	C = 46.7577 m
Long straight (4)	ℓ_S = 4.0 m
Dipole (8)	ρ = 1.6666 m
	θ = 45°
	ℓ_D = 1.309 m
Quadrupole (12)	ℓ_Q = 0.5 m
Q_F (8)	G_F = 3.6977 T/m
Q_D (4)	G_D = -4.1769 T/m
Tune	ν_x = 2.3088; ν_y = 2.2744
Chromaticity	ξ_x = -6.1846; ξ_y = -1.524
Beta function	
Dipole	$\hat{\beta}_x$ = 11.4 m; $\hat{\beta}_y$ = 5.7 m
Quadrupole	$\hat{\beta}_x$ = 12.2 m; $\hat{\beta}_y$ = 5.0 m
Straight	$\check{\beta}_x$ = 10.5 m; $\check{\beta}_y$ = 4.9 m
Dispersion function	
Dipole	$\hat{\eta}_x$ = 0.49 m
Quadrupole	$\hat{\eta}_x$ = 1.51 m
Straight	η_x = 0 m

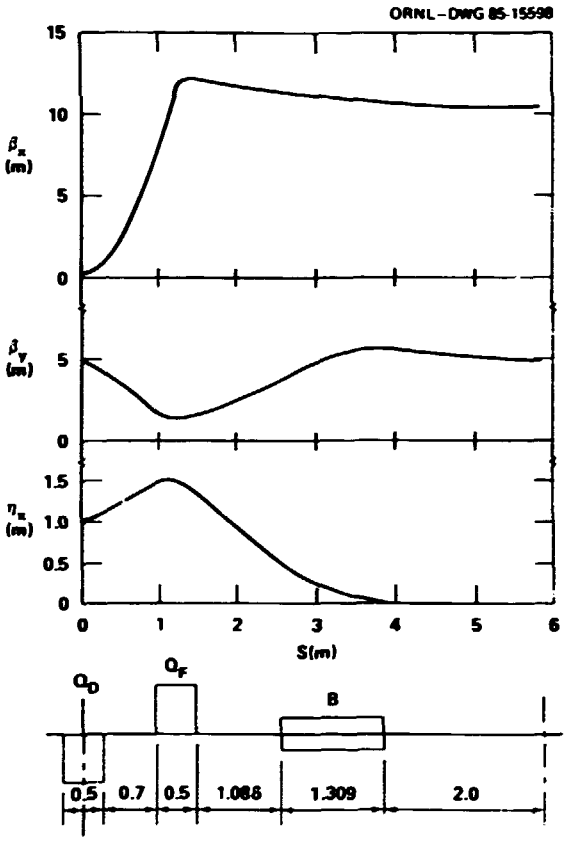

Fig. 10.6. Lattice functions for the 2-Tm ring.

11. PUBLICATIONS

List Prepared by Shirley J. Ball

The following list of publications includes primarily those articles by Physics Division staff members and associates which appeared in print from October 1984 through September 1985. Articles pending publication as of September 30, 1985, are listed immediately following this section.

BOOK, JOURNAL, AND PROCEEDINGS ARTICLES

Aichelin, J., and G. Bertsch
"Numerical Simulation of Medium-Energy Heavy-Ion Reactions," Phys. Rev. C 31, 1730-38 (1985)

Albrecht, R., R. Bock, G. Claesson, H. H. Gutbrod, B. Kolb, R. Schmidt, R. Schulze, M. Doss, P. Kristiansson, A. M. Poskanzer, H. G. Ritter, S. Garpman, H. A. Gustafsson, A. Oskarsson, I. Otterlund, S. Persson, K. Soderstrom, E. Stenlund, P. Beckmann, F. Berger, L. Dragon, R. Glasow, K. H. Kampert, H. Lohner, T. Peitzmann, M. Purschke, R. Santo, R. Wienke, T. Awes, C. Baktash, J. Beene, R. Ferguson, E. Gross, J. Johnson, I. Y. Lee, F. Obenshain, F. Plasil, G. Young, S. Sorensen, T. Siemiarczuk, Y. Stepaniak, and I. Zielinski
Study of Relativistic Nucleus-Nucleus Collisions at the CERN SPS, CERN Report CERN/SPSC/85-39 (August 1985), 33 pages

Alton, G. D., R. N. Compton, and D. J. Pegg
"Electron-Detachment Spectroscopy of 20-100 keV H⁻ Projectiles Interacting with Thin Ar Targets," Phys. Rev. A 31, 2129-36 (1985)

Andrews, M. C., F. D. McDaniel, J. L. Duggan, R. Mehta, G. Lapicki, P. D. Miller, P. L. Pepmiller, H. Krause, T. M. Rosseel, and L. A. Rayburn
"L-Shell X-Ray Production Cross Sections in Nd, Gd, Ho, Yb, Au, and Pb for 25-MeV Carbon and 32-MeV Oxygen Ions," Proceedings, Eighth Conference on the Application of Accelerators in Research and Industry, Denton, Texas, November 12-14, 1984, Nucl. Instrum. Methods Phys. Res. B10/11, 181-85 (1985)

Andrews, M. C., F. D. McDaniel, J. L. Duggan, P. D. Miller, P. L. Pepmiller, H. F. Krause, T. M. Rosseel, L. A. Rayburn, R. Mehta, and G. Lapicki
"M-Shell Electron Capture and Direct Ionization of Gold by 25-MeV Carbon and 32-MeV Oxygen Ions," Proceedings, Eighth Conference on the Application of Accelerators in Research and Industry, Denton, Texas, November 12-14, 1984, Nucl. Instrum. Methods Phys. Res. B10/11, 186-89 (1985)

Aronson, S., G. Igo, B. Pope, A. Shor, and G. Young (Invited Talk)
"A Detector for Dimuons Produced in the Relativistic Heavy Ion Collider," pp. 171-205 in Proceedings, RHIC Workshop on Experiments for a Relativistic Heavy-Ion Collider, Upton, New York, April 15-19, 1985, Brookhaven National Laboratory Report, BNL 51921 (1985)

Attaway, R., C. E. Bemis, Jr., P. Brobst, B. Crump, E. Evans, J. Fussell, V. Guthrie, J. Hogan, D. Lorenzo, F. W. Maxwell, T. Monk, B. Neimann, J. Parson, D. Peterson, J. Rooney, and J. Watson
AGC Critique of AVLIS Data Package II Areas of Interest/Uncertainty, (Title-U, Report-SRD), Centrifuge Program Team Report, K/CPT-74 (October 15, 1984), 189 pages

Attaway, R., C. E. Bemis, Jr., P. Brobst, B. Crump, E. Evans, J. Fussell, V. Guthrie, J. Hogan, D. Lorenzo, F. W. Maxwell, T. Monk, B. Neimann, J. Parson, D. Peterson, J. Rooney, and J. Watson
Detailed Assessment of the AVLIS Program, (Title-U, Report-SRD), Centrifuge Program Team Report, K/CPT-210 (January 25, 1985), 369 pages

Auble, R. L., Editor
"Holifield Heavy Ion Research Facility Newsletter," Issue No. 26 (1984)

Auble, R. L., Editor
"Holifield Heavy Ion Research Facility Newsletter," Issue No. 27 (1985)

Auble, R. L., Editor
"Holifield Heavy Ion Research Facility Newsletter," Issue No. 28 (1985)

Awes, T. C., R. L. Ferguson, R. Novotny, F. E. Obenshain, F. Plasil, V. Rauch, G. R. Young, and H. Sann
"Fission Decay of Reaction Products with A < 150," Phys. Rev. Lett. 55, 1062-65 (1985)

Baktash, C., Y. Schutz, I. Y. Lee, F. K. McGowan, N. R. Johnson, M. L. Halbert, D. C. Hensley, M. P. Fewell, L. Courtney, A. J. Larabee, L. L. Riedinger, A. W. Sunyar, E. der Mateosian, O. C. Kistner, and D. G. Sarantites
"Quasivibrational Bands at High Spins in ^{158}Yb," Phys. Rev. Lett. 54, 978-81 (1985)

Balantekin, A. B.
"Accidental Degeneracies and Supersymmetric Quantum Mechanics," Ann. Phys. (N.Y.) 164, 277-87 (1985)

Balantekin, A. B., and B. R. Barrett
"Collective M1 States in the Classical Limit of the Neutron-Proton Interacting Boson Model," Phys. Rev. C 32, 288-92 (1985)

Balantekin, A. B., C. Bottcher, M. R. Strayer, and S. J. Lee
"Production of New Particles in Heavy-Ion Collisions," Phys. Rev. Lett. 55, 461-64 (1985)

Barnett, C. F.
"Status of the U.S. Effort in Atomic Physics Research Relevant to the Magnetically Confined Fusion Program," Atomnaya Teknika za Rubezom 3, 28 (1984)

Barnett, C. F., and M.F.A. Harrison, Editors
Applied Atomic Collision Physics, Vol. 2: Plasmas, Academic Press, New York, 1984

Becker, R. L. (Invited Paper)
"Vacancy-Rearrangement Theory in the First Magnus Approximation," pp 131-37 in High-Energy Ion-Atom Collisions 2 (Proceedings, Second Workshop on High-Energy Ion-Atom Collision Processes, Debrecen, Hungary, August 27-28, 1984), ATOMKI, Debrecen, Hungary, 1985

Becker, R. L. (Invited Paper)
"Theory of K^nL^v Multiple Vacancy Production by Heavy Ions," Proceedings, Eighth Conference on the Application of Accelerators in Research and Industry, Denton, Texas, November 12-14, 1984, Nucl. Instrum. Methods Phys. Res. B10/11, 1-6 (1985)

Becker, R. L., A. L. Ford, and J. F. Reading (Invited Paper)
"Multiple Vacancy Production by High-Energy Heavy Ions," pp. 141-54 in High-Energy Ion-Atom Collisions 2 (Proceedings, Second Workshop on High-Energy Ion-Atom Collision Processes, Debrecen, Hungary, August 27-28, 1984), ATOMKI, Debrecen, Hungary, 1985

Becker, R. L., and A. D. MacKellar
"Theoretical Initial ℓ Dependence of Ion-Rydberg Atom Collision Cross Sections," J. Phys. B17, 3923-42 (1984)

Beene, J. R., F. E. Bertrand, and M. L. Halbert (Invited Paper)
"Crystal Ball Studies of Giant Resonance Gamma Decay ," pp. 623-35 in Capture Gamma-Ray Spectroscopy and Related Topics (Proceedings, International Symposium on Capture Gamma-Ray Spectroscopy and Related Topics, Knoxville, Tennessee, September 10-14, 1984), AIP Conf. Proc. No. 125, American Institute of Physics, New York, 1984

Beene, J. R., F. E. Bertrand, and M. L. Halbert (Invited Paper)
"Crystal Ball Studies of Giant Resonance Gamma Decay," Proceedings, 1984 INS-RIKEN International Symposium on Heavy-Ion Physics, Mt. Fuji, Japan, August 27-31, 1984, J. Phys. Soc. (Japan) 54, Suppl. II, 484-94 (1985)

Beene, J. R., F. E. Bertrand, M. L. Halbert, R. L. Auble, D. C. Hensley, D. J. Horen, R. L. Robinson, R. O. Sayer, and T. P. Sjoreen (Invited Paper)
"Electromagnetic Decay of Giant Resonances," pp. 503-17 in Proceedings, Niels Bohr Centennial Conference, "Nuclear Structure 1985," Copenhagen, Denmark, May 20-25, 1985, Elsevier Science Publishers, Amsterdam, 1985

Bemis, C. E., Jr.
AGC Proponent Team Critique of the AVLIS Program and Process Economic Model Review, (Title-U, Report-SRD), Centrifuge Program Team Report, K/CPT-248, Part 3 (February 6, 1985), 51 pages

Bemis, C. E., Jr., and J. R. Beene
Electron/Ion Recombination in the AVLIS Photoplasma: Modeling of Extractor Recombination Kinetics, (Title-U, Report-SRD), Centrifuge Program Team Report, K/CPT-170 (December 6, 1984), 34 pages

Bemis, C. E., Jr., and J. R. Beene
Simple Algorithms for Appropriate Boltzmann Partition Applications in Atomic Uranium: The AVLIS Integrated Process Model, (Title-U, Report-SRD), Centrifuge Program Team Report, K/CPT-181 (December 18, 1984), 9 pages

Bemis, C. E., Jr., J. R. Beene, J.L.C. Ford, Jr., D. Shapira, and B. Shivakumar (Invited Paper)
"Development of Polarized Targets for Subbarrier Fusion Studies," p. 339 in Lecture Notes in Physics 219, (Proceedings International Conference on Fusion Reactions Below the Coulomb Barrier, Cambridge, Massachusetts, June 13-15, 1984), Springer-Verlag, Berlin, 1985

Bemis, C. E., Jr., and M. R. Flannery
Update on Three-Body Recombination in the AVLIS Photoplasma, (Title-U, Report-SRD), Centrifuge Program Team Report, K/CPT-322 (March 25, 1985), 28 pages

Bemis, C. E., Jr., and J. T. Hogan
Supplementary Information — AVLIS Review Team, October 3, 1984, PEB Oral Presentations and Peer Discussions, (Title-U, Report-SRD), Centrifuge Program Team Report, K/CPT-116, (October 26, 1984), 235 pages

Bemis, C. E., Jr., and J. Hogan
Additional Information Presented at the Process Evaluation Board Meeting, (Title-U, Report-SRD), Centrifuge Program Team Report, K/CPT-228 (February 6, 1985), 20 pages

Bemis, Jr., C. E., J. T. Hogan, F. W. Maxwell, T. Monk, R. Attaway, P. Brobst, E. C. Evans, B. Neimann, J. W. Watson, D. K. Lorenzo, D. W. Peterson, D. F. Montague, B. Crump, and R. Hendricks
Final Review Team Response to the Process Evaluation Board on the AVLIS Process, (Title-U, Report-SRD), Centrifuge Program Team Report, K/CPT-347 (April 17, 1985), 41 pages

Bemis, C. E., Jr., J. Hogan, M. J. Ramsey, R. Attaway, P. Brobst, J. Watson, F. W. Maxwell, D. Lorenzo, E. Evans, T. Monk, B. Neimann, B. Crump, R. Hendricks, J. Rooney, and M. Robinson
Final Assessment Update of the AVLIS Program, (Title-U, Report-SRD), Centrifuge Program Team Report, K/CPT-296 (March 26, 1985), 219 pages

Bemis, C. E., Jr., J. T. Hogan, and J. Whealton
Additional Information Presented at Process Evaluation Board Meeting, (Title-U, Report-SRD), Centrifuge Program Team Report, K/CPT-309 April 2, 1985), 37 pages

Bemis, C. E., Jr., J. Watson, J. Hogan, D. Lorenzo, E. Evans, T. Monk, V. Guthrie, and F. W. Maxwell
AVLIS Review Team PEB Additional Information; Response to PEB 3 Rebuttal — Results of Continuing Analysis, (Title-U, Report-SRD), Centrifuge Program Team Report, K/CPT-288 (March 8, 1985), 159 pages

Berman, B. L., B. A. Dahling, S. Datz, J. O. Kephart, R. K. Klein, R. H. Pantell, and H. Park
"Channeling-Radiation Measurements at Lawrence Livermore National Laboratory," Proceedings, Eighth Conference on the Application of Accelerators in Research and Industry, Denton, Texas, November 12-14, 1984, Nucl. Instrum. Methods Phys. Res. B10/11, 611-17 (1985)

Bernstein, M. A., W. A. Friedman, W. G. Lynch, C. B. Chitwood, D. J. Fields, C. K. Gelbke, M. B. Tsang, T. C. Awes, R. L. Ferguson, F. E. Obenshain, F. Plasil, R. L. Robinson, and G. R. Young
"Statistical Emission of ^{2}He from Highly Excited Nuclear Systems," Phys. Rev. Lett. 54, 402-05 (1985)

Berry, S. D., G. A. Glass, I. A. Sellin, K.-O. Groeneveld, D. Hofmann, L. H. Andersen, M. Breinig, S. B. Elston, P. Engar, M. M. Schauer, N. Stolterfoht, H. Schmidt-Bocking, G. Nolte, and G. Schiwietz
"Shape of the Electron Capture to the Continuum Cusps for H, H_2, and He Targets in the Velocity Range 6.3-18.0 a.u.," Phys. Rev. A 31, 1392-98 (1985)

Bertrand, F. E., J. R. Beene, and M. L. Halbert (Invited Paper)
"Photon Decay of Giant Resonances," pp. 326-46 in Proceedings, International Symposium on Nuclear Spectroscopy and Nuclear Interactions, Osaka, Japan, March 21-24, 1984, World Scientific, Singapore, 1984

Biggerstaff, J. A., Guest Editor
Proceedings, 31st IEEE Nuclear Science Symposium and the 16th Symposium on Nuclear Power Reactors, Orlando, Florida, October 31-November 2, 1984, IEEE Trans. Nucl. Sci. NS-32, No. 1 (1985)

Bottcher, C. (Invited Paper)
"Time Dependent Hartree-Fock Theory of Ion-Atom Collisions: Application to F^{9+} + Ne," Proceedings, Eighth Conference on the Application of Accelerators in Research and Industry, Denton, Texas, November 12-14, 1984, Nucl. Instrum. Methods Phys. Res. B10/11, 7-11 (1985)

Bottcher, C., and M. R. Strayer
"Numerical Solution of the Time-Dependent Dirac Equation with Application to Positron Production in Heavy-Ion Collisions," Phys. Rev. Lett. 54, 669-72 (1985)

Carlton, R. F., J. A. Harvey, and C. H. Johnson
"Optical Model Scattering Functions for Low Energy Neutrons on ^{86}Kr," pp. 308-09 in A Probe of Nuclear Structure (Proceedings, Neutron-Nucleus Collisions Conference, Glouster, Ohio, September 5-8, 1984), AIP Conf. Proc. No. 124, American Institute of Physics, New York, 1985

Carvalho, J.L.S., F. M. Bernthal, R. M. Ronningen, N. R. Johnson, J. S. Hattula, I. Y. Lee, M. P. Fewell, L. L. Riedinger, and J. C. Wells
"High Spin States in ^{128}Ce," Phys. Rev. C 31, 1049-51 (1985)

Casson, W. H., D. P. Hutchinson, C. H. Ma, P. A. Staats, and J. B. Wilgen
"Far-Infrared Laser Diagnostic on ELMO Bumpy Torus and Extreme Far-Forward Laser Scattering on the Impurity Study Experiment," Proceedings, 5th Topical Conference on High Temperature Plasma Diagnostics, Tahoe City, California, September 16-20, 1984, Rev. Sci. Instrum. 56, 917-18 (1985)

Chitwood, C. T., J. Aichelin, D. H. Boal, G. Bertsch, D. J. Fields, C. K. Gelbke, W. G. Lynch, M. B. Tsang, J. C. Shillcock, T. C. Awes, R. L. Ferguson, F. E. Obenshain, F. Plasil, R. L. Robinson, and G. R. Young
"Final State Interactions Between Noncompound Light Particles for ^{16}O Induced Reactions on ^{197}Au at E/A = 25 MeV," Phys. Rev. Lett. 54, 302-05 (1985)

Clark, R. K., P. M. Barlow, R. N. Diamond, V. Hagopian, J. E. Lannutti, C. H. Spencer, M. Ferguson, T. Glanzmann, A. T. Goshaw, P. Lucas, N. Morgan, W. Robertson, W. D. Walker, W. Bugg, G. Condo, T. Handler, E. Hart, A. Rogers, H. O. Cohn, I. J. Kim, C. R. Sun, and R. Gearhart
"Triggered-Bubble-Chamber Study of the Reaction $\pi^+p \to \Delta^{++}\pi^0\pi^0$ at 16 GeV/c," Phys. Rev. D 32, 1061-70 (1985)

Cole, J. D., J. H. Hamilton, A. V. Ramayya, W. Lourens, B. van Nooijen, H. Kawakami, L. A. Mink, E. H. Spejewski, H. K. Carter, R. L. Mlekodaj, G. A. Leander, L. L. Riedinger, C. R. Bingham, E. F. Zganjar, J. L. Wood, R. W. Fink, K. S. Toth, B. D. Kern, and K.S.R. Sastry
"Decay of ^{188}Tl and Observed Shape Coexistence in the Bands of ^{188}Hg," Phys. Rev. C 30, 1267-76 (1984)

Cusson, R. Y., P.-G. Reinhard, M. R. Strayer, J. A. Maruhn, and W. Greiner
"Density as a Constraint and the Separation of Internal Excitation Energy in TDHF," Z. Phys. A320, 475-82 (1985)

Datz, S., C. Bottcher, L. H. Andersen, P. Hvelplund, and H. Knudsen (Invited Paper)
"Correlated Two-Electron Effects in Collisions of Multiply Charged Au Ions with He," Proceedings, Eighth Conference on the Application of Accelerators in Research and Industry, Denton, Texas, November 12-14, 1984, Nucl. Instrum. Methods Phys. Res. B10/11, 116-19 (1985)

Datz, S., and C. D. Moak
"Heavy-Ion Channeling," pp. 169-242 in Treatise on Heavy-Ion Science, Vol. 6, Plenum Press, New York, (1985)

Davies, K.T.R., K.R.S. Devi, S. E. Koonin, and M. R. Strayer
"TDHF Calculations of Heavy-Ion Collisions," pp. 3-80 in Treatise on Heavy-Ion Science, Vol. 3, Plenum Press, New York, 1985

Davies, K.T.R., and A. J. Sierk
"Conditional Saddle-Point Configurations," Phys. Rev. C 31, 915-22 (1985)

Davis, N. J., J. A. Kuehner, A. A. Pilt, A. J. Trudel, M. C. Vetterli, C. Bamber, E. K. Warburton, J. W. Olness, and S. Raman
"States of ^{38}S from the $^{36}S(t,p)^{38}S$ Reaction," Phys. Rev. C 32, 713-20 (1985)

Defrance, P., S. Chantrenne, F. Brouillard, S. Rachafi, D. Belic, J. Jureta, and D. Gregory
"Electron Impact Ionization of N^{4+} and N^{5+}, Proceedings, International Conference on the Physics of Highly Ionized Atoms, Oxford, England, July 2-5, 1984, Nucl. Instrum. Methods Phys. Res. B9, 400-02 (1985)

Demas, N. G., C. H. Ma, D. P. Hutchinson, and P. A. Staats
"Determination of Spatial Distribution of Plasma Electrons by Multibeam FIR Interferometry," IEEE Trans. Plasma Science PS-13, 41-44 (1985)

Dennis, L. C., and S. Raman
"Location of a Doorway State Using the Channel n + ^{207}Pb," pp. 495-97 in Capture Gamma-Ray Spectroscopy and Related Topics (Proceedings, International Symposium on Gamma-Ray Spectroscopy and Related Topics, Knoxville, Tennessee, September 10-14, 1984), AIP Conf. Proc. No. 125, American Institute of Physics, New York, 1984

Ellis-Akovali, Y. A.
"Nuclear Data Sheets for A = 241," Nucl. Data Sheets 44, 407-61 (1985)

El-Samman, H., V. Barci, A. Gizon, J. Gizon, L. Hildingsson, D. Jerrestam, W. Klamra, R. Kossakowski, Th. Lindblad, T. Bengtsson, and G. A. Leander
"On the Difference of the Dynamic Moment of Inertia $\mathcal{J}_{band}^{(2)}$ for Xe and Ba Nuclei," Nucl. Phys. A427, 397-412 (1984)

El-Samman, H., V. Barci, A. Gizon, J. Gizon, L. Hildingsson, D. Jerrestam, W. Klamra, R. Kossakowski, Th. Lindblad, Y. Gono, T. Bengtsson, and G. A. Leander
"Dynamic Moments of Inertia in Xe, Cs, and Ba Nuclei," p. 177 in Proceedings, International Symposium on In-Beam Nuclear Spectroscopy, Debrecen, Hungary, May 14-18, 1984, Akademiai Kiado, Budapest, 1984

Elston, S. B., S. D. Berry, M. Breinig, R. DeSerio, C. E. Gonzalez Lepera, I. A. Sellin, K.-O. Groeneveld, D. Hoffman, P. Koschar, I. B. Nemirovski, and L. I. Liljeby
"Doubly Differential Emission Distributions from Electron Loss to the Continuum from Fast Heavy Projectiles in Gas Targets," pp. 75-78 in Lecture Notes in Physics 213 (Proceedings, Symposium on the Physics of Electron Ejection in Ion-Atom and Ion-Solid Collisions, Aarhus, Denmark, June 29-30, 1984), Springer-Verlag, Berlin, 1984

Erb, K. A. (Invited Paper)
"Quasi-Molecular Single-Nucleon Effects in Heavy-Ion Collisions," pp. 61-75 in Fundamental Problems in Heavy-Ion Collisions (Proceedings, 5th Adriatic International Conference on Nuclear Physics, Hvar, Yugoslavia, September 24-29, 1984), World Scientific, Singapore, 1984

Erb, K. A.
"Coulomb Excitation," pp. 135-37 in McGraw-Hill Yearbook of Science and Technology, McGraw-Hill, New York, 1985

Erb, K. A., and D. A. Bromley
"Heavy-Ion Resonances," pp. 201-310 in Treatise on Heavy-Ion Science, Vol. 3, Plenum Press, New York, 1985

Ernst, D. J., M. R. Strayer, and A. S. Umar
"Correlations Between Preequilibrium Nucleons," Phys. Rev. Lett. 55, 584-87 (1985)

Esbensen, H., and G. F. Bertsch
"Double Excitation in High Energy Inelastic Scattering," Phys. Rev. C 32, 553-55 (1985)

Farid, M. E., and G. R. Satchler
"One Effect of Using Relativistic Kinematics in the Analysis of Heavy-Ion Elastic Scattering," Phys. Lett. 146B, 389-91 (1984)

Farid, M. E., and G. R. Satchler
"A Density-Dependent Interaction in the Folding Model for Heavy-Ion Potentials," Nucl. Phys. A438, 525-35 (1985)

Farid, M. E., and G. R. Satchler
"Some Optical-Model Analyses of the Elastic Scattering of ^{40}Ar at 1760 MeV," Nucl. Phys. A441, 157-73 (1985)

Fewell, M. P., N. R. Johnson, F. K. McGowan, J. S. Hattula, I. Y. Lee, C. Baktash, Y. Schutz, J. C. Wells, L. L. Riedinger, M. W. Guidry, and S. C. Pancholi
"Collectivity of ^{160,161}Yb at High Spin," Phys. Rev. C 31, 1057-60 (1985)

Fogelberg, B., J. Harvey, M. Mizumoto, and S. Raman
"Observation of Extremely Low s-Wave Strength in the Reaction ^{136}Xe + n," pp. 493-94 in Capture Gamma-Ray Spectroscopy and Related Topics (Proceedings, International Symposium on Gamma-Ray Spectroscopy and Related Topics, Knoxville, Tennessee, September 10-14, 1984), AIP Conf. Proc. No. 125, American Institute of Physics, New York, 1984

Fogelberg, B., J. A. Harvey, M. Mizumoto, and S. Raman
"Test of Fermi Gas Model Predictions of Level Density in ^{137}Xe," Phys. Rev. C 31, 2041-48 (1985)

Ford, J.L.C. (Invited Paper)
"Heavy Ions, Targets, and Research at HHIRF," pp. 43-87 in Proceedings, 1983 Workshop of the International Nuclear Target Development Society, Argonne, Illinois, September 7-9, 1983, Argonne National Laboratory Report ANL/PHY-84-2 (1984)

Fulmer, C. B., G. R. Satchler, K. A. Erb, D. C. Hensley, R. L. Auble, J. B. Ball, F. E. Bertrand, and E. E. Gross
"Elastic and Inelastic Scattering of 158-MeV ^{9}Be Ions," Nucl. Phys. A427, 545-67 (1984)

Gacsi, Z., J. Sa, J. L. Weil, E. T. Jurney, and S. Raman
"Decay Scheme of ^{116}Sn from $(n,n'\gamma)$ and (n,γ) Results," pp. 539-41 in Capture Gamma-Ray Spectroscopy and Related Topics (Proceedings, International Symposium on Gamma-Ray Spectroscopy and Related Topics, Knoxville, Tennessee, September 10-14, 1984), AIP Conf. Proc. No. 125, American Institute of Physics, New York, 1984

Gavron, A., J. Boissevain, H. C. Britt, K. Eskola, P. Eskola, M. M. Fowler, H. Ohm, J. B. Wilhelmy, T. C. Awes, R. L. Ferguson, F. E. Obenshain, F. Plasil, G. R. Young, and S. Wald
"Fission Cross Sections up to 20 MeV/Nucleon," Phys. Rev. C 30, 1550-60 (1984)

Glass, G. A., P. Engar, S. D. Berry, M. Breinig, R. DeSerio, S. B. Elston, and I. A. Sellin
"Electron Capture to the Continuum from Atomic Hydrogen," Proceedings, Eighth Conference on the Application of Accelerators in Research and Industry, Denton, Texas, November 12-14, 1984, Nucl. Instrum. Methods Phys. Res. B10/11, 138-41 (1985)

Goodman, C. D., R. C. Byrd, I. J. Van Heerden, T. A. Carey, D. J. Horen, J. S. Larsen, C. Gaarde, J. Rapaport, T. P. Welch, E. Sugarbaker, and T. N. Taddeucci
"Measurements of Gamow-Teller Strength Distributions in Mass 13 and 15," Phys. Rev. Lett. 54, 877-80 (1985)

Gregory, D. C. (Invited Paper)
"Indirect Processes in Electron Impact Ionization of Multiply-Charged Ions," Proceedings, Eighth Conference on the Application of Accelerators in Research and Industry, Denton, Texas, November 12-14, 1984, Nucl. Instrum. Methods Phys. Res. B10/11, 87-91 (1985)

Griffin, D. C., M. S. Pindzola, and C. Bottcher
"Distorted-Wave Calculations of Dielectronic Recombination Cross Sections in the Li Isoelectronic Sequence," Phys. Rev. A 31, 568-75 (1985)

Guidry, M. W., R. W. Kincaid, and P. Donangelo
"Angular Momentum Transfer in Very Heavy-Ion Direct Reactions," Phys. Lett. 150B, 265-69 (1985)

Guidry, M. W., R. E. Neese, C. R. Bingham, L. L. Riedinger, J. A. Vrba, I. Y. Lee, N. R. Johnson, G. R. Satchler, P. A. Butler, R. Donangelo, J. O. Rasmussen, D. L. Hillis, and H. H. Kluge
"Heavy-Ion Inelastic Scattering from Deformed Nuclei," Nucl. Phys. A430, 485-524 (1984)

Harvey, J. A., C. H. Johnson, R. F. Carlton, and B. Castel
"$d_{5/2}$ Single-Particle Strength in ^{48}Ca + n," pp. 304-05 in A Probe of Nuclear Structure (Proceedings, Neutron-Nucleus Collisions Conference, Glouster, Ohio, September 5-8, 1984), AIP Conf. Proc. No. 124, American Institute of Physics, New York, 1985

Harvey, J. A., C. H. Johnson, R. F. Carlton, and B. Castel
"Single-Particle $2d_{5/2}$ Strength in the ^{48}Ca + n Reaction," Phys. Rev. C 32, 1114-17 (1985)

Hill, N. W., J. A. Harvey, D. J. Horen, G. L. Morgan, and R. R. Winters
"Majority-Logic NE-110 Detector for keV Neutrons," IEEE Trans. Nucl. Sci. NS-32, 367-72 (1985)

Hogan, J. T., C. E. Bemis, Jr., and C. R. Attaway
Supplementary Information — AVLIS Review Team, December 11, 1984, PEB Oral Presentations and Peer Discussions, (Title-U, Report-SRD), Centrifuge Program Team Report, K/CPT-194, (January 4, 1985), 215 pages

Horen, D. J., F. E. Bertrand, E. E. Gross, T. P. Sjoreen, D. K. McDaniels, J. R. Tinsley, J. Lisantti, L. W. Swenson, J. B. McClelland, T. A. Carey, S. J. Seestrom-Morris, and K. Jones
"Cross Sections and Analyzing Powers for Quenched Spin Excitations in ^{40,48}Ca at E_p = 334 MeV," Phys. Rev. C 31, 2049-53 (1985)

Hutchinson, D. P., C. H. Ma, P. A. Staats, and K. L. Vander Sluis
"Far-Infrared Interferometry/Polarimetry on the ISX-B Tokamak," pp. 633-34 in Proceedings, Third International Conference on Infrared Physics, Zurich, Switzerland, July 23-27, 1984, ETH, Zurich, 1984

Hutchinson, D. P., K. L. Vander Sluis, J. Sheffield, and D. J. Sigmar
"Feasibility of Alpha Particle Measurement by CO_2 Laser Thomson Scattering," Proceedings, 5th Topical Conference on High Temperature Plasma Diagnostics, Tahoe City, California, September 16-20, 1984, Rev. Sci. Instrum. 56, 1075-77 (1985)

Johnson, B. M., K. W. Jones, D. C. Gregory, J. O. Ekberg, L. Engstrom, T. H. Kruse, and J. L. Cecchi
"Lifetimes and Oscillator Strengths for the Resonance Transitions in Cu-Like Iodine, I XXV," Phys. Scr. 32, 210-15 (1985)

Johnson, C. H. (Invited Paper)
"Optical Models from Low-Energy s-, p-, and d-Wave Cross Sections," pp. 446-62 in A Probe of Nuclear Structure (Proceedings, Neutron-Nucleus Collisions Conference, Glouster, Ohio, September 5-8, 1984), AIP Conf. Proc. No. 125, American Institute of Physics, New York, 1985

Johnson, C. H., C. Mahaux, and R. R. Winters
"Energy Average of the Scattering Matrix in Picket-Fence Models," Phys. Rev. C 32, 359-67 (1985)

Juncar, P., C. R. Bingham, J. A. Bounds, D. J. Pegg, H. K. Carter, R. L. Mlekodaj, and J. D. Cole
"New Method to Measure the Relativistic Doppler Shift: First Results and a Proposal," Phys. Rev. Lett. 54, 11-13 (1985)

Kim, H. J., T. C. Awes, J. R. Beene, C. E. Bemis, Jr., R. L. Ferguson, I. Y. Lee, F. K. McGowan, F. E. Obenshain, F. Plasil, V. Rauch, R. L. Robinson, and S. Steadman
"Calibration and Initial Experiments with the ORNL-MIT Recoil Mass Spectrometer," pp. 323-24 in Lecture Notes in Physics 219 (Proceedings, International Conference on Fusion Reactions Below the Coulomb Barrier, Cambridge, Massachusetts, June 13-15, 1984), Springer-Verlag, Berlin, 1985

Klein, R. K., J. O. Kephart, R. H. Pantell, H. Park, B. L. Berman, R. L. Swent, S. Datz, and R. W. Fearick
"Electron Channeling Radiation from Diamond," Phys. Rev. B 31, 68-92 (1985)

Kobos, A. M., and G. R. Satchler
"A Global Optical Potential Analysis of $^{16}O + ^{28}Si$ Elastic Scattering," Nucl. Phys. A427, 589-613 (1984)

Krofcheck, E. Sugarbaker, J. Rapaport, D. Wang, J. N. Bahcall, R. C. Byrd, C. C. Foster, C. D. Goodman, I. J. Van Heerden, C. Gaarde, J. S. Larsen, D. J. Horen, and T. N. Taddeucci
"Gamow-Teller Strength Function in ^{71}Ge via the (p,n) Reaction at Medium Energies," Phys. Rev. Lett. 55, 1051-54 (1985)

Kvale, T. J., G. D. Alton, R. N. Compton, D. J. Pegg, and J. S. Thompson
"Experimental Determination of the Energy level of $Be^-(1s^2 2s2p^2)^4P$," Phys. Rev. Lett. 55, 484-87 (1985)

Lazarus, E. A., J. D. Bell, C. E. Bush, A. Carnevali, B. A. Carreras, W. H. Casson, J. L. Dunlap, P. H. Edmonds, A. C. England, W. L. Gardner, G. A. Hallock, J. T. Hogan, H. C. Howe, D. P. Hutchinson, R. R. Kindsfather, R. C. Isler, R. A. Langley, C. H. Ma, J. Mathew, P. K. Mioduszewski, M. Murakami, G. H. Neilson, V. K. Pare, D. J. Sigmar, C. E. Thomas, R. M. Wieland, J. B. Wilgen, W. R. Wing, A. J. Wootton, and K. E. Yokoyama
"Confinement in Beam-Heated Plasmas: The Effects of Low-Z Impurities," Nucl. Fusion 25, 135-49 (1985)

Lazarus, E. A., J. D. Bell, C. E. Bush, A. Carnevali, J. L. Dunlap, P. H. Edmonds, L. C. Emerson, O. C. Eldridge, W. L. Gardner, H. C. Howe, D. P. Hutchinson, R. R. Kindsfather, R. C. Isler, R. A. Langley, C. H. Ma, P. K. Mioduszewski, M. Murakami, L. E. Murray, G. H. Neilson, V. K. Pare, S. D. Scott, D. J. Sigmar, J. E. Simpkins, K. A. Stewart, C. E. Thomas, R. M. Wieland, J. B. Wilgen, A. L. Wintenberg, W. R. Wing, and A. J. Wootton
"Confinement Improvement in Beam Heated ISX-B Discharges with Low-Z Impurity Injection," J. Nucl. Mater. 121, 61-68 (1984)

Leander, G. A.
"Shell Effects on the E1 Moments of Ra-Th Nuclei," pp. 125-29 in Capture Gamma-Ray Spectroscopy and Related Topics (Proceedings, International Symposium on Gamma-Ray Spectroscopy and Related Topics, Knoxville, Tennessee, September 10-14, 1984), AIP Conf. Proc. No. 125, American Institute of Physics, New York, 1984

Leander, G. A., P. Möller, J. R. Nix, and W. M. Howard
"Calculated Masses and Half-Lives for Nuclei in the Region $100 < Z < 110$," pp. 466-71 in Proceedings, Seventh International Conference on Atomic Masses and Fundamental Constants AMCO-7, Darmstadt, West Germany, September 3-7, 1984, Technische Hochschule, Darmstadt, 1984

Leander, G. A., W. Nazarewicz, P. Olanders, I. Ragnarsson, and J. Dudek
"A New Region of Intrinsic Reflection Asymmetry in Nuclei Around ^{145}Ba?," Phys. Lett. 152B, 284-90 (1985)

Leander, G. A., P. B. Semmes, and F. Donau (Invited Paper)
"Unpaired Nucleons as Probes of Core Collective Fields," p. 167 in Proceedings, International Workshop on Interacting Boson-Boson and Boson-Fermion Systems, Gull Lake, Michigan, May 28-30, 1984, World Scientific Publishing, Singapore, 1985

Lisantti, J., J. R. Tinsley, D. M. Drake, I. Bergqvist, L. W. Swenson, D. K. McDaniels, F. E. Bertrand, E. E. Gross, D. J. Horen, and T. P. Sjoreen
"Analyzing Power for the Inelastic Continuum with 200-MeV Protons," Phys. Lett. 147B, 23-26 (1984)

Ludemann, C. A., and B. J. Casstevens
"Operator Interface to the ORIC Control System," pp. 491-96 in Lecture Notes in Physics 215 (Proceedings, European Physical Society Conference on Computing in Accelerator Design and Technolgy, Berlin, West Germany, September 20-23, 1983), Springer-Verlag, Berlin, 1984

Ma, C. H., D. P. Hutchinson, P. A. Staats, and K. L. Vander Sluis
"FIR Interferometer/Polarimeter System on ISX-B Tokamak," Proceedings, 5th Topical Conference on High Temperature Plasma Diagnostics, Tahoe City, California, September 16-20, 1984, Rev. Sci. Instrum. 56, 911-13 (1985)

Ma, C. H., D. P. Hutchinson, P. A. Staats, K. L. Vander Sluis, D. K. Mansfield, H. Park, and L. C. Johnson
"Submillimeter Wave Propagation in Tokamak Plasmas," pp. 157-60 in Proceedings, 1985 International Symposium on Antennas and Propagation, Kyoto, Japan, August 20-22, 1985, 1985

Ma, C. H., D. P. Hutchinson, P. A. Staats, K. L. Vander Sluis, D. K. Mansfield, H. Park, and L. C. Johnson
"Submillimeter Wave Propagation in Tokamak Plasmas," pp. 779-84 in Proceedings, 1985 International Symposium on Antennas and EM Theory, Beijing, China, August 25-27, 1985, 1985

Marston, J. B., and S. E. Koonin
"Mean-Field Calculations of Fluctuations in Nuclear Collisions," Phys. Rev. Lett. 54, 1139-41 (1985)

Martin, M. J.
"Nuclear Decay Data for Selected Radionuclides," Appendix A of A Handbook of Radioactivity Measurements, National Council on Radiation Protection and Measurements Report No. 58 (Second Edition), 1985

Maruhn, J. A., K.T.R. Davies, and M. R. Strayer
"Time-Dependent Hartree-Fock Studies of the Sensitivity of Dynamical Fusion Thresholds to the Effective Two-Body Interaction," Phys. Rev. C 31, 1289-96 (1985)

Maxwell, F. W., C. E. Bemis, Jr., and J. T. Hogan
Additional Information Presented at the Process Evaluation Board Meeting, (Title-U, Report-SRD), Centrifuge Program Team Report, K/CPT-177 (December 11, 1984), 7 pages

Maxwell, F. W., C. E. Bemis, Jr., J. Hogan, and C. R. Attaway
Advanced Gas Centrifuge Proponent Team Critique of the Atomic Vapor Laser Isotope Separation Program, (Title-U, Report-SRD), Centrifuge Program Team Report, K/CPT-72 (October 3, 1984), 145 pages

Maxwell, F. W., J. T. Hogan, C. E. Bemis, Jr., C. R. Attaway, W. May, and T. M. Lawthers
Advanced Gas Centrifuge Proponent Team Critique of the Atomic Vapor Laser Isotope Separation Program, (Title-U, Report-SRD), Centrifuge Program Team Report, K/CPT-156, (December 11, 1984), 190 pages

Maxwell, F. W., J. T. Hogan, C. E. Bemis, Jr., D. W. Peterson, and D. K. Lorenzo
Advanced Gas Centrifuge Proponent Team Critique of the Atomic Vapor Laser Isotope Separation Program and Process Economic Model Review, (Title-U, Report-SRD), Centrifuge Program Team Report, K/CPT-237 (February 6, 1985), 114 pages

Maxwell, F. W., D. W. Peterson, J. T. Hogan, C. E. Bemis, J. W. Watson, D. K. Lorenzo, D. F. Montague, E. C. Evans, P. R. Brobst, T. H. Monk, and B. Niemann
Advanced Gas Centrifuge Proponent Team Review of the Atomic Vapor Laser Isotope Separation Program, (Title-U, Report-SRD), Centrifuge Program Team Report, K/CPT-303 (April 2, 1985), 141 pages

Maxwell, F. W., D. W. Peterson, J. T. Hogan, C. E. Bemis, J. W. Watson, D. K. Lorenzo, D. F. Montague, E. C. Evans, P. R. Brobst, T. H. Monk, and B. Niemann
Advanced Gas Centrifuge Proponent Team Review of the Atomic Vapor Laser Isotope Separation Program, (Title-U, Report-SRD), Centrifuge Program Team Report, K/CPT-303, Part 1 Addendum (April 2, 1985), 24 pages

Maxwell, F. W., D. W. Peterson, J. T. Hogan, C. E. Bemis, J. W. Watson, D. K. Lorenzo, D. F. Montague, E. C. Evans, P. R. Brobst, T. H. Monk, and B. Niemann
Advanced Gas Centrifuge Proponent Team Review of the Atomic Vapor Laser Isotope Separation Program, (Title-U, Report-SRD), Centrifuge Program Team Report, K/CPT-303, Part 2 Addendum (April 2, 1985), 23 pages

Meyer, F. W. (Invited Paper)
"The ORNL ECR Multicharged Ion Source," Proceedings, International Conference on the Physics of Highly Ionized Atoms, Oxford, England, July 2-5, 1984, Nucl. Instrum. Methods Phys. Res. B9, 532-37 (1985)

Meyer, F. W.
"Status of the ORNL ECR Source," pp. 37-39 in Proceedings, Sixth International ECR Ion Source Workshop, Berkeley, California, January 17-18, 1985, Lawrence Berkeley Laboratory Report, LBL-5143 (1985)

Meyer, F. W., A. M. Howald, C. C. Havener, and R. A. Phaneuf
"Observation of Low-Energy Z Oscillations in Total Electron Capture Cross Sections for Bare Projectiles Colliding with H and H_2," Phys. Rev. Lett. 54, 2663-66 (1985)

Miller, P. D., C. J. Sofield, C. J. Woods, N.E.B. Cowern, L. B. Bridwell, C. D. Moak, D. C. Gregory, C. M. Jones, G. D. Alton, P. L. Pepmiller, and J. Hall (Invited Paper)
"Excited State Populations and Charge Exchange of Fast Ions in Solids," Proceedings, Eighth Conference on the Application of Accelerators in Research and Industry, Denton, Texas, November 12-14, 1984, Nucl. Instrum. Methods Phys. Res. B10/11, 225-27 (1985)

Milner, W. T., and J. A. Biggerstaff
"CHIL: A Comprehensive Histogramming Language," Proceedings, 1984 Nuclear Science Symposium, Orlando, Florida, October 31-November 2, 1984, IEEE Trans. Nucl. Sci. NS-32, 277-81 (1985)

Mioduszewski, P., L. C. Emerson, J. E. Simpkins, A. J. Wooton, C. E. Bush, A. Carnevali, J. L. Dunlap, P. H. Edmonds, W. L. Gardner, H. C. Howe, D. P. Hutchinson, K. C. Isler, R. R. Kindsfather, R. A. Langley, E. A. Lazarus, C. H. Ma, M. Murakami, G. H. Neilson, V. K. Pare, S. D. Scott, C. E. Thomas, J. B. Whitley, W. R. Wing, and K. Yokoyama
"Particle Removal with Pump Limiters in ISX-B," J. Nucl. Mater. 121, 285-93 (1984)

Mioduszewski, P. K., J. E. Simpkins, P. H. Edmonds, R. C. Isler, E. A. Lazarus, C. H. Ma, M. Murakami, and A. J. Wootton
"Studies on Impurity Control and Hydrogen Pumping with Chromium Gettering in ISX-B," J. Nucl. Mater. 128 & 129, 884-85 (1984)

Mishra, C. S., B. M. Preedom, B. G. Ritchie, R. S. Moore, M. Blecher, K. Gotow, R. L. Burman, M. V. Hynes, E. Piasetzky, N. S. Chant, P. G. Roos, F. E. Bertrand, T. Sjoreen, F. E. Obenshain, and E. E. Gross
"Isospin Effect in $\pi^{\pm}$ ^{14}C Elastic Scattering at 50 MeV," Phys. Rev. C 32, 995-98 (1985)

Moltz, D. M., J. D. Sullivan, R. E. Tribble, C. A. Gagliardi, K. S. Toth, and F. T. Avignone
"Neutron-Deficient Mass Surface Between the $1f_{7/2}$ and $1g_{9/2}$ Shells: The Masses of ^{77}Kr and ^{79}Kr," pp. 112-18 in Proceedings, Seventh International Conference on Atomic Masses and Fundamental Constants AMCO-7, Darmstadt, West Germany, September 3-7, 1984, Technische Hochschule, Darmstadt, 1984

Moltz, D. M., K. S. Toth, F. T. Avignone, III, H. Noma, B. D. Kern, R. E. Tribble, and J. P. Sullivan
"Beta Decay of ^{76}Rb and the Level Structure of ^{76}Kr," Nucl. Phys. A427, 317-31 (1984)

Mueller, D. W., T. J. Morgan, G. H. Dunn, D. C. Gregory, and D. H. Crandall
"Absolute Cross Section Measurements for Electron-Impact Ionization of Doubly Charged Ions Ti^{2+}, Fe^{2+}, Ar^{2+}, Cl^{2+}, and F^{2+}," Phys. Rev. A 31, 2905-13 (1985)

Murakami, M., P. H. Edmonds, G. A. Hallock, R. C. Isler, E. A. Lazarus, G. H. Neilson, A. J. Wootton, J. D. Bell, C. E. Bush, A. Carnevali, B. A. Carreras, J. L. Dunlap, A. C. England, W. L. Gardner, R. L. Hickok, H. C. Howe, D. P. Hutchinson, W. C. Jennings, R. R. Kindsfather, R. A. Langley, C. H. Ma, J. Mathew, P. K. Mioduszewski, J. K. Munro, V. K. Pare, M. J. Saltmarsh, S. D. Scott, D. J. Sigmar, M. L. Simpson, C. E. Thomas, R. M. Wieland, W. R. Wing, and K. E. Yokoyama
"Confinement of Beam-Heated Plasmas in ISX-B," pp. 87-102 in Vol. 1 of Proceedings, Tenth International Conference on Plasma Physics and Controlled Nuclear Fusion Research, London, England, September 12-19, 1984, IAEA, Vienna, 1985

Murphy, M. J., S. Gil, M. N. Harakeh, A. Ray, A. G. Seamster, R. Vandenbosch, and T. C. Awes
"Time Scale for Projectile Breakup into Coincident Heavy Fragments," Phys. Rev. Lett. 53, 1543-46 (1984)

Nagarajan, M. A., C. C. Mahaux, and G. R. Satchler
"Dispersion Relation and the Low-Energy Behavior of the Heavy-Ion Optical Potential," Phys. Rev. Lett. 54, 1136-38 (1985)

Nazarewicz, W., P. Olanders, I. Ragnarsson, J. Dudek, G. A. Leander, P. Moller, and E. Ruchowska
"Analysis of Octupole Instability in Medium-Mass and Heavy Nuclei," Nucl. Phys. A429, 269-95 (1984)

Neilson, G. H., A. J. Wootton, J. D. Bell, C. E. Bush, A. Carnevali, J. L. Dunlap, P. H. Edmonds, A. C. England, W. L. Gardner, H. C. Howe, D. P. Hutchinson, R. R. Kindsfather, R. C. Isler, R. A. Langley, E. A. Lazarus, C. H. Ma, M. Murakami, V. K. Pare, S. D. Scott, C. E. Thomas, R. M. Wieland, J. B. Wilgen, and W. R. Wing
"Experimental Results on Tokamak Beta Limits from ISX-B," Nucl. Fusion 25, 825-27 (1985)

Park, H., J. O. Kephart, R. K. Klein, R. H. Pantell, B. L. Berman, S. Datz, and R. L. Swent
"Electron Channeling Radiation from Diamonds with and without Platelets," J. Appl. Phys. 57, 1661-64 (1985)

Park, H., D. K. Mansfield, L. C. Johnson, and C. H. Ma
"MIRI: A Multichannel Far-Infrared Interferometer/Polarimeter for TFTR," Proceedings, 5th Topical Conference on High Temperature Plasma Diagnostics, Tahoe City, California, September 16-20, 1984, Rev. Sci. Instrum. 56, 938 (1985)

Pepmiller, P. L., and J. M. Loftus
"A Device for Handling Cesium Safely," Rev. Sci. Instrum. 56, 1832-33 (1985)

Phaneuf, R. A., M. Kimura, H. Sato, and R. E. Olson
"Electron Capture by Slow Al^{q+} Ions Colliding with Hydrogen," Phys. Rev. A 31, 2914-17 (1985)

Piercey, R. B., J. H. Hamilton, A. V. Ramayya, C. F. Maguire, R. L. Robinson, S. Frauendorf, and J. Eberth
"Effects of Reinforcing Shell Gap on Competition Between Spherical and Highly Deformed Shapes," J. Phys. G10, L87-L89 (1984)

Piercey, R. B., A. C. Rester, J. H. Hamilton, A. V. Ramayya, H. K. Carter, R. L. Robinson, H. J. Kim, J. C. Wells, and J. Lin
"Near-Spherical Band in ^{76}Kr Observed in the β Decay of Mass-Separated ^{76}Rb," Phys. Rev. C 32, 625-27 (1985)

Pindzola, M. S., D. C. Griffin, and C. Bottcher
"Resonance Contributions to the Electron-Impact Excitation of Ions in the Distorted-Wave Approximation," Phys. Rev. A 32, 822-28 (1985)

Plasil, F. (Invited Paper)
"Recent Advances in Heavy-Ion-Induced Fission," pp. 449-68 in Proceedings, International Conference on Nuclear Physics, Bombay, India, December 27-31, 1984, World Scientific Publishing, Singapore, 1985

Plasil, F. (Invited Paper)
"Recent Advances in Fusion-Fission Reactions," pp. 95-112 in Proceedings, Tsukuba International Symposium on Heavy-Ion Fusion Reactions, Ibaraki, Japan, September 3-5, 1984, World Scientific Publishing, Singapore, 1985

Ragnarsson, I., T. Bengtsson, W. Nazarewicz, J. Dudek, and G. A. Leander
"Band Termination at Very High Spin in ^{158}Yb," Phys. Rev. Lett. 54, 982-85 (1985)

Raman, S., Editor
"Actinide Newsletter," Issue No. 8 (March 1985)

Raman, S., Editor
Capture Gamma-Ray Spectroscopy and Related Topics-1984 (Proceedings, International Symposium, Knoxville, Tennessee, September 10-14, 1984), AIP Conf. Proc. No 125, American Institute of Physics, New York, 1984

Raman, S., R. F. Carlton, J. C. Wells, E. T. Jurney, and J. E. Lynn
"Thermal Neutron Capture Gamma Rays from Sulfur Isotopes: Experiment and Theory," Phys. Rev. C 32, 18-69 (1985)

Raman, S., and B. Fogelberg (Invited Paper)
"Overlapping β Decay and Resonance Neutron Spectroscopy," pp. 102-06 in Proceedings, International Symposium on Nuclear Spectroscopy and Nuclear Interactions, Osaka, Japan, March 21-24, 1984, World Scientific, 1984

Rapaport, J., R. Alarcon, B. A. Brown, C. Gaarde, J. Larsen, C. D. Goodman, C. C. Foster, D. Horen, T. Masterson, E. Sugarbaker, and T. N. Taddeucci
"The $^{51}V(p,n)^{51}Cr$ Reaction at E_p = 160 MeV," Nucl. Phys. A427, 332-56 (1984)

Rapaport, J., C. Gaarde, J. Larsen, C. Goulding, C. D. Goodman, C. Foster, D. J. Horen, T. Masterson, E. Sugarbaker, and T. N. Taddeucci
"The $^{19}F(p,n)^{19}Ne$ and $^{39}K(p,n)^{39}Ca$ Reactions at Intermediate Energies and Quenching of the Gamow-Teller Strength," Nucl. Phys. A431, 301-16 (1984)

Rapaport, J., P. Welch, J. Bahcall, E. Sugarbaker, T. N. Taddeucci, C. D. Goodman, C. F. Foster, D. Horen, C. Gaarde, J. Larsen, and T. Masterson
"Solar Neutrino Detection: Experimental Determination of Gamow-Teller Strengths via the ^{98}Mo and ^{115}In (p,n) Reactions," Phys. Rev. Lett. 54, 2325-28 (1985)

Robinson, M. T., and C. E. Bemis, Jr.
"Sputter Yield and Related Phenomena in the AVLIS Process," (Title-U, Report-SRD), Centrifuge Program Team Report, K/CPT-266 (February 21, 1985), 27 pages

Rosseel, T. M., J. M. Dale, L. D. Hulett, H. F. Krause, P. L. Pepmiller, S. Raman, C. R. Vane, and J. P. Young
"Effect of Chemical Environment on the L and M Heavy-Ion-Induced X-Ray Satellite Emission Spectra," Proceedings, Eighth Conference on the Application of Accelerators in Research and Industry, Denton, Texas, November 12-14, 1984, Nucl. Instrum. Methods Phys. Res. B10/11, 195-97 (1985)

Schmorak, M. R.
"Nuclear Data Sheets for A = 207," Nucl. Data Sheets 43, 383-479 (1984)

Schmorak, M. R.
"Nuclear Data Sheets for A = 205," Nucl. Data Sheets 45, 145-249 (1985)

Schmorak, M. R.
"Nuclear Data Sheets for A = 203," Nucl. Data Sheets 46, 287-377 (1985)

Scott, S. D., J. F. Lyon, J. K. Munro, D. J. Sigmar, S. C. Bates, J. D. Bell, C. E. Bush, A. Carnevali, J. L. Dunlap, P. H. Edmonds, W. L. Gardner, H. C. Howe, D. P. Hutchinson, R. C. Isler, R. R. Kindsfather, E. A. Lazarus, C. H. Ma, M. Murakami, L. E. Murray, G. H. Neilson, V. K. Pare, T. A. Staats, C. E. Thomas, R. M. Wieland, W. R. Wing, and A. J. Wootton
"Measurements of Periodic Ripple Transport in ISX-B Tokamak," Nucl. Fusion 25, 359-82 (1985)

Sellin, I. A. (Invited Paper)
"Convoy Electron Production by Heavy Ions in Solids," Proceedings, Eighth Conference on the Application of Accelerators in Research and Industry, Denton, Texas, November 12-14, 1984, Nucl. Instrum. Methods Phys. Res. B10/11, 156-60 (1985)

Sellin, I. A.
"Forward Electron Production in Heavy Ion-Atom and Ion-Solid Collisions," pp. 219-32 in Proceedings, International Conference on X-Ray and Inner Shell Processes in Atoms, Molecules, and Solids, Leipzig, East Germany, August 20-24, 1984, Karl-Marx-Universitat, Leipzig, 1984

Sellin, I. A., S. D. Berry, M. Breinig, C. Bottcher, R. Latz, M. Burkhard, H. Folger, H.-J. Frischkorn, K.-O. Groeneveld, D. Hofmann, and P. Koschar
"Anomalous Mean Free Paths for Scattering of Convoy Electrons Generated by Fast, Highly Ionized Ions in Thin Solid Targets," pp. 109-14 in Lecture Notes in Physics 213 (Proceedings, Symposium on the Physics of Electron Ejection in Ion-Atom and Ion-Solid Collisions, Aarhus, Denmark, June 29-30, 1984), Springer-Verlag, Berlin, 1984

Sellin, I. A., S. B. Elston, and S. D. Berry
"Recent Advances in Forward Electron Production Studies in Ion-Atom and Ion-Solid Collisions," pp. 249-61 in High-Energy Ion-Atom Collisions 2 (Proceedings, Second Workshop on High-Energy Ion-Atom Collision Processes, Debrecen, Hungary, August 27-28, 1984), ATOMKI, Debrecen, Hungary, 1985

Semmes, P. B., G. A. Leander, and J. L. Wood (Invited Paper)
"Particle-Core Coupling Calculations for the Positive Parity States in the Odd-Mass Hg Isotopes as a Test of IBA Core Descriptions," p. 208 in Proceedings, International Workshop on Interacting Boson-Boson and Boson-Fermion Systems, Gull Lake, Michigan, May 28-30, 1984, World Scientific Publishing, Singapore, 1985

Shalaby, M. M., and G. R. Satchler
"Optical Potential Ambiguities and Fusion Cross Sections for Heavy Ions," Nucl. Phys. A442, 469-77 (1985)

Shapira, D., Conference Chairman
Program and Abstracts for Conference on Instrumentation for Heavy-Ion Nuclear Research, Oak Ridge, Tennessee, October 22-24, 1984, ORNL-841005-Absts (1984)

Shapira, D., Editor
Instrumentation for Heavy Ion Nuclear Research (Proceedings, Conference on Instrumentation for Heavy Ion Nuclear Research, Oak Ridge, Tennessee, October 22-24, 1984), Harwood Academic, New York, 1985

Shapira, D., J.L.C. Ford, Jr., R. Novotny, B. Shivakumar, R. L. Parks, and S. T. Thornton
"The HHIRF Supersonic Gas-Jet Target Facility," Nucl. Instrum. Methods Phys. Res. A228, 259-66 (1985)

Shapira, D., J. Gomez del Campo, J.L.C. Ford, Jr., B. Shivakumar, P. H. Stelson, B. A. Harmon, R. A. Parks, and S. T. Thornton
"Nuclear Physics Experiments with the ORNL-HHIRF Supersonic Gas Jet Target," Proceedings, Eighth Conference on the Application of Accelerators in Research and Industry, Denton, Texas, November 12-14, 1984, Nucl. Instrum. Methods Phys. Res. B10/11, 436-40 (1985)

Shapira, D., D. Schull, J.L.C. Ford, Jr., B. Shivakumar, R. L. Parks, R. A. Cecil, and S. Thornton
"Observation of Angular Momentum Saturation in Deep-Inelastic Processes Involving Light Heavy Ions," Phys. Rev. Lett. 53, 1634-37 (1984)

Sherman, N. K., W. F. Davidson, S. Raman, W. Delbianco, and G. Kajrys
"Comparison of Photoabsorption by ^{16}O and ^{18}O," pp. 221-24 in Capture Gamma-Ray Spectroscopy and Related Topics (Proceedings, International Symposium on Gamma-Ray Spectroscopy and Related Topics Knoxville, Tennessee, September 10-14, 1984), AIP Conf. Proc. No. 125, American Institute of Physics, New York, 1984

Snell, A. H.
"Exciting Years!," Nucl. Sci. Eng. 90, 358-66 (1985)

Sofield, C. J., L. B. Bridwell, C. J. Woods, C. D. Moak, N.E.B. Cowern, P. D. Miller, D. Gregory, C. Jones, G. Alton, P. Pepmiller, and H. J. Hall
"Excited State Populations and Charge-Exchange of Fast Ions in Solids," Proceedings, X International Confernce on Atomic Collisions in Solids, Bad Iburg, West Germany, July 18-22, 1983, Nucl. Instrum. Methods Phys. Res., Sect. B, 230 [B2], 260-64 (1984)

Stachel, J., P. Braun-Munzinger, P. Paul, P. H. Zhang, F. E. Obenshain, F. Plasil, and G. R. Young
"Pion Production in Heavy-Ion Reactions near Absolute Thresholds," Proceedings, INS-RIKEN International Symposium on Heavy-Ion Physics, Mt. Fuji, Japan, August 27-31, 1984, J. Phys. Soc. (Japan) 54, Suppl. II, 400-09 (1985)

Stone, R. E., C. R. Bingham, L. L. Riedinger, R. W. Lide, H. K. Carter, R. L. Mlekodaj, and E. H. Spejewski
"The Decay of Mass-Separated $^{199}Po^{m}$ and $^{199}Po^{g}$," Phys. Rev. C 31, 582-92 (1985)

Strayer, M. R. (Invited Paper)
"Chaos near the Coulomb Barrier? — Nuclear Molecules," pp. 21-42 in Lecture Notes in Physics 219 (Proceedings, International Conference on Fusion Reactions Below the Coulomb Barrier, Cambridge, Massachusetts, June 13-15, 1984), Springer-Verlag, Berlin 1985

Strayer, M. R. (Invited Paper)
"Nuclear Molecules in TDHF," pp. 95-108 in Fundamental Problems in Heavy-Ion Collisions (Proceedings, 5th Adriatic International Conference on Nuclear Physics), Hvar, Yugoslavia, September 24-29, 1984, World Scientific Publishing, Singapore, 1984

Thorn, C. E., J. W. Olness, E. K. Warburton, and S. Raman
"$^{36}S(d,p)^{37}S$ and $^{34,36}S(d,^{3}He)^{33,35}P$ Reactions," Phys. Rev. C 30, 1442-53 (1984)

Thornton, S. T., R. L. Parks, D. Shapira, J.L.C. Ford, Jr., B. Shivakumar, and R. Novotny (Invited Paper)
"The ORNL Gas-Jet Target," pp. 1-10 in Instrumentation for Heavy Ion Research (Proceedings, Conference on Instrumentation for Heavy Ion Nuclear Research, Oak Ridge, Tennessee, October 22-24, 1984), Harwood Academic, New York, 1985

Toth, K. S., Y. A. Ellis-Akovali, F. T. Avignone III, R. S. Moore, D. M. Moltz, J. M. Nitschke, P. A. Wilmarth, P. K. Lemmertz, D. C. Sousa, and A. L. Goodman
"Single-Particle States in ^{149}Er and ^{149}Ho and the Effect of the Z = 64 Closure," Phys. Rev. C 32, 342-45 (1985)

Toth, K. S., Y. A. Ellis-Akovali, C. R. Bingham, D. M. Moltz, H. K. Carter, R. L. Mlekodaj, E. H. Spejewski, and D. C. Sousa
"Decay Properties of ^{186}Pb and the Lead Alpha-Decay Rate Anomaly," pp. 265-71 in Proceedings, Seventh International Conference on Atomic Masses and Fundamental Constants AMCO-7, Darmstadt, West Germany, September 3-7, 1984, Technische Hochschule, Darmstadt, 1984

Toth, K. S., Y. A. Ellis-Akovali, C. R. Bingham, D. M. Moltz, D. C. Sousa, H. K. Carter, R. L. Mlekodaj, and E. H. Spejewski
"Evidence from α Decay That Z = 82 Is Not Magic for Light Pb Isotopes," Phys. Rev. Lett. 53, 1623-26 (1984)

Toth, K. S., D. M. Moltz, E. C. Schloemer, M. D. Cable, F. T. Avignone, III, and Y. A. Ellis-Akovali
"Beta-Delayed Proton Activities: ^{147}Dy and ^{149}Er," pp. 237-43 in Proceedings, Seventh International Conference on Atomic Masses and Fundamental Constants AMCO-7, Darmstadt, West Germany, September 3-7, 1984, Technische Hochschule, Darmstadt, 1984

Tsang, M. B., W. G. Lynch, C. B. Chitwood, D. J. Fields, D. R. Klesch, C. K. Gelbke, G. R. Young, T. C. Awes, R. L. Ferguson, F. E. Obenshain, F. Plasil, and R. L. Robinson
"Azimuthal Correlations Between Light Particles Emitted in ^{16}O-Induced Reactions on ^{12}C and ^{197}Au at 400 MeV," Phys. Lett. 148B, 265-69 (1984)

Uchai, W., G. Lapicki, W. T. Milner, S. Raman, P. V. Rao, and C. R. Vane
"L X-Ray Emission from High-Z Elements after Ionization by 1 MeV u^{-1} Ag Ions," J. Phys. B18, L389-L394 (1985)

Umar, A. S.
"A Time-Dependent Mean-Field Theory for Prompt Nucleon Emission in Heavy-Ion Reactions," pp. 284-87 in Lecture Notes in Physics 219, (Proceedings, International Conference on Fusion Reactions Below the Coulomb Barrier, Cambridge, Massachusetts, June 13-15, 1984), Springer-Verlag, Berlin, 1985

Umar, A. S., M. R. Strayer, R. Y. Cusson, P.-G. Reinhard, and D. A. Bromley
"Time-Dependent Hartree-Fock Calculations of $^{4}He + ^{14}C$, $^{12}C + ^{12}C(0^{+})$, and $^{4}He + ^{20}Ne$ Molecular Formations," Phys. Rev. C 32, 172-83 (1985)

Umar, A. S., M. R. Strayer, D. J. Ernst, and K.R.S. Devi
"Mean-Field Theory of Prompt, High-Energy Nucleon Emission," Phys. Rev. C 30, 1934-48 (1984)

Vane, C. R., E. Kallne, J. Kallne, G. Morford, S. Raman, and M. S. Smith (Invited Paper)
"Ultrahigh-Resolution Studies of Heavy-Ion-Induced X-Ray Satellite Emission," Proceedings, Eighth Conference on the Application of Accelerators in Research and Industry, Denton, Texas, November 12-14, 1984, Nucl. Instrum. Methods Phys. Res. B10/11, 190-94 (1985)

Watson, J. W., C. E. Bemis, Jr., and J. Hogan
Update Addendum to Detailed Assessment of AVLIS Program, (Title-U, Report-SRD), Centrifuge Program Team Report, K/CPT-278 (February 22, 1985), 29 pages

Wells, J. C., N. R. Johnson, J. Hattula, M. P. Fewell, D. R. Haenni, I. Y. Lee, F. K. McGowan, J. W. Johnson, and L. L. Riedinger
"Evidence for Collective Behavior in ^{128}Ce from Lifetime Measurements," Phys. Rev. C 30, 1532-37 (1984)

Whealton, J., J. T. Hogan, and C. E. Bemis, Jr.
Advanced Gas Centrifuge Proponent Team Report Review of the Atomic Vapor Laser Isotope Separation Program: Off-Line Physics Discussions, (Title-U, Report-SRD), Centrifuge Program Team Report, K/CPT-305 (April 2, 1985), 29 pages

Winters, R. R., C. H. Johnson, and A. D. MacKellar
"Optical Model for Low-Energy Neutrons on ^{60}Ni," Phys. Rev. C 31, 384-91 (1985)

Wong, C. Y.
"Rotating Torodial Nuclei in Heavy-Ion Reactions," Phys. Rev. C 30, 1949-52 (1984)

Wong, C. Y.
"Nucleon-Nucleus Reactions at Ultrarelativistic Energies," Phys. Rev. D 32, 94-114 (1985)

Wootton, A. J., C. E. Bush, P. H. Edmonds, H. C. Howe, E. A. Lazarus, C. H. Ma, M. Murakami, and G. H. Neilson
"The Effects of Varying Wall Conditions, Minor and Major Radii on Confinement Properties in ISX-B," Nucl. Fusion 25, 479-84 (1985)

Young, G. R. (Invited Paper)
"Accelerator-Colliders for Relativistic Heavy Ions or in Search of Luminosity," pp. 169-75 in Intersections Between Particle and Nuclear Physics (Proceedings, Conference on the Intersections Between Particle and Nuclear Physics, Steamboat Springs, Colorado, May 23-30, 1984), AIP Conf. Proc. No. 123, American Institute of Physics, New York, 1984

Young, G. R. (Invited Paper)
"How to Work with RHIC (Really Highly Interesting Collider)," pp. 27-46 in Proceedings, RHIC Workshop on Experiments for a Relativistic Heavy-Ion Collider, Upton, New York, April 15-19, 1985, Brookhaven National Laboratory Report, BNL 51921 (1985)

Young, G. R. (Invited Paper)
"Internal Targets for RHIC," pp. 283-86 in Proceedings, RHIC Workshop on Experiments for a Relativistic Heavy-Ion Collider, Upton, New York, April 15-19, 1985, Brookhaven National Laboratory Report, BNL 51921 (1985)

Ziegler, N. F., E. G. Richardson, J. E. Mann, P. K. Kloeppel, R. C. Juras, C. M. Jones, J. A. Biggerstaff, J. A. Benjamin, and G. D. Alton
"Status of the Oak Ridge 25URC Accelerator," pp. 36-38 in Proceedings, 1983 Symposium of Northeastern Accelerator Personnel, Rochester, New York, October 3-5, 1983, 1984

Zumbro, J. D., E. B. Shera, Y. Tanaka, C. E. Bemis, Jr., R. A. Naumann, M. V. Hoehn, W. Reuter, and R. M. Steffen
"E2 and E4 Deformations in $^{233,234,235,238}U$," Phys. Rev. Lett. 53, 1888-92 (1984)

PROGRESS REPORT

Ball, J. B., S. Datz, E. E. Gross, C. M. Jones, J. B. McGrory, and R. L. Robinson
Physics Division Progress Report for Period Ending September 30, 1984, ORNL-6120 (January 1985)

TOPICAL REPORTS

Barnett, C. F., D. H. Crandall, H. B. Gilbody, D. C. Gregory, M. I. Kirkpatrick, E. W. McDaniel, R. H. McKnight, F. W. Meyer, T. J. Morgan, R. A. Phaneuf, M. S. Pindzola, and E. W. Thomas
1983 Bibliography of Atomic and Molecular Processes, ORNL-6095 (October 1984)

Barnett, C. F., H. B. Gilbody, D. C. Gregory, P. M. Griffin, C. C. Havener, A. M. Howald, M. I. Kirkpatrick, E. W. McDaniel, F. W. Meyer, T. J. Morgan, R. A. Phaneuf, M. S. Pindzola, and E. W. Thomas
1984 Bibliography of Atomic and Molecular Processes, ORNL-6157 (April 1985)

Gregory, D. C., D. H. Crandall, R. A. Phaneuf, A. M. Howald, G. H. Dunn, R. A. Falk, D. W. Mueller, and T. J. Morgan
Electron Impact Ionization of Multicharged Ions at ORNL: 1980-1984, ORNL/TM-9501 (May 1985)

Griffin, D. C., M. S. Pindzola, and C. Bottcher
The Effect of External Electric Fields on the Dielectronic Recombination Cross Section of Lithium- and Sodium-Like Ions, ORNL/TM-9478 (March 1985)

Hutchinson, D. P., K. L. Vander Sluis, J. Sheffield, and D. J. Sigmar
Feasibility of Alpha Particle Measurement by CO_2 Laser Thomson Scattering, ORNL/TM-9090 (December 1984)

Pindzola, M. S., D. C. Griffin, C. Bottcher, D. C. Gregory, A. M. Howald, R. A. Phaneuf, D. H. Crandall, G. H. Dunn, D. W. Mueller, and T. J. Morgan
Survey of Experimental and Theoretical Electron-Impact Ionization Cross Sections for Transition Metal Ions in Low Stages of Ionization, ORNL/TM-9436 (March 1985)

Thomas, E. W.
Atomic Data for Controlled Fusion Research. Volume III. Particle Interactions with Surfaces, ORNL-6088/V3 (February 1985)

Wells, J. W., M. P. Fewell, and M. R. Johnson
"LIFETIME": A Computer Program for Analyzing Doppler-Shift Recoil-Distance Nuclear Lifetime Data, ORNL/TM-9105 (October 1985)

Wiese, R. L., Editor
Atomic Data for Controlled Fusion Research. Volume IV. Spectroscopic Data for Iron, ORNL-6089/V4 (February 1985)

ARTICLES PENDING PUBLICATION AS OF SEPTEMBER 30, 1985

Abe, K., R. Armenteros, T. C. Bacon, J. Ballam, H. H. Bingham, J. E. Brau, K. Braune, D. Brick, W. M. Bugg, J. M. Butler, W. Cameron, H. O. Cohn, D. C. Colley, G. T. Condo, P. Dingus, R. Erickson, R. C. Field, B. Franek, R. Gearhart, T. Glanzman, I. M. Godfrey, J. J. Goldberg, G. Hall, E. R. Hancock, H. J. Hargis, E. L. Hart, M. J. Harwin, K. Hasegawa, M. Jobes, T. Kafka, G. E. Kalmus, D. P. Kelsey, T. Kitagaki, W. A. Mann, R. Merenyi, R. Milburn, K. C. Moffeit, J. J. Murray, A. Napier, V. R. O'Dell, P. Rankin, H. Sagawa, J. Schneps, S. J. Sewell, J. Shank, A. M. Shapiro, J. Shimony, K. Tamai, S. Tanaka, D. A. Waide, M. Widgoff, S. Wolbers, C. A. Woods, A. Yamaguchi, G. P. Yost, and H. Yuta
"Charm Photoproduction at 20 GeV Including Preliminary Lifetime Results with Improved Optical Resolution," Proceedings, XXII International Conference on High-Energy Physics, Leipzig, East Germany, July 19-25, 1984

Abe, K., R. Armenteros, T. C. Bacon, J. Ballam, H. H. Bingham, J. E. Brau, K. Braune, D. Brick, W. M. Bugg, J. M. Butler, W. Cameron, H. O. Cohn, D. C. Colley, G. T. Condo, P. Dingus, R. Erickson, R. C. Field, B. Franek, R. Gearhart, T. Glanzman, I. M. Godfrey, J. J. Goldberg, G. Hall, E. R. Hancock, H. J. Hargis, E. L. Hart, M. J. Harwin, K. Hasegawa, M. Jobes, T. Kafka, G. E. Kalmus, D. P. Kelsey, T. Kitagaki, W. A. Mann, R. Merenyi, R. Milburn, K. C. Moffeit, J. J. Murray, A. Napier, V. R. O'Dell, P. Rankin, H. Sagawa, J. Schneps, S. J. Sewell, J. Shank, A. M. Shapiro, J. Shimony, K. Tamai, S. Tanaka, D. A. Waide, M. Widgoff, S. Wolbers, C. A. Woods, A. Yamaguchi, G. P. Yost, and H. Yuta
"Comparison of Lambda and Antilambda Inclusive Photoproduction at 20 GeV with Quark-Diquark Fusion Model," Proceedings, XXII International Conference on High-Energy Physics, Leipzig, East Germany, July 19-25, 1984

Aichelin, J.
"Heavy Systems at Intermediate Energies in the Boltzmann-Uehling-Uhlenbeck Approach," Physical Review C

Aichelin, J.
"Subthreshold π^0 Production in the Boltzmann-Uehling-Uhlenbeck Theory," Physical Review Letters

Alton, G. D.
"An Axial Geometry Cesium Sputter Negative Ion Source with Continuous Tungsten Surface Ionizer," Proceedings, Fourth International Conference on Electrostatic Accelerator Technology, Buenos Aires, Argentina, April 15-19, 1985

Alton, G. D., R. M. Beckers, and J. W. Johnson
"A Radial Geometry Cesium Plasma Source with Improved Mechanical Features," Proceedings, Fourth International Conference on Electrostatic Accelerator Technology, Buenos Aires, Argentina, April 15-19, 1985

Alton, G. D., and C. M. Jones
"Pulsed Mode Evaluation of an Axial Geometry Cesium Sputter Negative Ion Source," Proceedings, Fourth International Conference on Electrostatic Accelerator Technology, Buenos Aires, Argentina, April 15-19, 1985

Alton, G. D., T. J. Kvale, R. N. Compton, D. J. Pegg, and J. S. Thompson
"The Production of Ca^- Through Sequential Charge Exchange with Li Vapor," Proceedings, Fourth International Conference on Electrostatic Accelerator Technology, Buenos Aires, Argentina, April 15-19, 1985

Alton, G. D., and G. D. Mills
"Negative Ion Sources Equipped with Continuous Annular and Spherical Geometry Surface Ionizers," Proceedings, 1985 Particle Accelerator Conference, Vancouver, Canada, May 13-16, 1985

Balantekin, A. B.
"Accidental Degeneracies, Hidden Supersymmetries, and Spectrum Generating Superalgebras," Proceedings, Nuclear Shell Models: A Symposium on Contemporary Research, Honoring I. Talmi, Philadelphia, Pennsylvania, October 31-November 3, 1984

Balantekin, A. B., C. Bottcher, M. R. Strayer, and S. J. Lee (Invited Paper)
"Phenomenology of New Particle Production in Heavy-Ion Collisions," Proceedings, Atomic Theory Workshop on Relativistic and QED Effects in Heavy Atoms, Washington, D.C., May 23-24, 1985

Ballon, D., Y. Niv, S. Vajda, N. Benczer-Koller, L. Zamick, and G. A. Leander
"Magnetic Moments of the Lowest $3/2_1^-$ and $5/2_1^-$ States in $^{107,109}Ag$," Physical Review C

Beckerman, M. (Invited Paper)
"Fusion Reactions at Low Energy," Proceedings, Niels Bohr Centennial Symposia, North-Holland, Amsterdam

Beene, J. R., G. F. Bertsch, P. F. Bortignon, and R. A. Broglia
"Direct and Compound Gamma Decay of the Giant Quadrupole Resonance of ^{208}Pb," Physics Letters B

Berman, B. L., and S. Datz
"Channeling-Radiation Experiments," Topics in Current Physics: Coherent Radiation Sources

Bertrand, F. E., E. E. Gross, D. J. Horen, R. O. Sayer, T. P. Sjoreen, D. K. McDaniels, J. Lisantti, J. R. Tinsley, L. W. Swenson, J. B. McClelland, T. A. Carey, K. Jones, and S. J. Seestrom-Morris
"A High Resolution Study of Giant Resonance Structure in ^{208}Pb Using the (p,p') Reaction at 334 MeV," Physical Review C

Bertrand, F. E., R. O. Sayer, R. L. Auble, M. Beckerman, J.L. Blankenship, B.L. Burks, M A.G. Fernandes, C. W. Glover, E. E. Gross, D. J. Horen, D. Shapira, and H. P. Morsch
"Excitation of the High Energy Nuclear Continuum in ^{208}Pb by 22 MeV/Nucleon ^{17}O and ^{32}S," Physical Review C

Bertsch, G. F. (Invited Paper)
"Nonrelativistic Theory of Heavy-Ion Collisions," Proceedings, School on Heavy-Ion Physics, Erice, Sicily, July 17-23, 1984

Bertsch, G., and W. Ekardt
"Application of Sum Rules to the Response of Small Metal Particles," Physical Review B

Bertsch, G., and H. Esbensen
"The Classical Limit of the Surface Response in Fermi Liquids," Physics Letters B

Bottcher, C.
"Transition State Theory for Nonstationary Atomic and Molecular Systems," Proceedings of the Royal Society of London A

Bottcher, C., and M. R. Strayer (Invited Paper)
"Pair Production at GeV/u Energies," Proceedings, Atomic Theory Workshop on Relativistic and QED Effects in Heavy Atoms, Gaithersburg, Maryland, May 23-24, 1985

Bounds, J. A., C. R. Bingham, P. Juncar, H. K. Carter, G. A. Leander, R. L. Mlekodaj, E. H. Spejewski, and W. M. Fairbank, Jr.
"Role of Deformation in the Intrusion of the $h_{9/2}$ Levels below the Z = 82 Proton Shell," Physical Review Letters

Broglia, R. A., and M. Gallardo (Invited Paper)
"Random Phase Approximation Treatment of the Pairing Phase Transition in Strongly Rotating Nuclei," Proceedings, Second International Conference on Nucleus-Nucleus Collisions, Visby, Sweden, June 10-14, 1985

Burgdorfer, J.
"The Width of the Electron Loss to Continuum Cusp for He^+ Colliding with He," Journal of Physics B

Burgdorfer, J. (Invited Paper)
"Final-State Angular Momentum Distributions in Charge Transfer Collisions at High Energies," Proceedings, Second Workshop on Cross Sections for Fusion and Other Applications, College Station, Texas, November 8-10, 1984

Burgdorfer, J.
"Statistical Multipoles for Cusp Electrons and Rydberg Electrons," Physical Review

Burgdorfer, J., and K. Taulbjerg
"Distorted Wave Methods for Electron Capture in Ion-Atom Collisions," Physical Review

Carvalho, J., R. Le Blanc, M. Vassanji, D. J. Rowe, and J. B. McGrory
"The Symplectic Shell Model Theory of Collective States," Nuclear Physics A

Church, D. A., H. M. Holzscheiter, R. A. Kenefick, C. S. O, R. T. Short, S. D. Berry, S. B. Elston, M. Breinig, R. DeSerio, I. A. Sellin, and B. Thomas
"Recoil Ion Confinement in a Radio-Frequency Quadrupole Ion Trap," Applied Physics Letters

Crandall, D. H., R. A. Phaneuf, D. C. Gregory, A. M. Howald, D. W. Mueller, T. J. Morgan, G. H. Dunn, and R.J.W. Henry
"Electron Impact Ionization of O^{2+} and O^{6+}: Excitation-Autoionization in Li-Like Ions," Physical Review A

Cusson, R. Y., P. G. Reinhard, J. J. Molitoris, H. Stocker, M. R. Strayer, and W. Greiner
"The Time Dependent Dirac Equation (TDDE) with Relativistic Mean Field Dynamics Applied to Heavy Ion Scattering," Physical Review Letters

Cusson, R. Y., P. G. Reinhard, H. Stoecker, M. R. Strayer, and W. Greiner
"Mean Field Model for Relativistic Heavy Ion Collisions," Zeitschrift fuer Physik

Dabbs, J.W.T., and C. E. Bemis, Jr.
"Measurement of the ^{249}Cf Neutron Fission Cross Section," Nuclear Science and Engineering

Datz, S. (Invited Paper)
"Experimental Approaches to the Measurement of Dielectronic Recombination," Atomic Excitation and *Recombination in External Fields*

Datz, S., P. F. Dittner, P. D. Miller, and P. L. Pepmiller (Invited Paper)
"Dielectronic Recombination Measurements in a Single Pass Experiment," Proceedings, Workshop on Electron Cooling and Related Applications, ECOOL 84, Karlsruhe, F.R.G., September 24-26, 1984

Dittner, P. F., S. Datz, P. D. Miller, and P. L. Pepmiller
"Dielectronic Recombination Measurements on Multicharged Ions," Atomic Excitation and Recombination in External Fields

Dittner, P. F., S. Datz, P. D. Miller, P. L. Pepmiller, and C. M. Fou
"Dielectronic Recombination Measurements of P^{4+}, S^{5+}, and Cl^{6+}," Physical Review A

Engar, P., M. Breinig, R. DeSerio, C. E. Gonzalez-Lepera, and I. A. Sellin
"Quantitative Determination of the Fraction of Rydberg Electrons in a Convoy Electron Cusp," Physical Review A

Gregory, D. C. (Invited Paper)
"The Role of Indirect Processes in Electron-Impact Ionization of Multicharged Ions," Proceedings, XIV International Conference on the Physics of Electronic and Atomic Collisions, Palo Alto, California, July 24-30, 1985

Griffin, D. C., M. S. Pindzola, and C. Bottcher (Invited Paper)
"Trends in the Electric Field Enhancement of Dielectronic Recombination Cross Sections," Atomic Excitation and Recombination in External Fields

Guidry, M. W., S. Juutinen, X. T. Liu, C. R. Bingham, A. J. Larabee, L. L. Riedinger, C. Baktash, I. Y. Lee, M. L. Halbert, D. Cline, B. Kotlinski, W. J. Kernan, T. M. Semkow, D. G. Sarantites, K. Honkanen, and M. Rajagopalan
"Population of High Spin States in Transfer Reactions," Physics Letters B

Hall, J., P. Richard, P. L. Pepmiller, D. C. Gregory, P. D. Miller, C. D. Moak, C. M. Jones, G. D. Alton, L. B. Bridwell, and C. J. Sofield
"Energy Systematics of Single and Double K-Shell-Vacancy Production in Titanium Bombarded by Chlorine Ions," Physical Review A

Honkanen, K., H. C. Griffin, D. G. Sarantites, V. Abenante, L. A. Adler, C. Baktash, Y. S. Chen, O. Dietzsch, M. L. Halbert, D. C. Hensley, N. R. Johnson, A. Larabee, I. Y. Lee, L. L. Riedinger, J. X. Saladin, T. Semkow, and Y. Schutz
"High-Spin Structure of ^{163}Lu," Proceedings, ACS Symposium on Recent Advances in the Study of Nuclei off the Line of Stability, Chicago, Illinois, September 8-13, 1985

Horen, D. J.
"Isotopes," McGraw-Hill Encyclopedia of Science and Technology, Sixth Edition

Horen, D. J., C. H. Johnson, and A. D. MacKellar
"J-Dependence of the Real Optical Potential Near Neutron Threshold," Physics Letters B

Hudson, E. D., J. A. Martin, and R. S. Lord
"A Variable Field Magnetic Extraction Channel for ORIC," Proceedings, 1985 Particle Accelerator Conference, Vancouver, Canada, May 13-16, 1985

Johnson, N. R. (Invited Paper)
"Information on Nuclear Shapes at High Spins from Lifetime Measurements," Proceedings, Symposium on Electromagnetic Properties of High Spin States, Stockholm, Sweden, May 28-31, 1985

Johnson, N. R. (Invited Paper)
"Evolution of Nuclear Shapes at High Spins," Proceedings, ACS Symposium on Recent Advances in the Study of Nuclei off the Line of Stability, Chicago, Illinois, September 8-13, 1985

Jones, C. M., G. D. Alton, J. B. Ball, J. A. Biggerstaff, D. T. Dowling, K. A. Erb, D. E. Hoglund, E. D. Hudson, R. C. Juras, S. N. Lane, C. A. Ludemann, J. A. Martin, S. W. Mosko, D. K. Olsen, E. G. Richardson, and N. F. Ziegler
"The Holifield Heavy Ion Research Facility," Proceedings, Fourth International Conference on Electrostatic Accelerator Technology, Buenos Aires, Argentina, April 15-19, 1985

Ko, C. M., G. F. Bertsch, and J. Aichelin
"Lambda Production from Antiproton Annihilation in Nuclei," Physical Review C

Ko, C. M., and C. Y. Wong
"Photon Bremsstrahlung from Ultra-relativistic Nuclear Collisions," Physical Review C

Kratz, J. V., W. Bruchle, H. Folger, H. Gaggeler, M. Schadel, K. Summerer, G. Wirth, N. Greulich, G. Herrmann, U. Hickmann, P. Peuser, N. Trautmann, E. K. Hulet, R. W. Lougheed, J. M. Nitschke, R. L. Ferguson, and R. L. Hahn
"Search for Superheavy Elements in Damped Collisions Between ^{238}U and ^{248}Cm," Physical Review C

Leander, G. A., P. Moller, and J. R. Nix
"Calculated Masses and Decay Properties for Heavy and Superheavy Elements," Proceedings, International Workshop on Gross Properties of Nuclei and Nuclear Excitations XIII, Hirschegg, Austria, January 7-11, 1985

Lee, I. Y., C. Baktash, J. R. Beene, M. P. Fewell, M. L. Halbert, N. R. Johnson, F. K. McGowan, W. T. Milner, H. Kim, R. O. Sayer, and D. G. Sarantites
"Gamma-Decay Pathways of Nuclei with High Angular Momentum and High Excitation Energy," Physical Review Letters

Mahaux, C., H. Ngo, and G. R. Satchler
"Causality and the Threshold Anomaly of the Nucleus-Nucleus Potential," Nuclear Physics A

Martin, J. A., R. L. Auble, K. A. Erb, C. M. Jones, and D. K. Olsen
"Charge-State Distributions of 100, 175, 275, and 352 MeV Gold Ions Emerging from Thin Carbon Foils, Proceedings, Fourth International Conference on Electrostatic Accelerator Technology, Buenos Aires, Argentina, April 15-19, 1985

McDaniels, D. K., J. Lisantti, J. Tinsley, I. Bergqvist, L. W. Swenson, F. E. Bertrand, E. E. Gross, and D. J. Horen
"On the Validity of Microscopic Calculations for Inelastic Proton Scattering," Physics Letters B

McDaniels, D. K., J. R. Tinsley, J. Lisantti, D. M. Drake, I. Bergqvist, L. W. Swenson, F. E. Bertrand, E. E. Gross, D. J. Horen, T. Sjoreen, R. Liljestrand, and H. Wilson
"Cross Section and Analyzing Power Measurements for the Giant Resonance Region in ^{208}Pb with 200-MeV Protons," Physical Review C

McGowan, F. K., N. R. Johnson, I. Y. Lee, W. T. Milner, C. Roulet, J. Hattula, M. P. Fewell, Y. A. Ellis-Akovali, R. M. Diamond, F. S. Stephens, and M. W. Guidry
"Test of the Triaxial Rotor Model and the IBFA Model Description of Collective States in ^{191}Ir," Physical Review C

Meyer, F. W., A. M. Howald, C. C. Havener, and R. A. Phaneuf
"Low Energy Electron Capture Cross Sections for Fully-Stripped and H-Like Projectiles Incident on H and H_2," Physical Review A

Nazarewicz, W., P. Olanders, I. Ragnarsson, J. Dudek, and G. A. Leander
"Octupole Shapes in Nuclei and Some Rotational Consequences Thereof," Proceedings, XIX Winter School on Physics Selected Topics in Nuclear Structure, (Zakopane, Poland, April 1984)

Neskovic, N.
"The Effect of Transverse Correlations in Ion Channeling in Very Thin Crystals," Physical Review Letters

Petitt, G. A., A. Gavron, J. R. Beene, B. Cheynis, R. L. Ferguson, F. E. Obenshain, F. Plasil, G. R. Young, M. Jaaskelainen, D. G. Sarantites, and C. F. Maguire
"Neutron Emission in Inelastic Reactions of $^{12}C + ^{158}Gd$ and $^{20}Ne + ^{150}Nd$," Physical Review C

Phaneuf, R. A. (Invited Paper)
"Many-Electron Effects in Electron-Impact Ionization of Multiply Charged Ions," Proceedings, Second Workshop on Cross Sections for Fusion and Other Applications, College Station, Texas, November 8-10, 1984

Phaneuf, R. A., and D. H. Crandall
"Collisions of Low-Energy Multiply Charged Ions," Proceedings, Atomic Physics Contractors' Workshop, Gaithersburg, Maryland, April 26-27, 1984

Raatz, J. E., R. D. Rathmell, P. H. Stelson, and N. F. Ziegler
"Tests of Compressed Geometry NEC Acceleration Tubes," Proceedings, Fourth International Conference on Electrostatic Accelerator Technology, Buenos Aires, Argentina, April 15-19, 1985

Raman, S. (Invited Paper)
"Summary Talk," Proceedings, Fourth International Symposium on Neutron-Induced Reactions, Smolenice, Czechoslovakia, June 17-21, 1985

Raman, S., and J. E. Lynn
"Comment on 'Evidence for a Nucleus-Nucleus Spin-Spin Interaction in ^{9}Be'," Physical Review Letters

Raman, S., and J. E. Lynn (Invited Paper)
"Applications and Misapplications of the Channel-Capture Formalism of Direct Neutron Capture," Proceedings, Fourth International Symposium on Neutron-Induced Reactions, Smolenice, Czechoslovakia, June 17-21, 1985

Raman, S., and C. W. Nestor (Invited Paper)
"$B(E2)\uparrow$ for the 2_1^+ States of Collective Nuclei off the Line of Stability," Proceedings, ACS Symposium on Recent Advances in the Study of Nuclei off the Line of Stability, Chicago, Illinois, September 8-13, 1985

Ramayya, A. V., W. C. Ma, J. H. Hamilton, S. J. Robinson, K. Zhao, J. D. Cole, E. F. Zganjar, and E. H. Spejewski
"Competing Nuclear Structures in $^{182-188}Hg$," Proceedings, International Symposium on In-Beam Nuclear Spectroscopy, Debrecen, Hungary, May 14-18, 1984

Sa, B.-H., and C.-Y. Wong
"Transverse Momentum Distribution of Produced Particles in Ultra-relativistic Nucleus-Nucleus Collisions, Physical Review D

Satchler, G. R.
"Absorption Cross Sections and the Use of Complex Potentials in Coupled-Channels Models," Physical Review C

Schuck, C., F. Hannachi, R. Chapman, J. C. Lisle, J. N. Mo, E. Paul, D.J.G. Love, P. J. Nolan, A. H. Nelson, P. M. Walker, Y. Ellis-Akovali, N. R. Johnson, N. Bendjaballah, R. M. Diamond, M. A. Deleplanque, F. S. Stephens, G. Dines, and J. Draper (Invited Paper)
"Gamma-Spectrometry with Compton Suppressed Detector Arrays," Proceedings, XXIII International Meeting on Nuclear Physics, Bormio, Italy, January 21-26, 1985

Stelson, P. H., J. R. Raatz, and R. D. Rathmell
"Hydrogen Arc Discharge Cleaning of Accelerator Tubes," Proceedings, Fourth International Conference on Electrostatic Accelerator Technology, Buenos Aires, Argentina, April 15-19, 1985

Taddeucci, T. N., C. D. Goodman, R. C. Byrd, T. A. Carey, D. J. Horen, J. Rapaport, and E. Sugarbaker
"A Neutron Polarimeter for (p,n) Measurements at Intermediate Energies," Nuclear Instruments and Methods in Physics Research

Taddeucci, T. N., C. D. Goodman, R. C. Byrd, I. J. Van Heerden, T. A. Carey, D. J. Horen, J. S. Larsen, C. Gaarde, J. Rapaport, T. P. Welch, and E. Sugarbaker
"Spin-Flip Decomposition of the Spectrum for $^{90}Zr(p,n)$ at E_p = 160 MeV," Physical Review C

Toth, K. S. (Invited Paper)
"Particle Studies at or near Closed Shells," Proceedings, ACS Symposium on Recent Advances in the Study of Nuclei off the Line of Stability, Chicago, Illinois, September 8-13, 1985

Uchai, W., C. W. Nestor, Jr., S. Raman, and C. R. Vane
"Energy Shifts of L X Rays from 70 < Z < 90 Elements due to Multiple M Vacancies," Atomic Data and Nuclear Data Tables

Umar, A. S., and M. R. Strayer
"Nuclear Shape-Isomeric Vibrations," Physical Review Letters

Wille, U., and R. Hippler
"Mechanisms of Inner-Shell Vacancy Production in Slow Ion-Atom Collisions," Physics Reports

Wong, C. Y.
"Transverse Momentum Distributions of π^0 and Its Product Gamma Rays," Physical Review D

Wong, C. Y.
"Rapidity Distribution of Produced Particles in Nucleon-Nucleon Collisions," Physical Review D

Wong, C. Y.
"Hot Toroidal and Bubble Nuclei," Physical Review Letters

Wong, C. Y.
"Stopping of Heavy Nuclei in Relativistic Heavy-Ion Collisions," Physical Review C

Wong, C. Y.
"Anomalous Positron Peak in Heavy-Ion Collisions," Physical Review Letters

Wu, J. Q., G. Bertsch, and A. B. Balantekin
"Channel Coupling Effects in Subbarrier Fusion of Oxygen + Oxygen," Physical Review C

Young, G. R., F. E. Obenshain, F. Plasil, P. Braun-Munzinger, R. Freifelder, P. Paul, and J. Stachel
"Production of Neutral Pions in Heavy-Ion Collisions at E_{lab}/A = 25 MeV," Physical Review C

Ziegler, N. F., E. G. Richardson, J. E. Mann, R. C. Juras, C. M. Jones, D. L. Haynes, J. A. Benjamin, and G. D. Alton
"Status Report on the ORNL 25 URC Accelerator," Proceedings, 1984 Symposium of Northeastern Accelerator Personnel with Postaccelerator Workshop, Stony Brook, New York, October 15-18, 1984

Ziegler, N. F., P. H. Stelson, W. Carli, H. Munzer, and G. Korschinek
"Observations on the Munich MP Arc Discharge Conditioning Test," Proceedings, 1984 Symposium of Northeastern Accelerator Personnel with Postaccelerator Workshop, Stony Brook, New York, October 15-18, 1984

Ziegler, N. F., P. H. Stelson, C. M. Jones, and J. E. Raatz
"Arc Discharge Conditioning Test on the Oak Ridge 25 URC Accelerator," Proceedings, Fourth International Conference on Electrostatic Accelerator Technology, Buenos Aires, Argentina, April 15-19, 1985

Zumbro, J. D., R. A. Naumann, M. V. Hoehn, W. Reuter, E. B. Shera, C. E. Bemis, Jr., and Y. Tanaka
"E2 and E4 Deformations in ^{232}Th and $^{239,240,242}Pu$," Physics Letters B

12. PAPERS PRESENTED AT SCIENTIFIC AND TECHNICAL MEETINGS

October 1984 Through September 1985

List Prepared by Shirley J. Ball

1984

1984 Symposium of Northeastern Accelerator Personnel Stony Brook, New York, October 15-18, 1984

N. F. Ziegler, E. G. Richardson, J. E. Mann, R. C. Juras, C. M. Jones, D. L. Haynes, J. A. Benjamin, and G. D. Alton
"Status Report on the ORNL 25 URC Accelerator"

N. F. Ziegler, P. H. Stelson, W. Carli, H. Munzer, and G. Korschinek
"Observations on the Munich MP Arc Discharge Conditioning Test"

American Physical Society Meeting, Division of Nuclear Physics, Nashville, Tennessee, October 18-20, 1984

C. Baktash, Y. Schutz, I. Y. Lee, M. Oshima, N. R. Johnson, E. der Mateosian, O. C. Kistner, A. W. Sunyar, D. Horn, C. J. Lister, C. Y. Chen, O. Dietzsch, J. X. Saladin, K. Honkanen, D. G. Sarantites, T. Semkov, and A. J. Larabee
"Discrete and Continuum γ Ray Study of ^{154}Er at High Spins," Bull. Am. Phys. Soc. 29, 1042 (1984)

J. A. Bounds, C. R. Bingham, D. J. Pegg, M. L. Gaillard, P. Juncar, H. K. Carter, R. L. Mlekodaj, E. H. Spejewski, W. M. Fairbank, Jr., J. D. Cole, P. M. Griffin, and C. E. Bemis, Jr.
"Hyperfine Structures and Isotope Shifts of ^{201,203,205}Tl by Collinear Laser Spectroscopy at UNISOR," Bull. Am. Phys. Soc. 29, 1045 (1984)

B. L. Burks, D. J. Horen, R. L. Auble, F. E. Bertrand, J. L. Blankenship, J.L.C. Ford, Jr., E. E. Gross, D. C. Hensley, R. O. Sayer, D. Shapira, and T. P. Sjoreen
"A Coupled Channels Analysis of Elastic and Inelastic Scattering of ^{18}O from ^{28}Si," Bull. Am. Phys. Soc. 29, 1026 (1984)

R. F. Carlton, C. H. Johnson, and J. A. Harvey
"Total Cross Sections for Low Energy Neutrons on ^{86}Kr," Bull. Am. Phys. Soc. 29, 1037 (1984)

Z. Gacsi, S. Ja, J. L. Weil, E. T. Jurney, and S. Raman
"Energy Levels of ^{116}Sn from (n,n'γ) and (n,γ) Reactions," Bull. Am. Phys. Soc. 29, 1041 (1984)

B. A. Harmon, S. T. Thornton, M. Beckerman, J. Gomez del Campo, and D. Shapira
"Study of Evaporation Residues from ^{28}Si + ^{12}C Induced Reactions," Bull. Am. Phys. Soc. 29, 1047 (1984)

D. J. Horen, F. A. Harrison, D. Wang, R. Alarcon, P. Welch, J. Rapaport, T. N. Taddeucci, C. D. Goodman, E. Sugarbaker, and C. Gaarde
"Observation of L = 0 Strength in the ^{52}Cr(p,n)^{52}Mn Reaction at 120 MeV," Bull. Am. Phys. Soc. 29, 1050 (1984)

N. R. Johnson, F. K. McGowan, Y. Schutz, I. Y. Lee, C. Baktash, A. J. Larabee, and J. C. Wells
"Lifetimes of High-Spin States in ^{162}Yb," Bull. Am. Phys. Soc. 29, 1043 (1984)

S. Juutinen, M. W. Guidry, C. R. Bingham, A. Larabee, X. T. Liu, L. L. Riedinger, C. Baktash, I. Y. Lee, M. L. Halbert, M. P. Fewell, D. Cline, B. Kotlinski, A. Baklin, D. Sarantites, T. M. Semkow, K. Honkanen, and M. Rajagopalan
"The Reaction Mechanism for One and Two-Particle Transfer with Very Heavy Ions," Bull. Am. Phys. Soc. 29, 1027 (1984)

X. T. Liu, S. Juutinen, C. R. Bingham, L. L. Riedinger, M. W. Guidry, C. Baktash, I. Y. Lee, D. Cline, and B. Kotlinski
"Cross Sections for Population of High-Spin States in Transfer Reactions," Bull. Am. Phys. Soc. 29, 1027 (1984)

W. C. Ma, A. V. Ramayya, S. J. Robinson, J. H. Hamilton, J. D. Cole, E. F. Zganjar, E. H. Spejewski
"High Spin States and Lifetimes in ^{184}Hg," Bull. Am. Phys. Soc. 29, 1049 (1984)

C. F. Maguire, H. C. Mogul, Z. Kui, W. C. Ma, S. J. Robinson, D. Watson, A. V. Ramayya, J. H. Hamilton, D. G. Kovar, H. Ikezoe, G. Rosner, G. Stephans, E. Ungricht, B. Wilkins, T. Awes, and G. R. Young
"Proton and α-Particle Emission in Fusion and Deep-Inelastic Reactions of 252-MeV ^{28}Si + ^{40}Ca," Bull. Am. Phys. Soc. 29, 1048 (1984)

F. K. McGowan, N. R. Johnson, I. Y. Lee, W. T. Milner, C. Roulet, J. Hattula, M. P. Fewell, Y. A. Ellis-Akovali, R. M. Diamond, F. S. Stephens, and M. W. Guidry
"A Test of the Triaxial Rotor Model and the IBFM Description of the States from Coulomb Excitation of ^{191}Ir," Bull. Am. Phys. Soc. 29, 1049 (1984)

M. Oshima, N. R. Johnson, F. K. McGowan, I. Y. Lee, C. Baktash, R. V. Ribas, Y. Schutz, and J. C. Wells
"Lifetimes of High-Spin States in ^{158}Er," Bull. Am. Phys. Soc. 29, 1043 (1984)

Y. Schutz, C. Baktash, I. Y. Lee, N. R. Johnson, F. McGowan, M. P. Fewell, M. L. Halbert, D. C. Hensley, L. Courtney, A. Larabee, L. L. Riedinger, and D. G. Sarantites
"Study of ^{158}Yb at High Spin and Excitation Energy," Bull. Am. Phys. Soc. 29, 1043 (1984)

K. M. Teh, C. F. Maguire, W. C. Ma, F. E. Bertrand, R. L. Auble, R. O. Sayer, D. Shapira, and B. L. Burks
"Test of the Optical Potential Spin-Orbit Coupling Term in the ^{28}Si(^{11}B,^{10}B[3$^+$,1$^+$])^{29}Si Reactions at 170 MeV," Bull. Am. Phys. Soc. 29, 1026 (1984)

A. S. Umar
"Fast Particle Emission in Heavy-Ion Reactions," Bull. Am. Phys. Soc. 29, 1053 (1984)

G. R. Young (Invited Talk)
"Production of Neutral Pi Mesons at Near-Threshold Bombarding Energies in Heavy-Ion Reactions," Bull. Am. Phys. Soc. 29, 1039 (1984)

E. F. Zganjar, J. D. Cole, J. L. Wood, G. Gowdy, and L. L. Reidinger
"A New Class of Low-Energy Structure at Closed Shells: Levels in $^{187-191}$Tl," Bull. Am. Phys. Soc. 29, 1049 (1984)

Workshop on Atomic Spectra and Collisions in External Fields, Gaithersburg, Maryland, October 22-23, 1984

S. Datz (Invited Talk)
"Experimental Approaches to the Measurement of Dielectronic Recombination"

P. F. Dittner, S. Datz, P. D. Miller, and P. L. Pepmiller (Invited Talk)
"Dielectronic Recombination Measurements on Multicharged Ions"

D. C. Griffin, M. S. Pindzola, and C. Bottcher (Invited Talk)
"Trends in the Electric Field Enhancement of Dielectronic Recombination Cross Sections

Conference on Instrumentation for Heavy-Ion Nuclear Research, Oak Ridge, Tennessee, October 22-24, 1984

T. C. Awes, R. L. Ferguson, F. E. Obenshain, F. Plasil, G. R. Young, P. Braun-Munzinger, R. Freifelder, P. Paul, L. Ricken, J. Stachel, P. DeYoung, and P.-H. Zhang
"A Large Acceptance Spectrometer for π^0 Mesons"

C. E. Bemis, Jr. (Invited Paper)
"The ORNL Polarized Target"

H. J. Kim, T. C. Awes, M. Beckerman, J. R. Beene, C. E. Bemis, Jr., R. L. Ferguson, I. Y. Lee, F. K. McGowan, F. E. Obenshain, F. Plasil, R. L. Robinson, D. Shapira, and P. H. Stelson
"ORNL-MIT Recoil Mass Separator"

S. T. Thornton, R. L. Parks, D. Shapira, J.L.C. Ford, Jr., B. Shivakumar, and R. Novotny (Invited Talk)
"The ORNL Gas-Jet Target"

1984 Meeting of the Southeastern Section of the American Physical Society, Memphis, Tennessee, October 25-28, 1984

F. E. Bertrand (Invited Talk)
"Studies of the Nuclear Giant Resonances Using Heavy Ions," Bull. Am. Phys. Soc. 29, 1486 (1984)

K. M. Teh, C. F. Maguire, W. C. Ma, F. E. Bertrand, R. L. Auble, R. O. Sayer, D. N. Shapira, and B. L. Burks
"Test of the Optical Potential Spin-Orbit Coupling Term in the $^{28}Si(^{11}B,^{10}B[3^+,1^+])^{29}Si$ Reactions at 170 MeV," Bull. Am. Phys. Soc. 29, 1502 (1984)

American Physical Society Meeting, Division of Plasma Physics, Boston, Massachusetts, October 29-November 2, 1984

D. K. Mansfield, H. Park, L. C. Johnson, and C. H. Ma
"A Multichannel Far-Infrared Interferometer/Polarimeter for TFTR," Bull. Am. Phys. Soc. 29, 1304 (1984)

1984 Nuclear Science Symposium, Orlando, Florida, October 31-November 2, 1984

W. T. Milner and J. A. Biggerstaff
"CHIL: A Comprehensive Histogramming Language"

Nuclear Shell Models: A Symposium on Contemporary Research, Honoring I. Talmi, Philadelphia, Pennsylvania, October 31-November 3, 1984

A. B. Balantekin
" 'Accidental' Degeneracies and Hidden Supersymmetries"

Second Workshop on Cross Sections for Fusion and Other Applications, College Station, Texas, November 8-10, 1984

J. Burgdorfer (Invited Talk)
"Final-State Angular Momentum Distributions in Charge Transfer Collisions at High Energies"

R. A. Phaneuf (Invited Talk)
"Many-Electron Effects in Electron-Impact Ionization of Multiply Charged Ions"

Eighth Conference on the Application of Accelerators in Research and Industry, Denton, Texas, November 12-14, 1984

M. C. Andrews, F. D. McDaniel, J. L. Duggan, R. Mehta, P. D. Miller, H. Krause, P. L. Pepmiller, T. M. Rosseel, L. A. Rayburn, and G. Lapicki
"M-Shell Electron Capture and Direct Ionization of Selected Events with Z = 60 to 82 by Incident 25-MeV Carbon and 32-MeV Oxygen Ions," Bull. Am. Phys. Soc. 29, 1104 (1984)

M. C. Andrews, F. D. McDaniel, J. L. Duggan, R. Mehta, P. D. Miller, H. Krause, P. L. Pepmiller, T. M. Rosseel, L. A. Rayburn, and G. Lapicki
"L-Shell X-Ray Production Cross Sections of Selected Elements with Z = 60 to 82 for Incident 25-MeV Carbon and 32-MeV Oxygen Ions," Bull. Am. Phys. Soc. 29, 1103 (1984)

R. L. Becker (Invited Talk)
"Theory of K^nL^v Multiple Vacancy Production by Heavy Ions," Bull. Am. Phys. Soc. 29, 1084 (1984)

C. Bottcher (Invited Talk)
"Time-Dependent Hartree-Fock Studies of Heavy-Ion Collisions," Bull. Am. Phys. Soc. 29, 1120 (1984)

M. Breinig (Invited Talk)
"Observation of the Thomas Peak in the Transfer of Atoms Between Molecules," Bull. Am. Phys. Soc. 29, 1075 (1984)

S. Datz
"Correlated Two-Electron Effects in Highly Charged Ion-Atom Collisions," Bull. Am. Phys. Soc. 29, 1120 (1984)

P. F. Dittner (Invited Talk)
"Dielectronic Recombination: A Status Report," Bull. Am. Phys. Soc. 29, 1074 (1984)

S. B. Elston (Invited Talk)
"Application of Position-Sensitive Detectors to the Spectrometry of Collision Produced Forward-Ejected Electrons," Bull. Am. Phys. Soc. 29, 1126 (1984)

P. Engar, M. Breinig, C. E. Gonzalez-Lepera, S. D. Berry, R. DeSerio, and I. A. Sellin
"Rydberg State and Convoy Electron Production by Fast Oxygen Ions in Foil Targets," Bull. Am. Phys. Soc. 29, 1103 (1984)

G. A. Glass, P. Engar, S. D. Berry, M. Breinig, R. DeSerio, S. B. Elston, and I. A. Sellin
"Electron Capture to the Continuum from Atomic Hydrogen," Bull. Am. Phys. Soc. 29, 1103 (1984)

D. C. Gregory (Invited Talk)
"Indirect Processes in Electron-Impact Ionization of Multiply Charged Ions," Bull. Am. Phys. Soc. 29, 1091 (1984)

P. D. Miller
"Excited State Populations and Charge Exchange of Fast Ions in Solids," Bull. Am. Phys. Soc. 29, 1064 (1984)

S. Raman (Invited Talk)
"Ultrahigh-Resolution Studies of Heavy-Ion-Induced X-Ray Satellite Emission," Bull. Am. Phys. Soc. 29, 1084 (1984)

T. M. Rosseel, J. M. Dale, L. D. Hulett, H. F. Krause, P. L. Pepmiller, S. Raman, C. R. Vane, and J. P. Young
"Effect of Chemical Environment on the L and M Heavy-Ion-Induced X-Ray Satellite Emission (HIXSE)," Bull. Am. Phys. Soc. 29, 1105 (1984)

I. A. Sellin (Invited Talk)
"Progress in Forward Electron Production in Ion-Atom and Ion-Solid Collisions," Bull. Am. Phys. Soc. 29, 1119 (1984)

D. Shapira (Invited Talk)
"A Windowless Supersonic Gas Jet Target for Nuclear Physics Experiments," Bull. Am. Phys. Soc. 29, 1086 (1984)

International Conference on Nuclear Physics, Bombay, India, December 27-31, 1984

F. Plasil (Invited Talk)
"Recent Advances in Heavy-Ion-Induced Fission"

1985

International Workshop on Gross Properties of Nuclei and Nuclear Excitations XIII, Hirschegg, Austria, January 7-11, 1985

G. A. Leander, P. Moller, and J. R. Nix
"Calculated Masses and Decay Properties for Heavy and Superheavy Elements"

Sixth International ECR Ion Source Workshop, Berkeley, California, January 17-18, 1985

F. W. Meyer
"Status of the ORNL ECR Source"

XXIII International Meeting on Nuclear Physics, Bormio, Italy, January 21-26, 1985

C. Schuck, F. Hannachi, R. Chapman, J. C. Lisle, J. N. Mo, E. Paul, D.J.G. Love, P. J. Nolan, A. H. Nelson, P. M. Walker, Y. Ellis-Akovali, N. R. Johnson, N. Bendjaballah, R. M. Diamond, M. A. Deleplanque, F. S. Stephens, G. Dines, and J. Draper (Invited Talk)
"Gamma-Spectrometry with Compton Suppressed Detector Arrays"

Fifth APS Topical Conference on Atomic Processes in High-Temperature Plasmas, Pacific Grove, California, February 25-28, 1985

C. F. Barnett, R. A. Phaneuf, H. T. Hunter, M. I. Kirkpatrick, W. L. Wiese, E. W. Thomas, J. W. Gallagher, M. S. Pindzola, and R. K. Janev
"Atomic Data for High Temperature Plasmas," Bull. Am. Phys. Soc. 30, 1131 (1985)

C. Bottcher (Invited Talk)
"Rydberg Atoms in External Fields: How to Interpret Experiments on Dielectronic Recombination," Bull. Am. Phys. Soc. 30, 1128 (1985)

A. M. Howald, D. C. Gregory, R. A. Phaneuf, A. Muller, N. Djuric, and G. H. Dunn
"Electron Impact Ionization of Mg-Like Ions," Bull. Am. Phys. Soc. 30, 1120 (1985)

F. W. Meyer (Invited Talk)
"EBIC and ECRIS: New Sources of High Charge State Ions for Atomic Collision Research," Bull. Am. Phys. Soc. 30, 1125 (1985)

R. A. Phaneuf (Invited Talk)
"Recent Developments in Charge-Exchange Measurements at ORNL," Bull. Am. Phys. Soc. 30, 1126 (1985)

American Physical Society Meeting, Baltimore, Maryland, March 25-29, 1985

W. Beezhold, T.W.L. Sanford, H. Park, J. O. Kephart, R. K. Klein, R. H. Pantell, B. L. Berman, and S. Datz
"Channeling Radiation from Tungsten," Bull. Am. Phys. Soc. 30, 374 (1985)

B. L. Berman, S. Datz, J. O. Kephart, R. K. Klein, R. H. Pantell, H. Park, R. L. Swent, M. J. Alguard, and M. V. Hynes
"Channeling Radiation from LiH and LiD," Bull. Am. Phys. Soc. 30, 373 (1985)

S. Datz, B. L. Berman, B. A. Dahling, J. O. Kephart, R. K. Klein, R. H. Pantell, and H. Park
"Channeling Radiation from Damaged LiF Crystals," Bull. Am. Phys. Soc. 30, 373 (1985)

J. O. Kephart, R. K. Klein, R. H. Pantell, H. Park, S. Datz, M. J. Alguard, R. L. Swent, and B. L. Berman
"Occupation Lengths for Electrons and Positrons Channeled in Silicon Crystals," Bull. Am. Phys. Soc. 30, 374 (1985)

H. Park, J. O. Kephart, R. K. Klein, R. H. Pantell, M. V. Hynes, B. L. Berman, B. A. Dahling, S. Datz, R. L. Swent, and M. J. Alguard
"Temperature Dependence of Channeling Radiation," Bull. Am. Phys. Soc. 30, 374 (1985)

Niels Bohr Centennial Symposium on Semiclassical Descriptions of Atomic and Nuclear Collisions, Copenhagen, Denmark, March 25-30, 1985

J. O. Rasmussen, M. W. Guidry, and L. F. Canto (Invited Talk)
"Transfer Involving Deformed Nuclei"

M. Beckerman (Invited Talk)
"Fusion Reactions at Low Energy"

Fourth International Conference on Electrostatic Accelerator Technology, Buenos Aires, Argentina, April 15-19, 1985

G. D. Alton
"Development of a Pulsed-Mode Negative Ion Source"

G. D. Alton
"A High Brightness Axial Geometry Negative Ion Source with Solid Surface Ionizer"

G. D. Alton, R. M. Beckers, and J. W. Johnson
"An Improved Radial Geometry Cesium Plasma Negative Ion Source"

G. D. Alton, T. J. Kvale, D. J. Pegg, and J. S. Thompson
"Production of Ca^- Through Double Charge Exchange with Li Vapor"

C. M. Jones, G. D. Alton, J. B. Ball, J. A. Biggerstaff, D. T. Dowling, K. A. Erb, D. E. Hoglund, E. D. Hudson, R. C. Juras, S. N. Lane, C. A. Ludemann, J. A. Martin, S. W. Mosko, D. K. Olsen, E. G. Richardson, and N. F. Ziegler
"The Holifield Heavy Ion Research Facility"

J. A. Martin, R. L. Auble, K. A. Erb, C. M. Jones, and D. K. Olsen
"Charge-State Distributions of Gold Ions Emerging from Thin Carbon Foils at Energies of 100, 175, 275, and 352 MeV"

J. R. Raatz, R. D. Rathmell, P. H. Stelson, and N. F. Ziegler
"Tests of Compressed Geometry NEC Acceleration Tubes"

P. H. Stelson, J. R. Raatz, and R. D. Rathmell
"Hydrogen Arc Discharge Cleaning of Accelerator Tubes"

N. F. Ziegler, P. H. Stelson, C. M. Jones, and J. R. Raatz
"Arc Discharge Conditioning Test on the Oak Ridge 25 URC Accelerator"

Workshop on Experiments for a Relativistic Heavy-Ion Collider, Upton, New York, April 15-19, 1985

S. Aronson, G. Igo, B. Pope, A. Shor, and G. Young (Invited Talk)
"A Detector for Dimuons Produced in the Relativistic Heavy Ion Collider"

G. R. Young (Invited Talk)
"How to Work with RHIC (Really Highly Interesting Collider)"

G. R. Young (Invited Talk)
"Internal Targets for RHIC"

Second European Conference on Atomic and Molecular Physics, Amsterdam, The Netherlands, April 19-23, 1985

P. Defrance, S. Chantrenne, S. Rachafi, D. Belic, J. Cureta, D. Gregory, and F. Brouillard
"Electron Impact Ionization of N^{6+} and O^{6+}"

American Physical Society Meeting, Washington, D.C., April 24-27, 1985

T. C. Awes, R. L. Ferguson, R. Novotny, F. E. Obenshain, F. Plasil, V. Rauch, G. R. Young, and H. Sann
"Equilibrium Fission Decay of Reaction Products with $A \lesssim 150$," Bull. Am. Phys. Soc. 30, 708 (1985)

A. B. Balantekin and B. R. Barrett
"Collective M1 States in the Classical Limit of the IBM-2," Bull. Am. Phys. Soc. 30, 729 (1985)

J. A. Bounds, C. R. Bingham, H. K. Carter, G. A. Leander, R. L. Mlekodaj, and E. H. Spejewski
"Hyperfine Structure and Isotope Shifts of $^{189-193m}$Tl," Bull. Am. Phys. Soc. 30, 777 (1985)

M. P. Carpenter, C. R. Bingham, L. H. Courtney, S. Juutinen, A. J. Larabee, Z. M. Liu, L. L. Riedinger, C. Baktash, M. L. Halbert, N. R. Johnson, I. Y. Lee, Y. Schutz, A. Johnson, J. Nyberg, K. Honkanen, D. G. Sarantites, and D. R. Haenni
"High Spin States in ^{184}Pt," Bull. Am. Phys. Soc. 30, 762 (1985)

L. H. Courtney, M. P. Carpenter, A. J. Larabee, L. L. Riedinger, C. Baktash, M. L. Halbert, D. C. Hensley, N. R. Johnson, I. Y. Lee, M. Oshima, R. Ribas, Y. Schutz, L. Adler, K. Honkanen, and D. G. Sarantites
"High Spin States of ^{159}Yb," Bull. Am. Phys. Soc. 30, 761 (1985)

Y. A. Ellis-Akovali, K. S. Toth, F. T. Avignone, R. S. Moore, J. M. Nitschke, P. A. Wilmarth, P. K. Lemmertz, D. M. Moltz, and D. C. Sousa
"Single-Neutron and Single-Proton States in ^{149}Er and ^{149}Ho," Bull. Am. Phys. Soc. 30, 743 (1985)

C. W. Glover, E. E. Gross, A. W. Carpenter, J. A. Carr, R. J. Philpott, F. Petrovich, P. Schwandt, W. W. Jacobs, and H. O. Meyer
"Elastic p + ^{9}Be Scattering at 200 MeV," Bull. Am. Phys. Soc. 30, 701 (1985)

E. E. Gross, R. L. Auble, F. E. Bertrand, J. L. Blankenship, B. L. Burks, C. W. Glover, R. O. Sayer, D. Shapira, and M. Beckerman
"Quasi-Elastic Scattering of ^{208}Pb with 15.7-MeV/A ^{58}Ni Ions," Bull. Am. Phys. Soc. 30, 709 (1985)

B. A. Harmon, S. T. Thornton, D. Shapira, M. Beckerman, and J. Gomez del Campo
"An Entrance Chanrel Limit on the Fusion of $^{28}Si + ^{12}C$ at High Energy," Bull. Am. Phys. Soc. 30, 732 (1985)

S. Juutinen, M. W. Guidry, C. R. Bingham, A. J. Larabee, X. T. Liu, L. L. Riedinger, L. H. Courtney, C. Baktash, I. Y. Lee, M. L. Halbert, D. Cline, and B. Kotlinski
"Multiparticle Transfer in Heavy-Ion Collisions," Bull. Am. Phys. Soc. 30, 733 (1985)

A. J. Larabee, L. L. Riedinger, C. R. Bingham, L. H. Courtney, C. Baktash, M. L. Halbert, D. C. Hensley, N. R. Johnson, I. Y. Lee, Y. Schutz, S. A. Hjorth, A. Johnson, K. J. Nyberg, B. Herskind, A. Dilmanian, M. Rajagopolan, D. G. Sarantites, D. R. Haenni, J. C. Waddington, J. S. Hattula, and G. A. Leander
"Entry State Dependence of High Spin Population in ^{160}Yb," Bull. Am. Phys. Soc. 30, 761 (1985)

M. J. Murphy, T. Awes, S. Gil, M. Harakeh, D. Leach, A. Ray, A. Seamster, and R. Vandenbosch
"Projectile Breakup into Multiple Heavy Fragments," Bull. Am. Phys. Soc. 30, 747 (1985)

F. E. Obenshain, F. Plasil, G. R. Young, P. Braun-Munzinger, R. Freifelder, and J. Stachel
"Measurement of Neutral Pion Production Cross Section for $^{16}O + ^{27}Al$ at 25 MeV/Nucleon," Bull. Am. Phys. Soc. 30, 768 (1985)

D. Shapira, R. Novotny, and S. T. Thornton
"Coincidence Measurements of Complex Fragments from $^{28}Si + ^{12}C$ Induced Reactions," Bull. Am. Phys. Soc. 30, 746 (1985)

P. H. Stelson, H. J. Kim, M. Beckerman, D. Shapira, and R. L. Robinson
"Fusion Cross Sections for Beams of $^{46,50}Ti$ on Targets ^{90}Zr and ^{93}Nb," Bull. Am. Phys. Soc. 30, 732 (1985)

K. M. Teh, C. F. Maguire, W. C. Ma, F. E. Bertrand, R. L. Auble, R. O. Sayer, D. N. Shapira, and B. L. Burks
"Heavy-Ion Spin Orbit Interaction in $^{28}Si(^{11}B,^{10}B)^{29}Si$ at E_{lab} = 170 MeV," Bull. Am. Phys. Soc. 30, 733 (1985)

K. S. Toth, Y. A. Ellis-Akovali, F. T. Avignone, J. M. Nitschke, P. A. Wilmarth, P. K. Lemmertz, and D. M. Moltz
"Identification of ^{151}Tb," Bull. Am. Phys. Soc. 30, 760 (1985)

W. Uchai, P. Venugopala Rao, S. Raman, C. R. Vane, W. T. Milner, P. H. Stelson, and G. Lapicki
"L X-Ray Transitions from Multiply Ionized Thin Targets of Yb, Ta, W, Pt, Au, Pb, and Th Bombarded by 107-MeV Ag(6+) Ions," Bull. Am. Phys. Soc. 30, 734 (1985)

J. C. Wells, N. R. Johnson, F. K. McGowan, M. P. Fewell, J. S. Hattula, I. Y. Lee, C. Baktash, Y. Schutz, L. L. Riedinger, M. W. Guidry, and S. C. Pancholi
"Lifetimes of High-Spin States of ^{159}Yb," Bull. Am. Phys. Soc. 30, 761 (1985)

J. D. Zumbro, R. A. Naumann, M. V. Hoehn, W. Reuter, E. B. Shera, C. E. Bemis, Jr., and Y. Tanaka
"Precision Muonic-Atom Determinations of the Charge Parameters for ^{232}Th and $^{239,240,242}Pu$," Bull. Am. Phys. Soc. 30, 778 (1985)

American Chemical Society Meeting, Division of Nuclear Chemistry and Technology, Miami Beach, Florida, April 28-May 3, 1985

L. G. Sobotka, D. G. Sarantites, F. A. Dilmanian, M. Jaaskelainen, H. Puchta, R. Woodward, M. L. Halbert, J. H. Barker, J. R. Beene, R. L. Ferguson, D. C. Hensley, and G. R. Young
"Excited State Yields of Light Fragments Produced in the Reaction: 180-MeV $^{19}F + ^{159}Tb$"

J. Stachel, P. Braun-Munzinger, P. Paul, F. E. Obenshain, F. Plasil, and G. R. Young
"Pion Production in Heavy-Ion Reactions Near Absolute Thresholds"

BES Atomic Physics Program Contractor's Workshop, Chapel Hill, North Carolina, May 13-14, 1985

C. C. Havener, H. F. Krause, and R. A. Phaneuf
"Multicharged Ion-Atom Merged-Beams Apparatus"

1985 Particle Accelerator Conference, Vancouver, Canada, May 13-16, 1985

G. D. Alton and G. D. Mills
"A Negative Ion Source with a Solid Tungsten Surface Ionizer," Bull. Am. Phys. Soc. 30, 964 (1985)

E. D. Hudson, J. A. Martin, and R. S. Lord
"A Variable Field Magnetic Extraction Channel for ORIC," Bull. Am. Phys. Soc. 30, 978 (1985)

International Conference on Nuclear Data for Basic and Applied Science, Santa Fe, New Mexico, May 13-17, 1985

R. Kohler, L. Mewissen, F. Poortmans, S. Raman, H. Wartena, and H. Weigmann
"Doorways in the Reaction $^{207}Pb + n$"

"Growth Point" Meeting on Correlated Electron Phenomena Arising in Heavy-Ion Atom Collisions, Chapel Hill, North Carolina, May 15, 1985

R. L. Becker, A. L. Ford, and J. F. Reading
"Single and Double K-Shell-Vacancy Production in Nearly Symmetric Systems: IFPM Theory and OHCE Calculations for $Cl^{(15-17)+} + Ti$"

Niels Bohr Centennial Conference, Nuclear Structure 1985, Copenhagen, Denmark, May 20-25, 1985

J. R. Beene, F. E. Bertrand, M. L. Halbert, R. L. Auble, D. C. Hensley, D. J. Horen, R. L. Robinson, R. O. Sayer, and T. P. Sjoreen (Invited Talk)
"Electromagnetic Decay of Giant Resonances"

W. Nazarewicz, G. A. Leander, Ph. Quentin, and J. Dudek
"BCS Pairing with Approximate Particle Number Projection Before Variation"

Atomic Theory Workshop on Relativistic and QED Effects in Heavy Atoms, Washington, D.C., May 23-24, 1985

A. B. Balantekin, C. Bottcher, M. R. Strayer, and S. J. Lee (Invited Talk)
"Phenomenology of New Particle Production in Heavy-Ion Collisions"

C. Bottcher and M. R. Strayer (Invited Talk)
"Pair Production at GeV/u Energies"

Symposium on Electromagnetic Properties of High Spin States, Stockholm, Sweden, May 28-31, 1985

N. R. Johnson (Invited Talk)
"Information on Nuclear Shapes at High Spins from Lifetime Measurements"

American Physical Society Meeting, Division of Electron and Atomic Physics, Norman, Oklahoma, May 29-31, 1985

D. A. Church, H. M. Holzscheiter, R. A. Kenefick, C. S. O, R. T. Short, S. B. Elston, M. Breinig, R. DeSerio, and I. A. Sellin
"Multicharged Recoil Ion Storage in a Radio-Frequency Quadrupole Ion Trap," Bull. Am. Phys. Soc. 30, 862 (1985)

J. Hall, P. Richard, P. L. Pepmiller, D. C. Gregory, P. D. Miller, C. D. Moak, C. M. Jones, G. D. Alton, L. B. Bridwell, and C. J. Sofield
"Energy Systematics of Single and Double K-Shell Vacancy Production in Titanium Bombarded by Chlorine Ions," Bull. Am. Phys. Soc. 30, 885 (1985)

F. W. Meyer (Invited Talk)
"Low Energy Electron Capture by Fully Stripped Light Ions from Atomic Hydrogen," Bull. Am. Phys. Soc. 30, 846 (1985)

M. R. Strayer (Invited Talk)
"Finite Element Studies of the Dirac Equation for Heavy-Ion Collisions," Bull. Am. Phys. Soc. 30, 854 (1985)

Second International Conference on Nucleus-Nucleus Collisions, Visby, Sweden, June 10-15, 1985

T. C. Awes, R. L. Ferguson, R. Novotny, F. E. Obenshain, F. Plasil, V. Rauch, G. R. Young, and H. Sann
"Equilibrium Fission Decay of Reaction Products with A < 150"

R. A. Broglia and M. Gallardo (Invited Talk)
"Random Phase Approximation Treatment of the Pairing Phase Transition in Strongly Rotating Nuclei"

B. R. Fulton, D. W. Banes, J. S. Lilley, M. A. Nagarajan, I. J. Thompson, and G. R. Satchler,
"Energy Variation of the $^{16}O + ^{60}Ni$ Potential and the Optical Model Dispersion Relation"

F. E. Obenshain, T. C. Awes, R. L. Ferguson, F. Plasil, G. R. Young, P. Braun-Munzinger, R. Freifelder, P. Paul, and J. Stachel
"Near-Threshold Neutral Pion Production with Heavy Ions"

Fourth International Symposium on Neutron-Induced Reactions, Smolenice, Czechoslovakia, June 17-21, 1985

S. Raman (Invited Talk)
"Summary Talk"

S. Raman and J. E. Lynn (Invited Talk)
"Applications and Misapplications of the Channel-Capture Formalism of Direct Neutron Capture"

Atomic Physics of Highly Charged Ions (Satellite Meeting of the XIV International Conference on the Physics of Electronic and Atomic Collisions), Palo Alto, California, July 22-23, 1985

F. W. Meyer (Invited Talk)
"ECR Ion Sources for Producing Highly Charged Ions"

XIV International Conference on the Physics of Electronic and Atomic Collisions, Palo Alto, California, July 24-30, 1985

R. L. Becker
"Multiple-Electron Processes in H^+ + (He,Ne) Collisions at 300 keV"

C. Bottcher
"Towards Numerical Solution of the Threshold Ionization Problem"

C. Bottcher and M. R. Strayer
"Galerkin Methods for Solving the Schrodinger and Dirac Equations"

M. Breinig, S. E. Lasley, and C. C. Gaither, III (Invited Talk)
"Atom Capture and Loss in Ion Molecule Collisions"

J. Burgdorfer
"Statistical Multipoles for Cusp Electrons and Rydberg Electrons"

P. F. Dittner, S. Datz, P. D. Miller, and P. L. Pepmiller
"Dielectronic Recombination Measurements of P^{4+}, S^{5+}, and Cl^{6+}"

S. B. Elston (Invited Talk)
"Doubly Differential Cross Sections of Collision-Produced Forward Electron Emission"

D. C. Gregory (Invited Talk)
"The Role of Indirect Processes in Electron-Impact Ionization of Multicharged Ions"

C. C. Havener, H. F. Krause, and R. A. Phaneuf
"Multicharged Ion-Atom Merged Beams Apparatus"

R. Hippler, S. Datz, P. D. Miller and P. L. Pepmiller
"Double and Single Electron Capture in 1-2 MeV/u O^{8+}-He Collisions"

H.-P. Hulskotter, M. Breinig, J. Burgdorfer, S. B. Elston, P. Engar, and I. A. Sellin
"Threshold Law for Simultaneous Rydberg Electron and Convoy Electron Production"

T. J. Kvale, G. D. Alton, R. N. Compton, D. J. Pegg, and J. S. Thompson
"An Experimental Investigation of the Metastable States of Beryllium Anions"

F. W. Meyer, A. M. Howald, C. C. Havener, and R. A. Phaneuf
"Low Energy Electron Capture by Fully Stripped Light Ions from H and H_2"

C. S. O, R. T. Short, S. B. Elston, M. Breinig, R. DeSerio, I. A. Sellin, and B. Thomas
"Storage of Heavy-Ion-Generated Multiply-Charged Recoil Ions in a Radio-Frequency Quadrupole Ion Trap"

Seminar on Atomic Processes in Fusion Plasmas, Santa Cruz, California, July 31-August 2, 1985

C. F. Barnett (Invited Talk)
"The Next Decade of Atomic Physics in Fusion Research"

R. A. Phaneuf (Invited Talk)
"Single Ionization of Multiply Charged Ions by Electron Impact"

M. S. Pindzola (Invited Talk)
"Theoretical Studies of Electric Field Effects of Dielectronic Recombination"

11th International Conference on Atomic Collisions in Solids, Washington, D.C., August 4-9, 1985

S. Datz, J. O. Kephart, H. Park, R. K. Klein, R. H. Pantell, B. L. Berman, B. A. Dahling, M. V. Hynes, R. L. Swent, and M. J. Alguard (Invited Talk)
"On the Temperature and Length Dependence of Channeling Radiation from 54-MeV Electrons in Silicon"

H. F. Krause, S. Datz, P. F. Dittner, J. Gomez del Campo, P. D. Miller, C. D. Moak, N. Neskovic, and P. L. Pepmiller (Invited Talk)
"Rainbow Scattering in Axial Ion-Channeling Involving Very Thin Crystals"

P. D. Miller, H. F. Krause, C. D. Moak, J. Gomez del Campo, J. A. Biggerstaff, S. Datz, P. L. Pepmiller, P. F. Dittner, O. H. Crawford, N. Neskovic, and M. D. Brown (Invited Talk)
"Resonant Coherent Excitation of O^{7+}, F^{8+}, and C^{5+} in Au <100> Channel"

1985 International Symposium on Antennas and Propagation, Kyoto, Japan, August 20-22, 1985

C. H. Ma, D. P. Hutchinson, P. A. Staats, K. L. Vander Sluis, D. K. Mansfield, H. Park, and L. C. Johnson
"Submillimeter Wave Propagation in Tokamak Plasmas"

1985 International Symposium on Antennas and EM Theory, Beijing, China, August 25-27, 1985

C. H. Ma D. P. Hutchinson, P. A. Staats, K. L. Vander Sluis, D. K. Mansfield, H. Park, and L. C. Johnson
"Submillimeter Wave Propagation in Tokamak Plasmas"

ACS Symposium on Recent Advances in the Study of Nuclei off the Line of Stability, Chicago, Illinois, September 8-13, 1985

A. B. Balantekin, T. Hubsch, and V. Paar (Invited Talk)
"Boson Fermion Symmetries and Dynamical Supersymmetries for Odd-Odd Nuclei"

K. K. Carter, G. A. Leander, J. A. Bounds, and C. R. Bingham
"First Results from the UNISOR Collinear Laser Facility"

K. Honkanen, H. C. Griffin, D. G. Sarantites, V. Abenante, L. A. Adler, C. Baktash, Y. S. Chen, O. Dietzsch, M. L. Halbert, D. C. Hensley, N. R. Johnson, A. Larabee, I. Y. Lee, L. L. Riedinger, J. X. Saladin, T. Semkow, and Y. Schutz
"High-Spin Structure of ^{163}Lu"

N. R. Johnson (Invited Talk)
"Evolution of Nuclear Shapes at High Spins"

G. A. Leander
"Low-Energy Collective El Mode in Nuclei"

J. B. McGrory (Invited Talk)
"A Study of the Weak-Coupling Truncation Scheme for Large Shell Model Calculations"

R. L. Mlekodaj, G. A. Leander, R. A. Braga, B. D. Kern, K. S. Toth, and B. E. Gnade
"Decay of ^{138}Eu and Deformation in the Light Sm Region"

S. Raman and C. W. Nestor (Invited Talk)
"B(E2)↑ for the 2_1^+ States of Collective Nuclei off the Line of Stability"

K. S. Toth (Invited Talk)
"Particle Decay Studies at or near Closed Shells"

J. B. Wilhelmy, C. Albiston, J. P. Bocquet, J. Boissevain, H. C. Britt, Y. D. Chan, R. L. Ferguson, M. M. Fowler, A. Gavron, A. Gayer, S. Gazes, A. Guessous, B. V. Jacak, P. Lysaght, G. Mamone, F. E. Obenshain, F. Plasil, C. Ristori, R. Schmidt, R. G. Stokstad, and S. Wald
"Saddle to Scission: Time Scales and Dissipative Mechanisms"

E. F. Zganjar, C. D. Papanicolopoulos, J. L. Wood, R. A. Braga, R. W. Fink, A. J. Larabee, M. Carpenter, D. Love, C. R. Bingham, L. L. Riedinger, J. C. Waddington
"Shape Coexistence in ^{185}Au"

IAEA Advisory Group Meeting on Atomic Data for Fusion Plasma Modelling, Vienna, Austria, September 18-20, 1985

R. A. Phaneuf
"Charge Exchange Processes Involving Iron Ions"

NATO Advanced Study Institute on Physics of Electron-Ion and Ion-Ion Collisions, Han sur Lesse, Belgium, September 30-October 12, 1985

R. A. Phaneuf
"Experiments on Electron-Impact Excitation and Ionization of Ions"

13. GENERAL INFORMATION

PERSONNEL CHANGES

New Staff Members

A. Scientific Staff

B. A. Harmon, University of Virginia, Charlottesville, Virginia (part-time)
D. K. Olsen (transferred from Engineering Physics and Mathematics Division)
S. P. Sorensen, University of Tennessee, Knoxville, Tennessee (part-time)
R. L. Varner, Jr., University of North Carolina, Chapel Hill, North Carolina

B. Administrative and Technical Staff

S. L. Birch, Accelerator Operations
M. E. Whitley, Laboratory Technician (transferred from Centrifuge Division)

Staff Transfers and Terminations

A. Scientific Staff

C. F. Barnett (retirement)
P. M. Griffin (retirement)
C. D. Moak (retirement)
P. A. Staats (retirement)
G. F. Wells (retirement)

B. Administrative and Technical Staff

J. T. Martin, Laboratory Technician (transferred to Information Division)
B. F. McHargue, Secretary (retirement)

TEMPORARY ASSIGNMENTS

Short-Term Assignments

Scientific Staff

R. O. Hippler, University of Bielefeld, Bielefeld, Federal Republic of Germany
N. R. Stolterfoht, Hahn-Meitner-Institut, Berlin, Federal Republic of Germany

Guest Assignments

A. Joint Institute for Heavy Ion Research

M. A. Beckerman, Joint Institute for Heavy Ion Research, Oak Ridge, Tennessee
A. Bracco, University of Milano, Milano, Italy
P. A. Butler, University of Liverpool, Liverpool, England
Y. S. Chen, Institute of Atomic Energy, Beijing, China
N. Cindro, Ruder Boskovic Institute, Crostia, Yugoslavia
M. I. F. Gallardo, Niels Bohr Institute, Copenhagen, Denmark
I. Hamamoto-Kuroda, University of Lund, Lund, Sweden
D. J. G. Love, University of Liverpool, Liverpool, England
U. B. Mosel, Justus-Liebig-University, Giessen, Federal Republic of Germany
W. Nazarewicz, Niels Bohr Institute, Copenhagen, Denmark
J. Pacheco, Niels Bohr Institute, Copenhagen, Denmark
F. B. Paulano, Niels Bohr Institute, Copenhagen, Denmark
J. M. Quesada, University of Sevilla, Sevilla, Spain
P-G. Reinhard, Institut fur Theoretische Physik, Universitat Erlangen, Erlangen, Federal Republic of Germany

B. Graduate Students

S. D. Berry, University of Tennessee, Knoxville, Tennessee
M. J. Bloemer, University of Tennessee, Knoxville, Tennessee
W. G. Campbell, University of Tennessee, Knoxville, Tennessee
M. P. Carpenter, University of Tennessee, Knoxville, Tennessee
L. H. Courtney, University of Tennessee, Knoxville, Tennessee
P. P. Engar, University of Tennessee, Knoxville, Tennessee
J. P. Gibbons, University of Tennessee, Knoxville, Tennessee
J. C. Griffin, Georgia Institute of Technology, Atlanta, Georgia
J-N. Juang, Tennessee Technological University, Cookeville, Tennessee
R. W. Kincaid, University of Tennessee, Knoxville, Tennessee
A. J. Larabee, University of Tennessee, Knoxville, Tennessee
S. E. Lasley, University of Tennessee, Knoxville, Tennessee
S-J. Lee, Yale University, New Haven, Connecticut
X. T. Liu, University of Tennessee, Knoxville, Tennessee
K. J. Nyberg, University of Tennessee, Knoxville, Tennessee
R. T. Short, University of Tennessee, Knoxville, Tennessee
K. M. Teh, Vanderbilt University, Nashville, Tennessee
J. S. Thompson, University of Tennessee, Knoxville, Tennessee
W. Uchai, Emory University, Atlanta, Georgia
S. A. Umar, Yale University, New Haven, Connecticut
T. A. Underwood, University of Tennessee, Knoxville, Tennessee

C. Co-op Students

D. E. Hoglund, Virginia Polytechnic Institute and State University, Blacksburg, Virginia
M. A. Walker, Morehouse College, Atlanta, Georgia

D. ORAU Graduate Research Participant

J. A. Bounds, University of Tennessee, Knoxville, Tennessee

E. ORAU Postgraduate Research Training Program

W. H. Casson, University of Tennessee, Knoxville, Tennessee
A. M. Howald, University of Wisconsin, Madison, Wisconsin

F. ORAU Faculty Research Participants

C. A. Bennett, Jr., University of North Carolina, Asheville, North Carolina
J. E. Purcell, Georgia State University, Atlanta, Georgia
P. A. Schulz, Georgia Institute of Technology, Atlanta, Georgia

G. ORAU Student Research Participants

J. L. Chance, New College of the University of South Florida, Sarasota, Florida
A. J. Collison, Louisiana State University, Shreveport, Louisiana
L. I. Maliner, Union College, Schenectady, New York
J. T. Mitchell, Louisiana State University, Shreveport, Louisiana
G. J. Nelson, Gustavus Adolphus College, St. Peter, Minnesota
P. E. Reimer, Bethel College, North Newton, Kansas
F. V. Weber, Grinnell College, Grinnell, Iowa
S. A. Williamson, Elon College, Elon College, North Carolina

H. Great Lakes College Association Science Program

J-M. Perelmuter, Beloit College, Beloit, Wisconsin
D. M. Schmidt, Denison University, Granville, Ohio
K. B. Smith, Rollins College, Winter Park, Florida

Summer Assignments

A. 1985 Summer Program for High School Teachers

R. A. Core, South-Young High School, Knoxville, Tennessee
D. E. Morrison, Maryville High School, Maryville, Tennessee

B. University of Tennessee/ORNL Science Alliance Program

J. Boyle, University of Wisconsin, Kenosha, Wisconsin
V. Carmichael, Francis Marion College, Florence, South Carolina
B. Cox, Bridgewater College, Bridgewater, Virginia
M. Craycraft, University of Dayton, Dayton, Ohio
C. Gaither, University of Southwestern Louisiana, LaFayette, Louisiana
C. Holly, Western Michigan University, Kalamazoo, Michigan
J. Houser, Widener University, Chester, Pennsylvania
I. Krucke, Eckerd College, St. Petersburg, Florida
P. Rollins, Loyola College, Baltimore, Maryland
J. Stasko, University of Dallas, Irving, Texas
G. Tweed, Middle Tennessee State University, Murfreesboro, Tennessee
G. Ulrich, Moorhead State University, Moorhead, Minnesota
W. Wester, Xavier University, Cincinnati, Ohio

PHYSICS DIVISION SEMINARS: OCTOBER 1984-SEPTEMBER 1985

Those seminars arranged by the Physics Division and announced in the ORNL Technical Calendar are listed below. During the period of this report, I. Y. Lee served as Seminar Chairman.

Date	Speaker	Title
1984		
Oct. 24	Philippe Quentin Los Alamos National Lab. and University of Bordeaux, France	Nuclear Thermostatic Properties: Fission Barrier and Giant Resonances
Oct. 25	Thomas Lindblad Research Inst. of Physics Stockholm, Sweden	Development of Liquid Xenon Detectors
Oct. 25	Enchin Wu Institute of Modern Physics Lanzhou, China	Recent Research Activities at Institute of Modern Physics at Lanzhou
Oct. 29	Hans A. Weidenmüller Max-Plank Institut für Kernphysik Heidelberg Federal Republic of Germany	Statistical Method in Nuclear Physics
Oct. 31	Helmut Winter University of Münster Münster Federal Republic of Germany	Recent Results in Ion Beam Sources Interaction at Grazing Incidence
Nov. 5	Gordon H. Dunn Joint Inst. for Lab. Astrophysics Univ. of Colorado and National Bureau of Standards Boulder, Colorado	Product Rydberg States from Dielectronic Recombination of Mg^+
Nov. 5	Bernward Jenschke Fachinformationszentrum Energie Physik, Mathematik (FIZ) Karlsruhe Federal Republic of Germany	Bibliographic and Numeric On-Line Data Bases in Science and Technology
Nov. 8	J. L. Egido University of Madrid Madrid, Spain	Gamma Decay of Highly Excited Nuclei
Nov. 13	David Ward Chalk River Nuclear Laboratories Chalk River, Canada	Perturbed Angular Correlation Measurements on High Spin States - Past, Present, and Future
Nov. 16	H. J. Hay The Australian National Univ. Canberra, Australia	Beam-Foil Spectroscopy of Partially-Stripped Heavy Ions
Nov. 19	Steven E. Koonin California Inst. of Technology Pasadena, California	Subsaturation Phases of Nuclear Matter
Nov. 19	L. J. Morford University of Illinois Urbana, Illinois	Investigation of the Giant Isoscalar Quadrupole Resonance in ^{206}Pb and ^{208}Pb
Nov. 19	Y. Yamazaki Tokyo Inst. of Technology Tokyo, Japan	Convoy Electron Production

Date	Speaker	Title
Nov. 20	Paul Mokler Gesellschaft für Schwerionenforschung Darmstadt Federal Republic of Germany	Experiments with Decelerated Heavy Ions
Nov. 21	R. Schuch Univ. of Heidelberg Heidelberg Federal Republic of Germany	Atomic Collision of Nearly Bare Atoms
Nov. 21	Horst Schmidt-Bocking Univ. of Frankfurt Frankfurt Federal Republic of Germany	High Charge State Ions and Heavy Ion Storage Ring
Dec. 7	Carl Sofield Atomic Energy Research Establishment Harwell, England	High Order Terms and Charge Exchange Contributions to Stopping Power
Dec. 13	Chia-Cheng Shih Univ. of Tennessee Knoxville, Tennessee	Correlations in Hadronic Multiplicity
1985		
Jan. 8	Malvin H. Kalos Courant Institute, New York Univ., New York	The NYU Ultra Computer - Its Architecture and Its Applications
Jar. 25	Osvaldo Goscinski Univ. of Uppsala Sweden	Statistical, and Nonstatistical Features in Collisions and Laser Stimulated Processes
Jan. 28	Sa Ban-Hao Inst. of Atomic Energy Beijing, Peoples Republic of China	Transverse Momentum Distribution in Ultra-relativistic Heavy-Ion Collisions
Jan. 29	Wolfgang Trautmann Brookhaven National Lab. Upton, New York	Alignment in Heavy Ion Reactions
Feb. 7	K. Langanke Calif. Inst. of Technology Pasadena, California	Gamma Decay of Heavy Ion Resonances
Feb. 15	Franco Iachello Yale Univ. New Haven, Connecticut	New Class of Collective State in Nuclei
Feb. 14	Cleland H. Johnson Physics Div. Staff, ORNL	Neutron Scattering Fine Structure and Optical Model Parameters
Mar. 11	Turgay Uzer Univ. of Colorado, Boulder	State Selected Reaction Theory and Application
Mar. 28	Helmut Poth Kernforschungszentrum, Inst. für Kernphysik, Karlsruhe, F.R.G. and Org. Européene pour la Recherche Nucléaire, Geneva, Switzerland	Physics with Anti-Protonic Atoms
Apr. 19	Shimon Levit MIT Cambridge, Massachusetts	Stability of Hot Nuclei

Date	Speaker	Title
May 9	Jean Blachot Centre d'etudes Nucleaires de Grenoble, Grenoble, France	Linear Momentum Transfer in ^{12}C, ^{20}Ne, ^{40}Ar Heavy Ion Reactions on ^{124}Sn at 20-50 MeV/u; Experimental Evidence for a Limiting Excitation Energy in the Nucleus
May 9	Nikola Cindro Ruder Boskovic Institute Zagreb, Yugoslavia	Thermodynamics, Degrees of Freedom, and the Description of a Nucleus-Nucleus Colision
May 17	Jolie Cizewski Yale University	Structure of Light Actinides
May 29	Wolfram Westmeier Philipps Universität Marburg Federal Republic of Germany	Reaction Mechanism in Very Heavy Ion Systems
June 7	Ralph Z. Roskies Univ. of Pittsburgh Pennsylvania	Phase Transitions in Quark-Gluon Matter
June 11	Marc Huyse Instituut Voor Kern-en Stralinfysika Katholieke Universiteit Leuven, Belgium	α and β Decay Studies of Shell Model Intruder States in Tl and Bi Isotopes
July 11	Pierre Defrance Catholic Univ. of Louvain-la-Neuve Belgium	Electron-Impact Ionization of Li-like Ions
July 15	Valeriu I. Zoran The Central Inst. of Physics Bucharest, Rumania	L-Vacancy Production, Propagation and Decay in Asymmetric Ion-Atom Collisions
July 16	Benoet Morel California Inst. of Technology Pasadena, California	X-Ray Lasers and Their Possibilities
July 17	K.-H. Schartner PhysiKalisches Institut der Justus-Liebig-Universität Giessen Federal Republic of Germany	VUV-Spectroscopy of Rare Gas Ions Produced in Atomic Collisions
July 18	Hans Klapdor Max-Planck-Institute Heidelberg Federal Republic of Germany	Nuclear Beta Strength, Neutrino Mass, and Cosmology
Aug. 8	Erhard Salzborn Institut für Kernphysik Justus-Liebig-University Giessen Federal Republic of Germany	Charge Transfer and Ionization in Ion-Ion Collisions
Aug. 12	H. Knudsen Institute of Physics Univ. of Arhus Arhus, Denmark	On the Creation of Projectile Continuum Electrons in Fast Ion-Atom Collision
Aug. 13	Yoel Tikochinsky Racah Institute of Physics Hebrew Univ. of Jerusalem Israel	Estimation of Inverse Temperature and Other Lagrange Multipliers-The Dual Distribution

Date	Speaker	Title
Aug. 13	H. O. Lutz Univ. of Bielefeld Bielefeld Federal Republic of Germany	Atomic Collision Processes from Inner Shell Ionization to Laser Assisted Collision
Aug. 14	George Eichler Hahn-Meitner Institute Berlin Federal Republic of Germany	Relativistic Eikonal Theory for Electron Transfer
Aug. 15	William P. Kells Fermi National Accelerator Lab. Batavia, Illinois	Trapping Anti-Protons
Aug. 19	K. A. Snover Univ. of Washington Seattle, Washington	Giant Dipole Resonances Based on Excited Nuclear States
Aug. 27	A. M. Lane AERE Harwell, England	Disturbance of a Series of Resonances by a Broad Level
Sept. 13	Amand Faessler Univ. of Tübingen Tübingen Federal Republic of Germany	Recent Results from the Monster
Sept. 19	Knud Taulbjerg Univ. of Arhus Arhus, Denmark	Electron Capture in Ion-Atom Collisions
Sept. 26	Emilio Migneco Laboratorio Nazionale del Sud (LNS) Catania, Italy	Status and Programs of the Heavy Ion Facility at the LNS in Catania
Sept. 27	George Contopoulos Univ. of Athens Athens, Greece and Univ. of Florida Gainesville, Florida	Dynamical Systems of Two and Three Degrees of Freedom

SCIENTIFIC MEETINGS SPONSORED BY THE PHYSICS DIVISION AND HELD DURING THE REPORTING PERIOD

Holifield Theory Users Group Meeting
Oak Ridge, Tennessee, October 12-13, 1984
G. A. Leander, J. B. McGrory, and K. T. R. Davies, organizers

Instrumentation for Heavy Ion Research
Oak Ridge, Tennessee, October 22-26, 1984
D. Shapira, organizer

Holifield Theory Users Group Meeting
Oak Ridge, Tennessee, May 10-11, 1985
J. B. McGrory, G. A. Leander, and M. R. Strayer, organizers

UNISOR Brainstorm Workshop
Oak Ridge, Tennessee, June 26-27, 1985
H. K. Carter, organizer

High Spin Workshop (ORNL/JIHIR)
Oak Ridge, Tennessee, July 11-12 and 15-16, 1985
N. R. Johnson and L. L. Riedinger, organizers

Workshop on Intermediate Energy Heavy Ion Physics (ORNL/JIHIR)
Oak Ridge, Tennessee, September 23-25, 1985
R. L. Robinson, organizer

INFORMATION MEETING

The most recent Physics Division Information Meeting was held on September 9-10, 1985. The members of the Advisory Committee were:

M. Macfarlane, Indiana University

E. Merzbacher, University of North Carolina

R. E. Pollock, Indiana University

L. C. Teng, Fermi National Accelerator Laboratory

PHYSICS DIVISION

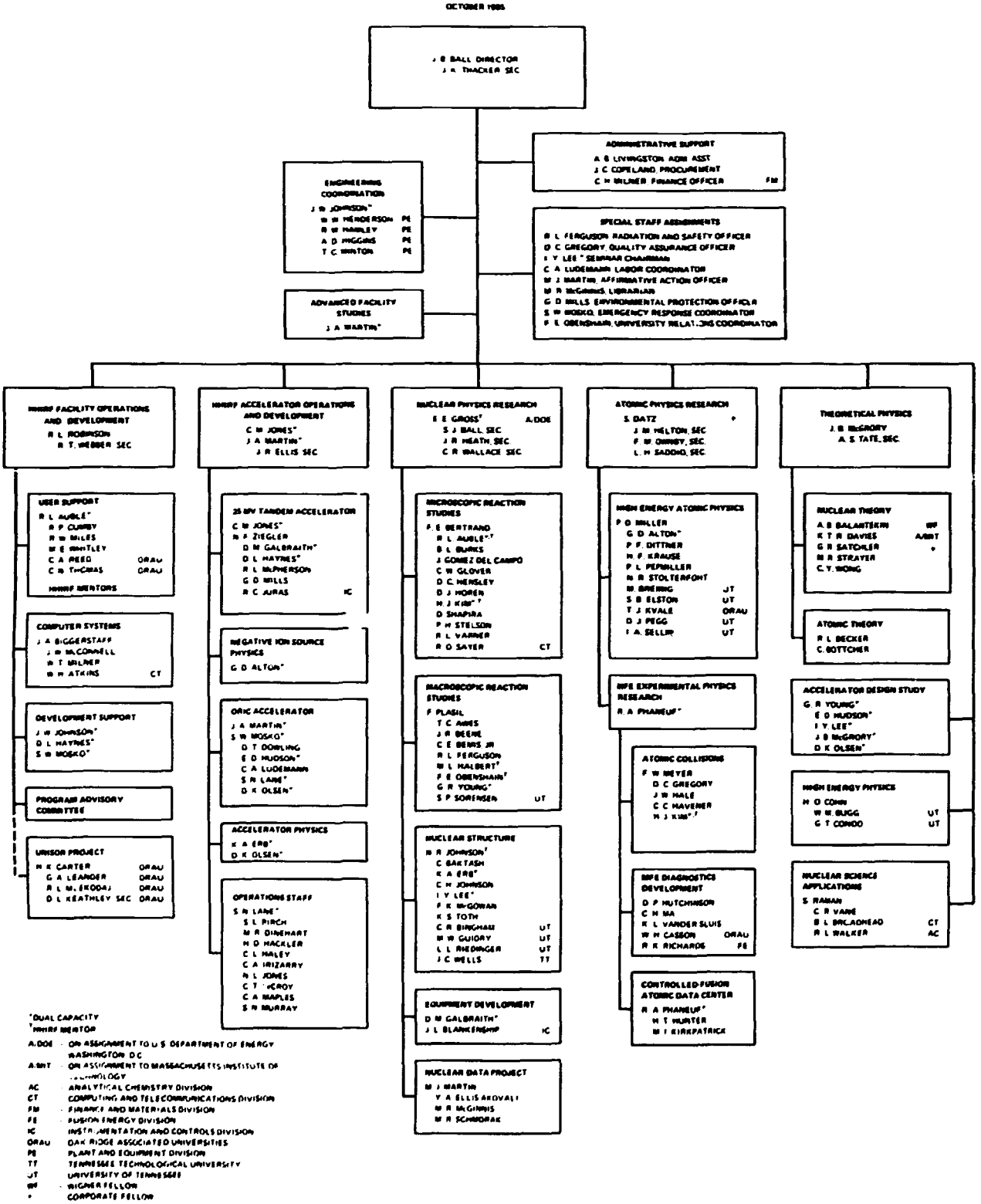

*DUAL CAPACITY
†HHIRF MENTOR

A,DOE - ON ASSIGNMENT TO U S DEPARTMENT OF ENERGY WASHINGTON D C
A,MIT - ON ASSIGNMENT TO MASSACHUSETTS INSTITUTE OF TECHNOLOGY
AC - ANALYTICAL CHEMISTRY DIVISION
CT - COMPUTING AND TELECOMMUNICATIONS DIVISION
FM - FINANCE AND MATERIALS DIVISION
FE - FUSION ENERGY DIVISION
IC - INSTRUMENTATION AND CONTROLS DIVISION
ORAU - OAK RIDGE ASSOCIATED UNIVERSITIES
PE - PLANT AND EQUIPMENT DIVISION
TT - TENNESSEE TECHNOLOGICAL UNIVERSITY
UT - UNIVERSITY OF TENNESSEE
WF - WIGNER FELLOW
* - CORPORATE FELLOW

ORNL-6233
Distribution Category
UC-34

INTERNAL DISTRIBUTION

1. G. D. Alton
2. T. D. Anderson
3. R. R. Appleton
4. R. L. Auble
5. T. C. Awes
6. C. Baktash
7. A. B. Balantekin
8-178. J. B. Ball
179. S. J. Ball
180. C. F. Barnett
181. R. L. Becker
182. M. Beckerman
183. J. R. Beene
184. C. E. Bemis, Jr.
185. F. E. Bertrand
186. J. A. Biggerstaff
187. C. R. Bingham
188. Biology Library
189. C. Bottcher
190. W. M. Bugg
191. B. L. Burks
192. H. K. Carter
193-194. Central Research Library
195. H. O. Cohn
196. R. P. Cumby
197. S. Datz
198. K. T. R. Davies
199. P. F. Dittner
200. D. T. Dowling
201. J. R. Ellis
202. Y. A. Ellis-Akovali
203. S. B. Elston
204. K. A. Erb
205. R. L. Ferguson
206. C. W. Glover
207. J. Gomez del Campo
208. D. C. Gregory
209. E. E. Gross
210. M. W. Guidry
211. R. L. Hahn
212. M. L. Halbert
213. B. A. Harmon
214. J. A. Harvey
215. L. J. Hawkins-Saddiq
216. D. L. Haynes
217. J. R. Heath
218. J. M. Helton
219. D. C. Hensley
220. D. J. Horen
231. E. D. Hudson
232. H. T. Hunter
223. D. P. Hutchinson
224. L. H. Jenkins
225. C. H. Johnson
226. J. W. Johnson
227. N. R. Johnson
228. C. M. Jones
229. P. R. Kasten
230. S. V. Kaye
231. H. J. Kim
232. H. F. Krause
233. E. H. Krieg, Jr.
234-235. Laboratory Records Department
236. Laboratory Records, ORNL R.C.
237. G. A. Leander
238. I. Y. Lee
239. A. B. Livingston
240. C. A. Ludemann
241. C. H. Ma
242. J. A. Martin
243. M. J. Martin
244. J. W. McConnell
245. F. K. McGowan
246. J. B. McGrory
247. G. S. McNeilly
248. F. W. Meyer
249. R. W. Miles
250. P. D. Miller
251. W. T. Milner
252. R. L. Mlekodaj
253. S. W. Mosko
254. F. R. Mynatt
255. F. E. Obenshain
256. D. K. Olsen
257. ORNL - Y-12 Technical Library
Document Reference Section
258. F. M. Ownby
259. D. C. Parzyck
260. R. W. Peelle
261. D. J. Pegg
262. P. L. Pepmiller
263. F. G. Perey
264. R. A. Phaneuf
265. Physics Division Library
266. F. Plasil
267. H. Postma
268. M. L. Poutsma
269. S. Raman
270. L. L. Riedinger
271. R. L. Robinson
272. T. M. Rosseel
273. M. J. Saltmarsh
274. G. R. Satchler
275. R. O. Sayer
276. M. R. Schmorak
277. I. A. Sellin
278. D. Shapira
279. J. Sheffield
280. B. Shivakumar
281. W. D. Shults
282. T. P. Sjoreen
283. A. H. Snell
284. S. P. Sorenson
285. P. H. Stelson
286. N. R. Stolterfoht
287. M. R. Strayer
288. A. S. Tate
289. J. K. Thacker
290. K. S. Toth
291. D. B. Trauger
292. K. L. Vander Sluis
293. C. R. Vane
294. R. L. Varner
295. C. R. Wallace
296. K. M. Wallace
297. R. T. Webber

298. J. C. Wells, Jr.
299. M. Whitley
300. M. K. Wilkinson
301. C-Y. Wong
302. G. R. Young
303. N. F. Ziegler
304. A. Zucker

EXTERNAL DISTRIBUTION

305. B. J. Allen, Physics Division, Australian Atomic Energy Commission, Sutherland, N.S.W., Australia
306. Sakir Ayik, Tennessee Technological University, Physics Department, Cookeville, TN 38505
307. Charles A. Barnes, Division of Physics and Astronomy, California Institute of Technology, Pasadena, CA 91125
308. G. A. Bastin, Centre de Spectrometrie Nucleaire et de Spectrometrie de Masse, B. P. 104, 91406 Orsay, France
309. Bates Linear Accelerator, P. O. Box 95, Middleton, MA 01949
310. H. Behrens, Zentralstelle fur Atomkernenergie-Dokumentation, Kernforschungszentrum Karlsruhe 7514, Eggenstein-Leopoldshafen-2, Federal Republic of Germany
311. Ingmar Bergstrom, Nobel Institute of Physics, Stockholm 50, Sweden
312. Biblioteca do Depto. de Fisica Nuclear, Instituto de Fisica da USP, Caixa Postal 20516, 0100 - Sao Paulo, SP, Brasil
313. Bibliotheque - Madame Belle, Universite de Grenoble, Institut des Sciences Nucleaires, 53, rue des Martyrs, B. P. 21, 38 Grenoble, France
314. J. P. Blaser, Swiss Institute for Nuclear Research (SIN), CH-5234 Villigen, Switzerland
315. S. D. Bloom, University of California, Lawrence Livermore National Laboratory, P. O. Box 808, Livermore, CA 94550
316. H. G. Blosser, Cyclotron Laboratory, Michigan State University, East Lansing, MI 48824
317. H. Bohn, Physik-Department E12, Technische Universitat, 8046 Garching bei Munchen, Federal Republic of Germany
318 A. Bohr, Copenhagen University, Niels Bohr Institute, Blegdamsvej 17, Copenhagen, Denmark
319. J. S. Briggs, Theoretical Physics Division, Atomic Energy Research Establishment, Harwell, Didcot, Oxfordshire OX 11 ORA, England
320. David Brink, Oxford University, Oxford, England
321. J. A. Brink, Library Division, The Merensky Institute of Physics, University of Stellenbosch, Stellenbosch, Republic of South Africa
322. Ricardo Americo Broglia, Niels Bohr Institute, Blegdamsvej 17, 2100 Copenhagen O, Denmark
323. D. A. Bromley, Nuclear Structure Laboratory, Yale University, New Haven, CT 06520
324. Peter Anthony Butler, University of Liverpool, P. O. Box 147, Liverpool L69 3X, United Kingdom
325. T. A. Cahill, Director, Crocker Nuclear Laboratory, University of California, Davis, CA 95616
326. Jose L. S. Carvalho, Instituto de Radioprotecao e Dosimetria, C.N.E.N., Av. das Americas km 11,5 Barra de Tijuca - R. J., 22700 - Rio de Janeiro, R. J. Brazil
327. Yong Shou Chen, Institute of Atomic Energy, Academia Sinica, P. O. Box 275, Beijing, China
328. David Clark, Lawrence Berkeley Laboratory, University of California, Berkeley, CA 94720
329. Douglas Cline, Nuclear Structure Research Laboratory, University of Rochester, Rochester, NY 14627
330. University of Colorado, Department of Physics, Boulder, CO 80309
331. D. H. Crandall, Branch Chief for Experimental Research, Applied Plasma Physics Division, Office of Fusion Energy, ER 542, G-226, GTN, U.S. Department of Energy, Washington, DC 20545
332. F. L. Culler, Office of the President, Electric Power Research Institute, P. O. Box 10412, 3412 Hillview Avenue, Palo Alto, CA 94303
333. T. J. Curtin, Director, Office of Research and Grants Administration, Texas Women's University, Box 22939, TWU Station, Denton, TX 76204
334. R. Y. Cusson, Physics Department, Duke University, Durham, NC 27706
335. Cyclotron Library, Indiana University Cyclotron Facility, 2401 Milo B. Sampson Lane, Bloomington, IN 47405
336. Solange de Barros, Head, Department of Nuclear Physics, Universidade Federal do Rio de Janeiro, Instituto de Fisica - Department Fisica Nuclear, Centro de Technologia - Bloco A, Ilha do Fundao - Rio de Janeiro, Brasil
337. Adriano de Lima, Physics Laboratory, University of Coimbra, Coimbra, Portugal
338. R. M. Diamond, Chemistry Division, Lawrence Berkeley Laboratory, Berkeley, CA 94720
339. Olacio Dietzsch, Depto. de Fisica Experimental, Instituto de Fisica, Universidade de Sao Paulo, Cx. Postal 20516, Sao Paulo, S.P., Brazil
340. John R. Erskine, U.S. Department of Energy, Division of Nuclear Physics, ER-23, GTN, Washington, DC 20545
341. U. Facchini, Physics Department, University of Milan, Via Saldini 50, Milan, Italy
342. Amand Faessler, Institut fur Theoretische Physik, Universitat Tubingen, Auf der Morgenstelle 14, D-7400 Tubingen, West Germany
343. M. P. Fewell, Australian National University, Canberra, 2600 Australia
344. G. N. Flerov, Laboratory for Nuclear Reactions, Dubna Joint Institute for Nuclear Research, Dubna, Moscow Oblast, U.S.S.R.
345. J. D. Fox, Department of Physics, Florida State University, Tallahassee, FL 32306

346. I. M. Frank, Laboratory for Nuclear Reactions, Dubna Joint Institute for Nuclear Research, Dubna, Moscow Oblast, U.S.S.R.
347. Claus-Konrad Gelbke, National Superconducting Cyclotron Laboratory, Michigan State University, East Lansing, MI 48824
348-357. GLCA-ORS, Attention: R. R. Winters, Denison University, Granville, OH 43023
358. Alan Goodman, Department of Physics, Tulane University, New Orleans, LA 70118
359. Harvey A. Gould, Lawrence Berkeley Laboratory, 1 Cyclotron Blvd., Berkeley, CA 94720
360. H. E. Gove, Nuclear Structure Laboratory, University of Rochester, Bldg. 510A, Rochester, NY 14627
361. Walter Greiner, Institut fur Theoretische Physik der Universitat Frankfurt Main, Robert Mayer-Strasse 8-10, West Germany
362. H. Grunder, Lawrence Berkeley Laboratory, Berkeley, CA 94720
363. M. Grypeos, University of Thessaloniki, Department of Theoretical Physics, Thessaloniki, Greece
364. J. H. Hamilton, Department of Physics, Vanderbilt University, Nashville, TN 37203
365. Ole Hansen, Brookhaven National Laboratory, Bldg. 901A, Upton, NY 19973
366. J. S. Hattula, Department of Physics, University of Jyvaskyla, Seminaarinkatu 15, SF-40100 Jyvaskyla 10, Finland
367. R. L. Heath, Idaho National Engineering Laboratory, EG&G Idaho, Inc., P. O. Box 1625, Idaho Falls, ID 83401
368. David L. Hendrie, Director, Division of Nuclear Physics, ER 23, Mail Station J-309, U.S. Department of Energy, Washington, DC 20545
369. Harry D. Holmgren, Department of Physics, University of Maryland, College Park, MD 20742.
370. H. R. McK. Hyder, Nuclear Physics Laboratory, Oxford University, Keble Road, Oxford OX1 3RH, England
371. Francesco Iachello, Yale University, Department of Physics, New Haven, CT 06520
372. University of Illinois at Urbana-Champaign, Department of Physics, Urbana, IL 61801
373. Institute for Energy Analysis, P. O. Box 117, Oak Ridge, TN 37830
374. Institute of Physics, High Energy and Nuclear Physics Library, C. Postal 20.516,0100 - Sao Paulo, S.P., Brasil
375. Iowa State University, Department of Physics, Ames, IA 50011
376. Beth Jinkerson, ORAU/UPD, Oak Ridge, TN 37831-0117
377. R. Kamermans, Fysisch Laboratorium, Rijksuniversiteit Utrecht, P. O. Box 80.000, 3508 TA UTRECHT, The Netherlands
378. H. Kamitsubo, Head, Cyclotron Laboratory, Institute of Physical and Chemical Research, Wako-shi, Saitama, 351 Japan
379. D. G. Kanke, Ruhr-Universitat Bochum, Dynamitron Tandem Laboratory, Universitattstr, 150 Gibaunde NT, Postfach 1021 48, 4360 Bochum 1, Federal Republic of Germany
380. University of Kansas, Department of Physics, Lawrence, KS 66045
381. H. Kawakami, Institute for Nuclear Study, University of Tokyo, Midori-cho, Tokyo, Japan
382. P. K. Kloeppel, Continuous Electron Beam Accelerator Facility, 12070 Jefferson Avenue, Newport News, VA 23606
383. Steven E. Koonin, Kellogg Radiation Laboratory, California Institute of Technology, Pasadena, CA 91125
384. J. A. Lenhard, DOE-ORO, Federal Office Building, Oak Ridge, TN 37830
385. Michel LeTournel, Centre de Recherches Nucleaires, Service des Accelerateurs, B. P. 20 CRO, 67037 Strasbourg Cedex, France
386. Librarian, Atomic Energy Centre, P. O. Box No. 164, Ramna, Dacca, Bangladesh
387. Librarian, Chen Kin-hai, Institute of Modern Physics, Academia Sinica, P. O. Box 31, Lanzhou, People's Republic of China
388. Librarian, Cyclotron Laboratory, Michigan State University, East Lansing, MI 48824
389. Librarian, Cyclotron Laboratory, RIKEN (The Institute of Physical and Chemical Research), Wako-shi, Saitama 351, Japan
390. Librarian, Department of Physics, Georgia State University, Atlanta, GA 30303
391. Librarian, GANIL, B. P. No. 5027, 14004 Caen Cedex, France
392. Librarian, GSI, Postfach 11 05 41, 6100 Darmstadt, Federal Republic of Germany
393. Library of the Institute of Atomic Energy, Beijing, People's Republic of China
394. Librarian, MERT Division Library, Oak Ridge Associated Universities, P. O. Box 117, Oak Ridge, TN 37831-0117
395. Librarian, Physics Department, 374 Bausch and Lomb Building, University of Rochester, Rochester, NY 14627
396. Librarian, Institut des Sciences Nucleaires, B. P. No. 257 - Centre de Tri, 38044 Grenoble Cedex, France
397. A. D. MacKellar, Department of Physics and Astronomy, University of Kentucky, Lexington, KY 40506-0055
398. G. Madurga, Departameto de Fisica Atomica y Nuclear, Facultad de Ciencias, Universidad de Sevilla, Sevilla, Spain
399. Malcolm Macfarlane, Department of Physics, Indiana University, Bloomington, IN 47405
400. Claude Charles Mahaux, Institut de Physique B5 Universite de Liege, Sait Tilman, B-4000 Liege 1, Belgium

401. Mario Mariscotti, Comision Nacional de Energia Atomica, Departmento de Fisica, Avenida del Libertador 8250, 1429 Buenos Aires, Argentina
402. Niels Marquardt, Institut fur Experimentalphysik III der Ruhr-Universitat Bochum, Postfach I02148 Gebaude NB/3, 4630 Bochum, Federal Republic of Germany
403. J. V. Martinez, Division of Chemical Sciences, Mail Stop J309 GTN, U.S. Department of Energy, Washington, DC 20545
404. W. R. McMurray, Deputy Chief Scientist, Kerninstituut Van Die Suidelike Universiteite, Southern Universities Nuclear Institute, Republic of South Africa
405. G. K. Mehta, Professor of Physics, Van de Graaff Laboratory, Indian Institute of Technology Kanpur, Kanpur 208 016, India
406. Eugen Merzbacher, University of North Carolina, Department of Physics and Astronomy, Chapel Hill, NC 27514
407. R. J. Meyer, Nuclear Physics Department, Fysisch Laboratorium Rijksuniversiteit, P. O. Box 80 000, 3508 TA Utrecht, The Netherlands
408. A. Michaudon, Chef du Service de Physique Nucleaire, Commissariat a l'Energie Atomique, Centre d'Etudes de Bruyeres le Chatel, P. O. Box 61, Montrouge 92120, France
409. R. Middleton, Department of Physics, University of Pennsylvania, Philadelphia, PA 19104
410. E. Migneco, INFN Laboratorio Nazionale del Sud, Corso Italia 57, 95127 Catania, Italy
411. Alice C. Mignerey, Department of Chemistry, University of Maryland, College Park, MD 20742
412. J. C. D. Milton, Physics Division, Atomic Energy of Canada Ltd., Chalk River, Canada K0J 1J0
413. University of Minnesota, Physics Department, 116 Church Street SW, Minneapolis, MN 55455
414. G. C. Morrison, Department of Physics, University of Birmingham, Birmingham B15 2TT, England
415. U. Mosel, Institut fur Theoretische Pysik, Universitat Giessen, 6300 Giessen, West Germany
416. S. C. Mukherjee, Librarian, Saha Institute of Nuclear Physics, 92, Acharya Prafulla Chandra Road, Calcutta - 9, India
417. Y. Nakamura, JPL, Systems Analysis Section, California Institute of Technology, 4800 Oak Grove Drive, Pasadena, CA 91103
418. Witek Nazarewicz, Institute of Physics, Politechnika Warszawska ul. Koszykowa 75, PL-00662 Warszawa, Poland
419. Ray Nix, Nuclear Theory, T-9, MS 8279, Los Alamos National Laboratory, Los Alamos, NM 87545
420. Ranier W. Novotny, II. Physikalisches Institut, Justus-Liebig Universitat, Heinrich-Buff-Ring 16, 6300 Giessen, West Germany
421. Oregon State University, Department of Physics, Boulder, CO 80309
422. Masumi Oshima, Japan Atomic Energy Research Institute. Tokai Establishment, Tokai-mura, Naka-gun, Ibaraki-ken 319-11, Japan
423. Peter Paul, Department of Physics, S.U.N.Y. at Stony Br , Stony Brook, NY 11794
424. Max Peisach, Southern Universities Nuclear Institute, P. Box 17, Faure, 7131, Republic of South Africa
425. Elliott S. Pierce, Assistant Director, Molecular Sciences, Department of Energy, Washington, DC 20545
426. A. A. Pilt, Tandem Accelerator Laboratory, McMaster University, Hamilton, Ontario, Canada L8S 4K1
427. University of Pittsburgh, Department of Physics, Pittsburgh, PA 15260
428. R. E. Pollock, Department of Physics, Indiana University, Bloomington, IN 47405
429. B. Povh, Max Planck Institut fur Kernphysik, 69 Heidelberg, Saupfercheckweg, Postfach 1248, Federal Republic of Germany
430. James Purcell, Department of Physics, Georgia State University, Atlanta, GA 30303
431. Jacobo Rapaport, Department of Physics, Ohio University, Athens, OH 45701-0640
432. John Rasmussen, Lawrence Berkeley Laboratory, Building 70A, Berkeley, CA 94720
433. Patrick Richard, Physics Department, Kansas State University, Manhattan, KS 66506
434. L. Rosen, Los Alamos National Laboratory, P. O. Box 1663, Los Alamos, NM 87544
435. Ranier Santo, Sektion Physik der Universitat Munchen, 8046 Garching, Beschleunigerlaboratorium (Forschungsgelande), Federal Republic of Germany
436. D. G. Sarantites, Department of Chemistry, Washington University, St. Louis, MO 63130
437. V. Sarantseva, Head, Publishing Department, Joint Institute for Nuclear Research, Head Post Office, P. O. Box 79, Moscow, U.S.S.R.
438. J. P. Schiffer, Physics Division, Argonne National Laboratory, 9700 South Cass Avenue, Argonne, IL 60439
439. A. Schwarzschild, Brookhaven National Laboratory, Upton, NY 11973
440. Hermann Schweickert, Cyclotron Laboratory, Kernforschungszentrum Karlsruhe, Institut fur Applied Physik, P. O. Box 3640, D-7500 Karlsruhe 1, Federal Republic of Germany
441. David K. Scott, National Superconducting Cyclotron Laboratory, Michigan State University, East Lansing, MI 48824
442. S. Seki, Tandem Accelerator Center, University of Tsukuba, Ibaraki 305, Japan
443. Paul Semmes, School of Chemistry, Georgia Institute of Technology, Atlanta, GA 30332
444. J. C. C. Sharp, Information Officer, Daresbury Laboratory, Science Research Council, Daresbury, Warrington WA4 4AD, England
445. N. Shikazono, Division of Physics, Japan Atomic Energy Research Institute, Tokai Research Institute, Postal Area Number 319-11, Tokai-mura, Naka-gun, Ibaraki-ken, Japan

446. R. H. Siemssen, Kernfysisch Versneller Instituit der Rijksuniversiteit Zernikelaan 25, 9747 AA Groningen, The Netherlands
447. C. Signorini, INFN Laboratorio Nazionale di Legnaro, Via Romea 4, 35020 Legnaro-Padova, Italy
448. S. J. Skorka, Tandem Accelerator Laboratory, University of Munich, Munich, Federal Republic of Germany
449. Hsu Loke Soo, Department of Physics, Nanyang University, Singapore 22, Republic of Singapore
450. C. Speth, Institut fur Kernphysik, KFA, Julich, Postfach 1913, D-5170 Julich, Federal Republic of Germany
451. T. Springer, Institut Max von Laue - Paul Langevin, 156 X Centre de Tri, 38402 Grenoble Cedex, France
452. Stanford University, Department of Physics, Stanford, CA 94305
453. Stephen G. Steadman, Massachusetts Institute of Technology, Room 26-411, Cambridge, MA 02139
454. R. G. Stokstad, Lawrence Berkeley Laboratory, Bldg. 88, Berkeley, CA 94720
455. T. T. Sugihara, College of Science, Oregon State University, Corvallis, OR 97331
456. Kazusuke Sugiyama, Department of Nuclear Engineering, Faculty of Engineering, Tohoku University, Sendai, Japan
457. Shigyea Tanaka, Japan Atomic Energy Research Institute, Tokai-mura, Ibaraki-ken, Japan
458. J. Teillac, Laboratoire de Physique Nucleaire d'Orsay, Facultes des Sciences, B. P. No. 1, Orsay (S. and O.), France
459. Lee C. Teng, Fermi National Accelerator Laboratory, Accelerator Division, P. O. Box 500, Batavia, IL 60510
460. S. T. Thornton, Physics Department, University of Virginia, Charlottesville, VA 22901
461. T. A. Tombrello, Division of Physics and Astronomy, California Institute of Technology, 106-38, Pasadena, CA 91125
462. Mauro Donizette Tonasse, Faculdades Integradad de Uberaba, Avenida Afranio de Azevedo no. 115, UBERABA - MG - Brazil
463. P. J. Twin, Daresbury Nuclear Physics Laboratory, Daresbury, Nr. Warrington, Lancashire, England
464. J. P. Unik, Argonne National Laboratory, Building 200, Argonne, IL 60439
465. Robert Vandenbosch, Department of Chemistry, University of Washington, Seattle, WA 98195
466. A. van der Woude, Kernfysisch Versneller Institut der Rijksuniversiteit, Universiteitscomplex Paddepoel, Groningen, The Netherlands
467. H. Verheul, Natuurkundig Laboratorium der Vrije Universiteit de Boelelaan 1081, Amsterdam, The Netherlands
468. VICKSI, Sekretariat, Hahn-Meitner Institut fur Kernforschung Berlin GmbH, Postfach 39 01 28, D-1000 Berlin 39, Federal Republic of Germany
469. Virginia Polytechnic Institute and State University, Department of Physics, Blacksburg, VA 24061
470. W. von Oertzen, Hahn-Meitner Institut fur Kernforschung, Berlin GmbH, Federal Republic of Germany
471. George Vourvopoulos, Department of Physics, Western Kentucky University, Bowling Green, KY 42101
472. A. H. Wapstra, Institute Voor Kernphysisch Onderzoek, Ooster Ringdijk 18, Amsterdam, The Netherlands
473. David Ward, Nuclear Physics Branch, Chalk River Nuclear Laboratories, Ontario, Canada KOJ 1JO
474. Harlan L. Watson, Deputy Staff Director, Subcommittee on Energy Development and Applications, Committee on Science and Technology, U.S. House of Representatives, B374 Rayburn House Office Building, Washington, DC 20515
475. H. E. Wegner, Department of Physics, 901A, Brookhaven National Laboratory, Upton, NY 11973
476. D. C. Weisser, Department of Nuclear Physics, Institute of Advanced Studies, The Australian National University, P. O. Box 4, Canberra ACT 2600, Australia
477. W. G. Weitkamp, Nuclear Physics Laboratory, G-10, University of Washington, Seattle, WA 98195
478. Joseph Weneser, Department of Physics, Bldg. 510, Brookhaven National Laboratory, Upton, NY 11973
479. E. P. Wigner, Department of Physics, Princeton University, Princeton, NJ 08540
480. B. H. Wildenthal, Department of Physics, Drexel University, Philadelphia, PA 19104
481. H. B. Willard, Program Director for Intermediate Energy Physics, National Science Foundation, 1800 G Street NW, Washington, DC 20050
482. University of Wisconsin, Department of Physics, Madison, WI 53706
483. Alexander Xenoulis, Van de Graaff Laboratory, Nuclear Research Center, Demokridos, Aghia Paraskevi Attikis, Athens, Greece
484. Takashi Yamazaki, Research Center for Nuclear Physics, Osaka University (Suita Campus), Ibaraki, Osaka, 567 Japan
485. D. Youngblood, Cyclotron Institute, Texas A&M University, College Station, TX 77940
486. E. F. Zganjar, Department of Physics and Astronomy, Louisiana State University, Baton Rouge, LA 70803
487. K. Ziegler, Hahn-Meitner Institut fur Kernforschung Berlin GmbH, Postfach 39 01 28, D-1000 Berlin 39, Federal Republic of Germany

488-584. Given distribution as shown in TID-4500 under Physics category (25 copies - NTIS)